

REACTION MECHANISMS INVOLVED IN CROSS COUPLING PROCESSES CATALYSED BY COPPER AND NICKEL

Mireia Rovira Coll

Per citar o enllaçar aquest document:

Para citar o enlazar este documento:

Use this url to cite or link to this publication:

<http://hdl.handle.net/10803/403434>

ADVERTIMENT. L'accés als continguts d'aquesta tesi doctoral i la seva utilització ha de respectar els drets de la persona autora. Pot ser utilitzada per a consulta o estudi personal, així com en activitats o materials d'investigació i docència en els termes establerts a l'art. 32 del Text Refós de la Llei de Propietat Intel·lectual (RDL 1/1996). Per altres utilitzacions es requereix l'autorització prèvia i expressa de la persona autora. En qualsevol cas, en la utilització dels seus continguts caldrà indicar de forma clara el nom i cognoms de la persona autora i el títol de la tesi doctoral. No s'autoritza la seva reproducció o altres formes d'explotació efectuades amb finalitats de lucre ni la seva comunicació pública des d'un lloc aliè al servei TDX. Tampoc s'autoritza la presentació del seu contingut en una finestra o marc aliè a TDX (framing). Aquesta reserva de drets afecta tant als continguts de la tesi com als seus resums i índexs.

ADVERTENCIA. El acceso a los contenidos de esta tesis doctoral y su utilización debe respetar los derechos de la persona autora. Puede ser utilizada para consulta o estudio personal, así como en actividades o materiales de investigación y docencia en los términos establecidos en el art. 32 del Texto Refundido de la Ley de Propiedad Intelectual (RDL 1/1996). Para otros usos se requiere la autorización previa y expresa de la persona autora. En cualquier caso, en la utilización de sus contenidos se deberá indicar de forma clara el nombre y apellidos de la persona autora y el título de la tesis doctoral. No se autoriza su reproducción u otras formas de explotación efectuadas con fines lucrativos ni su comunicación pública desde un sitio ajeno al servicio TDR. Tampoco se autoriza la presentación de su contenido en una ventana o marco ajeno a TDR (framing). Esta reserva de derechos afecta tanto al contenido de la tesis como a sus resúmenes e índices.

WARNING. Access to the contents of this doctoral thesis and its use must respect the rights of the author. It can be used for reference or private study, as well as research and learning activities or materials in the terms established by the 32nd article of the Spanish Consolidated Copyright Act (RDL 1/1996). Express and previous authorization of the author is required for any other uses. In any case, when using its content, full name of the author and title of the thesis must be clearly indicated. Reproduction or other forms of for profit use or public communication from outside TDX service is not allowed. Presentation of its content in a window or frame external to TDX (framing) is not authorized either. These rights affect both the content of the thesis and its abstracts and indexes.



DOCTORAL THESIS

REACTION MECHANISMS INVOLVED IN CROSS
COUPLING PROCESSES CATALYSED BY COPPER
AND NICKEL

Mireia Rovira Coll

2017

Doctoral programme in Chemistry

Supervised by: Dr. Xavi Ribas

Tutor: Dr. Xavi Ribas

Presented in partial fulfilment of the requirements for a doctoral degree from the
University of Girona



Dr. Xavi Ribas, from Universitat de Girona,

I DECLARE:

That the thesis entitled “Reaction mechanisms involved in cross coupling processes catalysed by copper and nickel”, presented by Mireia Rovira Coll to obtain a doctoral degree, has been completed under my supervision.

For all intents and purposes, I hereby sign this document.

Dr. Xavi Ribas

Girona, January 25, 2017

En definitiva, l'important és començar.

No importa com, després hi haurà temps

per pensar en els detalls

Alain

FULL LIST OF PUBLICATIONS

This thesis is based on a compendium of the following publications:

Chapter III

Model Csp²-Csp³ Hurdley Coupling Catalysis that Operates through a Well-Defined Cu^I/Cu^{III} Mechanism. Mireia Rovira, Marc Font, and Xavi Ribas in *Chem. Cat. Chem.*, **2013**, 5, 687 - 691. (Impact factor: 4.724, position 29/144 in Chemistry, Physical, 1st quartile)

Chapter IV

Aryl-Copper(III)-Acetylides as a Key Intermediates in Csp²-Csp Couplings under Mild conditions. Mireia Rovira, Marc Font, Ferran Acuña-Parés, Teodor Parella, Josep M. Luis, Julio Lloret-Fillol and Xavi Ribas in *Chem. Eur. J.* **2014**, 20, 10005 - 10010. (Impact factor: 5.771, position 24/163 in Chemistry, Multidisciplinary, 1st quartile)

Chapter V

Mechanistic insight in the trifluoromethylation of a well-defined aryl-Ni^{II} complex involving a SET step and a Ni^{IV}-CF₃ intermediate species. Mireia Rovira, Steven Roldán-Gómez, Vlad Martin-Diaconescu, Christopher J. Whiteoak, Anna Company, Josep M. Luis and Xavi Ribas. (*Submitted and under revision*)

Chapter VI

Orthogonal Discrimination among Functional Groups in Ullmann-type C-O and C-N Couplings. Mireia Rovira, Marta Soler, Imma Güell, Ming-Zheng Wang, Laura Gómez, and Xavi Ribas in *J. Org. Chem.* **2016**, 81, 7315 – 7325. (Impact factor: 4.785, position 7/59 in Chemistry, Organic, 1st quartile)

Three of these papers have been published in journals that belong to the first quartile according to JCR and the other one is submitted and under revision

Publications not included in this thesis

Characterization and Reactivity Studies of a Terminal Copper-Nitrene Species. Teresa Corona, Lidia Ribas, Mireia Rovira, Dr. Erik R Farquhar, Dr. Xavi Ribas, Prof. Dr. Kallol Ray, Dr. Anna Company. *Angew. Chem. Int. Ed.* **2016**, 55, 14005- 14008. (Impact factor: 11.709, position 13/157 in Chemistry, Multidisciplinary, 1st quartile).

LIST OF ABBREVIATIONS

Å	Angstrom
Abs	Absorbance
Ar	Aryl
AT	Atom Transfer
B	Base
BINAP	1,1'-(Binaphthalene-2,2'-diyl)bis(diphenylphosphine)
BTMABr ₃	Benzyltrimethylammonium tribromide
CF ₃	Trifluoromethyl group
CIO ₄	Perchlorate anion
CO	Carbon monoxide
COD	1,5-Cyclooctadiene
CODH/ACS	Carbon monoxide dehydrogenase/acetyl-CoA Synthase
COSY	Homonuclear correlation spectroscopy
CMD	Concerted metalation-deprotonation
CV	Cyclic Voltammetry
DFT	Density functional theory
DMF	<i>N, N</i> -dimethylformamide
DMSO	Dimethylsulfoxide
dppf	1,1'-Bis(diphenylphosphino)ferrocene
EPR	Electron Paramagnetic Resonance
EXAFS	Extended X-ray absorption fine structure
equiv	Equivalents
HRMS	High Resolution Mass Spectrometry
hν	The energy of photons
HMBC	Heteronuclear multiple-bond correlation spectroscopy
HOMO	Highest Occupied Molecular Orbital
HSQC	Heteronuclear single-quantum correlation spectroscopy
IAT	Ionic Atom Transfer
Kcal	Kilocalorie
L	Ligand
LUMO	Lowest Unoccupied Molecular Orbital
M	Metal
Me	Methyl
MCR	Methyl-coenzyme M reductase
MeOH	Methanol
MeCN	Acetonitrile
min	Minutes

mL	Millilitre
mM	millimolar
MW	Molecular weight
MS	Mass Spectrometry
n.d.	Not-detected
NFTPT	N-Fluoro-2, 4,6-trimethylpyridinium triflate
NMP	<i>N</i> -methylpyrrolidone
NMR	Nuclear Magnetic Resonance
NO ₃	Nitrate anion
NOESY	Nuclear Overhauser effect spectroscopy
NPA	Natural Population Analysis
Nu	Nucleophile
OTf	CF ₃ SO ₃ anion
p.	Page
PCET	Proton Coupled electron transfer
PCy ₃	Tricyclohexylphosphine
Phen	1,10-phenanthroline
PhICl ₂	Iodobenzene dichloride
PhI(OAc) ₂	Iodobenzene diacetate
ppm	Part per million
Ref.	Reference
r.t.	Room temperature
SET	Single Electron Transfer
S _E Ar	Electrophilic Aromatic Substitution
T	Temperature
TEMPO	2,2,6,6-Tetramethylpiperidin-1-yl)oxyl
TDTT	<i>S</i> -(trifluoromethyl)dibenzothiophenium triflate
THF	Tetrahydrofuran
TOCKSY	Total Correlation Spectroscopy
TON	Turn Over Number
UV-Vis	Ultraviolet-Visible spectroscopy
V	Volts
XANES	X-ray absorption near edge structure
XAS	X-ray absorption spectroscopy
X-ray	X-ray diffraction data

LIST OF FIGURES

Figure I.1. Earth-abundant first-row transition metals – catalysed C-C and C-Heteroatom bond formation, which are present in a wide range of interesting molecules. (p. 7)

Figure I.2. The number of publications on the topic of cross-coupling (blue bars) and on the cross-coupling reactions catalysed by Cu and Ni (purple line) between 2000 and 2015. Data for the bar chart were obtained by a Web of Knowledge search in September 2016 using keyword cross-coupling. Data for the line chart were obtained by the sum of refining search using keywords copper-catalysed and nickel-catalysed, respectively. (p. 8)

Figure I.3. Current challenges for the development of new cross-coupling methodologies based on first-row transition metals. (p. 10)

Figure I.4. Reversible reductive elimination/oxidative addition under pH control and the UV-Vis monitoring (p.19)

Figure VII.1. Progressive UV/Vis spectra of the cross-coupling reaction between compounds **L₁-Br** and malononitrile to form **P1**, catalysed by [Cu(CH₃CN)₄]OTf, which shown a disappearance of the characteristic band of the aryl-Cu^{III}-Br (**1_{Br}**) at 550 nm. Conditions: [**L₁-Br**] = 10 mM, [[Cu(CH₃CN)₄]OTf] = 1.4 mM, [malononitrile] = 100 mM, CH₃CN, 40°C, N₂ atmosphere. (p. 107)

Figure VII.2. ¹H NMR monitoring of the Cu^I-catalysed coupling of **L₁-Br** and malononitrile to produce **P1** quantitatively. (a) Overlaid spectra showing the consumption of substrate **L₁-Br** signals (circles) and growing of **P1** signals (stars). (b) Plot of the concentration changes of both substrate **L₁-Br** and product **P1** based on the integration of selected peaks. Conditions: [**L₁-Br**] = 9.6 mM, [[Cu^I(CH₃CN)₄]OTf] = 0.9 mM, [malononitrile] = 17 mM, [TMB] = 0.76 mM, CH₃CN, 40 °C, N₂ atmosphere. Spectra registered every 15 min (selected spectra are shown for clarity). (p. 108)

Figure VII.3. ¹H NMR monitoring study showing full formation of C_{aryl}-C_{sp} coupling intermediate species **I_{CF3}** upon reaction of **1_{ClO4}** with 2 equiv. of **S_{CF3}**. General conditions: [**1_{ClO4}**] = 78.6 mM, [**S_{CF3}**] = 157.2 mM, CD₃CN, 0 °C, N₂ atmosphere. (p. 111)

Figure VII.4 Plot of the concentration changes versus time of both **I_{CF3}** and product **P_{CF3}**, with and without sequestering Cu^I by the addition of phen. General conditions: [**1_{ClO4}**] = 78.6 mM, [**S_{CF3}**] = 157.2 mM, CD₃CN, 0 °C, N₂ atmosphere. (p. 112)

Figure VII.5. DFT Gibbs energy profile of the reaction of **1_{ClO4}** with **S_H** in the presence Et₂NH as external model base (ΔG in kcal·mol⁻¹). Et₂NH and Et₂NH₂⁺ molecules are necessary to ensure the correct energetic balance in all the steps of the reaction, and the external base was only explicitly modelled in the TS1 structure. Irrelevant hydrogen atoms are omitted for clarity. (p. 114)

Figure VII.6. Mulliken (green) and NPA (red) charges on the alkyne and amine moieties for **I_H·Cu^I** and **I_{NO2}·Cu^I** species. Conditions: B3LYP(6-31G* (C,N,H,Cu), SCRF = (SMD, acetonitrile), Grimme-D2). (p. 115)

Figure VII.7. (a) Representation of the frontier molecular orbitals; the highest-energy occupied and lowest-energy unoccupied molecular orbitals (the HOMO and LUMO) for **I_H·Cu^I** and **I_{NO2}·Cu^I** species.

(b) LUMO frontier orbitals for $\text{I}_\text{H}\cdot\text{Cu}^\text{I}$ and $\text{I}_{\text{NO}_2}\cdot\text{Cu}^\text{I}$ species and simplified scheme of the possible nucleophilic attacks in each molecule (Cu^I cation is omitted for clarity). (p. 117)

Figure VII.8. (a) XANES spectra of $[\text{L}_1\text{-H}\cdots\text{Ni}^\text{II}\text{-MeCN}]^{2+}$ (blue) and 1_{NO_3} in solution (black); Inset: highlight of the pre-edge region. (b) EXAFS analysis of $[\text{L}_1\text{-H}\cdots\text{Ni}^\text{II}\text{-MeCN}]^{2+}$. Shown are Fourier-transformed EXAFS spectra (no phase correction, FT, window as shown in the inset); Inset: k^2 -weighted unfiltered EXAFS spectra) and comparison of selected EXAFS derived and theoretical bond distances. (p. 122)

Figure VII.9. X-Ray crystal structures of 1_{ClO_4} (left) and 5_{OTf} (right) at 50% probability level. H atoms and counter anions omitted for clarity. Selected bond distances [Å] and angles [°] for 1_{ClO_4} : Ni(1)-C(1) 1.840(4), Ni(1)-N(3) 1.953(3), Ni(1)-N(1) 1.955(3), Ni(1)-N(2) 2.032(4); C(1)-Ni(1)-N(3) 83.33(18), C(1)-Ni(1)-N(1) 83.68(18), N(3)-Ni(1)-N(1) 164.53(16), C(1)-Ni(1)-N(2) 176.15(16), N(3)-Ni(1)-N(2) 96.68(15), N(1)-Ni(1)-N(2) 95.71(16). Selected bond distances [Å] and angles [°] for 5_{OTf} : Ni(1)-C(1) 1.838(7), Ni(1)-N(3) 1.98(3), Ni(1)-N(1) 1.94(3), Ni(1)-N(2) 2.062(6); C(1)-Ni(1)-N(3) 80.6(11), C(1)-Ni(1)-N(1) 84.2(8), N(3)-Ni(1)-N(1) 163.0(13), C(1)-Ni(1)-N(2) 178.3(10), N(3)-Ni(1)-N(2) 98.9(10), N(1)-Ni(1)-N(2) 96.5(8). (p. 123)

Figure VII.10. Cyclic voltammetry (CV) of complexes 1_{OTf} (blue chart) and 5_{OTf} (purple chart). Conditions used [1_{OTf}] = 0.5 mM, [$n\text{-Bu}_4\text{NPF}_6$] = 0.05 M and [5_{OTf}] = 1 mM, [$n\text{-Bu}_4\text{NPF}_6$] = 0.1 M, CH_3CN , 298 K, scan rate = 0.1 V/s, using non-aqueous Ag/AgNO₃ reference electrode. (p. 125)

Figure VII.11. Reaction progress of the formation of trifluoromethylated compound and consumption of 1_{OTf} monitored by ^1H NMR spectroscopy at low temperature in CD_3CN . Compounds 1_{OTf} , TDDT, trifluoromethylated product $\text{L}_1\text{-CF}_3$ and the byproduct of the oxidant (dibenzothophene) are tagged. (a) Complex 1_{OTf} at -40°C ; (b) Reaction crude, 45 min, -40°C ; (c) 1.45 h, 0°C and (e) Overnight 0°C . Only selected spectra are shown for clarity. General conditions: [1_{OTf}] = 13.2 mM, [CF_3^+] = 13.2 mM, CD_3CN , -40°C to 0°C . (p. 127)

Figure VII.12. Free energy profile for the proposed mechanism **A** computed at B3LYP/cc-pVTZ//B3LYP/TZPV level. TS_1 and $\text{TS}_{1\text{-Alt}}$ correspond to the two plausible transitions states that connects the Nickel (II) and Nickel (IV) species through an oxidative addition-like step. The former represents an $\text{S}_\text{N}2$ -like attack between the species, while the latter describes a sort-of-lateral attack. TS_2 is the transition state of the reductive elimination final step of the pathway **A**. Blue lines represent the singlet state pathway, whereas magenta ones describe the triplet profile. Atomic color code: Carbon, Nitrogen, Fluor, Sulphur; In the case of Nickel, different colors are assigned to different oxidation states: Nickel (III), Nickel (IV). (p. 129)

Figure VII.13. Energy profile computed at B3LYP-GD3BJ/TZPV level and snapshots sequence of the trifluoromethyl radical attack of the Nickel (III) to generate Nickel (IV). The plot (a) shows the electronic energy profile of the barrierless approach of the radical to the Ni^III . The spin density allows us to locate the bond distance at which the $\text{Ni}^\text{IV}\text{-CF}_3$ can be initially formed (no spin density on the CF_3). The sequence of IRC snapshots in scheme (b) illustrates the attack on the Nickel center. Atomic color code: Carbon, Nitrogen, Fluor, Sulphur; In the case of Nickel, different colors are assigned to different oxidation states: Nickel (III), Nickel (IV). (p. 129)

Figure VII.14. Free Energy profile for the Mechanism **C**. Free energy values were calculated at (B3LYP/cc-pVTZ//B3LYP/TZPV). The blue profiles correspond to open and close shell singlet systems while the triplets are represented by the fuchsia lines. The determining-step barrier free energy of the mechanism **A** (TS1, magenta color) is depicted to contrast with the value of the single electron transfer Marcus barrier. The zero Gibbs free energy value of the profile correspond to the free energies of reactants at infinite distance. The following color code illustrates the kind of atoms in the figure: Carbon, Nitrogen, Fluor, Sulphur, Nickel (II), Nickel (III), Nickel (IV). (p. 130)

Figure VII.15. Bidentate and tridentate auxiliary ligands chosen in this work. (p. 132)

LIST OF TABLES

Table VII.1. Attempts to synthesize P_{NO_2} under catalytic amounts of Cu^{I} sources. General conditions for catalytic reactions: $[\text{L}_1\text{-X}] = 5 \text{ mM}$, $[\text{nucleophile}] = 10 \text{ mM}$, $[\text{Cu}^{\text{I}} \text{ source}] = 0.5 \text{ mM}$, N_2 , CD_3CN (p. 118)

Table VII.2. Attempts to synthesize I'_{CF_3} under catalytic amounts of Cu^{I} sources. General conditions for catalytic reactions: $[\text{L}_5\text{-X}] = 5 \text{ mM}$, $[\text{nucleophile}] = 10 \text{ mM}$, $[\text{Cu}^{\text{I}} \text{ source}] = 0.5 \text{ mM}$ and 1 mM , N_2 , CD_3CN . (p. 119)

Table VII.3. Screening of amides for N-arylation with iodobenzene. [a] Reaction conditions: **1** (0.88 mmol, 0.9 M), **2** (1.79 mmol); [b] Yield was determined by GC. [c] Reaction temperature of 80°C . [d] Reaction temperature of 130°C . [e] 2% yield N,N-diphenylacetamide. [f] Isolated yield. $^{\dagger} \text{L}_3$ refers to the hydrochloric salt $\text{L}_3\cdot(\text{HCl})_2$. (p. 133)

Table VII.4. Mild O-arylation of alcohols with iodobenzene. [a] Reaction conditions: **1** (0.88 mmol, 0.9 M), **4** (1.79 mmol); [b] Yield was determined by GC. (p. 134)

Table VII.5. Mild N-arylation of amines with iodobenzene. [a] Reaction conditions: **1** (0.88 mmol, 0.9 M), **4** (1.79 mmol); [b] Yield was determined by GC. [c] Yield was determined by ^1H NMR. (p. 135)

Table VII.6. Arylation of different nucleophiles with bromobenzene. [a] Reaction conditions: **1** (0.88 mmol, 0.9 M), nucleophile (1.79 mmol); [b] Yield was determined by GC. [c] CsF was used as a base. (p. 136)

Table VII.7. Optimized conditions for ligand-dependent arylation of nucleophile (A or B) with iodobenzene in competition reactions with orthogonal selectivity. Standard reaction conditions: iodobenzene (0.88 mmol, 0.9M), **A** and **B** (1.79 mmol), 24 h, DMSO under an inert atmosphere (yields given in parenthesis). (p. 144)

Table VII.8. Optimized conditions for ligand-dependent arylation of nucleophile (A or B) with iodobenzene in competition reactions with high selectivity for one of the competing nucleophiles (Column A). Standard reaction conditions: iodobenzene (0.88 mmol, 0.9M), **A** and **B** (1.79 mmol), 24 h, DMSO under an inert atmosphere (yields given in parenthesis). (p. 145)

LIST OF SCHEMES

Scheme I.1. (a) Common Pd-mediated cross-coupling C-C and C-Heteroatom bond-forming processes. (b) General mechanism for Pd-catalysed cross-coupling reactions, which is initiated by oxidative addition of an organic halide at Pd⁰, continues through transmetallation and finishes by reductive elimination. (p. 10)

Scheme I.2. General reaction scheme of Ullmann-type coupling reactions and some representative auxiliary ligands used. (p.12)

Scheme I.3. Radical and non-radical intermediates proposed for Ullmann coupling reactions. (p. 13)

Scheme I.4. Proposed mechanistic pathways for (a) single electron transfer (SET) mechanism and (b) atom transfer (AT) mechanism both based in a Cu^I/Cu^{II} catalytic cycle. (p. 14)

Scheme I.5. (a) Photoinduced Ullmann C-N coupling reactions of copper-carbazolide complex with aryl halides. (b) Cyclization, followed by C-N bond formation, through a photoinduced Ullmann reaction using an allyloxyiodobenzene (radical clock) as a substrate. (p. 15)

Scheme I.6. Two proposed pathways for the Ullmann reaction depending on the relative order of oxidative addition/nucleophile coordination events. (p. 16)

Scheme I.7. Taillefer's mechanistic proposal for the Ullmann-Goldberg reactions using bidentate N, N-based auxiliary ligands. (p. 17)

Scheme I.8. Synthesis of well-defined high-valent copper (III) complexes, based on a macrocyclic model substrates. X-ray structures of aryl-Cu^{III} complexes (ellipsoid representation at 50% probability and hydrogens and corresponding counter anions are omitted for clarity). (a) Using triazamacrocyclic ligands described by Ribas group. (b) Using heterocalixarene-type ligands described by Wang. (p. 18)

Scheme I.9. General mechanism for the C-C and C-Heteroatom bond formation in copper-catalysed cross-coupling reaction within triazamacrocyclic model aryl halide platforms. (p. 20)

Scheme I.10. Possible intermediates resulting from coordination of Cu^I with bidentate ionic and anionic ligands. (p. 21)

Scheme I.11. (a) Selective ligand-dependent copper-mediated N-arylation and O-arylation of 5-amino-1-pentanol with 3-bromiodobenzene and bidentate ligands. (b) Computed mechanism reported by Fu for the selective arylation between aryl iodide and 5-amino-1-pentanol, using β-diketone and 1,10-phenanthroline as an auxiliary ligands, involving Cu^I/Cu^{III} oxidative addition/reductive elimination catalytic cycle. (p. 23)

Scheme I.12. Prototypical examples of elementary organometallic reaction steps, highlighting changes in oxidation state at nickel. Ligands and additives are omitted for clarity. M = metal; Me = methyl. (p. 26)

Scheme I.13. Radical and non-radical intermediates proposed for Ni-assisted cross-coupling reactions. (p. 27)

Scheme I.14. (a) General reaction scheme of cross-coupling reactions involving oxidative addition to C(sp³) electrophiles and some used ligands. (b) Mechanism proposed for C(sp³)-C(sp³) cross-coupling reactions catalysed by Ni. (p. 29)

Scheme I.15. Plausible mechanism involving Ni^I/Ni^{III} catalytic pathway using a well-defined Ni^I-NHC as a catalyst. (p. 30)

Scheme I.16. (a) General reaction scheme of Ni-assisted cross coupling reactions. (b) Possible mechanistic scenarios for Ni-Catalysed cross-coupling of aryl ethers consisting on a Ni⁰/ Ni^{II} catalytic cycle. (p. 31)

Scheme I.17. Proposed mechanism for Ni-catalysed direct arylation of unactivated C-H bonds in presence of bidentate directing group. (p. 33)

Scheme I.18. Proposed mechanism for photoredox/Ni dual catalytic cycle for cross-coupling reactions. (p. 34)

Scheme I.19. Synthesis of well-defined nickel(II) complex, based on a macrocyclic model substrates and X-ray structure of aryl-Ni^{II} complex using heterocalixarene-type ligands described by Wang. (p. 36)

Scheme I.20. (a) Synthesis of well-defined Ni^{III} distorted octahedral complexes through the oxidative addition of tetradentate (^tBuN3CBr) ligand to Ni(COD)₂ in THF at RT. (b) Formation of C-O bonds from the reductive elimination of aryl-Ni^{III} intermediate species. (p. 37)

Scheme I.21. (a) Synthesis of well-defined diamagnetic Ni^{IV} octahedral complex through the oxidation of [(Py₃CH)Ni^{II}(CH₂CMe₂-o-C₆H₄)] with TDDT, using a facial tridentate ligand tris(2-pyridyl)methane (Py₃CH). (b) Reactivity of aryl-Ni^{IV} complex forming a C(sp²)-C(sp³) or C(sp³)-O coupling products. (p. 38)

Scheme I.22. Synthesis of (Me₃tacn)Ni(CH₂CMe₂-o-C₆H₄) complexes. (p. 39)

Scheme I.23. Metal-mediated C-H bond activation aided by bidentate directing groups. (p. 41)

Scheme I.24. (a) Cu^{II}-mediated several C-H functionalization reactions using various nucleophilic anion sources. (b) Cu^{II}-catalysed acetoxylation of aryl C-H bonds. (c) Mechanism proposal for the selective formation of mono functionalized compounds. (p. 42)

Scheme I.25. Selective *meta*-arylation C-H activation reaction catalysed by Cu^{II} salts and the proposal of most favorable intermediated based on four-membered transition state found by DFT. (p. 43)

Scheme I.26. (a) Copper-mediated C(sp²)-H/C(sp³)-H coupling of benzoic acid derivatives with activated methylenes. (b) Copper-catalysed C-H activation based arene/alkyne annulations. (p.43)

Scheme I.27. (a) Copper-mediated direct C(sp³)-H acyloxylation. (b) Copper-mediated direct C(sp³)-H acetoxylation. (c) Copper-catalysed aryloxylation of β-C(sp³)-H. (p.44)

Scheme I.28. Divergent reactivity in Cu^{II}-mediated C-H oxidation reaction using the *N*-(8-quinoliny)-benzamide substrate. (p. 45)

Scheme I.29. Examples of nickel-catalysed C-H arylation reactions. (a) C-H arylation of 1,3-azoles with aryl halides. (b) Nickel-catalysed chelation-assisted selective *ortho* C-H activation reaction, using 8-aminoquinoline as a directing group. (p. 47)

Scheme I.30. Synthesis of well-defined nickel(II) complex based on a macrocyclic model substrate, *via* direct C-H activation, and X-ray structure of aryl-Ni^{II} (right). (p. 47)

Scheme I.31. C(*sp*²)-H activation mediated by high-valent Ni^{III} species, using macrocyclic model systems. (p. 48)

Scheme II.1. Study of the C-C bond formation using macrocyclic model systems based on high valent Cu^{III} and Ni^{II} intermediate species. (p.57)

Scheme II.2. Investigation of the role of auxiliary ligands on the chemoselective formation of C-heteroatom bonds and the plausible involvement of high valent copper(III) species as reaction intermediates. (p. 58)

Scheme VII.1. (a) Formation of C_{aryl}-C_{alkynyl} and C_{aryl}-C_{alkyl} bonds from the cross coupling reaction between macrocyclic model aryl-Cu^{III} complexes and alkynyl and alkyl lithium reagents. (b) Wang's model system involving an aryl-Cu^{III} intermediate species for Stephens-Castro reaction. (p. 103)

Scheme VII.2. Stoichiometric reaction between 1_{ClO4} and activated methylene substrates, which undergo C(*sp*²)-C(*sp*³) coupling product and subsequent intramolecular reorganization. General conditions for stoichiometric reactions: [1_{ClO4}] = 12 mM, [nucleophile] = 24 mM, CH₃CN, 25°C. For P2 product the reaction was carried out at 50°C and, for the P3 product, the addition of 2.2 eq. of Cs₂CO₃ was required. Yields of C-C coupling products are calculated by ¹H NMR using 1,3,5-trimethoxybenzene as internal standard. (p. 104)

Scheme VII.3. Proposed mechanism for the C-arylation of (a) malononitrile, (b) acetylacetone and (c) dimethyl malonate via aryl-Cu^{III} species and further intramolecular reorganization to afford the desired heterocyclic **P1-P3** compounds. (p. 106)

Scheme VII.4. Copper-catalysed Hurtley reactions with model aryl bromide (L₁-Br) to form P1-P3; highlight the detection of aryl-Cu^{III}-Br intermediate species, which undergo C(*sp*²)-C(*sp*³) coupling product and subsequent intramolecular reorganization. General conditions for catalytic reactions: [L₁-Br] = 5 mM, [[Cu(CH₃CN)₄]OTf] = 0.5 mM, [nucleophile] = 10 mM, CH₃CN, 25°C. For P2 product the reaction was carried out in presence of 2.2 equiv. of K₂CO₃ and molecular sieves and for the P3 product the reaction was performed in presence of 8.8 equiv. of K₂CO₃. Yields of C-C coupling products are calculated by ¹H NMR using 1,3,5-trimethoxybenzene as internal standard. (p. 107)

Scheme VII.5. General proposed mechanism of copper-mediated C(*sp*²)-C(*sp*³) bond formation through the intermediacy of aryl-Cu^{III} complexes within a model triazamacrocyclic aryl bromide substrate. (p. 109)

Scheme VII.6. Stoichiometric reaction between **1_{ClO4}** and phenylacetylene derivatives substrates (**S_R**), which undergo C(sp²)-C(sp) coupling product and further intramolecular reorganization to form 2H-isoindole (**P_{CF3}**, **P_{NO2}** and **P_{Ha}**) or 1,2-dihydroisoquinoline (**P_{Hb}**) scaffolds. General conditions for stoichiometric reactions: [**1_{ClO4}**] = 12 mM, [nucleophile] = 24 mM, CH₃CN, 25°C; product yields were calculated by ¹H NMR spectroscopy integration related to the internal. (p. 110)

Scheme VII.7. Reaction of **L₅-Cl** with *p*-CF₃-phenylacetylide copper(I) complex to afford the stable **I'_{CF3}** product. (p. 113)

Scheme VII.8. Mechanistic proposal for the formation of **P_R** products from the **1_{ClO4}** complex and *p*-phenylacetylene derivatives, with the intermediacy of aryl-Cu^{III}-acetylide species, and subsequent intramolecular cyclization following divergent pathways depending on **R**. (p. 115)

Scheme VII.9. Sequential addition of macrocyclic model substrate (**L₁-Br**) on a catalytic reaction in order to understand the catalytic operative mechanism. General conditions for the reaction: [**L₁-Br**] = 20 mM (each addition of 25 μL), [**S_{NO2}**] = 200 mM, [Cu^I source] = 20 mM, [TMB] = 2.4 mM N₂, CD₃CN; product yields were calculated by ¹H NMR spectroscopy integration related to the internal. (p. 119)

Scheme VII.10. Synthesis of organometallic aryl-Ni^{II} complexes (**1_{OTf}**, **1_{ClO4}**, **1_{NO3}** or **5_{OTf}**) via (a) oxidative addition at Ni⁰ and (b) direct C-H activation by Ni^{II}. (DFT optimized structure of [**L₁-H**...Ni^{II}-ACN]²⁺ is depicted). (p. 120)

Scheme VII.11. Reactivity of **1_{OTf}** and **5_{OTf}** in the presence of widely used “CF₃⁺” oxidants, TDTT and Togni reagent to obtain **L₁-CF₃** and **L₅-CF₃**. General conditions for stoichiometric reactions: [**1_{OTf}**] = 29.3 mM, [**CF₃⁺**] = 58.6 mM, CH₃CN, 25°C, 4h and [**5_{OTf}**] = 27.7 mM, [**CF₃⁺**] = 55.4 mM, CH₃CN, 70°C, 48h. (p. 126)

Scheme VII.12. Brief description of the three proposed mechanisms, **A**, **B** and **C**. Mechanism **A** implies the transfer or flow of two electrons during the reaction (oxidative addition-like step, followed by a reductive elimination step); Mechanism **B** can be described as Single Electron Transfer (SET), followed by a direct radical CF₃ addition on the aryl group. Mechanism **C** is a combination of **A** and **B**. (p. 128)

Scheme VII.13. Competitive reactions among nucleophiles using iodobenzene with a sharp switch of chemoselectivity. Conversions are given in parentheses; standard experimental conditions used. (p. 138)

Scheme VII.14. Competition reactions among nucleophiles with strong preference for one nucleophile independent of the auxiliary ligand used. Conversions are given in parentheses; standard experimental conditions used. (p. 139)

Scheme VII.15. (a) Competitive reactions using *p*-iodotoluene. (b) Competitive reactions using *p*-iodonitrobenzene. Conversions are given in parentheses; standard experimental conditions used. (p. 140)

Scheme VII.16. Competition reactions using bifunctional nucleophiles **8a** - **8c**. Conversions are given in parentheses; standard experimental conditions used. (p. 141)

Scheme VII.17. Competition reactions among nucleophiles using bromobenzene with sharp switch of chemoselectivity. Conversions are given in parentheses; standard experimental conditions used. (p. 142)

Scheme VII.18. Selected coupling reactions using radical clock (**rc**) as a substrate. (p. 146)

AGRAÏMENTS

Doncs bé família, tot l'ho bo s'acaba i no m'agradaria acabar sense dedicar-vos unes paraules. Vaig entrar al Qbis a fer el projecte final de carrera el setembre del 2011 i ara, gener del 2017 estic escrivint els agraïments de la tesi. Podria omplir fulls i més fulls amb historietes i vivències de tot tipus amb tots vosaltres, però intentaré ser breu.

Xavi, m'agradaria començar per tu, només puc donar-te les GRÀCIES per l'oportunitat que em vas donar, per ajudar-me, per animar-me, per ensenyar-me tot el que saps i més. Miquel i Anna gràcies per ser-hi sempre, per la vostra ajuda i el vostre suport. Els tres formeu un gran equip i, creieu-me és molt difícil expressar amb paraules la gratitud que sento cap a vosaltres.

Josep Maria, moltíssimes gràcies per supervisar tots els càlculs DFT i per les idees aportades. Moltes gràcies a les "Belles glòries" del Qbis que em vau adoptar de seguida i em vareu fer sentir com a casa i, encara ara em feu costat: Julio i Isaac, molta sort amb els nous grups. Alícia, la reina del Cu, moltes gràcies per la teva ajuda. A en David, a l'Irene, a en Zoel (aprofita ara per córrer, perquè se't gira feina!!!) i a la Mercè, des de que vau marxar ja no és el mateix. L'Imma i la Marta, el Cu^{III} team, va ser maco mentre va durar, ehh. A en Ferran, moltes gràcies per el càlculs DFT i molta sort per Tarragona. A l'Arnauet de Vidreres, molta sort per Japó i, sempre pots patentar el ranxo!!! A la Carla, molta sort amb el PhD guapa!!

A la Laura, la que viu més bé, moltíssimes gràcies per la teva ajuda sobretot amb el Cu^{III} i per colar-me alguna mostra de tant en tant. Dr. Marc Font gràcies per ajudar-me des de bon principi, i sobretot per els acudits de l'Eugenio (que mai podies acabar d'explicar perquè et parties de riure!!!). Espero que continuïs siguent tant Modernet de merda com sempre. Sir Christopher J. Whiteoak, thanks for all your super/crazy ideas, for domesticate Oriol and absolutely for the wine clubs. En Joan, un crack que sempre té un meme o un video apunt per enviar. Espero que et vagi molt i molt per Suïssa, et trobarem molt a faltar!!! A la Cristina, la més trempada, la més treballadora i la més cuqui del Qbis. Espero que tot et vagi molt i molt bé perquè t'ho mereixes; ole tu mujer!!! El Monsieur Colombar que sempre està disposat a anar a fer un coffee. A l'Orioloooo, un altre crack que sempre disposat a molestar o entrenir el personal (depen de com es miri), però saps que et trobaré molt a faltar tontorron!! Gràcies per ajudar-me, donar-me idees, escoltar les meves paranoies i, per instal·lar-me els programes a l'ordinador. Jordi, un fanàtic de la ratafia i l'independència, et desitjo molta sort i continua anant a les classes de gimnàs de la meva amiga, ehh. En Màrius, un homínid únic en la seva espècie (menys mal!), només d'arribar ja va esberar el galliner amb el seu flow. Et desitjo molta sort en el teu post-doc i, sinó sempre et pots apuntar a Masterchef o Gran Hermano, total ja ets famós!!! A en Carles, el més guapo i el més trempat del parc!! Et desitjo tota la sort del món, estic segura que et sortirà una gran tesi. I els que acabeu de començar Lorena, Carla, Cristian, Pau i Marc us desitjo tota la sort i la paciència del món (sobretot a la Lorena que ha d'aguantar en Màrius tot el dia).

Als tallers també són tots molt macus com l'Olaf un altre crack que a primera vista no sembla, però està com una cabra!! A la Michela, la *Madonna* de la mafia italiana, la més bella i brava de tots, te voy a echar mucho de menos, suerte con tu super tesis *sdruffy*. En Giorgio, otro crack que siempre tiene respuesta a tus preguntas, espero que tengas mucha suerte, porque te lo mereces. A la Tere, la meva

compi d'habitació, molts ànims en la defensa (segur que ho faras molt bé) i moltíssima sort per Berlín!! En Diego, puro nervio, sempre disposat a ajudar i a fer coses (serà per la coca-cola?), molta sort amb els cavitands! En Marco, el Giorgio Armani de Girona, un super currante y fan de la química orgánica, te deseo mucha suerte y estoy segura que lo haras top. A la Carlota, et desitjo molta sort en la recta final de la tesi, tu pots amb això i molt més!! Els que comenceu Mago i Laia us desitjo molta sort; Mago posa'ls tots a ratlla. Vlad, the synchrotron guy thanks for all the XAS, XANES and EXAFS analysis.

Raquel, la pesadilla de Sigma Aldrich, que habriamos hecho sin tí!! Muchas gracias por cuidarnos tanto y siempre con una sonrisa, eres la mejor!!! En Gerard el jefe del taller 13 i el trenca portes, que tinguis molta sort amb la tesi i no estiguis tant serio home!!! La Mònica i el seu bon dia rialler que t'alegra el dia. La Ilaria, la reina del UV que siempre está contenta, espero que tengas mucha suerte guapa. La Valeria, la más nueva la mafia italiana y que siempre sonrie, te deseo mucha suerte en el PhD. Steven, que más pues, muchas gracias por los cálculos del níquel y te deseo toda la suerte del mundo.

I would like to aknowledge Prof. Dr. Gwilherm Evano for taking care of me during my stay at the université Libre de Bruxelles. It was a great pleasure working in your labs and I keep really good memories of the time that I spent in Brussels. I would like to thank Sara, Cédric, Celine, Morgan, Antoine, Christopher, Phideline and Jianjun for the great time on the lab, for taking care of me and for the french lessons. Ludo and Marylou, thanks for the great time on the lab and also for the thousands of beers on l'Atelier and le Tavernier it was amazing! I thank all of you most sincerely and I look forward to seeing you again!

Dr. Jana Roithová, Erik and Lucie thanks for all the He@IRPD spectroscopy and for all the mass spectroscopy experiments, it was a great time in Prague.

Finalment, m'agradaria agrair als meus pares i les meves germanes, la seva ajuda i el seu suport incondicional, tot i no entendre gaire el que faig. També els més petits de casa que fan que cada dia sigui una superaventura i t'oblidis dels problemes. A l'Anna Vicu per aquesta super portada que m'ha ajudat a fer i, per ser tant valenta i lluitadora. A les meves cuquis i els sopars de divendres que arreglen la setmana i el món, us estimo molt a totes!! I recordeu que tenim un viatge pendent. A la família del cau, que no para de créixer, per totes les vivències i els bons moments viscuts. Tot i que costa veure'ns tots sempre ser que esteu allà, us estimo molt a tots.

I ara si que per acabar, m'agradaria agrair-li a en David, tota la paciència i tot el seu suport, que creu-me han sigut molt importants. Moltes gràcies pel teu bon humor, tots el bons moments viscuts i per aguantar totes les meves presentacions orals. Gràcies per cuidar-me i estimar-me tant, les coses són més boniques i fàcils quan sumem dos!

Moltíssimes gràcies a tots de tot cor,

Mireia

ACKNOWLEDGEMENTS

This work would have not been possible without the following collaborations:

- Serveis Tècnics de Recerca from Universitat de Girona for technical support, with especial remark to Dr. Laura Gómez and her dedication in setting up the cryospray mass spectrometer.
- Dr. Julio Lloret, Dr. Ferran Acuña Parés from ICIQ and Dr. Josep M. Luis and Steven Roldán from IQCC for the DFT calculations
- Dr. Teodor Parella from Servei de RMN at Universitat Autònoma de Barcelona for NMR experiments and fruitful discussions.
- Prof. Dr. Gwilherm Evano from the Université Libre de Bruxelles (ULB) for hosting a scientific visit and the collaborative research in the mechanistic investigations on Ullmann-type trifluoromethylation and amination reactions.
- Dr. Christopher J. Whiteoak (Sheffield Hallam University) for collaboration in the synthesis and reactivity of organometallic aryl-Ni^{II} complexes.
- Dr. Vlad Martin-Diaconescu from IQCC for XAS study and EXAFS analysis.
- Financial support from the European Research Council (ERC-2011-StG- 277801), and from the Spanish MICINN (CTQ2013-43012-P).

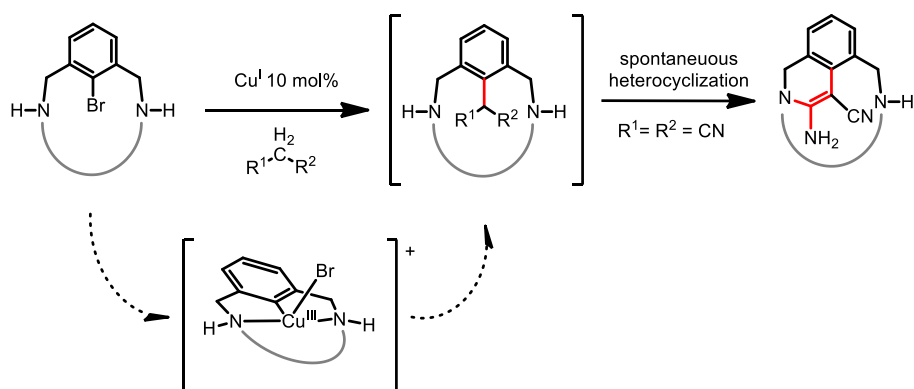
GRAPHICAL ABSTRACT

Summary (p. 1)

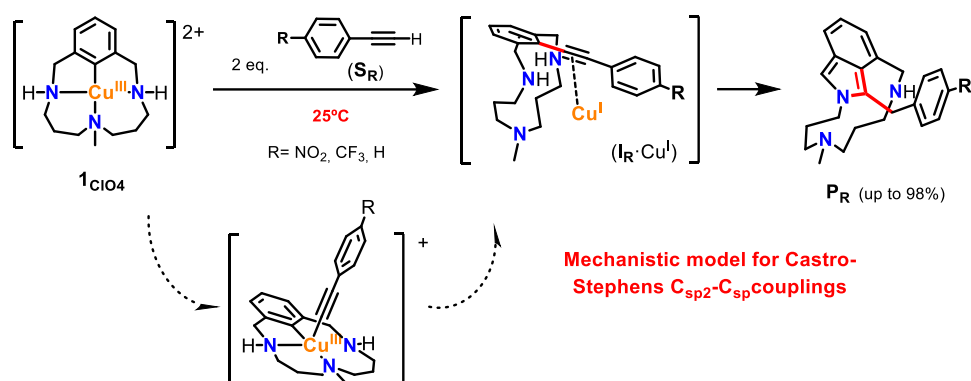
Chapter I. General Introduction (p. 5)

Chapter II. Main Objectives (p. 55)

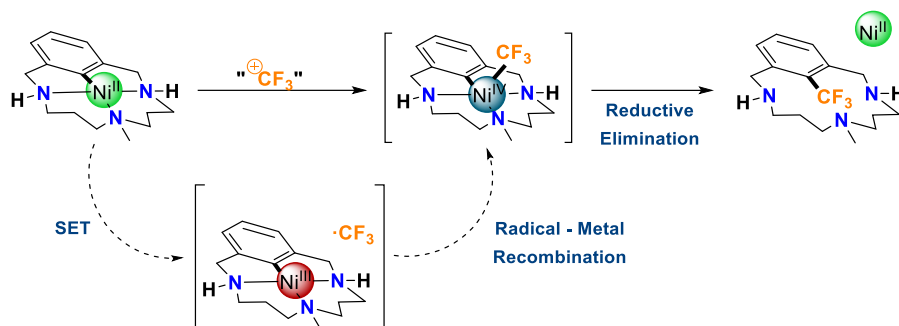
Chapter III. Model Csp^2 - Csp^3 Hurtley Coupling Catalysis that Operates through a Well-Defined Cu^I/Cu^{III} Mechanism (p. 59)



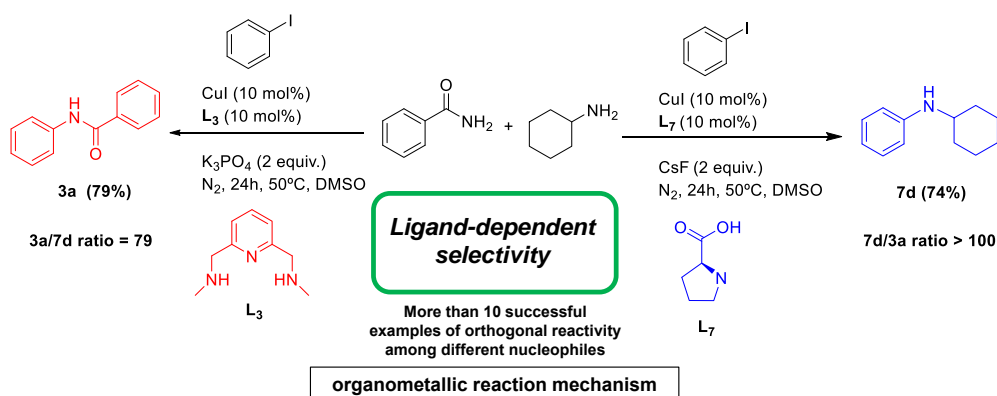
Chapter IV. Aryl-Copper(III)-Acetylides as Key Intermediates in Csp^2 - Csp Model Couplings under Mild Conditions (p. 67)



Chapter V. Mechanistic insight in the trifluoromethylation of a well-defined aryl-Ni^{II} complex involving a SET step and a Ni^{IV}-CF₃ intermediate species (p. 75)



Chapter VI. Orthogonal Discrimination among Functional Groups in Ullmann-Type C-O and C-N Couplings (p. 83)



Chapter VII. Results and Discussion (p. 99)

Chapter VIII. General Conclusions (p. 151).

ANNEX 1. (p. 155).

ANNEX 2. (p. 179).

ANNEX 3. (p. 209).

ANNEX 4. (p. 247).

TABLE OF CONTENTS

Summary	1
Resum	2
Resumen	3
Chapter I. General Introduction	5
I.1. First row transition metals in organic synthesis	7
I.2. Cross-Coupling Catalysis	8
I.3. Copper in Cross-Coupling Catalysis	11
I.3.1. Coinage metals	11
I.3.2. Overview and background	11
I.3.3. Mechanistic features of Copper-Catalysed Cross-Coupling reactions	12
I.3.4. One-electron redox processes Cu ^I /Cu ^{II}	13
I.3.5. Oxidative addition/reductive elimination Cu ^I /Cu ^{III}	16
I.3.5.1. The role of high-valent organometallic Copper(III) species	18
I.3.5.2. Mechanistic insights on Ullmann-type Cross-Coupling reactions	20
I.3.6. Dependence on ancillary ligands	21
I.3.6.1. Chemoselectivity	21
I.3.7. General Conclusions and industrial applications	23
I.4. Nickel in Cross-Coupling Catalysis	24
I.4.1. Group 10 metals	24
I.4.2. Overview and background	25
I.4.3. Mechanistic features of Nickel-assisted Cross-Coupling reactions	27
I.4.3.1. Ni ^I /Ni ^{III} Catalytic Cycle	28
I.4.3.2. Ni ⁰ /Ni ^{II} Catalytic Cycle	30
I.4.3.3. Ni ^{II} /Ni ^{IV} Catalytic Cycle	32

I.4.4. Photoredox Catalysis	33
I.4.5. Deeper mechanistic insight on Ni-Catalysed Cross-Coupling reactions	35
I.4.5.1. Chelation-assisted stabilisation of high-valent nickel species	35
I.4.6. General Conclusions and applications.....	39
I.5. C-H bond functionalization	39
I.5.1. Copper catalysed C-H activation	41
I.5.1.1. Intramolecular C-H activation using macrocyclic model substrates	44
I.5.2. Nickel catalysed C-H activation	46
I.5.2.1. Intramolecular C-H activation using macrocyclic model substrates	47
I.6. References	48
 Chapter II. Main Objectives	 55
 Chapter III. Model Csp²-Csp³ Hurtley Coupling Catalysis that Operates through a Well-Defined Cu^I/Cu^{III} Mechanism	 59
 Chapter IV. Aryl-Copper(III)-Acetylides as a Key Intermediates in C(sp²)-C(sp) Couplings under Mild conditions.	 67
 Chapter V. Mechanistic insight in the trifluoromethylation of a well-defined aryl-Ni^{II} complex involving a SET step and a Ni^{IV}-CF₃ intermediate species.	 75
 Chapter VI. Orthogonal Discrimination among Functional Groups in Ullmann-type C-O and C-N Couplings.	 83
 Chapter VII. Results and discussion.....	 99
VII.1. Copper(III)-mediated C(sp ²)-C(sp ³) and C(sp ²)-C(sp) bond formation under milder conditions	102
VII.1.1. Reactivity of aryl-Cu ^{III} (1 _{C104}) with activated methylene substrates (Hurtley Catalysis).....	103

VII.1.1.1. Mechanistic insight into the C(sp ²)-C(sp ³) bond formation.....	105
VII.1.2. Reactivity of aryl-Cu ^{III} (1 _{C104}) with <i>p</i> -R-phenylacetylene (S_R) (Stephens-Castro couplings)	109
VII.1.2.1. Mechanistic insight into the C(sp ²)-C(sp) bond formation.....	111
VII.1.2.2. DFT calculations and mechanistic proposal	113
VII.2. Mechanistic insight in the trifluoromethylation of a well-defined aryl-Ni ^{II} complex involving a SET step and a Ni ^{IV} -CF ₃ intermediate species	120
VII.2.1. Synthesis and characterization of [L _n -Ni ^{II}](X).....	120
VII.2.2. Reactivity of [L _n -Ni ^{II}](X) towards common nucleophiles	124
VII.2.3. Reactivity of [L _n -Ni ^{II}](X) towards 1e ⁻ and 2e ⁻ oxidants	125
VII.2.4. Mechanistic insight. DFT calculations	127
VII.3. Orthogonal discrimination among functional group in Ullmann-type C-O and C-N Couplings	131
VII.3.1. Optimization of the single arylation of nucleophiles	132
VII.3.2. Ligand-dependent selectivities in competition reaction using iodobenzene.....	136
VII.3.3. Ligand-dependent selectivities in competition reaction using bifunctional nucleophiles and iodobenzene.....	139
VII.3.4. Ligand-dependent selectivities in competition reaction using bromobenzene.....	140
VII.3.5. Ligand-dependent selectivities in competition reaction using <i>para</i> -substituted bromobenzene	141
VII.3.6. Practical orthogonal nucleophile discrimination summary	143
VIII.4. References.....	147
Chapter VIII. General conclusions.....	151
ANNEX 1. Supporting information Chapter III	155
ANNEX 2. Supporting information Chapter IV	179
ANNEX 3. Supporting information Chapter V	209
ANNEX 4. Supporting information Chapter IV	247

SUMMARY

The development of efficient synthetic strategies have been one of the key challenges in synthetic organic chemistry. Many types of cross-coupling reactions have been known for several decades, however, advances in recent years have led to the development of many of the catalytic organometallic processes used today. One of the most relevant cross-coupling process is the Ullmann-Goldberg coupling, in which stoichiometric or catalytic amounts of a copper complex were used. Besides, the use of nickel-based catalysts in cross-coupling reactions is emerging as a powerful tool providing very rich, versatile and innovative chemical transformations. Despite such methodologies have been extensively developed, the fundamental mechanistic steps that govern such transformations are not clearly understood. It is noteworthy that an improved understanding of the reaction mechanisms should facilitate the development of improved methodologies as well as the catalyst design. This doctoral dissertation is focused on the use of copper and nickel-based synthetic model systems in order to gain insight into the formation of C-C bonds and also, on the role of the auxiliary ligands imparting chemoselectivity in Ullmann chemistry.

In the first part of this thesis, we take advantage of the feasibility of well-defined aryl-Cu^{III} complexes as intermediated species in several C(sp²)-Heteroatom bond formation reactions, to further develop their reactivity in presence of activated methylenes (Hurtley couplings) and terminal acetylenes (Stephens-Castro couplings) to form C(sp²)-C(sp³) and C(sp²)-C(sp) bonds, respectively. The results obtained indicate the intermediacy of aryl-Cu^{III} species in such reactions and provide insight on the fundamental understanding of the elementary steps of these transformations.

Subsequently, we explored the reactivity of the analogue well-defined aryl-Ni^{II} complexes using the same macrocyclic model system. The reactivity of the aryl-Ni^{II} complexes in presence of the widely used trifluoromethylating sources provided us a nicely mechanistic pathway initiated by a SET step followed by a recombination of the aryl-Ni^{III} and the CF₃[•] radical to afford an aryl-Ni^{IV}-CF₃ intermediate which easily evolved into reductive elimination step. This square planar platform was able to support the formation of nickel complexes in three oxidation states (II, III, IV) and thus could be of great help on the reactivity studies, trying to understand the role of each oxidation state in several organometallic transformations.

In the last part of the thesis we have turned our attention on the effect of the auxiliary ligand choice on the chemoselectivity and on the operative pathway in a standard Ullmann systems. We studied the chemoselective arylation of a wide-range of nucleophiles oxygen- and nitrogen-based nucleophiles in competition reactions using different well-known and available chelating ligands and aryl iodides and bromides, obtaining in the most of the cases excellent selectivity and high yields. The orthogonal selectivity is mainly governed by the nature of the auxiliary ligand. The mechanistic details of these processes are also discussed.

RESUM

El desenvolupament d'estratègies sintètiques més eficients i sostenibles esdevé un dels reptes més importants en el camp de la síntesi orgànica. Es coneixen diversos tipus de reaccions d'acoplament creuat, i a més a més, els recent avenços en aquest camp han permès el desenvolupament de diversos processos basats en química organometàl·lica de gran utilitat en els nostres temps. La reacció d'Ullmann-Goldberg, basada en l'ús de catalitzadors de coure, és una de la més important en l'àmbit dels acoblaments creuats. Per altra banda, l'ús de catalitzadors basats en níquel està emergint d'una forma molt potent, ja que posseix una química molt novedosa i altament versàtil. Tot i els avenços en aquestes metodologies, els passos fonamentals que regeixen aquests processos continuen encara generant controvèrsia. Caldria destacar que una millor comprensió dels mecanismes de reacció facilitaria el desenvolupament de metodologies innovadores i un disseny més acurat dels catalitzadors. Aquesta tesi doctoral es centra en el desenvolupament de sistemes sintètics models basats en coure i níquel amb l'objectiu d'entendre la formació d'enllaços C-C, a més també s'estudia la selectivitat dirigida pels lligands auxiliars en la química de tipus Ullmann.

En la primera part de la tesi, estudiem la reactivitat d'un complex ben definit aril-Cu^{III} davant de metilens activats (Reacció de Hurtley) i d'acetilens terminals (Reacció de Stephens-Castro) per formar C(sp²)-C(sp³) i C(sp²)-C(sp), respectivament. Els resultats obtinguts indiquen la directa implicació d'espècies aril-Cu^{III} en el transcurs de les reaccions i aporten coneixament sobre els paràmetres fonamentals que dominen aquestes reaccions.

Seguidament, s'estudia la reactivitat dels complexos anàlegs ben definits aril-Ni^{II}, amb l'objectiu d'entendre d'una forma més clara la química redox del níquel, utilitzant el mateix system model. La reactivitat d'aquests complexos en presència de fonts trifluorometilans ens proporciona un interessant mecanisme de reacció iniciat per un procés SET, seguit per la recombinació de l'aril-Ni^{III} i el CF₃· radical per obtenir l'espècie intermèdia aril-Ni^{IV}-CF₃, que evoluciona favorablement per donar lloc a un procés d'eliminació reductiva. Per tant, aquest sistema amb geometria plano-quadrada és compatible amb la formació de complexos de níquel en tres estats d'oxidació (II, III, IV). Fet molt important, que ajuda a entendre el rol del níquel en cada estat d'oxidació en diverses reaccions organometàl·liques.

En l'última part de la tesi, ens centrem en com afecta la naturalesa del lligand auxiliar coordinat al centre de coure i la selectivitat que presenten envers diferents nucleòfils. També estudiarem l'efecte que presenten en el mecanisme de reacció operatiu en els sistemes estàndards de tipus Ullmann. S'estudia la quimioselectivitat entre nucleòfils basats en oxigen i nitrogen en reaccions de competició utilitzant diversos lligands auxiliars i halurs d'aril, obtinguent en la majoria de casos una alta selectivitat i uns rendiments excel·lents. En la majoria dels casos, la selectivitat obtinguda és deguda a la natura del lligand. També es discuteixen els aspectes mecanístics que governen aquests processos.

RESUMEN

El desarrollo de estrategias sintéticas más eficientes y sostenibles es uno de los retos más importantes en el campo de la síntesis orgánica. Se conocen diversos tipos de reacciones de acoplamiento cruzado que, gracias a los recientes avances en este campo, ha permitido el desarrollo de innumerables procedimientos basados en química organometálica de gran utilidad en nuestros días. La reacción de Ullmann-Goldberg, basada en el uso de catalizadores de cobre, es una de las más importantes en el ámbito de los acoplamientos cruzados. Por su parte, el uso de catalizadores basados en níquel está emergiendo de una forma muy potente, ya que posee una química muy novedosa y altamente versátil. A pesar de los avances conseguidos en estas metodologías, los pasos fundamentales que rigen estos procesos, aún siguen generando controversia. Vale la pena destacar que una mejor comprensión de los mecanismos de reacción facilitaría el desarrollo de metodologías innovadoras y un diseño más preciso de los catalizadores. Esta tesis doctoral se centra en el desarrollo de sistemas sintéticos modelo basados en cobre y níquel con el objetivo de entender la formación de enlaces C-C, además también se estudia la selectividad dirigida por los ligandos auxiliares en la química de tipo Ullmann.

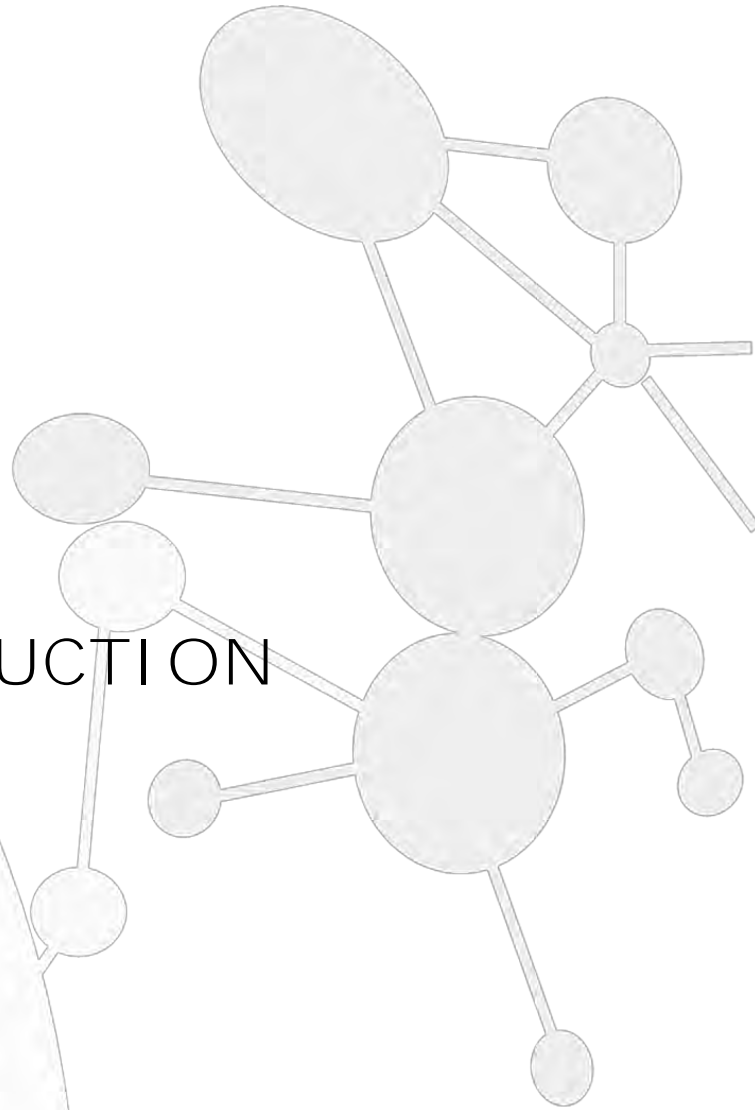
En la primera parte de la tesis, se estudia la reactividad de un complejo bien definido arilo-Cu^{III} en presencia de metilenos activos (Reacción de Hurtley) y de acetilenos terminales (Reacción de Stephens-Castro) para formar enlaces C(sp²)-C(sp³) y C(sp²)-C(sp), respectivamente. Los resultados obtenidos indican la directa implicación de especies arilo-Cu^{III} en el transcurso de las reacciones y aportan conocimiento sobre los parámetros fundamentales que rigen estas reacciones.

A continuación, se estudia la reactividad de los complejos bien definidos análogos arilo-Ni^{II}, con el objetivo de entender más claramente la química redox del níquel utilizando el mismo sistema modelo. La reactividad de estos complejos en presencia de agente trifluorometilantes nos proporciona un interesante mecanismo de reacción iniciado por un proceso SET, que seguido de la recombinación entre la especie arilo-Ni^{III} y el radical CF₃·, para obtener la especie intermedia aril-Ni^{IV}-CF₃, que evoluciona favorablemente a un proceso de eliminación reductora. Por lo tanto, este sistema plano-cuadrado es compatible con la formación de complejos de níquel en tres estados de oxidación (II, III, IV). Los resultados obtenidos, pueden ser de gran ayuda para entender el rol del níquel en cada estado de oxidación en diversas reacciones organometálicas.

En la última parte de la tesis, nos centramos en el estudio de las propiedades estéricas de los ligandos auxiliares y la selectividad ante diversos nucleófilos. También estudiaremos el efecto que presentan en el mecanismo de reacción operativo en los sistemas estándar de tipo Ullmann. Se estudia la quimioselectividad entre nucleófilos basados en oxígeno y nitrógeno en reacciones de competición utilizando diversos ligandos auxiliares y haluros de arilo, obteniendo en la mayoría de los casos una alta selectividad y unos rendimientos excelentes.

CHAPTER I.

GENERAL INTRODUCTION



I.1 First row transition metals in organic synthesis

Natural products, pharmaceuticals, agrochemicals and polymers are built from organic molecules and many of these compounds are structurally complex, possessing a high percentage of diverse C-C, C-H and C-Heteroatom bonds as well as multiple stereogenic centres. Organic compounds have played a central role in the development of the field of organic chemistry by providing challenging synthetic targets.

Activation of C-H, C-C and C-Heteroatom bonds has received a great attention over the last decades as the preferred way to increase molecular complexity and find new applications. The development of efficient methods and novel synthetic strategies, which not only avoid the tedious synthetic procedures and emission of undesirable waste, remains one of the top challenges in organic chemistry. Oftentimes, older reactions are rediscovered and improved in order to solve several disadvantages.^{1,2} Transition metal catalysis has revolutionized organic synthesis, enabling transformations that would be either difficult or impossible by other means, providing concise and practical approaches for the preparation of various organic compounds. Elementary transition metal-mediated reactions to form and cleave bonds in organic molecules are of fundamental importance in homogeneous catalysis.³⁻⁵

In the past decades, a great number of well-defined catalysts based on late noble transition metals were broadly employed, because they played a key role being powerful catalysts for inert bonds activations. From an industrial point of view, the high toxicity and high cost of these metals limit their broad applications. In contrast, the earth-abundant first-row transition metals, such as iron, cobalt, nickel and copper, are attractive alternatives to the traditional precious metals, due to their lower toxicity, their high abundance and in consequently, lower cost.^{4,6} For example, the natural abundance of Fe, Ni, Co and Cu on earth is about 32%, 1.8%, 0.88% and 0.31%, respectively. In recent years, the assumption of toxic heavy metals and benign early metals should not be exactly considered, nonetheless, there is no single parameter to describe the general toxicity of a metal because it is strongly depended on the solubility, oxidation state, and the nature of coordinated ligands, among others.⁷

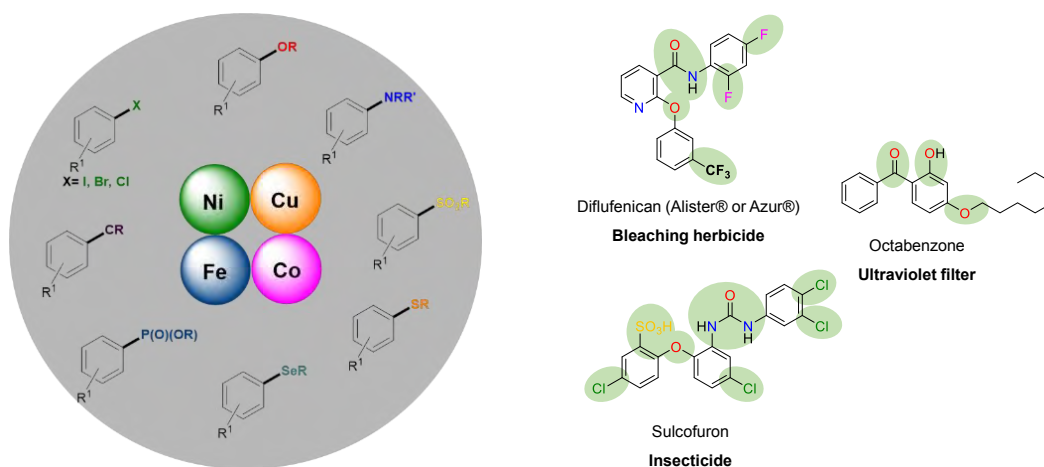


Figure I.1. Earth-abundant first-row transition metals – catalysed C-C and C-Heteroatom bond formation, which are present in a wide range of interesting molecules.

On the other hand, first row transition-metal based catalysts usually show totally different or complementary catalytic reactivities owing to their unique electronic configuration structures (Figure I.1). Chemists have employed iron^{8,9}, cobalt¹⁰⁻¹², nickel¹³⁻¹⁵ and copper¹⁶⁻¹⁸ in organic transformations for more than a century, especially in catalysis, leading to the development of greener approaches towards organic molecules. Among these elements, copper and nickel are the most extensively used in organometallic chemistry. Moreover, and although copper is the most well-known first row transition metal capable of catalysing cross-coupling reactions either through C-H or C-X (X= halide, metal) bond activation, nickel-catalysed cross-coupling reactions have been emerging as an attractive method for the formation of C-C and C-Heteroatom bonds. Several key properties of nickel have allowed the development of a broad range of innovative reactions. The concept of *cross-coupling* has gained significant attention due to the enormous potential that this transformations enclose for the formation of C-C and C-Heteroatom bonds. Indeed, the number of publications on the topic has remarkably increased in the last few years, with approximately 7000 publications in 2015 (Figure I.2). Furthermore, the development of new cross-coupling reactions based on copper and nickel catalysts have grown exponentially, with approximately 700 publications in 2015 (Figure 2, purple line).

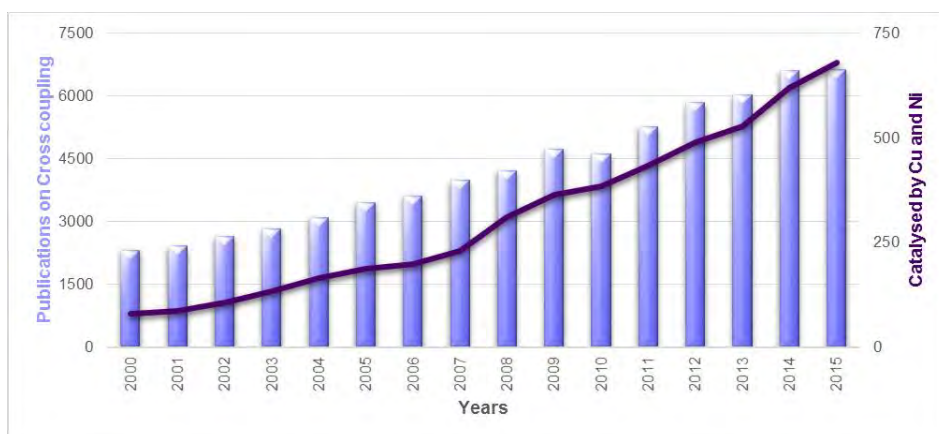


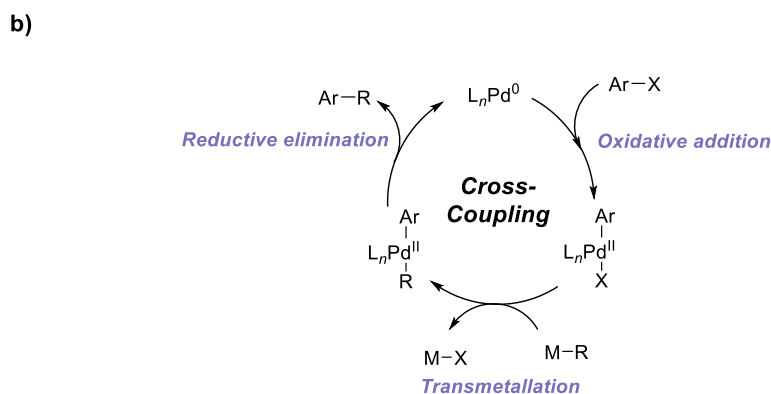
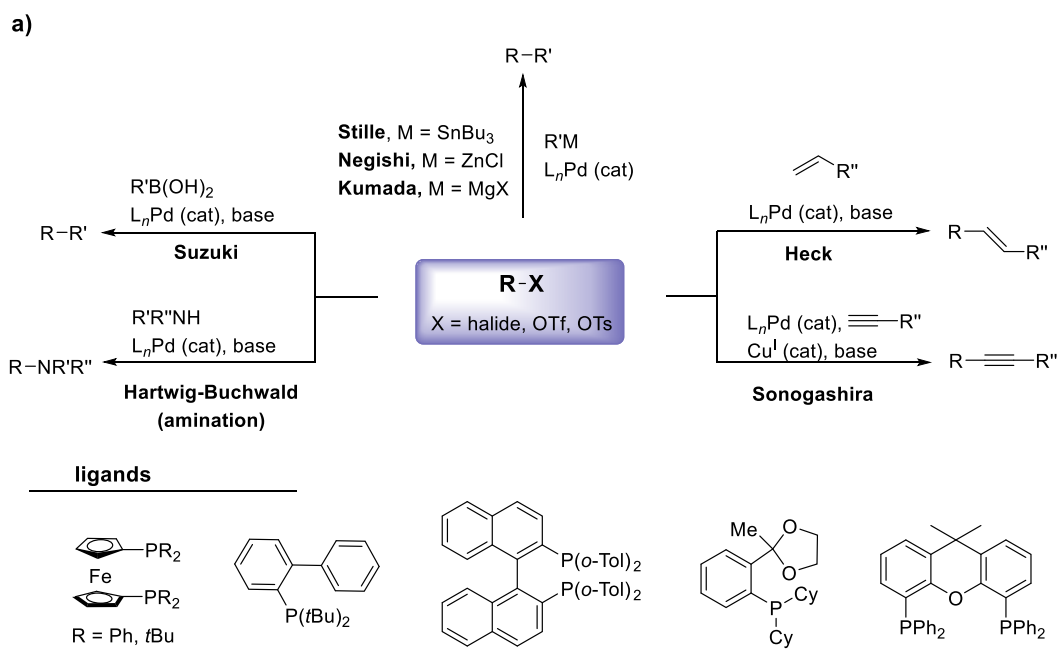
Figure I.2. The number of publications on the topic of cross-coupling (blue bars) and on the cross-coupling reactions catalysed by Cu and Ni (purple line) between 2000 and 2015. Data for the bar chart were obtained by a Web of Knowledge search in September 2016 using keyword cross-coupling. Data for the line chart were obtained by the sum of refining search using keywords copper-catalysed and nickel-catalysed, respectively.

I.2 Cross-Coupling Catalysis

Cross-coupling chemistry involves the formal substitution of an aryl, vinyl, or alkyl halide or pseudohalide (such as trifluoromethylsulfonate, isocyanide ...) by a nucleophile, assisted by a transition metal catalyst. While many types of cross-coupling reactions have been known for several decades, advances in recent years have greatly increased their scope and applications.^{19,20} Since then, cross-coupling processes have been a breakthrough in the field of organic synthesis and have provided a new approach for the construction of molecules of interest such as pharmaceuticals, agrochemicals, polymers, etc. This progress not only has had a

significant impact on academic research but also in industrial applications.²¹ A continuous search for highly efficient catalytic systems led to the development of new methodologies with extremely low catalyst loadings. The emergence of cross-coupling as a popular method in synthesis arised from both the diversity of reagents utilized in these reactions and the broad range of functional groups which can be incorporated into these reagents. Among other metals, palladium-catalysed cross-coupling reactions to form C-C and C-Heteroatom bonds have emerged as a powerful tool in synthetic chemistry.^{22,23}

However, it was not until the early seventies, when the first reports on palladium-catalysed cross-coupling reactions appeared.²⁴ Cross-coupling processes were first applied only to C-C bond formation which includes a wide range of reactions based in C-nucleophiles, such as aryl, vinyl or alkyl derivatives of magnesium (Kumada-Corriu)^{25,26}, boron (Suzuki-Miyaura)²⁷, tin (Stille-Migita)²⁸, zinc (Negishi)²⁹, or silicon (Hiyama).³⁰ In another very important cross-coupling process, a terminal alkyne serves as a nucleophile in the presence (Sonogashira)³¹ or absence (Heck alkynylation)³² of a copper co-catalyst (Scheme I.1a). Indeed, the significance of palladium-catalysed C-C bond formation was awarded in 2010 with the Nobel Prize to Akira Suzuki, Ei-ichi Negishi and Richard F. Heck.³³ The generally proposed mechanism begins with the oxidative addition of the organo halide to the catalyst. Subsequently, the second partner undergoes transmetalation, which places both coupling partners on the same metal centre while eliminating the functional groups. The final step is reductive elimination of the two coupling fragments to regenerate the catalyst and results in the organic product formation (Scheme I.1b).²⁰ At the beginning of the nineties, Hartwig and Buchwald groups made substantial contributions to the area, developing cross-coupling methodologies based on palladium catalysts for the formation of C-N.^{34,35} Over the course of its development, several sorts of catalytic systems have been developed, allowing the expansion of the scope including a wide variety of amine-based, sulphide-based and oxygen-based nucleophiles and aryl halides as a coupling partners.^{36,37} Studies involving more complex systems have remained an active area of research. Despite the remarkable results obtained using palladium-based catalysts, several drawbacks begun to appear, such as the high costs associated to the use and removal of palladium catalysts, as well as their toxicity and the use of sophisticated (and expensive) ligands. Moreover, pursuing greener and more sustainable procedures remains one of the top challenges in organic chemistry, thus the exploration of alternative processes provided several methodologies for the replacement of palladium with first-row transition metals, most frequently copper and nickel, which shown highlight performance in these transformations (Figure I.3).³⁸



Scheme I.1. (a) Common Pd-mediated cross-coupling C-C and C-Heteroatom bond-forming processes. (b) General mechanism for Pd-catalysed cross-coupling reactions, which is initiated by oxidative addition of an organic halide at Pd⁰, continues through transmetalation and finishes by reductive elimination.

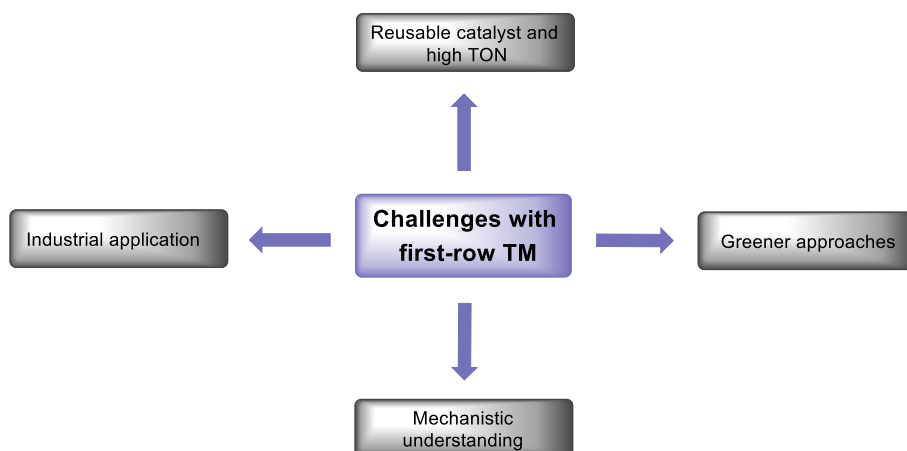


Figure I.3. Current challenges for the development of new cross-coupling methodologies based on first-row transition metals.

1.3 Copper in Cross-Coupling Catalysis

1.3.1 Coinage metals

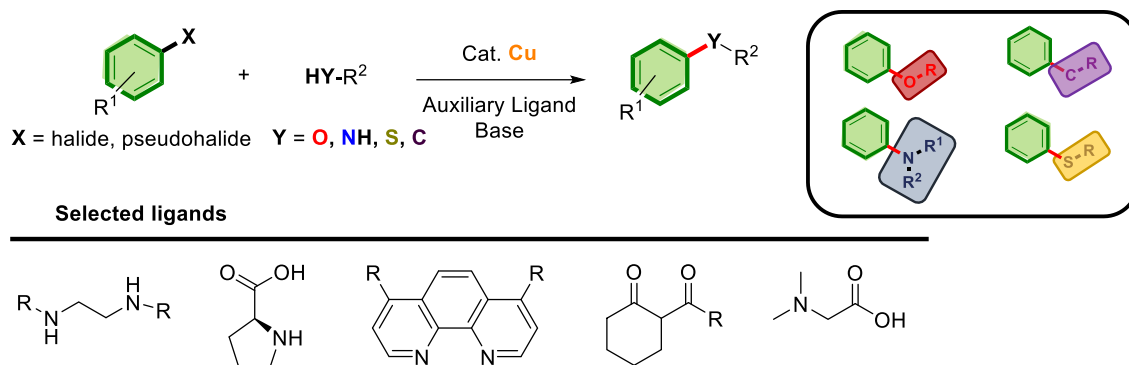
Coinage metals consist of the three non-radioactive members of group 11 of the periodic table: copper, silver and gold. All three metals have been extensively used in homogeneous catalysis reactions. Among the three elements, copper is the most used in cross-coupling and organometallic chemistry. However, silver has increasingly gained interest as a catalyst or co-catalyst in various cross-coupling reactions. The applications of silver salts, mainly, Ag^+ , in organic synthesis are indeed mostly driven by its Lewis acidity. Another important feature is the insolubility of the corresponding halide salts (halogenophilicity), which are driving reactions to trigger the precipitation of AgX salts ($\text{X} = \text{Cl}, \text{Br}, \text{I}$).^{39,40} The gold chemistry has grown substantially over past few years. Gold catalysis exhibits excellent performance for the cross-coupling chemistry, their inherent properties, like air and moisture tolerance as well as the strong Lewis acidity, led to conduct several transformations involving C-C and C-Heteroatom bond formation, under mild reaction conditions.^{41,42}

While silver-catalysed cross-coupling reactions are hardly developed, gold-catalysis field are experiencing a period of special interest, showing satisfactory results in several transformations, especially in C-H functionalisation area. Besides this, copper is the most versatile, cheap and productive metal of coinage metals. Copper-assisted cross-coupling methods allow to the development of improved protocols for the formation of wide range of C-C and C-Heteroatom bonds. In addition, the copper-mediated chemistry is environmentally friendly, one of the essential goal of modern organic chemistry.

1.3.2 Overview and background

The copper-catalysed arylation of nucleophiles, known as Ullmann-type condensations, has been known for more than a century as an efficient method for the formation of C-C and C-Heteroatom bonds. However, after the discovery of palladium-mediated cross-coupling reactions, the practicality of these processes was very limited due to several drawbacks, such as the requirement of highly polar solvents, high temperature ($>200^\circ\text{C}$) and long reaction times, as well as the narrow range of nucleophiles tolerated as coupling partners. Additionally, in most of the cases stoichiometric amounts of copper were needed.^{43,44}

At the beginning of the twentieth century, Ullmann-Goldberg chemistry experienced a renaissance, basically due to the development of new and improved auxiliary ligands. The use of these auxiliary ligands in combination of inorganic bases led to much milder chemistry (milder reaction temperatures, faster reaction rates and lower catalyst loadings) with a broadened substrate scope (Scheme 1.2).



Scheme I.2. General reaction scheme of Ullmann-type coupling reactions and some representative auxiliary ligands used.

Usually, nitrogen and oxygen-based bidentate ligands have been used and it was thought that these auxiliary ligands increased the solubility and stability of the copper catalyst, but their exact role was not well established. Since then, several research groups focused on the development of new copper/ligand systems for the formation C-C and C-Heteroatom bond formation.⁴⁵

Many approaches and methods have been reported since then, nonetheless the optimization of the experimental conditions is crucial to achieve good performance, and more efforts in this area are also valuable. In this regard, several “ligand free” procedures have been described as an efficient catalytic systems in Ullmann coupling reactions, basically in C-N bond formation and more recently in C-O bond formation.⁴⁶ This chemistry usually involve the use of chelating substrates (such as amino acids, amino alcohols ...), which can act as a ligand. Moreover, the non-requirement of auxiliary ligands and the use of solvents with coordinating abilities such as *N*-methylpyrrolidone (NMP), *N,N*-dimethylformamide (DMF) or dimethylsulfoxide (DMSO), provide to this methodology a chance to find some applications in current organic synthesis.⁴⁷ Despite the versatility and the simplicity of these catalytic systems, several drawbacks need to be overcome, such as the low reproducibility of these transformations as well as the high temperature conditions.⁴⁸

Finally, a complementary approach was recently reported, based on photoirradiation. Peters, Fu and co-workers demonstrated that performing the coupling reactions in presence of light and a simple copper catalysts, a wide variety of C-Nucleophiles (such as nitrogen, oxygen, sulphur, or carbon) can be accomplished under unusual mild conditions (see below).⁴⁹

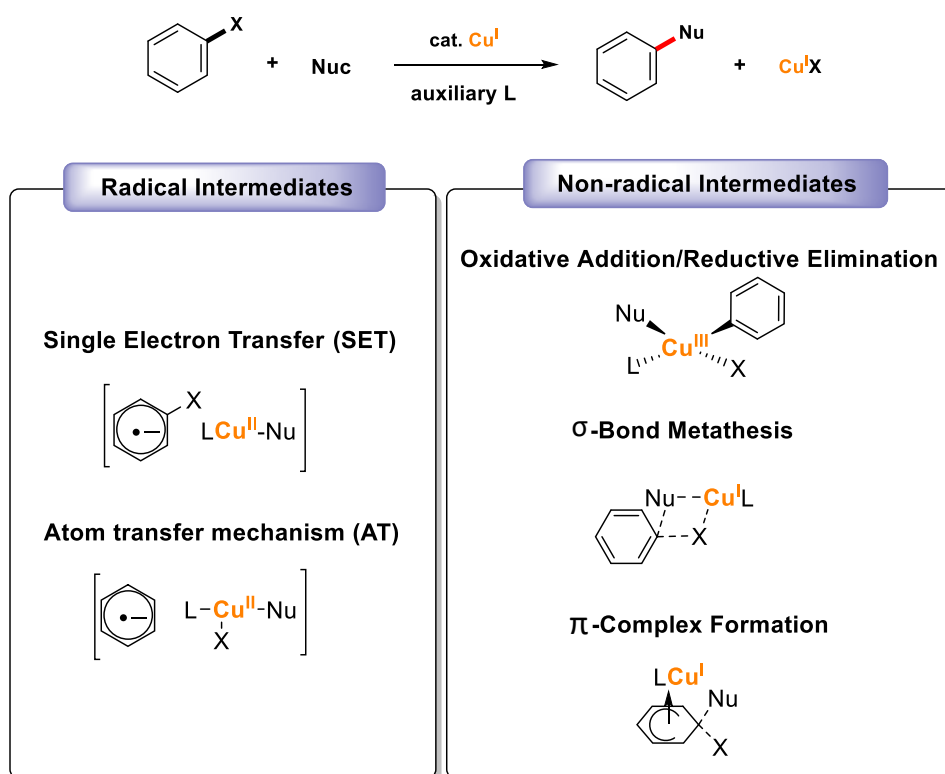
The most essential drawback of copper-mediated cross-coupling chemistry as a whole is the lack of mechanistic understanding to fundament and design further developments.

I.3.3 Mechanistic features of copper-catalysed cross-coupling reactions

The great diversity of catalytic systems as well as the different nature of nucleophiles, suggests that Ullmann couplings might proceed via different mechanisms. In this sense, many proposals

were drawn, including radical and non-radical processes (Scheme I.3).^{17,50} The radical-based mechanisms include SET (*Single Electron Transfer*) and AT (*Atom Transfer*), both involve the formation of aryl radicals that react with the Cu^{II}-nucleophile species to form the coupling product and Cu^I.⁵⁰⁻⁶⁰ For the non-radical processes, concerted mechanisms *via* σ -bond metathesis^{61,62} and S_EAr^{63,64} procedures, which involve π -complexation of Cu^I on the aryl halide have been reported, although only few experimental evidences are described. Among the non-radical based mechanisms, the most generally proposed is based on oxidative addition/reductive elimination, a two-electron redox Cu^I/Cu^{III} catalytic cycle.

However, the recent progress in copper-assisted cross-coupling reactions shows that these transformations are extremely dependent on experimental conditions, such as the nature of the ligand, the solvent choice, the sterically hindrance as well as the electronic effect of the substrates and nucleophiles, and the operating mechanism can differ among distinct experimental setups.

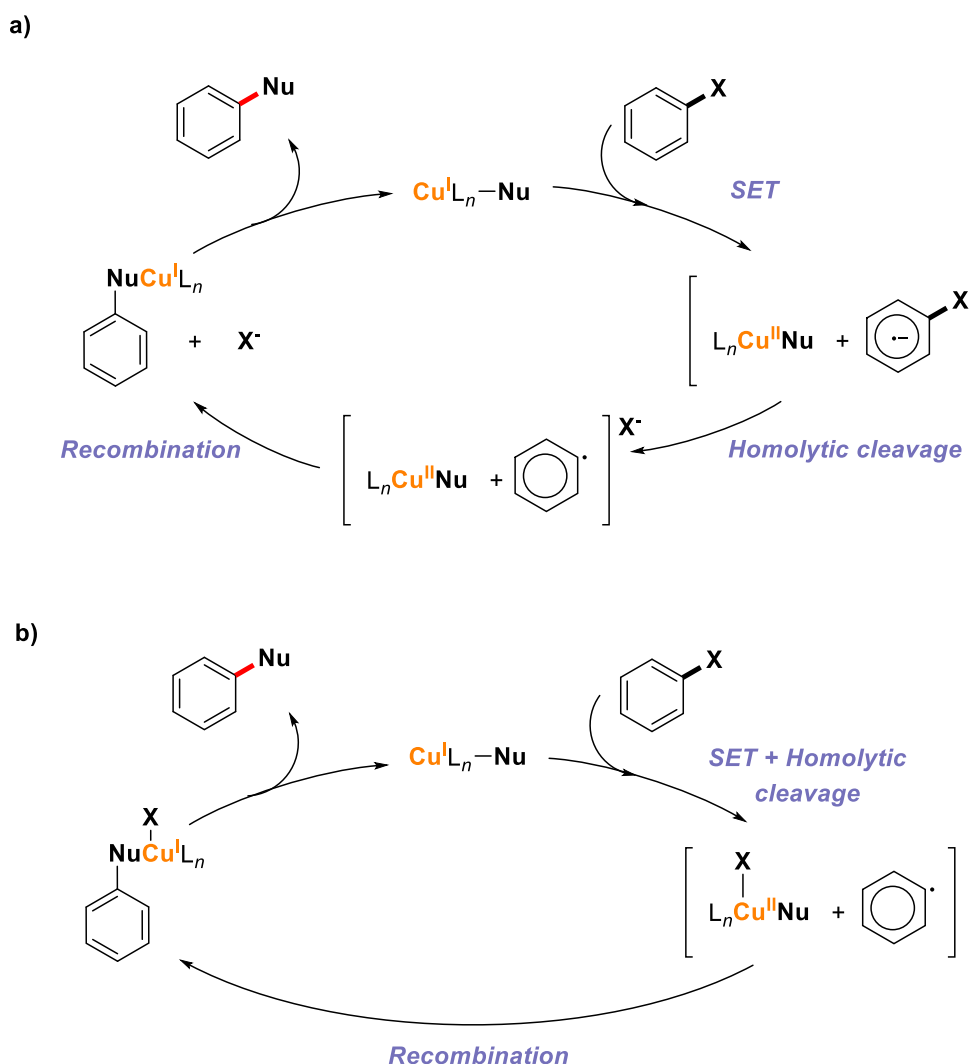


Scheme I.3. Radical and non-radical intermediates proposed for Ullmann coupling reactions.

I.3.4 One-electron redox processes Cu^I/Cu^{II}

Several studies postulate a Cu^I/Cu^{II} catalytic cycle involving a radical intermediated species formed *via* a single electron transfer (SET) mechanism, which is initiated by the oxidation of the copper(I) complex by inner-sphere one-electron process from the aryl halide, producing an aryl halide radical anion. This haloarene radical intermediate reacts with the Cu^{II}-nucleophile complex, forming the coupling product and regenerating the copper(I) (Scheme I.4a). Since the postulation of the plausibility of radical intermediates, many proposals appeared in the literature suggesting

that the free radical reacts rapidly with the Cu^{II} species *via* atom transfer, which involve the transfer of the halide to the copper atom to form the aryl radical (Scheme I.4b). Classical radical scavengers have been used in order to identify the presence or absence of radical intermediates in Ullmann condensation reactions. It was found that in many catalytic systems the reaction performance was not inhibited by the presence of the radical scavengers, supporting an alternative non-radical-based mechanism. However, these results cannot exclude the formation of short-lived radicals during the reaction outcome. To probe this radical pathway, several research groups synthesised and conducted the reactions using a radical clock as aryl halides, which undergoes a fast cyclisation in presence of radicals. The lack of cyclisation products formation was attributed to against the involvement of radical intermediates in the reaction mechanism.⁶⁵

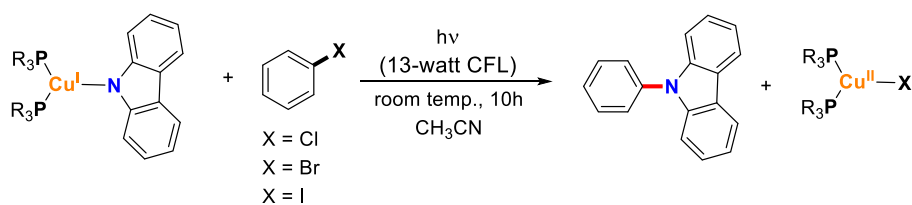


Scheme I.4. Proposed mechanistic pathways for (a) single electron transfer (SET) mechanism and (b) atom transfer (AT) mechanism both based in a $\text{Cu}^{\text{I}}/\text{Cu}^{\text{II}}$ catalytic cycle.

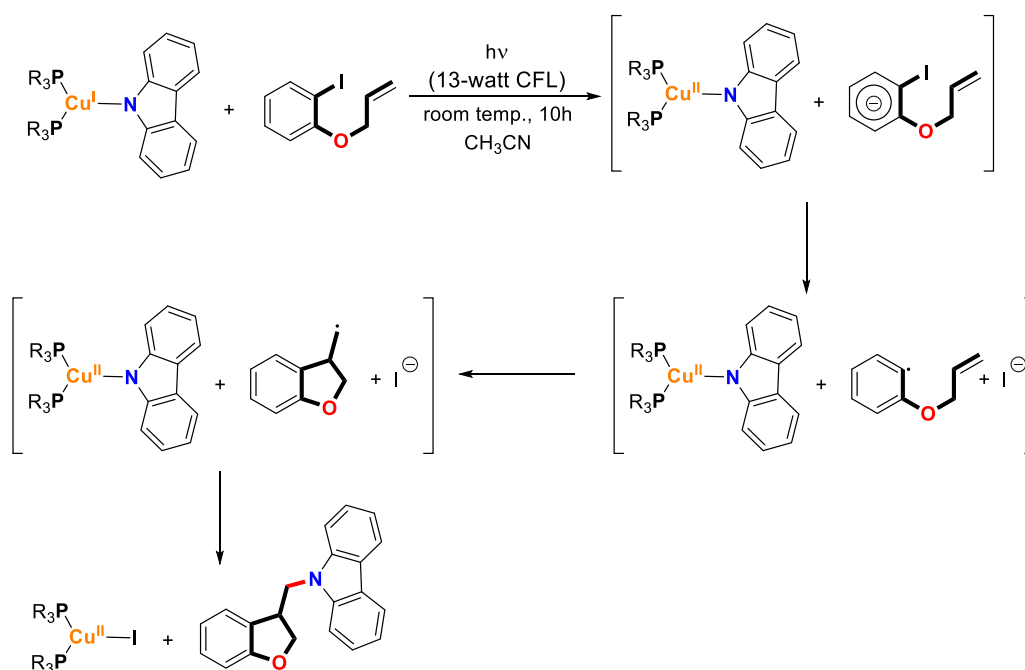
In 2012, J. Peters and G. Fu reported the first experimental evidence of $\text{Cu}^{\text{I}}/\text{Cu}^{\text{II}}$ in Ullmann-Goldberg chemistry, demonstrating the viability of the SET pathway.⁵¹ This study introduces a photoinduced variant of this powerful transformation, through the investigation of the formation of

the C-N couplings between a photoluminescent copper-carbazolide complex and aryl halides. Upon the irradiation of the mixture, a radical from copper-carbazolide complex was formed (detected by EPR spectroscopy). This radical intermediate reacts with aryl halides *via* single electron transfer to afford the corresponding C-N coupling product. To provide further support for radical intermediates in these photoinduced Ullmann reactions, they further investigate the copper-carbazolide complex with a radical clock (2-(allyloxy)iodobenzene). Interestingly, cyclised products were exclusively observed, providing the first evidence of the involvement of radical intermediates. Moreover, deuterium-labelled experiments of the same test were carried out, generating a mixture 1:1 of cyclised diastereoisomer compounds and any noncyclic products are observed, which is fully consistent with a radical pathway (Scheme I.5). Otherwise, this contribution opens the door to the new development of practical and mild photoinduced protocols for the Ullmann-type reactions. The scope of these methodologies has also been broaden with a range of nucleophiles and electrophiles, since the photochemical irradiation can lead, under mild conditions, the formation of several C-N, C-O, C-S and C-C.^{49,53,56}

a)



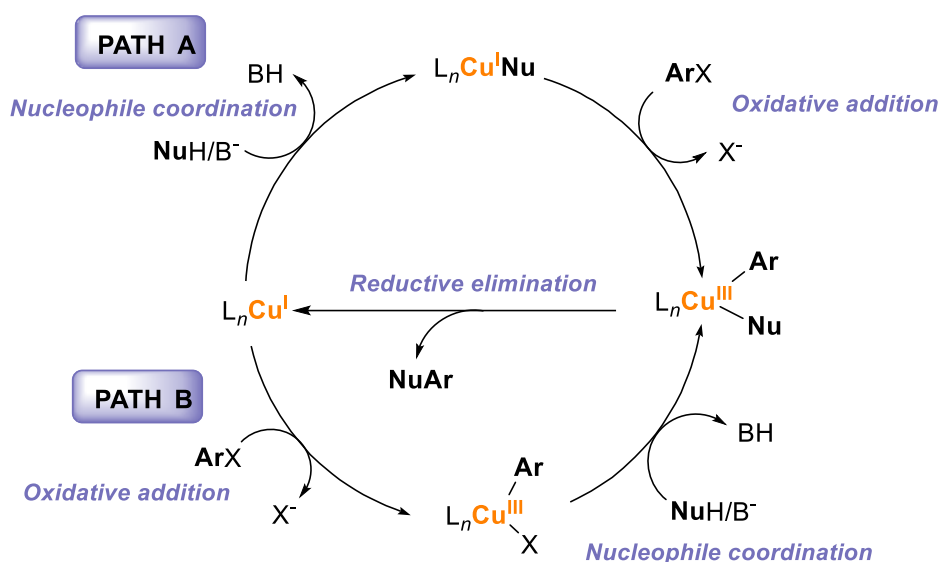
b)



Scheme I.5. (a) Photoinduced Ullmann C-N coupling reactions of copper-carbazolide complex with aryl halides. (b) Cyclisation, followed by C-N bond formation, through a photoinduced Ullmann reaction using an allyloxyiodobenzene (radical clock) as a substrate.

I.3.5 Oxidative addition/reductive elimination $\text{Cu}^{\text{I}}/\text{Cu}^{\text{III}}$

Most of the recent studies proposed a catalytic cycle based on $\text{Cu}^{\text{I}}/\text{Cu}^{\text{III}}$ two-electron redox process for Ullmann-Goldberg condensation. This proposal involves first the formation of the $\text{L}_n\text{Cu}^{\text{I}}\text{Nu}$ complex via deprotonation of the NuH by a base, followed by an aryl halide oxidative addition at the copper(I) centre, increasing the oxidation state and the coordination number of the metal centre, forming an aryl- Cu^{III} intermediate species. Finally, this aryl- Cu^{III} complex undergoes to the formation of the coupling product through reductive elimination step and regenerates the copper(I) catalyst. However, two formal representations can be proposed for the copper-catalysed arylation of nucleophiles (Scheme I.6). In the first one, the nucleophile coordination occurs in the first step, before the activation of aryl halide (path A). In the second proposal, the oxidative addition step proceeds before the nucleophile coordination (path B).



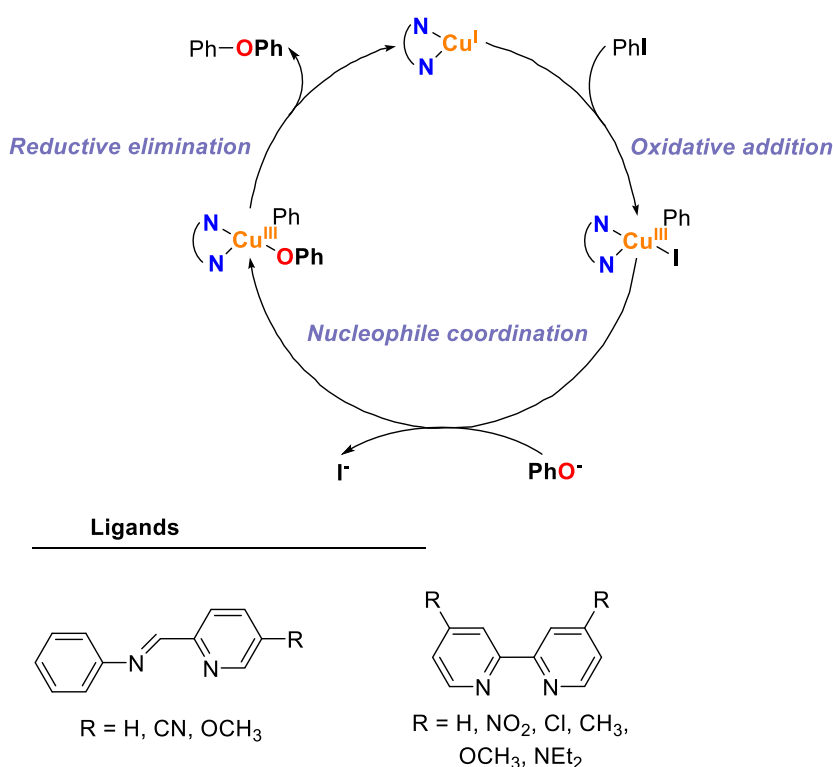
Scheme I.6. Two proposed pathways for the Ullmann reaction depending on the relative order of oxidative addition/nucleophile coordination events.

However, experimental data supports pathway A as the most plausible mechanism in these couplings. Basically, the proposal of $\text{Cu}^{\text{I}}/\text{Cu}^{\text{III}}$ catalytic cycle is mainly supported by the lack of rate inhibition with radical scavengers and computational studies. Cohen proposed for the first time in the 1970s, a copper(III) complex as a key intermediate species in Ullmann-type chemistry, studying the mechanism of the copper mediated homocoupling reaction of *o*-bromonitrobenzene. Moreover, the presence of radical intermediates were rejected by the lack of rate inhibition in the presence of radical scavengers.^{66,67} Since then, several research groups have suggested the involvement of putative aryl- Cu^{III} species in copper-mediated C-C and C-Heteroatom bond formation and their detection became a challenging subject.

Taillefer and co-workers⁶⁸ studied the copper-mediated arylation of phenols using several *N, N*-based bidentate chelating ligands, in order to get better understanding on the catalytic activity conferred by the structure of the auxiliary ligand. According to their results, oxidative

addition/reductive elimination catalytic cycle was the most favourable operative pathway. The most effective ligands contain one imine or one pyridine coordinating groups in a synergistic manner. By tuning the electronic properties of pyridine moiety of the ligand, they found that more electro-donating groups in the *para* position in the pyridine ring improved the catalytic activity owing to a more favourable oxidative addition, as indicated by the lower oxidation potential. In contrast, the more electron-withdrawing *para*-substituents in the imine coordinating groups favoured the arylation reaction, suggesting that this binding site is related to the ligand exchange and/or reductive elimination steps, which are more favourable in electron deficient copper(III) intermediates (Scheme I.7). These results suggest that the reaction pathway is extremely dependent on the ligand electronic properties. However, the putative aryl-Cu^{III} intermediates were not observed during the reaction outcomes, only the non-inhibition of the coupling reaction upon the use of radical scavengers.

Therefore, different research groups supported the plausibility of the putative copper(III) intermediates using DFT computational studies, in order to get further mechanistic information.^{65,69,70}

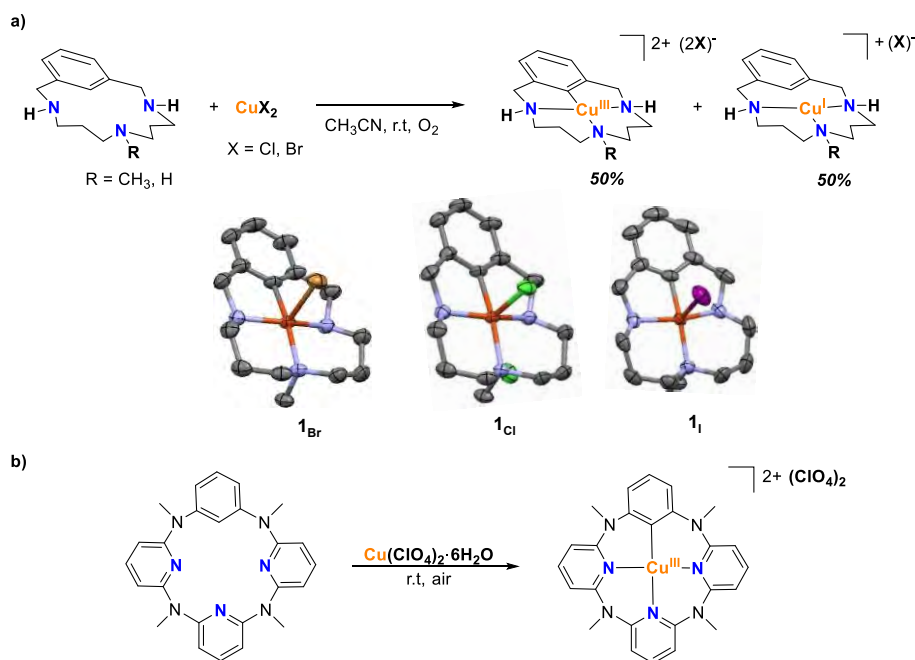


Scheme I.7. Taillefer's mechanistic proposal for the Ullmann-Goldberg reactions using bidentate *N, N*-based auxiliary ligands.

1.3.5.1 The role of high-valent organometallic copper(III) species

Despite the long history of the Ullmann coupling chemistry, mechanistic investigations of a plausible catalytic cycle remained ambiguous and speculative, mainly due to the short-lived aryl-Cu^{III} intermediate species usually formed after the C-halogen bond cleavage, which is generally the rate-determining step.

In 2002 Ribas, Stack and Llobet^{71,72} provided a new strategy for the investigation of the feasibility of aryl-Cu^{III} complexes. A well-defined organometallic copper(III) complex based on a macrocyclic model substrate, was synthesised, isolated and fully characterised. These ligands hold an aliphatic chain with three amine coordinating groups capable to stabilize high-valent copper species by the σ -donor properties of the secondary amines. It was not until 2010 when Ribas in collaboration with Stahl⁷³ observed for the first time the fundamental Cu^I/Cu^{III} redox step in Ullmann-type couplings. A family of square pyramidal complexes aryl-Cu^{III}-X (X = Cl, Br, I) were prepared by reacting CuX₂ salts with a triazamacrocyclic ligand containing an arene moiety *via* proton coupled electron transfer (PCET) C-H activation process.^{72,74} These complexes were spectroscopic and structurally characterized (Scheme I.8a). Similarly, Wang and co-workers⁷⁵ reported the synthesis and full characterization of a monoaryl copper(III) complex based in a heterocalixarene ligand, which provides an electron-donating environment suitable for the stabilization of high-valent copper species (Scheme I.8b) through C-H activation.



Scheme I.8. Synthesis of well-defined high-valent copper(III) complexes, based on a macrocyclic model substrates. X-ray structures of aryl-Cu^{III} complexes (ellipsoid representation at 50% probability and hydrogens and corresponding counter anions are omitted for clarity). (a) Using triazamacrocyclic ligands described by Ribas group. (b) Using heterocalixarene-type ligands described by Wang.

The isolation of the complexes **1_x** (X = Cl, Br and I) provided an unprecedented opportunity to study the reactivity of these putative aryl-Cu^{III}-X key intermediate species in Ullmann-type reactions. The reaction with nucleophiles proceeded fairly rapidly without the addition of base, indicating the high reactivity of the copper(III) complex.⁷³ This result strongly suggested that the mechanism proceeds *via* reductive elimination. Initial studies revealed that the addition of one equivalent of triflic acid triggered the reductive elimination at **1_x** to form the intramolecular C-X bond and releasing Cu^I. Moreover, upon the addition of one equivalent of proton sponge[®] as a non-coordinating base, the aryl-Cu^{III}-halide was regenerated through an oxidative addition step. The interconversion between the two redox states, Cu^I/L-X-H⁺ and aryl-Cu^{III}-X, was demonstrated via sequential additions of acid and base, and the cycle could be repeated several times without significant loss of **1_x** (Figure I.4). In order to gain more mechanistic insight into this process a DFT calculations were performed. Interestingly, the acid-triggered reductive elimination involved the protonation of one amine of the complex causing its decoordination from the electron deficient copper(III) centre and in consequence, the reductive elimination occurred due to the destabilization of the complex. Additionally, another effective strategy was described by the same authors, in which the reductive elimination was promoted by the addition of an external ligand able to trap copper(I) ions. The equilibrium towards coupling product was achieved by adding excess of 1,10-phenanthroline, that presents a high affinity for copper(I) ions.

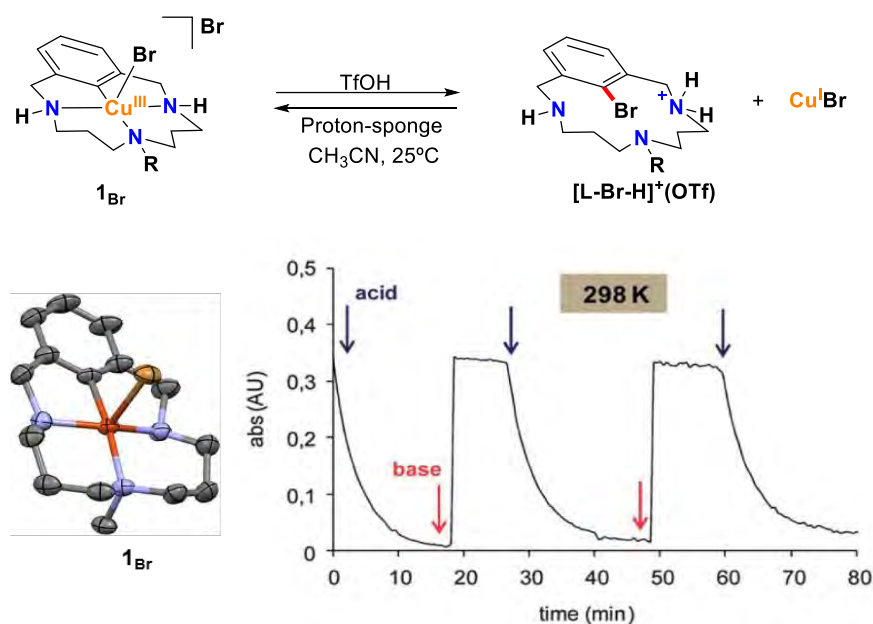
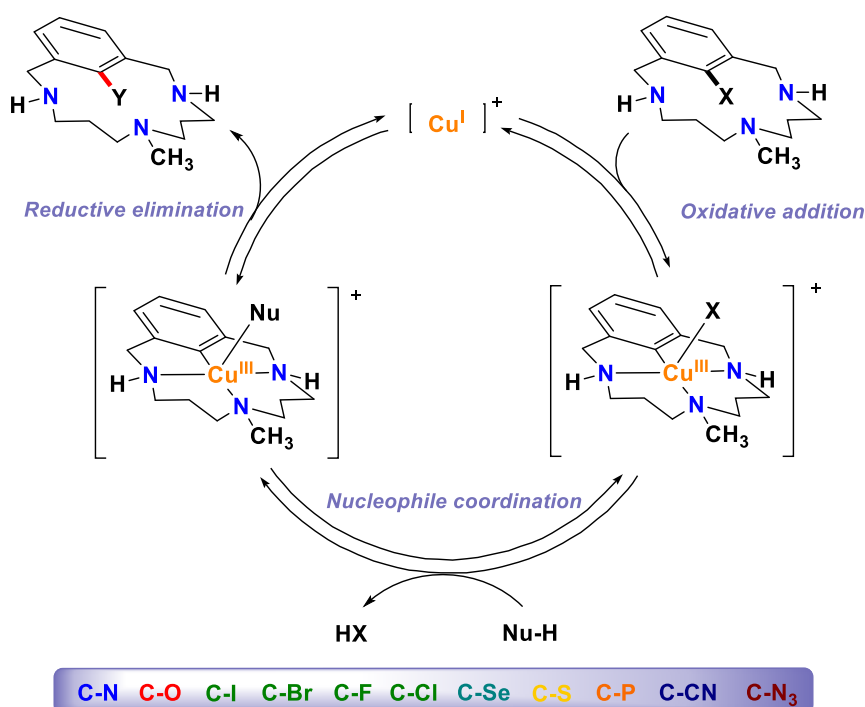


Figure I.4. Reversible reductive elimination/oxidative addition under pH control and the UV-Vis monitoring.

Shortly after, Wang and co-workers⁷⁶ reported in 2011 the reactivity of the well-defined aryl-Cu^{III} complex based in azacalix[1]arene[3]pyridine, which readily reacts with a wide range of nucleophiles, including halides, cyanide, isothiocyanate and carboxylates to form C-X, C-C, C-S and C-O bonds, respectively achieving almost quantitative yields under mild conditions.

I.3.5.2 Mechanistic insights on Ullmann-type cross-coupling reactions

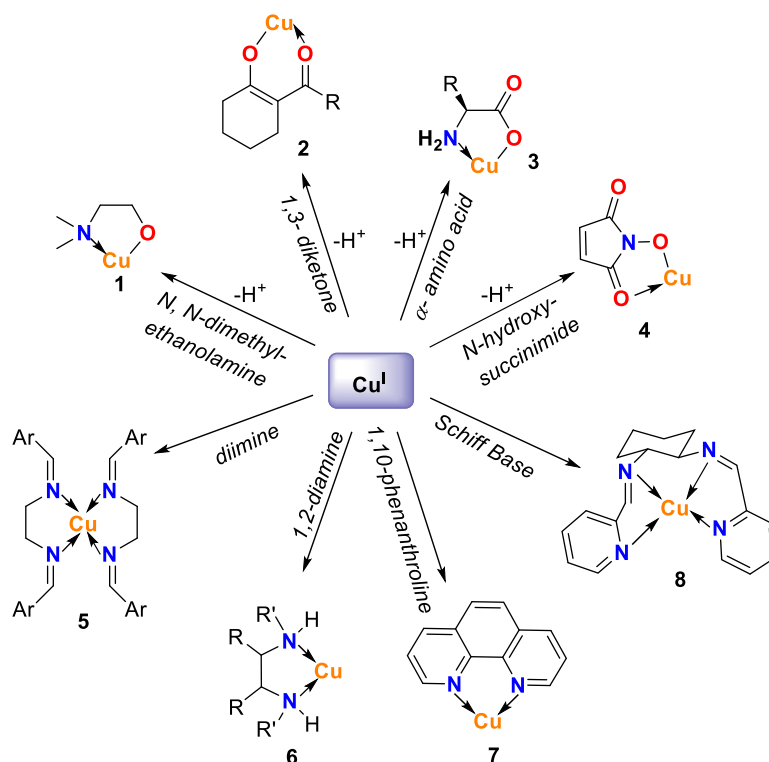
Improved understanding of the fundamental reactivity of high-valent organocopper(III) species should facilitate the development of new and improved methodologies based on copper catalysis. Nonetheless, Ribas, Stahl and co-workers studied in detail the formation of a cationic $[\text{ArCu}^{\text{III}}\text{Br}]^+\text{Br}^-$ complex and demonstrated that the mentioned species can be plausible intermediates in copper-mediated C-N, C-O, C-S and C-halide bond formation.^{77,78} These macrocyclic model systems allowed the study of reductive elimination and oxidative addition steps independently. In an early report, Stahl reported the reactivity between the macrocyclic model systems (using a perchlorate salt) with several amides to afford the C-N bond formation under mild conditions. They could observe that the more acidic N-based nucleophiles reacted faster than the less acidic ones, which also yielded a by-product (the intramolecular C-N formation). The trend suggests that the nitrogen nucleophile undergoes deprotonation before or during the rate-limiting step of the reaction. Ribas and Stahl demonstrated that the aryl- Cu^{III} also underwent coupling in presence of carboxylic acids, phenols, aliphatic alcohols⁷⁸, halides⁷⁹, amides⁷³, sulphides⁸⁰, among others (Scheme I.9). This model system also proved to be catalytic and aryl- Cu^{III} -halide intermediate species were unequivocally characterized under catalytic conditions with a wide range of nucleophiles. This observation was the first example of the experimental feasibility of $\text{Cu}^{\text{I}}/\text{Cu}^{\text{III}}$ catalytic cycle, undergoing an initial aryl halide oxidative addition to form aryl- $\text{Cu}^{\text{III}}\text{-X}$, followed by halide exchange and final reductive elimination, thus supporting the path B of the Scheme I.6 for the biased model substrate.



Scheme I.9. General mechanism for the C-C and C-Heteroatom bond formation in copper-catalysed cross-coupling reaction within triazamacrocyclic model aryl halide platforms.

I.3.6 Dependence on ancillary ligands

As discussed before, the Ullmann condensation has been improved notably through the addition of auxiliary ligands, which enabled faster reactions and allowed milder conditions. This effect has initially been explained through the improvement of the solubility and stability of the active copper species. Since the 1990s a great number of chelating ligands, typically bidentate based on *N,N*-, *N,O*- and *O,O*- bonding moieties have shown excellent performance on promoting this kind of transformations. Moreover, the ligand choice plays a key role enhancing the chemoselectivity and also influencing on the operative mechanism. The use of these additives not only speeded up the reactions but also made them more reproducible and safer in terms of operating conditions and residual toxicity. It is believed that these ligands coordinate to the copper(I) centre changing the electronic properties of the active species and some proposed LCu^{I} intermediates are outlined in Scheme I.10. The complexes **1** - **4** are formed by the coordination of ionic ligands⁸¹⁻⁸³ and the complexes **5** - **8** results of the coordination of non-ionic ligand.^{68,84} Furthermore, the nature of the auxiliary ligand, as well as the nature of the nucleophiles, can determine a distinct selectivity towards sterically different aryl halides substrates.



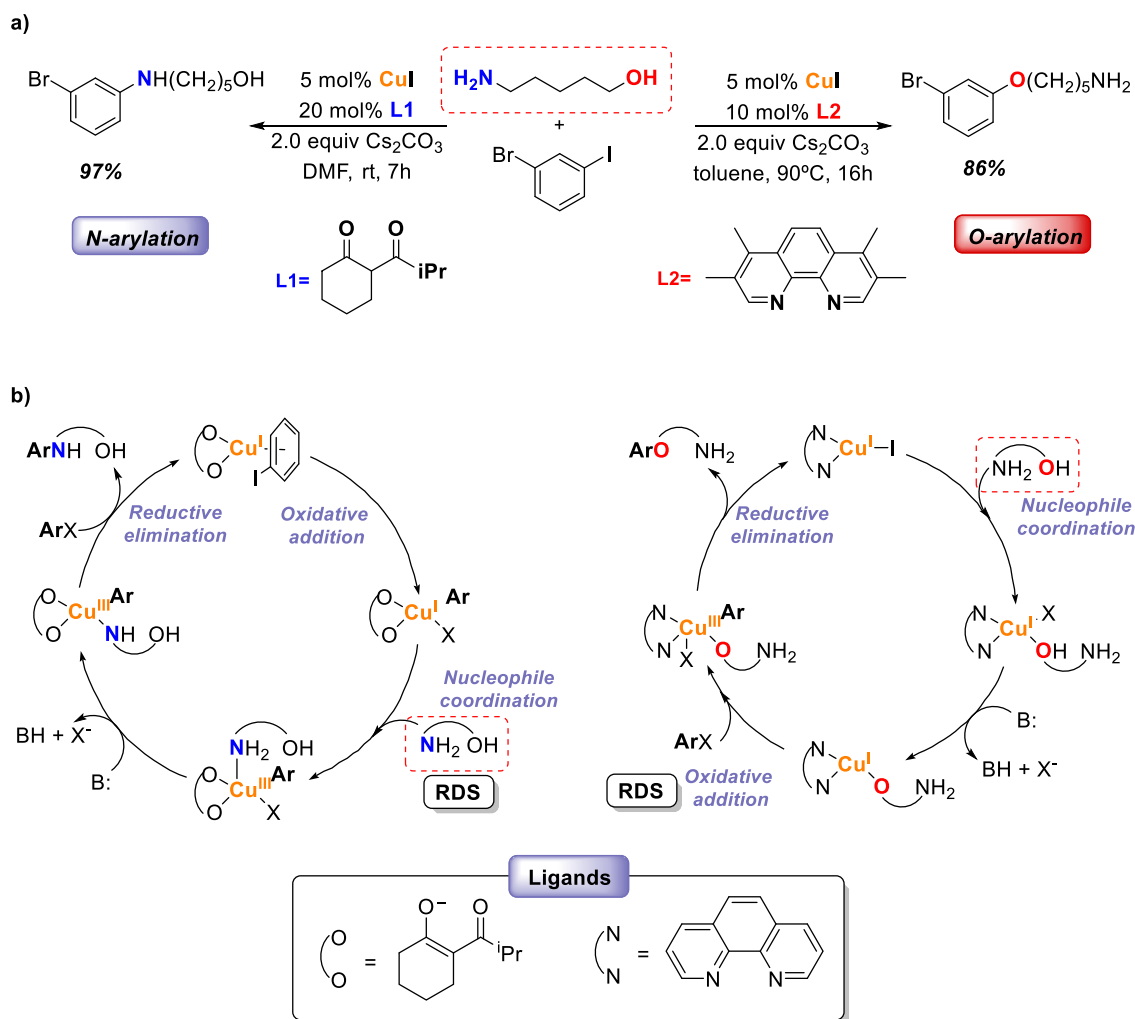
Scheme I.10. Possible intermediates resulting from coordination of Cu^{I} with bidentate ionic and anionic ligands.

I.3.6.1 Chemoselectivity

Buchwald and co-workers studied the ligand-directed chemoselective *N*- or *O*- arylation of aminoalcohols by using different auxiliary ligands. Whereas, the β -diketone ligand promoted the formation of *N*-arylated product in DMF at room temperature, tetramethylphenanthroline ligand promoted the selective *O*-arylation in toluene at 90°C (Scheme I.11a).⁸⁵ Later on, the same

authors concluded, through computational studies that the pathways which showed lower energy barrier were SET and IAT mechanisms, in which short-lived radical pairs are formed. Computational investigations were performed on distinct reactions of iodobenzene, methanol and methylamine, as a simplified model systems. The reactions involving Cu^I complexes and either β -diketone or tetramethylphenanthroline ligands were studied. The results suggest that the electron-rich β -diketone ligand promotes the SET mechanism, in which the electron is transferred from the copper(I) complex. Although the *N*-bound copper(I) complex is less stable and the amino substituent is better electron donor, which facilitates electron transfer. In contrast, when the neutral and less electron-rich phenanthroline ligand was used, the IAT and SET mechanisms have similar barriers and either may occur depending on the nucleophile. The results suggest that the observed selectivities arise in the aryl halide activation step of the reaction.⁸⁶

However, Fu and co-workers proposed an alternative computational pathway, based on Cu^I/Cu^{III} catalytic cycle, using the real 5-amino-1-pentanol, instead of methanol and methylamine as a theoretical model substrates.⁸⁷ Surprisingly, it was found that oxidative addition/reductive elimination pathway was the most plausible one. It was found that the chemoselectivity came from the steps involving the nucleophile coordination and oxidative addition. Therefore, the calculations performed with β -diketone ligand indicated that before the oxidative addition step, a number of Cu^I complexes exist in equilibrium through ligand exchange in the reaction mixture. Oxidative addition produced a tetra-coordinated Cu^{III} intermediate that coordinates to the nucleophile in a rate determining step forming a five-coordinated Cu^{III} complex. It was shown that the formation of the amine-coordinated intermediate is more favourable than the formation of the alcohol-coordinated intermediate. Finally, the removal of the proton from the amino alcohol took place, before the reductive elimination step (Scheme I.11b). In contrast, calculations performed with 1,10-phenanthroline ligand indicated that the coordination of the nucleophile, being the rate determining step, happened before of the oxidative addition. The most favourable transition state consisted in a penta-coordinated copper(III) complex bound to the deprotonated alcohol of the substrate that lead to the C-O coupling product by reductive elimination (Scheme I.11b).



Scheme I.11. (a) Selective ligand-dependent copper-mediated N-arylation and O-arylation of 5-amino-1-pentanol with 3-bromiodobenzene and bidentate ligands. (b) Computed mechanism reported by Fu for the selective arylation between aryl iodide and 5-amino-1-pentanol, using β -diketone and 1,10-phenanthroline as an auxiliary ligands, involving Cu^I/Cu^{III} oxidative addition/reductive elimination catalytic cycle.

In this sense, computational studies are a very useful tool for the detailed understanding of reaction mechanisms at a molecular level, nevertheless a slight change in the computational methods can render different results, even for the same reaction.

I.3.7 General Conclusions and industrial applications

The great challenge for the synthetic organic chemists is the development of a sustainable, robust and economically feasible synthetic pathways for all target molecules. The palladium-catalysed cross-coupling reactions have attracted tremendous attention over the past years. However, in the late 1990s, several research groups turned out the interest in copper-assisted cross-coupling chemistry providing new more effective and more sustainable procedures, which emerged powerfully in many areas of special interest. This development, was basically driven by the introduction of auxiliary ligands in combination of copper salts, which were able to conduct the

coupling reactions under milder conditions with excellent performance. This modern Ullmann-Goldberg chemistry really grabbed attention in industrial laboratories and pilot plants. The low costs of the copper catalysts and their powerful catalytic activity have been a key success in industrial processes. Several applications were found in material science, providing strategic approaches to scale-up and optimize several processes, such as the improvement on polymers⁸⁸⁻⁹⁰ and electroluminescent compounds synthesis as well as the production of high-tech materials.⁹¹ On pharmaceutical industry, copper-assisted cross-coupling reactions have been a breakthrough providing economically feasible approaches for the replacement of well-established old ones. The ligand modification allowed a reduction of metal loadings, an increase of the solubility and an easy way to remove it (copper scavengers). These improvements provided alternative methodologies for the design of several drugs, antibiotics and biological active compounds, among others, as well as an easy way to scale-up these processes.^{92,93} Finally, in the field of crop science, copper-mediated transformations have proved to be highly valuable for a high amount of coupling reactions, such as cyanation reactions. There is no doubt that Ullmann chemistry will assert its position in industrial catalysis over the coming decades.

Although major achievements were reported for the development of copper-catalysed Ullmann reactions in the past decade, this area is still active and numerous challenges remain. The experimental and computational data do not reach an agreement concerning the mechanism, even for the same reaction. Nevertheless, the diversity of nucleophiles and catalytic systems render the comprehension of the molecular mechanisms as a difficult task. A deeper understanding on the mechanism of copper-mediated cross-coupling reactions will lead to development of more efficient methodologies as well as the catalyst design.

I.4 Nickel in Cross-Coupling Catalysis

I.4.1 Group 10 metals

Nickel (Ni), Palladium (Pd) and Platinum (Pt) are the three non-radioactive elements that conform group 10. Like other groups, their members show patterns in electron configuration especially in the outermost shells. Nickel just lies above palladium and it can readily perform many of the same elementary reactions as their group counterparts. Both Pd and Pt were extensively used in both homogeneous and heterogeneous catalysis. From the perspective of economic sustainability, nickel has emerged as a very promising alternative to the other elements in the d¹⁰ group, being its costs 2000 times lower than palladium and 10000 times lower than platinum. Nickel is a relatively electropositive late transition metal, thus the oxidative addition tends to occur easily allowing its use in several couplings, showing better efficiencies than Pd in some cases.^{13,14} Palladium-catalysed cross-coupling reactions have transformed synthetic organic chemistry and the relevant and exceptional features of this methodology were recognised with the Nobel Prize in Chemistry in 2010. The success of palladium-catalysed cross-coupling is mainly due to the

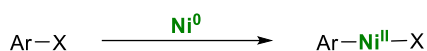
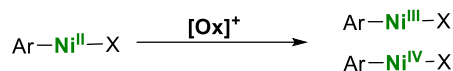
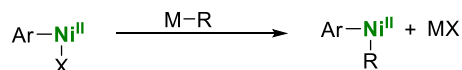
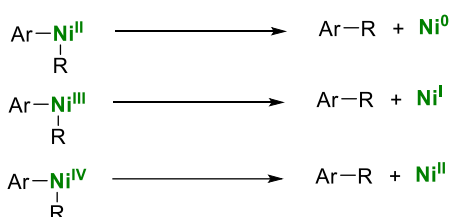
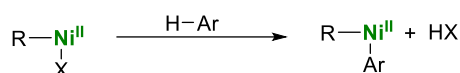
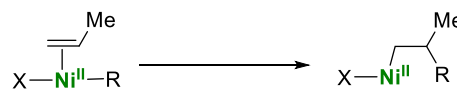
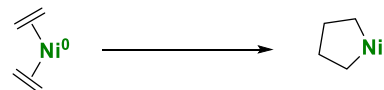
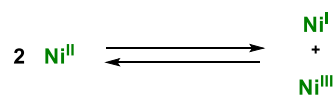
extensive and systematic investigations of reaction mechanisms.³³ Such mechanistic studies have been crucial in the development of new catalyst structures and novel transformations.⁹⁴ The vast majority of these processes involve low-valent Pd⁰/Pd^{II} catalytic cycles, nevertheless, the readily accessibility to high-valent palladium species, such as Pd^{III} and Pd^{IV} have been recently reported.^{95,96} On the contrary, only few studies on platinum-catalysed C-C bond formation have been reported. Compared to the corresponding Ni- or Pd- compounds, Pt shows low reactivity towards organic halides presumably due to the diffused d-orbitals (5d-orbitals). Platinum is chemically dissimilar from its partners, the most common oxidation states are Pt^{II} and Pt^{IV}, which are often stabilised by metal bonding in bimetallic (or polymetallic) species. The easy access to the higher oxidation states makes the platinum chemistry more suitable in other processes than cross-coupling, such as oxidation reactions.⁹⁷

Besides this, the facile oxidation and readily access to multiple oxidation states have allowed the development of a broad range of innovative protocols based on homogenous nickel catalysis. In addition, nickel becomes a privileged reagent for cross-coupling chemistry from the standpoints of economic sustainability and versatility.

1.4.2 Overview and background

Historically, the use of nickel in organometallic reactions pre-dates many other metals, since it was isolated in 1751. However, it was not until 1899 when Günter Wilke made a substantial contribution to this area, providing the structure and reactivity of nickel complexes as well as the synthesis of Ni(COD)₂ and the investigation of olefin oligomerization.⁹⁸ Indeed, in 1912 Sabatier was honoured with the Nobel Prize in Chemistry, for his pioneering work on the hydrogenation of ethylene using nickel.

At the beginning of the seventies, nickel found extensive use both for cross-coupling and reactions of alkenes and alkynes, such as nucleophilic allylation, oligomerization, cycloisomerization and reductive couplings. However, in the following years great attention was devoted in the development of Pd-based catalysis. Over the past decade, academic and industrial focus has moved toward efficient chemistry using low-cost and green reagents in transformations leading a resurgence of nickel chemistry, which is experiencing a period of special interest. In addition, the intrinsic properties of nickel could enable challenging transformations and also it has proved to be extremely effective catalyst for cross-coupling.¹⁴ Alongside palladium, nickel has been shown excellent performance in a wide range of C-C bond-forming reactions, such as Negishi, Suzuki-Miyaura, Stille, Kumada and Hiyama couplings. Through the years, the development of new catalysts, ligands, and substrates have greatly improved the scope of this transformation. Despite the tremendous advances in C-C bond formation, some C-Heteroatom couplings still remain a challenge.

Oxidative addition*Oxidation reactions**Transmetallation**Reductive elimination**C-H activation**β-migratory insertion**β-hydride elimination**Oxidative cyclization**Disproportionation/ Comproportionation*

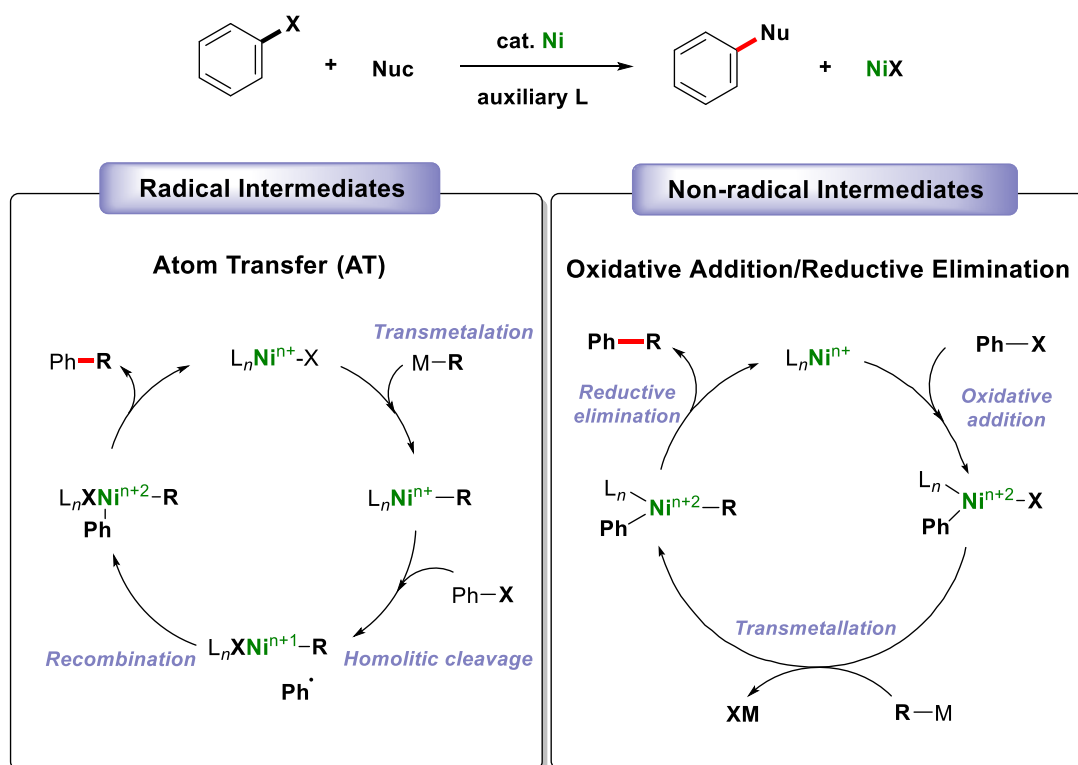
Scheme I.12. Prototypical examples of elementary organometallic reaction steps, highlighting changes in oxidation state at nickel. Ligands and additives are omitted for clarity. M = metal; Me = methyl.

The organometallic chemistry of nickel is rich and varied including numerous catalytic processes,⁹⁹ such as oxidative addition,¹⁰⁰ reductive elimination,¹⁰¹ migratory insertion, transmetallation among others (Scheme I.12).¹³ Nickel has a number of readily accessible oxidation states (from 0 to +4) and thus provides an excellent opportunity to develop a wide range of new catalytic protocols by exploiting these oxidation states. Ni⁰/Ni^{II} catalytic cycle is the most widespread one in catalysis, although the easy access to Ni^I and Ni^{III} oxidation states allows different ways of reactivity, including radical mechanisms. Finally, the accessibility to high-valent Ni^{IV} oxidation states have been definitely established, mainly providing an unprecedented distinct reactivity from the more common oxidation states. Ni⁰ is stabilized by soft and π-acceptor ligands such as CO, phosphine, N-heterocyclic carbene, 2,2'-bipyridine and olefins. Ni(COD)₂ and Ni(PPh₃)₄ are commonly used as a Ni⁰ sources, both have a tetrahedral geometry and are labile. Ni^I complexes often contain phosphine or carbene ligands, therefore, mononuclear Ni^I complexes are paramagnetic. Ni^{II} complexes are ubiquitous; the square planar Ni^{II} complexes are diamagnetic, tetrahedral Ni^{II} are paramagnetic and finally, 5 and 6- coordinate Ni^{II} complexes are generally paramagnetic. There are fewer Ni^{III} and Ni^{IV} complexes, most of them are octahedral, however formal Ni^{III} complexes with pincer ligands are known in square planar geometry.¹⁰²

The mechanisms of nickel-catalysed transformations are in general less studied and a high variability, system dependent pathways, have been shown.

1.4.3 Mechanistic features of nickel-assisted cross-coupling reactions

The readily available oxidation states of the nickel species renders the mechanistic understanding of these transformations as a challenging enterprise. Ni-based catalysts are the most versatile in terms of substrate scope and group tolerance. It appears that there are multiple reaction pathways and also the mechanism of the catalysis depends on the specific ligands employed. With redox active ligands such as pyridine or imines the assignment of the oxidation states of Ni is not straightforward due to the formally Ni^{I} complexes. According to the simple charge balances consideration, could be in fact a Ni^{II} complex bound to a radical-anionic ligand.¹⁰³ Whether redox-active ligands facilitate Ni-assisted catalytic transformations is an open and interesting issue. Several mechanisms have been suggested for the nickel-assisted cross-coupling reactions. Some of them involve the formation of radical intermediates and the others are based on oxidative addition/reductive elimination catalytic cycle (Scheme I.13).¹⁰⁴



Scheme I.13. Radical and non-radical intermediates proposed for Ni-assisted cross-coupling reactions.

However, to overcome several limitations of Ni-mediated cross-coupling reactions, such as excess of base, high temperatures and the use of stoichiometric amount of less reactive nucleophiles, a novel methodology based on a combination of visible light photoredox catalysis has been developed.¹⁰⁵ The combination of visible light and several Ni-based catalysts has become a powerful tool for cross-coupling, allowing new and improved reactivity partners, as well as the capability of the photocatalyst to activate the nucleophiles by generating a high-energy radical intermediates.^{105,106}

Thus, in addition to $\text{Ni}^0/\text{Ni}^{\text{II}}$ pathways, fascinating transformations involving $\text{Ni}^{\text{I}}/\text{Ni}^{\text{III}}$, $\text{Ni}^0/\text{Ni}^{\text{II}}/\text{Ni}^{\text{III}}/\text{Ni}^{\text{I}}$, or all Ni^{I} catalytic cycles are also possible.¹⁰⁷ Moreover, more detailed mechanistic studies for the Ni-mediated reactions should be performed, which not only provide insight into the reaction process but may also inspire the design of new reactions and new catalysts.

I.4.3.1 $\text{Ni}^{\text{I}}/\text{Ni}^{\text{III}}$ catalytic cycle

Although insightful understanding of the reaction mechanisms still requires demanding studies, it is now well accepted that alkyl halides participate in the Ni-catalysed reductive coupling reactions through a radical process using redox-active ligands, such as pybox, N-heterocyclic carbenes or terpyridyl ligands.¹⁰³ Early proposals were described by Kochi in 1978, in which a series of aryl- Ni^{II} complexes were synthesised. The study of the kinetics of the reductive elimination step provided an evidence of the involvement of aryl- Ni^{I} and aryl- Ni^{III} intermediate species in the reaction pathway.^{108,109} The intermediacy of alkyl- Ni^{III} species were proposed in those reactions, but it was not until Tilley¹¹⁰ and co-workers reported the first $\text{Ni}^{\text{I}}/\text{Ni}^{\text{III}}$ catalytic system in which the oxidative addition led to an isolable Ni^{III} compound.

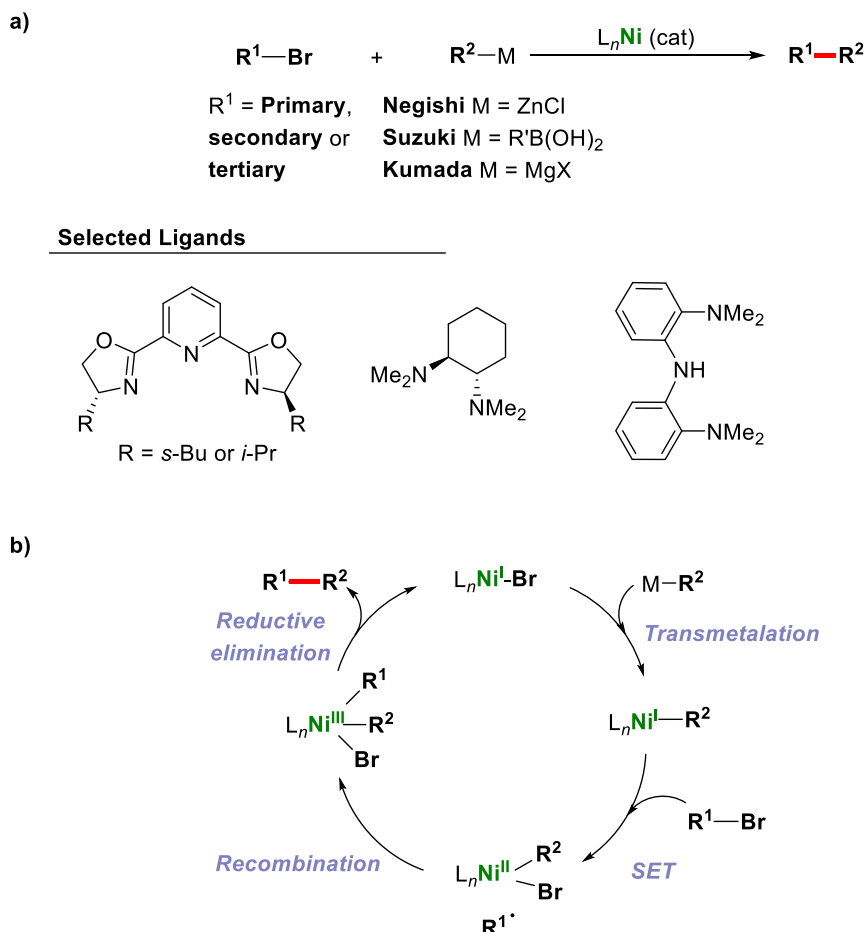
- **Formal oxidative addition step consisting of SET + Recombination**

Cross-coupling reactions with a variety of $\text{C}(\text{sp}^3)$ -metal reagents can also be accomplished using nickel-based catalysis; for example Suzuki, Negishi and Kumada couplings among others can be carried out under mild conditions (room temperature and low catalyst loading), using unactivated alkyl electrophiles, which remains challenging in palladium cross-coupling chemistry. In addition, it is believed that the chelating nature of these redox-active ligands made the β -elimination and other side reactions unfavourable, due to the coordinative saturation.

During the past several years, Fu and co-workers have endeavoured to increase the scope of cross-coupling reactions of alkyl electrophiles to form C-C bonds, focusing on couplings of primary, secondary and unactivated tertiary electrophiles (Scheme I.14a).^{111,112} Preliminary mechanistic studies of these reactions are consistent with an inner-sphere electron-transfer pathway as initial step. Moreover, Vicić group¹⁰³ demonstrated experimentally and computationally, the involvement of radical species in these systems and also the role of the redox-active ligands. The first step of the proposed mechanism involved a transmetalation of Ni^{I} complex and the metal reagent, then the activation of electrophile proceeds through a single electron transfer (SET) process to give an alkyl radical and an alkyl- Ni^{II} complex. The alkyl radical recombines with the alkyl- Ni^{II} species to give a bis(alkyl)- Ni^{III} complex. Finally, the reductive elimination from the bis(alkyl)- Ni^{III} species leads to the formation of coupling product and a Ni^{I} -halide complex (Scheme I.14b).

Hu and co-workers¹¹³ developed nickel-catalysed alkyl-alkyl Kumada coupling reactions as well as Sonogashira couplings of alkynes with primary aryl halides using preformed nickel pincer complexes as catalysts. A bimetallic oxidative addition mechanism involving radical intermediates

has been proposed, evidenced by the use of radical clock substrate, radical scavengers and computational studies, highlighting the formation of a coordinated Ni^{III} -pincer complex as intermediated species in the turnover-determining step of the catalysis. In addition, several publications on asymmetric reactions providing tertiary and quaternary stereocentres with high enantioselectivity have been reported, solving an ongoing challenge in this field.¹¹⁴⁻¹¹⁶

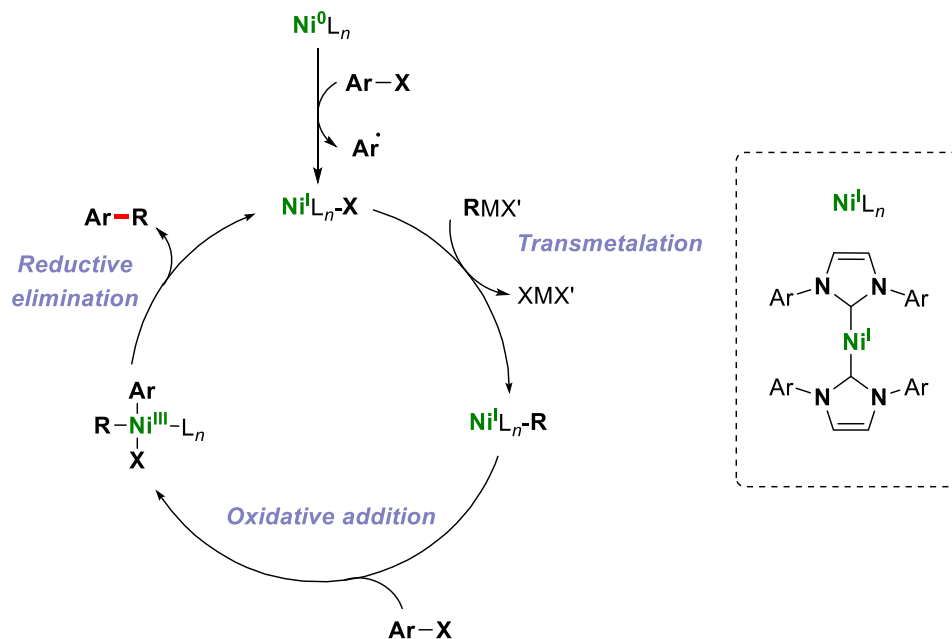


Scheme I.14. (a) General reaction scheme of cross-coupling reactions involving oxidative addition to $\text{C}(\text{sp}^3)$ electrophiles and some used ligands. (b) Mechanism proposed for $\text{C}(\text{sp}^3)\text{—C}(\text{sp}^3)$ cross-coupling reactions catalysed by Ni.

- **Oxidative addition step without the presence of radical intermediates**

Notwithstanding, the chemistry of *N*-heterocyclic carbene species has blossomed at the beginning of this century. The rapid evolution of this chemistry has led to an increasing number of applications in C-C and C-heteroatom bond formation field.^{117,118} Recently, several authors reported the Ni-catalysed coupling reactions of diphenylamine¹¹⁹ and Grignard¹²⁰⁻¹²² reagents among others with several aryl and alkyl halides using carbene-based ligands. Under these conditions, the coupling reactions were achieved at room temperature with moderate to good yields. The authors proposed a $\text{Ni}^{\text{I}}/\text{Ni}^{\text{III}}$ catalytic cycle, which starts with a transmetalation step of the Ni^{I} halide species with the nucleophile to form a nickel(I) nucleophile intermediate followed by oxidative addition of aryl halide to generate a Ni^{III} intermediate and subsequent reductive

elimination to provide the coupling product and the regeneration of the initial Ni^{I} species. Nevertheless, no experimental data were given to support this assumption and also, in several transformations, control experiments run with radical scavengers suggested that radical intermediates are implied in the reaction. Some authors attributed it to the formation of the active Ni^{I} catalyst (Scheme I.15).^{121,122}



Scheme I.15. Plausible mechanism involving $\text{Ni}^{\text{I}}/\text{Ni}^{\text{III}}$ catalytic pathway using a well-defined $\text{Ni}^{\text{I}}\text{-NHC}$ as a catalyst.

Significant progress have been made in Ni-catalysed cross-coupling of alkyl and aryl halides. Several methods are available for all main types of reactions, such as Suzuki, Hiyama, Negishi, Stille among others. The mechanism of these nickel-catalysed coupling reactions is complex and not fully understood. It appears that there are multiple reaction pathways, and the mechanism for a particular system depends on multiple factors.

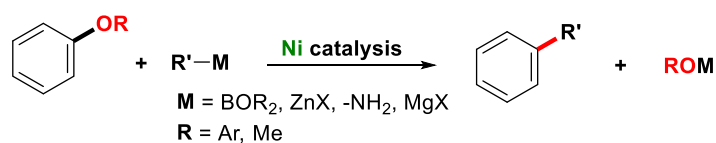
I.4.3.2 $\text{Ni}^0/\text{Ni}^{\text{II}}$ catalytic cycle

Cross-coupling reactions of aryl or vinyl halides (or pseudohalides) with nucleophiles, including organoboron¹²³, organozinc reagents¹²⁴, amines^{125,126}, hydrosilanes¹²⁷, or Grignard reagents¹²⁸ among others, can be accomplished under nickel catalysis. Despite the advances in this area, progress in this field was relatively slow until the introduction of auxiliary ligands bearing bulky substituents, such as carbene derivatives, dppf, PCy_3 or BINAP among others. The use of these ligands have enabled faster reactions under milder conditions (Scheme I.16a). In 1979, Wenkert and co-workers reported nickel-catalysed cross-coupling reactions involving Grignard reagents and aryl ethers rather than aryl halides. Owing to their general low-cost, readily availability and high thermal stability, aromatic ether derivatives have emerged as versatile and cost-efficient alternatives to aryl halides. This pioneering work indicated that oxidative addition of C-O bonds to nickel(0) species can readily occur. Since then, several research groups reported

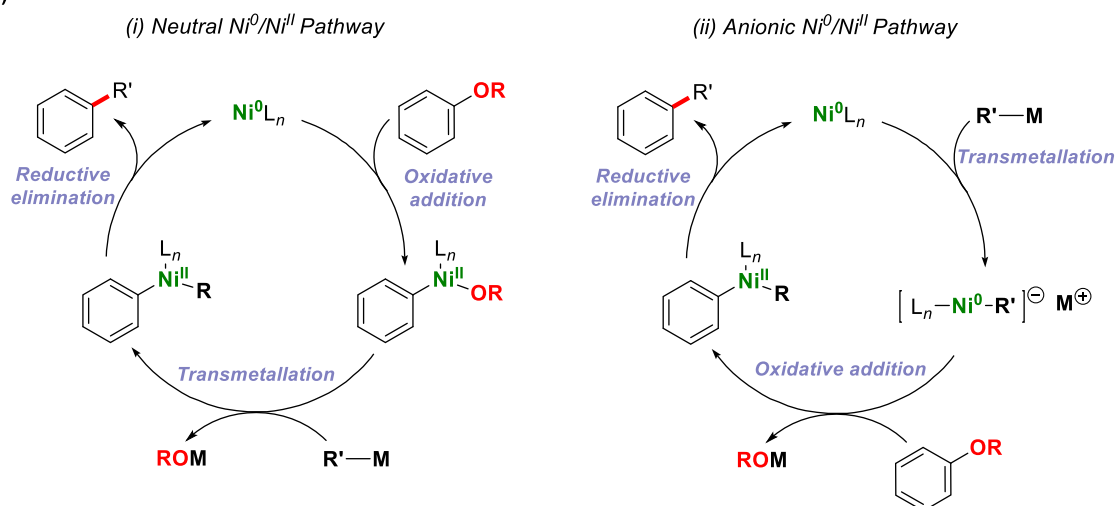
transformations of aromatic C-O bonds including aryl carbamates, carbonates, esters, sulfonates and even aryl triflates, mesylates or tosylates.^{1,129-133}

From the mechanistic point of view the most accepted pathway for these methodologies follows the classical oxidative addition/reductive elimination steps (Scheme I.16b(i)). Two possible scenarios are postulated, depending on the nature of the nucleophile. The generally accepted one involve a sequence of oxidative addition / Transmetalation / reductive elimination, $\text{Ni}^0/\text{Ni}^{\text{II}}$ catalytic cycle. Moreover, another plausible scenario was proposed based on the generation of an anionic nickelate species by the reaction of the nickel(0) precursor with Grignard reagents, which can potentially operate as a competent catalyst, making a more reactive catalyst due the increase of electron density around the nickel centre (Scheme I.16b(ii)).¹³⁴ Although the formation of anionic nickelate species was experimentally proved when Grignard reagents were used,¹³⁵ its generation by the reaction with less reactive nucleophiles, such as organoboron reagents, is unlikely. The change in the substrate scope as well as the nature of the nucleophiles might cause the switch between the neutral and anionic mechanisms, but further mechanistic studies are required to prove the feasibility of these proposals. Despite recent advances in this field, a mechanistic understanding of the Ni-catalysed C-OR bonds cleavage still remains ambiguous and uncertain.

a)



b)



Scheme I.16. (a) General reaction scheme of Ni-assisted cross-coupling reactions. (b) Possible mechanistic scenarios for Ni-Catalysed cross-coupling of aryl ethers consisting on a $\text{Ni}^0/\text{Ni}^{\text{II}}$ catalytic cycle.

Notwithstanding, Martin group reported an extensive mechanistic study on the Ni-catalysed C-OR bond-cleavage using hydrosilanes. Experimental and computational data demonstrate that the reaction does not operate *via* putative Ni^{II}-oxidative addition complexes and pointed at a Ni^I-SiR₃ species as a responsible of the observed reactivity. This work strongly suggest that oxidative addition is not always a suitable pathway for the activation of inert C-O bonds and other mechanistic scenarios could be conceivable.¹²⁷

1.4.3.3 Ni^{II}/Ni^{IV} catalytic cycle

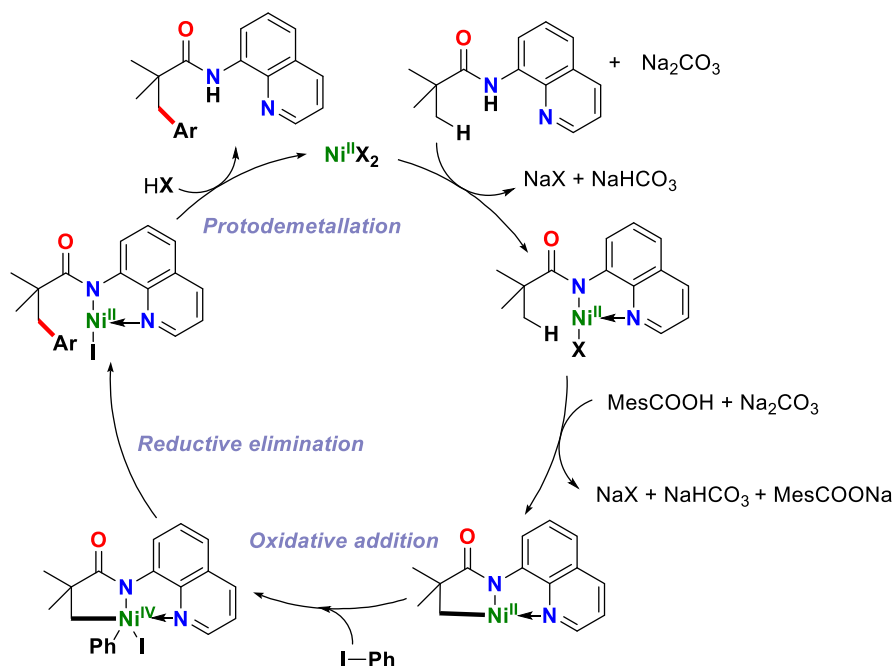
Over the past decades, despite the continued development on nickel catalysis, the higher oxidation states in nickel chemistry were mainly dominated by Ni^{III} complexes, but relatively few example of Ni^{IV} compounds were reported. These organonickel(IV) compounds, mainly contain polydentate nitrogen ligands (amide and deprotonated oximes). Klein¹³⁶⁻¹³⁸ et al. reported the isolation of octahedral Ni^{IV} species by oxidative addition of methyl iodide onto Ni^{II}-acylphenolate tris(phosphine) complexes. Dimitrov and co-workers reported the isolation of a pseudotetrahedral bromotris(1-norbornyl)nickel (IV) complex and Turro and co-workers reported the first isolated tetraalkyl Ni^{IV} complex.¹³⁹

So far, the vast majority of C-C and C-Heteroatom coupling reactions catalysed by nickel mainly involve Ni⁰/Ni^I/Ni^{II}/Ni^{III} species in the catalytic pathway, although no reliable evidence for the generation of Ni^{IV} species as a part of catalytic cycle has been provided thus far. More recently, Ni^{IV} intermediate species are being proposed in transformations involving the Ni^{II}/Ni^{IV} redox couple,¹⁴⁰⁻¹⁴² although well-characterised species have been only reported using model substrates designed for octahedral environments.¹⁴³⁻¹⁴⁵ This hypothesis is fully supported by several studies that revealed the involvement of organometallic Pd^{IV} intermediate species, which can be easily accessed with many common oxidants. Furthermore, the reactivity of these high-valent Pd^{IV} complexes in C-C and C-Heteroatom bond formation processes have led to the development of various Pd^{II}/Pd^{IV} catalytic cycles.⁹⁶ Inspired by the emergence of high valent palladium chemistry, a pursuit for a similar organometallic high-valent nickel chemistry becomes a challenging target.

In 2009, Nakamura et. al¹⁴⁶ reported a very efficient methodology for the coupling of aryl and heteroaryl halides with aryl magnesium bromides using a combination of nickel difluoride catalyst and several NHC. Experimental results and theoretical calculations suggest that the reaction proceed via a Ni^{II}/Ni^{IV} catalytic cycle. Importantly, this work arose several questions about the possibility of accessing to high-valent Ni^{IV} species and also the way of reactivity, which will probably be complementary to their low-valent Ni counterparts.

Recently, Chatani and co-workers^{141,147} reported the C-H arylation reactions using aryl iodides and diaryliodonium electrophiles, and the authors proposed the involvement of Ni^{IV} intermediate species (Scheme I.17). Nevertheless, these putative aryl-Ni^{IV} intermediate species were not

directly detected, but the use of radical scavengers did not affect the reaction outcome, providing an evidence of the non-involvement of radical species.



Scheme I.17. Proposed mechanism for Ni-catalysed direct arylation of unactivated C-H bonds in presence of bidentate directing group.

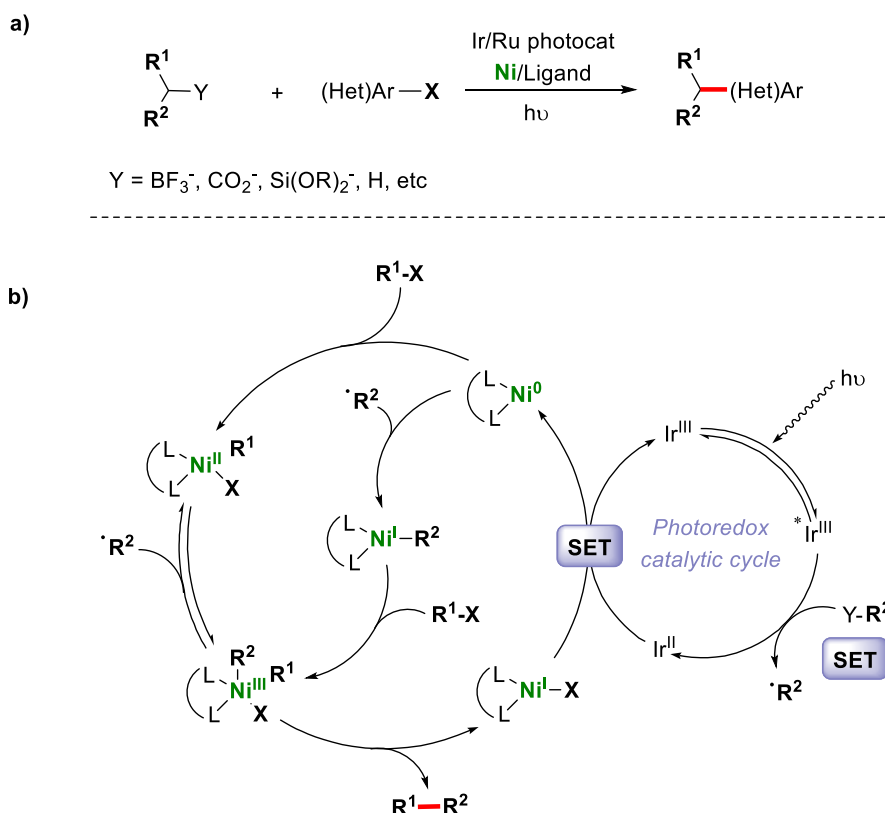
Very recently, Fout and co-workers¹⁴⁵ reported the first example of the isolation of high-valent Ni^{IV} organometallic complexes supported by a monoanionic bis(carbene) pincer ligand platform, which were obtained through the oxidation of Ni^{II} precursor with several halogen surrogates, such as iodobenzene dichloride (PhICl_2), elemental bromine (Br_2) or benzyltrimethylammonium tribromide (BTMABr_3). These complexes promote halogenation of organic substrates via reductive elimination pathway, featuring a $\text{Ni}^{\text{II}}/\text{Ni}^{\text{IV}}$ redox catalytic cycle.

I.4.4 Photoredox catalysis

Visible light photoredox catalysis has emerged in recent years as a powerful methodology in organic synthesis. Nickel has become an ideal transition metal for the photochemical procedures due to its ability to participate in one-electron processes. The combination of photoredox catalysis with nickel catalysis has enabled C-C, C-O and C-S bond formation through the formation of reactive radical intermediates and a prototypical mechanistic scenario for these processes has been proposed (Scheme I.18a).^{105,106,148} The feasibility of these reactions arises from the ability of photocatalysts to act as both strong single-electron oxidants and reductants upon irradiation with visible light.

The radical precursor is generated from single electron oxidation of a suitable precursor by an excited-state photocatalyst complex. This radical can enter the cross-coupling cycle in two different pathways: radical addition to an organonickel(II) species, which is formed after oxidative

addition of an aryl halide to a Ni^0 catalyst, or direct radical addition to the Ni^0 catalyst to form a $\text{Ni}^{\text{I}}\text{-R}$ species, followed by oxidative addition of the aryl halide. Both pathways provide a common Ni^{III} intermediate that can rapidly dissociate the stabilized radical or more slowly undergo reductive elimination to afford the desired coupled product and a Ni^{I} species. The latter can be reduced by the iridium complex to regenerate both the Ni^0 and the photocatalyst (Scheme I.18b).^{149,150}



Scheme I.18. Proposed mechanism for photoredox/Ni dual catalytic cycle for cross-coupling reactions.

Recently, MacMillan and Doyle¹⁵¹ explored the combination of visible-light photoredox and nickel transition metal catalysis to create a dual catalysis platform for the formation of C-C and C-Heteroatom bonds, using non-traditional leaving groups, such as $\text{C}(\text{sp}^3)\text{-COOH}$ or $\text{C}(\text{sp}^3)\text{-H}$ bonds, as a coupling partners. This strategy enable the formation $\text{C}(\text{sp}^3)\text{-C}(\text{sp}^2)$ and $\text{C}(\text{sp}^3)\text{-C}(\text{sp}^3)$ bonds, which are not currently possible using either photoredox or transition metal catalysis alone. Otherwise, these contribution opens the door to the development of new and practical methodologies for C-C and C-Heteroatom bond formation. The photoredox/Ni dual catalysis not only has enabled transformations that were extremely challenging, but these reactions can also be carried out under mild conditions with minimal by-products compared to the traditional cross-coupling reactions. The use of visible light could overcome the high-energy transition state barriers associated with the transmetallation from less nucleophilic coupling partners. Complementary studies, based on an enantioselective version of photoredox Ni catalysis of several cross-coupling reactions were also performed, obtaining in most of the cases excellent performances. This strategy represents a complementary approach to traditional cross-coupling processes, which will likely be applicable across a range of different substrates. However, deeper

understanding of the operative mechanism should provide opportunities to extend the reaction to less reactive C-H bonds and/or new halide or pseudohalide partners.¹⁵²

1.4.5 Deeper mechanistic insight on Ni-catalysed cross-coupling reactions

Over the past decades, multiple generations of ligands have been designed to improve the catalytic systems, not only in terms of promoting elementary catalytic steps, but also favouring desired oxidation states of nickel, given the established viability of $\text{Ni}^0/\text{Ni}^{\text{II}}$, $\text{Ni}^{\text{I}}/\text{Ni}^{\text{III}}$ and $\text{Ni}^{\text{II}}/\text{Ni}^{\text{IV}}$ catalytic cycles.¹⁰⁷ The ligand frameworks often employ a few key design elements, such as sterically encumbered architectures, hemilabile coordinating groups, electronically-tuned substituents among others, to achieve high catalytic efficiency. The ancillary ligand design strategy contributes towards the development of high-performance nickel catalysis for use in a wide range of important cross-coupling reactions in a more sustainable way.

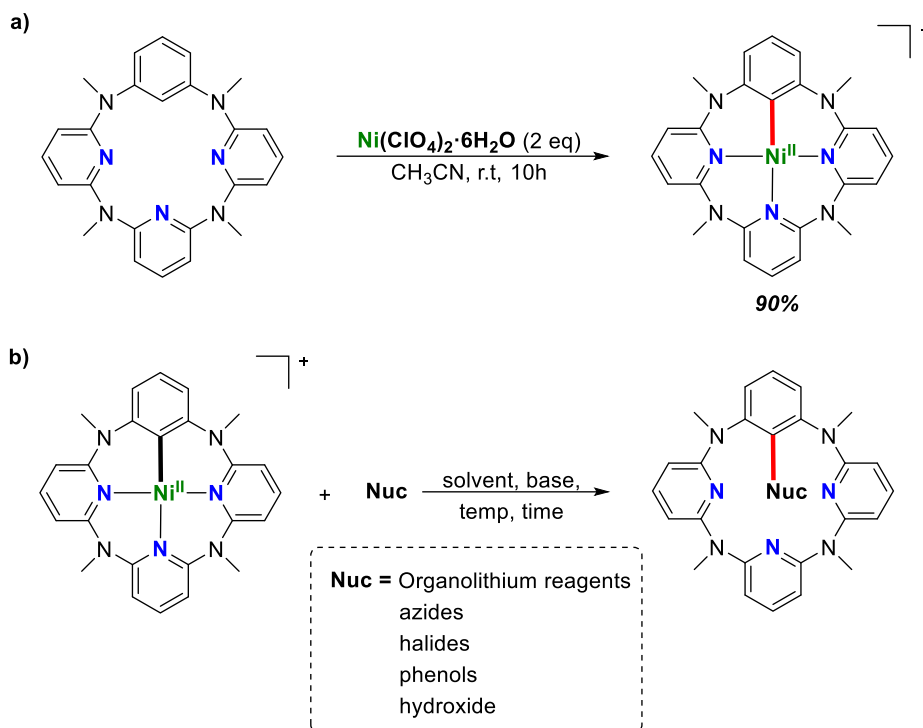
1.4.5.1 Chelation-assisted stabilisation of high-valent nickel species

Despite the continued development of nickel catalysis, isolated and well-characterised organometallic high-valent nickel complexes still remains a challenging target. Most of the proposed mechanistic pathways lacked of direct experimental evidences to confirm the mechanistic proposals, most of them are only supported by computational and radical trapping studies.

- **Well-defined aryl- Ni^{II} complexes**

Nickel-mediated cross-coupling reactions and C-H bond functionalisation are extremely versatile and also can promote coupling reactions of challenging substrates. It is believed that most of these methodologies follow a classical $\text{Ni}^0/\text{Ni}^{\text{II}}$ catalytic cycle consisting of an initial oxidative addition, transmetalation and final reductive elimination. Nevertheless, to date reactivity studies of aryl- Ni^{II} complexes remained very poor. In 2010 Ribas and co-workers⁷² reported the synthesis of well-defined organometallic nickel(II) complex based on model macrocyclic arene substrates through the C-H bond activation by Ni^{II} salts (see in section 1.5.2). However, the chemistry of this well-defined macrocyclic aryl- Ni^{II} species was not studied to date (see Chapter V). More recently, Wang and co-workers¹⁵³ reported the synthesis and fully characterization of a well-defined aryl- Ni^{II} complexes formed through the direct electrophilic metalation of macrocyclic azacalix[m]arene[n]pyridine ligands (Scheme 1.19a). Both of them exhibit a typical square planar coordination and the isolation of these complexes provides an unprecedented chance to study the stoichiometric reactivity of aryl- Ni^{II} species in cross-coupling reactions. Furthermore, Wang and co-workers studied the reactivity of the monoaryl- Ni^{II} compounds against several nucleophiles such as organolithium reagents, azide, halide, phenol and hydroxide, obtaining from good to excellent results, observing in some cases β -hydride elimination as a side-reaction. These

results suggested that the reaction proceeds *via* reductive elimination under optimized conditions depending on the nucleophile. However, further mechanistic studies for these transformations need to be done. The authors did not provide the catalytic version of these couplings (Scheme I.19b).



Scheme I.19. Synthesis of well-defined nickel(II) complex, based on a macrocyclic model substrates and X-ray structure of aryl-Ni^{III} complex using heterocalixarene-type ligands described by Wang.

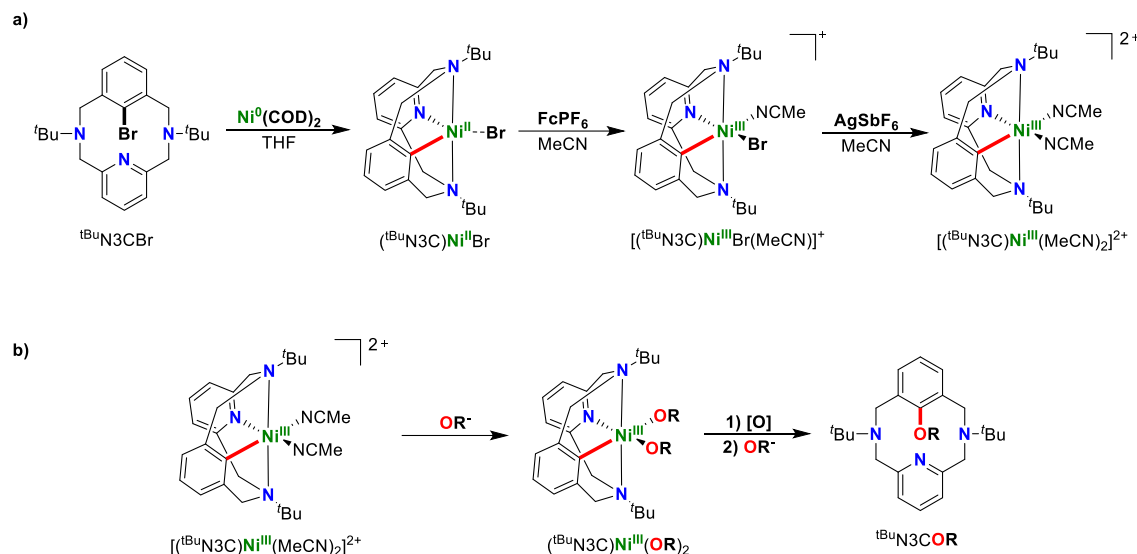
• *Well-defined aryl-Ni^{III} complexes*

Since the seminal work of Kochi and co-workers, many experimental and computational reports have proposed the involvement of organometallic Ni^{III} intermediates in cross-coupling reactions, although a few high-valent Ni^{III} species have been isolated and characterised.

On the other hand, high-valent organometallics have also been proposed as catalytically active intermediates in metalloenzymes such as methyl-coenzyme M reductase (MCR)¹⁵⁴, which have been characterised by EPR and carbon monoxide dehydrogenase/ acetyl-CoA synthetase (CODH/ACS).¹⁵⁵ Interestingly, organometallic Ni^{III} intermediates have also been recently proposed to play a key role in the C-H activation step during the anaerobic oxidation of methane.^{156,157}

Mirica and co-workers¹⁵⁸⁻¹⁶⁰ reported the first isolation and characterization of a mononuclear aryl-Ni^{III} complexes stabilised by a tetradentate ligand, presenting a distorted octahedral geometry of the Ni^{III} centre (Scheme I.20). These complexes can easily undergo C-C and C-Heteroatom bond formation at room temperature and generating an unstable Ni^I species that undergoes rapid disproportionation to Ni⁰ and Ni^{II} species, providing an evidence that such Ni^{III} species are active

intermediates. Overall, these studies provide a strong evidence for the direct involvement of organometallic Ni^{III} complexes in Ni-mediated cross-coupling reactions.



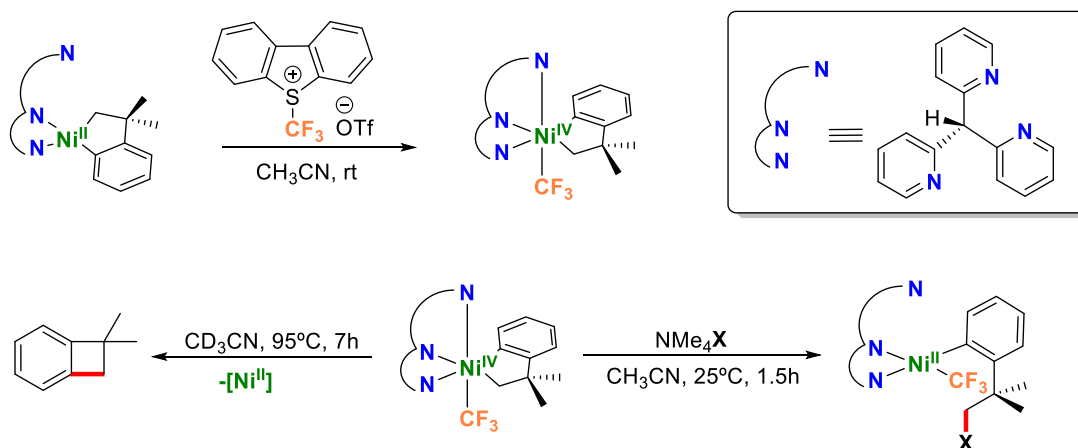
Scheme I.20. (a) Synthesis of well-defined Ni^{III} distorted octahedral complexes through the oxidative addition of tetradentate $(\text{tBuN}_3\text{CBr})$ ligand to $\text{Ni}(\text{COD})_2$ in THF at RT. (b) Formation of C-O bonds from the reductive elimination of aryl- Ni^{III} intermediate species.

Moreover, further mechanistic and spectroscopic studies will be crucial for the development of more efficient and selective catalysts for several C-C and C-Heteroatom organic transformations.

• Well-defined aryl- Ni^{IV} complexes

In the recent years, the interest in the feasibility of a $\text{Ni}^{\text{II}}/\text{Ni}^{\text{IV}}$ redox catalytic cycle for bond-forming reactions and also the plausible reactivity of those Ni^{IV} complexes compared to other oxidation states have grown. Cross-coupling reactions are possible candidates for the involvement of Ni^{IV} intermediates by oxidative addition, which could be initiated by radical processes from the starting Ni^{II} compound. Very recently, Sanford and co-workers,^{143,161} finding inspiration on their previous studies on Pd^{IV} chemistry, reported the isolation and full characterization of octahedral Ni^{IV} complexes featuring the tris(2-pyridyl)methane and tris(pyrazolyl)borate ligand platforms, capable of reductively eliminating C-X ($\text{X} = \text{O}, \text{S}, \text{N}, \text{CF}_3$). These high-valent Ni^{IV} complexes can be prepared by the oxidation of Ni^{II} precursors with several inner sphere oxidants that are known to promote the $2e^-$ oxidation of other group 10 metal complexes, such as *N*-fluoro-2,4,6-trimethylpyridinium triflate (NFTPT), iodobenzene diacetate ($\text{PhI}(\text{OAc})_2$) and iodobenzene dichloride (PhICl_2). However, these intermediates could not be spectroscopically detected at room or even at low temperature with any of these oxidants, suggesting that this putative intermediate is highly reactive. Interestingly, the use of *S*-(trifluoromethyl)dibenzothiophenium triflate (TDTT) as an oxidant resulted in a transfer of a CF_3 to Ni to obtain a long-lived Ni^{IV} intermediate, which can be isolated and fully characterised (Scheme I.21). The reactivity of this Ni^{IV} complex was further investigated and upon heating at 95°C , it underwent to $\text{C}(\text{sp}^2)\text{-C}(\text{sp}^3)$ bond formation through reductive elimination step in a quantitative yield. In contrast, upon the addition of

exogenous reagents, such as tetrabutyl ammonium salts, resulted in selective C(sp^3)-heteroatom bond formation to afford Ni^{II} product. These results provided the first evidence of the formation of Ni^{IV} intermediate species under mild conditions using bidentate nitrogen donor ligands, through the oxidative addition of the respective Ni^{II} precursor. Additional studies, mechanistic and spectroscopic, of high-valent nickel systems will provide even more insight into the oxidants that enable selective access to Ni^{IV} (rather than Ni^{III}) as well as the reactivity of Ni^{IV} species. A fundamental understanding of these transformations will lead to the development of new and improved methodologies.

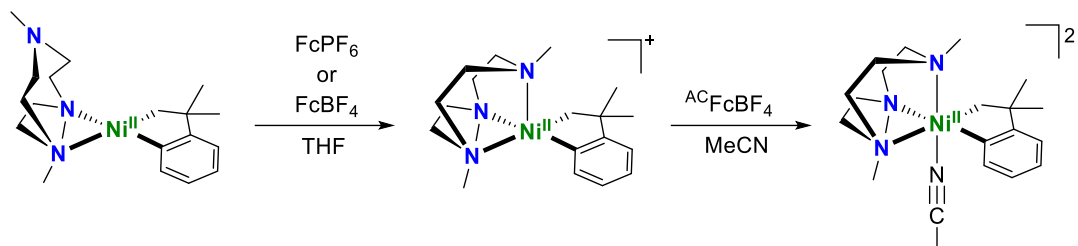


Scheme I.21. (a) Synthesis of well-defined diamagnetic Ni^{IV} octahedral complex through the oxidation of $[(Py_3CH)Ni^{II}(CH_2CMe_2-o-C_6H_4)]$ with TDTT, using a facial tridentate ligand tris(2-pyridyl)methane (Py_3CH). (b) Reactivity of aryl- Ni^{IV} complex forming a C(sp^2)-C(sp^3) or C(sp^3)-O coupling products.

Very recently, Mirica and co-workers¹⁴⁴ reported the potential involvement of high-valent Ni^{III} and Ni^{IV} intermediate species in Ni-mediated cross-coupling reactions, especially for transformations involving alkyl substrates. They reported the synthesis of the *N, N'*-dimethyl-2,11-diaza[3.3](2,6)pyridinophane ligand, which is able to stabilise a Ni^{III} -dialkyl complex. The isolation of this Ni^{III} -dialkyl complex allowed a detailed mechanistic investigation. Interestingly, this high-valent Ni^{III} species undergoes the reductive elimination quite slowly; in contrast, upon the addition of one equivalent of oxidant, the reductive elimination evolved faster, suggesting the involvement of a Ni^{IV} intermediate. Moreover, the Ni^{IV} intermediate species was spectroscopically characterised, confirming the strong potential of Ni^{IV} species in the oxidatively induced C-C and C-Heteroatom bond formation.

Most recently, the same authors reported the first organometallic Ni complexes supported by a triazacyclononane-derived ligand.¹⁶² Besides the presence the alkyl/aryl C-donor cycloneophyl ligand allowed the isolation of uncommon organometallic Ni^{II} , Ni^{III} , and Ni^{IV} complexes (Scheme I.22). The five-coordinated Ni^{III} complex was stable both in solution and solid state, albeit it exhibited limited C-C bond formation reactivity. In contrast, the six-coordinated Ni^{IV} complex has a MeCN molecule bound to Ni and it undergoes rapid C-C bond formation upon exposure to light, which is in according to the dual Ni/photoredox catalysis discussed above. Furthermore, the

(Me₃tacn)Ni^{III}(cycloneophyl) complex undergoes oxidative addition with alkyl halides, as well as rapid oxidation by O₂, to generate detectable Ni^{III} and Ni^{IV} intermediates and followed by reductive elimination to form new C-C bonds.



Scheme I.22. Synthesis of (Me₃tacn)Ni(CH₂CMe₂-o-C₆H₄) complexes.

Overall, these facial ligands platforms were able to support the formation of nickel complexes in three oxidation states (II, III, IV) and thus could be of great help on the reactivity studies, trying to understand the role of each oxidation state in several organometallic transformations, especially those relevant to cross-coupling reactions.

I.4.6 General Conclusions and applications

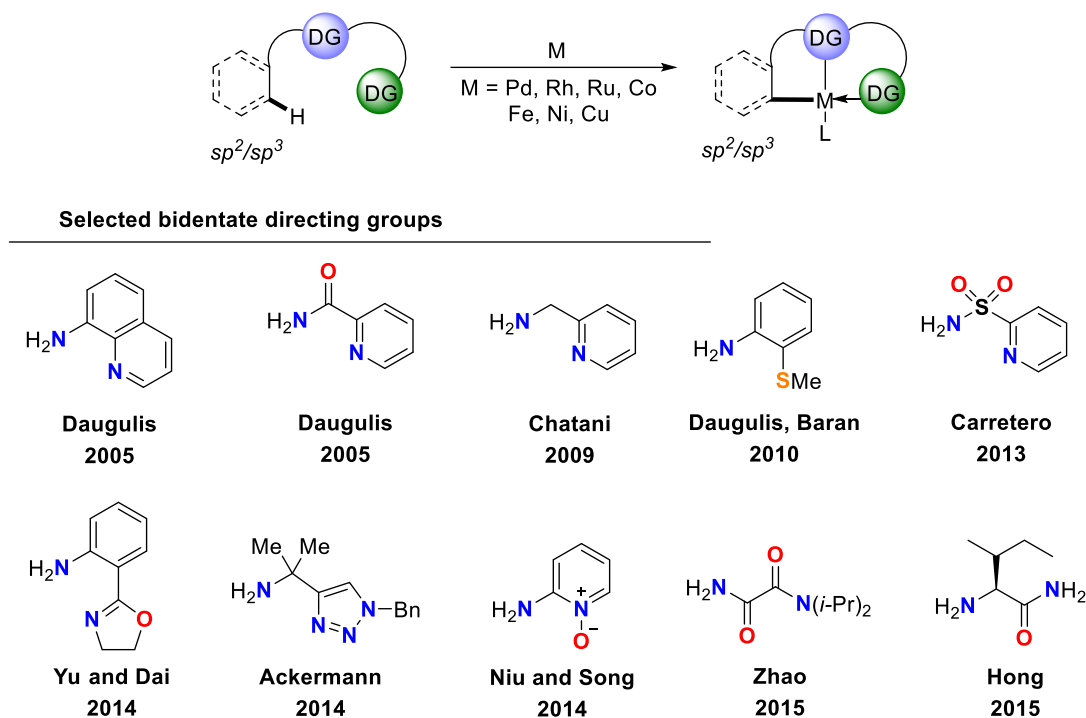
In the last decades, the paradigm of C-C and C-Heteroatom bond formation has allowed to assemble complex molecular frameworks with an impact in natural product synthesis, medicinal chemistry and industrial process development. Nickel catalysis has been at the forefront of this expansion and progressively it is evolving into a suitable and effective alternative to precious metal catalysts for several key transformations. Nevertheless, the extensive mechanistic investigations done resulted in a complex chemistry, due to the rich coordination chemistry of nickel that allows it to adopt a variety of geometries and oxidation states.¹⁶³ Nickel is between hard and soft transition metals and could interact with a variety of ligands that not only stabilize all the oxidation states, which commonly range from +1 to +4, but also allow the fine tuning of the redox potential at the metal centre. Therefore, most of the key challenges of nickel catalysis relies on a clear understanding of how such systems work and gathering more detailed knowledge of the plausible mechanisms involved in such transformations. These further information of nickel chemistry should not only provide insight into the reaction processes, but also inspire the design of new catalysts and new transformations with broaden substrate scope.

I.5 C-H bond functionalisation

Nowadays, the C-H functionalisation is one of the mainstream topic of synthetic chemistry and one of the most investigated approaches for the development of new synthetic methodologies. The C-H bonds are ubiquitous in organic species, from natural simple feedstocks to the more elaborated natural products and material sciences. Therefore, the use of substrates containing only C-H bonds have emerged as a very powerful tool and sustainable strategy, since the synthesis of prefunctionalised substrates is no longer necessary. The C-H bonds are relatively

inert, requiring a high amount of energy to dissociate it, however, the use of transition metals provide a new approach for enabling these transformations in an easier way. Moreover, the knowledge gained insight the plausible mechanisms for the C-H bonds cleavage assisted by transition metals has caused a dramatic impact in synthetic organic chemistry.¹⁶⁴⁻¹⁶⁶ An extensive C-C and C-heteroatom functionalisation of a wide range of arenes was developed using palladium, ruthenium, iridium and rhodium catalysts, among others, with varying degree of success.¹⁶⁷⁻¹⁶⁹ However, from the viewpoint of the practicality of these transformations tremendous challenges lie ahead in the development of new approaches based on inexpensive and earth-abundant first row transition metals that endowed with high catalytic performance, versatility and excellent chemo- and regioselectivity. In light with the remarkable progress achieved using these type of metals, research into new processes and new applications using iron, copper, nickel and cobalt based catalysts as an alternative methodologies has been in a continuous progress.

Therefore, the control of the selectivity of C-H bond functionalisation has been a challenging issue, due to the fact that most of the molecules contains many C-H bonds enable to be activated at the same time, obtaining different isomers, or even multifunctionalisation. Several strategies to overcome the problem of selectivity were reported; for instance, the introduction of directing groups (DG), which direct the metal to a specific position reducing the amount of available positions and providing a high degree of selectivity.¹⁷⁰⁻¹⁷² Chelation-assisted transformations have become a common and powerful methodology for the regioselective functionalisation of *ortho* C-H bonds.^{173,174} In this sense, there is an extended number of directing groups with specific electronic and steric properties as well as with chiral groups (Scheme I.23). Bidentate directing groups have been exhaustively studied, offering the chance to developed new strategies for C-H functionalisation. In 2005, Daugulis and co-workers¹⁷⁵ reported the arylation of unactivated C(*sp*³)-H bonds using 8-aminoquinolines scaffolds and picolinamide as *N, N*-bidentate directing group using Pd(OAc)₂ as a catalyst. Since the Daugulis pioneering work, several groups focused their research on the study of new possibilities that this detachable and rigid system could offered, using different transition metals to explore new catalytic reactions based on C-H activation.



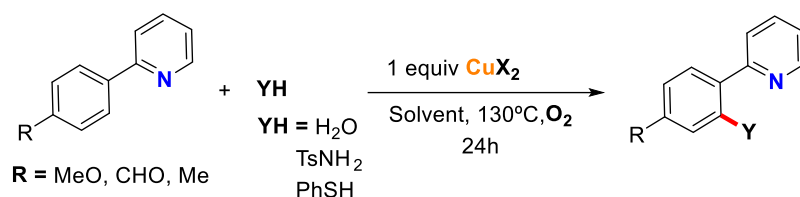
Scheme I.23. Metal-mediated C-H bond activation aided by bidentate directing groups.

I.5.1 Copper catalysed C-H activation

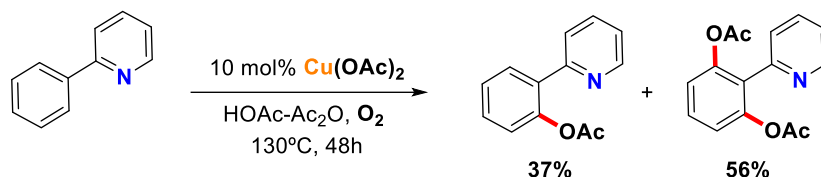
Several reports highlight the feasibility of copper to achieve oxidative functionalisation of C-H bonds, including chelated-directed and non-directed examples.

There are a number of Cu-catalysed C-H activation processes reported in the literature, for which the mechanism of C-H activation is not well established. In some examples it is suggested that the use of sacrificial oxidants led to obtain highly electrophilic Cu^{III} intermediates, which may be the responsible for the C-H activation. In this sense, in 2006 Yu and coworkers¹⁷⁶ reported a seminal work on the use of directing groups in which, inexpensive Cu^I salts can catalyse the *ortho*-selective C-H functionalisation of 2-arylpyridines, using O₂ as a terminal oxidant at 130°C. Interestingly, the stoichiometric reaction gave the selective formation of mono-functionalised compounds and remarkably this reaction could be extended to cyanation, amination, halogenation, esterification and thioesterification of C-H bonds using various nucleophilic anions (Scheme I.24a). Nevertheless, the reduction of catalyst loading to 10 mol% in presence of O₂ resulted in a mixture of mono- and diacetoxylation products (Scheme I.24b). A radical-cation pathway was proposed to explain the data obtained from the mechanistic studies. A single electron transfer (SET) from the aryl ring to the coordinated Cu^I leading to the cation-radical intermediate is the rate-limiting step. The observed *ortho*-selectivity is explained by an intramolecular anion transfer from a nitrogen-bound Cu^I complex (Scheme I.24c).

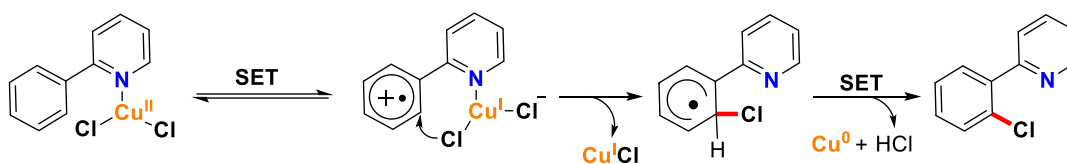
a)



b)



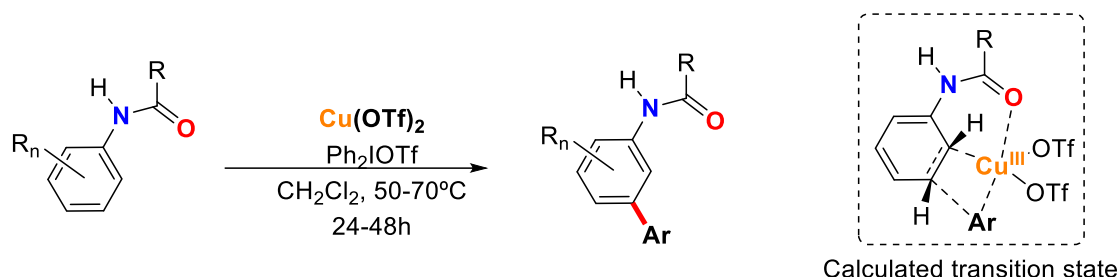
c)



Scheme I.24. (a) Cu^{II} -mediated several C-H functionalisation reactions using various nucleophilic anion sources. (b) Cu^{II} -catalysed acetoxylation of aryl C-H bonds. (c) Mechanism proposal for the selective formation of mono functionalised compounds.

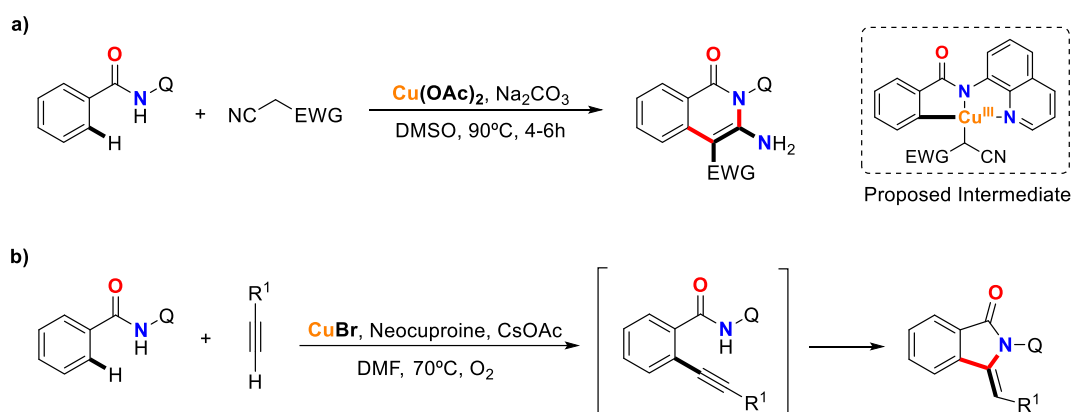
The use of inexpensive and environmental aware reagents jointly with the high tolerance to several functionalities made this protocol a very promising tool in transition-metal-mediated C-H functionalisation chemistry.

In 2009 Phipps and Gaunt¹⁷⁷ reported the *meta*-selective electrophilic arylation reaction, when substituted anilides were used as a directing group (Scheme I.25). This result became very interesting, due to the fact that anilido groups orientate to *ortho* position. The reaction proceeds under mild conditions using Cu^{II} salts as a catalyst and $\text{I}(\text{III})$ salts as an oxidant. Interestingly, this methodology is tolerant with the presence of several functional groups, therefore many tri- and tetra- substituted anilides, which are difficult to obtain by classical pathways, could be synthesised. The mechanism for the *meta* C-H activation reaction is poorly understood and the obtained data are controversial, however the involvement of aryl- Cu^{III} intermediate species are proposed. Later on, it was found that the carbonyl group was suggested as the truly responsible for the selectivity in *meta* position.¹⁷⁸



Scheme I.25. Selective *meta*-arylation C-H activation reaction catalysed by Cu^{II} salts and the proposal of most favorable intermediated based on four-membered transition state found by DFT.¹⁷⁸

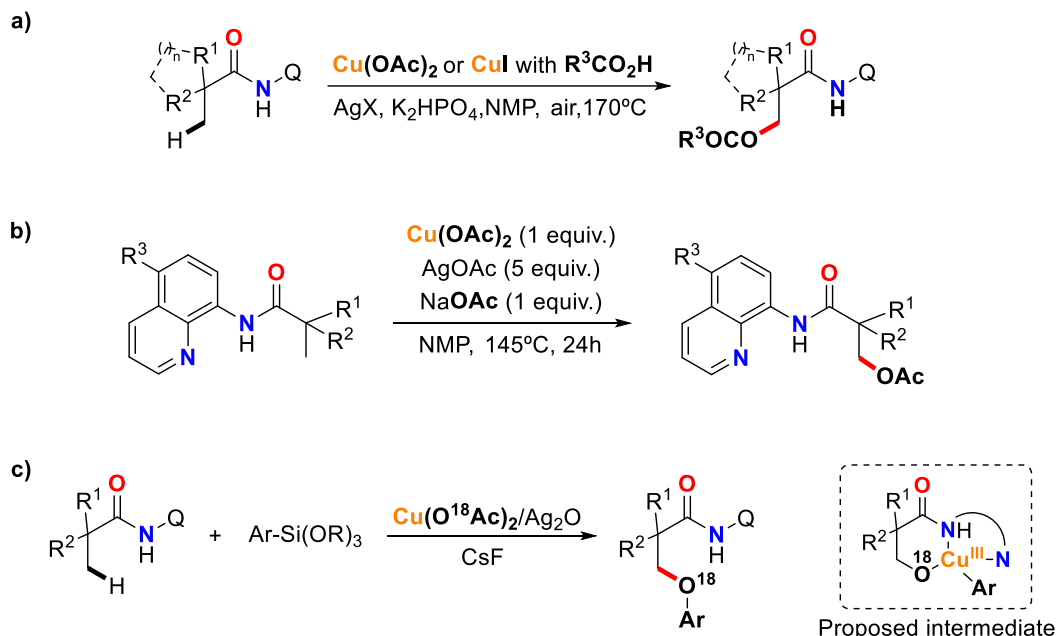
In 2014, Liu group reported the first Cu^{II} -mediated oxidative coupling of benzamide with ethylcyanoacetate using 8-aminoquinoline as a directing group (Scheme I.26a).¹⁷⁹ This tandem reaction provides a straightforward approach for the construction of isoquinoline scaffolds. In this system, the best yield could be achieved when 3 equiv. of Cu^{II} was used under argon atmosphere. In the same year, You and co-workers reported another example of intramolecular annulation reaction, in which a copper-promoted the oxidative cross-coupling of arenes with terminal alkynes.¹⁸⁰ In this oxidative coupling process, $\text{Cu}(\text{OAc})_2$ acts as both the promoter and terminal oxidant; an excess of alkyne were used in order to minimize the yield of the homocoupling side reaction. Shortly after, Huang and Yu reported the same reaction and the optimization studies indicated that the choice of the ligand had a significant impact on the reaction outcome (Scheme I.26b). Finally, the use of catalytic amount of copper salts and molecular oxygen as a green oxidant, represent an important improvement in the preparation of indole derivatives *via* C-H functionalisation reactions.¹⁸¹



Scheme I.26. (a) Copper-mediated $\text{C}(\text{sp}^2)\text{-H}/\text{C}(\text{sp}^3)\text{-H}$ coupling of benzoic acid derivatives with activated methylenes. (b) Copper-catalysed C-H activation based arene/alkyne annulations.

In order to increase the scope of copper-mediated C-H activation, further studies using unactivated $\text{C}(\text{sp}^3)\text{-H}$ were done. In 2014, Ge group reported a copper-assisted site-selective acyloxylation of unactivated $\text{C}(\text{sp}^3)\text{-H}$ directed by 8-aminoquinoline bidentate ligand (Scheme I.27a).¹⁸² Interestingly, the reaction proceeded exclusively at the β -methyl C-H bonds in a highly regioselective manner and when α,α -dimethyl-substituted amides were used, both mono- and bis-

acyloxylation products were observed. Noteworthy, several linear and cyclic aliphatic acids and benzoic acids were applicable to the acyloxylation reaction. Shortly after, Kuninobu and Kanai also developed a copper-mediated direct C(sp^3)-H acetoxylation using 8-aminoquinoline as the chelation directing group and AgOAc as oxidant (Scheme I.27b).¹⁸³



Scheme I.27. (a) Copper-mediated direct C(sp^3)-H acyloxylation. (b) Copper-mediated direct C(sp^3)-H acetoxylation. (c) Copper-catalysed aryloxylation of β -C(sp^3)-H.

More recently, Zhang and co-workers investigated a copper-promoted aryloxylation and vinyloxylation of β -C(sp^3)-H bond with organosilanes and directed by 8-aminoquinoline bidentate ligand (Scheme I.27c). Preliminary mechanistic studies revealed that the $\text{Cu}(\text{OAc})_2$ acts as both the promoter and the source of oxygen in the final products. The proposed reaction mechanism starts with the coordination of the aminoquinoline substrate to the $\text{Cu}(\text{OAc})_2$, followed by C-H activation and disproportionation generates an organocopper(III) intermediate species, which undergoes reductive elimination to deliver the acetoxylation product.^{184,185}

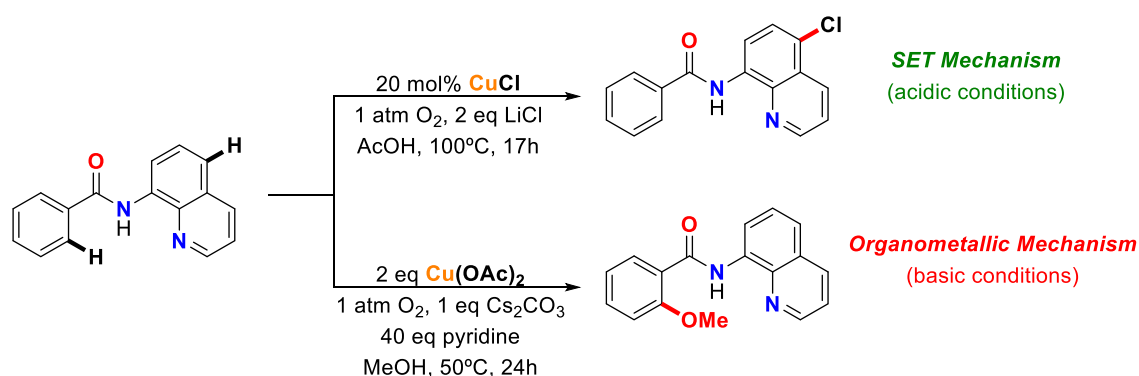
I.5.1.1 Intramolecular C-H activation using macrocyclic model substrates

A growth on the understanding of the copper-mediated C-H bond activation will lead the design of new copper catalysts and new strategies for conducting the C-H activation reactions under milder conditions.

Ribas and co-workers⁷² reported the stoichiometric C-H bond activation of macrocyclic model substrates, using CuX_2 salts. Mechanistic studies of these transformations suggested a Cu^{II} disproportionation pathway that yields aryl- Cu^{III} and Cu^{I} products (see Scheme I.8a), providing the first evidence for organometallic pathway in C-H activation reactions under oxidative

conditions. The involvement of the aryl-Cu^{III} species was also supported, by conducting the C-H activation reaction in presence of TEMPO, quantitative and fast formation of aryl-Cu^{III} and TEMPO-H were observed. Mechanistic and spectroscopic studies suggested a three-centre, three electron C-H...Cu^{II} interaction and further kinetic studies showed the C-H bond cleavage as rate-determining step of the proton-coupled electron transfer (PCET) mechanism. Moreover, complementary results were reported by Wang and co-workers¹⁸⁶, who performed the reaction using calixerene-type ligands and Cu(ClO₄)₂ salt (see Scheme I.8b). The same authors proposed, based on extensive experimental data and theoretical calculations, that the arene C-H bond activation would proceed through an electrophilic aromatic metalation pathway to form an unprecedented phenylcopper(II) organometallic compound, which was isolated and fully characterized. Such arylcopper(II) compounds led to the formation of arylcopper(III) compounds in excellent yields through its oxidation by a free Cu^{II} source or an oxidant like oxone.¹⁸⁷

Recently, Stahl and co-workers,¹⁸⁸ finding inspiration on the macrocyclic model systems mentioned above, investigated the plausible involvement of organometallic Cu^{III} intermediates with the *N*-(8-quinoliny)-benzamide substrate, first used by Daugulis. Interestingly, this substrate exhibits different reactivity, functionalising the *ortho*-directed C-H bond versus the functionalisation of the directing group (quinoline), depending on the reaction conditions (Scheme I.28). Experimental and computational studies are consistent with the operation of organometallic and SET mechanistic pathways upon changing from basic to acidic reaction conditions. When a Brønsted basic ligand was used the C-H activation proceeds through an organometallic pathway, whereas the use of acidic conditions favoured the SET pathway. The results demonstrate the involvement of high-valent Cu^{III} species as a key intermediates of the oxidative C-H activation as it was shown using macrocyclic model systems.



Scheme I.28. Divergent reactivity in Cu^{II}-mediated C-H oxidation reaction using the *N*-(8-quinoliny)-benzamide substrate.

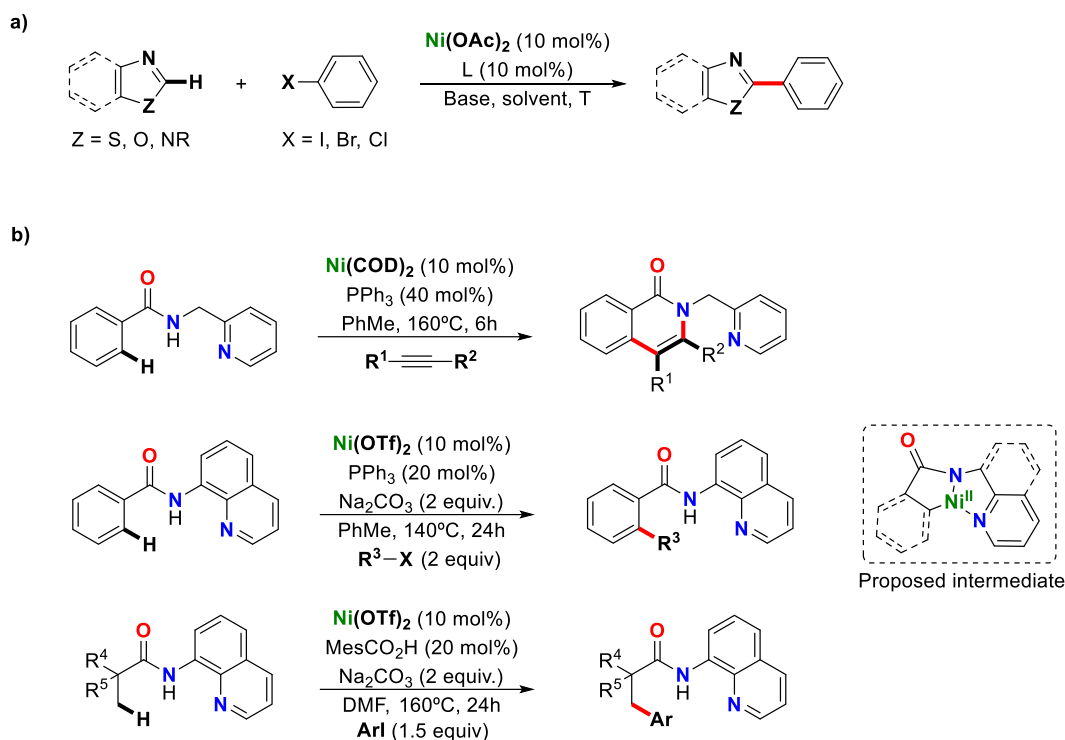
In conclusion, the different strategies showed above for copper-catalysed C-H functionalisation protocols, showed divergent operative mechanistic pathways, which emphasized the high complexity of copper-mediated C-H activation processes and the extreme dependence on the reaction conditions as well as on the nature of chelating-directing group.

I.5.2 Nickel catalysed C-H activation

In the recent years, considerable progress has been accomplished in Ni-catalysed C-H functionalisation chemistry, thereby important contributions have been done by many research groups providing several methodologies, including chelated-directed and non-directed, for the activation of inert C-H bonds. From a synthetic point of view, nickel-catalysed direct C-H bond functionalisation provides novel an efficient tools for constructing molecules of special interest. Early reports on nickel-assisted C-H activation of aromatic compounds date back to 1963¹⁸⁹, however it was not until 2009, when Itami¹⁹⁰ and Miura¹⁹¹ independently reported the first example of nickel-catalysed C-H arylation of 1,3-azoles with aryl halides. Importantly, this procedure enabled catalytic direct arylation with aryl iodides, bromides as well as chlorides as electrophiles (Scheme I.29a). Since these seminal studies, a variety of C-H bond transformations based on nickel catalysts have been developed.

Chatani and co-workers highly contributed to the field of Ni-catalysed C-H activation reactions. While most of the examples involve the coupling of activated C(*sp*²)-H bonds, they become interested on the challenging coupling of unactivated alkyl groups (Scheme I.29b). In 2011, they reported the first nickel-mediated oxidative cycloaddition of alkynes to aromatic amides catalytic system, which take advantage of a 2-pyridylmethylamine moiety as chelating bidentate directing group, for the activation of *ortho* aromatic C-H bonds. Subsequently, in 2013 they reported the *ortho* C-H activation using *N*-(8-quinolinyl)-benzamide as a substrate for the direct alkylation of C-H aromatic bonds with unactivated alkyl halides, a challenging transformation due to fact of the unfavourable oxidative addition of alkyl halides in favour of the β -hydride elimination side reaction. In a parallel study, the same authors reported the β -arylation of aliphatic amides, containing the same directing group with aryl iodides *via* the cleavage of unactivated C(*sp*³)-H bonds.

In order to increase the scope of Ni-assisted C-H activation, further studies using unactivated secondary alkyl halides were also performed by Chatani and Ackermann¹⁹² groups, using the same 8-quinolinyl-amine as a bidentate directing group. This chelation-assisted group with the 8-aminoquinoline moiety, enabled the use of not only primary alkyl and allyl halides but also secondary alkyl halides. Mechanistic studies were done for this transformations, it is hypothesized that the reaction starts with the coordination of nickel centre to the 1,2 diamine moiety of the directing group, followed by a metalation step to form a putative aryl-Ni^{II} intermediate complex, probably via a concerted metalation-deprotonation (CMD) mechanism. The oxidative addition of aryl- or alkyl-halide takes place forming a putative Ni^{IV} intermediate specie, which rapidly evolved to the formation of desired product and regeneration of Ni^{II} catalyst through reductive elimination step. However, any of the intermediate species proposed were directly detected, further mechanistic studies need to be done in order to get more insight into the operative pathways of the Ni-assisted C-H activation chemistry.^{140,141,147,193-195} However, although tremendous progress has been made, the development of new types of directing groups continues to be important in terms of exploring novel types of transformations of C-H bonds that cannot be achieved when conventional directing groups were used.

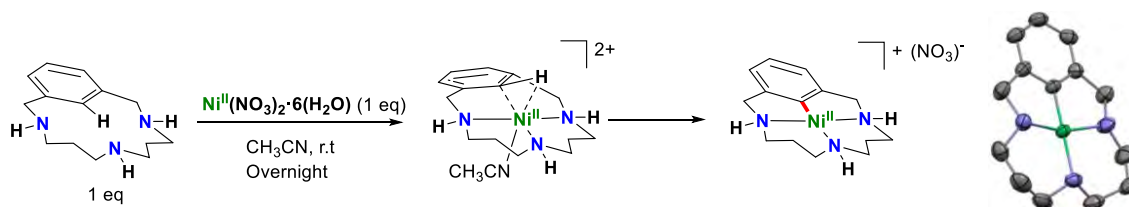


Scheme I.29. Examples of nickel-catalysed C-H arylation reactions. (a) C-H arylation of 1,3-azoles with aryl halides. (b) Nickel-catalysed chelation-assisted selective *ortho* C-H activation reaction.

I.5.2.1 Intramolecular C-H activation using macrocyclic model substrates

Over the past decades, there has been an important growth in the development of methods for C-H functionalisation. Gathering mechanistic insights could provide better understanding on the nature of these reactions, leading the development of new transformations.

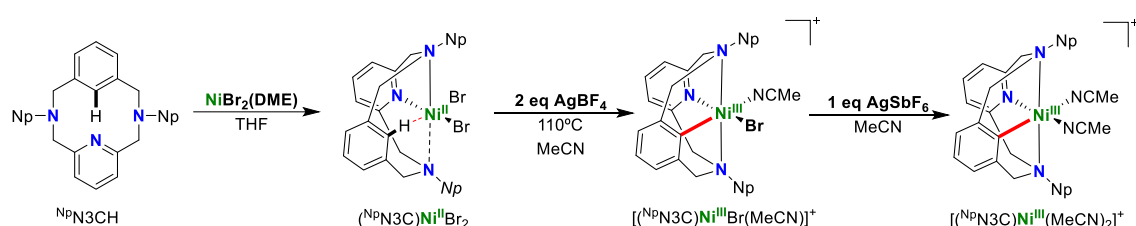
As mentioned before, Ribas and co-workers reported the stoichiometric C-H of macrocyclic model substrates, using NiX_2 salts. Interestingly, nickel does not change its oxidation state, affording a well-defined aryl- Ni^{III} complex⁷², probably through concerted-metalation-deprotonation (CMD) pathway; however, no direct mechanistic insights were reported (Scheme I.30).



Scheme I.30. Synthesis of well-defined nickel(II) complex based on a macrocyclic model substrate, *via* direct C-H activation, and X-ray structure of aryl- Ni^{III} (right).

Mechanistic studies of these transformations were discussed in the previous sections. Complementary results were reported by Wang and co-workers, who performed the reaction using heterocalixerene-type ligands and $\text{Ni}(\text{ClO}_4)_2$ salt (see Scheme I.19a).¹⁵³

Very recently, Mirica and co-workers¹⁶⁰ reported the first example of the C-H activation mediated by high-valent Ni^{III} species, using macrocyclic model systems. Mechanistic studies for the C-H activation processes revealed the coordination of the NiX_2 salts to the NpN3CH ligand and upon the addition of two equivalents of oxidant the $\text{C}(\text{sp}^2)\text{-H}$ activation was observed, generating a distorted octahedral high-valent Ni^{III} complex (Scheme I.31). Further studies, indicate that the C-H activation step likely operates through an oxidative-induced mechanism at Ni^{III} centre, in which less steric hindered substituents, on secondary amines, enable an agostic interaction between the Ni centre and the C-H to be activated.



Scheme I.31. $\text{C}(\text{sp}^2)\text{-H}$ activation mediated by high-valent Ni^{III} species, using macrocyclic model systems.

There are still some major challenges that need to be overcome in the field of Ni-catalysed C-H bond functionalisation. Most of the mechanistic proposals reported so far are preliminary and lack insightful experimental and theoretical studies to validate them. Therefore, a deeper understanding of the fundamental reactivity of these transformations will provide the basis for the development of new and fruitful methodologies based on C-H activation.

I.6 References

- (1) Yamaguchi, J.; Yamaguchi, A. D.; Itami, K. *Angew. Chem. Int. Ed.* **2012**, *51*, 8960.
- (2) Li, C.-J. *Acc. Chem. Res.* **2009**, *42*, 335.
- (3) Trost, B. M.; Czabaniuk, L. C. *Angew. Chem. Int. Ed.* **2014**, *53*, 2826.
- (4) Su, B.; Cao, Z.-C.; Shi, Z.-J. *Acc. Chem. Res.* **2015**, *48*, 886.
- (5) Crabtree, R. H. *The Organometallic Chemistry of the Transition Metals*; New York: Wiley, 2009.
- (6) Miao, J.; Ge, H. *Eur. J. Org. Chem.* **2015**, 2015, 7859.
- (7) Egorova, K. S.; Ananikov, V. P. *Angew. Chem. Int. Ed.* **2016**, *55*, 12150.
- (8) Bolm, C.; Legros, J.; Le Pailh, J.; Zani, L. *Chem. Rev.* **2004**, *104*, 6217.
- (9) Sun, C.-L.; Li, B.-J.; Shi, Z.-J. *Chem. Rev.* **2011**, *111*, 1293.
- (10) Gosmini, C.; Begouin, J.-M.; Moncomble, A. *Chem. Commun.* **2008**, 3221.
- (11) Cahiez, G.; Moyer, A. *Chem. Rev.* **2010**, *110*, 1435.
- (12) Gao, K.; Yoshikai, N. *Acc. Chem. Res.* **2014**, *47*, 1208.

- (13) Tasker, S. Z.; Standley, E. A.; Jamison, T. F. *Nature* **2014**, 509, 299.
- (14) Rosen, B. M.; Quasdorf, K. W.; Wilson, D. A.; Zhang, N.; Resmerita, A.-M.; Garg, N. K.; Percec, V. *Chem. Rev.* **2011**, 111, 1346.
- (15) Tobisu, M.; Chatani, N. *Acc. Chem. Res.* **2015**, 48, 1717.
- (16) Evano, G.; Blanchard, N.; Toumi, M. *Chem. Rev.* **2008**, 108, 3054.
- (17) Casitas, A.; Ribas, X. *Chem. Sci.* **2013**, 4, 2301.
- (18) Beletskaya, I. P.; Cheprakov, A. V. *Coord. Chem. Rev.* **2004**, 248, 2337.
- (19) Buchwald, S. L. *Acc. Chem. Res.* **2008**, 41, 1439.
- (20) Hartwig, J. F. *Nature* **2008**, 455, 314.
- (21) Magano, J.; Dunetz, J. R. *Chem. Rev.* **2011**, 111, 2177.
- (22) Schlummer, B.; Scholz, U. *Adv. Synth. Catal.* **2004**, 346, 1599.
- (23) Buchwald, S. L.; Mauger, C.; Mignani, G.; Scholz, U. *Adv. Synth. Catal.* **2006**, 348, 23.
- (24) Masanori, K.; Masayuki, K.; Toshihiko, M. *Chem. Lett.* **1983**, 12, 927.
- (25) Tamao, K.; Sumitani, K.; Kumada, M. *J. Am. Chem. Soc.* **1972**, 94, 4374.
- (26) Corriu, R. J. P.; Masse, J. P. *J. Chem. Soc., Chem. Commun.* **1972**, 144a.
- (27) Miyauchi, N.; Yamada, K.; Suzuki, A. *Tetrahedron Lett.* **1979**, 20, 3437.
- (28) Milstein, D.; Stille, J. K. *J. Am. Chem. Soc.* **1978**, 100, 3636.
- (29) King, A. O.; Okukado, N.; Negishi, E.-i. *J. Chem. Soc., Chem. Commun.* **1977**, 683.
- (30) Hatanaka, Y.; Hiyama, T. *J. Org. Chem.* **1988**, 53, 918.
- (31) Sonogashira, K. *J. Organomet. Chem.* **2002**, 653, 46.
- (32) Heck, R. F.; Nolley, J. P. *J. Org. Chem.* **1972**, 37, 2320.
- (33) Johansson Seechurn, C. C. C.; Kitching, M. O.; Colacot, T. J.; Snieckus, V. *Angew. Chem. Int. Ed.* **2012**, 51, 5062.
- (34) Paul, F.; Patt, J.; Hartwig, J. F. *J. Am. Chem. Soc.* **1994**, 116, 5969.
- (35) Guram, A. S.; Buchwald, S. L. *J. Am. Chem. Soc.* **1994**, 116, 7901.
- (36) Wolfe, J. P.; Wagaw, S.; Marcoux, J.-F.; Buchwald, S. L. *Acc. Chem. Res.* **1998**, 31, 805.
- (37) Hartwig, J. F. *Acc. Chem. Res.* **1998**, 31, 852.
- (38) Beletskaya, I. P.; Ananikov, V. P. *Chem. Rev.* **2011**, 111, 1596.
- (39) Weibel, J.-M.; Blanc, A. I.; Pale, P. *Chem. Rev.* **2008**, 108, 3149.
- (40) Font, M.; Acuña-Parés, F.; Parella, T.; Serra, J.; Luis, J. M.; Lloret-Fillol, J.; Costas, M.; Ribas, X. *Nat. Commun.* **2014**, 5, 4373.
- (41) Wang, Y.-M.; Lackner, A. D.; Toste, F. D. *Acc. Chem. Res.* **2014**, 47, 889.
- (42) Hashmi, A. S. K. *Chem. Rev.* **2007**, 107, 3180.
- (43) Krause, N. *Modern Organocopper Chemistry*; Wiley-VCH: Weinheim: Germany, 2002.
- (44) Cotton, F. A.; Wilkinson, G. *Advanced Inorganic Chemistry*; 5th ed.; Wiley: New York, 1988.
- (45) Surry, D. S.; Buchwald, S. L. *Chem. Sci.* **2010**, 1, 13.
- (46) Correa, A.; Bolm, C. *Adv. Synth. Catal.* **2007**, 349, 2673.
- (47) Güell, I.; Ribas, X. *Eur. J. Org. Chem.* **2014**, 2014, 3188.
- (48) Monnier, F.; Taillefer, M. *Angew. Chem. Int. Ed.* **2009**, 48, 6954.

- (49) Johnson, M. W.; Hannoun, K. I.; Tan, Y.; Fu, G. C.; Peters, J. C. *Chem. Sci.* **2016**, 7, 4091.
- (50) Sperotto, E.; Klink, G. P. M. v.; Koten, G. v.; Vries, J. G. d. *Dalton Trans.* **2010**, 39, 10338.
- (51) Creutz, S. E.; Lotito, K. J.; Fu, G. C.; Peters, J. C. *Science* **2012**, 338, 647.
- (52) Ziegler, D. T.; Choi, J.; Muñoz-Molina, J. M.; Bissember, A. C.; Peters, J. C.; Fu, G. C. *J. Am. Chem. Soc.* **2013**, 135, 13107.
- (53) Kainz, Q. M.; Matier, C. D.; Bartoszewicz, A.; Zultanski, S. L.; Peters, J. C.; Fu, G. C. *Science* **2016**, 351, 681.
- (54) Bissember, A. C.; Lundgren, R. J.; Creutz, S. E.; Peters, J. C.; Fu, G. C. *Angew Chem. Int. Ed.* **2013**, 52, 5129.
- (55) Uyeda, C.; Tan, Y.; Fu, G. C.; Peters, J. C. *J. Am. Chem. Soc.* **2013**, 135, 9548.
- (56) Do, H.-Q.; Bachman, S.; Bissember, A. C.; Peters, J. C.; Fu, G. C. *J. Am. Chem. Soc.* **2014**, 136, 2162.
- (57) Sadao, A.; Mitsuhiro, H.; Takamichi, Y. *Bull. Chem. Soc. Jpn.* **1978**, 51, 277.
- (58) Sperotto, E.; van Klink, G. P. M.; de Vries, J. G.; van Koten, G. *Tetrahedron* **2010**, 66, 9009.
- (59) Kochi, J. K. *J. Am. Chem. Soc.* **1957**, 79, 2942.
- (60) Kochi, J. K.; Subramanian, R. V. *J. Am. Chem. Soc.* **1965**, 87, 1508.
- (61) Bacon, R. G. R.; Hill, H. A. O. *J. Chem. Soc.* **1964**, 1097.
- (62) Bacon, R. G. R.; Hill, H. A. O. *J. Chem. Soc.* **1964**, 1112.
- (63) Weingarten, H. *J. Org. Chem.* **1964**, 29, 977.
- (64) Weingarten, H. *J. Org. Chem.* **1964**, 29, 3624.
- (65) Tye, J. W.; Weng, Z.; Johns, A. M.; Incarvito, C. D.; Hartwig, J. F. *J. Am. Chem. Soc.* **2008**, 130, 9971.
- (66) Cohen, T.; Cristea, I. *J. Am. Chem. Soc.* **1976**, 98, 748.
- (67) Cohen, T.; Cristea, I. *J. Am. Chem. Soc.* **1975**, 40, 3649.
- (68) Ouali, A.; Spindler, J.-F.; Jutand, A.; Taillefer, M. *Adv. Synth. Catal.* **2007**, 349, 1906.
- (69) Giri, R.; Hartwig, J. F. *J. Am. Chem. Soc.* **2010**, 132, 15860.
- (70) Tye, J. W.; Weng, Z.; Giri, G.; Hartwig, J. F. *Angew Chem. Int. Ed.* **2010**, 49, 2185.
- (71) Ribas, X.; Jackson, D. A.; Donnadieu, B.; Mahía, J.; Parella, T.; Xifra, R.; Hedman, B.; Hodgson, K. O.; Llobet, A.; Stack, T. D. P. *Angew. Chem. Int. Ed.* **2002**, 41, 2991.
- (72) Ribas, X.; Calle, C.; Poater, A.; Casitas, A.; Gómez, L.; Xifra, R.; Parella, T.; Benet-Buchholz, J.; Schweiger, A.; Mitrikas, G.; Solà, M.; Llobet, A.; Stack, T. D. P. *J. Am. Chem. Soc.* **2010**, 132, 12299.
- (73) Casitas, A.; King, A. E.; Parella, T.; Costas, M.; Stahl, S. S.; Ribas, X. *Chem. Sci.* **2010**, 1, 326.
- (74) King, A. E.; Huffman, L. M.; Casitas, A.; Costas, M.; Ribas, X.; Stahl, S. S. *J. Am. Chem. Soc.* **2010**, 132, 12068.
- (75) Yao, B.; Wang, D.-X.; Huang, Z.-T.; Wang, M.-X. *Chem. Commun.* **2009**, 2899.
- (76) Wang, Z.-L.; Zhao, L.; Wang, M.-X. *Org. Lett.* **2011**, 13, 6560.

- (77) Huffman, L. M.; Stahl, S. S. *J. Am. Chem. Soc.* **2008**, *130*, 9196.
- (78) Huffman, L. M.; Casitas, A.; Font, M.; Canta, M.; Costas, M.; Ribas, X.; Stahl, S. S. *Chem. Eur. J.* **2011**, *17*, 10643
- (79) Casitas, A.; Canta, M.; Solà, M.; Costas, M.; Ribas, X. *J. Am. Chem. Soc.* **2011**, *133*, 19386.
- (80) Font, M.; Parella, T.; Costas, M.; Ribas, X. *Organometallics* **2012**, *31*, 7976.
- (81) Ma, D.; Zhang, Y.; Yao, J.; Wu, S.; Tao, F. *J. Am. Chem. Soc.* **1998**, *120*, 12459.
- (82) Ma, H.-C.; Jiang, X.-Z. *J. Org. Chem.* **2007**, *72*, 8943.
- (83) Lu, Z.; Twieg, R. J. *Tetrahedron* **2005**, *61*, 903.
- (84) Ouali, A.; Taillefer, M.; Spindler, J.-F.; Jutand, A. *Organometallics* **2007**, *26*, 65.
- (85) Shafir, A.; Lichtor, P. A.; Buchwald, S. L. *J. Am. Chem. Soc.* **2007**, *129*, 3490.
- (86) Jones, G. O.; Liu, P.; Houk, K. N.; Buchwald, S. L. *J. Am. Chem. Soc.* **2010**, *132*, 6205.
- (87) Yu, H.-Z.; Jiang, Y.-Y.; Fu, Y.; Liu, L. *J. Am. Chem. Soc.* **2010**, *132*, 18078.
- (88) Ritter, J. C. 2008; Vol. PCT Int. Appl. WO 2008079225 A1.
- (89) Ritter, J. C. 2009; Vol. WO 2009018504 (A1).
- (90) Wibaut, J. P.; Nicolai, J.R *Recl. Trav. Chim. Pays-Bas*, *58*.
- (91) Kubo, S.; Shintou, T.; Aoki, H. 2004; Vol. PCT Int. Appl. WO 2004024670.
- (92) Corbet, J.-P.; Mignani, G. *Chem. Rev.* **2006**, *106*, 2651.
- (93) Ghosh, A.; Sieser, J. E.; Caron, S.; Couturier, M.; Dupont-Gaudet, K.; Girardin, M. *J. Org. Chem.* **2006**, *71*, 1258.
- (94) Hickman, A. J.; Sanford, M. S. *Nature* **2012**, *484*, 177.
- (95) Dick, A. R.; Kampf, J. W.; Sanford, M. S. *J. Am. Chem. Soc.* **2005**, *127*, 12790.
- (96) Ball, N. D.; Kampf, J. W.; Sanford, M. S. *J. Am. Chem. Soc.* **2010**, *132*, 2878.
- (97) Oh, C. H.; Lim, Y. M.; You, C. H. *Tetrahedron Lett.* **2002**, *43*, 4645.
- (98) Wilke, G. *Angew. Chem. Int. Ed.* **1988**, *27*, 185.
- (99) Montgomery, J. *Angew. Chem. Int. Ed.* **2004**, *43*, 3890.
- (100) Tsou, T. T.; Kochi, J. K. *J. Am. Chem. Soc.* **1979**, *101*, 6319.
- (101) de Meijere, A.; Diederich, F. *Metal-Catalyzed Cross-Coupling Reactions*; Wiley-VCH, 2004; Vol. 1.
- (102) Gossage, R. A.; van de Kuil, L. A.; van Koten, G. *Acc. Chem. Res.* **1998**, *31*, 423.
- (103) Jones, G. D.; Martin, J. L.; McFarland, C.; Allen, O. R.; Hall, R. E.; Haley, A. D.; Brandon, R. J.; Konovalova, T.; Desrochers, P. J.; Pulay, P.; Vivic, D. A. *J. Am. Chem. Soc.* **2006**, *128*, 13175.
- (104) Takahashi, T. a. K., K In *Modern Organonickel Chemistry*; Wiley, Ed. 2005, p 41.
- (105) Corcoran, E. B.; Pirnot, M. T.; Lin, S.; Dreher, S. D.; DiRocco, D. A.; Davies, I. W.; Buchwald, S. L.; MacMillan, D. W. C. *Science* **2016**, *353*, 279.
- (106) Shaw, M. H.; Shurtleff, V. W.; Terrett, J. A.; Cuthbertson, J. D.; MacMillan, D. W. C. *Science* **2016**, *352*, 1304.

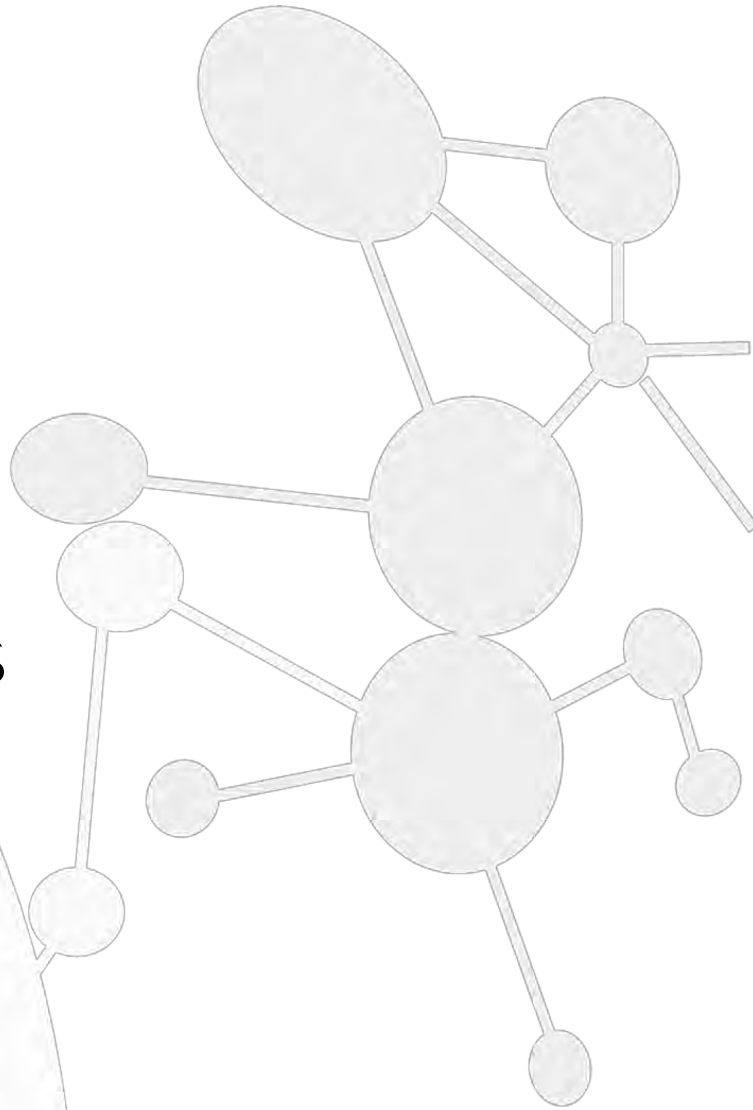
- (107) Lavoie, C. M.; MacQueen, P. M.; Rotta-Loria, N. L.; Sawatzky, R. S.; Borzenko, A.; Chisholm, A. J.; Hargreaves, B. K. V.; McDonald, R.; Ferguson, M. J.; Stradiotto, M. *Nat. Commun.* **2016**, *7*.
- (108) Tsou, T. T.; Kochi, J. K. *J. Am. Chem. Soc.* **1978**, *100*, 1634.
- (109) Tsou, T. T.; Kochi, J. K. *J. Am. Chem. Soc.* **1979**, *101*, 7547.
- (110) Lipschutz, M. I.; Yang, X.; Chatterjee, R.; Tilley, T. D. *J. Am. Chem. Soc.* **2013**, *135*, 15298.
- (111) Dudnik, A. S.; Fu, G. C. *J. Am. Chem. Soc.* **2012**, *134*, 10693.
- (112) Zultanski, S. L.; Fu, G. C. *J. Am. Chem. Soc.* **2013**, *135*, 624.
- (113) Breitenfeld, J.; Ruiz, J.; Wodrich, M. D.; Hu, X. *J. Am. Chem. Soc.* **2013**, *135*, 12004.
- (114) Fischer, C.; Fu, G. C. *J. Am. Chem. Soc.* **2005**, *127*, 4594.
- (115) Zultanski, S. L.; Fu, G. C. *J. Am. Chem. Soc.* **2011**, *133*, 15362.
- (116) Tollefson, E. J.; Hanna, L. E.; Jarvo, E. R. *Acc. Chem. Res.* **2015**, *48*, 2344.
- (117) Henrion, M.; Ritleng, V.; Chetcuti, M. J. *ACS Catal.* **2015**, *5*, 1283.
- (118) Ritleng, V.; Henrion, M.; Chetcuti, M. J. *ACS Catal.* **2016**, *6*, 890.
- (119) Shinya, N.; Taisuke, M.; Yuji, K.; Kouki, M. *Chem. Lett.* **2011**, *40*, 1036.
- (120) Joshi-Pangu, A.; Wang, C.-Y.; Biscoe, M. R. *J. Am. Chem. Soc.* **2011**, *133*, 8478.
- (121) Miyazaki, S.; Koga, Y.; Matsumoto, T.; Matsubara, K. *Chem. Commun.* **2010**, *46*, 1932.
- (122) Zhang, K.; Conda-Sheridan, M.; R. Cooke, S.; Louie, J. *Organometallics* **2011**, *30*, 2546.
- (123) Tobisu, M.; Shimasaki, T.; Chatani, N. *Angew. Chem. Int. Ed.* **2008**, *47*, 4866.
- (124) Wang, C.; Ozaki, T.; Takita, R.; Uchiyama, M. *Chem. Eur. J.* **2012**, *18*, 3482.
- (125) Mamoru, T.; Toshiaki, S.; Naoto, C. *Chem. Lett.* **2009**, *38*, 710.
- (126) Kampmann, S. S.; Sobolev, A. N.; Koutsantonis, G. A.; Stewart, S. G. *Adv. Synth. Catal.* **2014**, *356*, 1967.
- (127) Cornella, J.; Gómez-Bengoa, E.; Martin, R. *J. Am. Chem. Soc.* **2013**, *135*, 1997.
- (128) Guan, B.-T.; Xiang, S.-K.; Wu, T.; Sun, Z.-P.; Wang, B.-Q.; Zhao, K.-Q.; Shi, Z.-J. *Chem. Commun.* **2008**, 1437.
- (129) Fujihara, T.; Nogi, K.; Xu, T.; Terao, J.; Tsuji, Y. *J. Am. Chem. Soc.* **2012**, *134*, 9106.
- (130) Correa, A.; Cornella, J.; Martin, R. *Angew. Chem. Int. Ed.* **2013**, *52*, 1878.
- (131) Mesganaw, T.; Garg, N. K. *Org. Process Res. Dev.* **2013**, *17*, 29.
- (132) Yu, D.-G.; Li, B.-J.; Shi, Z.-J. *Acc. Chem. Res.* **2010**, *43*, 1486.
- (133) Li, B.-J.; Yu, D.-G.; Sun, C.-L.; Shi, Z.-J. *Chem. Eur. J.* **2011**, *17*, 1728.
- (134) Terao, J.; Kambe, N. *Acc. Chem. Res.* **2008**, *41*, 1545.
- (135) Kaschube, W.; Pörschke, K.-R.; Angermund, K.; Krüger, C.; Wilke, G. *Chem. Ber.* **1988**, *121*, 1921.
- (136) Klein, H.-F.; Bickelhaupt, A.; Jung, T.; Cordier, G. *Organometallics* **1994**, *13*, 2557.
- (137) Dimitrov, V.; Linden, A. *Angew. Chem. Int. Ed.* **2003**, *42*, 2631.
- (138) Carnes, M.; Buccella, D.; Chen, J. Y. C.; Ramirez, A. P.; Turro, N. J.; Nuckolls, C.; Steigerwald, M. *Angew. Chem. Int. Ed.* **2009**, *48*, 290.
- (139) Mitra, R.; Pörschke, K.-R. *Angew. Chem. Int. Ed.* **2015**, *54*, 7488.

- (140) Aihara, Y.; Chatani, N. *J. Am. Chem. Soc.* **2013**, *135*, 5308.
- (141) Aihara, Y.; Chatani, N. *J. Am. Chem. Soc.* **2014**, *136*, 898.
- (142) Wu, X.; Zhao, Y.; Ge, H. *J. Am. Chem. Soc.* **2014**, *136*, 1789.
- (143) Camasso, N. M.; Sanford, M. S. *Science* **2015**, *347*, 1218.
- (144) Schultz, J. W.; Fuchigami, K.; Zheng, B.; Rath, N. P.; Mirica, L. M. *J. Am. Chem. Soc.* **2016**, *138*, 12928.
- (145) Martinez, G. E.; Ocampo, C.; Park, Y. J.; Fout, A. R. *J. Am. Chem. Soc.* **2016**, *138*, 4290.
- (146) Hatakeyama, T.; Hashimoto, S.; Ishizuka, K.; Nakamura, M. *J. Am. Chem. Soc.* **2009**, *131*, 11949.
- (147) Iyanaga, M.; Aihara, Y.; Chatani, N. *J. Org. Chem.* **2014**, *79*, 11933.
- (148) Terrett, J. A.; Cuthbertson, J. D.; Shurtleff, V. W.; MacMillan, D. W. C. *Nature* **2015**, *524*, 330.
- (149) Gutierrez, O.; Tellis, J. C.; Primer, D. N.; Molander, G. A.; Kozlowski, M. C. *J. Am. Chem. Soc.* **2015**, *137*, 4896.
- (150) Heitz, D. R.; Tellis, J. C.; Molander, G. A. *J. Am. Chem. Soc.* **2016**, *138*, 12715.
- (151) Zuo, Z.; Ahneman, D. T.; Chu, L.; Terrett, J. A.; Doyle, A. G.; MacMillan, D. W. C. *Science* **2014**, *345*, 437.
- (152) Cavalcanti, L. N.; Molander, G. A. *Top. Curr. Chem.* **2016**, *374*, 1.
- (153) Yang, C.; Wu, W.-D.; Zhao, L.; Wang, M.-X. *Organometallics* **2015**, *34*, 5167.
- (154) Ermler, U.; Grabarse, W.; Shima, S.; Goubeaud, M.; Thauer, R. K. *Science* **1997**, *278*, 1457.
- (155) Evans, D. J. *Coord. Chem. Rev.* **2005**, *249*, 1582.
- (156) Scheller, S.; Goenrich, M.; Boecher, R.; Thauer, R. K.; Jaun, B. *Nature* **2010**, *465*, 606.
- (157) Scheller, S.; Goenrich, M.; Mayr, S.; Thauer, R. K.; Jaun, B. *Angew. Chem. Int. Ed.* **2010**, *49*, 8112.
- (158) Zheng, B.; Tang, F.; Luo, J.; Schultz, J. W.; Rath, N. P.; Mirica, L. M. *J. Am. Chem. Soc.* **2014**, *136*, 6499.
- (159) Zhou, W.; Schultz, J. W.; Rath, N. P.; Mirica, L. M. *J. Am. Chem. Soc.* **2015**, *137*, 7604.
- (160) Zhou, W.; Zheng, S.; Schultz, J. W.; Rath, N. P.; Mirica, L. M. *J. Am. Chem. Soc.* **2016**, *138*, 5777.
- (161) Bour, J. R.; Camasso, N. M.; Sanford, M. S. *J. Am. Chem. Soc.* **2015**, *137*, 8034.
- (162) Watson, M. B.; Rath, N. P.; Mirica, L. M. *J. Am. Chem. Soc.* **2017**, *139*, 35.
- (163) Martin-Diaconescu, V.; Maroney, M. J. In *Comprehensive Inorganic Chemistry II (Second Edition)*; Poeppelmeier, K., Ed.; Elsevier: Amsterdam, 2013, p 295.
- (164) Ackermann, L.; Vicente, R.; Kapdi, A. R. *Angew. Chem. Int. Ed.* **2009**, *48*, 9792.
- (165) Wencel-Delord, J.; Droge, T.; Liu, F.; Glorius, F. *Chem. Soc. Rev.* **2011**, *40*, 4740.
- (166) Hartwig, J. F. *J. Am. Chem. Soc.* **2016**, *138*, 2.
- (167) Chen, X.; Engle, K. M.; Wang, D.-H.; Yu, J.-Q. *Angew. Chem. Int. Ed.* **2009**, *48*, 5094.
- (168) Shi, W.; Liu, C.; Lei, A. *Chem. Soc. Rev.* **2011**, *40*, 2761.
- (169) Liu, C.; Zhang, H.; Shi, W.; Lei, A. *Chem. Rev.* **2011**, *111*, 1780.

- (170) Brückl, T.; Baxter, R. D.; Ishihara, Y.; Baran, P. S. *Acc. Chem. Res.* **2012**, *45*, 826.
- (171) Newhouse, T.; Baran, P. S. *Angew. Chem. Int. Ed.* **2011**, *50*, 3362.
- (172) Engle, K. M.; Mei, T.-S.; Wasa, M.; Yu, J.-Q. *Acc. Chem. Res.* **2012**, *45*, 788.
- (173) Albrecht, M. *Chem. Rev.* **2010**, *110*, 576.
- (174) Rouquet, G.; Chatani, N. *Angew. Chem. Int. Ed.* **2013**, *52*, 11726.
- (175) Zaitsev, V. G.; Shabashov, D.; Daugulis, O. *J. Am. Chem. Soc.* **2005**, *127*, 13154.
- (176) Chen, X.; Hao, X.-S.; Goodhue, C. E.; Yu, J.-Q. *J. Am. Chem. Soc.* **2006**, *128*, 6790.
- (177) Phipps, R. J.; Gaunt, M. J. *Science* **2009**, *323*, 1593.
- (178) Chen, B.; Hou, X.-L.; Li, Y.-X.; Wu, Y.-D. *J. Am. Chem. Soc.* **2011**, *133*, 7668.
- (179) Zhu, W.; Zhang, D.; Yang, N.; Liu, H. *Chem. Commun.* **2014**, *50*, 10634.
- (180) Dong, J.; Wang, F.; You, J. *Org. Lett.* **2014**, *16*, 2884.
- (181) Zhang, Y.; Wang, Q.; Yu, H.; Huang, Y. *Organic & Biomolecular Chemistry* **2014**, *12*, 8844.
- (182) Wu, X.; Zhao, Y.; Ge, H. *Chemistry – An Asian Journal* **2014**, *9*, 2736.
- (183) Wang, Z.; Kuninobu, Y.; Kanai, M. *Org. Lett.* **2014**, *16*, 4790.
- (184) Zhang, J.; Chen, H.; Wang, B.; Liu, Z.; Zhang, Y. *Org. Lett.* **2015**, *17*, 2768.
- (185) Liu, J.; Chen, G.; Tan, Z. *Adv. Synth. Catal.* **2016**, *358*, 1174.
- (186) Yao, B.; Wang, D.-X.; Huang, Z.-T.; Wang, M.-X. *Chem. Commun.* **2009**, 2899.
- (187) Zhang, H.; Yao, B.; Zhao, L.; Wang, D.-X.; Xu, B.-Q.; Wang, M.-X. *J. Am. Chem. Soc.* **2014**, *136*, 6326.
- (188) Suess, A. M.; Ertem, M. Z.; Cramer, C. J.; Stahl, S. S. *J. Am. Chem. Soc.* **2013**, *135*, 9797.
- (189) Kleiman, J. P.; Dubeck, M. *J. Am. Chem. Soc.* **1963**, *85*, 1544.
- (190) Canivet, J.; Yamaguchi, J.; Ban, I.; Itami, K. *Org. Lett.* **2009**, *11*, 1733.
- (191) Hachiya, H.; Hirano, K.; Satoh, T.; Miura, M. *Org. Lett.* **2009**, *11*, 1737.
- (192) Song, W.; Lackner, S.; Ackermann, L. *Angew. Chem. Int. Ed.* **2014**, *53*, 2477.
- (193) Shiota, H.; Ano, Y.; Aihara, Y.; Fukumoto, Y.; Chatani, N. *J. Am. Chem. Soc.* **2011**, *133*, 14952.
- (194) Aihara, Y.; Tobisu, M.; Fukumoto, Y.; Chatani, N. *J. Am. Chem. Soc.* **2014**, *136*, 15509.
- (195) Ayana, Y.; Naoto, C. *Chem. Lett.* **2015**, *44*, 902.

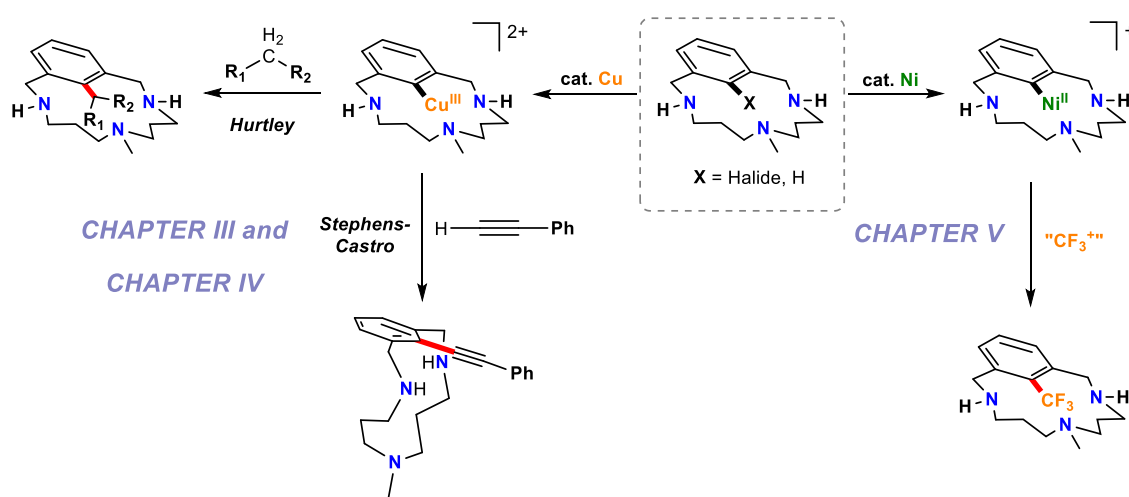
CHAPTER II.

MAIN OBJECTIVES



Earth-abundant first-row transition metal-catalysed cross-coupling chemistry has blossomed over the last decades, allowing the design of renewed and practical protocols for the formation of C-C and C-Heteroatom bonds. The rapid evolution of this chemistry as well as the great success of several transformations, undoubtedly redirected the face of synthetic organic chemistry towards environmental tolerant and lower-cost alternative strategies. Among effectiveness of several transition metals, copper and nickel have been extensively used in cross-coupling chemistry since the introduction of chelating auxiliary ligands, which led to the development of improved and more sustainable methodologies. However, the most essential drawback of copper- and nickel-mediated cross-coupling reactions is the lack of mechanistic understanding of these processes. Indeed, the operative pathways are extremely dependent on the reaction conditions.

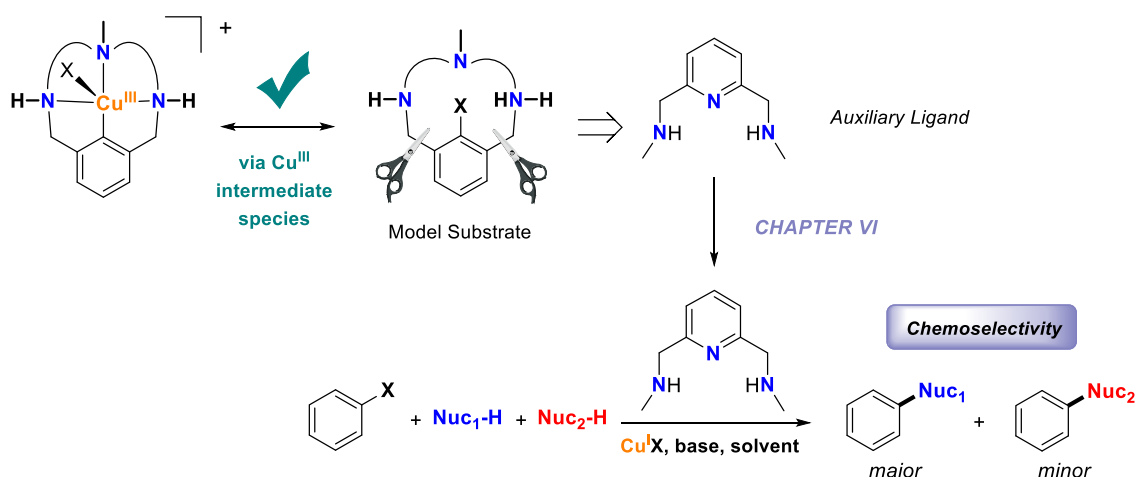
The recent advances in copper-catalysed cross-coupling chemistry also had a strong impact on the development of new, milder and improved copper-based methodologies towards the formation of C-C bonds, which are found in a large number of natural products and they are really important precursors in pharmaceutical industry. However, no consensus on the mechanistic details of these reactions has been reached and many questions remains unanswered. Therefore, more clear understanding on the mechanistic pathways for these transformations is of fundamental importance to facilitate the design of more efficient methodologies. Chapters III and IV of this thesis are focused on this topic, and we study in depth the plausible mechanism involved in Hurltley condensations (activated methylene compounds) and Stephens-Castro reactions (palladium-free Sonogashira couplings using terminal acetylenes), within well-defined macrocyclic model aryl-Cu^{III} complexes. For this purpose, we took advantage of the previously results reported by our group, in which the intermediacy of aryl-Cu^{III} species was demonstrated in a wide range of C-Heteroatom bond formation, using a family of well-defined copper(III) complexes (Scheme II.1).



Scheme II.1. Study of the C-C bond formation using macrocyclic model systems based on high valent Cu^{III} and Ni^{II} intermediate species.

In Chapter V, we turn our attention towards organometallic nickel chemistry. Since nickel can accommodate multiple geometries and oxidation states, we are interested in gaining mechanistic insight in the Ni redox chemistry involved in cross coupling reactions using macrocyclic model systems in atypical non-octahedral environments. Finding inspiration in the previous work performed in our group using macrocyclic model systems, we explore the synthesis of well-defined macrocyclic aryl-Ni^{II} complex and its trifluoromethylation with TDDT and Togni reagent. Furthermore, we will evaluate the capability of these complexes to participate in one and two electron redox processes as well as the plausibility of accessing to high-valent nickel species (Scheme II.1).

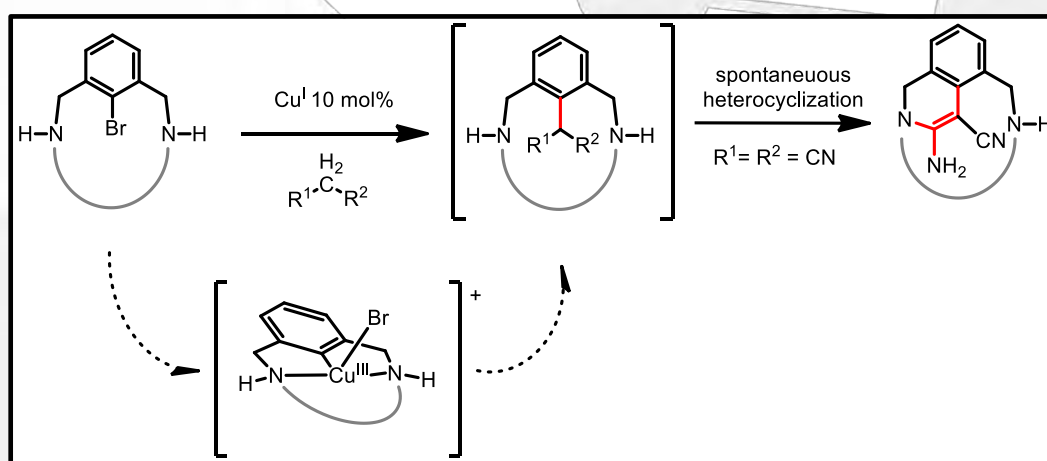
In the last part of this thesis (Chapter VI), we focus on the development of Ullmann coupling reactions using standard systems based on simple aryl halides and auxiliary ligands. Considering the recent progress in modern Ullmann chemistry and bearing in mind the role of auxiliary ligands, we become interested on achieving enhanced selectivity towards several functional groups. In Chapter VI we studied the chemoselective arylation of a wide-range of nucleophiles oxygen- and nitrogen-based in competitive reactions using different well-known and available auxiliary ligands and iodobenzene or bromobenzene (Scheme II.2).



Scheme II.2. Investigation of the role of auxiliary ligands on the chemoselective formation of C-heteroatom bonds and the plausible involvement of high valent copper(III) species as reaction intermediates.

CHAPTER III.

Model Csp²-Csp³ Hurtley Coupling Catalysis that Operates through a Well-Defined Cu^I/Cu^{III} Mechanism



This chapter corresponds to the following publication:

Mireia Rovira, Marc Font, and Xavi Ribas*. *ChemCatChem*. **2013**, 5, 687 – 691

DOI: 10.1002/cctc.201200885

For this publication M. R. performed the synthesis and characterization of all compounds, as well as the reactivity studies. Additionally, M. R. participated in all the discussions and was involved in writing the paper.

DOI: 10.1002/cctc.201200885

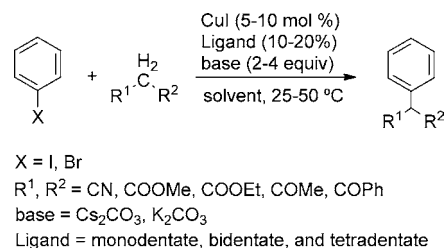
Model $C_{sp^2}-C_{sp^3}$ Hurtley Coupling Catalysis that Operates through a Well-Defined Cu^I/Cu^{III} Mechanism

Mireia Rovira, Marc Font, and Xavi Ribas^{*[a]}

Hurtley-type coupling reactions, which were first discovered more than 80 years ago, involve the copper-catalyzed α -arylation of activated methylene compounds by using aryl-halide substrates.^[1–3] These reactions afford $C_{sp^2}-C_{sp^3}$ coupling products, usually as their α -aryl-ketone derivatives. These compounds are important because they are found in a large number of natural products and they have also found wide application in pharmaceutical chemistry.^[4] Importantly, there is not a clear understanding of the mechanistic details of copper-based Hurtley catalysis; therefore, unraveling the mechanistic pathways is of fundamental importance to facilitate the design of more-sustainable methodologies.

From a broader perspective, copper catalysis is receiving significant attention, owing to its lower cost and complementary reactivity compared to palladium-based catalytic processes.^[5] Among the numerous cross-coupling reactions that are catalyzed by copper, C–heteroatom Ullmann condensation reactions have been well-studied.^[2,3,6] Although the exact mechanism of these processes is not completely understood, a Cu^I/Cu^{III} redox catalytic cycle has been implied for a long time and, recently, it has been experimentally verified in selected systems.^[7–9] The nucleophilic role of the activated methylene substrate suggests that Hurtley copper-catalyzed couplings might share common mechanistic features with Ullmann couplings.

Several methods for Hurtley coupling reactions have been reported (Scheme 1),^[10,11] the most successful of which requires the use of bidentate ancillary ligands, such as L-proline,^[12–14] picolinic acid,^[15] and 1,10-phenanthroline.^[16] Monodentate ligands, such as 2-phenylphenol,^[17] or tetradentate ligands, such as Schiff bases,^[18] have also been used. Temperatures between 25–70 °C and soft bases, such as CS_2CO_3 , have been used, thereby affording the coupling products in good yields. However, until now, no consensus on the mechanistic details of these reactions has been reached and two main questions still remain: 1) What is the mechanism of the aryl-halide-activation step? 2) What is the coordination mode of the activated methylene compound? On one hand, Setsune et al. proposed an electron-transfer mechanism to explain the activation of the aryl halide,^[19] whereas, on the other hand, Hennessy and Buchwald proposed that the bidentate coordination of a deproton-



Scheme 1. General procedure and conditions for the Hurtley $C_{sp^2}-C_{sp^3}$ coupling reaction.

ated dimethyl malonate substrate through two oxygen atoms to the Cu^I center was required.^[17]

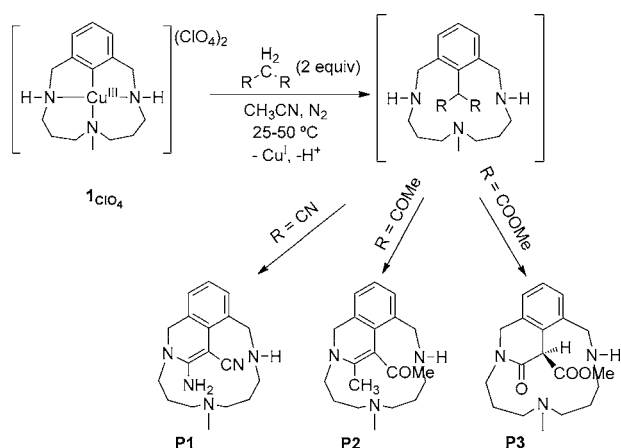
Very recently, Huang and Hartwig attempted to answer both questions by studying the Hurtley coupling reactions between aryl iodides and isolated Cu^I -enolate complexes.^[16] These latter complexes were synthesized by a direct reaction between $CuOtBu$ and β -dicarbonyl compounds. The use of radical clocks ruled out the presence of radical intermediates, thus indicating that the electron-transfer mechanism for the activation of the aryl halide was not favored. Instead, with the aid of DFT calculations, the same authors proposed the aryl halide oxidative addition at a carbon-bound form of the Cu^I complex, that is, $LCu^I(CHR_2)$.

Therefore, more efforts are clearly needed to unravel the detailed mechanistic pathways behind Hurtley-type reactions. Our approach is based on evaluating the reactivity of well-defined aryl- Cu^{III} species as pertinent intermediate species in Hurtley catalysis. To this end, herein we report the stoichiometric reactions between complex **1**_{ClO₄} and malononitrile, dimethyl malonate, and acetylacetone (Scheme 2), as well as the corresponding catalytic reactions with model aryl halide **L**₁-Br (see below).

Interestingly, the reactions between compound **1**_{ClO₄} and the activated methylene substrates afforded 1,2-dihydroisoquinoline (compounds **P1** and **P2**) and 1,2-dihydroisoquinolin-3(4H)-one products (compound **P3**). These scaffolds are necessarily formed through a very favorable intramolecular reorganization of the expected aryl-methylene C–C coupling species. The chemical structures of compounds **P1–P3** were unequivocally established by 1D and 2D NMR spectroscopy and by MS (ESI). The full ¹H NMR assignment of compound **P1** is shown in Figure 1 (for the assignment of compounds **P2** and **P3**, see the Supporting Information). The yields of the heterocyclic products range from quantitative (**P1**) to good or modest (**P2**: 80% yield, **P3**: 56% yield) and they correlate with the pK_a value of the corresponding activated methylene substrate (Table 1). The most acidic substrate reacts in less than 3 h at room tempera-

[a] M. Rovira, M. Font, Dr. X. Ribas
QBIS Research Group, Departament de Química
Universitat de Girona
Campus Montilivi, Girona E-17071, Catalonia (Spain)
Fax: (+34) 972418150
E-mail: xavi.ribas@udg.edu

Supporting information for this article is available on the WWW under <http://dx.doi.org/10.1002/cctc.201200885>.



Scheme 2. Stoichiometric reactions between aryl- Cu^{III} complex 1_{ClO_4} and activated methylene substrates, which undergo $\text{C}_{\text{sp}^2}\text{-C}_{\text{sp}^3}$ coupling and subsequent intramolecular reorganization.

ture to afford compound **P1** in quantitative yield, whereas, upon increasing the pK_a value, higher temperatures (50°C) and longer reaction times (24 h) are required. Despite these more favorable conditions, lower yields are obtained (80% and 37% for compounds **P2** and **P3**, respectively). In addition, at temperatures above 40°C , intramolecular aryl- NCH_3 coupling occurred as an important side-reaction, which was responsible for the lower yield of compound **P3**.^[20] For this latter reaction, the addition of 2.2 equivalents of Cs_2CO_3 as a base was beneficial for the reaction at room temperature and afforded an increase in the yield of the product from 37% to 56%.

The structural characterization of compounds **P1–P3** was challenging and required extensive 2D NMR experiments. As an example, the rigidity of the 1,2-dihydroisoquinoline scaffold of compound **P1** and its macrocyclic structure caused most of the protons in the molecule to become diastereotopic. Based on these studies, the assignment of each proton signal is shown in Figure 1 (for a complete explanation of the structural

Table 1. Experimental yields for the stoichiometric and catalytic syntheses of compounds **P1–P3**.^[a]

Activated methylene nucleophile (pK_a in DMSO)	Malononitrile (11.1)	Acetylacetone (13.3)	Dimethyl malonate (16.4)
product	P1	P2	P3
yield (stoichiometric reaction) ^[b]	99	80 ^[c]	56 ^[d]
yield (catalytic reaction) ^[e]	95	37 ^[f]	67 ^[g]

[a] The yields of the C–C coupling products were calculated by integration of the ^1H NMR spectra with 1,3,5-trimethoxybenzene as an internal standard; [b] general conditions for the stoichiometric reactions: $[1_{\text{ClO}_4}] = 12\text{ mm}$, [nucleophile] = 24 mm, 25°C , CD_3CN ; [c] 50°C ; [d] 25°C , Cs_2CO_3 (2.2 equiv; the highest yield, which was obtained without base at 50°C , was 37%); [e] general conditions for the catalytic reactions: $[L_1\text{-Br}] = 5\text{ mm}$, $[[\text{Cu}(\text{CH}_3\text{CN})_4]\text{CF}_3\text{SO}_3] = 0.5\text{ mm}$, [nucleophile] = 10 mm, 25°C , MeCN ; [f] molecular sieves and K_2CO_3 (2.2 equiv); [g] K_2CO_3 (8.8 equiv).

determination of compounds **P1–P3**, see the Supporting Information). Interestingly, a former NH proton and the methylenic proton of deprotonated malononitrile are formally transferred to form the NH_2 group at the 3-position of the 1,2-dihydroisoquinoline heterocycle (see below).

In the case of acetylacetone as the activated methylenic substrate, product **P2** is obtained. Compound **P2** also contains a 1,2-dihydroisoquinoline scaffold, although a methyl group is found at the 3-position on the heterocycle and a water molecule must be eliminated to allow for its formation. In the case of dimethyl malonate, compound **P3** is obtained, which contains a 1,2-dihydroisoquinolin-3(4H)-one scaffold, owing to the attack of a secondary amine on one ester moiety of the C-inserted substrate, to finally release one MeOH molecule. In compound **P3**, a new chiral carbon center is formed, as shown in Scheme 2. The proposed mechanisms for the formation of compounds **P2** and **P3** are shown in the Supporting Information, Figures S29 and S30.

The proposed mechanism for the synthesis of compound **P1** is shown in Scheme 3. The pK_a dependence of the reactivity of

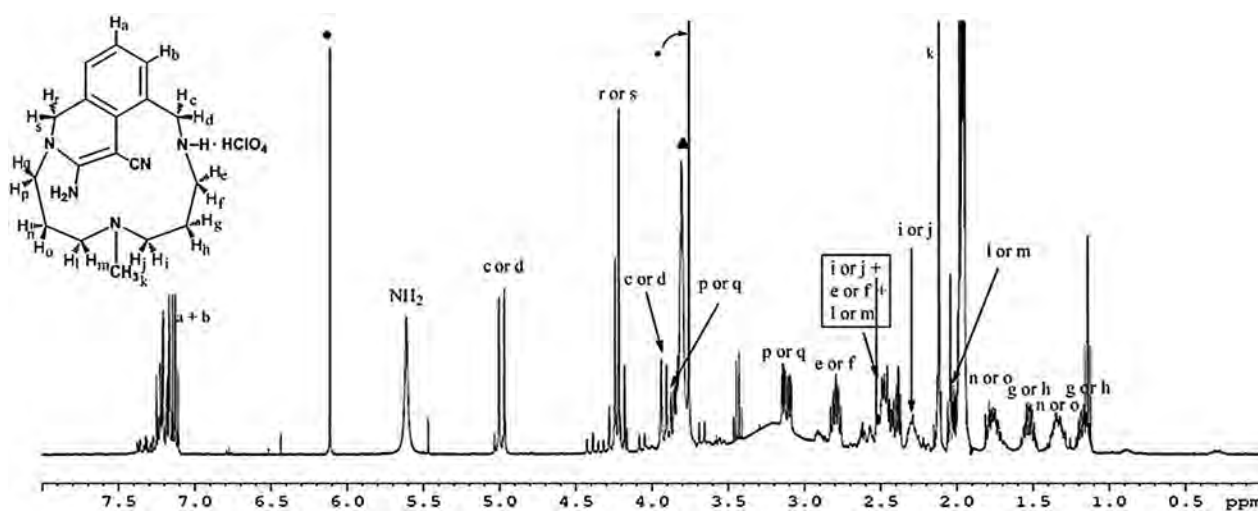
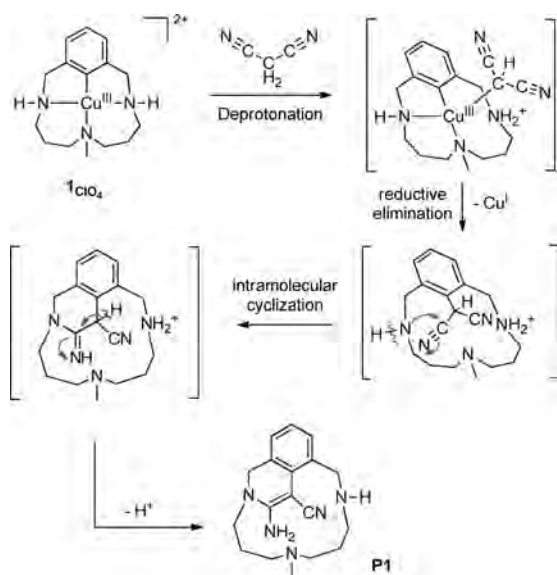


Figure 1. ^1H NMR spectrum (CD_3CN , 25°C , 400 MHz) of compound **P1** with proton assignment. ● 1,3,5-trimethoxybenzene (internal standard); ▲ excess malononitrile.



Scheme 3. Proposed mechanism for the C-arylation of malononitrile through an aryl-Cu^{III} species and subsequent intramolecular reorganization to afford heterocycle **P1**.

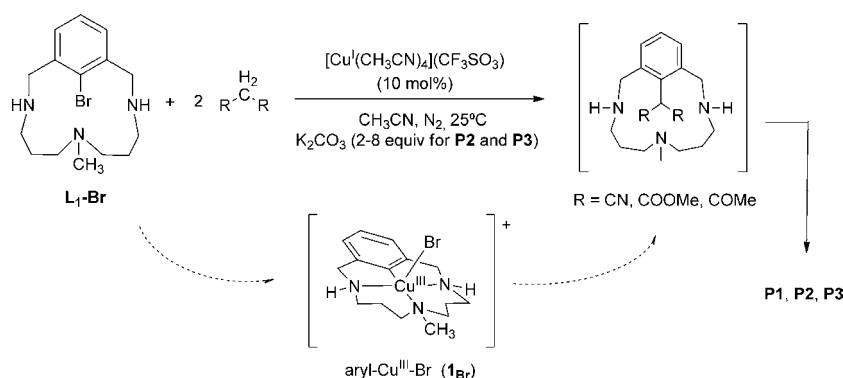
compound **1**_{ClO₄} with different C nucleophiles, as well as the fact that no intermediate species is observed during ¹H NMR analysis of the reaction at low temperatures (only the disappearance of the signals of aryl-Cu^{III} complex and the appearance of signals of compound **P1** are observed), suggest an initial rate-limiting deprotonation of malononitrile, similar to what was recently reported for other nucleophiles, such as alkyl and aryl thiols or phenols.^[8–9] Based on previous work with other heteroatom nucleophiles, we propose that these reactions are initiated by an apical coordination of the deprotonated C nucleophile, which then rapidly undergoes reductive elimination to afford the C_{sp²}-C_{sp³} coupling product. At this point, the benzylic secondary amine rapidly attacks one of the nitrile moieties to trigger an intramolecular domino cyclization, which is also a downhill process. For compounds **P2** and **P3**, a similar mechanism is proposed, although the intramolecular cyclization differs in the nature of the molecule that is released (either H₂O or MeOH; see the Supporting Information, Figures S29 and S30). Similar intramolecular heterocyclization reactions that involve malononitrile or β-ketoesters have been reported.^[21–24] Interestingly, if the bulkier activated methylene substrate 1,3-diphenylpropane-1,3-dione (pK_a in DMSO = 13.4) was added to compound **1**_{ClO₄}, no reaction was observed; thus, steric properties also play a clear role in (at least) the rate-limiting deprotonation step.

The stoichiometric reactivity shown above points towards the

possible implication of aryl-Cu^{III} species in Hurtley-type reactivity.^[25] To explore the catalytic version of this transformation within our model system, we investigated the copper-catalyzed reaction (10 mol% Cu^I source) of a model aryl halide, **L1-Br**, with malononitrile under ambient conditions. Pleasingly, we found that compound **P1** was formed in quantitative yield (> 95%) within 24 h (Scheme 4). Indeed, UV/Vis monitoring of this catalytic reaction revealed the formation of the well-defined aryl-Cu^{III}-Br species **1**_{Br} (band at 550 nm)^[7] as the resting state of the catalyst under the reaction conditions (Figure 2). Furthermore, the ¹H NMR kinetics of the catalytic reaction showed equal rates of the consumption of substrate **L1-Br** and the formation of product **P1** (see the Supporting Information, Figure S1). These observations indicate that, under these catalytic conditions, the rate-limiting step corresponds to the removal of the apical halide ligand by the C nucleophile, with its concomitant deprotonation by a secondary amine.

The analogous copper-catalyzed formation of compounds **P2** and **P3** from the reactions of **L1-Br** with acetylacetone and dimethyl malonate, respectively, were more challenging and moderate-to-good yields were only obtained upon the addition of a base to overcome the lower acidity of these two substrates (K₂CO₃ afforded the best results; Table 1 and Scheme 4). Furthermore, the catalytic synthesis of compound **P2** required the presence of molecular sieves to achieve yields of up to 37%. One possible explanation for this result is that the trapping of the released water helps to prevent the oxidation of the Cu^I catalysts.

Overall, these data clearly indicate the presence of aryl-Cu^{III} species in Hurtley-type reactions on our model platform. The stepwise sequence starts with the direct oxidative addition of the aryl halide at a Cu^I center, followed by the rate-limiting interaction of the aryl-Cu^{III}-halide complex with the activated methylene substrate. The exact nature of the coordination mode of the deprotonated C nucleophile to the aryl-Cu^{III} species is still unclear, because, after the rate-determining deprotonation and coordination of the nucleophile, all of the subsequent steps occur very rapidly. The formation of compounds **P1–P3** also shows that such Hurtley-type reactivity could be a useful synthetic strategy for the synthesis of valuable hetero-



Scheme 4. Copper-catalyzed Hurtley reactions with model aryl bromide (**L1-Br**) to form compounds **P1–P3**; the detection of an intermediate aryl-Cu^{III}-Br species is highlighted. An inorganic base (K₂CO₃) was required to facilitate the catalytic conversion with less-acidic substrates (R = COOMe, COMe).

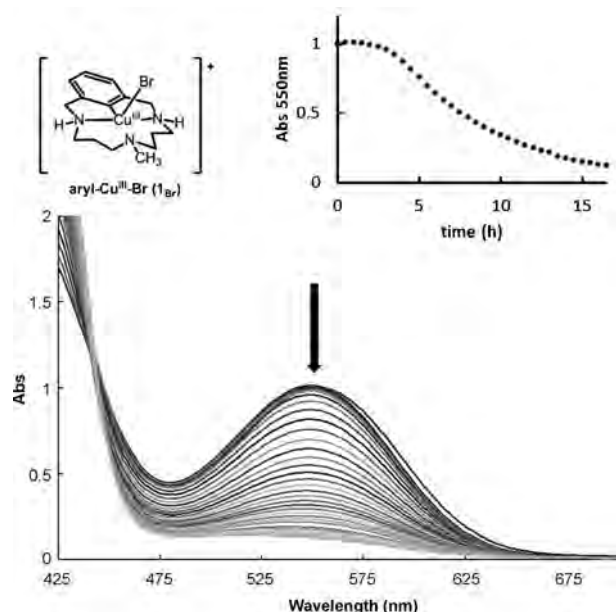


Figure 2. Progressive UV/Vis spectra of the cross-coupling reaction between compound **L₁-Br** and malononitrile to form compound **P1**, catalyzed by $[\text{Cu}^{\text{I}}(\text{CH}_3\text{CN})_4]\text{CF}_3\text{SO}_3$, which show the disappearance of the characteristic band of the aryl- Cu^{III} -Br species (**1_{Br}**) at 550 nm. Conditions: $[\text{L}_1-\text{Br}] = 10 \text{ mM}$, $[[\text{Cu}^{\text{I}}(\text{CH}_3\text{CN})_4]\text{CF}_3\text{SO}_3] = 1.4 \text{ mM}$, $[\text{malononitrile}] = 100 \text{ mM}$, MeCN, 40°C , N_2 atmosphere.

cycles.^[2,23–24] To the best of our knowledge, the reactions reported herein constitute the first experimental examples of copper-catalyzed $\text{C}_{\text{sp}^2}-\text{C}_{\text{sp}^3}$ cross-coupling with the direct involvement of a $\text{Cu}^{\text{I}}/\text{Cu}^{\text{III}}$ catalytic cycle.

Experimental Section

Stoichiometric synthesis of compounds **P1–P3**

Under an inert atmosphere inside a glove box, a sample of aryl- Cu^{III} complex **1_{ClO₄}** (14.2 mg, 28 μmol) was dissolved in CD_3CN (1.6 mL) and 0.4 mL of a solution of 1,3,5-trimethoxybenzene (TMB) in CD_3CN (3.34 μmol) was added as an internal standard. An aliquot of this solution (0.6 mL) was placed inside an NMR tube and two equivalents of the corresponding activated methylene nucleophile (0.1 mL, 168 mM) were added. Final concentrations: $[\text{1}_{\text{ClO}_4}] = 12 \text{ mM}$, $[\text{active methylene nucleophile}] = 24 \text{ mM}$, $[\text{TMB}] = 1.43 \text{ mM}$. The tube was sealed with a screw-cap and the reaction was allowed to proceed at RT (for malononitrile) or at 50°C (for acetylacetone and dimethyl malonate) with monitoring by ^1H NMR spectroscopy until the reaction had completed. Final yields: compound **P1** (99%), compound **P2** (80%), and compound **P3** (37%). In the reaction of dimethyl malonate, the presence of Cs_2CO_3 (8.8 equiv) enhanced the yield of compound **P3** from 37% to 56%. ^1H , COSY, NOESY, TOCSY, $^1\text{H}-^{13}\text{C}$ HSQC, $^1\text{H}-^{13}\text{C}$ HMBC, and ^{13}C NMR spectra and mass spectrometry were obtained directly from crude reactions. Reaction yields were obtained from integration of the ^1H NMR signals relative to the internal standard.

General procedure for the catalytic reactions

Under an inert atmosphere inside a glove box, a vial was loaded with ligand **L₁-Br** (0.5 mL, 30 mM in MeCN) and $[\text{Cu}^{\text{I}}(\text{CH}_3\text{CN})_4]\text{CF}_3\text{SO}_3$ (10 mol%, 0.2 mL of a 7.5 mM stock solution in MeCN) was added. The colorless solution became slightly red, thus indicating that oxidative addition had taken place to afford the corresponding aryl- Cu^{III} -Br complex. Then, a solution of the active methylene nucleophile (2.3 mL, 13 mM in MeCN) was added by a syringe pump over 3 h. For the coupling reactions of dimethyl malonate and acetylacetone, the presence of K_2CO_3 (8.8 equivalents and 2.2 equivalents, respectively) was required and, for the coupling of acetylacetone, the presence of molecular sieves increased the yield of the reaction. Final concentrations: $[\text{L}_1-\text{Br}] = 5 \text{ mM}$, $[[\text{Cu}^{\text{I}}(\text{CH}_3\text{CN})_4]\text{CF}_3\text{SO}_3] = 0.5 \text{ mM}$, $[\text{active methylene nucleophile}] = 10 \text{ mM}$. After stirring the crude mixture at room temperature for 24 h, a solution of 1,3,5-trimethoxybenzene (150 μL , 1.67 mM in MeCN) was added as an internal standard and the solvent was removed. The sample was re-dissolved in CD_3CN (0.5 mL) and the yield was determined from the relative integration of the benzylic protons with respect to those of 1,3,5-trimethoxybenzene in the ^1H NMR spectrum. The yields of compounds **P1**, **P2**, and **P3** were 95%, 37%, and 67%, respectively.

Acknowledgements

We acknowledge financial support from the European Research Council for a Starting Grant Project to X.R. (ERC-2011-StG-277801), the MICINN of Spain (CTQ2009-08464/BQU to Dr. Costas and a PhD FPI grant to M.F.), the Consolider-Ingenio (CSD2010-00065), and the Catalan DIUE of the Generalitat de Catalunya (2009SGR637). X.R. acknowledges an ICREA-Acadèmia award. We also thank Dr. M. Costas, Dr. A. Casitas, and Dr. A. Company for their fruitful discussions.

Keywords: copper • cross-coupling • reaction mechanisms • rearrangement • structure elucidation

- [1] W. R. H. Hurtley, *J. Chem. Soc.* **1929**, 1870.
- [2] G. Evano, N. Blanchard, M. Toumi, *Chem. Rev.* **2008**, *108*, 3054–3131.
- [3] F. Monnier, M. Taillefer, *Angew. Chem.* **2009**, *121*, 7088–7105; *Angew. Chem. Int. Ed.* **2009**, *48*, 6954–6971.
- [4] B. Wang, B. Lu, Y. Jiang, Y. Zhang, D. Ma, *Org. Lett.* **2008**, *10*, 2761–2763.
- [5] I. P. Beletskaya, A. V. Cheprakov, *Coord. Chem. Rev.* **2004**, *248*, 2337–2364.
- [6] S. V. Ley, A. W. Thomas, *Angew. Chem.* **2003**, *115*, 5558–5607; *Angew. Chem. Int. Ed.* **2003**, *42*, 5400–5449.
- [7] A. Casitas, A. E. King, T. Parella, M. Costas, S. S. Stahl, X. Ribas, *Chem. Sci.* **2010**, *1*, 326–330.
- [8] L. M. Huffman, A. Casitas, M. Font, M. Canta, M. Costas, X. Ribas, S. S. Stahl, *Chem. Eur. J.* **2011**, *17*, 10643–10650.
- [9] M. Font, T. Parella, M. Costas, X. Ribas, *Organometallics* **2012**, *31*, 7976–7982.
- [10] Y. Gao, T. R. Burke, Jr., *Synlett* **2000**, 134–136.
- [11] G. J. Quallich, T. W. Makowski, A. F. Sanders, F. J. Urban, E. Vazquez, *J. Org. Chem.* **1998**, *63*, 4116–4119.
- [12] X. Xie, G. Cai, D. Ma, *Org. Lett.* **2005**, *7*, 4693–4695.
- [13] Y. Jiang, N. Wu, H. Wu, M. He, *Synlett* **2005**, 2731–2734.
- [14] X. Xie, Y. Chen, D. Ma, *J. Am. Chem. Soc.* **2006**, *128*, 16050–16051.
- [15] S. F. Yip, H. Y. Cheung, Z. Zhou, F. Y. Kwong, *Org. Lett.* **2007**, *9*, 3469–3472.
- [16] Z. Huang, J. F. Hartwig, *Angew. Chem.* **2012**, *124*, 1052–1056; *Angew. Chem. Int. Ed.* **2012**, *51*, 1028–1032.
- [17] E. J. Hennessy, S. L. Buchwald, *Org. Lett.* **2002**, *4*, 269–272.

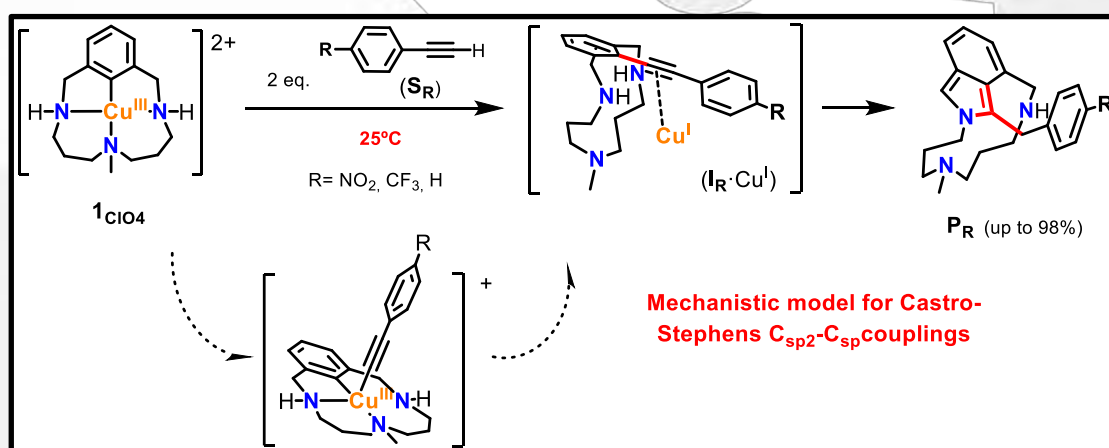
- [18] H.-J. Cristau, P. P. Cellier, J.-F. Spindler, M. Taillefer, *Chem. Eur. J.* **2004**, *10*, 5607–5622.
- [19] J.-i. Setsune, T. Ueda, K. Shikata, K. Matsukawa, T. Iida, T. Kitao, *Tetrahedron* **1986**, *42*, 2647–2656.
- [20] L. M. Huffman, S. S. Stahl, *Dalton Trans.* **2011**, *40*, 8959–8963.
- [21] B. Rajarathinam, G. Vasuki, *Org. Lett.* **2012**, *14*, 5204–5206.
- [22] Y. Chen, X. Xie, D. Ma, *J. Org. Chem.* **2007**, *72*, 9329–9334.
- [23] K. Okuro, M. Furuune, M. Miura, M. Nomura, *J. Org. Chem.* **1993**, *58*, 7606–7607.
- [24] S. Tanimori, H. Ura, M. Kirihata, *Eur. J. Org. Chem.* **2007**, 3977–3980.
- [25] Z.-L. Wang, L. Zhao, M.-X. Wang, *Chem. Commun.* **2012**, *48*, 9418–9420.

Received: November 30, 2012

Published online on February 19, 2013

CHAPTER IV.

Aryl-Copper(III)-Acetylides as Key Intermediates in Csp²-Csp Model Couplings under Mild Conditions



This chapter corresponds to the following publication:

Mireia Rovira, Marc Font, Ferran Acuña-Parés, Teodor Parella, Josep M. Luis, Julio Lloret-Fillol, and Xavi Ribas*. *Chem. Eur. J.* **2014**, *20*, 10005 – 10010

DOI: 10.1002/chem.201402711

For this publication M. R. performed all the experimental work concerning with this publication. Besides, M. R. participated in all the discussions and was involved in writing the paper.

Cu^{III} Intermediates

Aryl-Copper(III)-Acetylides as Key Intermediates in C_{sp}²–C_{sp} Model Couplings under Mild Conditions

Mireia Rovira,^[a] Marc Font,^[a] Ferran Acuña-Parés,^[a] Teodor Parella,^[b] Josep M. Luis,^[a] Julio Lloret-Fillol,^[a] and Xavi Ribas^{*[a]}

Abstract: The mechanism of copper-mediated Sonogashira couplings (so-called Stephens–Castro and Miura couplings) is not well understood and lacks clear comprehension. In this work, the reactivity of a well-defined aryl-Cu^{III} species (1_{Cu}) with *p*-R-phenylacetylenes (R = NO₂, CF₃, H) is reported and it is found that facile reductive elimination from a putative aryl-Cu^{III}-acetylide species occurs at room temperature to afford the C_{aryl}–C_{sp} coupling species (I_R), which in turn undergo an intramolecular reorganisation to afford final heterocyclic products containing 2*H*-isoindole (P_{NO₂}, P_{CF₃}, P_{Ha}) or

1,2-dihydroisoquinoline (P_{Hb}) substructures. Density Functional Theory (DFT) studies support the postulated reductive elimination pathway that leads to the formation of C_{sp}²–C_{sp} bonds and provide the clue to understand the divergent intramolecular reorganisation when *p*-H-phenylacetylene is used. Mechanistic insights and the very mild experimental conditions to effect C_{aryl}–C_{sp} coupling in these model systems provide important insights for developing milder copper-catalysed C_{aryl}–C_{sp} coupling reactions with standard substrates in the future.

Introduction

The transition-metal catalysed couplings of aryl halides and terminal acetylenes is a fundamental reaction for providing access to highly versatile aryl alkyne scaffolds, which are very important precursors in the pharmaceutical industry, as well as in total synthesis and production of organic materials.^[1] The palladium-copper co-catalysed methodology (Sonogashira–Hagihara reaction) is the most widely used, and is thought to proceed through a Pd⁰/Pd^{II} catalytic cycle for effecting the aryl-acetylide coupling. The role of copper as transmetallating agent from Cu^I-acetylides is generally proposed.^[2] However, this coupling reaction can also proceed under copper catalysis (palladium-free) as reported by Miura's seminal report in 1993.^[3] In fact, Castro and Stephens first demonstrated that Cu^I-acetylides could directly react with aryl iodides to provide the desired phenyl acetylenes, back in 1963.^[4]

More recently, renewed interest in palladium-free methodologies is motivated by economic and toxicity reasons, thus copper-based Sonogashira couplings appear as an attractive alternative.^[5] However, copper is known to catalyse the homo-

coupling of terminal alkynes (Glaser–Hay reaction),^[6] a clear drawback that steps down its synthetic utility. Recently, Bolm and co-workers reported that sub-mol% copper loading and a large excess of DMEDA constituted a good methodology to afford the coupling products in quantitative yields,^[7] thus avoiding the undesired acetylene homocoupling.

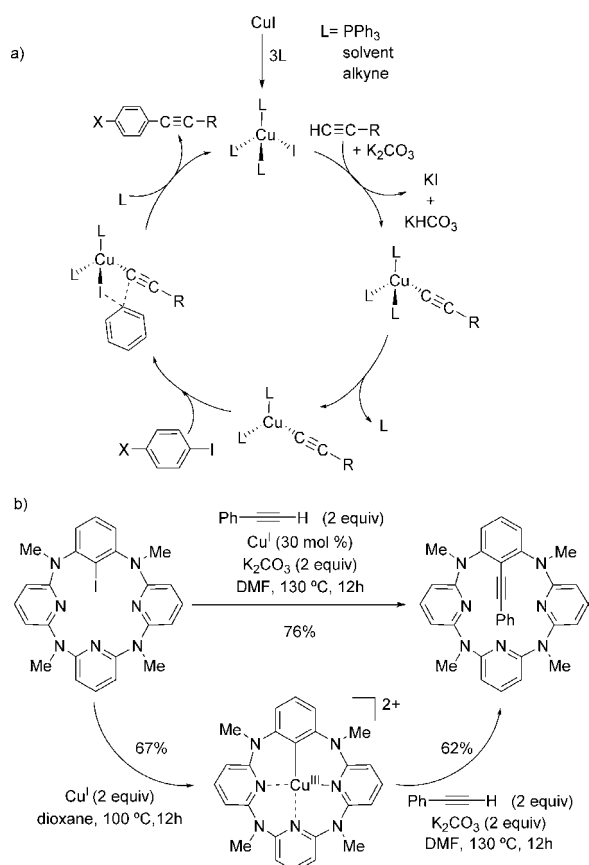
The mechanism of copper-mediated Sonogashira couplings is far from being well-understood. The Stephens and Miura groups supported a mechanism involving the formation of a mononuclear Cu^I-acetylide species that reacted with aryl iodide in a concerted manner through a 4-centre transition state, although no experimental proof was provided (Scheme 1 A).^[3a,4b] Bolm and co-workers performed kinetic investigations with their methodology using DMEDA in excess and supported also that a monomeric Cu^I-acetylide complex was the active species that reacts with aryl iodide, but no further details were provided to explain the key coupling step.^[7] More recently, Wang and co-workers shed more light on the mechanism of this reaction by showing that an aryl iodide moiety embedded in azacalix-[1]arene[3]pyridine can effectively couple with phenylacetylene, in a process catalysed by Cu^I (30 mol%) at 130 °C, where aryl-Cu^{III} species were clearly shown as intermediates (Scheme 1 B).^[8]

In view of the minor mechanistic information available for Cu-based Sonogashira couplings, and in our experience demonstrating that aryl-Cu^{III} species are valid intermediates in model copper-catalysed C_{aryl}-heteroatom (C–N, C–O, C–S, C–Se, C–P and C–halide)^[9] and C_{aryl}–C_{sp}³ coupling reactions,^[10] we decided to investigate in depth the reactivity of well-defined aryl-Cu^{III} species with terminal acetylenes. Here we report on the ability of aryl-Cu^{III} species to react with phenylacetylene derivatives at room temperature to afford the C_{sp}²–C_{sp} coupling

[a] M. Rovira, M. Font, F. Acuña-Parés, Dr. J. M. Luis, Dr. J. Lloret-Fillol, Dr. X. Ribas
Institut de Química Computacional i Catàlisi (IQCC) and
Departament de Química, Universitat de Girona
Campus Montilivi, Facultat Ciències, E17071 Girona (Catalonia, Spain)
E-mail: xavi.ribas@udg.edu

[b] Dr. T. Parella
Servei de RMN, Facultat de Ciències
Universitat Autònoma de Barcelona (UAB)
Campus UAB, E-08193 Bellaterra (Catalonia, Spain)

Supporting information for this article is available on the WWW under
<http://dx.doi.org/10.1002/chem.201402711>.



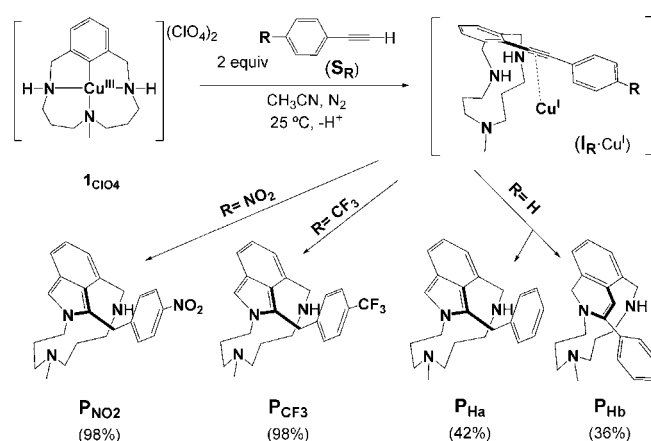
Scheme 1. Mechanistic proposals for the Cu-catalysed Sonogashira coupling reaction. a) Stephens–Castro and Miura's 4-centre transition state proposal, and b) Wang's model system involving an aryl-Cu^{III} species.

products, which in turn evolve to 2*H*-isoindole final products through an intramolecular cyclisation due to nucleophilic attack of secondary amines over the inserted alkyne. Experimental and theoretical evidence showing that monomeric aryl-Cu^{III}-acetylides undergo reductive elimination as the key step of this reaction are presented, and therefore, we provide a mechanistic basis to suggest that these species are plausible intermediates in Pd-free copper-mediated Sonogashira couplings.

Results and Discussion

Reactivity of aryl-Cu^{III} (**1**_{CIO₄}) with *p*-R-phenylacetylene (**S_R**)

This study is inspired by our previous experience with C-heteroatom and C_{aryl}–C_{sp³} cross-coupling catalysis involving the well-defined aryl-Cu^{III} species.^[10] Here we report on the reactivity of aryl-Cu^{III} complex **1**_{CIO₄} with *p*-R-phenylacetylene (**R** = NO₂, CF₃, H) derivatives (**S_R**, Scheme 2). Since we have reported that the oxidative addition step within these model aryl halide substrates is extremely favoured,^[9g] we concentrated our efforts on finding the experimental conditions to achieve a putative C_{aryl}–C_{sp} reductive elimination step. We were pleased to observe that the reaction of **1**_{CIO₄} with the three *p*-R-phenylacetylene derivatives tested afforded the desired arylated phenyla-



Scheme 2. Reaction between the well-defined aryl-Cu^{III} complex (**1**_{CIO₄}) and phenylacetylene derivatives (**S_R**) that undergo C_{sp²}–C_{sp} coupling and further intramolecular cyclisation to form products containing 2*H*-isoindole (**P**_{NO₂}, **P**_{CF₃}, **P**_{Ha}) or 1,2-dihydroisoquinoline (**P**_{Hb}) scaffolds (general conditions: [**1**_{CIO₄}] = 12 mM, [nucleophile] = 24 mM, 25 °C, CD₃CN; product yields were calculated by ¹H NMR spectroscopy integration related to the internal standard).

cetylene compounds at room temperature in less than 2 h, although these were unstable and underwent intramolecular cyclisation through the attack of one of the secondary amines of the substrate scaffold over the alkyne moiety (Scheme 2) in an overall 8 h reaction time.

Final cyclised products contained 2*H*-isoindole (**P**_{NO₂}, **P**_{CF₃}, **P**_{Ha}) or 1,2-dihydroisoquinoline (**P**_{Hb}) substructures. Yields were excellent for *p*-NO₂ and *p*-CF₃ derivatives whereas a global aryl-Cu^{III} conversion of 78% was found for the reaction with **S_H** (**P**_{Ha} 42%, **P**_{Hb} 36%, in almost a 1:1 ratio). No C_{sp}–C_{sp} Glaser–Hay homocoupling side products were detected in any of these reactions. The chemical structure of **P**_{NO₂} and **P**_{CF₃} has been unequivocally established by means of NMR spectroscopy and ESI-MS studies. In the case of **P**_{Ha} and **P**_{Hb}, their separation has not been possible but a complete structure characterisation and unambiguous chemical-shift assignment of both molecules has been successfully performed from the careful analysis of multidimensional NMR spectra of the mixture. As an example, the ¹H NMR spectrum of **P**_{CF₃} is depicted in Figure 1. Intramolecular cyclisation imposes rigidity in the molecule and converts all methylene protons into diastereotopic pair signals, which are assigned from COSY and ¹H-¹³C HSQC spectra. The main features that identify the 2*H*-isoindole moiety in **P**_{CF₃} were deduced from the analysis of NOESY and ¹H-¹³C HMBC spectra. The NOESY experiment allowed us to assign H^c and H^d due to its through-space connectivity with H^e, H^f and the aromatic H^b protons. NOE data were also observed between the benzylic H^s and H^t protons with the aromatic H^u protons from the *p*-CF₃-phenyl moiety, which evidenced the loss of the triple bond. A key point to elucidate the compound structure was the singlet resonance (Hⁱ proton) resonating at 7.47 ppm and directly attached to the carbon resonating at 115.6 ppm (via HSQC), a characteristic value for a C_{sp²}. This Hⁱ proton showed NOE with the aromatic H^b and the methylene H^m and Hⁿ protons. On the other hand, the connectivities observed in the

HMBC spectrum allowed the assignment of all quaternary carbons and indicated the formation of 5-membered cyclised ring corresponding to a 2*H*-isindole type. Thus, the benzylic H^t proton presented HMBC cross-peaks with C₁₈, C₁₉, C₁₆ and C₁₅ carbons, whereas Hⁱ were correlated with C₃, C₁₂, C₁₄, C₁₅ and C₁₆.

Analogous structural characterisation of **P**_{NO₂} and **P**_{Ha_r} bearing the same 2*H*-isindole substructure, is fully detailed in the Supporting Information. On the other hand, **P**_{Hb} has been characterised by NMR spectroscopy and found to contain a 6-membered 1,2-dihydroisoquinoline moiety; full characterisation details are also given in the Supporting Information.

It is worth mentioning that copper-catalysed alkynylation–cyclisation cascade reactions had been described for the synthesis of 1*H*-indole substructures,^[11] but the synthesis of 2*H*-isindole using this strategy is, to our knowledge, unprecedented. On the other hand, Cu-catalysed cascade reactions involving aryl–acetylide coupling followed by intramolecular reorganisation for the synthesis of isoquinoline derivatives has been recently reported using phenyl-pyrazoles as substrates.^[12]

Characterisation of C_{aryl}–C_{sp} coupling intermediate species (I_R)

The structural characterisation of final products immediately suggests the initial formation of a C_{aryl}–C_{sp} coupling intermediate species (I_R) as depicted in Figure 2, which suffers an intramolecular reorganisation to form **P**_R (vide infra). In order to prove this hypothesis, we attempted the isolation or accumulation of I_{CF₃} by monitoring the reaction of **1**_{ClO₄} with **S**_{CF₃} by NMR spectroscopy at low temperature. Upon optimisation of the conditions we found that the reaction of **1**_{ClO₄} with **S**_{CF₃} at 0 °C allowed the accumulation of I_{CF₃} during 30 min without any sign of evolution to the intramolecularly cyclised final product **P**_{CF₃} (Figure 2). This species was fully characterised by 1D and 2D NMR spectroscopy studies and by high resolution mass spectrometry (HRMS) using a cryospray device to inject the sample at –40 °C, thus warranting the integrity of I_{CF₃} during the measurement (see the Supporting Information). Subsequently, compound I_{CF₃} underwent reorganisation to finally form **P**_{CF₃} quantitatively in 18 h at 0 °C (see the Supporting Information).

To further substantiate the plausible implication of aryl–Cu^{III}–acetylide species as key intermediates for the formation of C_{aryl}–C_{sp} coupling species (I_R) we undertook a theoretical DFT study on the reaction of **1**_{ClO₄} with **S**_H as depicted in Figure 3 (see the Supporting Information for computational details). A first intermediate species **B** was identified, consisting of the axial π-coordination of the alkyne to the Cu^{III} centre. As a first attempt to explain the reactivity, an intramolecular deprotonation of phenylacetylene by one of the secondary amines of the complex was found to be too high in energy (Δ*G* = 47.1 kcal mol^{–1}), suggesting that the Cu^{III} oxidation state cannot be stabilised upon decoordination of one of the amine sites (Figure S40 in

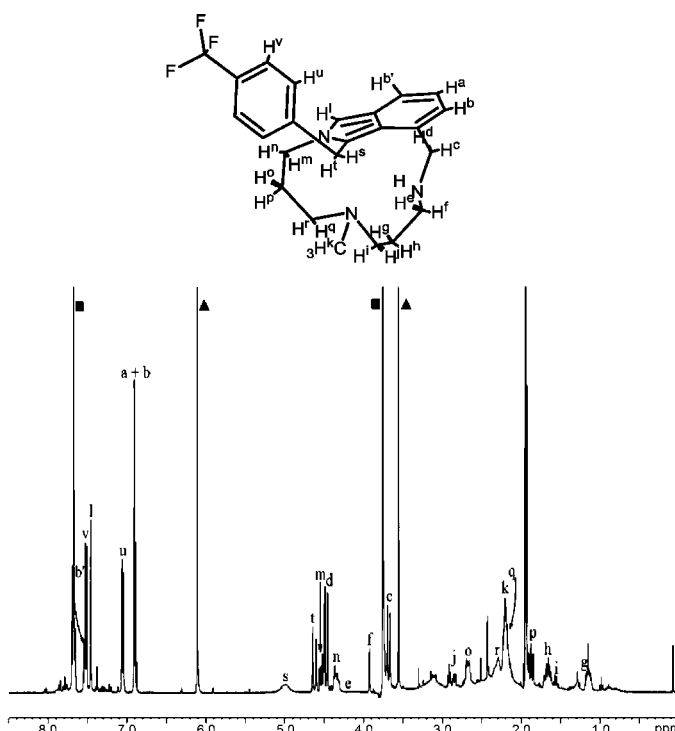


Figure 1. ¹H NMR spectrum (CD₃CN, 25 °C, 400 MHz) of compound **P**_{CF₃} with proton assignment. ▲: 1,3,5-trimethoxybenzene (internal standard); ■: excess of *p*-CF₃-phenylacetylene.

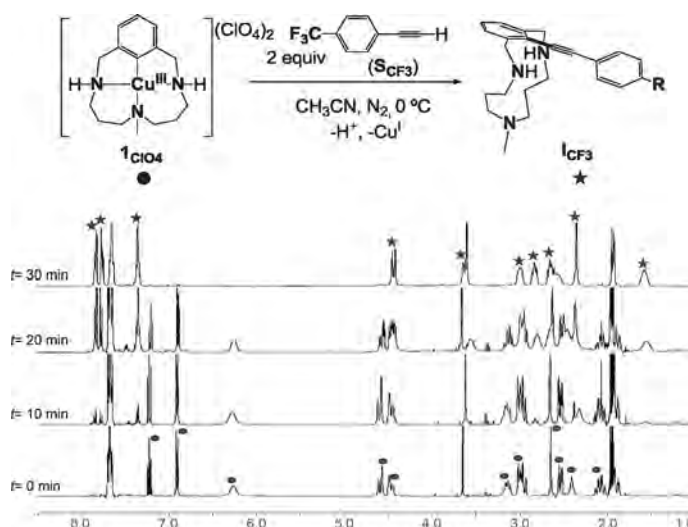


Figure 2. ¹H NMR monitoring study showing full formation of C_{aryl}–C_{sp} coupling intermediate species I_{CF₃} upon treatment of **1**_{ClO₄} with 2 equiv of **S**_{CF₃} (general conditions: [1_{ClO₄}] = 78.6 mM, [nucleophile] = 157.2 mM, CD₃CN, 0 °C, 400 MHz; ●: **1**_{ClO₄}; ★: I_{CF₃}).

the Supporting Information). On the contrary, by using an external model base (i.e., Et₂NH was selected as modelled base owing to the possibility that minor amounts of free ligand are available in the reaction mixture), a much smaller barrier was found leading to aryl–Cu^{III}–acetylide (intermediate **C**; Δ*G*[‡] = 13.0 kcal mol^{–1}). This species rapidly undergoes reductive elimination to form I_H–Cu^I, which corresponds to I_H with the Cu^I

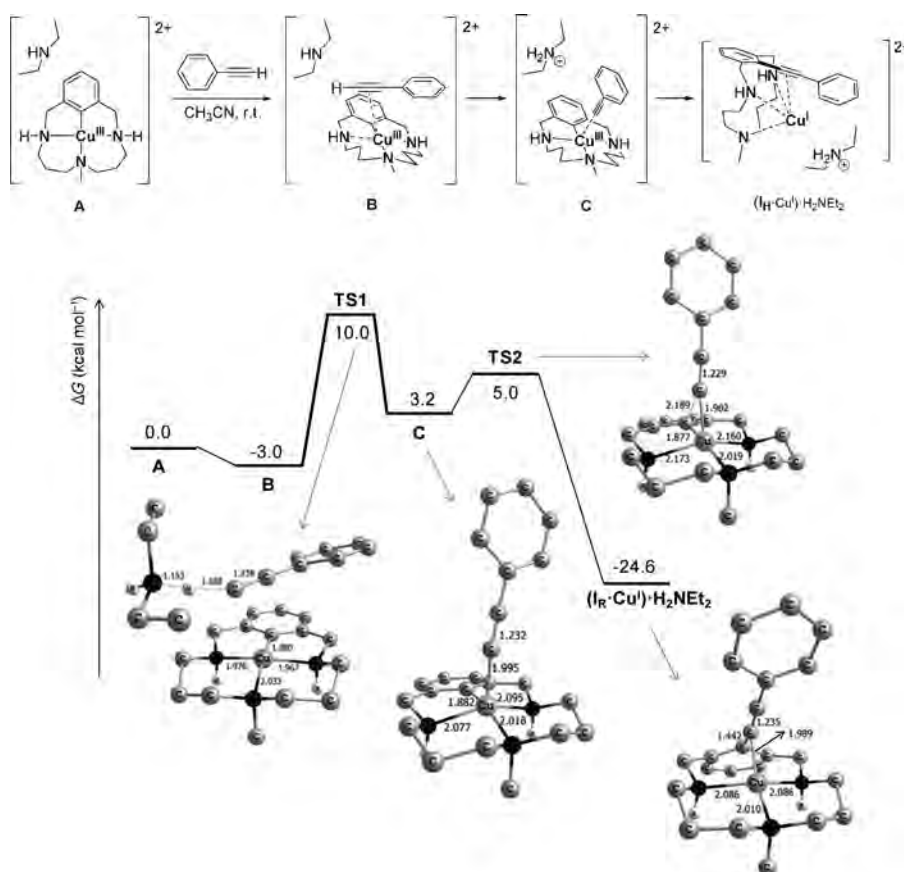


Figure 3. DFT Gibbs energy profile of the reaction of 1_{CuO_4} with S_{H} in the presence of Et_3NH as external model base (ΔG in kcal mol^{-1}). Et_3NH and Et_3NH_2^+ molecules are necessary to ensure the correct energetic balance in all the steps of the reaction, and are included in the calculation. The interaction between the copper complex and the external base was only explicitly modelled in the TS1 structure. Irrelevant hydrogen atoms in the figures are omitted for clarity.

cation still coordinated in the macrocyclic pocket. DFT calculations nicely agree with the experimental isolation of analogous I_{CF_3} starting from the well-defined aryl- Cu^{III} species (1_{CuO_4}).

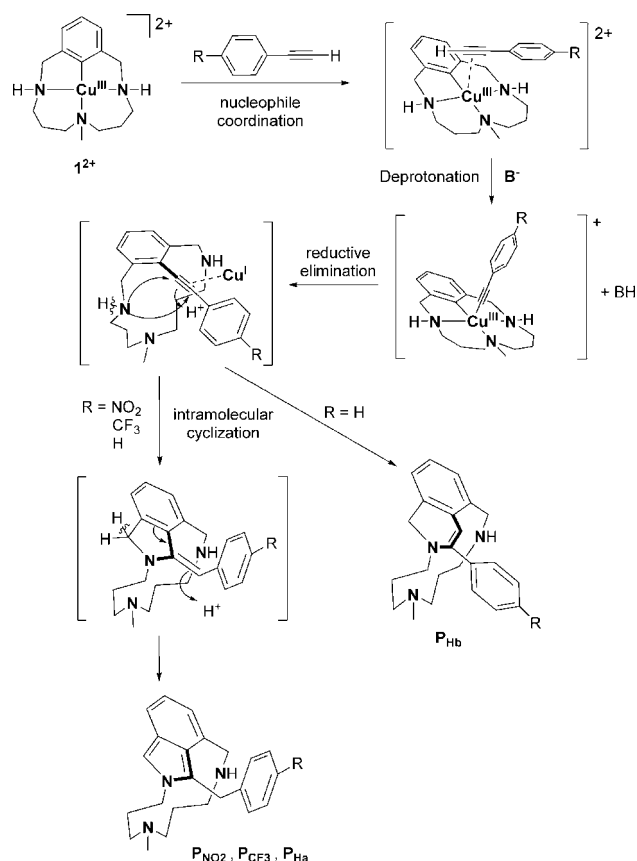
Altogether this constitutes a solid argument to the proposal that the aryl- Cu^{III} -acetylide species is involved in Cu-based Sonogashira couplings. However, in our model system I_{R} undergoes further reorganisation to P_{R} . We propose that an initial nucleophilic attack of a NH group occurs over the triple bond of the inserted acetylide, as depicted in Scheme 3. This attack can in principle take place at both carbons of the triple bond of I_{R} , although we have clearly observed that for $\text{R}=\text{NO}_2$ or CF_3 , the attack exclusively occurs at the proximal carbon to afford 5-membered ring 2*H*-isoindole products (P_{NO_2} , P_{CF_3} , P_{Ha}), whereas for $\text{R}=\text{H}$ the attack occurs equally at both C_{sp} atoms, thus affording almost 1:1 ratios of P_{Ha} and six-membered ring 1,2-dihydroisoquinoline P_{Hb} . In either case, proton shifts and/or rearomatisation arrangements are envisioned to finally afford the structure of the end products (Scheme 3).

At this stage, we were intrigued by three important mechanistic aspects concerning the evolution of I_{R} to P_{R} . On one hand, we wondered if the initial nucleophilic attack of NH over the triple bond requires its electrophilic activation by the coordination of the Cu^{I} cation formed in solution. To check this hy-

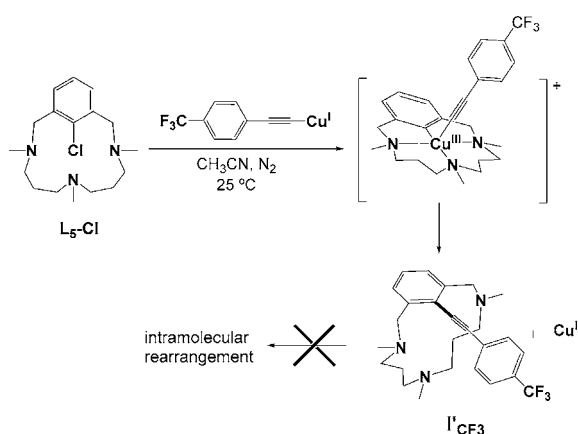
pothesis, we fully formed I_{CF_3} exclusively at 0°C and we compared the time consumed to form P_{CF_3} with and without the addition of 1,10-phenanthroline (phen) in excess (2.5 equiv), owing to the high affinity of phen to complexate Cu^{I} as the highly stable $[\text{Cu}^{\text{I}}(\text{phen})_2]^+$.^[13] We observed that upon sequestering Cu^{I} by the addition of phen, the formation of P_{CF_3} from I_{CF_3} was slowed down by twofold (see the Supporting Information). This result clearly points to a substantial activation of the triple bond by Cu^{I} coordination, which is reminiscent of the chemistry of silver(I) and gold(I),^[14] although it also argues in favour of a slower intramolecular rearrangement in the absence of an electrophilic activation of the alkyne moiety.

Another consideration to take into account is the occurrence of a secondary amine moiety to initiate the nucleophilic attack over the triple bond. To verify that an NH group is essential for the intramolecular reorganisation to proceed, we performed the reaction of a triazamacrocyclic model aryl halide bearing three permethylated tertiary amines ($L_5\text{-Cl}$) with 1 equiv of the $[\text{Cu}^{\text{I}}(\text{CC-Ph-}p\text{-CF}_3)]$ complex prepared independently (Scheme 4).^[15] The reaction afforded 76% yield of the I'_{CF_3} product, which remained stable in solution for days with no signs of intramolecular rearrangement. Therefore, we can conclude that the nucleophilic attack of the amine over the alkyne is effective only if proton shifts are allowed.

Finally, the third important question was related to the comprehension of the regioselective attack to one C_{sp} atom for $\text{R}=\text{NO}_2$, CF_3 , whereas for $\text{R}=\text{H}$ both C_{sp} atoms suffer the nucleophilic attack indistinctly. We calculated theoretical charge densities (natural population analysis (NPA) and Mulliken charges) on the alkyne moiety for the $I_{\text{R}}\text{-Cu}^{\text{I}}$ species, but no significant differences were found (Figure S41 in the Supporting Information). However, the representation of the frontier molecular orbitals for $I_{\text{H}}\text{-Cu}^{\text{I}}$ and $I_{\text{NO}_2}\text{-Cu}^{\text{I}}$ species nicely showed that when an electron-withdrawing group, such as $-\text{NO}_2$, is present in the molecule, the LUMO orbital that receives the nucleophilic attack of the amine completely excludes any orbital participation of the C_{sp} atom closer to the electron-withdrawing centre, thus exclusively allowing for a 5-membered ring formation (Figure 4). On the contrary, if $\text{R}=\text{H}$, both C_{sp} atoms of the alkyne do participate in the corresponding LUMO equally,



Scheme 3. Global mechanistic proposal for the formation of P_R products through aryl-Cu^{III}-acetylide species, and subsequent intramolecular cyclisations following divergent pathways depending on R.



Scheme 4. Reaction of L_5 -Cl with p -CF₃-phenylacetylide copper(I) complex to afford the stable I'_{CF_3} product.

which is translated to the almost equimolar formation of 5-membered ring P_{Ha} and 6-membered ring P_{Hb} products.

All information extracted from the above-reported experiments using 1_{ClO_4} as our starting reactant provided the fundamental basis to attempt a catalytic version for producing a $C_{aryl}-C_{sp}$ coupling product within our model system. Exhaustive experimental optimisation of the catalysis of L_1 -Br with

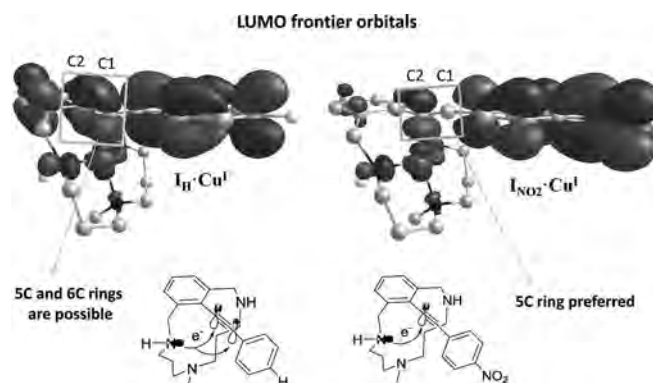


Figure 4. LUMO frontier orbitals for I_H -Cu^I and I_{NO_2} -Cu^I species and simplified scheme of the possible nucleophilic attacks in each molecule (Cu^I cation omitted for clarity).

2 equiv of S_{NO_2} employing 10 mol% $[Cu^I(CH_3CN)_4]OTf$ did not afford any trace of P_{NO_2} (Table S1 in the Supporting Information), although L_1 -Br was completely consumed. We reasoned that the heterocyclic nature of the P_{NO_2} product is unstable under catalytic conditions and decomposes completely. Therefore, we screened the copper-catalysed reaction using L_5 -Br or L_5 -Cl with 2 equiv of S_{CF_3} and 4 equiv of base (to assist the acetylene deprotonation) to form the nonheterocyclic coupling product I'_{CF_3} (Table S2 in the Supporting Information). We found yields of product close to the copper(I) loading used, thus indicating that only stoichiometric amounts of product were obtained. Similar results were found when Cu^I-acetylide was used as copper catalyst. These observations suggest the inhibition or entrapment of Cu^I released upon reductive elimination. At present we have not been able to overcome the inactivation of the Cu^I released in solution to achieve catalytic turnover, despite the fact that different strategies have been explored (see the Supporting Information).

Conclusion

In summary, here we report the feasibility of aryl-Cu^{III} species as key intermediates in copper-mediated $C_{sp^2}-C_{sp}$ coupling reactions by studying the reactivity of well-defined aryl-Cu^{III} (1_{ClO_4}) with phenylacetylene derivatives to afford P_{NO_2} , P_{CF_3} , P_{Ha} and P_{Hb} coupling products at room temperature. The latter heterocyclic products are formed by intramolecular reorganisation of biaryl acetylene species I_R , in which the nucleophilic attack of the secondary amine is facilitated via Lewis activation of the alkyne moiety by Cu^I. This reorganisation is blocked if tertiary amines are present in the model aryl halide substrates (L_5 -X). Catalytic turnover was not possible in these model systems due to inhibition or entrapment of Cu^I released upon reductive elimination. Most importantly, the copper-mediated $C_{sp^2}-C_{sp}$ reductive elimination step was proven to easily occur at room temperature, thus adding mechanistic understanding to copper-mediated Stephens–Castro (stoichiometric)^[4] and Miura's (catalytic)^[3] reactions. Along with Wang's reported precedent,^[8] this work is relevant in the mechanistic comprehension of Pd-free Cu-mediated Sonogashira couplings and

covers strategies and limitations to be translated in copper-catalysed $C_{sp^2}-C_{sp}$ couplings. Ongoing studies are focused on applying the insights learned from these studies to Miura's catalysis with standard substrates. Furthermore, this study may be used as a fundamental basis to extend the Cu-catalysed alkylation-cyclisation cascade reactions to produce 2*H*-isoindole products using (2-halophenyl)methanamine-type of substrates.

Experimental Section

Synthesis of products P_{NO_2} , P_{CF_3} , P_{Ha} and P_{Hb}

In an inert-atmosphere glove box, a sample of the aryl-Cu^{III} complex **1**_{ClO₄} (14.2 mg, 28 μmol) was dissolved in CD₃CN (1.6 mL) and a solution of 1,3,5-trimethoxybenzene (0.4 mL) was added as an internal standard. A portion of this solution (0.6 mL) was loaded into an NMR tube, and 2 equivalents of the corresponding acetylene nucleophile were added to the tube (0.1 mL, 168 mM). Final concentrations: [**1**_{ClO₄}] = 12 mM, [*p*-R-phenylacetylene] = 24 mM. The tube was sealed with a screw-cap and the reaction was allowed to proceed at room temperature and was monitored by ¹H NMR spectroscopy until reaction completion. Final yields were: P_{NO_2} (98%), P_{CF_3} (98%), P_{Ha} (42%) and P_{Hb} (36%). ¹H, COSY, NOESY, TOCSY, ¹H-¹³C HSQC, ¹H-¹³C HMBC and ¹³C NMR spectra and mass spectrometric analysis were obtained directly from crude reactions. Reaction yields were obtained by relative integration of the ¹H NMR signals to the internal standard. Full characterisation details can be found in the Supporting Information.

Acknowledgements

We acknowledge financial support from European Research Council for Starting Grant Project ERC-2011-StG-277801 to X.R., MICINN of Spain (INNPLANTA project INP-2011-0059-PCT-420000-ACT1 to X.R., CTQ2012-32436 to T.P., CTQ2012-37420-C02-01/BQU to Dr. M. Costas, RyC contract to J.Ll.-F. and PhD FPI grant to M.F.), Consolider-Ingenio CSD2010-00065, and the Catalan DIUE of the Generalitat de Catalunya (2009SGR637). X.R. thanks an ICREA-Acadèmia award.

Keywords: $C_{aryl}-C_{sp}$ cross coupling • copper(III) • density functional calculations • reaction mechanisms • Pd-free Sonogashira

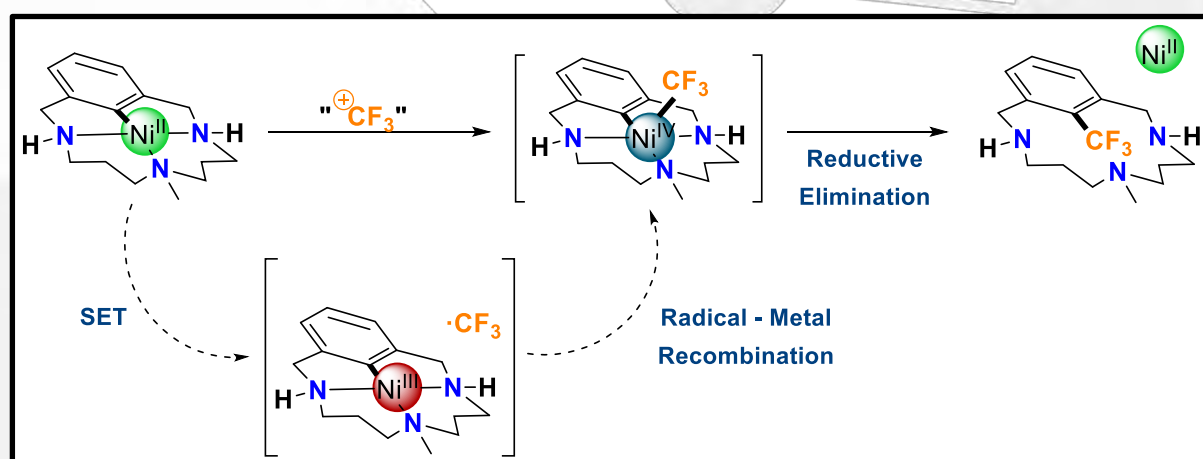
- [1] a) R. Chinchilla, C. Nájera, *Chem. Rev.* **2007**, *107*, 874–922; b) T. Truong, O. Daugulis, *Org. Lett.* **2011**, *13*, 4172–4175; c) E.-i. Negishi, L. Anastasia, *Chem. Rev.* **2003**, *103*, 1979–2018; d) A. S. Dudnik, V. Gevorgyan, *Angew. Chem.* **2010**, *122*, 2140–2142; *Angew. Chem. Int. Ed.* **2010**, *49*, 2096–2098.
- [2] a) K. Sonogashira, Y. Tohda, N. Hagihara, *Tetrahedron Lett.* **1975**, *16*, 4467–4470; b) K. Sonogashira, in *Metal-Catalyzed Cross-Coupling Reactions* (Eds.: F. Diederich, P. J. Stang), Wiley-VCH, Weinheim, **1998**, pp. 203–229; c) M. S. Viciu, S. P. Nolan, in *Modern Arylation Methods* (Ed.: L. Ackermann), Wiley-VCH, Weinheim, **2009**, pp. 183–220.
- [3] a) K. Okuro, M. Furuune, M. Miura, M. Nomura, *J. Org. Chem.* **1993**, *58*, 7606–7607; b) K. Okuro, M. Furuune, M. Enna, M. Miura, M. Nomura, *J. Org. Chem.* **1993**, *58*, 4716–4721.
- [4] a) C. E. Castro, R. D. Stephens, *J. Org. Chem.* **1963**, *28*, 2163; b) R. D. Stephens, C. E. Castro, *J. Org. Chem.* **1963**, *28*, 3313–3315.
- [5] a) A. Sagadevan, K. C. Hwang, *Adv. Synth. Catal.* **2012**, *354*, 3421–3427; b) D. Ma, F. Liu, *Chem. Commun.* **2004**, 1934–1935; c) Y. Zhang, T. F. Jamison, S. Patel, N. Mainolfi, *Org. Lett.* **2010**, *12*, 280–283; d) R. K. Gujadhur, C. G. Bates, D. Venkataraman, *Org. Lett.* **2001**, *3*, 4315–4317.
- [6] a) C. Glaser, *Ber. Dtsch. Chem. Ges.* **1869**, *2*, 422; b) A. S. Hay, *J. Org. Chem.* **1962**, *27*, 3320–3321.
- [7] E. Zuidema, C. Bolm, *Chem. Eur. J.* **2010**, *16*, 4181–4185.
- [8] Z.-L. Wang, L. Zhao, M.-X. Wang, *Org. Lett.* **2012**, *14*, 1472–1475.
- [9] a) X. Ribas, I. Güell, *Pure Appl. Chem.* **2014**, *86*, 263–467; b) A. Casitas, X. Ribas, *Chem. Sci.* **2013**, *4*, 2301–2318; c) A. Casitas, X. Ribas, in *Copper-Mediated Cross-Coupling Reactions* (Eds.: G. Evano, N. Blanchard), Wiley, Hoboken, **2013**, pp. 253–279; d) M. Font, T. Parella, M. Costas, X. Ribas, *Organometallics* **2012**, *31*, 7976–7982; e) L. M. Huffman, A. Casitas, M. Font, M. Canta, M. Costas, X. Ribas, S. S. Stahl, *Chem. Eur. J.* **2011**, *17*, 10643–10650; f) A. Casitas, M. Canta, M. Solà, M. Costas, X. Ribas, *J. Am. Chem. Soc.* **2011**, *133*, 19386–19392; g) A. Casitas, A. E. King, T. Parella, M. Costas, S. S. Stahl, X. Ribas, *Chem. Sci.* **2010**, *1*, 326–330.
- [10] M. Rovira, M. Font, X. Ribas, *ChemCatChem* **2013**, *5*, 687–691.
- [11] a) P. Saejueng, C. G. Bates, D. Venkataraman, *Synthesis* **2005**, 2005, 1706–1712; b) G. Evano, N. Blanchard, M. Toumi, *Chem. Rev.* **2008**, *108*, 3054–3131; c) F. Liu, D. Ma, *J. Org. Chem.* **2007**, *72*, 4844–4850; d) S. Cacchi, G. Fabrizi, L. M. Parisi, *Org. Lett.* **2003**, *5*, 3843–3846.
- [12] Y. Yang, H. Ren, D. Wang, F. Shi, C. Wu, *RSC Adv.* **2013**, *3*, 10434–10441.
- [13] X. Ribas, D. A. Jackson, B. Donnadieu, J. Mahía, T. Parella, R. Xifra, B. Hedman, K. O. Hodgson, A. Llobet, T. D. P. Stack, *Angew. Chem.* **2002**, *114*, 3117–3120; *Angew. Chem. Int. Ed.* **2002**, *41*, 2991–2994.
- [14] A. S. K. Hashmi, in *Silver in Organic Chemistry* (Ed.: M. Harmata), Wiley, **2010**, pp. 357–379.
- [15] K. Jouvin, J. Heimbürger, G. Evano, *Chem. Sci.* **2012**, *3*, 756–760.

Received: March 21, 2014

Published online on July 10, 2014

CHAPTER V.

Mechanistic insight in the trifluoromethylation of a well-defined aryl-Ni^{II} complex involving a SET step and a Ni^{IV}-CF₃ intermediate species



This chapter corresponds to the following publication:

Mireia Rovira, Steven Roldán-Gómez, Christopher J. Whiteoak, Vlad Martin-Diaconescu, Anna Company, Josep M. Luis, and Xavi Ribas*.

Manuscript under revision

For this publication M. R. synthesised and characterized aryl-Ni^{II} complexes and also performed all the reactivity studies. Additionally, M. R. was involved in argumentations and discussions, as well as in writing the manuscript.

Mechanistic insight into the trifluoromethylation of a well-defined aryl-Ni^{II} complex involving Ni^{III}/CF₃· and Ni^{IV}-CF₃ intermediate species

Mireia Rovira, Steven Roldán-Gómez, Vlad Martin-Diaconescu, Christopher J. Whiteoak, Anna Company, Josep M. Luis*, Xavi Ribas*

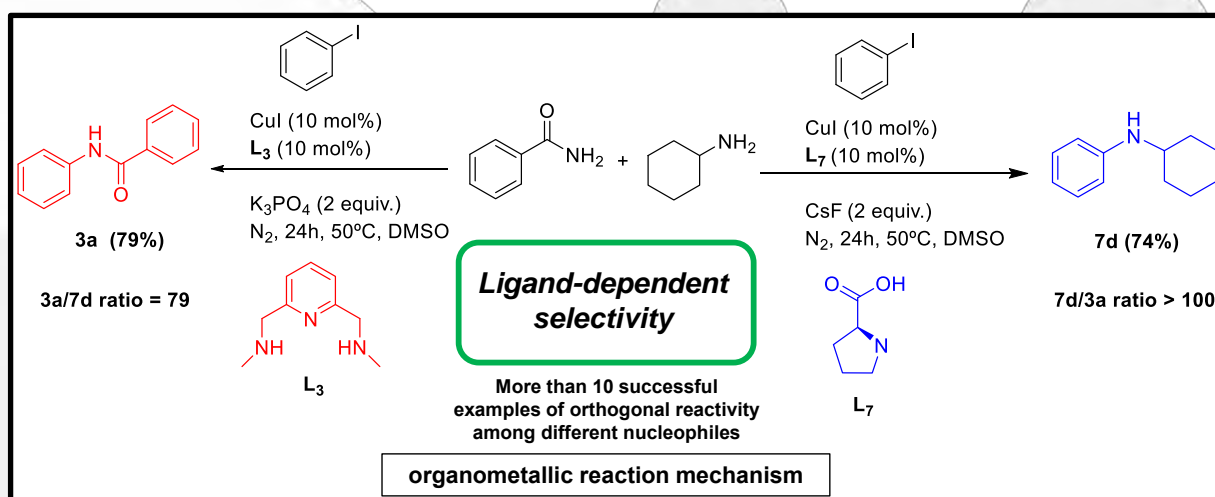
Institut de Química Computacional i Catàlisi (IQCC) and Departament de Química, Universitat de Girona, Campus de Montilivi, E-17071 Girona, Catalonia, Spain

ABSTRACT: Nickel mediated trifluoromethylation of an aryl-Br bond in a model macrocyclic ligand (**L_n-Br**, n = 1 or 5) has been thoroughly studied, starting with an oxidative addition at Ni⁰ to obtain well-defined aryl-Ni^{II}-Br complexes (**[L_n-Ni^{II}]Br**). Removal of the halide with AgX (X = OTf or ClO₄⁻) thereafter provides **[L_n-Ni^{II}](OTf)** (**1_{OTf}**, **5_{OTf}**). The nitrate analogue has been obtained through a direct C-H activation of an aryl-H bond using Ni^{II} salts, and this route has been studied by XAS. Crystallographic (XRD) and XAS characterization has shown aryl-Ni^{II} bond distances among the shortest reported in the literature, which hampers their direct reaction with nucleophiles. On the contrary, enhanced reactivity is observed with oxidants, and the reaction of complexes **1_{OTf}**, **5_{OTf}** with a CF₃⁺ sources afforded the trifluoromethylation products, **L₁-CF₃** and **L₅-CF₃**, in quantitative yield. A combined experimental and theoretical mechanistic study was performed, providing new insights into the operative mechanism for this transformation. Computational analysis indicate the occurrence of an initial SET to 5-(trifluoromethyl)dibenzothiophenium triflate (TDTT) furnishing a transient L₁-Ni^{III}/CF₃· adduct, which rapidly evolves towards a **[L₁-Ni^{IV}-CF₃](X)₂** intermediate species. A final facile reductive elimination affords the trifluoromethylation product **L₁-CF₃**. This mechanistic study exemplifies that the well-defined square-planar model system studied encompasses all of the rich redox chemistry of nickel for this transformation, from Ni⁰ to Ni^{IV}.

EMBARGOED UNTIL PUBLICATION

CHAPTER VI.

Orthogonal Discrimination among Functional Groups in Ullmann-Type C–O and C–N Couplings



This chapter corresponds to the following publication:

Mireia Rovira, Marta Soler, Imma Güell, Ming-Zheng Wang, Laura Gómez, and Xavi Ribas*. *J.*

Org. Chem. **2016**, *81*, 7315 – 7325

DOI: 10.1021/acs.joc.6b01035

For this publication M. R. did all the optimization reactions and also she performed the competition reactions and mechanistic investigations. Besides, M. R. participated in all the discussions and was involved in writing the paper.

JOC

The Journal of Organic Chemistry

MARCH 18, 2016 VOLUME 81, NUMBER 6 pubs.acs.org/joc



ACS Publications
Most Trusted. Most Cited. Most Read.

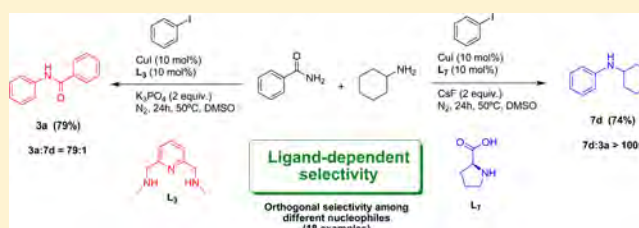
www.acs.org

Orthogonal Discrimination among Functional Groups in Ullmann-Type C–O and C–N Couplings

Mireia Rovira,[†] Marta Soler,[†] Imma Güell,[†] Ming-Zheng Wang,[†] Laura Gómez,^{†,‡} and Xavi Ribas^{*,†}[†]Institut de Química Computacional i Catàlisi (IQCC) and Departament de Química, Universitat de Girona, Campus de Montilivi, E-17003 Girona, Catalonia, Spain[‡]Serveis Tècnics de Recerca (STR), Universitat de Girona, Parc Científic i Tecnològic de la UdG, Pic de Peguera 15, E17003 Girona, Catalonia, Spain

S Supporting Information

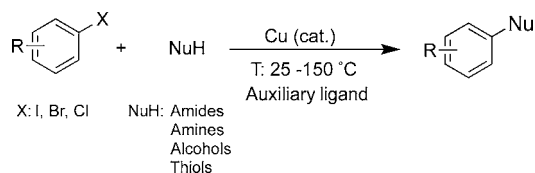
ABSTRACT: The copper-catalyzed arylation of nucleophiles has been established as an efficient methodology for the formation of C–C and C–heteroatom bonds. Considering the advances during the last two decades, the ligand choice plays a key role in such transformations and can strongly influence the catalytic efficiency. The applicability of these Ullmann-type coupling reactions regarding the orthogonal selectivity of different functional groups constitutes a challenging subject for current synthetic strategies. Herein, we report a useful toolkit of Cu-based catalysts for the chemoselective arylation of a wide-range of nucleophiles in competitive reactions using aryl iodides and bromides. We show in this work that the arylation of all kinds of amides can be orthogonal to that of amines (aliphatic or aromatic) and phenol derivatives. This high chemoselectivity can be governed by the use of different ligands, yielding the desired coupling products under mild conditions. The selectivity trends are maintained for electronically biased iodobenzene and bromobenzene electrophiles. Radical clock experiments discard the occurrence of radical-based mechanisms.



■ INTRODUCTION

Modern copper-catalyzed cross-coupling reactions have recently evolved into reliable and efficient methods for the formation of C–C and C–heteroatom bonds, which are present in a large number of natural and pharmaceutical products. Recent progress in modern catalytic Ullmann coupling reactions has led to the emergence of numerous methods to combine aryl halides (mainly iodides and bromides) with aliphatic amines, amino alcohols, amides, anilines, phenols, and other derivatives (Scheme 1).^{1–7}

Scheme 1. Copper-Catalyzed Ullmann-Type C–Heteroatom Couplings



The first reports on Ullmann–Goldberg reactions originally required relatively harsh conditions such as high temperatures and sometimes the use of stoichiometric amounts of copper salts.^{8–10} Interestingly, several “ligand-free” procedures have also been reported as effective catalytic systems for Ullmann-type reactions, taking advantage of the coordinating abilities of solvents such as DMF, DMP, and TEOS, albeit under high

temperature conditions.^{11–20} On the other hand, since the late 1990s, much effort has been devoted to the use of chelating ligands such as diamines, amino acids, phenanthroline derivatives, and β -diketones to perform coupling reactions under milder conditions while achieving enhanced yields.^{3,7,21} Moreover, the employment of auxiliary ligands not only accelerates the reactions but also affords more reproducible and safer reactions in terms of operating conditions and residual toxicity.

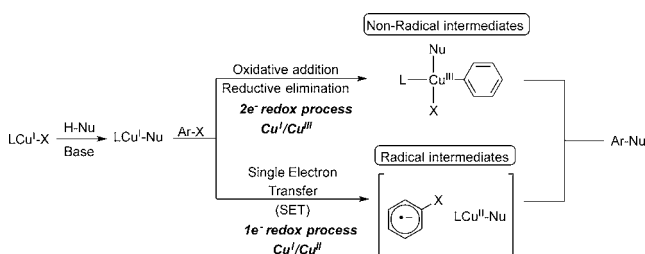
In thermal-based Ullmann couplings the detection of intermediate species after the activation of the aryl halide, which is usually rate-limiting, is very limited, and most mechanistic proposals are derived from kinetic and computational studies.^{22–26} The most invoked mechanism for Ullmann couplings is based on two-electron redox processes via a Cu^{I} / Cu^{III} catalytic cycle,⁶ although some computational reports point toward one-electron redox processes through radical intermediates (Scheme 2)²² and some MS studies suggest competing mechanisms.^{27–30} On the other hand, Peters, Fu, and co-workers recently reported a photoinduced, nonthermal process involving a copper–carbazole complex for promoting the radical-based C–N bond forming reaction.^{31–36}

The ligand choice could play a determinant role in the selectivity of the arylation reaction as well as in the operative mechanism for such a transformation. Indeed, Buchwald and

Received: May 3, 2016

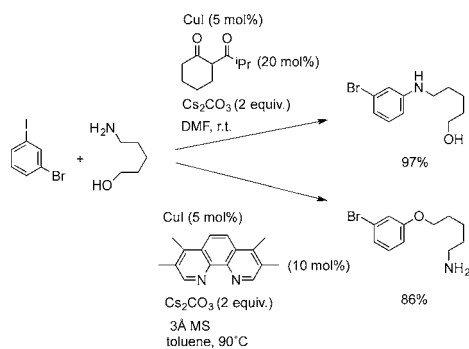
Published: June 1, 2016

Scheme 2. Two Main Mechanistic Proposals for Ullmann-Type Couplings



co-workers reported the first example of chemoselective arylation of amino alcohols by using different auxiliary ligands.^{37,38} While the β -diketone ligand promoted the formation of N-arylated product in DMF at room temperature, tetramethylphenanthroline ligand promoted selective O-arylation in toluene at 90 °C (Scheme 3).

Scheme 3. First Selective Ligand-Dependent Cu-Catalyzed Arylation of a Bifunctional Nucleophile Reported by Buchwald



Bearing in mind the importance of achieving selective reactivity among functional groups in current synthetic strategies, in this work we employed different well-known and available ligands coordinating to Cu^I with the aim of diverting the selective arylation of different nucleophiles at will. As a result, herein we disclose a useful toolkit of Cu-based catalytic systems for the highly chemoselective arylation of a wide range of nucleophiles in competitive reactions using aryl iodides and bromides.

RESULTS AND DISCUSSION

We recently described a practical ligand-free protocol for the N- and O-arylation of a wide range of amides, alcohols, and amines under common optimized reaction conditions.²⁰ Based on that experimental protocol and employing the base/solvent combination of K₃PO₄/DMSO with 10 mol % of CuI, in this work we explored the arylation of N- and O-nucleophiles using N,N-, N,O-, or O,O-bidentate or N,N,N-tridentate ligands (L₁–L₁₀) with aryl halides under mild conditions (Figure 1).^{3,7} The K₃PO₄ base is substituted in selected cases by CsF or K₂CO₃ to further improve the yield of the desired products. We used this common experimental protocol for all kinds of nucleophiles to visualize the impact of the ligand nature.

First, iodobenzene (1) was subjected to N-arylation with different primary and secondary amides (2) (see Scheme 4 and Table S1). Aromatic primary amides (2a and 2f; Table S1, entries 1 and 6) rendered good-to-excellent yields using di- or

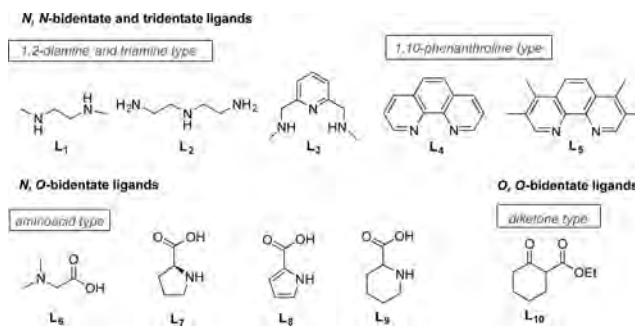
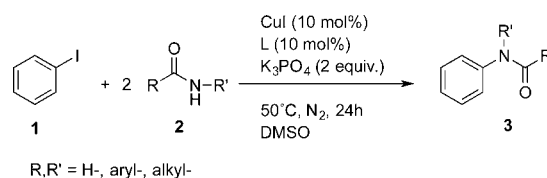


Figure 1. Bidentate and tridentate auxiliary ligands used in this work.

Scheme 4. Screening of Amides for N-Arylation with Iodobenzene

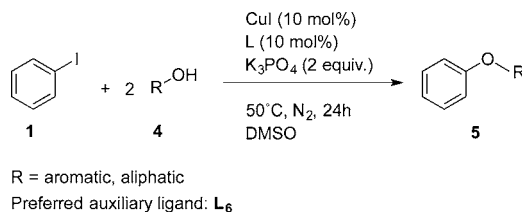


Preferred Auxiliary Ligands: L₁, L₂, L₃ (for primary aromatic amides)
L₇ (for primary aliphatic amides)
L₄/130 °C (for secondary amides)

triamine ligands (L₁–L₃). The use of *L*-proline (L₇) was found to be the most suitable ligand for the arylation of the primary aliphatic amide 2g in excellent yield at 80 °C (Table S1, entry 7). Due to the low reactivity of secondary amides, the use of 1,10-phenanthroline (L₄) as a ligand at 130 °C was necessary to reach good performance in the arylation of aliphatic secondary amides (3h and 3j; Table S1, entries 8 and 10). However, an exception was found for pyrrolidin-2-one (2b), a cyclic secondary amide, which afforded the N-arylated product 3b in 80–91% using di- or triamine ligands (L₁–L₃) or 1,10-phenanthroline (L₄) under mild conditions (Table S1, entry 2).

Next, we explored the arylation of alcohols under the same reaction conditions (Scheme 5 and Table S2). As expected

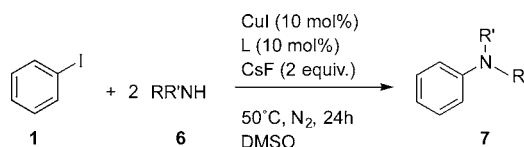
Scheme 5. Mild O-Arylation of Alcohols with Iodobenzene



from previous studies, the O-arylation of phenols using dimethylglycine (L₆) as a Cu-chelating ligand gave excellent coupling yields (82–97% 5a, 5b, 5c, 5d; Table S2, entries 1–4).^{39,40} Phenols with electron-withdrawing groups and aliphatic alcohols gave poor yields irrespective of the auxiliary ligand used.

After screening the O-arylation of different alcohols, we were also interested in exploring the reactivity of amines as nucleophiles (Scheme 6 and Table S3). In line with the literature, the N,O-bidentate ligands such as proline (L₇) or pyrrole-2-carboxylic acid (L₈) were found to be the most suitable chelating moieties when the arylation of amines is targeted.^{7,40–42,7,39–41} In addition, the employment of CsF as a

Scheme 6. Mild N-Arylation of Amines with Iodobenzene



R, R' = H-, aromatic, aliphatic

Preferred auxiliary ligands: L₇, L₈

base instead of K₃PO₄ rendered better results for these coupling reactions. In particular, the use of L₈ for the N-arylation of aromatic amines afforded moderate to good yields (62–76%, 7a and 7c; Table S3, entries 1 and 3), while the N-arylated *p*-nitro-substituted aniline (7b) was obtained only in 22% yield (Table S3, entry 2). On the contrary, the N-arylation of primary aliphatic amines (6d and 6e) was very effective using ligand L₇, and excellent yields and conversions were observed (89–95%; Table S3, entries 4 and 5). Regarding secondary aliphatic amines, cyclic piperidine (6g) afforded the desired product 7g in excellent yield (86% yield, Table S3, entry 7), while under the same reaction conditions, a very poor yield of the arylated product 7f was observed (Table S3, entry 6). In contrast, conjugated N-heterocyclic secondary amine 6h rendered the N-arylated product 7h in excellent yield using L₁ (96%; Table S3, entry 8). In particular, this latter product was also formed in excellent yields and conversions employing other ligands such as L₂, L₃, L₄, or L₆ or even working at rt with L₁.

Eventually, we also examined the arylation of different N- and O-nucleophiles employing the aryl bromide as a substrate (Table S4). Excellent yields (88–100%) were obtained for aromatic alcohols (5a and 5c; Table S4, entries 6 and 7), and moderate-to-good yields (50–80%) were found for aromatic and aliphatic amines (7a, 7c and 7d; Table S4, entries 8–10). Nevertheless, very poor reactivity was observed for the arylation of amides and only the use of pyrrole derivative L₈ afforded the arylation of the cyclic amide pyrrolidin-2-one (2b) in 26% yield (Table S4, entries 1–5).

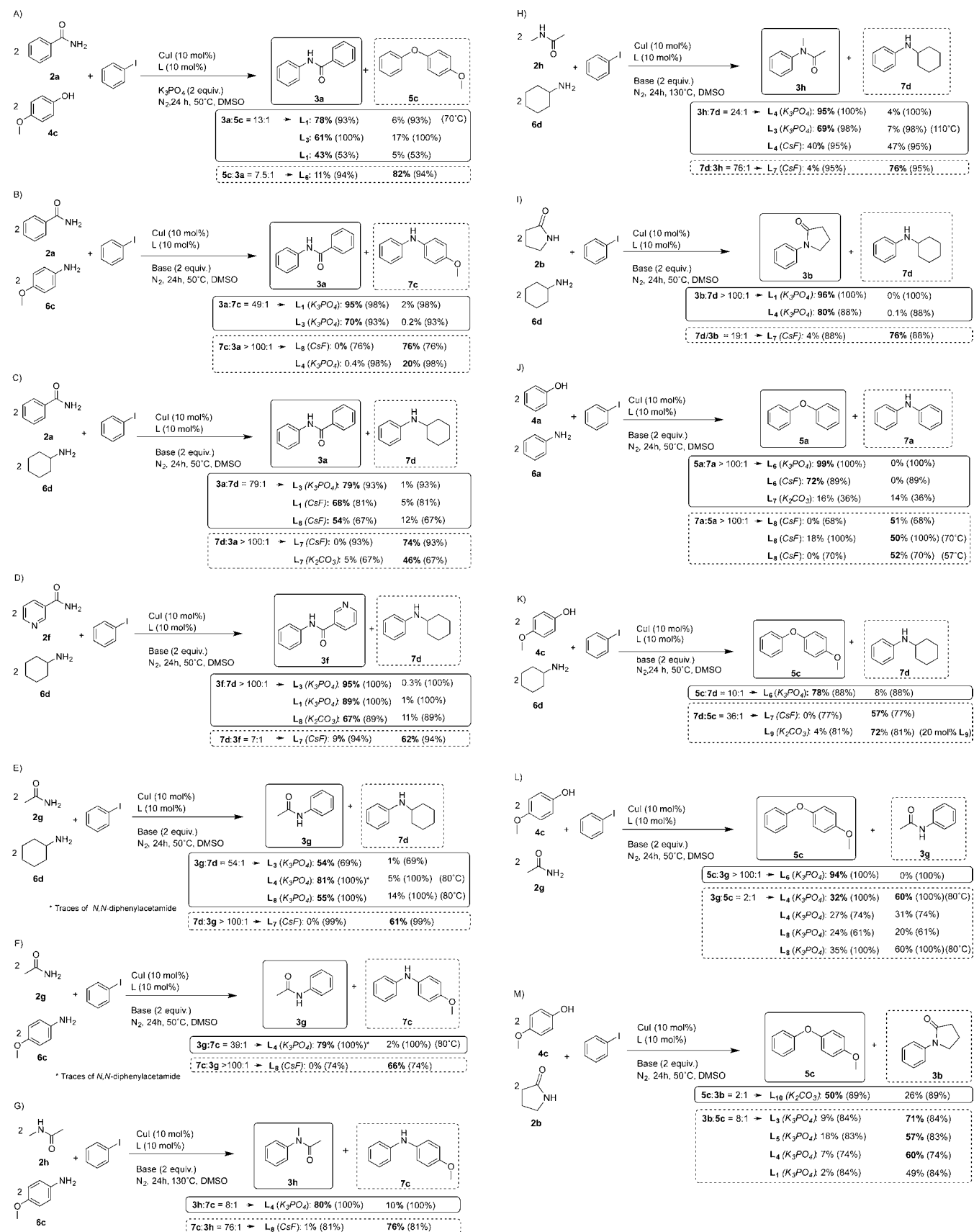
Ligand-Dependent Selectivities in Competition Reactions Using Iodobenzene. Considering the trends observed from the different ligands previously tested, we focused our attention on the study of the selective arylation of a wide-range of nucleophiles in competition reactions under mild conditions (50 °C). Thus, we performed competitive experiments combining amides, amines, and phenols under standard conditions (1 equiv of iodobenzene, 2 equiv of each nucleophile), aiming to find out the most suitable ligand for the arylation of each nucleophile in high selectivity and yield (Scheme 7).

In general trends, we have found that the arylation of aromatic amides is favored over that of phenols and amines when tridentate N-based auxiliary ligands and mild temperatures are used, with L₁ and L₃ being the best ones (Scheme 7, A–D). Owing to its well-known poor reactivity, the arylation of noncyclic aliphatic amides requires higher temperatures and is favored in front of the arylation of amines when L₄ is used (Scheme 7, E–H). Moreover, noncyclic primary aliphatic amides can be slightly favored in front of the arylation of phenols with L₄ (Scheme 7, L), but noncyclic secondary aliphatic amides cannot compete with phenols (Scheme 8, C). On the other hand, the arylation of cyclic aliphatic amides is sharply chemoselective in front of aliphatic amines, phenols and

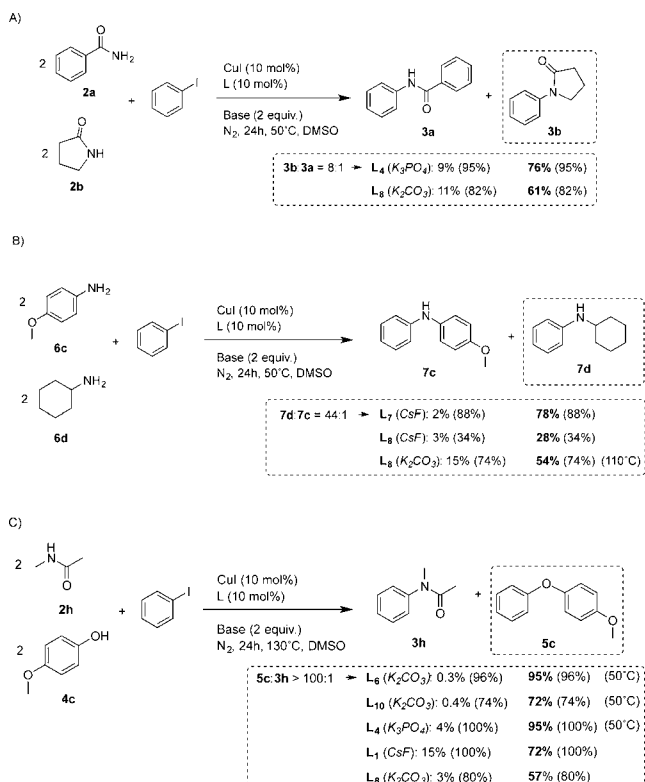
aromatic amides when L₁ or L₄ are used (Scheme 7, I, M, and Scheme 8, A). Moreover, the arylation of phenols is especially favored in competition with amines and amides when L₆ is used (Scheme 7, A, J–M and Scheme S1). Finally, anilines are arylated selectively before phenols and amides (Scheme 7, B, F, G, J) when L₈ is used. The product ratios are in general higher than 7 and in many cases above 20, showing an orthogonal selectivity in most of the competitions explored. The nonarylated nucleophile remained unconverted and could be recovered at the end of the reaction. Due to the low reactivity of aliphatic alcohols, no competition studies have been undertaken since those nucleophiles are clearly more challenging than the studied above (entries 6 and 7, Table S2).

Some nucleophiles present a strong preference toward arylation irrespective of the competing nucleophile or the auxiliary ligand used. Specifically, only minor changes in the selectivity could be achieved when the same family of nucleophiles is used, for example, the competitive reaction between two types of amides, benzamide (2a) and the cyclic amide pyrrolidin-2-one (2b) (Scheme 8, A). In this reaction, we were only able to set out conditions to render the N-arylation of 2b in excellent yield and conversion using L₄ at 50 °C (76% 3b; 3b/3a ratio = 8). Despite performing the reaction with other type of ligands such as L₈, a very low yield of 3a was obtained. Similarly, a competitive reaction of two types of amines (6c and 6d) afforded the N-arylated cyclohexylamine 7d as the major product in all cases tested (Scheme 8, B). Best results were observed by submitting proline ligand L₇ as a ligand (78% 7d; 7d/7c ratio = 44). Along the same line, when the competition is performed between N-methylacetamide (2h) and *p*-methoxyphenol (4c) (Scheme 8, C, and Scheme S1), the O-arylated 5c was successfully formed employing the glycine derivative L₆ and K₂CO₃ in high yield and conversion at 50 °C (98% 5c; 5c/3h ratio >100). Additionally, the O,O-bidentate ligand L₁₀ also led to the selective formation of 5c under the same conditions. However, we were unable to find the appropriate conditions to tilt the balance in favor of the arylation of the secondary amide 2h. Despite using the most suitable ligand for the formation of 3h (L₄), we found a very high selectivity for the O-arylated coupling product in all cases tested. The use of L₁ with K₃PO₄ or CsF or L₈ with K₂CO₃ at 50 °C significantly reduced the yield of the O-arylated product (37% and 57% yield, respectively); however, the reaction likewise proceeded in low yields for the formation N-arylacetamide 3h. We rationalize that the facile arylation of phenol and the high temperatures that are required for achieving reactivity toward secondary amides prevent us from establishing suitable conditions for such competition reactions.

Ligand-Dependent Selectivities in Competition Reactions Using Para-Substituted Iodobenzenes. Additionally, in order to broaden the aryl iodide scope, we checked the effect of electron-donating and electron-withdrawing substituents at the *para* position. Thus, *p*-iodotoluene and *p*-nitroiodobenzene were selected as aryl halides in competition reactions analogous to Scheme 7, C (Scheme S2 and S3 in the SI). Regarding *p*-iodotoluene (Scheme S2), the arylation of benzamide 2a was significantly suppressed using pincer ligand L₃. On the contrary, the arylation of the same nucleophile using pyrrole derivative L₈ was successfully improved up to 92% yield of 3n as a single arylated product in complete conversion (3n/7o ratio = 92). On the other hand, the formation of the coupling product 7o was also a bit suppressed when proline L₇ was used; however, it was effectively formed as a unique

Scheme 7. Competition Reactions among Nucleophiles Using Iodobenzene with a Sharp Switch of Chemoselectivity^a^aConversions are given in parentheses; standard experimental conditions used.

Scheme 8. Competition Reactions among Nucleophiles with Strong Arylation Preference for One Nucleophile Irrespective of the Auxiliary Ligand Used^a

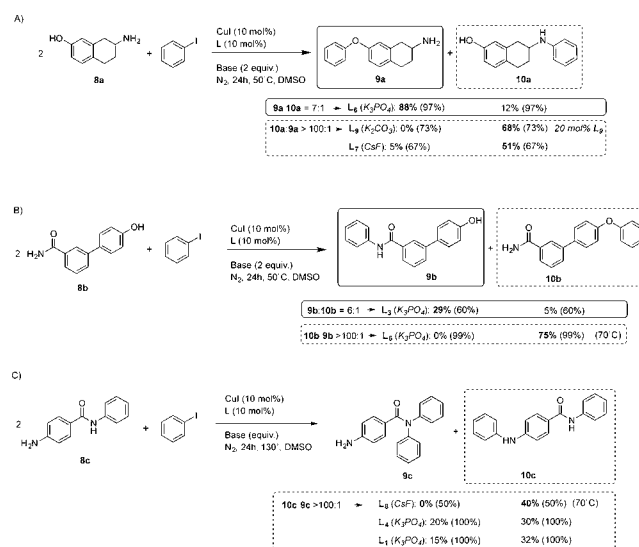


^aConversions are given in parentheses; standard experimental conditions used.

product (55% **7o**, **7o/3n** ratio >100). When *p*-nitroiodobenzene was used as a substrate (Scheme S3), we observed a reactivity similar to that of the iodobenzene. It is noteworthy that pincer-type ligand L₃ improved the formation of **3l**, which was obtained almost as a single product in good yield (64% **3l**, **3l/7m** ratio = 32). Additionally, the employment of proline L₇ also gave rise to the coupling product **7m** as single product (66% **7m**, **7m/3l** ratio = 66). Therefore, both electron-rich and electron-deficient aryl iodides underwent arylation with excellent selectivities.

Ligand-Dependent Selectivities in Competition Reactions Using Bifunctional Nucleophiles and Iodobenzene. To further probe the orthogonality of our Cu-based catalytic systems, we next evaluated the selective arylation of different bifunctional nucleophiles (**8a**, **8b**, and **8c**) (Scheme 9). First, the aminophenol **8a** could be selectively O-arylated with dimethylglycine L₆ (Scheme 9, A) to give the coupling product **9a** in excellent yield and with high chemoselectivity (88% **9a**; **9a/10a** ratio = 7). On the other hand, the N-arylation of **8a** was highly favored when L₇ was used as a ligand and CsF as a base (**10a**, 51%). Very notably, running the same reaction with N,O-bidentate ligand L₉ (20 mol %) in combination with K₂CO₃ improved the formation of **10a** as a unique product up to 68% yield (**10a/9a** ratio >100). We also succeeded in the competition reaction between the bifunctional nucleophile **8b** (bearing aromatic amide and phenol functional groups) and iodobenzene (Scheme 9, B). Not surprisingly, the presence of the dimethylglycine L₆ at 70 °C led to the O-arylation of **8b**, yielding **10b** as a sole coupling product (75% **10b**; **10b/9b**

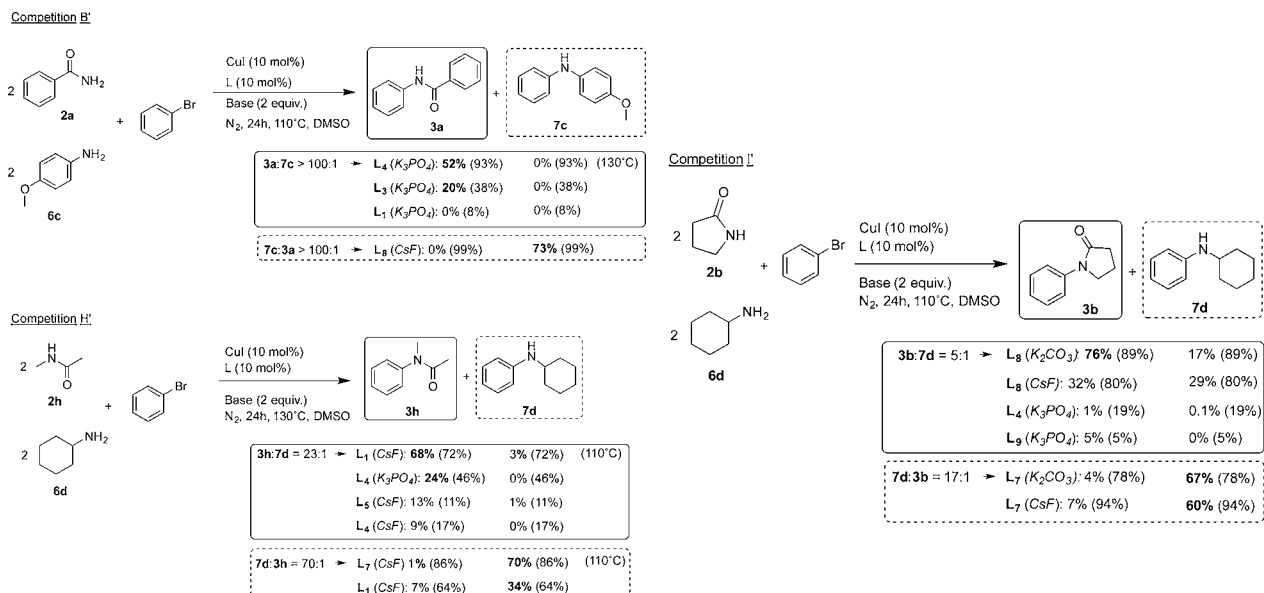
Scheme 9. Competition Reactions Using Bifunctional Nucleophiles **8a–8c^a**



^aConversions are given in parentheses; standard experimental conditions used.

ratio >100). On the contrary, this trend successfully switched to the formation of the N-arylated product **9b** in the presence of L₃, even though the yield was modest (29% **9b**; **9b/10b** ratio = 6). In the arylation reaction of 4-amino-*N*-phenylbenzamide (**8c**) with iodobenzene (Scheme 9, C), only the N-arylation of the amino group was observed as the major product, irrespective of the auxiliary ligand used. Compound **10c** was obtained as a single product in moderate yield and high selectivity when the pyrrole derivative ligand L₈ using CsF as a base (40% **10c**; **10c/9c** ratio >100) was used. Presumably, the arylation of the secondary amide was hampered by steric effects, and even when high temperatures (130 °C) together with L₁ or L₄ as ligands were used, the formation of **10c** was unavoidable in both cases tested.

Ligand-Dependent Selectivities in Competition Reactions Using Bromobenzene. With these good results in hand, we decided to conduct most of the competition reactions described above using bromobenzene. Because of the low reactivity of bromobenzene, reactions were undertaken at 110 or 130 °C. Among them and as shown in Scheme 10, competitions B', H', and I' were those in which excellent selectivities and yields were observed. First, when the competitive reaction was run between benzamide (**2a**) and anisidine (**6c**) (Scheme 10, competition B', equivalent to Scheme 7, B), we were very pleased to observe the single formation of N-arylamide **3a** in good yield using phenanthroline ligand L₄ at 130 °C (52% **3a**; **3a/7c** ratio >100). Remarkably, the selectivity was effectively turned to the unique arylation of **6c** in excellent yield when the pyrrole derivative L₈ (73% **7c**; **7c/3a** ratio >100) was employed. On the other hand, when the competitive reaction was run between N-methylacetamide (**2h**) and cyclohexylamine (**6d**) (Scheme 10, competition H', equivalent to Scheme 7, H), the presence of DMEDA (L₁) at 110 °C yielded **3h** almost exclusively in remarkable yield and selectivity (68%, **3h/7d** ratio = 23). Surprisingly, all of the attempts using phenanthroline-type ligands (L₄ and L₅) aiming to promote the same coupling product failed. However, using proline as chelating ligand (L₇)

Scheme 10. Competition Reactions among Nucleophiles Using Bromobenzene with a Sharp Switch of Chemoselectivity^a

^aConversions are given in parentheses.

at 110 °C successfully led to the almost exclusive formation of **7d** in 70% yield (**7d/3h** ratio = 70). In line with these results, we observed similar reactivity when facing the cyclic amide pyrrolidin-2-one (**2b**) and cyclohexylamine (**6d**) (Scheme 10, competition I', equivalent to Scheme 7, I). While **L₇** provided the arylation of the aliphatic amine to yield **7d** in good yields (67% **7d**; **7d/3b** ratio = 17), the pyrrole derivative **L₈** using K₂CO₃ as a base favored the arylation of the cyclic amide in good yield and moderate selectivity (76% **3b**, **3b/7d** ratio = 5). We noticed an important base effect in the latter case, since the use of CsF as a base instead of K₂CO₃ prevented the chemoselectivity between both nucleophiles. Furthermore, competitive reactions A', C', D', G', and J' and bifunctional **8a** employing bromobenzene also led to the selective arylation one of the nucleophiles, although most of them were in lower yields and moderate to good selectivities (Scheme S4, SI). Some unexpected effects were found, such as the fact that all reactions combining bromobenzene and aromatic amides **2a** and **2f** with **L₁** ligand completely failed in any competition tested (Scheme 10, competition B', and Scheme S4, competitions A', C', and D'). Moreover, 1,10-phenanthroline (**L₄**) showed a chemoselective behavior with bromobenzene different from that with iodobenzene when facing primary amides and aliphatic or aromatic amines with other nucleophiles (competitions B/B' and H/H', Schemes 7 and 10).

Ligand-Dependent Selectivities in Competition Reactions Using Chlorobenzene. Several reactions were also attempted using chlorobenzene as arylating agent and several nucleophiles and auxiliary ligands; however, the reactivity was almost suppressed for all nucleophiles tested at 130 °C (Scheme S5, SI).

Practical Orthogonal Nucleophile Discrimination Summary. Table 1 summarizes the most important results of all tested competition reactions, and the best conditions found to achieve the arylation of a given nucleophile in the presence of another are highlighted. In general, highly selective arylation of any nucleophile can be performed under mild

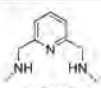
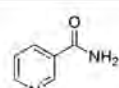
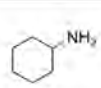
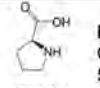
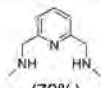
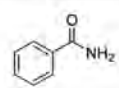
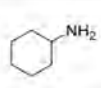
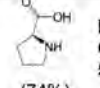
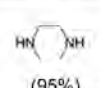
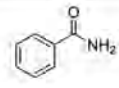
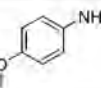
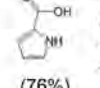
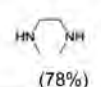
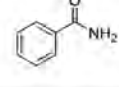
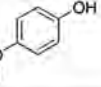
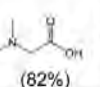
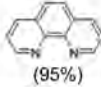
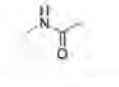
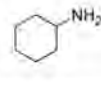
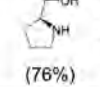
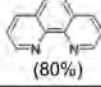
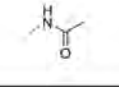
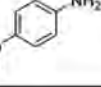
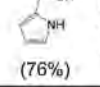
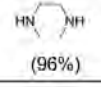
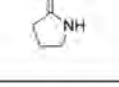
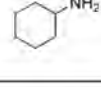
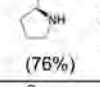
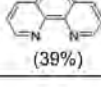
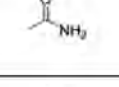
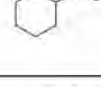
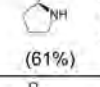
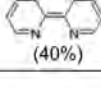
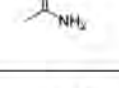
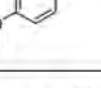
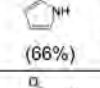
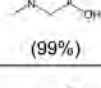
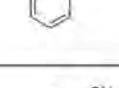
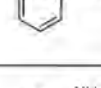
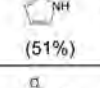
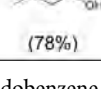
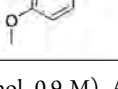
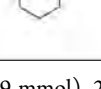
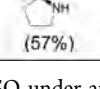
conditions in the presence of another nucleophile, provided careful selection of the auxiliary ligand and experimental conditions is made. Therefore, Table 1 is a practical recipe for mild and chemoselective C–O and C–N Ullmann-type couplings. Note that this high selectivity has also been successfully translated into bifunctional substrates (Scheme 10). However, the limitations of the methodology in terms of selectivity are shown in Table 2. The nonpreferred nucleophile in these competitions is arylated as a mixture with the arylation of the preferred nucleophile, so the corresponding reaction conditions are not included in Table 2.

Finally, to gain insight into the mechanism of the cross-coupling reactions with different auxiliary ligands, we have selected the most successful combinations of nucleophiles and ligands and used the radical clock 1-allyloxy-2-iodobenzene (**rc**) as substrate in the coupling reactions (Scheme 11). In all reactions, a significant amount of **rc-H** was observed, suggesting a protodecupration side reaction as previously observed by Cohen,⁴³ Hartwig,²⁵ and in the reactivity of well-defined model aryl-Cu^{III} complexes.⁴⁴ No traces were found of the cyclized coupling product, thus pointing toward a prototypical Cu^I/Cu^{III} mechanism for thermal-based Ullmann couplings and discarding a radical pathway. Given the fact that protodecupration product **rc-H** was found in important amounts when **rc** was used as a substrate, we wondered if this mechanism has also some contribution when iodobenzene is used. If so, benzene should be found as the product of a putative protodecupration. As suspected, low but significant amounts of benzene (from 4 to 8%) were found in several coupling reactions of anilines **6a**, **6b**, **6c**, and methylacetamide **2h**, indicating that the protodecupration pathway is generally spread as a side reaction in Ullmann couplings (see Scheme S6).

CONCLUSION

In light of the tremendous interest in finding a practical Cu-catalyzed methodology that allows orthogonal discrimination among N- or O-based functional groups, we have demonstrated that this is now possible with multiple combinations of

Table 1. Optimized Conditions for Ligand-Dependent Arylation of Nucleophiles (A or B) with Iodobenzene in Competition Reactions with Orthogonal Selectivity^a

Conditions for A arylation	A	B	Conditions for B arylation
L_3 K_3PO_4 50°C  (95%)			L_7 CsF 50°C  (62%)
L_3 K_3PO_4 50°C  (79%)			L_7 CsF 50°C  (74%)
L_1 K_3PO_4 50°C  (95%)			L_8 CsF 50°C  (76%)
L_1 K_3PO_4 50°C  (78%)			L_6 K_3PO_4 50°C  (82%)
L_4 K_3PO_4 50°C  (95%)			L_7 CsF 50°C  (76%)
L_4 K_3PO_4 50°C  (80%)			L_8 CsF 50°C  (76%)
L_1 K_3PO_4 50°C  (96%)			L_7 CsF 50°C  (76%)
L_4 K_3PO_4 80°C  (39%)			L_7 CsF 50°C  (61%)
L_4 K_3PO_4 80°C  (40%)			L_8 CsF 50°C  (66%)
L_6 K_3PO_4 50°C  (99%)			L_8 CsF 50°C  (51%)
L_6 K_3PO_4 50°C  (78%)			L_7 CsF 50°C  (57%)

^aStandard reaction conditions: iodobenzene (0.88 mmol, 0.9 M), A and B (1.79 mmol), 24 h, DMSO under an inert atmosphere (yields given in parentheses).

nucleophiles using a common experimental methodology and a preferred auxiliary ligand for each nucleophile. The exact role of each auxiliary ligand in switching the selectivity requires already ongoing in-depth computational studies. So far, the precise, simple methodologies to be used for the arylation of any of the nucleophiles tested should be a precious practical guide in organic synthesis laboratories. Indeed, by means of using a radical clock substrate (rc), no signs of radical-mediated mechanism were found in any of the coupling reactions tested in this work, reinforcing the occurrence of a nonradical mechanism in the thermal-based copper-catalyzed cross-coupling reactions.

EXPERIMENTAL SECTION

General Methods. The reagents and solvents used were commercially available unless indicated otherwise. Solvents were purchased and were purified and dried by passing them through an activated alumina purification system. The preparation and handling of air-sensitive materials were performed in a N_2 drybox with O_2 and H_2O concentrations of <1 ppm. 4'-Hydroxy(1,1'-biphenyl)-3-carboxamide (8b) was synthesized following the published procedures.⁴⁵

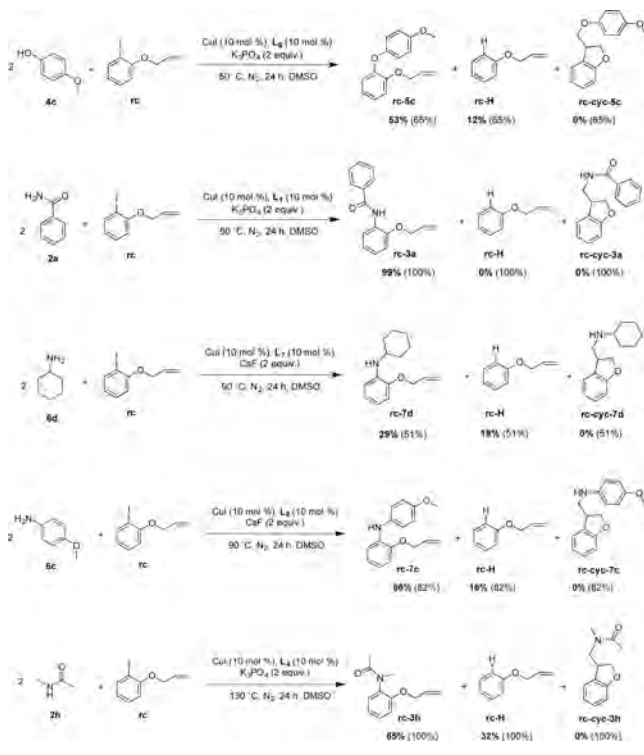
General Procedure for Catalytic Experiments. A vial was loaded with the base (1.8 mmol), the solid nucleophile (1.8 mmol), and the corresponding auxiliary ligand (10 mol %). Then, in an inert-atmosphere glovebox, copper(I) (10 mol %) in DMSO and the aryl iodide (0.9 mmol) were added. Liquid nucleophiles were added after

Table 2. Optimized Conditions for Ligand-Dependent Arylation of Nucleophiles with Iodobenzene in Competitive Reactions with High Selectivity for One of the Competing Nucleophiles (Column A)^a

Conditions for A arylation	A	B
L_6 K_3PO_4 50 °C 		
L_6 K_3PO_4 50 °C 		
L_4 K_3PO_4 50 °C 		
L_3 K_3PO_4 50 °C 		
L_7 CsF 50 °C 		

^aStandard reaction conditions: iodobenzene (0.88 mmol, 0.9 M), A and B (1.79 mmol), 24 h, DMSO under an inert atmosphere (yields are given in parentheses).

Scheme 11. Selected Coupling Reactions Using Radical Clock *rc* as Substrate



the aryl iodide. The vial was sealed, and the reaction mixture was kept under an inert atmosphere and placed in a preheated oil bath at the required temperature. After the reaction mixture was stirred for 24 h,

1,3,5-trimethoxybenzene (200 μ L, 1.5 M in DMSO) as internal standard was added. Subsequently, the reaction was quenched by the addition of AcOEt (5 mL). The workup consisted of the filtration of 400 μ L of the crude product through silica gel using AcOEt as eluent. All samples were analyzed by gas chromatography. The GC yields were obtained through calibration curves obtained with authentic sample of all products with 1,3,5-trimethoxybenzene as an internal standard.

Benzanilide (3a).^{46,47} 1H NMR (300 MHz, DMSO- d_6 , 25 °C) δ (ppm): 7.17–7.23 (m, 1H), 7.43–7.48 (m, 2H), 7.60–7.72 (m, 3H), 7.86–7.89 (m, 2H), 8.03–8.07 (m, 2H), 10.34 (s, 1H, NH). $^{13}C\{^1H\}$ NMR (75 MHz, DMSO- d_6 , 25 °C) δ (ppm): 120.3, 123.7, 127.6, 128.4, 128.6, 131.6, 134.9, 139.2, 165.5. HRMS (ESI-TOF (m/z)): calcd for $C_{13}H_{11}NONa$ 220.0733, found 220.0725, calcd for $(C_{13}H_{11}NO)_2Na$ 417.1573, found 417.1571.

1-Phenyl-2-pyrrolidone (3b).^{46,47} 1H NMR (300 MHz, $CDCl_3$, 25 °C) δ (ppm): 2.14–2.22 (m, 2H), 2.59–2.65 (m, 2H), 3.87 (t, 2H, $^2J_{HH} = 6.9$ Hz), 7.59–7.63 (m, 2H), 7.34–7.40 (m, 2H), 7.12–7.17 (m, 1H). $^{13}C\{^1H\}$ NMR (75 MHz, $CDCl_3$, 25 °C) δ (ppm): 18.0, 32.7, 48.8, 119.9, 124.5, 128.8, 139.4, 174.2. HRMS (ESI-TOF (m/z)): calcd for $C_{10}H_{11}NONa$ 184.0733, found 184.0720, calcd for $(C_{10}H_{11}NO)_2Na$ 345.1573, found 345.1559.

N-phenoxindole (3c).⁴⁸ 1H NMR (300 MHz, DMSO- d_6 , 25 °C) δ (ppm): 3.86 (s, 2H), 6.79–6.81 (m, 1H), 7.16 (td, 1H, $^2J_{HH} = 7.43$ Hz, $^4J_{HH} = 1$ Hz), 7.31 (td, 1H, $^2J_{HH} = 7.8$ Hz, $^4J_{HH} = 1.5$ Hz), 7.44–7.46 (m, 1H), 7.50–7.58 (m, 3H), 7.64–7.70 (m, 2H). $^{13}C\{^1H\}$ NMR (75 MHz, DMSO- d_6 , 25 °C) δ (ppm): 35.9, 108.6, 122.4, 124.7, 124.8, 126.8, 127.5, 127.9, 129.6, 134.5, 144.8, 173.9. HRMS (ESI-TOF (m/z)): calcd for $C_{14}H_{11}NONa$ 232.0733, found 232.0726, calcd for $(C_{14}H_{11}NO)_2Na$ 441.1573, found 441.1577.

Salicylanilide (3d).⁴⁷ 1H NMR (400 MHz, DMSO- d_6 , 25 °C) δ (ppm): 7.04–7.09 (m, 2H), 7.22–7.26 (m, 1H), 7.45–7.50 (m, 2H), 7.52–7.56 (m, 1H), 7.79–7.82 (m, 2H), 8.06 (dd, 1H, $^2J_{HH} = 7.8$ Hz, $^4J_{HH} = 1.4$ Hz), 10.50 (s, 1H, NH), 11.90 (br s, 1H, OH). $^{13}C\{^1H\}$ NMR (100 MHz, DMSO- d_6 , 25 °C) δ (ppm): 117.2, 117.5, 119.0, 120.9, 124.2, 128.7, 129.0, 133.6, 138.1, 158.5, 166.6. HRMS (ESI-TOF (m/z)): calcd for $C_{13}H_{11}NO_2Na$ 236.0682, found 236.0679, calcd for $(C_{13}H_{11}NO_2)_2Na$ 419.1472, found 419.1471.

N-phenyl-4-hydroxybenzamide (3e).⁴⁷ 1H NMR (300 MHz, DMSO- d_6 , 25 °C) δ (ppm): 6.93–6.98 (m, 2H), 7.13–7.19 (m, 1H), 7.40–7.46 (m, 2H), 7.82–7.86 (m, 2H), 7.92–7.97 (m, 2H), 10.07 (s, 1H, NH). $^{13}C\{^1H\}$ NMR (75 MHz, DMSO- d_6 , 25 °C) δ (ppm): 115.3, 120.6, 123.6, 125.7, 128.9, 130.1, 139.9, 160.9, 165.5. HRMS (ESI-TOF (m/z)): calcd for $C_{13}H_{11}NO_2Na$ 236.0682, found 236.0679, calcd for $(C_{13}H_{11}NO_2)_2Na$ 449.1472, found 449.1479.

Nicotinilide (3f).⁴⁷ 1H NMR (300 MHz, DMSO- d_6 , 25 °C) δ (ppm): 7.20–7.26 (m, 1H), 7.44–7.50 (m, 2H), 7.67 (ddd, 1H, $^2J_{HH} = 7.8$ Hz, $^3J_{HH} = 4.8$ Hz, $^4J_{HH} = 0.9$ Hz), 7.85–7.89 (m, 2H), 8.39 (ddd, 1H, $^2J_{HH} = 8.03$ Hz, $^3J_{HH} = 2.33$ Hz, $^4J_{HH} = 1.73$ Hz), 8.86 (dd, 1H, $^3J_{HH} = 4.8$ Hz, $^4J_{HH} = 1.8$ Hz), 9.20 (dd, 1H, $^3J_{HH} = 2.25$ Hz, $^4J_{HH} = 0.75$ Hz), 10.54 (s, 1H, NH). $^{13}C\{^1H\}$ NMR (75 MHz, DMSO- d_6 , 25 °C) δ (ppm): 120.4, 123.5, 124.0, 128.7, 130.6, 135.5, 138.8, 148.7, 152.1, 164.1. HRMS (ESI-TOF (m/z)): calcd for $C_{12}H_{10}N_2ONa$ 221.0685, found 221.0674, calcd for $(C_{12}H_{10}N_2O)_2Na$ 419.1478, found 419.1464.

Acetanilide (3g).^{46,47} 1H NMR (300 MHz, DMSO- d_6 , 25 °C) δ (ppm): 2.13 (s, 3H), 7.08–7.14 (m, 1H), 7.34–7.41 (m, 2H), 7.65–7.68 (m, 2H), 10.01 (s, 1H, NH). $^{13}C\{^1H\}$ NMR (75 MHz, DMSO- d_6 , 25 °C) δ (ppm): 29.0, 118.9, 123.0, 128.7, 139.3, 168.3. HRMS (ESI-TOF (m/z)): calcd for C_9H_9NONa 158.0576, found 158.0566.

N-Methylacetanilide (3h).⁴⁹ 1H NMR (300 MHz, $CDCl_3$, 25 °C) δ (ppm): 1.87 (s, 3H), 3.27 (s, 3H), 7.18–7.21 (m, 2H), 7.31–7.36 (m, 1H), 7.39–7.45 (m, 2H). $^{13}C\{^1H\}$ NMR (75 MHz, $CDCl_3$, 25 °C) δ (ppm): 22.4, 37.2, 127.1, 127.7, 129.7, 144.6, 170.6. HRMS (ESI-TOF (m/z)): calcd for $C_9H_{11}NONa$ 172.0733, found 172.0722, calcd for $(C_9H_{11}NO)_2Na$ 321.1573, found 321.1572.

N,N-Diphenylbenzamide (3i).⁵⁰ 1H NMR (300 MHz, $CDCl_3$, 25 °C) δ (ppm): 7.14–7.32 (m, 13H), 7.44–7.47 (m, 2H). $^{13}C\{^1H\}$ NMR (75 MHz, $CDCl_3$, 25 °C) δ (ppm): 126.6, 127.7, 128.1, 129.4, 129.4, 130.4, 136.3, 144.3. HRMS (ESI-TOF (m/z)): calcd for

$C_{19}H_{16}NO$ 274.1226, found 274.1234, calcd for $C_{19}H_{15}NONa$ 296.1046, found 296.1064, calcd for $(C_{19}H_{13}NO)_2Na$ 569.2199; found 569.2221.

N,N-Ethylphenylacetamide (**3j**).⁵¹ 1H NMR (300 MHz, $CDCl_3$, 25 °C) δ (ppm): 1.10 (t, 3H, $^2J_{HH} = 7.2$ MHz), 1.82 (s, 3H), 3.75 (q, 3H, $^2J_{HH} = 7.2$ MHz), 7.13–7.17 (m, 2H), 7.31–7.45 (m, 3H). $^{13}C\{^1H\}$ NMR (75 MHz, $CDCl_3$, 25 °C) δ (ppm): 13.3, 23.1, 44.1, 128.1, 128.5, 129.9, 143.2, 170.2. HRMS (ESI-TOF (m/z)): calcd for $C_{10}H_{14}NO$ 164.1070, found 164.1067, calcd for $C_{10}H_{13}NONa$ 186.0889, found 186.0889, calcd for $(C_{10}H_{13}NO)_2Na$ 349.1886, found 349.1869.

Diphenyl Ether (**5a**).⁵² 1H NMR (300 MHz, $CDCl_3$, 25 °C) δ (ppm): 7.03–7.07 (m, 4H), 7.10–7.16 (m, 2H), 7.33–7.40 (m, 4H). $^{13}C\{^1H\}$ NMR (75 MHz, $CDCl_3$, 25 °C) δ (ppm): 119.2, 123.5, 130.1, 157.6. GCMS: t_R 9.220. MS ($C_{12}H_{10}O$): 170.0.

1-Methyl-4-phenoxybenzene (**5b**).⁵² 1H NMR (400 MHz, $CDCl_3$, 25 °C) δ (ppm): 2.40 (s, 3H), 6.97–6.99 (m, 2H), 7.04–7.08 (m, 2H), 7.10–7.15 (m, 1H), 7.18–7.21 (m, 2H), 7.35–7.39 (m, 2H). $^{13}C\{^1H\}$ NMR (100 MHz, $CDCl_3$, 25 °C) δ (ppm): 20.9, 118.5, 119.3, 122.9, 129.8, 130.5, 133.1, 154.9, 158.0. GCMS: t_R 10.584. MS ($C_{12}H_{12}O$): 184.0.

1-Methoxy-4-phenoxybenzene (**5c**).⁵³ 1H NMR (400 MHz, $CDCl_3$, 25 °C) δ (ppm): 3.81 (s, 3H), 6.87–6.91 (m, 2H), 6.93–7.01 (m, 4H), 7.05 (t, 1H, $J = 7.4$ Hz), 7.28–7.33 (m, 2H). $^{13}C\{^1H\}$ NMR (100 MHz, $CDCl_3$, 25 °C) δ (ppm): 55.9, 115.1, 117.8, 121.0, 122.6, 129.8, 150.3, 156.1, 158.7. GCMS: t_R 12.359. MS ($C_{13}H_{12}O_2$): 200.1.

1,3-Dimethyl-5-phenoxybenzene (**5d**).⁵⁴ 1H NMR (300 MHz, $CDCl_3$, 25 °C) δ (ppm): 2.29 (s, 6H), 6.64–6.65 (m, 2H), 6.76 (sept, 1H, $^4J_{HH} = 0.7$ MHz), 6.99–7.03 (m, 2H), 7.07–7.12 (m, 1H), 7.30–7.37 (m, 2H). $^{13}C\{^1H\}$ NMR (75 MHz, $CDCl_3$, 25 °C) δ (ppm): 21.6, 116.8, 119.1, 123.2, 124.2, 129.9, 139.8, 157.4, 157.7. GCMS: t_R 11.596. MS ($C_{12}H_{12}O$): 198.1.

1-(4-Nitrophenoxy)benzene (**5e**).⁵³ 1H NMR (300 MHz, $CDCl_3$, 25 °C) δ (ppm): 7.00–7.06 (m, 2H), 7.09–7.14 (m, 2H), 7.22–7.32 (m, 1H), 7.43–7.51 (m, 2H), 8.20–8.25 (m, 2H). $^{13}C\{^1H\}$ NMR (75 MHz, $CDCl_3$, 25 °C) δ (ppm): 117.3, 120.8, 125.7, 126.2, 130.6, 154.9, 163.6. GCMS: t_R 14.180. MS ($C_{12}H_{12}O$): 215.0.

Ethoxybenzene (**5f**).⁵⁵ 1H NMR (400 MHz, $CDCl_3$, 25 °C) δ (ppm): 1.4 (t, 3H), 4.02 (q, 2H), 6.87–6.93 (m, 3H), 7.30–7.34 (m, 2H). GCMS: t_R 3.76. MS ($C_8H_{10}O$): 122.0.

N,N-Diphenylamine (**7a**).^{41,56} 1H NMR (400 MHz, $CDCl_3$, 25 °C) δ (ppm): 5.71 (s, 1H, NH), 6.96 (tt, 2H), 7.08–7.12 (m, 4H), 7.27–7.32 (m, 4H). $^{13}C\{^1H\}$ NMR (100 MHz, $CDCl_3$, 25 °C) δ (ppm): 117.9, 121.0, 129.4, 143.2. HRMS (ESI-TOF (m/z)): calcd for $C_{12}H_{12}N$ 170.0964, found 170.0948.

p-Nitro-*N*-phenylaniline (**7b**).⁵⁷ 1H NMR (300 MHz, $CDCl_3$, 25 °C) δ (ppm): 6.33 (s, 1H, NH), 6.92–6.97 (m, 2H), 7.14–7.26 (m, 3H), 7.35–7.42 (m, 2H), 8.09–8.11 (m, 2H). $^{13}C\{^1H\}$ NMR (75 MHz, $DMSO-d_6$, 25 °C) δ (ppm): 113.9, 122.2, 124.9, 126.5, 130.0, 139.7, 140.0, 150.4. HRMS (ESI-TOF (m/z)): calcd for $C_{12}H_{11}N_2O_2$ 215.0815, found 215.0813.

p-Methoxy-*N*-phenylaniline (**7c**).^{57,58} 1H NMR (400 MHz, $CDCl_3$, 25 °C) δ (ppm): 3.80 (s, 3H), 5.46 (s, 1H, NH), 6.81–6.92 (m, 5H), 7.05–7.09 (m, 2H), 7.18–7.23 (m, 2H). $^{13}C\{^1H\}$ NMR (100 MHz, $CDCl_3$, 25 °C) δ (ppm): 55.8, 114.9, 115.9, 119.8, 122.5, 129.5, 139.7, 140.0, 150.4. HRMS (ESI-TOF (m/z)): calcd for $C_{13}H_{14}NO$ 200.1070, found 200.1059.

N-Cyclohexylaniline (**7d**).⁵⁷ 1H NMR (400 MHz, $CDCl_3$, 25 °C) δ (ppm): 1.16–1.50 (m, 5H^{aliphatic}), 1.68–1.75 (m, 1H^{aliphatic}), 1.80–1.85 (m, 2H^{aliphatic}), 2.10–2.14 (m, 2H^{aliphatic}), 3.28–3.35 (m, 1H), 3.55 (m, 1H, NH), 6.63–6.66 (m, 2H), 6.72 (t, 1H, $^2J_{HH} = 7.2$ Hz, $^4J_{HH} = 0.93$ Hz), 7.19–7.24 (m, 2H). $^{13}C\{^1H\}$ NMR (100 MHz, $CDCl_3$, 25 °C) δ (ppm): 25.2, 26.1, 33.7, 51.8, 113.3, 117.0, 129.4, 147.6. HRMS (ESI-TOF (m/z)): calcd for $C_{12}H_{18}N$ 176.1434, found 176.1406, calcd for $C_{12}H_{17}NNa$ 198.1253, found 198.1226.

N-Propylaniline (**7e**).⁵⁹ 1H NMR (400 MHz, $CDCl_3$, 25 °C) δ (ppm): 1.03 (t, 3H, $^2J_{HH} = 7.39$ Hz), 1.67 (q, 2H, $^2J_{HH} = 7.28$ Hz), 3.11 (t, 2H, $^2J_{HH} = 7.01$ Hz), 3.64 (s, 1H, NH), 6.61–6.65 (m, 2H), 6.72 (tt, 1H, $^2J_{HH} = 14.71$ Hz, $^3J_{HH} = 7.24$ Hz, $^4J_{HH} = 1.07$ Hz), 7.17–

7.24 (m, 2H). $^{13}C\{^1H\}$ NMR (100 MHz, $CDCl_3$, 25 °C) δ (ppm): 11.7, 22.8, 45.9, 112.7, 117.1, 129.2, 148.6. HRMS (ESI-TOF (m/z)): calcd for $C_9H_{14}N$ 136.1121, found 136.1126.

N,N-Diethylaniline (**7f**).⁶⁰ This compound was obtained in a low yield. It was detected by GCMS: t_R 6.834. MS ($C_{10}H_{15}N$): 149.1.

1-Phenylpiperidine (**7g**).⁵⁸ 1H NMR (300 MHz, $CDCl_3$, 25 °C) δ (ppm): 1.55–1.62 (m, 2H), 1.68–1.75 (m, 4H), 3.14–3.17 (m, 4H), 6.79–6.85 (m, 1H), 6.92–6.97 (m, 2H), 7.21–7.28 (m, 2H). $^{13}C\{^1H\}$ NMR (75 MHz, $CDCl_3$, 25 °C) δ (ppm): 24.3, 25.9, 50.7, 116.5, 119.2, 129.0, 152.3. HRMS (ESI-TOF (m/z)): calcd for $C_{11}H_{16}N$ 162.1277, found 162.1265.

1-Phenyl-1H-imidazole (**7h**).⁶¹ 1H NMR (400 MHz, $CDCl_3$, 25 °C) δ (ppm): 7.21 (s, 1H), 7.29 (s, 1H), 7.35–7.41 (m, 3H), 7.47–7.52 (m, 2H), 7.86 (s, 1H). $^{13}C\{^1H\}$ NMR (100 MHz, $CDCl_3$, 25 °C) δ (ppm): 118.1, 121.2, 127.3, 129.6, 130.1, 135.3, 137.1. HRMS (ESI-TOF (m/z)): calcd for $C_9H_9N_2$ 145.0760, found 145.0771, calcd for $C_9H_8N_2Na$ 167.0580, found 167.0580, calcd for $(C_9H_8N_2)_2Na$ 311.1267, found 311.1262.

7-Phenoxy-1,2,3,4-tetrahydronaphthalen-2-amine (**9a**). 1H NMR (400 MHz, $CDCl_3$, 25 °C) δ (ppm): 1.56 (s, 2H, NH), 1.60–1.66 (m, 1H, Hⁱ or H^j), 1.97–2.04 (m, 1H, Hⁱ or H^j), 2.53 (dd, $^2J_{HH} = 16.22$ Hz, $^3J_{HH} = 9.41$ Hz, 1H, H^f or H^g), 2.80–2.85 (m, 2H, H^k and H^l), 2.94 (dd, $^2J_{HH} = 16.41$ Hz, $^3J_{HH} = 5.14$ Hz, 1H, H^f or H^g), 3.15–3.24 (m, 1H, H^h), 6.73 (d, $^4J_{HH} = 2.54$ Hz, 1H, H^d), 6.78 (dd, $^3J_{HH} = 8.29$ Hz, $^4J_{HH} = 2.63$ Hz, 1H, H^e), 6.99 (dt, $^4J_{HH} = 7.64$, 1.12 Hz, 2H, H^a), 7.05 (dt, $^3J_{HH} = 7.69$ Hz, $^4J_{HH} = 1.12$ Hz, 2H, H^c and H^d), 7.31 (dd, $^3J_{HH} = 7.52$ Hz, $^4J_{HH} = 1.28$ Hz, 2H, H^b). $^{13}C\{^1H\}$ NMR (100 MHz, $CDCl_3$, 25 °C) δ (ppm): 27.4 (C₈), 29.7 (C₁₁), 31.0 (C₁₀), 52.9 (C₉), 117.1 (C₁₃), 118.4 (C₁), 119.4 (C₆), 122.9 (C₃), 129.6 (C₂), 19.8 (C₁₄), 131.0 (C₁₂), 136.0 (C₇), 155.1 (C₅) and 157.8 (C₄). HRMS (ESI-TOF (m/z)): calcd for $C_{16}H_{18}NO$ 240.1383, found 240.1395, calcd for $(C_{16}H_{17}NO)_2H$ 479.2693, found 479.2708.

7-(Phenylamino)-5,6,7,8-tetrahydronaphthalen-2-ol (**10a**). 1H NMR (400 MHz, $CDCl_3$, 25 °C) δ (ppm): 1.77 (m, 1H, H^e or H^f), 2.16 (m, 1H, H^e or H^f), 2.64 (ddd, $^2J_{HH} = 16.58$ Hz, $^3J_{HH} = 8.34$ Hz, 1H, H^b or H^c), 2.83 (m, 2H, H^d), 3.15 (ddd, $^2J_{HH} = 16.54$ Hz, $^3J_{HH} = 4.86$ Hz, 1H, Hⁱ or H^j), 3.75 (m, 1H, H^g), 4.58 (m, 1H, NH), 6.55 (d, $^4J_{HH} = 2.62$ Hz, 1H, H^a), 6.64 (dd, $^3J_{HH} = 8.66$ Hz, $^4J_{HH} = 1.06$ Hz, 3H, H^b and H^c), 6.70 (tt, $^3J_{HH} = 7.93$ Hz, $^4J_{HH} = 1.07$ Hz, 1H, Hⁱ), 6.98 (d, $^3J_{HH} = 8.41$ Hz, 1H, H^e), 7.18 (dd, $^3J_{HH} = 7.39$ Hz, $^4J_{HH} = 1.2$ Hz, 2H, H^k). $^{13}C\{^1H\}$ NMR (100 MHz, $CDCl_3$, 25 °C) δ (ppm): 26.6 (C₆), 29.3 (C₇), 36.6 (C₉), 48.5 (C₈), 113.5 (C₃ and C₁₂), 115.6 (C₁), 117.8 (C₁₄), 128.4 (C₅ or C₁₀), 129.3 (C₁₃), 129.9 (C₄), 136.0 (C₅ or C₁₀), 147.1 (C₁₁) and 153.6 (C₂). HRMS (ESI-TOF (m/z)): calcd for $C_{16}H_{18}NO$ 240.1383, found 240.1378, calcd for $(C_{16}H_{17}NO)_2Na$ 501.2515, found 501.2507.

4'-Hydroxy-*N*-phenyl(1,1'-biphenyl)-3-carboxamide (**9b**). 1H NMR (400 MHz, $DMSO-d_6$, 25 °C) δ (ppm): 6.90 (d, $^3J_{HH} = 8.61$ Hz, 2H, Hⁱ), 7.12 (t, $^3J_{HH} = 7.40$ Hz, $^4J_{HH} = 1.12$ Hz, 1H, H^a), 7.37 (t, $^3J_{HH} = 7.40$ Hz, 2H, H^b), 7.57 (t, $^3J_{HH} = 7.68$ Hz, 1H, H^f), 7.61 (dd, $^3J_{HH} = 8.70$ Hz, 2H, H^b), 7.79 (d, $^3J_{HH} = 8.61$ Hz, $^4J_{HH} = 1.17$ Hz, 3H, H^c and H^g), 7.85 (dt, $^3J_{HH} = 7.68$ Hz, $^4J_{HH} = 1.49$ Hz, 1H, H^e), 8.14 (t, $J = 3.32$, $^4J_{HH} = 1.67$ Hz, 1H, H^d), 9.66 (s, 1H, OH) and 10.31 (s, 1H, NH). $^{13}C\{^1H\}$ NMR (100 MHz, $DMSO-d_6$, 25 °C) δ (ppm): 116.3 (C₁₄), 120.9 (C₃), 124.2 (C₁), 125.5 (C₇), 126.2 (C₈), 128.5 (C₁₃), 129.1 (C₂), 129.4 (C₉ and C₁₀), 130.7 (C₁₂), 136 (C₆), 139.6 (C₄), 140.8 (C₁₁), 157.9 (C₁₅) and 166.1 (C₅). HRMS (ESI-TOF (m/z)): Positive mode (+): calcd for $C_{19}H_{15}NO_2Na$ 312.0995, found 312.0994; Negative mode (−): calcd for $C_{19}H_{14}NO_2$ 288.1025, found 288.1002, calcd for $(C_{19}H_{14}NO_2)(C_{19}H_{15}NO_2)$ 577.2127, found 577.2110.

4'-Phenoxy(1,1'-biphenyl)-3-carboxamide (**10b**). 1H NMR (400 MHz, $CDCl_3$, 25 °C) δ (ppm): 5.73 (s, 1H, NH), 6.17 (s, 1H, NH), 7.07–7.13 (m, 4H, H^f and H^g), 7.16 (tt, $^3J_{HH} = 7.42$, $^4J_{HH} = 1.15$ Hz, 1H, Hⁱ), 7.37–7.42 (m, 2H, H^b), 7.54 (t, $^3J_{HH} = 8.00$ Hz, $^4J_{HH} = 0.61$ Hz, 1H, H^c), 7.60 (dt, $^3J_{HH} = 8.85$ Hz, $^4J_{HH} = 2.18$ Hz, 2H, H^e), 7.76 (dt, $^3J_{HH} = 7.77$ Hz, $^4J_{HH} = 1.80$ Hz, 2H, H^a and H^d) and 8.06 (t, $^3J_{HH} = 3.75$ Hz, $^4J_{HH} = 1.92$ Hz, 1H, H^b). $^{13}C\{^1H\}$ NMR (100 MHz, $CDCl_3$, 25 °C) δ (ppm): 119.1 (C₁₀), 119.2 (C₁₃), 123.6 (C₁₅), 125.7

(C₆), 126.1 (C₄), 128.5 (C₉), 129.1 (C₅), 129.9 (C₁₄), 130.4 (C₁), 133.9 (C₂), 135.1 (C₃), 141.2 (C₇), 156.9 (C₁₂), 157.4 (C₁₁) and 169.2 (C₃). HRMS (ESI-TOF (*m/z*)): calcd for C₁₉H₁₅NO₂Na 312.1000, found 312.0993, calcd for (C₁₉H₁₅NO₂)₂Na 601.2103, found 601.2078, calcd for (C₁₉H₁₅NO₂)₃Na 890.3206, found 890.3186.

4-Amino-*N,N*-diphenylbenzamide (9c). ¹H NMR (400 MHz, CDCl₃, 25 °C) δ (ppm): 3.78–3.92 (m, 2H, NH), 6.44 (d, ³J_{HH} = 8.71 Hz, 2H, H^b), 7.11–7.19 (m, 6H, H^c or H^d and H^e), 7.23–7.33 (dd, ³J_{HH} = 7.87 Hz, ⁴J_{HH} = 2.05 Hz, 6H, H^a and H^c or H^d). ¹³C{¹H} NMR (100 MHz, CDCl₃, 25 °C) δ (ppm): 113.6 (C₄), 125.2 (C₂), 125.9 (C₉), 127.4 (C₇ or C₈), 129.1 (C₇ or C₈), 131.8 (C₃), 144.7 (C₆), 148.6 (C₅), 170.7 (C₁). (ESI-TOF (*m/z*)): calcd for C₁₉H₁₇N₂O 289.1335, found 289.1335, calcd for C₁₉H₁₆N₂O₂Na 311.1155, found 311.1163, calcd for (C₁₉H₁₆N₂O)₂Na 599.2417, found 599.2420.

***N*-Phenyl-4-(phenylamino)benzamide (10c).** ¹H NMR (400 MHz, CDCl₃, 25 °C) δ (ppm): 6.07 (s, 1H, NH_{amide}), 7.04 (d, ³J_{HH} = 8.65 Hz, 2H, H^b), 7.07 (d, ³J_{HH} = 7.20 Hz, 1H, H^e), 7.13 (t, ³J_{HH} = 7.46 Hz, ⁴J_{HH} = 1.04 Hz, 1H, H^b), 7.16 (d, ³J_{HH} = 7.72 Hz, ⁴J_{HH} = 1.18 Hz, 2H, H^c), 7.35 (dt, ³J_{HH} = 7.74 Hz, 4H, H^d and H^g), 7.63 (d, ³J_{HH} = 8.60 Hz, 2H, H^f), 7.77 (d, ³J_{HH} = 8.54 Hz, 2H, H^f), 7.80 (s, 1H, NH_{amide}). ¹³C{¹H} NMR (100 MHz, CDCl₃, 25 °C) δ (ppm): 115.2 (C₄), 120.1 (C₇ and C₁₁), 122.9 (C₉), 124.2 (C₁₃), 125.7 (C₂), 128.8 (C₈ or C₁₂), 129.0 (C₃), 129.5 (C₈ or C₁₂), 138.2 (C₁₀), 141.1 (C₆), 147.2 (C₅), 165.5 (C₁). HRMS (ESI-TOF (*m/z*)): calcd for C₁₉H₁₆N₂O₂Na 311.1155, found 311.1149, calcd for (C₁₉H₁₆N₂O)₂Na 599.2417, found 599.2407.

1-(Allyloxy)-2-iodobenzene (rc). rc was synthesized following published procedures.³⁶ The characterization of rc-H was performed by comparison to a commercially available sample.

1-(Allyloxy)-2-(4-methoxyphenoxy)benzene (rc-5c). ¹H NMR (300 MHz, CDCl₃, 25 °C) δ (ppm): 3.81 (s, 3H), 4.62 (dt, ³J_{HH} = 5.23 Hz, ⁴J_{HH} = 1.55 Hz, 2H), 5.24 (ddd, ²J_{HH} = 10.50 Hz, ³J_{HH} = 3.21 Hz, ⁴J_{HH} = 1.64 Hz, 1H), 5.34 (ddd, ²J_{HH} = 17.25 Hz, ³J_{HH} = 3.65 Hz, ⁴J_{HH} = 1.72 Hz, 1H), 5.94–6.08 (m, 1H), 6.84–6.97 (m, 6H), 7.01–7.09 (m, 2H). ¹³C{¹H} NMR (75 MHz, CDCl₃, 25 °C) δ (ppm): 55.6, 69.9, 114.6, 114.9, 117.5, 119.1, 119.9, 121.4, 123.8, 133.2, 146.9, 149.8, 151.3, 155.2. HRMS (ESI-TOF (*m/z*)): calcd for C₁₆H₁₆O₃Na 279.0992, found 279.0999, calcd for (C₁₆H₁₆O₃)₂Na 535.2091, found 535.2084.

***N*-(2-(Allyloxy)phenyl)benzamide (rc-3a).** ¹H NMR (300 MHz, CDCl₃, 25 °C) δ (ppm): 4.68 (dt, ³J_{HH} = 5.28 Hz, ⁴J_{HH} = 1.44 Hz, 2H), 5.37 (ddd, ²J_{HH} = 10.50 Hz, ³J_{HH} = 3.17 Hz, ⁴J_{HH} = 1.32 Hz, 1H), 5.46 (ddd, ²J_{HH} = 17.29 Hz, ³J_{HH} = 3.47 Hz, ⁴J_{HH} = 1.61 Hz, 1H), 6.05–6.12 (m, 1H), 6.95 (dd, ³J_{HH} = 7.25 Hz, ⁴J_{HH} = 2.37 Hz, 1H), 7.05–7.09 (m, 2H), 7.50–7.58 (m, 3H), 7.92 (dd, ³J_{HH} = 8.28 Hz, ⁴J_{HH} = 1.76 Hz, 1H). ¹³C{¹H} NMR (75 MHz, CDCl₃, 25 °C) δ (ppm): 69.6, 111.5, 118.2, 119.9, 121.5, 123.8, 127.0, 128.1, 128.8, 131.7, 132.8, 135.7, 147.1, 165.2. HRMS (ESI-TOF (*m/z*)): calcd for C₁₆H₁₅NO₂Na 276.0995, found 276.0991, calcd for (C₁₆H₁₅NO₂)₂Na 529.2098, found 529.2083.

2-(Allyloxy)-*N*-cyclohexylaniline (rc-7d). ¹H NMR (400 MHz, CDCl₃, 25 °C) δ (ppm): 1.15–1.31 (m, 3H), 1.31–1.48 (m, 3H), 1.61–1.73 (m, 1H), 1.73–1.86 (m, 2H), 2.09 (d, ³J_{HH} = 12.18 Hz, 2H), 3.22–3.34 (m, 1H), 4.19 (s, 1H, NH), 4.57 (dt, ³J_{HH} = 5.23 Hz, ⁴J_{HH} = 1.51 Hz, 2H), 5.30 (ddd, ²J_{HH} = 10.50 Hz, ³J_{HH} = 3.21 Hz, ⁴J_{HH} = 1.64 Hz, 1H), 5.42 (ddd, ²J_{HH} = 17.23 Hz, ³J_{HH} = 3.55 Hz, ⁴J_{HH} = 1.58 Hz, 1H), 6.04–6.18 (m, 1H), 6.63 (dd, ²J_{HH} = 10.50 Hz, ³J_{HH} = 8.17 Hz, ⁴J_{HH} = 1.44 Hz, 2H), 6.79 (dd, ³J_{HH} = 8.04 Hz, ⁴J_{HH} = 1.41 Hz, 1H), (ddt, ²J_{HH} = 15.35 Hz, ³J_{HH} = 7.69 Hz, ⁴J_{HH} = 1.31 Hz, 1H). ¹³C{¹H} NMR (100 MHz, CDCl₃, 25 °C) δ (ppm): 25.1, 26.0, 33.5, 51.4, 69.3, 110.5, 111.3, 115.7, 117.3, 121.5, 133.7, 137.7, 145.7. HRMS (ESI-TOF (*m/z*)): calcd for C₁₅H₂₂NO 232.1696, found 232.1705, calcd for C₁₅H₂₁NONa 254.1515, found 254.1514.

2-(Allyloxy)-*N*-(4-methoxyphenyl)aniline (rc-7c). ¹H NMR (400 MHz, CDCl₃, 25 °C) δ (ppm): 3.83 (s, 3H), 4.64 (dt, ³J_{HH} = 5.45 Hz, ⁴J_{HH} = 1.34 Hz, 2H), 5.33 (ddd, ²J_{HH} = 10.46 Hz, ³J_{HH} = 3.33 Hz, ⁴J_{HH} = 1.40 Hz, 1H), 5.45 (ddd, ²J_{HH} = 17.26 Hz, ³J_{HH} = 3.59 Hz, ⁴J_{HH} = 1.59 Hz, 1H), 6.03 (s, 1H, NH), 6.07–6.20 (m, 1H), 6.77 (td, ³J_{HH} =

7.69 Hz, ⁴J_{HH} = 1.73 Hz, 2H), 6.82–6.92 (m, 3H), 7.07 (dd, ³J_{HH} = 7.79 Hz, ⁴J_{HH} = 1.74 Hz, 2H) 7.17 (d, ³J_{HH} = 8.91 Hz, 2H). ¹³C{¹H} NMR (100 MHz, CDCl₃, 25 °C) δ (ppm): 55.6, 69.5, 111.8, 112.8, 114.6, 117.8, 118.4, 121.3, 123.0, 133.4, 135.4, 146.3, 155.4. HRMS (ESI-TOF (*m/z*)): calcd for C₁₆H₁₇NO₂Na 278.1151, found 278.1161.

***N*-(2-(Allyloxy)phenyl)-*N*-methylacetamide (rc-3h).** ¹H NMR (300 MHz, CDCl₃, 25 °C) δ (ppm): 1.84 (s, 3H), 3.21 (s, 3H), 4.60 (dt, ³J_{HH} = 4.98 Hz, ⁴J_{HH} = 1.65 Hz, 2H), 5.30 (ddd, ²J_{HH} = 10.57 Hz, ³J_{HH} = 4.36 Hz, ⁴J_{HH} = 1.50 Hz, 1H), 5.41 (ddd, ²J_{HH} = 17.27 Hz, ³J_{HH} = 4.90 Hz, ⁴J_{HH} = 1.68 Hz, 1H), 5.96–6.08 (m, 1H), 6.96–7.02 (m, 2H), 7.19 (dd, ³J_{HH} = 7.68 Hz, ⁴J_{HH} = 1.68 Hz, 1H) 7.85 (td, ³J_{HH} = 8.91 Hz, ⁴J_{HH} = 1.79 Hz, 2H). ¹³C{¹H} NMR (75 MHz, CDCl₃, 25 °C) δ (ppm): 21.6, 35.8, 68.6, 113.2, 117.6, 121.2, 129.0, 129.2, 132.5, 154.0, 171.4. (ESI-TOF (*m/z*)): calcd for C₁₂H₁₅NO₂Na 228.0995, found 228.0993, calcd for (C₁₂H₁₅NO₂)₂Na 433.2098, found 433.2095.

Synthesis of Auxiliary Ligand L₃. *N,N'*-Dimethyl-2,6-bis-(aminomethyl)pyridine as HCl Salt (L₃·(HCl)₂). 2,6-Bis-(chloromethyl)pyridine (1 g, 5.6 mmol) was added to aqueous methylamine (40%) (30 mL, 350 mmol) in a round-bottom flask, and the mixture was stirred at room temperature for 2–3 days. The reaction was monitored by ¹H NMR. Next, NaOH (0.470 g) was added, and the mixture was concentrated under reduced pressure. The crude was extracted with CH₂Cl₂, and the combined organic layers were dried with anhydrous MgSO₄. Finally, the solvent was evaporated under reduced pressure, obtaining L₃ as a yellow oil (0.920 g, 90% yield). Since the product is highly hygroscopic, the hydrochloric salt L₃·(HCl)₂ was prepared by dissolving the oil in CHCl₃ (1 mL) and hydrochloric acid 36.5% (0.85 mL). The aqueous phase was dried under vacuum to dryness, and the crystallization was performed with a mixture of MeOH and Et₂O (0.660 g, 55% yield). L₃·(HCl)₂ salt: ¹H NMR (400 MHz, D₂O, 25 °C) δ (ppm): 2.83 (s, 6 H), 4.43 (s, 4 H), 7.46 (d, 2 H), 7.93 (t, 1 H). HRMS (ESI-TOF (*m/z*)): calcd for C₉H₁₆N₃ 166.1339, found 166.1345. Anal. Calcd for (C₉H₁₇N₃Cl₂·1.15 H₂O): C, 41.76; H, 7.51; N, 16.23. Found: C, 41.78; H, 7.37; N, 16.10.

■ ASSOCIATED CONTENT

Supporting Information

The Supporting Information is available free of charge on the ACS Publications website at DOI: 10.1021/acs.joc.6b01035.

Experimental details; full characterization of chemical compounds; supplementary methods; supplementary schemes, figures, and tables (PDF)

■ AUTHOR INFORMATION

Corresponding Author

*E-mail: xavi.ribas@udg.edu.

Notes

The authors declare no competing financial interest.

■ ACKNOWLEDGMENTS

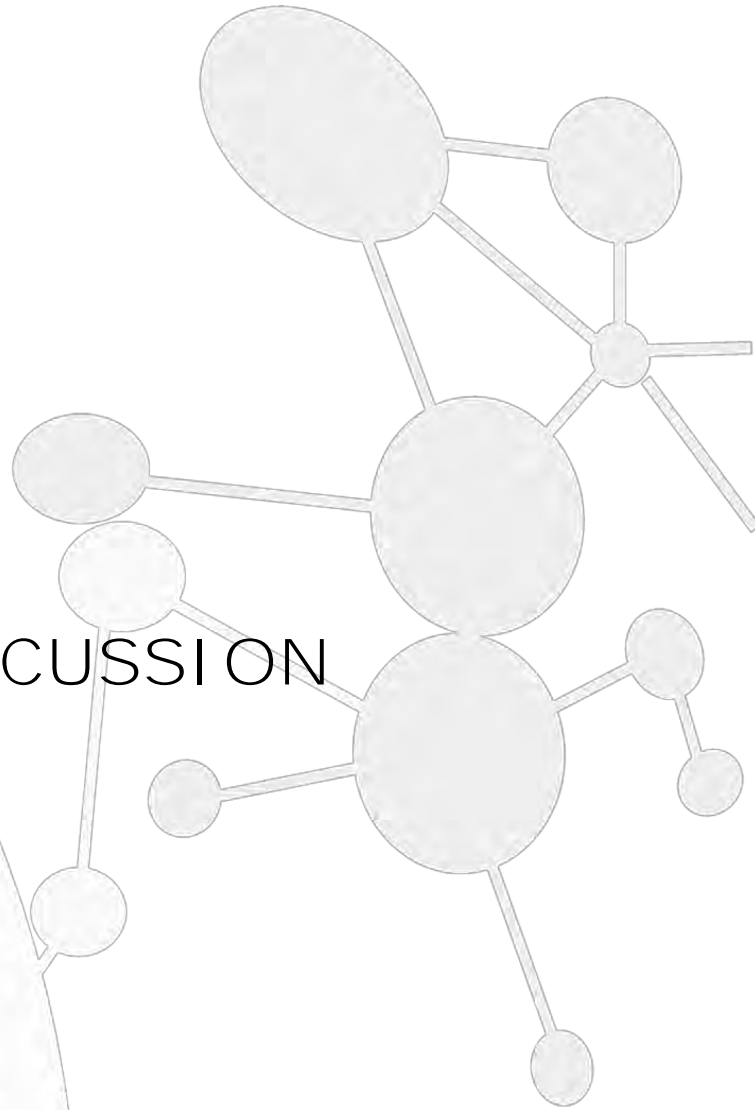
This work was supported by grants from the European Research Council (Starting Grant Project ERC-2011-StG-277801), the Spanish MICINN (CTQ2013-43012-P, Consolider-Ingenio CSD2010-00065, INNPLANTA project INP-2011-0059-PCT-420000-ACT1), and the Catalan DIUE of the Generalitat de Catalunya (2014SGR862). X.R. thanks ICREA for an ICREA-Acadèmia award. We thank STR from UdG for technical support. We also thank Prof. J. Roithová and Dr. JM. Luis for fruitful discussions. We also thank Xavi Amat for his help in preparing the cover art.

REFERENCES

- (1) Beletskaya, I. P.; Cheprakov, A. V. *Coord. Chem. Rev.* **2004**, *248*, 2337–2364.
- (2) Ley, S. V.; Thomas, A. W. *Angew. Chem., Int. Ed.* **2003**, *42*, 5400–5449.
- (3) Evano, G.; Blanchard, N.; Toumi, M. *Chem. Rev.* **2008**, *108*, 3054–3131.
- (4) Ma, D.; Cai, Q. *Acc. Chem. Res.* **2008**, *41*, 1450–1460.
- (5) Surry, D. S.; Buchwald, S. L. *Chem. Sci.* **2010**, *1*, 13–31.
- (6) Casitas, A.; Ribas, X. *Chem. Sci.* **2013**, *4*, 2301–2318.
- (7) Jiang, Y.; Xu, L.; Zhou, C.; Ma, D. Cu-Catalyzed Ullmann-Type C–Heteroatom Bond Formation: The Key Role of Dinucleating Ancillary Ligands. In *C–H and C–X Functionalization. Transition Metal Mediation*; Ribas, X., Ed.; RSC Publishing: Cambridge, 2013; Vol. Catalysis Series 11, pp 1–45.
- (8) Ullmann, F.; Bielecki, J. *Ber. Dtsch. Chem. Ges.* **1901**, *34*, 2174.
- (9) Ullmann, F. *Ber. Dtsch. Chem. Ges.* **1903**, *36*, 1017.
- (10) Goldberg, I. *Ber. Dtsch. Chem. Ges.* **1906**, *39*, 1691–1696.
- (11) Zhu, L.; Li, G.; Luo, L.; Guo, P.; Lan, J.; You, J. *J. Org. Chem.* **2009**, *74*, 2200–2202.
- (12) Sperotto, E.; de Vries, J. G.; van Klink, G. P. M.; van Koten, G. *Tetrahedron Lett.* **2007**, *48*, 7366–7370.
- (13) Taillefer, M.; Xia, N.; Ouali, A. *Angew. Chem., Int. Ed.* **2007**, *46*, 934–936.
- (14) Panda, N.; Jena, A. K.; Mohapatra, S.; Rout, S. R. *Tetrahedron Lett.* **2011**, *52*, 1924–1927.
- (15) Zhu, R.; Xing, L.; Wang, X.; Cheng, C.; Su, D.; Hu, Y. *Adv. Synth. Catal.* **2008**, *350*, 1253–1257.
- (16) Correa, A.; Bolm, C. *Adv. Synth. Catal.* **2007**, *349*, 2673–2676.
- (17) Chang, J. W. W.; Xu, X.; Chan, P. W. H. *Tetrahedron Lett.* **2007**, *48*, 245–248.
- (18) Yuan, Y.; Thomé, I.; Kim, S. H.; Chen, D.; Beyer, A.; Bonnamour, J.; Zuidema, E.; Chang, S.; Bolm, C. *Adv. Synth. Catal.* **2010**, *352*, 2892–2898.
- (19) Cano, R.; Ramón, D. J.; Yus, M. *J. Org. Chem.* **2011**, *76*, 654–660.
- (20) Güell, I.; Ribas, X. *Eur. J. Org. Chem.* **2014**, *2014*, 3188–3195.
- (21) Monnier, F.; Taillefer, M. *Angew. Chem., Int. Ed.* **2009**, *48*, 6954–6971.
- (22) Jones, G. O.; Liu, P.; Houk, K. N.; Buchwald, S. L. *J. Am. Chem. Soc.* **2010**, *132*, 6205–6213.
- (23) Tye, J. W.; Weng, Z.; Giri, G.; Hartwig, J. F. *Angew. Chem., Int. Ed.* **2010**, *49*, 2185–2189.
- (24) Giri, R.; Hartwig, J. F. *J. Am. Chem. Soc.* **2010**, *132*, 15860–15863.
- (25) Tye, J. W.; Weng, Z.; Johns, A. M.; Incarvito, C. D.; Hartwig, J. F. *J. Am. Chem. Soc.* **2008**, *130*, 9971–9983.
- (26) Zhang, S.-L.; Liu, L.; Fu, Y.; Guo, Q.-X. *Organometallics* **2007**, *26*, 4546–4554.
- (27) Tseng, C.-K.; Tseng, M.-C.; Han, C.-C.; Shyu, S.-G. *Chem. Commun.* **2011**, *47*, 6686–6688.
- (28) Tseng, C.-K.; Lee, C.-R.; Han, C.-C.; Shyu, S.-G. *Chem. - Eur. J.* **2011**, *17*, 2716–2723.
- (29) Cheng, S.-W.; Tseng, M.-C.; Lii, K.-H.; Lee, C.-R.; Shyu, S.-G. *Chem. Commun.* **2011**, *47*, 5599–5601.
- (30) Tseng, C.-K.; Lee, C.-R.; Tseng, M.-C.; Han, C.-C.; Shyu, S.-G. *Dalton Trans.* **2014**, *43*, 7020–7027.
- (31) Kainz, Q. M.; Matier, C. D.; Bartoszewicz, A.; Zultanski, S. L.; Peters, J. C.; Fu, G. C. *Science* **2016**, *351*, 681–684.
- (32) Do, H.-Q.; Bachman, S.; Bissember, A. C.; Peters, J. C.; Fu, G. C. *J. Am. Chem. Soc.* **2014**, *136*, 2162–2167.
- (33) Ziegler, D. T.; Choi, J.; Muñoz-Molina, J. M.; Bissember, A. C.; Peters, J. C.; Fu, G. C. *J. Am. Chem. Soc.* **2013**, *135*, 13107–13112.
- (34) Uyeda, C.; Tan, Y.; Fu, G. C.; Peters, J. C. *J. Am. Chem. Soc.* **2013**, *135*, 9548–9552.
- (35) Bissember, A. C.; Lundgren, R. J.; Creutz, S. E.; Peters, J. C.; Fu, G. C. *Angew. Chem., Int. Ed.* **2013**, *52*, 5129–5133.
- (36) Creutz, S. E.; Lotito, K. J.; Fu, G. C.; Peters, J. C. *Science* **2012**, *338*, 647–651.
- (37) Maiti, D.; Buchwald, S. L. *J. Am. Chem. Soc.* **2009**, *131*, 17423–17429.
- (38) Shafir, A.; Lichtor, P. A.; Buchwald, S. L. *J. Am. Chem. Soc.* **2007**, *129*, 3490–3491.
- (39) Cai, Q.; He, G.; Ma, D. *J. Org. Chem.* **2006**, *71*, 5268–5273.
- (40) Ma, D.; Cai, Q. *Org. Lett.* **2003**, *5*, 3799–3802.
- (41) Zhang, H.; Cai, Q.; Ma, D. *J. Org. Chem.* **2005**, *70*, 5164–5173.
- (42) Altman, R. A.; Shafir, A.; Choi, A.; Lichtor, P. A.; Buchwald, S. L. *J. Org. Chem.* **2008**, *73*, 284–286.
- (43) Cohen, T.; Cristea, I. *J. Org. Chem.* **1975**, *40*, 3649–3651.
- (44) Casitas, A.; Canta, M.; Solà, M.; Costas, M.; Ribas, X. *J. Am. Chem. Soc.* **2011**, *133*, 19386–19392.
- (45) De Simone, A.; Ruda, G. F.; Albani, C.; Tarozzo, G.; Bandiera, T.; Piomelli, D.; Cavalli, A.; Bottegoni, G. *Chem. Commun.* **2014**, *50*, 4904–4907.
- (46) Cristau, H.-J.; Cellier, P. P.; Spindler, J.-F.; Taillefer, M. *Chem. - Eur. J.* **2004**, *10*, 5607–5622.
- (47) Ma, F.; Xie, X.; Zhang, L.; Peng, Z.; Ding, L.; Fu, L.; Zhang, Z. *J. Org. Chem.* **2012**, *77*, 5279–5285.
- (48) Poondra, R. R.; Turner, N. J. *Org. Lett.* **2005**, *7*, 863–866.
- (49) Tobisu, M.; Nakamura, R.; Kita, Y.; Chatani, N. *J. Am. Chem. Soc.* **2009**, *131*, 3174–3175.
- (50) Barbe, G.; Charette, A. B. *J. Am. Chem. Soc.* **2008**, *130*, 18–19.
- (51) Li, Y.; Ma, L.; Jia, F.; Li, Z. *J. Org. Chem.* **2013**, *78*, 5638–5646.
- (52) Sreedhar, B.; Arundhathi, R.; Reddy, P. L.; Kantam, M. L. *J. Org. Chem.* **2009**, *74*, 7951–7954.
- (53) ¹H NMR spectra were compared to the commercial product.
- (54) Aranyos, A.; Old, D. W.; Kiyomori, A.; Wolfe, J. P.; Sadighi, J. P.; Buchwald, S. L. *J. Am. Chem. Soc.* **1999**, *121*, 4369–4378.
- (55) Shintou, T.; Mukaiyama, T. *J. Am. Chem. Soc.* **2004**, *126*, 7359–7367.
- (56) Guo, D.; Huang, H.; Xu, J.; Jiang, H.; Liu, H. *Org. Lett.* **2008**, *10*, 4513–4516.
- (57) Willis, M. C.; Brace, G. N.; Findlay, T. J. K.; Holmes, I. P. *Adv. Synth. Catal.* **2006**, *348*, 851–856.
- (58) Zhu, L.; Cheng, L.; Zhang, Y.; Xie, R.; You, J. *J. Org. Chem.* **2007**, *72*, 2737–2743.
- (59) Lee, Y.-H.; Chen, Y.-C.; Hsieh, J.-C. *Eur. J. Org. Chem.* **2012**, *2012*, 247–250.
- (60) Wu, Z.; Zhou, L.; Jiang, Z.; Wu, D.; Li, Z.; Zhou, X. *Eur. J. Org. Chem.* **2010**, *2010*, 4971–4975.
- (61) Lee, O.-Y.; Law, K.-L.; Ho, C.-Y.; Yang, D. *J. Org. Chem.* **2008**, *73*, 8829–8837.

CHAPTER VII.

RESULTS AND DISCUSSION



Since the discovery of the Buchwald-Hartwig coupling reaction, the development of renewed cross-coupling processes in a greener fashion has been a topic of interest over the last decades. The development of methodologies capable to compete with precious transition metals chemistry, which were slightly related with the judicious choice of ancillary ligand, is one of the most challenging aims in organic synthesis. The key of success of these transformations generally is a detailed mechanistic understanding of elementary steps, which depending on the reaction conditions could proceed via distinct reaction pathways. An array of synthetic model systems has been developed in the recent years in order to gain mechanistic insight. These model systems have successfully achieved the stabilization of high-valent metal intermediate species, which are key players in the reactions. Therefore, this thesis is focused on the investigation of the mechanistic features that govern copper- and nickel-catalysed C-C bond formation using well-defined model aryl halide substrates. Another goal of this thesis is to apply the mechanistic knowledge in model Cu-catalysed cross-couplings for standard Ullmann-type C-heteroatom bond forming reactions, paying especial attention to the chemoselective role of auxiliary ligands.

Chapter VII.1 depicts our progress in the investigation of a detailed mechanistic pathway behind copper-assisted Hurtley-type couplings for the formation of C(sp^2)-C(sp^3) bonds and Stephens-Castro (stoichiometric) or Miura (catalytic) couplings for the formation of C(sp^2)-C(sp) bonds, using well-defined copper(III) complexes. We evaluate the reactivity of these copper complexes towards activated methylenes (malononitrile, dimethyl malonate and acetylacetone) and terminal *p*-R-phenylacetylene derivatives (R = NO₂, CF₃, H). Interestingly, in the both cases we observe the formation of the desired product through the reductive elimination step and subsequently, these species undergo an intramolecular reorganization to afford the final heterocyclic products 2*H*-isoindole, 1,2-dihydroisoquinoline and 1,2-dihydroisoquinolin-3(4*H*)-one. *In situ* spectroscopic studies provide definitive evidence for the involvement of an aryl-Cu^{III}-halide intermediate as the resting state of the reaction. Our results in model aryl halide substrates provide evidences for the direct engagement of a redox Cu^I/Cu^{III} catalytic cycle involving oxidative addition and reductive elimination steps in copper-mediated Stephen-Castro and Hurtley-type coupling reactions.

In Chapter VII.2 we describe the recent advances on the development of well-defined nickel(II) complexes by oxidative addition at C-halide bonds or direct C-H activation, using macrocyclic model systems. The reactivity of these complexes towards widely used trifluoromethylating reagents (TDTT and Togni Reagent) is presented, obtaining near quantitative yields under mild conditions. Mechanistic investigations combining both experimental and DFT studies suggest an intriguing mechanistic pathway that combines Single Electron Transfer (SET) and reductive elimination processes, involving the formation of Ni^{II}, Ni^{III} and Ni^{IV} intermediate species.

Finally, in Chapter VII.3 we turned our attention on the investigation of the role of auxiliary ligands in Cu-catalysed Ullmann-type couplings for the chemoselective formation of C-heteroatom bonds. We present the selective arylation of a wide range O-based (phenols) and N-based (amines and

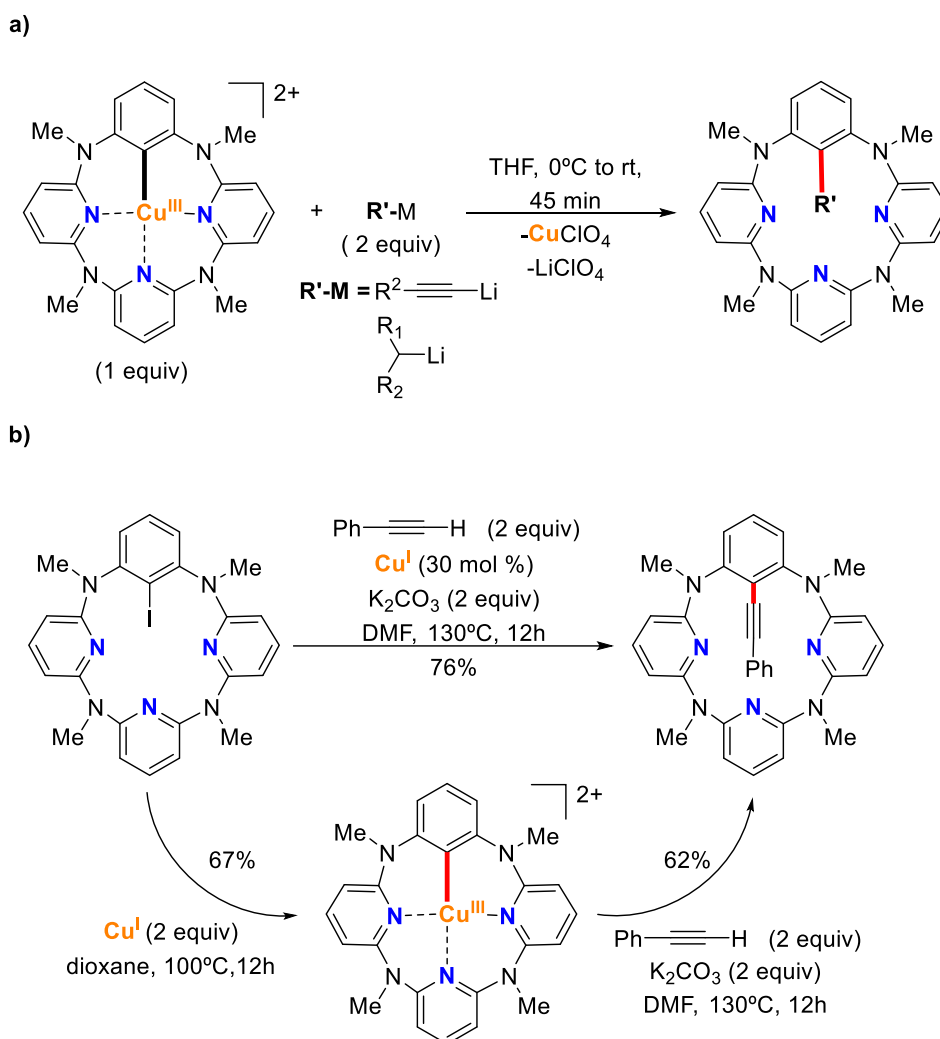
amides) nucleophiles in competitive reactions using aryl iodides and bromides. The sharp switch in the selectivity, in most of the combinations between amides, amines and phenols, mainly depends on the ligand choice. However, the exact role of these auxiliary ligands on the chemoselective arylation is not well understood. In addition, the formation of radical intermediates is not observed in any of the coupling reaction, reinforcing the general proposed $\text{Cu}^{\text{I}}/\text{Cu}^{\text{III}}$ redox catalytic cycle

VII.1 Copper(III)-mediated $\text{C}(\text{sp}^2)\text{-C}(\text{sp}^3)$ and $\text{C}(\text{sp}^2)\text{-C}(\text{sp})$ bond formation under milder conditions

This section corresponds to the contents of the manuscript by Rovira, M *et al.* *ChemCatChem*. **2013**, 5, 687 – 691 (subsection VII.1.1.) and Rovira, M *et al.* *Chem. Eur. J.* **2014**, 20, 10005 – 10010 (subsection VII.1.2.), which can be found in **Chapters III** and **IV** of this thesis, respectively.

The cross-coupling reaction of aryl halides with activated methylenes and terminal acetylenes are fundamental to provide access to high versatile aryl-alkyl and aryl-alkyne scaffolds, which are products amenable to further chemical transformations. In view of the scanty information into the mechanistic aspects that govern copper-based Hurltley and Stephens-Castro couplings and with the experience of our group demonstrating the feasibility of the aryl- Cu^{III} species as intermediate species in several $\text{C}_{\text{aryl}}\text{-Heteroatom}$ (C-N, C-O, C-S, C-Se, C-P and C-halide) coupling reactions,¹⁻⁶ we aimed to further developed the reactivity of well-defined aryl- Cu^{III} species with several activated methylenes and terminal phenylacetylene derivatives.

As was described on the introduction section, Wang and co-workers reported the synthesis of the well-defined aryl- Cu^{III} complex based in azacalix[1]arene[3]pyridine, which reacts readily with a wide range of nucleophiles to form C-X and C-C bonds in almost quantitative yields under mild conditions.^{7,8} More recently, the same authors reported the involvement of high valent organocopper intermediate species in the formation of C-C bonds. They have shown that the stable and well-defined aryl- Cu^{III} complex was able to undergo a cross-coupling reaction with various alkynyllithium and alkylolithium reagents to afford $\text{C}_{\text{aryl}}\text{-C}_{\text{alkynyl}}$ (Stephens-Castro-type reaction) and $\text{C}_{\text{aryl}}\text{-C}_{\text{alkyl}}$ (Hurtley-type reaction) bond forming products, respectively (Scheme VII.1a).^{9,10} In addition, they also have reported the catalytic version of the reaction, in which substoichiometric (30 mol%) amount of Cu^{I} can effectively perform the oxidative addition into C-I moiety to form the well-defined aryl- Cu^{III} complex. This intermediate species subsequently undergoes formation of $\text{C}_{\text{aryl}}\text{-C}_{\text{alkynyl}}$ product through a reductive elimination step, evidencing the direct involvement of high valent copper species in a model Stephens-Castro reaction (Scheme VII.1b).



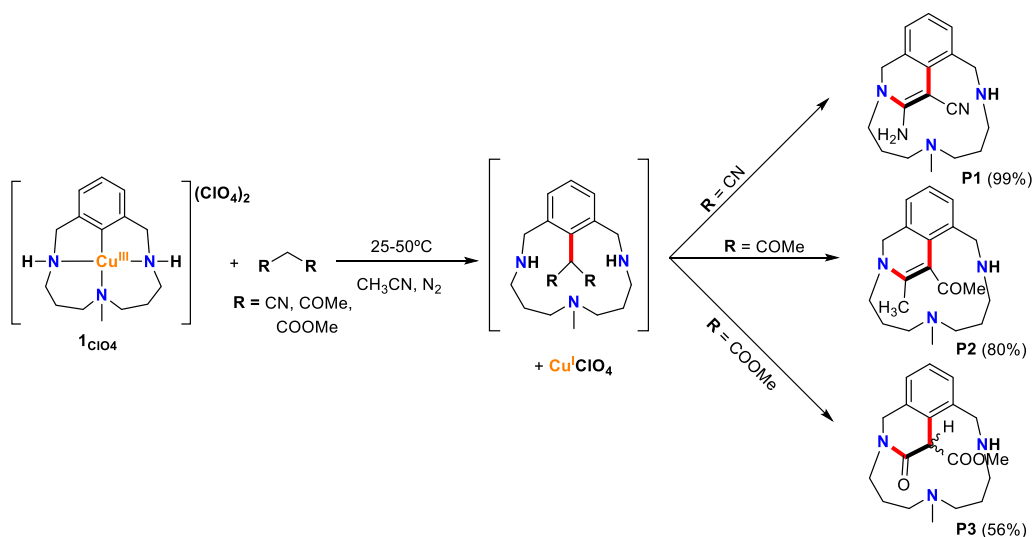
Scheme VII.1. (a) Formation of $\text{C}_{\text{aryl}}\text{-C}_{\text{alkynyl}}$ and $\text{C}_{\text{aryl}}\text{-C}_{\text{alkyl}}$ bonds from the cross-coupling reaction between macrocyclic model aryl- Cu^{III} complexes and alkynyl and alkyl lithium reagents. (b) Wang's model system involving an aryl- Cu^{III} intermediate species for Stephens-Castro reaction.

VII.1.1 Reactivity of aryl- Cu^{III} (1_{ClO_4}) with activated methylene substrates (Hurtley Catalysis)

Hurtley-type coupling reactions have been known for more than 80 years and this methodology has become of considerable importance for the preparation of $\text{C}(\text{sp}^2)\text{-C}(\text{sp}^3)$ coupling products in both laboratory and industry. Although significant progress has been achieved in the mechanistic understanding of Ullmann reactions, much remains uncovered. Indeed, the mechanisms of the copper-mediated C-H arylation seems to be significantly dependent on the reaction conditions and as a result several mechanisms have been proposed. Oxidative addition/reductive elimination pathway was the most proposed mechanism in the literature, indicating the involvement of Cu^{I} and Cu^{III} intermediates. However, the use of macrocyclic model systems can shed light to the plausible involvement of aryl- Cu^{III} key intermediate species in copper-catalysed Hurtley-type couplings.

Well-defined aryl-Cu^{III} complex (**1**_{CIO4}) readily reacts with stoichiometric amounts of activated methylene substrates (2 equiv) under mild conditions to afford the corresponding heterocyclic 1,2-dihydroisoquinoline (**P1** and **P2**) and 1,2-dihydroisoquinolin-3(4*H*)-one (**P3**) compounds (Scheme VII.2). These scaffolds are essentially formed through an intramolecular reorganization of the previously expected C(*sp*²)-C(*sp*³) coupling product, by the attack of one of the secondary amines of the substrate scaffold.

The obtained yields for the heterocyclic products were excellent for **P1** (99%), good for **P2** (80%) and modest for **P3** (56%); this decrease on the efficiency of the reaction performance correlates with the p*K*_a value of each activated methylene, indicating that the most acidic ones, can easily be deprotonated and react faster under milder conditions. The reaction of well-defined **1**_{CIO4} with malononitrile (p*K*_a = 11.1) occurs in less than 3 hours at room temperature obtaining quantitative yields of the desired product, whereas, the reaction of **1**_{CIO4} with acetylacetone (p*K*_a = 13.3) required higher temperatures (50 °C) and longer reaction times (24h) to achieved good performance and with a release of a water molecule during the spontaneous cyclisation. Despite the good results obtained with malononitrile and acetylacetone, the reaction of **1**_{CIO4} with dimethyl malonate (p*K*_a = 16.4) exhibited nearly poor results (37% of yield), favouring the formation of intramolecular aryl-NCH₃ side-coupling reaction at 50 °C, which often occurred when the working temperatures are above 40 °C.¹¹ In order to overcome this problem, the addition of 2.2 equivalents of Cs₂CO₃ as a base afforded the desired **P3** compound at room temperature with enhanced results, 56% of yield, which is still moderate and also a molecule of MeOH was released on the cyclisation step. In compound **P3** a new chiral carbon centre is formed as is shown in the Scheme VII.2.



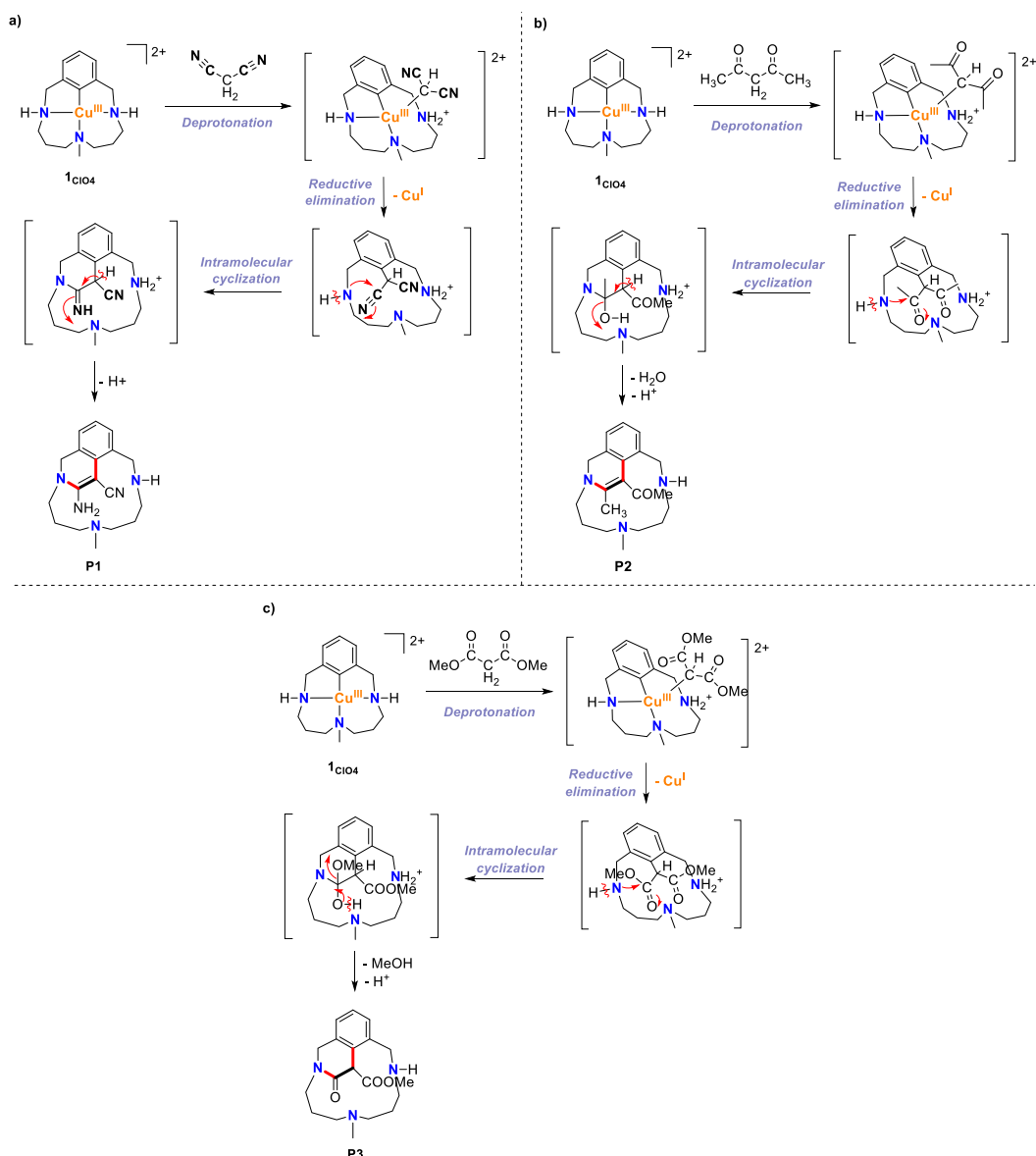
Scheme VII.2. Stoichiometric reaction between **1**_{CIO4} and activated methylene substrates, which undergo C(*sp*²)-C(*sp*³) coupling product and subsequent intramolecular reorganization. General conditions for stoichiometric reactions: [**1**_{CIO4}] = 12 mM, [nucleophile] = 24 mM, CH₃CN, 25°C. For **P2** product the reaction was carried out at 50°C and, for the **P3** product, the addition of 2.2 eq. of Cs₂CO₃ was required. Yields of C-C coupling products are calculated by ¹H NMR using 1,3,5-trimethoxybenzene as internal standard.

The structural characterization of the three compounds was challenging due to the loss of symmetry and the rigidity of the 1,2-dihydroisoquinoline (**P1** and **P2**) and 1,2-dihydroisoquinolin-3(4H)-one (**P3**) scaffolds, which make all the protons diastereotopic. For these reason, extensive two-dimensional NMR experiments such as COSY, NOESY, TOCSY, HSQC and HMBC were required (see Annex 1 for a complete explanation of the NMR structural determination of **P1-P3**).

VII.1.1.1 Mechanistic insight into the C(*sp*²)-C(*sp*³) bond formation

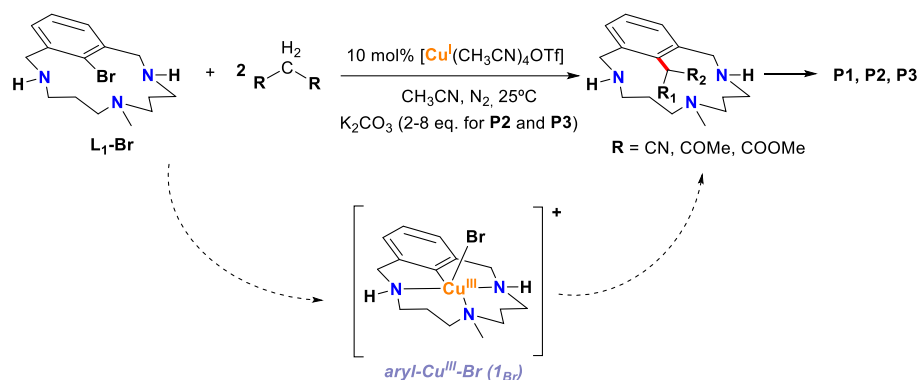
In order to get further insight into the reaction mechanism for the synthesis of **P1-P3** compounds, we were focused on the use of malononitrile as the nucleophile and monitored its reactivity with complex **1**_{C104} at low temperature, in order to trap the aryl-Cu^{III}...nucleophile adduct species analogous to the previously proposed for other nucleophiles, such as phenols or thiols.^{3,4} Indeed, low temperature ¹H NMR spectroscopy monitoring did not show the formation of any intermediate species, we could only observe the decrease of **1**_{C104} signals concomitant with the appearance of **P1** signals. Based on previous work with other heteroatoms as well as the p*K*_a dependence of the different nucleophiles in the reactivity, our mechanistic proposal starts with the rate-limiting deprotonation of the activated methylene, likely by one of the amines of the ligand. The following step was an apical coordination of the deprotonated C-nucleophile, which rapidly leads to reductive elimination to afford the C(*sp*²)-C(*sp*³) coupling product. Nevertheless, the benzylic secondary amine from macrocyclic substrate attacks a nitrile or carbonyl moiety to trigger an intramolecular spontaneous cyclisation, giving rise to the corresponding heterocyclic **P1-P3** compounds. The proposed mechanisms for the synthesis of **P1-P3** are depicted in Scheme VII.3.

Besides, the reaction between **1**_{C104} with a bulkier activated methylene substrate 1,3-diphenylpropane-1,3-dione (p*K*_a = 13.4) was also performed and no reactivity was observed, indicating that steric properties also play a clear role at least in the rate-limiting deprotonation step. Altogether, the stoichiometric reactivity shown above are consistent with the involvement of an aryl-Cu^{III} intermediate in a Hurtley-type reactivity.



Scheme VII.3. Proposed mechanism for the C-arylation of (a) malononitrile, (b) acetylacetone and (c) dimethyl malonate *via* aryl-Cu^{III} species and further intramolecular reorganization to afford the desired heterocyclic **P1-P3** compounds.

Remarkably, we also explored the catalytic copper-catalysed version of this transformation (10 mol%) within the model triazamacrocyclic aryl bromide **L1-Br** substrate affording the coupling products in quantitative yields for **P1** (>95% within 24h at 25°C), however, **P2** and **P3** were more challenging and moderate to good yields were afforded (37% and 67%, respectively for 24h at 25°C). The addition of K₂CO₃ as a base in order to overcome the lower acidity of acetylacetone and dimethyl malonate was essential to get enhanced yields. Furthermore, the catalytic synthesis of **P2** required to be performed in the presence of molecular sieves for getting better yields. This fact is probably due to the need of trapping the releasing water from the reaction, which can be the responsible of the oxidation of the Cu^I catalyst (Scheme VII.4).



Scheme VII.4. Copper-catalysed Hurtley reactions with model aryl bromide (**L1-Br**) to form **P1-P3**; highlight the detection of aryl-Cu^{III}-Br intermediate species, which undergo C(*sp*²)-C(*sp*³) coupling product and subsequent intramolecular reorganization. General conditions for catalytic reactions: [**L1-Br**] = 5 mM, [[Cu(CH₃CN)₄]OTf] = 0.5 mM, [nucleophile] = 10 mM, CH₃CN, 25°C. For **P2** product the reaction was carried out in presence of 2.2 equiv. of K₂CO₃ and molecular sieves and for the **P3** product the reaction was performed in presence of 8.8 equiv. of K₂CO₃. Yields of C-C coupling products are calculated by ¹H NMR using 1,3,5-trimethoxybenzene as internal standard.

To attain better understanding of the mechanism of the reactions described above, we monitored the catalytic transformations by UV/Vis and ¹H NMR (at low temperature) in attempt to trap intermediate species. Indeed, UV/Vis monitoring of this catalytic reaction revealed the formation of well-defined aryl-Cu^{III}-Br species (**1Br**) (band 550 nm) as a resting state of the catalyst under the reaction conditions. This observation indicates that the removal of the apical halide ligand by the C-nucleophile concomitantly with its deprotonation by a secondary amine is the rate-limiting step (Figure VII.1). Therefore, the ¹H NMR kinetics of the catalytic reaction showed equal rates of the consumption of **L1-Br** and the formation of product **P1** (Figure VII.2).

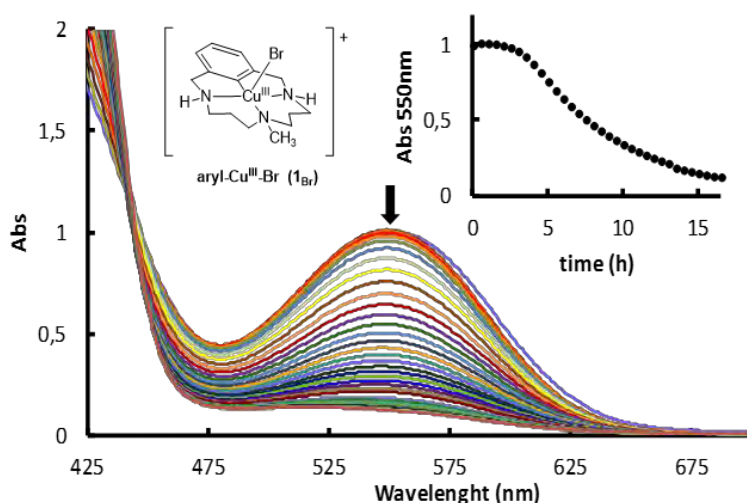


Figure VII.1. Progressive UV/Vis spectra of the cross-coupling reaction between compounds **L1-Br** and malononitrile to form **P1**, catalysed by [Cu(CH₃CN)₄]OTf, which shown a disappearance of the characteristic band of the aryl-Cu^{III}-Br (**1Br**) at 550 nm. Conditions: [**L1-Br**] = 10 mM, [[Cu(CH₃CN)₄]OTf] = 1.4 mM, [malononitrile] = 100 mM, CH₃CN, 40°C, N₂ atmosphere.

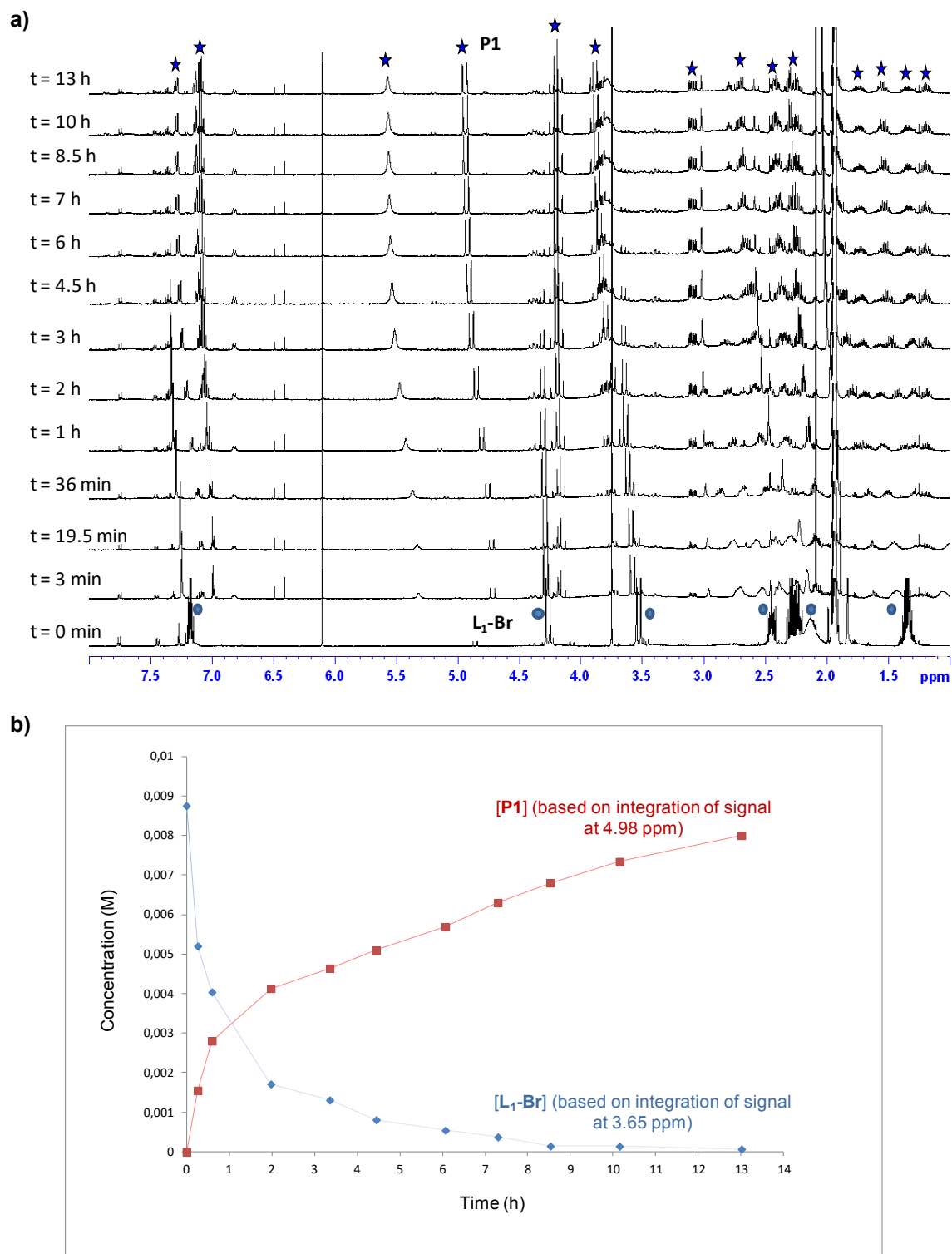
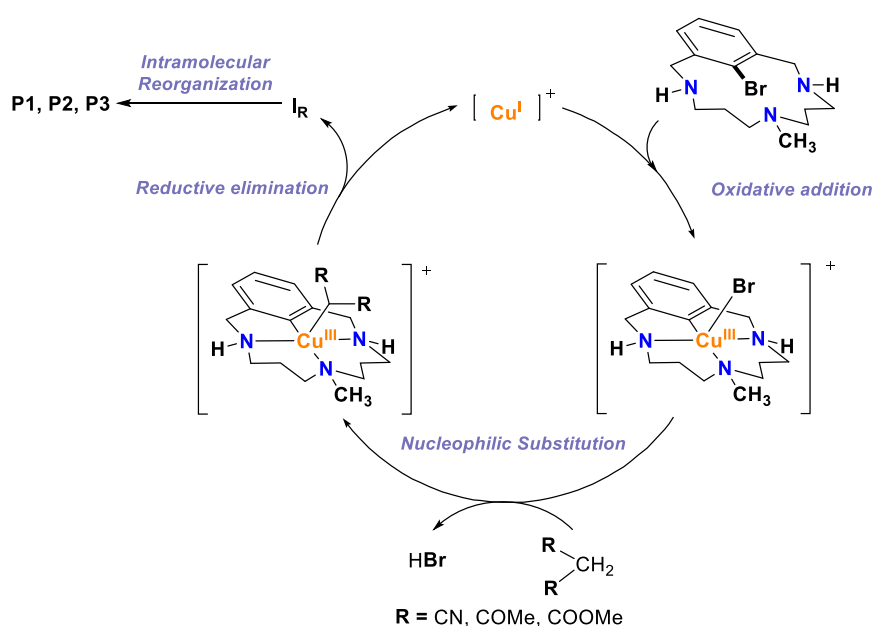


Figure VII.2. ^1H NMR monitoring of the Cu^{I} -catalysed coupling of **L₁-Br** and malononitrile to produce **P1** quantitatively. (a) Overlaid spectra showing the consumption of substrate **L₁-Br** signals (circles) and growing of **P1** signals (stars). (b) Plot of the concentration changes of both substrate **L₁-Br** and product **P1** based on the integration of selected peaks. Conditions: [**L₁-Br**] = 9.6 mM, [$[\text{Cu}^{\text{I}}(\text{CH}_3\text{CN})_4]\text{OTf}$] = 0.9 mM, [malononitrile] = 17 mM, [TMB] = 0.76 mM, CH_3CN , 40 °C, N_2 atmosphere. Spectra registered every 15 min (selected spectra are shown for clarity).

These observations enabled us to propose a catalytic cycle based on an aryl-Cu^{III} intermediate species depicted in Scheme VII.5. The catalytic reaction starts with the formation of aryl-Cu^{III}-halide through the direct oxidative addition of the aryl halide macrocyclic ligand at the Cu^I complex, followed by the rate-limiting step, in which the bromide is removed and simultaneously, the coordination and deprotonation of the activated methylene substrate occurs forming the corresponding aryl-Cu^{III}-C(*sp*³) complex. The exact nature of the coordination mode of the deprotonated C-nucleophile is still unclear, because after the rate-determining step, all the subsequent steps occurred readily fast.

Overall, we have described the first experimental example of the direct involvement of aryl-Cu^{III} species in Hurtley-type catalysis within our model platform. Moreover, the formation of heterocyclic scaffolds also constitute a valuable strategy for synthetic organic chemistry.



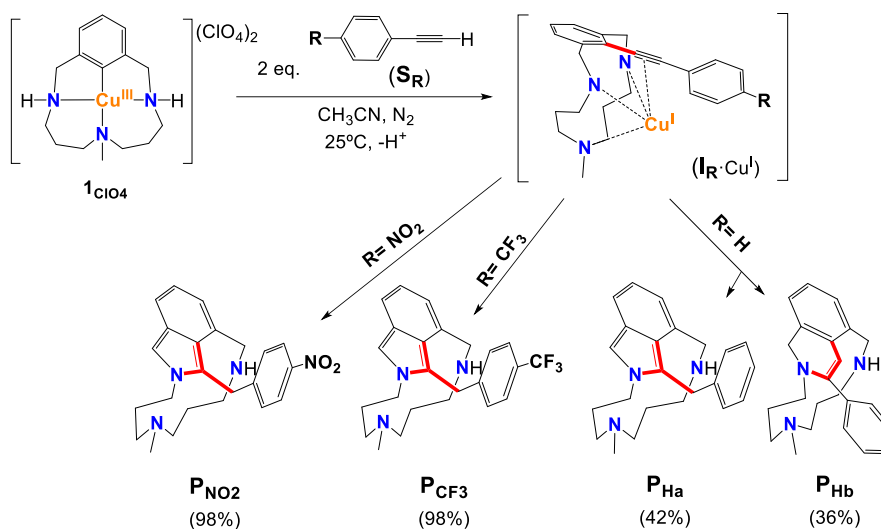
Scheme VII.5. General proposed mechanism of copper-mediated C(*sp*²)-C(*sp*³) bond formation through the intermediacy of aryl-Cu^{III} complexes within a model triazamacrocyclic aryl bromide substrate.

VII.1.2 Reactivity of aryl-Cu^{III} (1_{ClO4}) with *p*-R-phenylacetylene substrates (S_R) (Stephens-Castro Couplings)

The palladium-catalysed C(*sp*²)-C(*sp*) bond formation, called Sonogashira-Hagihara reaction, with the presence of Cu^I as a cocatalyst is one of the most widely used reaction in organic synthesis. Since the renewed interest in palladium-free methodologies, copper-mediated Sonogashira coupling, so called Stephens-Castro coupling and Miura's coupling in its catalytic version, has appeared as an attractive alternative. The mechanism of copper-mediated Stephens-Castro coupling is not well understood. Stephens and Miura groups proposed a mechanism involving the formation of a mononuclear Cu^I-acetylide species, which reacted with aryl halides in

a concerted manner through 4-centre transition state, although no experimental evidence has been provided. Inspired by our previous experience on C-Heteroatom and $C_{\text{aryl}}-C(sp^3)$ cross coupling catalysis involving well-defined aryl- Cu^{III} species, we turn our attention on the reactivity of aryl- Cu^{III} complex **1**_{ClO₄} with *p*-R-phenylacetylene (**S**_R, R = NO₂, CF₃, H) derivatives.

The stoichiometric reaction of well-defined **1**_{ClO₄} with *p*-R-phenylacetylene derivatives in CH₃CN at room temperature afforded the desired arylated compound in less than two hours, although the coupling products undergo an intramolecular spontaneous reorganization through the attack of one of the secondary amines of the macrocyclic model substrate over the alkyne moiety in an overall 8 hours of reaction time (Scheme VII.6). The final cyclised products contained 2*H*-isoindole (**P**_{NO₂}, **P**_{CF₃}, **P**_{Ha}) and 1,2-dihydroisoquinoline (**P**_{Hb}) scaffolds. It is worth to mention that no by-products were observed in any of the coupling reactions. The formation of the heterocyclic products was quantitative for **P**_{NO₂} and **P**_{CF₃}, obtaining more than 98% of yield in both cases. On the other hand, the reaction using **S**_H as a substrate could only achieve 78% of yield and interestingly, a mixture of **P**_{Ha} (42%) and **P**_{Hb} (36%) was observed in almost a 1:1 ratio. Their separation has not been possible, but a complete structural characterization of both molecules has been performed from extensive multidimensional NMR spectroscopy. According to this, the chemical structure of the obtained products has been established using NMR and ESI-MS techniques. The rigidity attained from the intramolecular reorganization transform all the methylene protons in diastereotopics. The main features that allowed us identifying the formation of 2*H*-isoindole moiety were on one hand, the observation of a singlet located 7.47 ppm, characteristic value of $C(sp^2)$ -H, which shows NOE with aromatic protons of the macrocyclic model ligand. On the other hand, the generation of benzylic protons by loss of the triple bond, are diagnostic since they show NOE signals with the aromatic protons of the phenylacetylene ring (see Annex 2 for a complete explanation of the NMR structural determination of **P**_{CF₃}, **P**_{NO₂} and **P**_H, bearing the same 2*H*-isoindole substructure as well as for **P**_H, which contain a 6-membered 1,2-dihydroisoquinoline moiety).



Scheme VII.6. Stoichiometric reaction between **1**_{ClO₄} and phenylacetylene derivatives substrates (**S**_R), which undergo $C(sp^2)-C(sp)$ coupling product and further intramolecular reorganization to form 2*H*-isoindole (**P**_{CF₃},

P_{NO2} and **P_{Ha}**) or 1,2-dihydroisoquinoline (**P_{Hb}**) scaffolds. General conditions for stoichiometric reactions: [**1_{ClO4}**] = 12 mM, [nucleophile] = 24 mM, CH₃CN, 25°C; product yields were calculated by ¹H NMR spectroscopy integration related to the internal standard.

The copper-catalysed alkynylation-cyclisation cascade reactions had been described for the synthesis of 1*H*-isoindole substructures,¹²⁻¹⁵ albeit the synthesis of 2*H*-isoindole using this strategy is unprecedented.

VII.1.2.1 Mechanistic insight into the C(*sp*²)-C(*sp*) bond formation

The structural characterization of the final products suggests that are essentially formed through an intramolecular reorganization of the expected C(*sp*²)-C(*sp*) coupling product. In order to prove our hypothesis, we monitored the reaction of **1_{ClO4}** complex with **S_{CF3}** at low temperature in an attempt to accumulate and isolate C(*sp*²)-C(*sp*) coupling product. Interestingly, we could observed the formation of a symmetric intermediate species during the time course of the reaction. Besides, we were able to accumulate this intermediate (**I_{CF3}**) at 0°C for 30 min without any sign of evolution to the formation of heterocyclic compound (Figure VII.3). This species was fully characterised by 1D and 2D NMR spectroscopy and also by HRMS using a cryospray device to inject the sample at -40°C, in order to keep the stability of the **I_{CF3}** during the measurement. Finally, the intermediate species undergo to intramolecular reorganization to form **P_{CF3}** after 18h at 0°C (see Annex 2).

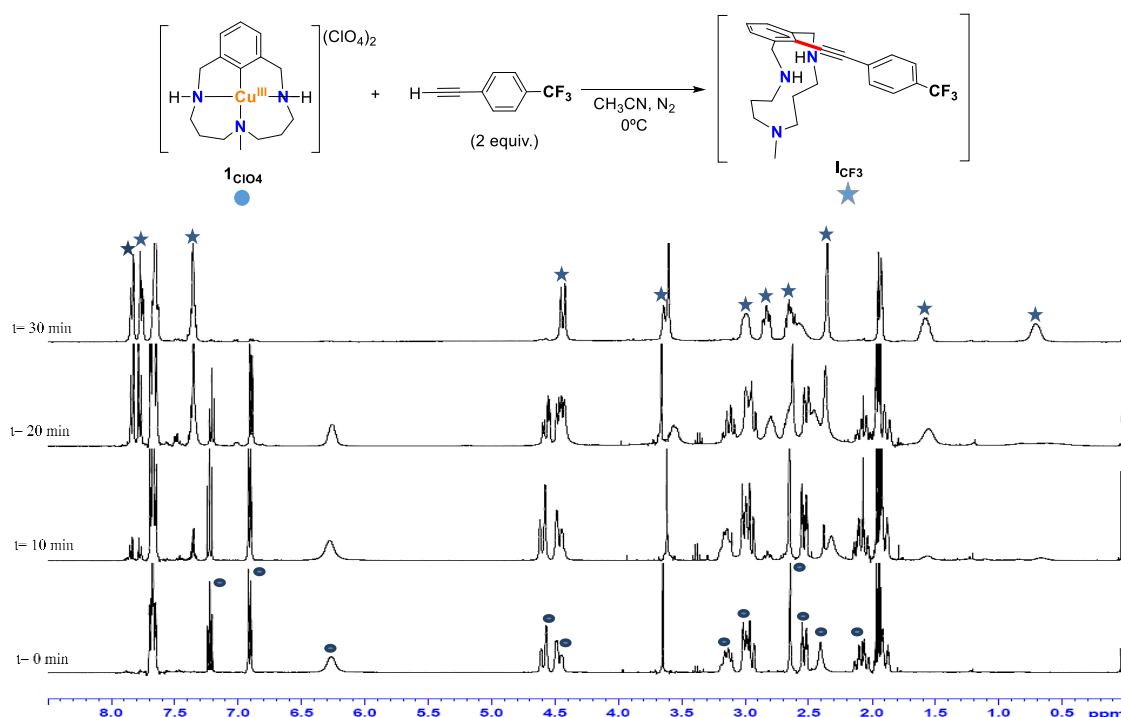


Figure VII.3. ¹H NMR monitoring study showing full formation of C_{aryl}-C_{sp} coupling intermediate species **I_{CF3}** upon reaction of **1_{ClO4}** with 2 equiv. of **S_{CF3}**. General conditions: [**1_{ClO4}**] = 78.6 mM, [**S_{CF3}**] = 157.2 mM, CD₃CN, 0 °C, N₂ atmosphere.

Bearing in mind the accumulation of the intermediate species and the moderate rate of the reorganization step, we wondered if the nucleophilic attack over the triple bond could be favoured by the coordination of Cu^{I} cation to the triple bond, activating this moiety in an electrophilic way. In order to check this hypothesis, upon accumulation of I_{CF_3} at 0°C we compared the time needed to form P_{CF_3} with and without the presence of the Cu^{I} cation in solution. To that end, we resorted to the addition of 2.5 eq. of 1,10-phenanthroline, owing to high affinity of phen to complexate Cu^{I} cation as a highly stable $[\text{Cu}^{\text{I}}(\text{phen})_2]^+$ complex. The obtained results clearly showed that the absence of electrophilic activation of alkyne moiety (by complexation of Cu^{I} cation) decreases the intramolecular reorganization rate, requiring more time for the formation of P_{CF_3} from I_{CF_3} . Altogether indicates that a substantial activation of the triple bond by Cu^{I} coordination, which is reminiscent of the chemistry of silver(I) and gold(I),¹⁶ occurs in our reaction. (Figure VII.4 and see Annex 2 for the overlaid spectra showing the consumption of reaction intermediate I_{CF_3} signals and growing of P_{CF_3} signals upon addition of 2.5 eq. of 1,10-phenanthroline).

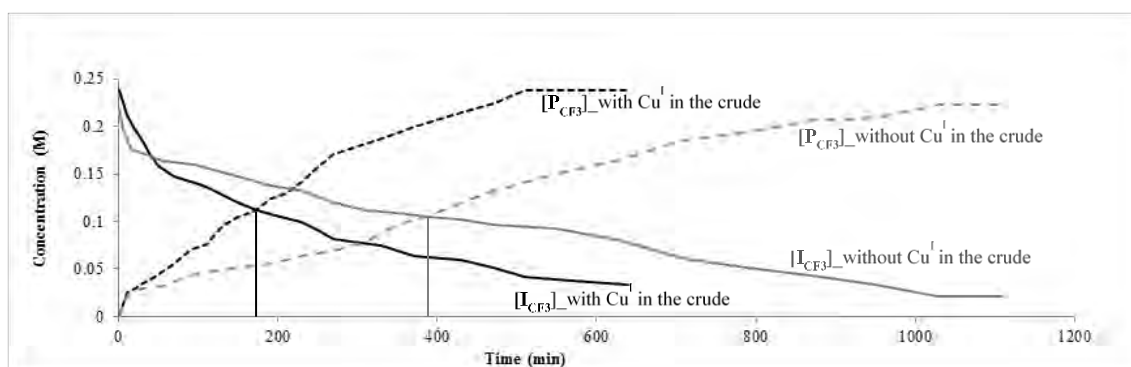
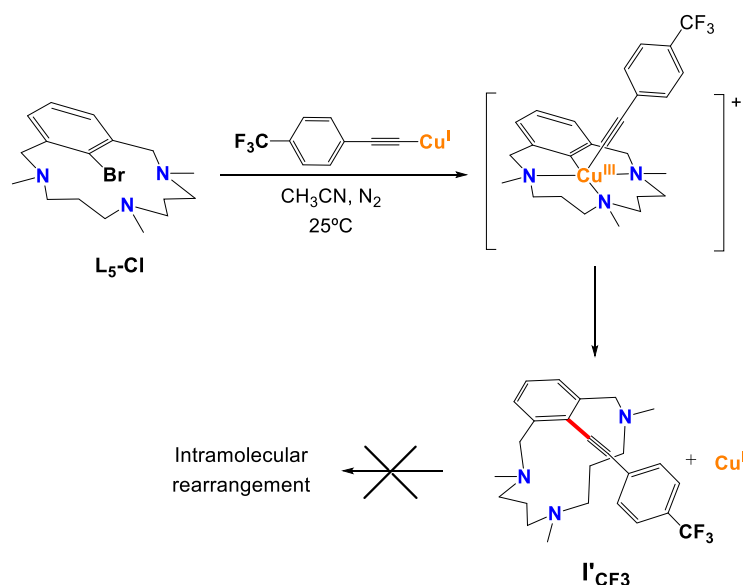


Figure VII.4. Plot of the concentration changes versus time of both I_{CF_3} and product P_{CF_3} , with and without sequestering Cu^{I} by the addition of phen. General conditions: $[\text{I}_{\text{ClO}_4}] = 78.6 \text{ mM}$, $[\text{S}_{\text{CF}_3}] = 157.2 \text{ mM}$, CD_3CN , 0°C , N_2 atmosphere.

Finally, in order to check the role of the secondary amine moiety in the cyclic reorganization step, the triazamacrocyclic model aryl bearing three permethylated tertiary amines (**L₅-Cl**) was synthesized and reacted with one equivalent of *p*- CF_3 -phenylacetylide copper(I) complex, affording 76% of yield of the I'_{CF_3} product. Interestingly, I'_{CF_3} product remains stable in solution for days without signs of intramolecular reorganization (Scheme VII.7).



Scheme VII.7. Reaction of **L₅-Cl** with *p*-CF₃-phenylacetylide copper(I) complex to afford the stable **I'_{CF3}** product.

Therefore, the formation of *2H*-isoindole or 1,2-dihydroisoquinoline scaffolds are only feasible when the model substrate bears secondary amines.

VII.1.2.2 DFT calculations and mechanistic proposal

We undertook a theoretical DFT study in order to get further insight into the general mechanism for the formation of the **P_{NO2}**, **P_{CF3}** and **P_H** coupling products.

We focused the theoretical study on the formation of **P_H** by reaction of **1⁺** and **S_H**. The first intermediate species named **B** consists of the axial π -coordination of the alkyne to the Cu^{III}. As an initial attempt to disclose the intramolecular deprotonation of the phenylacetylene by one of the secondary amines of the complex was found to be high in energy ($\Delta G = 47.1 \text{ kcal}\cdot\text{mol}^{-1}$), suggesting that the Cu^{III} oxidation state cannot be stabilized due to the decoordination of one of the amine sites (see Annex 2). In contrast, the use of an external model base (i.e. Et₂NH was selected as model base, owing to the possibility that minor amounts of free ligand are available in the reaction mixture), allowed the obtention of lower energy barriers for the formation of aryl-Cu^{III}-acetylide called intermediate **C** ($\Delta G^\ddagger = 13.0 \text{ kcal}\cdot\text{mol}^{-1}$). This species rapidly undergoes reductive elimination to form **I_H·Cu^I**, the Cu^I cation being coordinated to the macrocyclic product **I_H** (Figure VII.5). The theoretical study thus confirmed the implication of aryl-Cu^{III}-acetylide species as key intermediate species for the formation of C(*sp*²)-C(*sp*) coupling species (**I_H**).

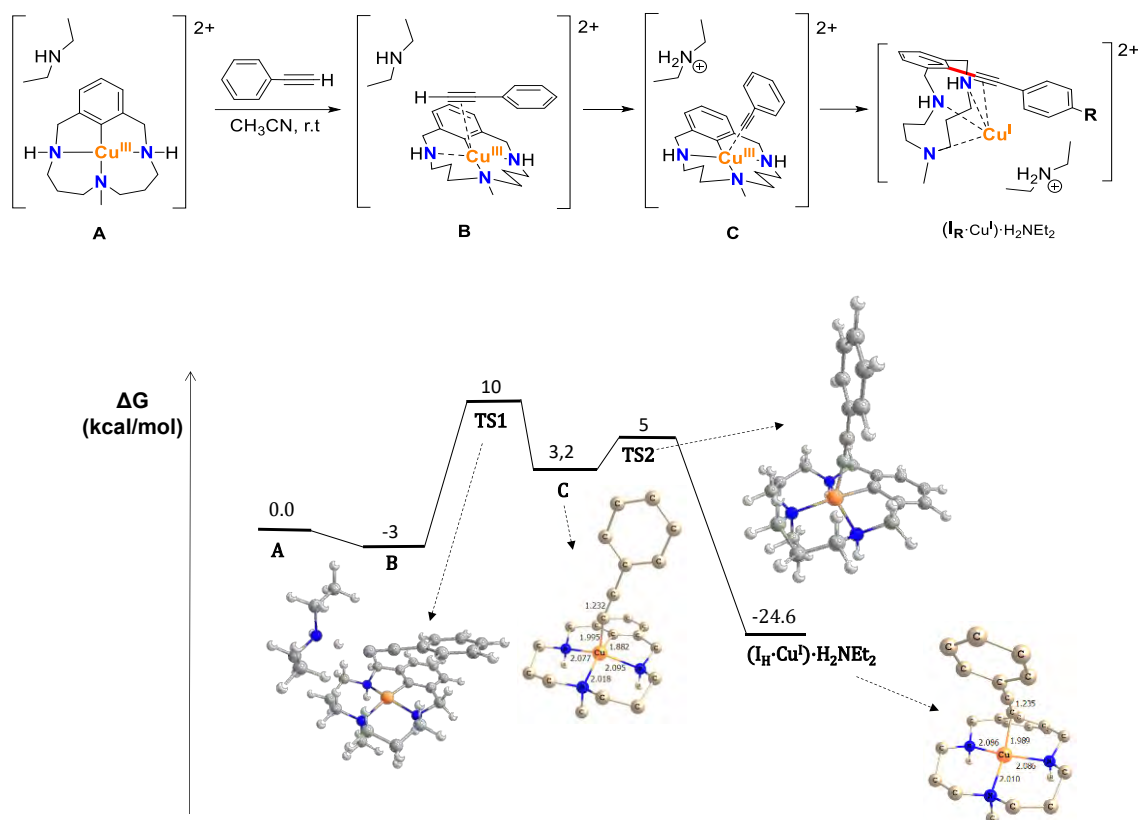
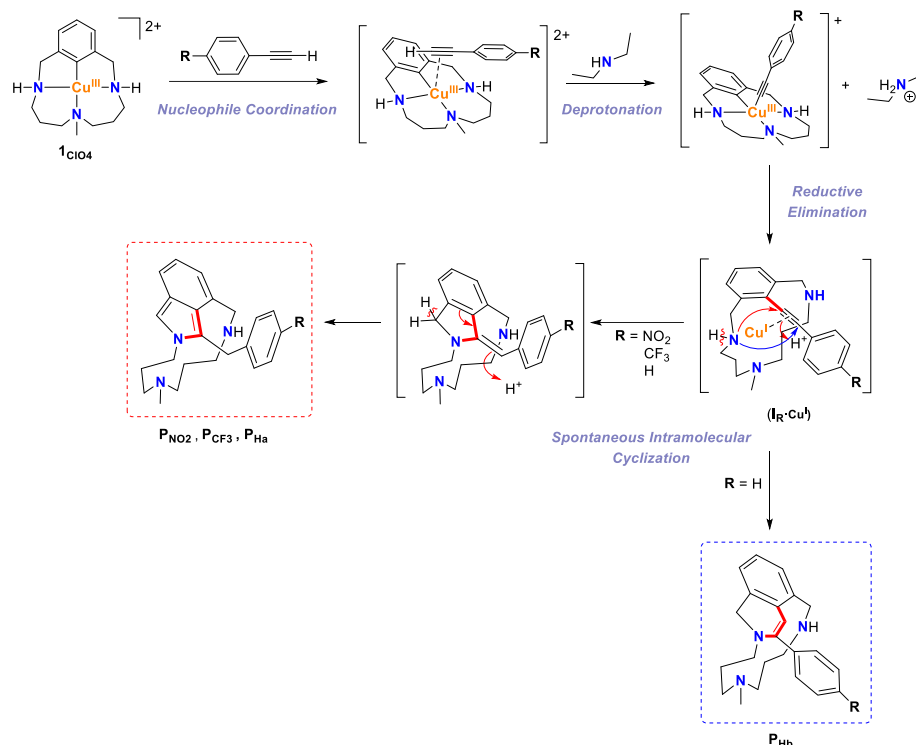


Figure VII.5. DFT Gibbs energy profile of the reaction of **1**_{ClO4} with **S**_H in the presence **Et**₂**NH** as external model base (ΔG in kcal·mol⁻¹). **Et**₂**NH** and **Et**₂**NH**₂⁺ molecules are necessary to ensure the correct energetic balance in all the steps of the reaction, and the external base was only explicitly modelled in the TS1 structure. Irrelevant hydrogen atoms are omitted for clarity.

Interestingly, we could observe that both DFT calculations and the experimental isolation of analogous **I**_{CF₃} species nicely correlate, furnishing relevant information to the puzzled mechanism of Stephens-Castro couplings. Thus, all the data gathered in this study establish a strong evidence for the clear involvement of an organometallic aryl-Cu^{III}-acetylide intermediate species in this transformations. A complete mechanistic proposal is depicted in Scheme VII.8. However, in our model system the intermediate species (**I**_R) undergoes further intramolecular reorganization to form the final products (**P**_R), which is initiated by the nucleophilic attack of one the secondary amines of the macrocyclic system over the triple bond moiety of the **I**_R compound through a Cu^I assisted intramolecular cyclisation. Nevertheless, despite the nucleophilic attack could happen at both carbons of triple bonds, we clearly observed that for the **R** = **NO**₂, **CF**₃ the attack exclusively occurs at the C2 (the farthest from **NO**₂ and **CF**₃ groups) affording exclusively the 5-membered ring forming the 2*H*-isoindole scaffold. On the other hand, for **R** = **H** the attack can occur equally at both C_{sp} atoms, thus affording almost 1:1 ratios of **P**_{Ha} (2*H*-isoindole; 5-membered ring product) and **P**_{Hb} (1,2-dihydroisoquinoline; 6-membered ring).



Scheme VII.8. Mechanistic proposal for the formation of P_R products from the 1_{CuI} complex and p - R -phenylacetylene derivatives, with the intermediacy of aryl- Cu^{III} -acetylide species, and subsequent intramolecular cyclisation following divergent pathways depending on R .

In an attempt to understand the divergent reactivity of the nucleophilic attack to the triple bond moiety depending on the substituent (R) of the phenylacetylene derivative, we performed some theoretical calculations. We calculate theoretical charge densities (Natural Population Analysis (NPA) and Mulliken charges) on the alkyne moiety for $I_R\cdot Cu^I$ species, but no significant differences in carbon atomic charges were found to rationalize the ring size preference (Figure VII.6).

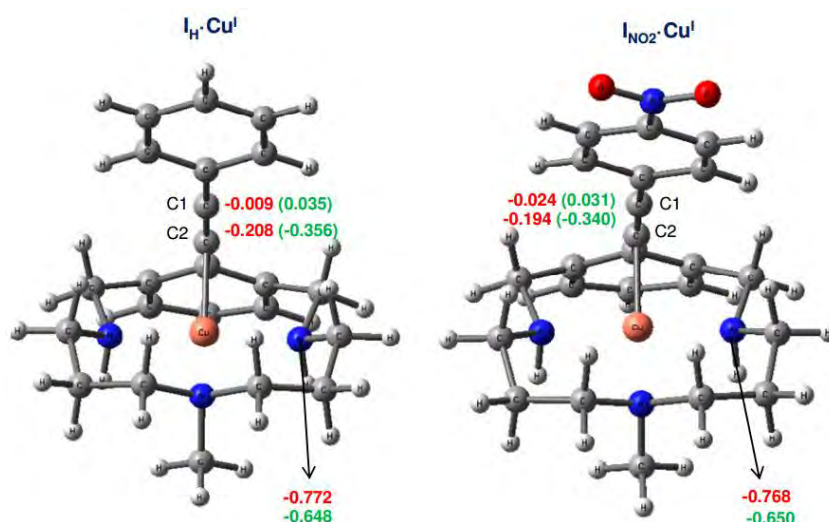
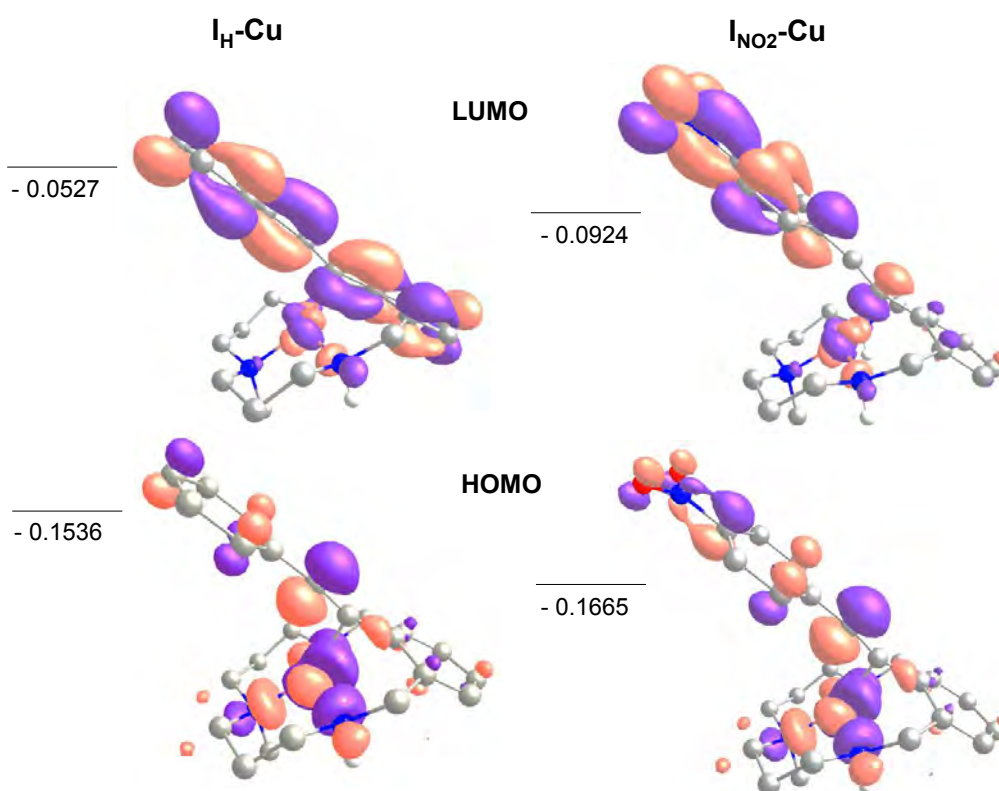


Figure VII.6. Mulliken (green) and NPA (red) charges on the alkyne and amine moieties for $I_H\cdot Cu^I$ and $I_{NO_2}\cdot Cu^I$ species. Conditions: B3LYP(6-31G* (C,N,H,Cu), SCRF = (SMD, acetonitrile), Grimme-D2).

With these uncertain results, we turned our attention to the frontier molecular orbitals theory (FMO theory), by observing the possible interactions between HOMO and LUMO orbitals of the triple bond and the secondary amine moieties. The representation of the frontier molecular orbitals for $I_H\cdot Cu^I$ and $I_{NO_2}\cdot Cu^I$ species showed that the HOMO orbital of the amine atom possess more electron density and can easily attack the LUMO orbital of the acetylene moiety (Figure VII.7a). Interestingly, when an electron-withdrawing group such as $-NO_2$ was present in the molecule, the nucleophilic attack of the amine is exclusively driven to the LUMO orbital located farthest from the electronwithdrawing center, thus allowing the single formation of 5-membered ring compound. Whereas, when the *para* substituent is a $-H$, the LUMO orbital of the acetylene is diffused, occupying both C_{sp} atoms and the nucleophilic attack could occur at both atoms equally, which is translated to the almost equimolar formation of 5-membered and 6-membered rings final products (Figure VII.7b).

a)



b)

LUMO frontier orbitals

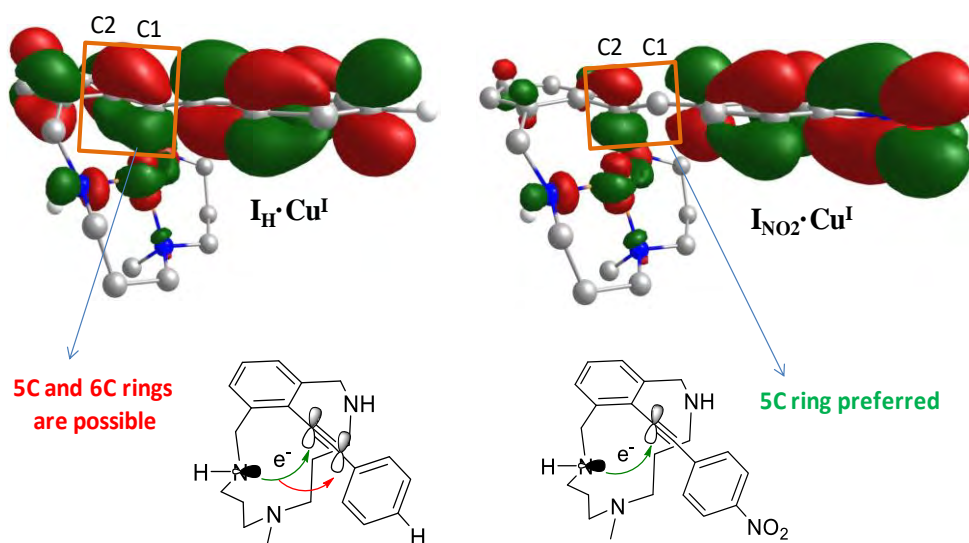


Figure VII.7. (a) Representation of the frontier molecular orbitals; the highest-energy occupied and lowest-energy unoccupied molecular orbitals (the HOMO and LUMO) for $I_H\cdot Cu^I$ and $I_{NO_2}\cdot Cu^I$ species. (b) LUMO frontier orbitals for $I_H\cdot Cu^I$ and $I_{NO_2}\cdot Cu^I$ species and simplified scheme of the possible nucleophilic attacks in each molecule (Cu^I cation is omitted for clarity).

All the information obtained from the above reported experiments using 1_{ClO_4} as our starting reactant provided the fundamental basis to attempt a catalytic version for producing $C(sp^2)-C(sp)$ coupling products within our model system.

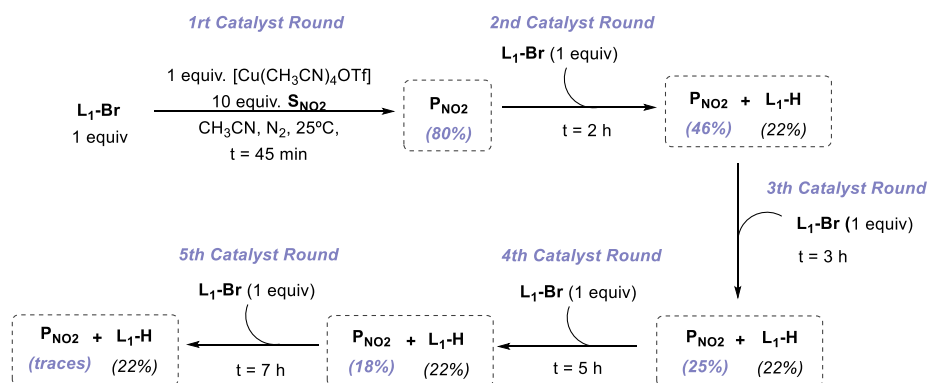
The reaction of L_1-X (Br, I, Cl) with S_{NO_2} (2 – 10 equiv) as a nucleophile under catalytic amounts of $[Cu(CH_3CN)_4OTf]$ (10 mol%) in acetonitrile solution and at room temperature, any trace of desired product were achieved, but in the most of the cases the starting material (L_1-X) was completely consumed (Table VII.1). A screening of temperature was performed, although no better performance was observed. Finally the use of some additives was also explored, the addition of base together with the addition of silver and gallium salts (halide coordination) did not show enhanced results. After exhaustive experimental optimization of the catalysis we reasoned that the heterocyclic nature of the P_{NO_2} product is unstable under catalytic conditions and its decomposition hampers the catalytic cycle.

Table VII.1. Attempts to synthesize **P_{NO2}** under catalytic amounts of Cu^I sources. General conditions for catalytic reactions: [**L1-X**] = 5 mM, [nucleophile] = 10 mM, [Cu^I source] = 0.5 mM, N₂, CD₃CN.

Ligand	Cu ^I (CH ₃ CN) ₄ OTf (mol%)	Base (equiv)	S _{NO2} (equiv)	Additive (equiv)	T (°C)	Yield (%)	Conversion (%)
L1-Br	(10)	-	2*	-	25	0	64%
	(10)	Proton Sponge (4)	2	-	25	0	100%
	(10)	-	2*	Ag(OTf) (2)	25	0	100%
	(10)	-	2*	-	50	0	82%
	(10)	Et ₃ N (2.2)	2*	-	25	0	100%
	(10)	K ₂ CO ₃ (2.2)	2	-	25	0	100%
	(10)	-	10*	-	25	0	75%
L1-I	(10)	-	2*	-	25	0	30%
	(10)	K ₂ CO ₃ (2.2)	2	-	50	0	100%
	(10)	K ₃ PO ₄ (2.2)	2	-	25	0	100%
L1-Cl	(10)	-	2*	GaCl ₃ (2)	25	0	0%
	(10)	-	10*	GaCl ₃ (2)	25	0	0%
	(10)	-	10	GaCl ₃ (2)	50	0	0%

*added by syringe pump in 3 hours.

The fact that the desired product was not obtained was puzzling. Taking into account that the starting material was fully consumed, we designed an experiment based on a sequential additions of the macrocyclic model substrate (Scheme VII.9). Our reaction started with the addition of 1 equiv of the aryl halide substrate (**L1-Br**), 1 equiv of Cu^I and 10 equiv of the **S_{NO2}** as a nucleophile, upon 45 min of the beginning of the reaction we undertook a NMR spectra and we could observed the formation of **P_{NO2}** in a 80% of yield. At this point, we added 1 equiv more of **L1-Br** substrate, after 2 h of the beginning of the reaction and 1 h and 15 min of the 2nd addition, we analysed the reaction crude, observing a decreasing on the yield of the **P_{NO2}** from 80% to 46% of yield, and in addition **L1-H** appeared as by-product. The 3th addition of another equivalent of **L1-Br** into the reaction mixture was done, after 3 h of the beginning of the reaction and 1 hour of the last addition, the same trend was observed, the yield of desired product was still decreasing (25%) and also new signals were growing, mainly due to decomposition. A subsequent addition of another equivalent of **L1-Br** was performed, after 5 hours of the beginning of the reaction and 2 hours of the last addition, only 18% of **P_{NO2}** was observed and the appearance of random signals was increasing, indicating a clear decomposition of the previously formed **P_{NO2}**. Finally, last addition of 1 equivalent of **L1-Br** was done, after 7 hours of the beginning of the reaction and 2 hours of the last addition, insignificant amounts of **P_{NO2}** was observed after 8 hours of starting the reaction, showing a completed decomposition of desired product.



Scheme VII. 9. Sequential addition of macrocyclic model substrate (**L₁-Br**) on a catalytic reaction in order to understand the catalytic operative mechanism. General conditions for the reaction: [**L₁-Br**] = 20 mM (each addition of 25 μ L), [**S_{NO2}**] = 200 mM, [**Cu^I** source] = 20 mM, [**TMB**] = 2.4 mM N_2 , CD_3CN ; product yields were calculated by 1H NMR spectroscopy integration related to the internal standard.

The obtained results suggests a possible inhibition or entrapment of Cu^I released upon reductive elimination, because the **P_{NO2}** yield did not increase during the reaction performance. Moreover, this experiment prove the low stability of this heterocyclic species, which rapidly decompose in the reaction mixture.

Therefore, we screened the copper-assisted reaction using **L₅-Br** and **L₅-Cl** as a macrocyclic model substrates with 2 equiv of **S_{CF3}** and 4 equiv of external base (to assist the acetylene deprotonation) to form the non-heterocyclic coupling product **I'_{CF3}** (Table VII.2). Interestingly we could observed that the obtained yields for the desired product were closed to the copper(I) loading used, indicating that only stoichiometric amounts of compounds can be obtained. Similar results were found when Cu^I -acetylide was used as copper catalyst (Table VII.2). However, we have not been able to develop the catalytic version of such reaction so far.

Table VII.2. Attempts to synthesize **I'_{CF3}** under catalytic amounts of Cu^I sources. General conditions for catalytic reactions: [**L₅-X**] = 5 mM, [nucleophile] = 10 mM, [Cu^I source] = 0.5 mM and 1 mM, N_2 , CD_3CN .

Ligand	Cu^I (mol%)	Base (equiv)	S_{CF3} (equiv)	T (°C)	Yield I'_{CF3} (%)
L₅-Cl	$Cu^I(CH_3CN)_4OTf$ (10)	-	2	25	10%
	$Cu^I(CH_3CN)_4OTf$ (10)	K_2CO_3 (4)	2	25	15%
	$Cu^I(CH_3CN)_4OTf$ (10)	K_3PO_4 (4)	2	60	0%
	$Cu^I-(C\equiv C-Ph-pCF_3)$ (20)	$tBuO^-K^+$ (0.2)	0.2	25	23%
L₅-Br	$Cu^I-(C\equiv C-Ph-pCF_3)$ (20)	K_3PO_4 (4)	2	70	0%
	$Cu^I(CH_3CN)_4OTf$ (20)	$tBuO^-K^+$ (4)	2	50	0%

These observations are in agreement with the previously proposal of the inhibition or entrapment of Cu^I . At present we have not been able to overcome the inactivation of the Cu^I released in solution to achieve catalytic turnover, despite different strategies that have been explored.

VII.2 Mechanistic insight in the trifluoromethylation of a well-defined aryl-Ni^{II} complex involving a SET step and a Ni^{IV}-CF₃ intermediate species

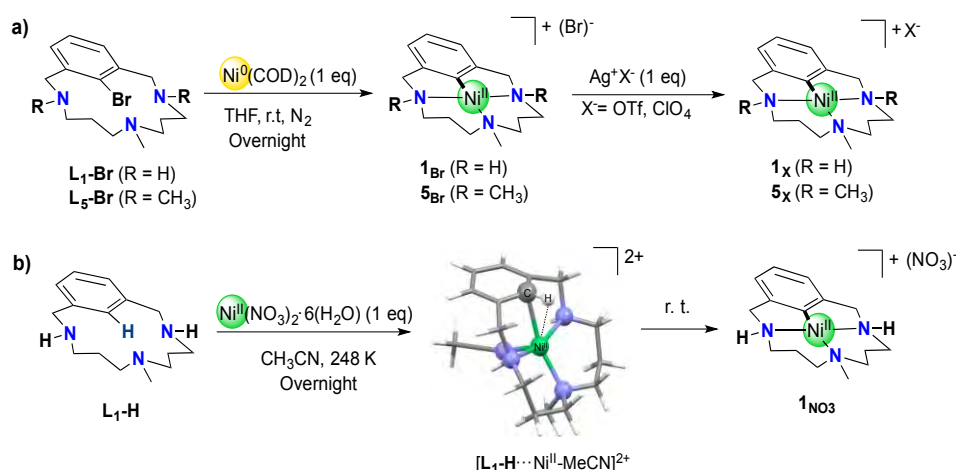
This section corresponds to the contents of **Chapter V** of this thesis (manuscript under revision).

*The compounds labelled as **1_x** ($X = \text{TfO}^-$, ClO_4^- or NO_3^-) in this section correspond to macrocyclic aryl-Ni^{II} complexes, and differ from the aryl-Cu^{III} complex labelled as **1_{ClO4}** in the section VII.1.*

Crucial challenges in nickel catalysis rely on a clear understanding of the plausible mechanisms involved in such transformations. In recent years, the interest in the feasibility of the involvement of high-valent Ni species as a putative intermediates in catalysis has grown. Therefore, several research groups designed and synthesised an array of an octahedral high valent aryl-Ni^{III} and Ni^{IV} model systems, capable to undergo *via* reductive elimination to the formation of C_{aryl}-Heteroatom and C_{aryl}-C bonds.¹⁷⁻²¹ In this sense, we are interested in gaining mechanistic insight in the redox chemistry of Ni using macrocyclic model systems in atypical non-octahedral environments, previously studied for copper. We synthesized an organometallic square planar aryl-Ni^{II} model system in order to evaluate its reactivity in front electrophilic trifluoromethylating agents, as well as the plausibility of accessing to high-valent nickel species.

VII.2.1 Synthesis and characterization of [L_n-Ni^{II}](X)

Organometallic aryl-Ni^{II} complexes [L_n-Ni^{II}](X) ($n = 1$ or 5 , $X = \text{TfO}^-$, ClO_4^- or NO_3^-) (**1_{Tf}**, **1_{ClO4}**, **1_{NO3}** and **5_{Tf}**) can be synthesised following two distinct procedures: a) through the oxidative addition of **L₁-Br** or **L₅-Br** (macrocyclic model substrate bearing permethylated tertiary amines) to Ni(COD)₂ and b) through the direct C-H activation of **L₁-H** using Ni(NO₃)₂ (Scheme VII.10).



Scheme VII.10. Synthesis of organometallic aryl-Ni^{II} complexes (**1_{Tf}**, **1_{ClO4}**, **1_{NO3}** or **5_{Tf}**) *via* (a) oxidative addition at Ni⁰ and (b) direct C-H activation by Ni^{II} (DFT optimized structure of $[\text{L}_1\text{-H} \cdots \text{Ni}^{\text{II}}\text{-MeCN}]^{2+}$ is depicted).

$[L_1-Ni^{II}](X)$ complexes (**1_X**, $X = TfO^-$, ClO_4^- or NO_3^-) and $[L_5-Ni^{II}](OTf)$ (**5_{OTf}**) can be synthesised through the oxidative addition of macrocyclic model system (**L₁-Br**) to $Ni(COD)_2$ in THF at room temperature, followed by treatment with AgX (TfO^- , ClO_4^-) in order to exchange the counter anion and increase the solubility, affording the desired complexes in quantitative yields. On the other hand, the **1_{NO₃}** complex can also be synthesised *via* direct $C(sp^2)$ -H activation of the macrocyclic model substrate (**L₁-H**) mediated by $Ni(NO_3)_2 \cdot 6H_2O$ as a nickel source in MeCN at room temperature, affording the desired product in 55% yield. After exhaustive screening of nickel(II) sources, solvents, bases and temperature, the reaction performance was not improved (see Annex 3). In addition, no $C(sp^2)$ -H activation was observed when **L₅-H** was used, even in the presence of several bases, evaluating several nickel(II) sources or screening different solvents and temperatures (see Annex 3). These results strongly suggest that the presence of secondary amines are essential for the $C(sp^2)$ -H activation process. As was mentioned in the introduction chapter, the C-H activation of macrocyclic model substrate by $Ni(NO_3)_2 \cdot 6H_2O$ salts probably proceed through concerted-metalation-deprotonation (CMD) mechanism, because nickel does not change its oxidation state; however, no direct mechanistic insights were reported yet.

Some years ago, our group reported the C-H activation reaction effected by Ni^{II} ligated to triazamacrocyclic ligands to afford an aryl- Ni^{II} complex. Accordingly with the experimental paramagnetic 1H NMR spectrum, that suggested a non-square planar d^8 high spin Ni^{II} species, an intermediate species based on three-electron $C-H \cdots Ni^{II}$ interaction $[Ni^{II}(H33m)(CH_3CN)]^{2+}$ was proposed and supported by DFT calculations.²² On the basis of this previously analogous complex featuring a trigonal bipyramidal geometry at the nickel centre, we further studied the geometry at the Ni^{II} centre and the interaction with the C-H bond by XAS. The paramagnetic nature of the species discards square planar, or square pyramidal geometry for the metal centre. In addition, the XANES region from the X-ray absorption spectrum of $[L_1-H \cdots Ni^{II}]^{2+}$ is consistent with either a trigonal bipyramidal or tetrahedral coordination environment.²³ The lack of any resolvable shoulder on the rising edge at around ~ 8337 eV, excludes the possibility of a square planar or square pyramidal geometry. Furthermore, the pre-edge at ~ 8332.1 eV correlates with the presence of a Ni^{II} centre with an intensity of 0.07 normalised units (Figure VII.8a and Figure S7 in Annex 3).

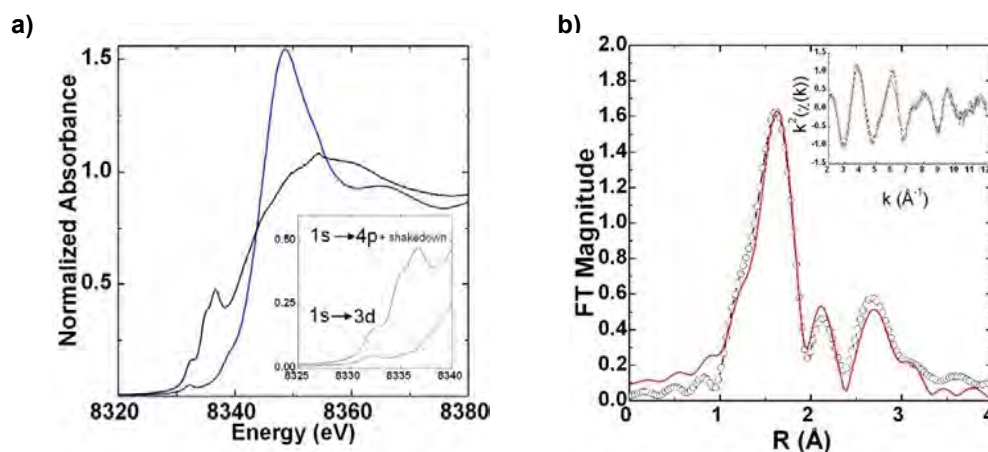


Figure VII.8. (a) XANES spectra of $[\text{L1-H}\cdots\text{Ni}^{\text{II}}\text{-MeCN}]^{2+}$ (blue) and $\mathbf{1NO}_3$ in solution (black); Inset: highlight of the pre-edge region. (b) EXAFS analysis of $[\text{L1-H}\cdots\text{Ni}^{\text{II}}\text{-MeCN}]^{2+}$. Shown are Fourier-transformed EXAFS spectra (no phase correction, FT, window as shown in the inset); Inset: k^2 -weighted unfiltered EXAFS spectra) and comparison of selected EXAFS derived and theoretical bond distances.

The pre-edge of $[\text{L1-H}\cdots\text{Ni}^{\text{II}}]^{2+}$ arising from $1s\rightarrow 3d$ transitions is too intense for that expected for octahedral environment and more in line with a trigonal bipyramidal (0.04 – 0.09 intensity units) or tetrahedral (0.08 – 0.11 intensity units) metal coordination. Finally, EXAFS analysis suggests a five coordinate metal centre, dismissing the possibility of a tetrahedral nickel centre (Figure VII.8b; see in Table S6 and Figure S8 in Annex 3). This results in a most probable trigonal bipyramidal geometry at the metal centre having 4 N/O scatters at an average distance of 2.09 Å (~ 2.09 Å from DFT) and a C_{aryl} scattering atom at 2.29 Å (~ 2.39 Å from DFT, see Scheme VII.10b). All the data is in agreement with the complex bearing a coordinated acetonitrile, and consistent with both the previously published DFT structure and our current *in silico* investigation (water ligation was also evaluated and found energetically unfavorable (see Table S7 in Annex 3)).

On the other hand, organometallic Ni^{II} complexes $\mathbf{1ClO}_4$, $\mathbf{1NO}_3$ and $\mathbf{5OTf}$ have been spectroscopically and crystallographically characterized (Figure VII.9 and Figure S1 - S3 in Annex 3) featuring a square planar geometry for Ni^{II} centre, which is coordinated to three amines and an aryl moiety. The $\text{Ni}^{\text{II}}\text{-C}$ (ranging from 1.83- 1.84 Å) and $\text{Ni}^{\text{II}}\text{-N}$ (ranging from 1.95- 2.06 Å) distances found are significantly shorter than analogous macrocyclic aryl- Ni^{II} using azacalix[1]arene[3]pyridine ligand scaffolds (1.88 Å), which also feature square planar geometry for the Ni^{II} centre.²⁴ The larger $\text{Ni}^{\text{II}}\text{-N}$ bonds for the *trans* coordinated tertiary amine in all three complexes show the stronger *trans* effect of the aryl moiety.

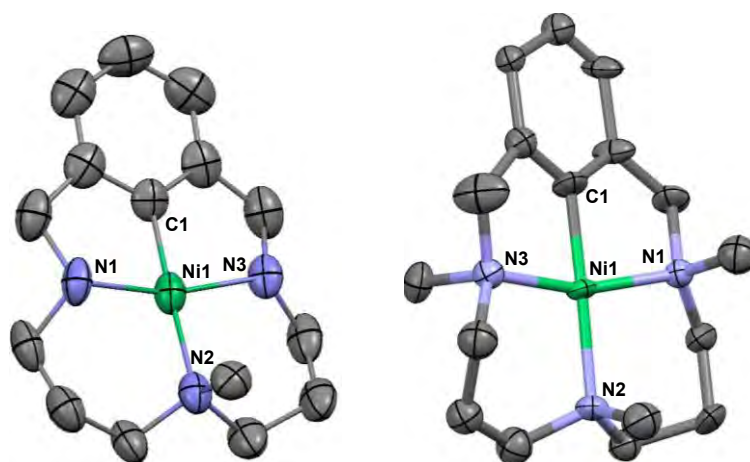


Figure VII.9. X-Ray crystal structures of **1ClO₄** (left) and **5OTf** (right) at 50% probability level. H atoms and counter anions omitted for clarity. Selected bond distances [Å] and angles [°] for **1ClO₄**: Ni(1)-C(1) 1.840(4), Ni(1)-N(3) 1.953(3), Ni(1)-N(1) 1.955(3), Ni(1)-N(2) 2.032(4); C(1)-Ni(1)-N(3) 83.33(18), C(1)-Ni(1)-N(1) 83.68(18), N(3)-Ni(1)-N(1) 164.53(16), C(1)-Ni(1)-N(2) 176.15(16), N(3)-Ni(1)-N(2) 96.68(15), N(1)-Ni(1)-N(2) 95.71(16). Selected bond distances [Å] and angles [°] for **5OTf**: Ni(1)-C(1) 1.838(7), Ni(1)-N(3) 1.98(3), Ni(1)-N(1) 1.94(3), Ni(1)-N(2) 2.062(6); C(1)-Ni(1)-N(3) 80.6(11), C(1)-Ni(1)-N(1) 84.2(8), N(3)-Ni(1)-N(1) 163.0(13), C(1)-Ni(1)-N(2) 178.3(10), N(3)-Ni(1)-N(2) 98.9(10), N(1)-Ni(1)-N(2) 96.5(8).

NMR studies and HRMS spectrometry analysis (see Annex 3) provided a conclusive evidence that in solution [**L_n**-Ni^{II}](X) complexes maintain the same structure observed in the solid state. To further explore the coordination environment of the metal centre in **1NO₃**, X-ray Absorption Spectroscopy (XAS) at the Ni K-edge was applied in order to probe the electronic structure for a solution sample of **1NO₃**. EXAFS analysis of **1NO₃** and **1OTf** is consistent with the crystal structure and shown the presence of four coordinate complexes having a short Ni-C bond of ~1.83 Å with 3 nitrogen scattering atoms in the ~1.97 Å range (Table S6 and Figure S8). Additionally, the XANES region of **1NO₃**, measured on a solid samples, exhibit a well resolved shoulder on the rising edge centred around 8335.9 eV, due to its 1s→4p + shakedown contributions as expected from a square planar geometry.^{23,25} Although the solid samples exhibit broader features, which are consistent with the resolved XANES spectra of the **1NO₃** solution sample as evidenced by second derivative plots. The **1NO₃** solution samples exhibits an intense pre-edge at 8332.3 eV from 1s→3d transitions, indicative of a Ni^{II} centre with a rising shoulder having two well resolved features at 8334.8 eV and 8336.7 eV (Figure S7 in Annex 3).

Interestingly, square planar complexes having centrosymmetric coordination environment are expected to have weak pre-edge intensities of below 0.02 normalised intensity units as exemplified by the spectra of [Ni(cyclam)](ClO₄)₂.²³ This is due to the dipole forbidden nature of the 1s→3d pre-edge transitions which can only gain intensity through p-d mixing, a process not favoured in square planar geometry.^{26,27} However, the pre-edge of **1NO₃** having an intensity of ~0.3 units is similar to the well resolved pre-edge of a previously reported square planar Ni^{II} complex, [(bpy)]Ni(Mes)Cl], having a C_{aryl}-Ni bond of 1.94 Å.²⁸ This can be explained by the highly covalent nature of the Ni-C bond, which facilitates p-d mixing through a configuration interaction

model, as previously described.^{29,30} Furthermore, the strenght of the C_{aryl}-Ni interaction in **1**_{NO₃} is further highlighted by the lower energy of the features due to 1s→4p + shakedown contributions which occur ~2 eV lower in energy than in either the previously reported [(bpy)]Ni(Mes)Cl] complex having a C_{aryl}-Ni bond of 1.94 Å or the [Ni(cyclam)](ClO₄)₂ analogue having no Ni-C bond.³¹

VII.2.2 Reactivity of [L_n-Ni^{II}](X) towards common nucleophiles

After fully characterization of aryl-Ni^{II} complexes, we studied their reactivity in front a broad range of nucleophiles of different nature, such as phenols, boronic acids, amines, and activated methylenes among others. Unfortunately, the aryl-Ni^{II} species showed to be very stable and C-Heteroatom reductive elimination was not observed, even under high temperatures. This is in contrast with the analogous macrocyclic aryl-Ni^{II} complexes described by Wang, using azacalix[1]arene[3]pyridine ligand scaffolds, which readily react with several nucleophiles, like phenols and sodium azides among others.²⁴ The most important difference between this two square planar nickel(II) systems is the Ni^{II}-C bond distance, suggesting that the stronger bond of the tighter macrocyclic coordination prevented the reductive elimination. The Ni^{II}-C_{aryl} bond distances in **1**_x and **5**_x are among the shortest reported^{22,32-35} in the Cambridge Crystallographic Database, which typically are larger than 1.89 Å.³⁶⁻³⁹ These findings suggested that the rigidity imposed by the macrocyclic environment might limit they reactivity, and the addition of oxidant reagents might allow to enhance or trigger their reactivity.

Due to the lack of reactivity of the aryl-Ni^{II} complexes using common nucleophiles and bearing in mind the idea of working with oxidants, we moved to study the electronic properties of **1**_{OTf} and **5**_{OTf} by Cyclic Voltammetry. We hypothesized that the highly donating chelating ligand platform might allow us to have access to high-valent nickel species. Interestingly, the accessibility to Ni^{III} oxidation state within the square planar platforms is clearly visible in the CV spectrum of **1**_{OTf} (Figure VII.10, blue chart) and **5**_{OTf} (Figure VII.10, purple chart) showing a chemically quasi-reversible 1e⁻ processes associated with Ni^{II}/Ni^{III} redox couples centered at E_{1/2} = 0.066 V and 0.227 V, respectively (vs Ag/AgNO₃). These results showed that nickel(III) oxidation state is more stabilized with secondary amines, due to their higher σ-donating ability in comparison to tertiary amines.

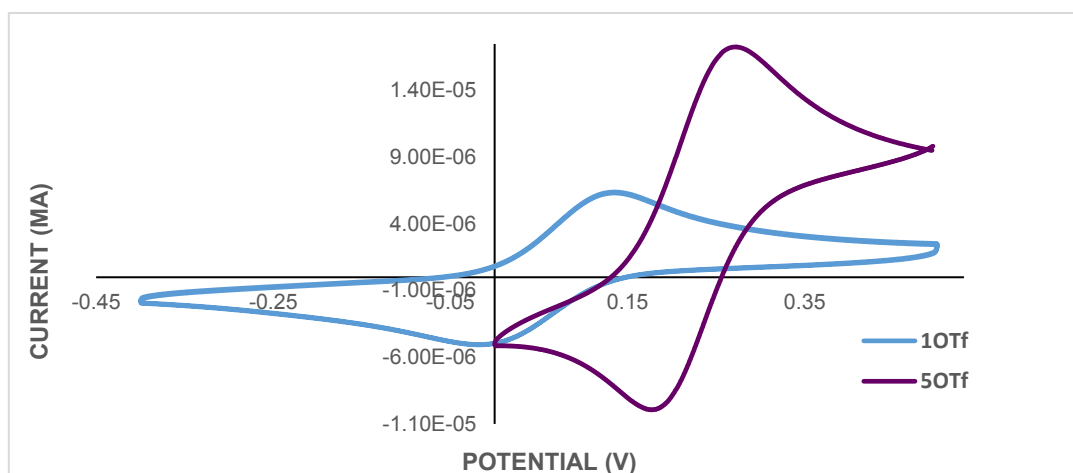


Figure VII.10. Cyclic voltammetry (CV) of complexes **1OTf** (blue chart) and **5OTf** (purple chart). Conditions used $[1_{OTf}] = 0.5$ mM, $[n\text{-Bu}_4\text{NPF}_6] = 0.1$ M and $[5_{OTf}] = 1$ mM, $[n\text{-Bu}_4\text{NPF}_6] = 0.1$ M, CH_3CN , 298 K, scan rate = 0.1 V/s, using non-aqueous Ag/AgNO_3 reference electrode.

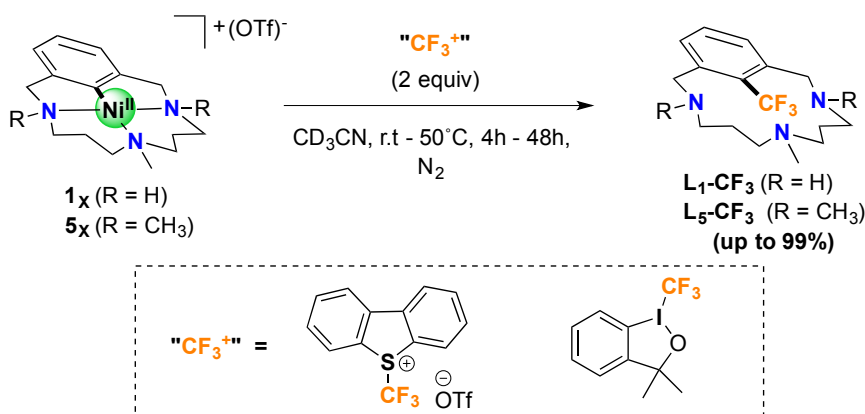
VII.2.3 Reactivity of $[\text{L}_n\text{-Ni}^{\text{II}}](\text{X})$ towards $1e^-$ and $2e^-$ oxidants

Since high-valent oxidation states of nickel can be accessed within our square planar macrocyclic model system, we evaluated their reactivity towards several $1e^-$ oxidants using MeOH as a nucleophile and solvent. However, the reactivity of **1OTf** and **5OTf** in front of Fc^+ , Ag^+ and NO^+ resulted in very complex reaction mixtures, due to the involvement of several side-reactions, such as the oxidation of amine-based ligands to imines, as well as the hydrogenation of the aryl moiety to arene. Similar results were obtained when malononitrile (active methylene), *p*-methoxyphenol and sodium cyanide were used as nucleophile.

Therefore, albeit generating a much more reactive species using $1e^-$ oxidants, we have not been able to control this enhanced reactivity to achieve a clean C-Heteroatom bond formation from the Ni^{III} reductive elimination. Accordingly to this observation, very recently Sanford and co-workers discussed about the uncontrolled side reactions of in situ generated Ni^{I} species.⁴⁰

In contrast, since Ni^{IV} species were reported to undergo reductive elimination with nucleophiles,^{17,18,21} we turned our attention on the use of $2e^-$ redox oxidants. We studied the reactivity of **1OTf** and **5OTf** with $\text{PhI}(\text{OAc})_2$ and F^+ reagents, such as N-fluoro-2,4,6-trimethylpyridinium triflate (NFTPT) and Selectfluor®, but we observed the same trend of multiple side-reactions, such as ligand oxidation and deprotonation, hydrogenation, among others, which resulted in the decomposition of **1OTf** and **5OTf** complexes. Subsequently, we changed the F^+ reagent for the CF_3^+ reagents, which are known to promote 2 electron oxidation of group 10 metal complexes and, we evaluated the reactivity of our complexes with 5-(trifluoromethyl)dibenzothiophenium trifluoromethanesulfonate (TDTT) and 3,3-Dimethyl-1-(trifluoromethyl)-1,2-benziodoxole (Togni reagent). To our delight, we observed quantitative formation of **L₁-CF₃** and **L₅-CF₃** products, respectively.

Initial tests were performed using stoichiometric amounts of **1_{OTf}** together with 2 equiv of corresponding trifluoromethyl oxidant in CD₃CN. At room temperature using TDDT as a trifluoromethyl source, the reaction shows excellent performance obtaining more than 99% yield in less than 4 hours. Otherwise, using Togni's reagent as an oxidant, quantitative yields (>99%) were also obtained, albeit in 12 hours. On the other hand, the reaction of **5_{OTf}** using both TDDT and Togni reagent as nucleophiles requires higher temperatures (70°C) and longer reaction times (48 hours) to reach almost quantitative yields (>95%) (Scheme VII.11).



Scheme VII.11. Reactivity of **1_{OTf}** and **5_{OTf}** in the presence of widely used "**CF₃⁺**" oxidants, TDDT and Togni reagent to obtain **L₁-CF₃** and **L₅-CF₃**. General conditions for stoichiometric reactions: [**1_{OTf}**] = 29.3 mM, [**CF₃⁺**] = 58.6 mM, CH₃CN, 25°C, 4h and [**5_{OTf}**] = 27.7 mM, [**CF₃⁺**] = 55.4 mM, CH₃CN, 70°C, 48h.

Initially we hypothesized that the trifluoromethylated product is likely generated *via* reductive elimination from a Ni^{IV} intermediated species in similarity to the work reported by Sanford and co-workers.¹⁸ In addition, the slower reactivity observed with **5_{OTf}**, suggests a lower stability of high oxidation states the nickel when tertiary amines are used (less σ-donor ability), as we could observe in the CV experiments of **1_{OTf}** and **5_{OTf}**.⁴¹

In an attempt to detect and characterise the putative aryl-Ni^{IV} intermediates species, we followed the reaction between **1_{OTf}** together with 1 equiv of TDDT by NMR at -40°C. We were not able to detect the formation of an intermediate species and the formation of **L₁-CF₃** occurred at equal rate of consumption of **1_{OTf}**, indicating that this putative aryl-Ni^{IV} intermediate is highly reactive (Figure VII.11).

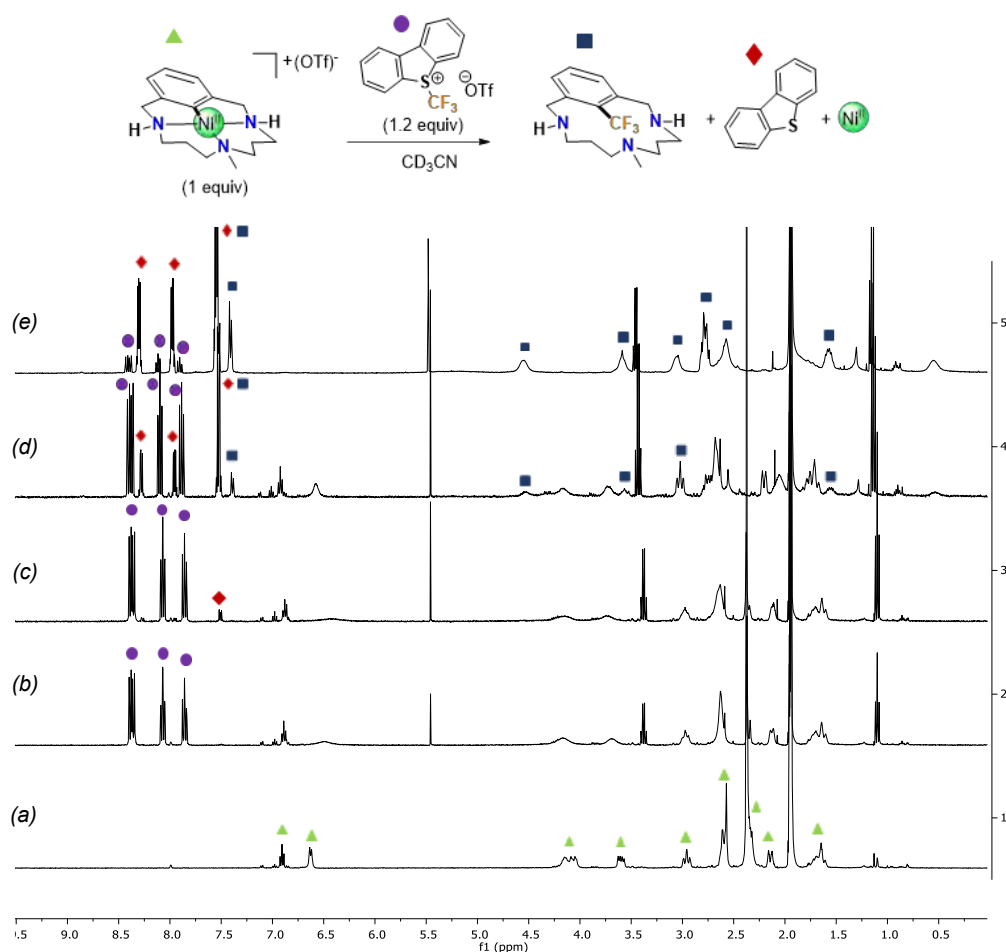
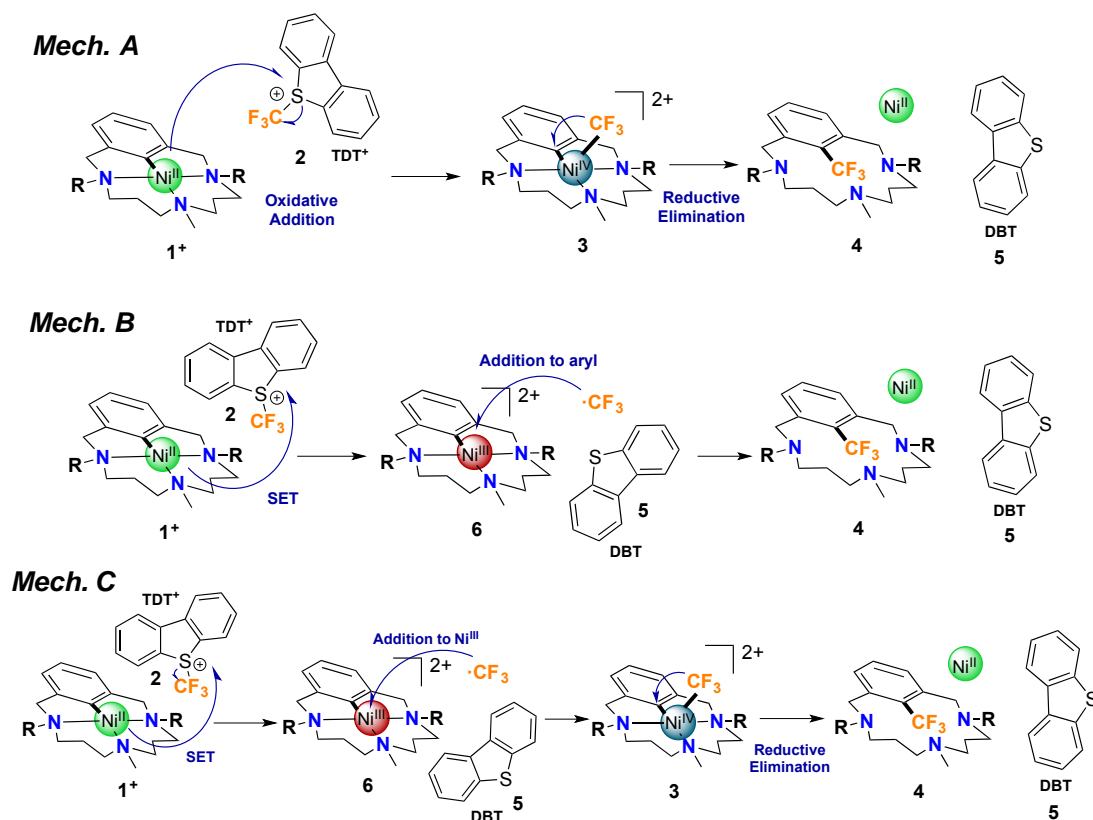


Figure VII.11. Reaction progress of the formation of trifluoromethylated compound and consumption of **1OTf** monitored by ^1H NMR spectroscopy at low temperature in CD_3CN . Compounds **1OTf**, TDTT, trifluoromethylated product **L1-CF₃** and the byproduct of the oxidant (dibenzothophene) are tagged. (a) Complex **1OTf** at -40°C ; (b) Reaction crude, 45 min, -40°C ; (c) 1.45 h, 0°C , (d) 4.45 h, 0°C and (e) Overnight 0°C . Only selected spectra are shown for clarity. General conditions: $[\mathbf{1OTf}] = 13.2 \text{ mM}$, $[\mathbf{CF}_3^*] = 13.2 \text{ mM}$, CD_3CN , -40°C to 0°C .

VII.2.4 Mechanistic insight. DFT calculations

We undertook a thorough computational DFT study to further elucidate the reaction mechanism. Based on recent literature concerning nickel complexes and their reactivity, we suggested two different pathways (Scheme VII.12) The first proposal (**A**) consisted on an oxidative-addition-like step ($\text{S}_{\text{N}}2$ -like attack or lateral attack) followed by a reductive-elimination step to obtain **L1-CF₃**. The second proposal (**B**) involves an initial Single Electron Transfer (SET) followed by a direct CF_3^\cdot radical recombination to the aryl group.



Scheme VII.12. Brief description of the three proposed mechanisms, **A**, **B** and **C**. Mechanism **A** implies the transfer or flow of two electrons during the reaction (oxidative addition-like step, followed by a reductive elimination step); Mechanism **B** can be described as Single Electron Transfer (SET), followed by a direct radical CF_3 addition on the aryl group. Mechanism **C** is a combination of **A** and **B**.

The mechanism **A** involved a high energetically demanding transition state to connect Ni^{II} and Ni^{IV} adducts by oxidative addition-like step **1**⁺ (34.0 kcal/mol). Different approaches of the CF_3 moiety ($\text{S}_{\text{N}}2$ -like and lateral) were also analysed, but again the oxidative addition barrier was too high (43.5 kcal/mol). So, mechanism **A**, based on oxidative addition pathway is not feasible from an energetic point of view (Figure VII.12).

Therefore, we turn our attention towards mechanism **B**, which consists in an initial Single Electron Transfer (SET) step to form an aryl- Ni^{III} species and a CF_3^\cdot radical. The DFT analysis showed that the Marcus Barrier for SET process was thermodynamically favorable (18.0 Kcal/mol) to form the transient aryl- $\text{Ni}^{\text{III}}/\text{CF}_3^\cdot$ adduct (**6**). Interestingly, the IRC calculations show no direct recombination between the CF_3^\cdot radical and aryl moiety was observed, even forcing the computed intermediate by approaching the CF_3^\cdot in close proximity to the aryl moiety (Figure VII.13 and Annex 3). On the contrary, the aryl- $\text{Ni}^{\text{III}}/\text{CF}_3^\cdot$ adduct (**6**) rapidly evolved to form an aryl- $\text{Ni}^{\text{IV}}\text{-CF}_3$ intermediate species (**3**), in a barrierless process, which underwent facile reductive elimination to form **L1- CF_3** product and Ni^{II} . Thus, we have found a more-favorable third mechanism (mechanism **C**), which consist of a combination of the both mechanistic proposals **A** and **B** (Figure VII.14 and Annex 3).

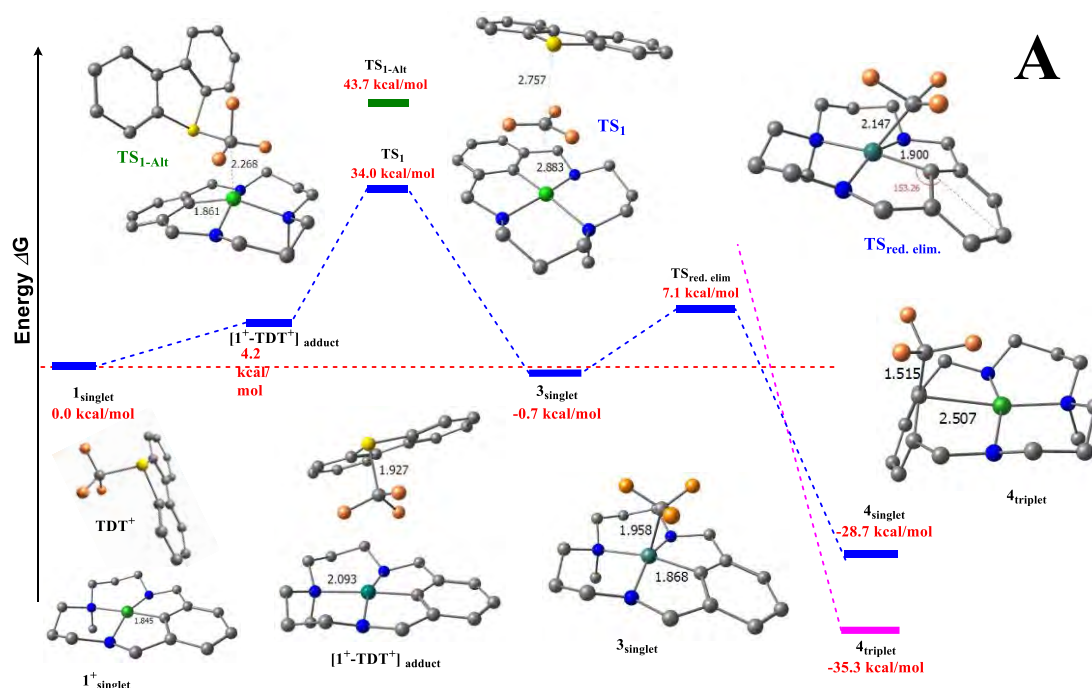
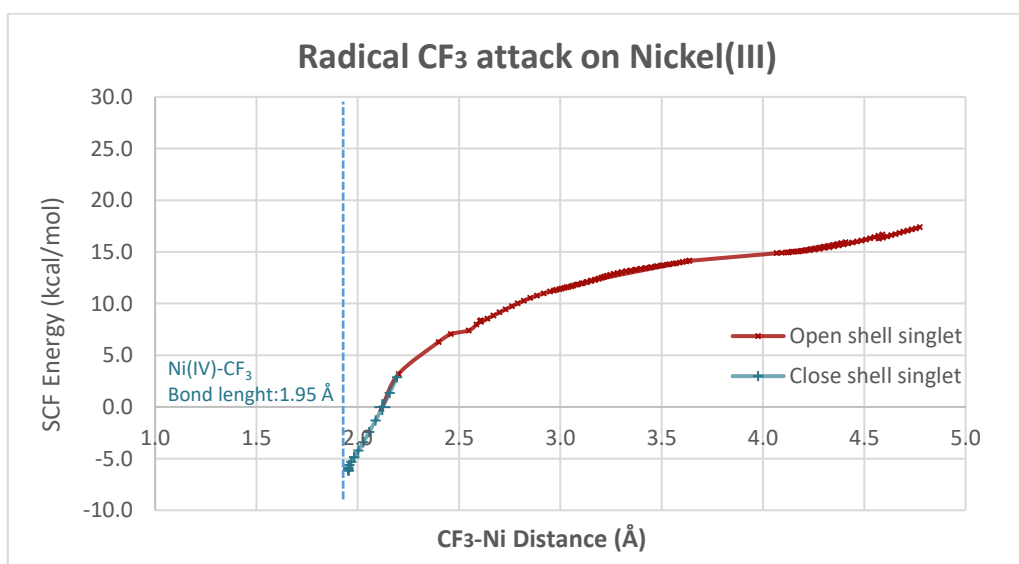


Figure VII.12. Free energy profile for the proposed mechanism **A** computed at B3LYP/cc-pVTZ//B3LYP/TZPV level. TS₁ and TS_{1-Alt} correspond to the two plausible transitions states that connects the nickel(II) and nickel(IV) species through an oxidative addition-like step. The former represents an S_N2-like attack between the species, while the latter describes a sort-of-lateral attack. TS₂ is the transition state of the reductive elimination final step of the pathway **A**. **Blue** lines represent the singlet state pathway, whereas **magenta** ones describe the triplet profile. Atomic colour code: **Carbon**, **Nitrogen**, **Fluor**, **Sulphur**; In the case of nickel, different colors are assigned to different oxidation states: **Nickel(II)**, **Nickel(IV)**.

a)



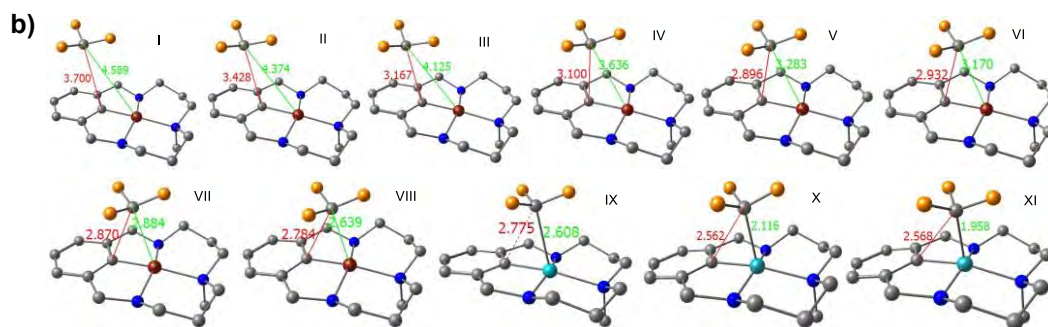


Figure VII.13. Energy profile computed at B3LYP-GD3BJ/TZPV level and snapshots sequence of the trifluoromethyl radical attack of the nickel(III) to generate nickel(IV). The plot (a) shows the electronic energy profile of the barrierless approach of the radical to the Ni^{III} . The spin density allows us to locate the bond distance at which the $\text{Ni}^{\text{IV}}\text{-CF}_3$ can be initially formed (no spin density on the CF_3). The sequence of IRC snapshots in scheme (b) illustrates the attack on the Nickel centre. Atomic color code: Carbon, Nitrogen, Fluor, Sulphur; In the case of Nickel, different colours are assigned to different oxidation states: Nickel(III), Nickel(IV).

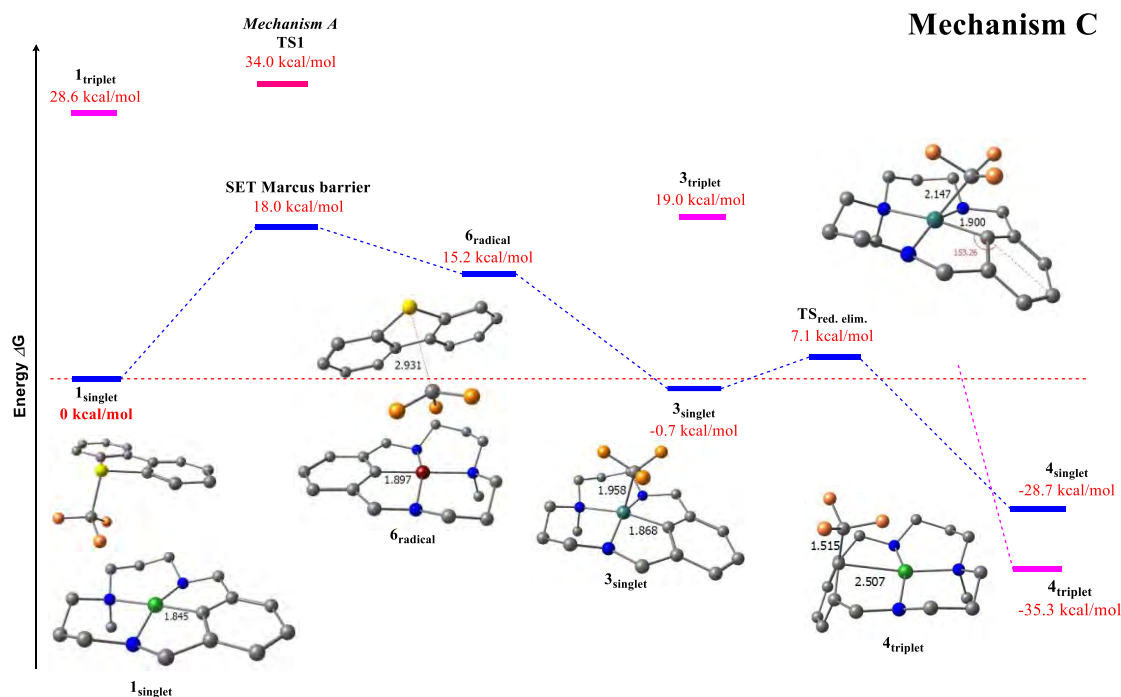


Figure VII.14. Free Energy profile for the Mechanism C. Free energy values were calculated at (B3LYP/cc-pVTZ/B3LYP/TZPV). The blue profiles correspond to open and close shell singlet systems while the triplets are represented by the fuchsia lines. The determining-step barrier free energy of the mechanism A (TS1, magenta colour) is depicted to contrast with the value of the single electron transfer Marcus barrier. The zero Gibbs free energy value of the profile correspond to the free energies of reactants at infinite distance. The following colour code illustrates the kind of atoms in the figure: Carbon, Nitrogen, Fluor, Sulphur, Nickel(II), Nickel(III), Nickel(IV).

This finding nicely correlates with the experimental data obtained and also explains why the experimental stabilization of high valent intermediates is precluded. The feasibility of the SET step is in line with the Cyclic Voltammetry experiments, easily accessing to Ni^{III} ($E_{1/2} = 0.066$ V vs

Ag/AgNO₃ for **1_{OTf}**) and the found in the literature -0.63 V for TDTT (vs Ag/AgNO₃).⁴² In fact, the ΔG° obtained (16.0 Kcal/mol) from the standard cell potential ($E^\circ_{\text{cell}} = -0.70$ V) closely matches the DFT thermodynamic energy difference between **1⁺** and the aryl-Ni^{III} species obtained by SET (15.2 Kcal/mol).

Besides, we performed some spin trap experiments in order to check the lifetime of the CF₃· radical generated in the SET step of the reaction. We carried out the reactions between **1_{OTf}** and **5_{OTf}** using both, TDTT and Togni Reagent in presence of spin trap reagent *N-tert*-butyl- α -phenylnitrone (PBN). The yield of the reactions was not affected and the radical trap reagent was not consumed, indicating that the life of CF₃· is very short (see Annex 3). These results are in line with DFT calculations, where the transient aryl-Ni^{III}/CF₃· adduct (**6**) rapidly evolved into the formation of aryl-Ni^{IV}-CF₃ intermediate (**3**) in a barrierless process.

Overall, we have described the synthesis and full characterization of well-defined organometallic aryl-Ni^{II} complexes (**1_x**, X = TfO⁻, ClO₄⁻ or NO₃⁻ and **5_{OTf}**) using macrocyclic model systems. These aryl-Ni^{II} complexes did not undergo reductive elimination with most common nucleophiles, whereas in the presence of electrophilic CF₃⁺ sources, quantitative yields of trifluoromethylated products were obtained under mild conditions. Further mechanistic investigations were performed combining experimental and DFT studies suggested an initial SET step followed by a recombination of aryl-Ni^{III}/CF₃· adduct, which evolved in a barrierless process to form an aryl-Ni^{IV}-CF₃ intermediate species, which easily underwent to the formation of trifluoromethylated product through reductive elimination. To the best of our knowledge, this is the first example of square planar model platform that allows to travel through the redox chemistry of nickel, from Ni⁰ to Ni^{IV}.

VII.3 Orthogonal Discrimination among Functional Group in Ullmann- Type C-O and C-N Couplings

This section corresponds to the contents of the manuscript by Rovira, M *et al.* *J. Org. Chem*, **2016**, 81, 7315 – 7325, which can be found in **Chapter VI** of this thesis.

The mechanistic investigations in thermal-based Ullmann couplings remained ambiguous and speculative, mainly due to the hardly detection of the putative aryl-Cu^{III} key intermediate species, nevertheless, the use of well-defined macrocyclic model systems demonstrate the feasibility of the aryl-Cu^{III} as intermediate species. We took advantage of the previously results reported in our group and employed them in model Cu-catalysed cross-couplings for standard Ullmann-type C-heteroatom bond forming reactions, paying especial attention to the chemoselective role of auxiliary ligands. L3 ligand design is inspired from a simplification of the macrocyclic model system used in sections VII.1-VII.3, while featuring its rigid tri-coordinating ability.

VII.3.1 Optimization of the single arylation of nucleophiles

Recently, our research group described a practical ligand-free protocol for the arylation of a wide range of amines, amides and phenols under optimized reaction conditions.⁴³ Based on that previous work, we explored the N-arylation and O-arylation of a wide range of amines, amides and phenols as a nucleophiles using several effective *N,N*-, *N,O*- or *O,O*- bidentate or *N,N,N*-tridentate ligands (**L**₁-**L**₁₀) (Figure VII.15).^{13,44} In this work, we employed the base/solvent combination K₃PO₄ / DMSO with 10 mol % of copper iodide using aryl iodides and aryl bromides as substrates under mild conditions.

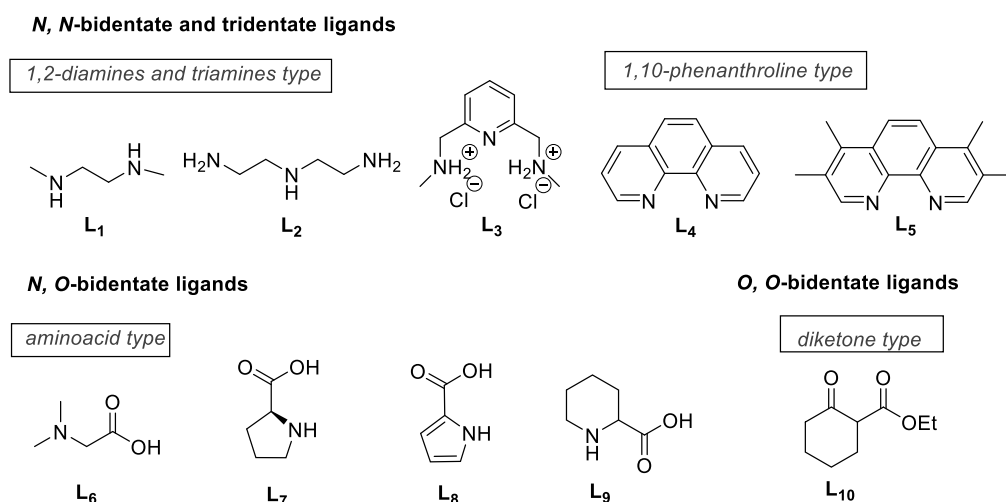
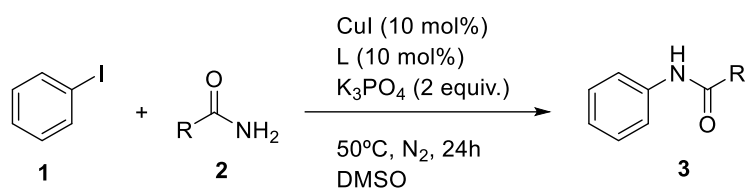


Figure VII.15. Bidentate and tridentate auxiliary ligands chosen in this work.

Firstly, iodobenzene (**1**) was subjected to N-arylation with different primary and secondary amides (**2**) (Table VII.3). Aromatic primary amides (**2a** and **2f**; Table VII.3, entries 1 and 6) rendered good-to-excellent yields using di- or triamine ligands (**L**₁-**L**₃). In contrast, the reaction seemed to be sensitive to the *ortho*-substituted benzamide in presence of the same ligands (**2d**; Table VII.3, entry 4) and almost no coupling product was observed with the *para*-substituted benzamide (**2e**; Table VII.3, entry 5). Besides, the use of L-proline (**L**₇) was found to be the most suitable ligand for the arylation of the primary aliphatic amide **2g** in good yield and excellent conversion (Table VII.3, entry 7). Taking into account the low reactivity of secondary amides, the use of 1,10-phenanthroline (**L**₄) as a ligand at 130°C significantly improved the arylation of aliphatic secondary amides (**3h** and **3j**; Table VII.3, entries 8 and 10). However, an exception was found for pyrrolidin-2-one (**2b**), which afforded the N-arylated product **3b** in 80-91% using di- or triamine ligands (**L**₁-**L**₃) or 1,10-phenanthroline (**L**₄) under milder conditions (Table VII.3, entry 2).

In summary, **L**₁, **L**₂, **L**₃ ligands are preferred for the arylation of primary aromatic amides, in contrast, **L**₇ was found the most suitable for the arylation of primary aliphatic amides. Finally, the use of 1,10-phenanthroline (**L**₄) at 130°C was essential to obtain good performance in the arylation of secondary amides.

Table VII.3. Screening of amides for N-arylation with iodobenzene.

Entry ^[a]	Amides	Product	Ligand [†]	Conv. (%)	Yield (%) ^[b]
1	2a	3a	L₁, L₂, L₃	100	100, 98, 75
2	2b	3b	L₁, L₂, L₃, L₄	90-100	91, 79, 80, 88
3	2c	3c	L₂	44	27
4	2d	3d	L₁	62	46
5	2e	3e	L₁, L₂, L₃	50	1, 3, 6
6	2f	3f	L₁, L₂	100	100, 76
7 ^[c]	2g	3g	L₇	96 ^[e]	91 ^[f]
8 ^[d]	2h	3h	L₄	98	91
9 ^[d]	2i*	3i	L₄	84	62
10 ^[d]	2j	3j	L₄	100	52

[a] Reaction conditions: **1** (0.88 mmol, 0.9 M), **2** (1.79 mmol); [b] Yield was determined by GC. [c] Reaction temperature of 80°C. [d] Reaction temperature of 130°C. [e] 2% yield *N,N*-diphenylacetamide. [f] Isolated yield. [†] **L₃** refers to the hydrochloric salt **L₃·(HCl)₂**. * **2i=3a**.

Thereafter, we explored the arylation of alcohols under the same reaction conditions (Table VII.4). As expected from the previous results reported in the literature, the O-arylation of phenols using dimethylglycine (**L**₆) as a Cu-chelating ligand displayed excellent performance (**5a**, **5b**, **5c**, **5d**; Table VII.4, entries 1-4).^{45,46} However, the presence of electron-withdrawing groups at *para*-position completely quenched the reaction (**5e**; Table VII.4, entry 5). On the other hand, aliphatic alcohols gave poor yields irrespective of the auxiliary ligand used (**5f** and **5g**; Table VII.4, entries 6 and 7).

Table VII.4. Mild O-arylation of alcohols with iodobenzene.

$ \begin{array}{c} \text{Cul (10 mol\%)} \\ \text{L (10 mol\%)} \\ \text{K}_3\text{PO}_4 \text{ (2 equiv.)} \\ \hline \text{50}^\circ\text{C, N}_2, 24\text{h} \\ \text{DMSO} \end{array} $					
Entry ^[a]	Alcohols	Product	Ligand	Conv. (%)	Yield (%) ^[b]
1			L ₆	93	82
2			L ₆	98	92
3			L ₆	100	97
4			L ₆	94	94
5			L ₆	3	3
6			L ₅	50	27
7			L ₅	2	traces

[a] Reaction conditions: **1** (0.88 mmol, 0.9 M), **4** (1.79 mmol); [b] Yield was determined by GC.

Eventually, we were also interested in exploring the reactivity of different amines as a nucleophile. In line with the literature, the *N,O*- bidentate ligands such as proline (**L**₇) or pyrrol-2-carboxylic acid (**L**₈) were found to be the most suitable chelating moieties for the arylation of amines.^{47,48} Besides, the employment of CsF as a base instead of K₃PO₄ rendered better results for these coupling reactions. Whereas the use of **L**₈ for the *N*-arylation of aromatic amines afforded moderate to good yields (**7a** and **7c**; Table VII.5, entries 1 and 3), the *N*-arylation of *para*-

nitro substituted aniline (**7b**) was obtained only in 22% of yield (Table VII.5, entry 2). Moreover, the N-arylation of primary aliphatic amines (**6d** and **6e**) was very effective using ligand **L₇** and excellent yield and conversions were observed (Table VII.5, entries 4 and 5). Concerning aliphatic amines, cyclic piperidine (**6g**) afforded the desired product in excellent yield and conversion (Table VII.5, entry 7), while under the same reaction conditions, a very poor yield of the arylated product **7f** was observed (Table VII.5, entry 6). Finally, conjugated N-heterocyclic secondary amine rendered the N-arylated product **7h** in excellent yield using **L₁** (Table VII.5, entry 8). Particularly, this latter product was also formed in excellent yields and conversions employing other ligands such as **L₂**, **L₃**, **L₄** or **L₆** or even working at room temperature with **L₁**.

Table VII.5. Mild N-arylation of amines with iodobenzene.

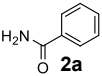
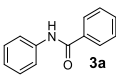
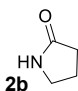
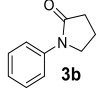
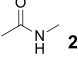
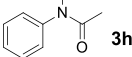
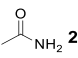
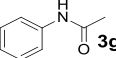
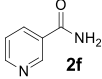
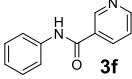
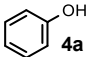
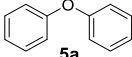
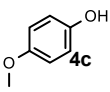
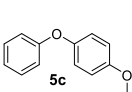
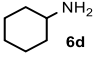
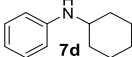
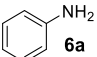
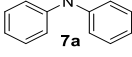
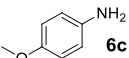
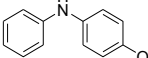
Entry ^[a]	Amines	Product	Ligand	Conv (%)	Yield (%) ^[b]
1	6a	7a	L₈	66	62
2	6b	7b	L₈	44	22
3	6c	7c	L₈	79	76
4	6d	7d	L₇	93	89
5 ^[c]	6e	7e	L₇	100	95
6	6f	7f	L₇	19	13
7	6g	7g	L₇	99	86
8	6h	7h	L₁	98	96

[a] Reaction conditions: **1** (0.88 mmol, 0.9 M), **4** (1.79 mmol); [b] Yield was determined by GC. [c] Yield was determined by ¹H NMR.

Furthermore, we also explored the N-arylation and O-arylation using aryl bromide as a substrate (Table VII.6). Due to the lower reactivity of bromobenzene compared to iodobenzene, the reactions were carried at 110°C. Excellent yields were obtained for the arylation of aromatic alcohols (**5a** and **5c**; Table VII.6, entries 6 and 7), and moderate to good yields were found for aromatic and aliphatic amines (**7a**, **7c** and **7d**; Table VII.6, entries 8-10). Nevertheless, poor

reactivity were observed for the arylation of amides and only the use of **L₈** afforded the arylation of cyclic amide pyrrolidin-2-one (**2b**) in a 26% of yield (Table VII.6, entries 1-5).

Table VII.6. Arylation of different nucleophiles with bromobenzene.

$ \begin{array}{c} \text{Cul (10 mol\%)} \\ \text{L (10 mol\%)} \\ \text{K}_3\text{PO}_4 \text{ (2 equiv)} \\ \text{N}_2, 24\text{h}, 110^\circ\text{C}, \text{DMSO} \end{array} $					
Entry ^[a]	Amines	Product	Ligand	Conv (%)	Yield (%) ^[b]
1			L₁	7	1
2			L₈	47	26
3			L₈	18	0
4			L₇	21	0
5			L₈	38	0
6			L₅	100	100
7			L₅	95	88
8 ^[c]			L₇	85	80
9 ^[c]			L₈	76	50
10 ^[c]			L₈	79	51

[a] Reaction conditions: **1** (0.88 mmol, 0.9 M), **nucleophile** (1.79 mmol); [b] Yield was determined by GC.

[c] CsF was used as a base.

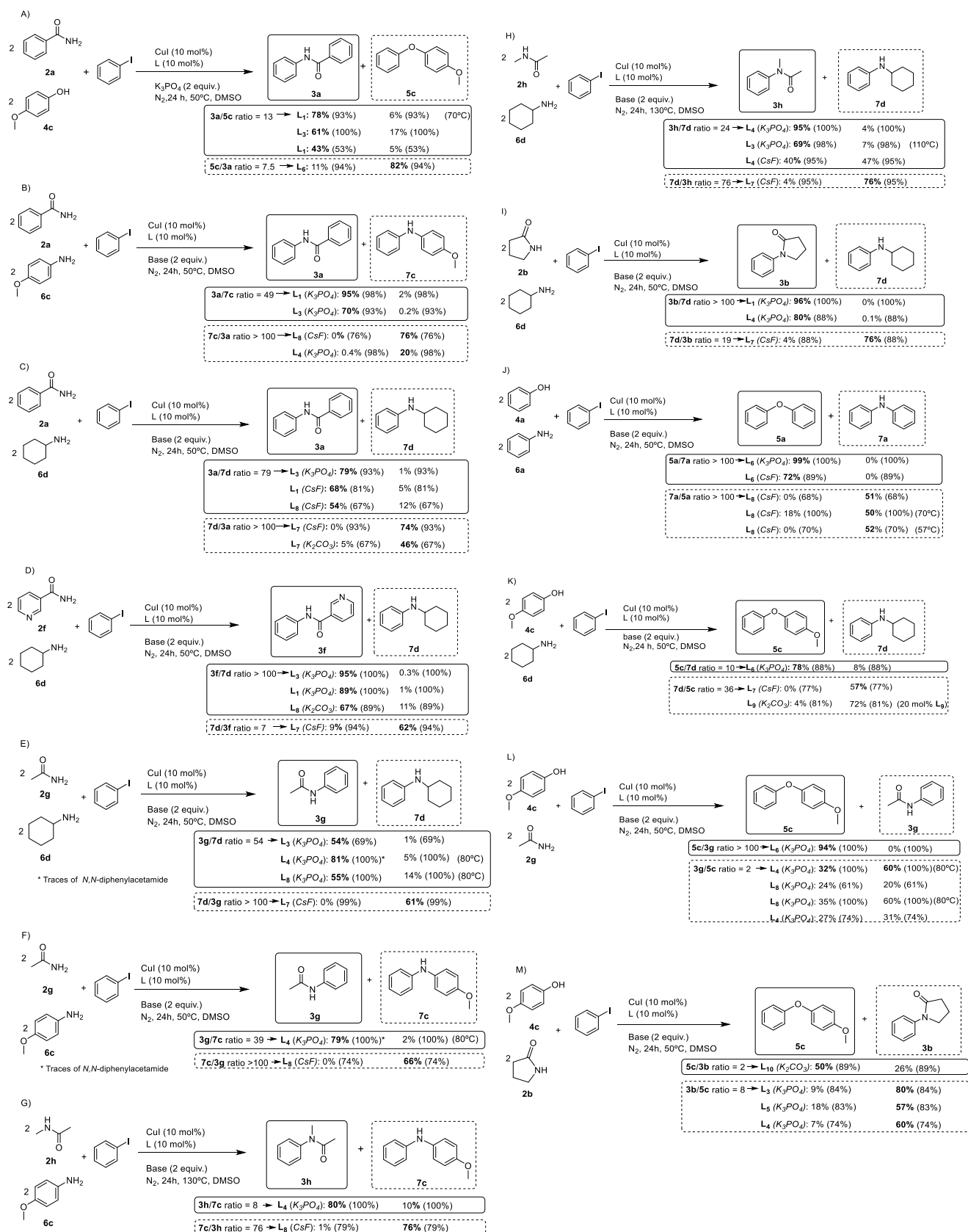
VII.3.2 Ligand-dependent selectivities in competition reactions using iodobenzene

Considering the trends observed from the different ligands previously tested, we turned our attention to the study of selective arylation of a wide range of nucleophiles in competition reactions. Thus, we performed competitive experiments combining amides, amines and phenols under standard conditions (1 equiv of iodobenzene and 2 equiv of each nucleophile), aiming to

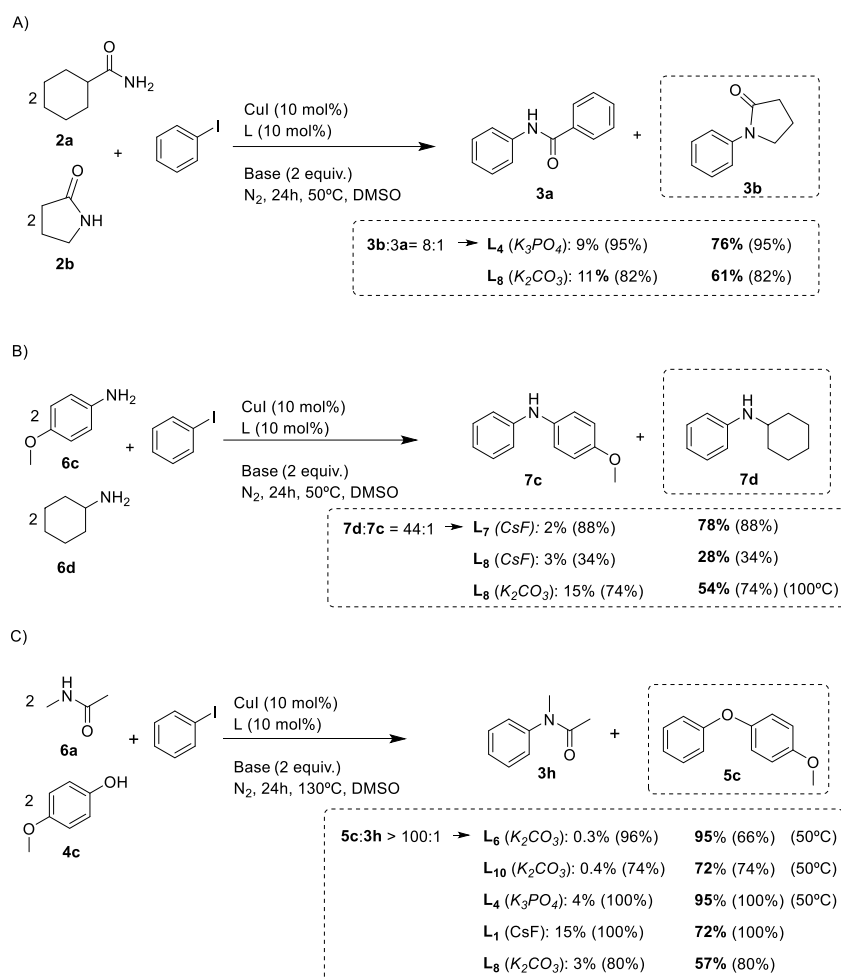
find out the most suitable ligand for the arylation of each nucleophile in high selectivity, yield and conversion (Scheme VII.13).

In general trends, we have found that the arylation of aromatic amides is favoured, over phenols and amines, when tridentate N-based auxiliary ligands are used, being **L**₁ and **L**₃ the best ones under mild temperatures (Scheme VII.13, A-D). Due to the poor reactivity of the non-cyclic aliphatic secondary amides, higher temperatures in combination of **L**₄ were required to favour them in front the arylation of amines (Scheme VII.13, G and H), in contrast they cannot compete with phenols (Scheme VII.14, C). Likewise, non-cyclic primary aliphatic amides can be clearly favoured in front of aromatic and aliphatic amines at 80°C using **L**₄ as a ligand (Scheme VII.13, E and F), although it can be slightly favoured in front of the arylation of phenols using the same conditions (Scheme VII.13, L).

On the other hand, the arylation of cyclic aliphatic amides is sharply chemoselective in front aliphatic amines, phenols and aromatic amides when **L**₁ or **L**₄ are used (Scheme VII.13, I, M and Scheme VII.14, A). Furthermore, the arylation of phenols is especially favoured in competition reaction with amides and amines when **L**₆ is used as an auxiliary ligand (Scheme VII.13, entries A, J-M; see also Annex 4). No competition studies have been undertaken with aliphatic alcohols (see Table VII.4), since their low reactivity made those nucleophiles more challenging than the ones studied in this work. Finally, anilines are selectively arylated towards amides and phenols when **L**₈ is used, showing an orthogonal selectivity in most of the competitions explored (Scheme VII.13, B, F, G, J). In the competitive reaction between two types of amides, benzamide (**2a**) and the cyclic amide pyrrolidin-2-one (**2b**) (Scheme VII.14, A), we were only able to set out conditions to render the N-arylation of **2b** in excellent yield and conversion using **L**₄ at 50°C. Despite submitting the reaction with other type of ligands such as **L**₈, very low yield of **3a** was observed. In the same line, in analogous reaction between aromatic and aliphatic amines (**6c** and **6d**), the N-arylation of cyclohexylamine **7d** was clearly favoured as a major coupling product in the competitions tested (Scheme VII.14, B), although the best results were obtained when **L**₇ was used as a ligand. Similarly results were observed when we tested the selectivity between the secondary amide *N*-methylacetamide (**6a**) and *p*-methoxyphenol (**4c**) (Scheme VII.14, C and Annex 4); the arylation of phenol was clearly favoured in all cases, including when *O,O*- bidentate **L**₁₀ ligand was used under the same conditions. We were unable to find suitable conditions for the selective arylation of the secondary amide. Additionally, the use of **L**₁ with K₃PO₄ or CsF and **L**₈ with K₂CO₃ significantly reduced the yield of the *O*-arylated product, however the reaction likewise afforded low yields of the *N*-arylated methylacetamide. We rationalise that due to the facile arylation of phenols and the high temperatures required for the arylation of secondary amides made difficult to establish the appropriate conditions for such arylation in competitive reactions.



Scheme VII.13. Competitive reactions among nucleophiles using iodobenzene with a sharp switch of chemoselectivity. Conversions are given in parentheses; standard experimental conditions used



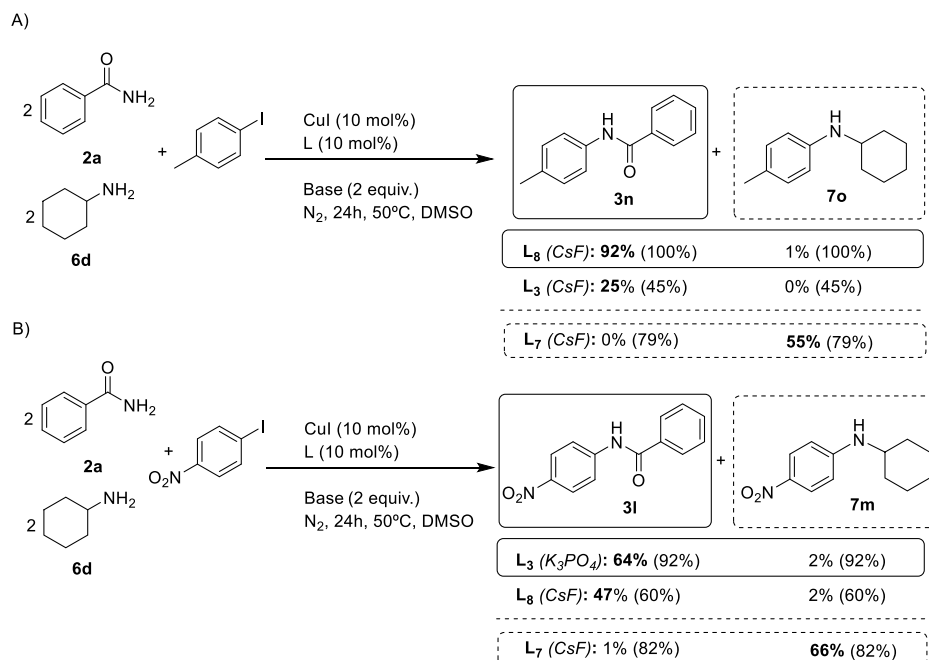
Scheme VII.14. Competition reactions among nucleophiles with strong preference for one nucleophile independent of the auxiliary ligand used. Conversions are given in parentheses; standard experimental conditions used.

VII.3.3 Ligand-dependent selectivities in competition reactions using *para*-substituted iodobenzenes

In order to broaden the scope of the electrophiles used, we turned our attention on the effect of the presence of electron-donating and electron-withdrawing substituents in *para* position of the aryl iodide derivatives. Thus, *p*-iodotoluene and *p*-nitrobenzene were chosen as substrates using the same standard conditions as the competitive experiments shown in the previous section.

For the competitive reaction between benzamide (**2a**) and cyclohexylamine (**6d**) using *p*-iodotoluene as a substrate, we could observe that the arylation of benzamide was significantly suppressed using the pincer ligand **L**₃. Besides this, the arylation of the same nucleophile using **L**₈ as an auxiliary ligand successfully improved the reaction performance (Scheme VII.15, A). On the other hand, the use of *L*-proline (**L**₇) favoured the single arylation of cyclohexylamine, but in a modest yield. Turning our attention to the use of *p*-nitrobenzene as a substrate, similar reactivity of the iodobenzene was observed. It is noteworthy that pincer-type ligand **L**₃ favoured the

formation of **3i** as an almost single product in good yield (Scheme VII.15, B). Additionally, the employment of *L*-proline **L**₇ also gave rise to the coupling product **7m** in good yield and also as a single product. Therefore, both electron-rich and electron-deficient aryl iodides underwent arylation with excellent chemoselectivities.

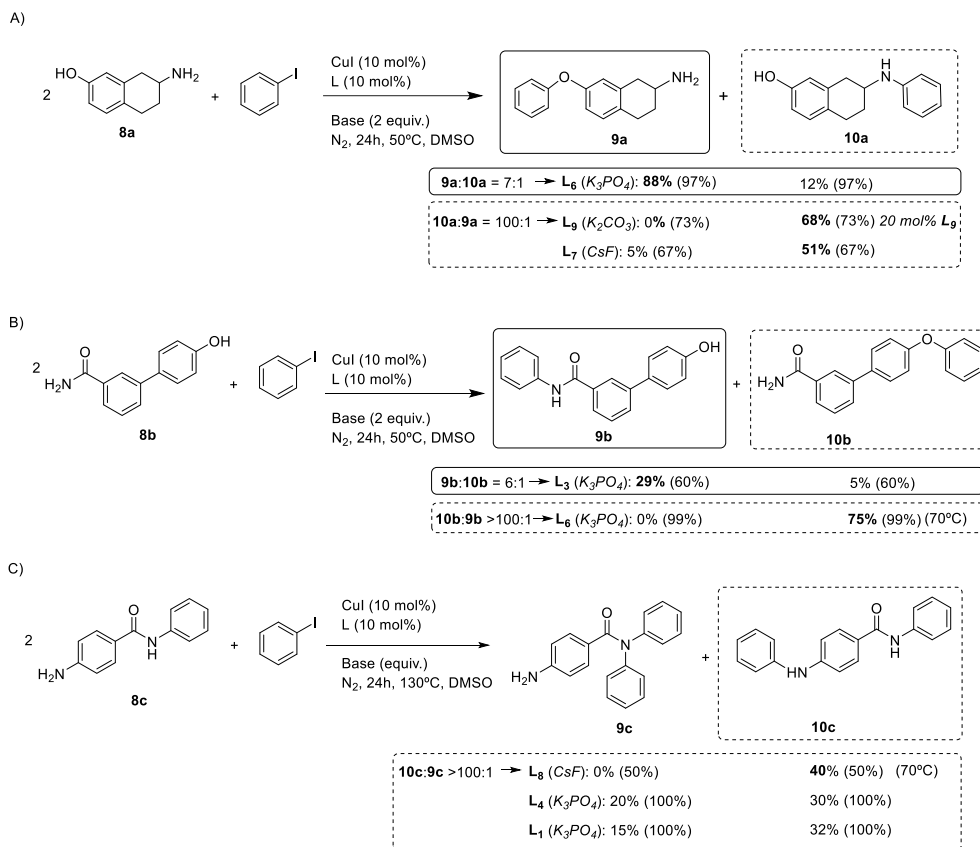


Scheme VII.15. (a) Competitive reactions using *p*-iodotoluene. (b) Competitive reactions using *p*-iodonitrobenzene. Conversions are given in parentheses; standard experimental conditions used.

VII.3.4 Ligand-dependent selectivities in competition reactions using bifunctional nucleophiles and iodobenzene

With these good results in hand, we further studied the orthogonal selectivity of our copper-based system using different bifunctional nucleophiles (**8a**, **8b** and **8c** of Scheme VII.16). The first bifunctional nucleophile tested was the aminophenol (**8a**): when dimethylglycine **L**₆ was used as an auxiliary ligand the O-arylated product was obtained in high yields and with high chemoselectivity (Scheme VII.16, A, **9a**). On the other hand, the selectivity was totally switched to the formation of N-arylated product with the use of *L*-proline (**L**₇) as a ligand. Very notably, performing the same reaction using *N,O*-bidentate **L**₉ ligand in combination of K₂CO₃ enhanced the formation of **10a** as a single reaction product. We also succeeded in the competition reaction between the bifunctional nucleophile **8b** (bearing aromatic amide and phenol functional groups) and iodobenzene (Scheme VII.16, B). According with the results obtained, the use of dimethylglycine (**L**₆) at 70°C led the single formation of O-arylated product (**10b**) in really good yields. In contrast, when the pincer **L**₃ ligand was used the selectivity was turned into the formation of N-arylated product (**9b**), even though the yield was modest. Finally, regarding the last coupling using 4-amino-*N*-phenylbenzamide (**8c**) as a nucleophile and iodobenzene (Scheme VII.16, C), only the arylation of amino group was achieved as a major product, independently of the auxiliary

ligand used. Compound **10c** was obtained as a unique product in moderate yield and high selectivity when the pyrrole derivative **L₈** ligand was used. We assumed that the arylation of secondary amide was hindered by steric effects, and even using high temperatures (130°C) together with **L₁** or **L₄** as a ligands, the formation of **10c** was unavoidable in both cases tested.

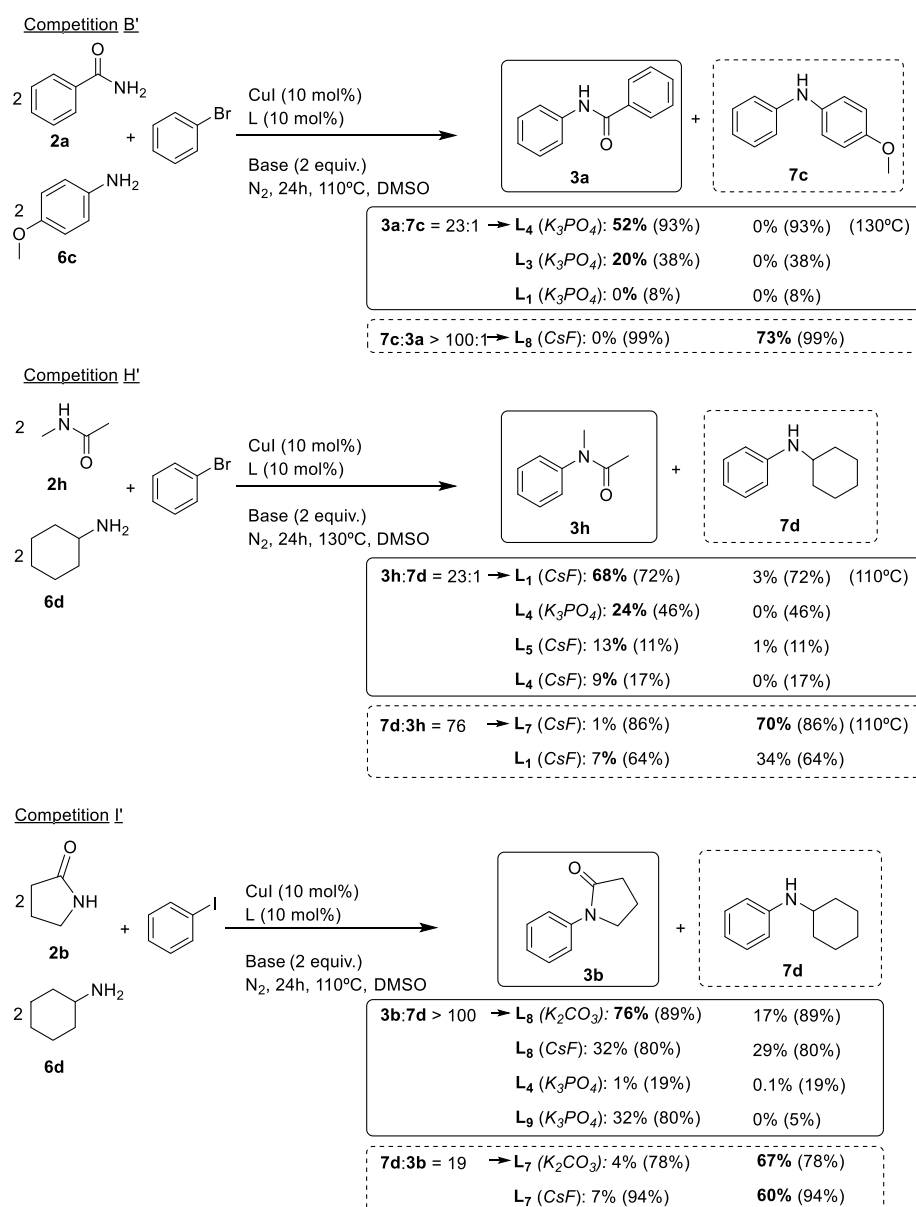


Scheme VII.16. Competition reactions using bifunctional nucleophiles **8a** - **8c**. Conversions are given in parentheses; standard experimental conditions used.

VII.3.5 Ligand-dependent selectivities in competition reactions using bromobenzene

With the valuable data acquired about the orthogonal selectivity among several N- and O- based nucleophiles using iodobenzene and *para*-substituted iodobenzenes, we focused our attention on conducting some of the competition reactions described above using bromobenzene. Due to the low reactivity of aryl bromides, the reactions required to be performed at 110°C or 130°C. The competitions B', H' and I' were chosen owing to the excellent selectivities and yields obtained with iodobenzene. In the first competitive reaction between benzamide (**2a**) and anisidine (**6c**) (Scheme VII.17, competition B', equivalent to Scheme VII.13, B), we could only observed the formation of benzamide arylated product when phenanthroline (**L₄**) was used at 130°C. Interestingly, the selectivity was completely switched leading the single arylation of aromatic amine (**6c**) compound when pyrrole derivative (**L₈**) ligand was employed. On the other hand, in next the competitive reaction investigated between *N*-methylacetamide (**2h**) and cyclohexylamine

(**6d**) (Scheme VII.17, competition H', equivalent to Scheme VII.13, H), the formation of **3h** in good yields and selectivity was obtained when DMEDA (**L**₁) ligand was used at 110°C. In contrast, all the attempts to promote the same reaction using (**L**₄ and **L**₅) ligands failed. However, the use of *L*-proline (**L**₇) as a chelating ligand at 110°C clearly favour the cyclohexylamine arylated product (**7d**) in excellent yield and selectivity. In line with this results we observed a similar trend in the last competitive reaction studied between the cyclic amide pyrrolidin-2-one (**2b**) and cyclohexylamine (**6d**) (Scheme VII.17, competition I', equivalent to Scheme VII.13, I).



Scheme VII.17. Competition reactions among nucleophiles using bromobenzene with sharp switch of chemoselectivity. Conversions are given in parentheses; standard experimental conditions used.

When **L**₇ was employed the arylation of aliphatic amine was clearly favoured obtaining excellent yield and selectivity, while the use of pyrrole derivative (**L**₈) in combination with *K*₂*CO*₃ as a base showed excellent performance for the arylation of cyclic amide (**3b**). In the latter competition we

could observed an important base effect, the use of CsF clearly suppressed the chemoselectivity between both nucleophiles, while the use of K_2CO_3 enhanced the chemoselectivity between them. Furthermore, competitive reaction were explored using bromobenzene as a substrate A', C', D', G', J' and with a bifunctional nucleophile **8a** (see Annex 4). In most of the cases poor yields and moderate to good selectivities were obtained, due some unexpected effects, like the different behaviour of some of the ligands, such as 1,10- phenanthroline when bromobenzene was used instead of iodobenzene when facing primary amides and aliphatic or aromatic amines with other nucleophiles (See competitions B/B' and H/H' from Scheme VII.13 and Scheme VII.17). Moreover, the competitive reactions using aryl bromide and aromatic amides **2a** and **2f** using **L₁** as a chelating ligand did not afford the arylated product either.

Several reactions using chlorobenzene as arylating agent were also attempted. Despite the screening of several nucleophiles and auxiliary ligands no reactivity was observed, even working at 130°C (see Annex 4).

VII.3.6 Practical orthogonal nucleophile discrimination summary

In Table VII.7 a practical methodology for the selective O-arylation and N-arylation in Ullmann-type couplings under milder conditions is depicted. Therefore, the most important results obtained for all competitive reactions tested are summarized in Table VII.7, together with the best conditions to achieve chemoselective arylation for each nucleophile. In a general trends, highly selective arylation of each nucleophile can be obtained in the most of competition reactions under mild conditions depending only on the ligand choice.

Nevertheless, we did not succeed in all the competitive reactions tested. In some cases we could only observed a single arylation one nucleophile, being the formation of the other one unfavourable, despite exhaustive screening of auxiliary ligands and reaction conditions. These limitations of the methodology in terms of selectivity are shown in Table VII.8.

Table VII.7. Optimised conditions for ligand-dependent arylation of nucleophile (A or B) with iodobenzene in competition reactions with orthogonal selectivity. Standard reaction conditions: iodobenzene (0.88 mmol, 0.9M), **A** and **B** (1.79 mmol), 24 h, DMSO under an inert atmosphere (yields given in parenthesis).

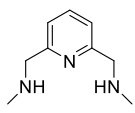
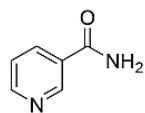
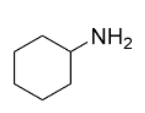
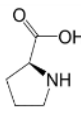
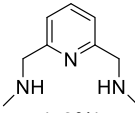
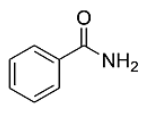
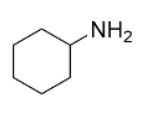
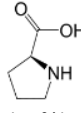
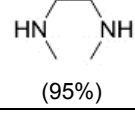
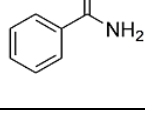
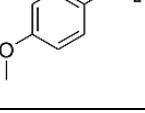
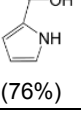
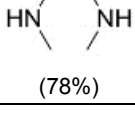
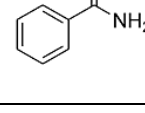
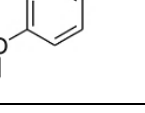
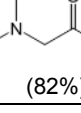
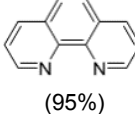
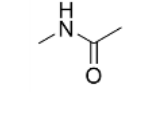
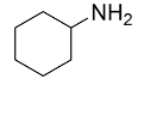
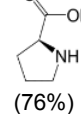
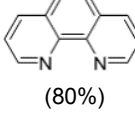
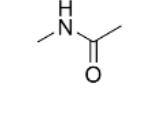
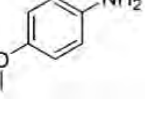
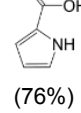
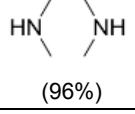
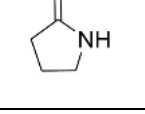
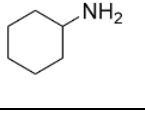
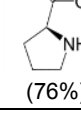
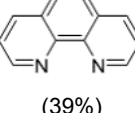
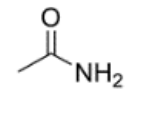
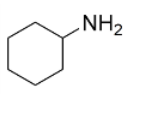
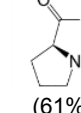
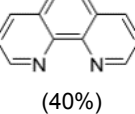
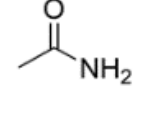
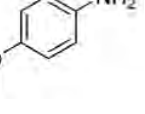
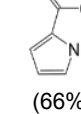
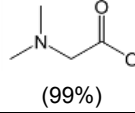
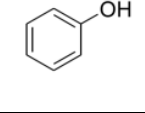
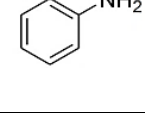
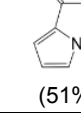
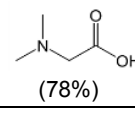
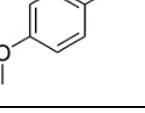
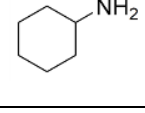
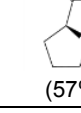
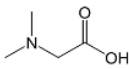
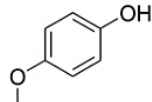
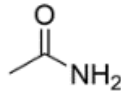
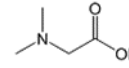
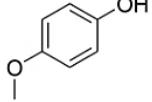
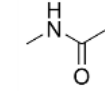
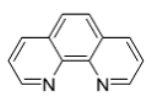
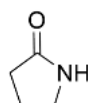
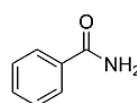
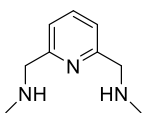
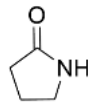
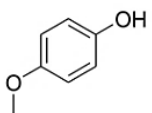
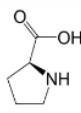
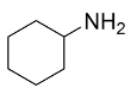
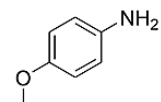
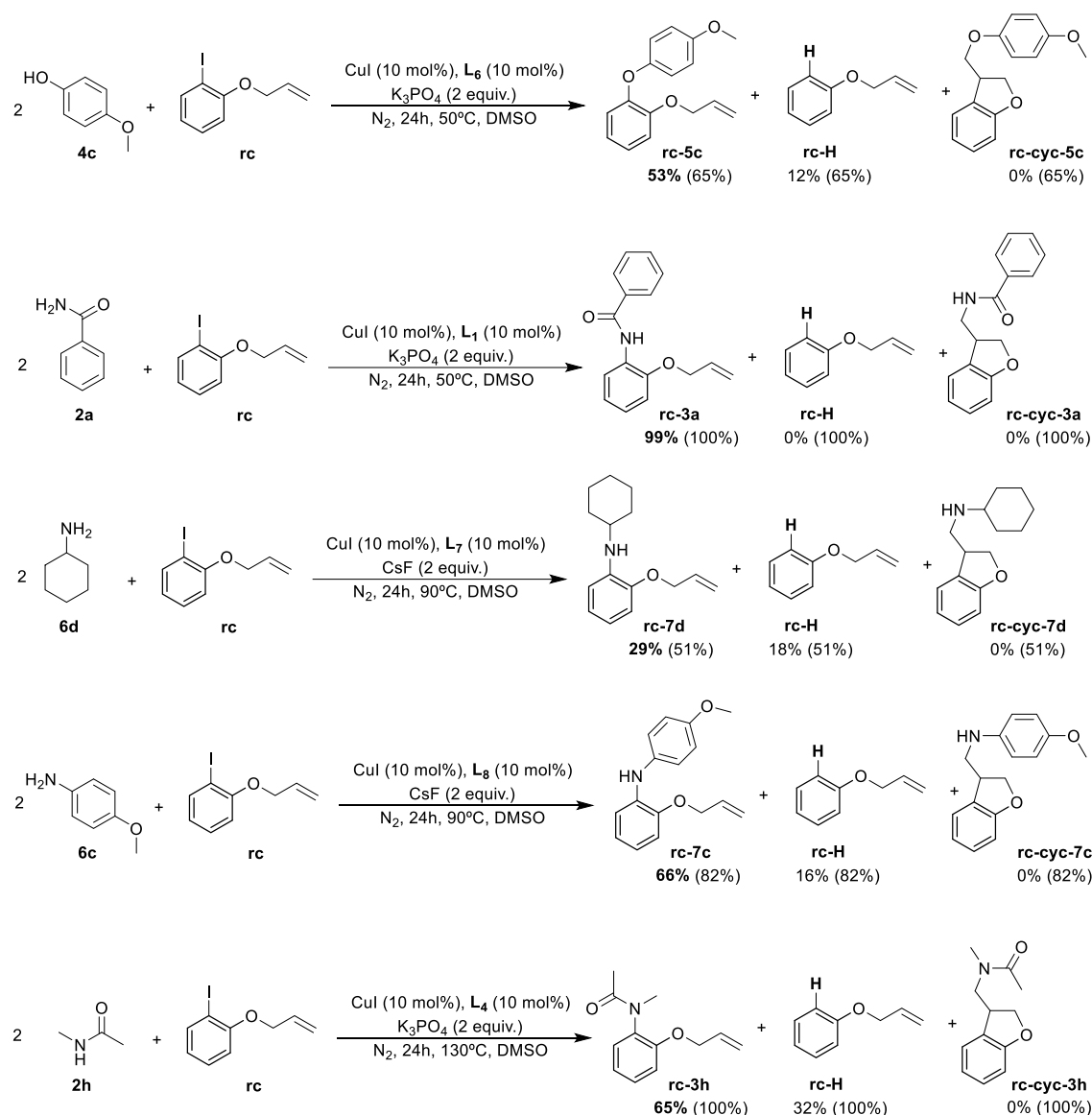
Conditions for A arylation	A	B	Conditions for B arylation
L₃ K_3PO_4 50°C  (95%)			 L₇ CsF 50°C (62%)
L₃ K_3PO_4 50°C  (79%)			 L₇ CsF 50°C (74%)
L₁ K_3PO_4 50°C  (95%)			 L₈ CsF 50°C (76%)
L₁ K_3PO_4 50°C  (78%)			 L₆ K_3PO_4 50°C (82%)
L₄ K_3PO_4 50°C  (95%)			 L₇ CsF 50°C (76%)
L₄ K_3PO_4 50°C  (80%)			 L₈ CsF 50°C (76%)
L₁ K_3PO_4 50°C  (96%)			 L₇ CsF 50°C (76%)
L₄ K_3PO_4 80°C  (39%)			 L₇ CsF 50°C (61%)
L₄ K_3PO_4 80°C  (40%)			 L₈ CsF 50°C (66%)
L₆ K_3PO_4 50°C  (99%)			 L₈ CsF 50°C (51%)
L₆ K_3PO_4 50°C  (78%)			 L₇ CsF 50°C (57%)

Table VII.8. Optimised conditions for ligand-dependent arylation of nucleophile (A or B) with iodobenzene in competition reactions with high selectivity for one of the competing nucleophiles (Column A). Standard reaction conditions: iodobenzene (0.88 mmol, 0.9M), **A** and **B** (1.79 mmol), 24 h, DMSO under an inert atmosphere (yields given in parenthesis).

Conditions for A arylation	A	B
L₆ K_3PO_4 $50^\circ C$  (94%)		
L₆ K_3PO_4 $50^\circ C$  (95%)		
L₄ K_3PO_4 $50^\circ C$  (76%)		
L₃ K_3PO_4 $50^\circ C$  (71%)		
L₇ CsF $50^\circ C$  (78%)		

Finally, in order to get further insight into the plausible mechanism, governing the cross-coupling reactions with the use of different chelating ligands, we have selected the most successful combinations of ligands and nucleophiles to be used with the radical clock 1-allyloxy-2-iodobenzene (**rc**) as a substrate (Scheme VII.15). Interestingly, no traces of cyclised product was observed, indicating the involvement of a prototypical Cu^I/Cu^{III} mechanism for thermal-based Ullmann couplings and discarding a radical pathway. However, in all the reactions we could observed the formation of a significant amount of hydrogenated compound (**rc-H**), suggesting a protodecupration side reaction as previously observed by Cohen⁴⁹ and Hartwig⁵⁰ and also in the reactivity of well-defined aryl- Cu^{III} macrocyclic model system.⁵ The formation of **rc-H** product was found in important amounts when **rc** was used as a substrate, so we checked if the protodecupration side reaction had the same contribution when iodobenzene was used as substrate. If so, benzene should be found as product of the putative protodecupration reaction. As we suspected, low but significant amounts of benzene were found (from 4% to 8%) in some coupling reactions, generally with aniline **6a**, **6b**, **6c** and methylacetamide **2h** (see Annex 4), being a strong evidence for the involvement of protodecupration pathway as a side reaction in Ullmann couplings.



Scheme VII.18. Selected coupling reactions using radical clock (**rc**) as a substrate.

Overall, we have described a practical Cu-based methodology for the highly selective arylation of a wide range of nucleophiles in competitive reactions using aryl iodides and bromides. The high selectivity and yields obtained are extremely dependent on nature of the chelating auxiliary ligand used. However, the exact role of these auxiliary ligands on the chemoselective arylation is not well understood. In the literature, we could find a large number of combinations of auxiliary ligands, nucleophiles and aryl halides, however a clear pattern cannot be established. In a pioneering work, Buchwald and co-workers explained the chemoselective N- or O-arylation of β -aminoalcohols (see Scheme I.11) by using different auxiliary ligands based on DFT studies, suggesting that the observed selectivities were closely based on the relative abilities of the ligands to donate electrons to the Cu^I centre.⁵¹ Some years later, Fu and co-workers proposed an alternative also computed pathway based on the formation and stability of the organometallic aryl-Cu^{III} intermediate species.⁵² Despite the tremendous effort concerning the exact role of auxiliary

ligands, several key challenges remained unanswered, mainly due to a clear lack of understanding of how such system work in such transformations.

The great diversity of nucleophiles and catalytic systems and the catalysis' strong dependence on the reaction conditions render the comprehension of the molecular mechanisms as a difficult task, however, in-depth mechanistic studies should be undertaken.

VII. 4. References

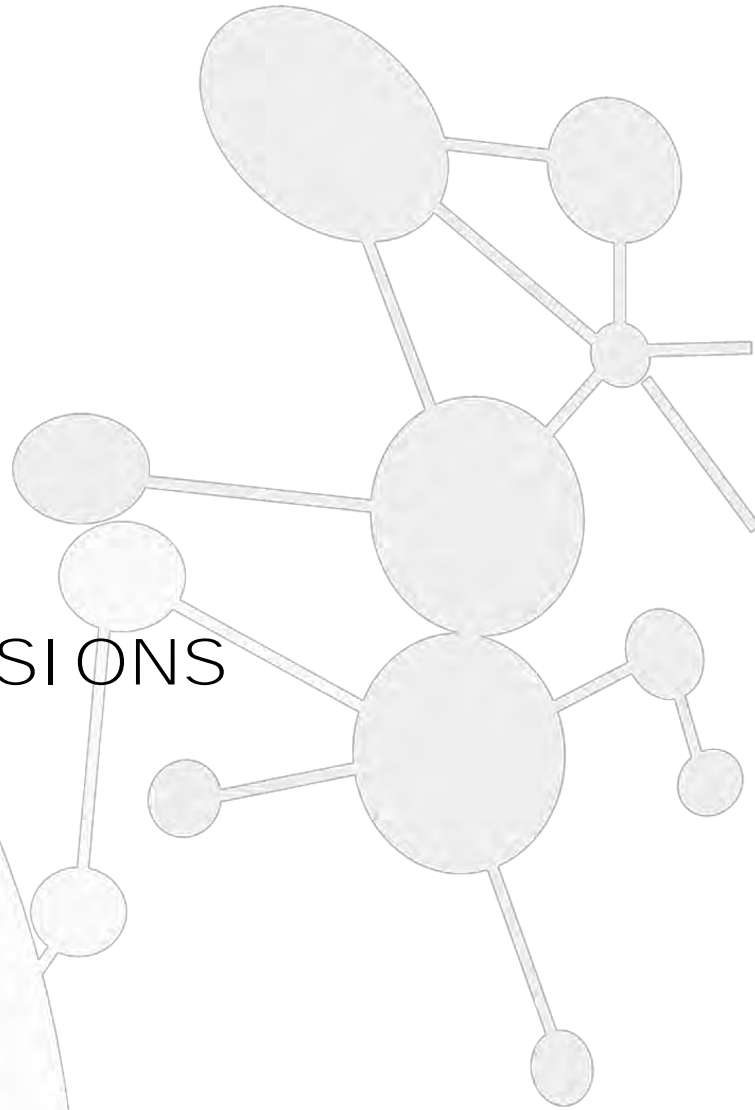
- (1) Casitas, A.; Ribas, X. *Chem. Sci.* **2013**, *4*, 2301.
- (2) Casitas, A.; Ribas, X. In *Copper-Mediated Cross-Coupling Reactions*; Evano, G., Blanchard, N., Eds.; John Wiley & Sons: Hoboken, 2013, p 253.
- (3) Font, M.; Parella, T.; Costas, M.; Ribas, X. *Organometallics* **2012**, *31*, 7976.
- (4) Huffman, L. M.; Casitas, A.; Font, M.; Canta, M.; Costas, M.; Ribas, X.; Stahl, S. S. *Chem. Eur. J.* **2011**, *17*, 10643
- (5) Casitas, A.; Canta, M.; Solà, M.; Costas, M.; Ribas, X. *J. Am. Chem. Soc.* **2011**, *133*, 19386.
- (6) Casitas, A.; King, A. E.; Parella, T.; Costas, M.; Stahl, S. S.; Ribas, X. *Chem. Sci.* **2010**, *1*, 326.
- (7) Yao, B.; Wang, D.-X.; Huang, Z.-T.; Wang, M.-X. *Chem. Commun.* **2009**, 2899.
- (8) Wang, Z.-L.; Zhao, L.; Wang, M.-X. *Org. Lett.* **2011**, *13*, 6560.
- (9) Wang, Z.-L.; Zhao, L.; Wang, M.-X. *Org. Lett.* **2012**, *14*, 1472.
- (10) Wang, Z.-L.; Zhao, L.; Wang, M.-X. *Chem. Commun.* **2012**, *48*, 9418.
- (11) Huffman, L. M.; Stahl, S. S. *Dalton Transactions* **2011**, *40*, 8959.
- (12) Saejueng, P.; Bates, C. G.; Venkataraman, D. *Synthesis* **2005**, *2005*, 1706.
- (13) Evano, G.; Blanchard, N.; Toumi, M. *Chem. Rev.* **2008**, *108*, 3054.
- (14) Liu, F.; Ma, D. *J. Org. Chem.* **2007**, *72*, 4844.
- (15) Cacchi, S.; Fabrizi, G.; Parisi, L. M. *Org. Lett.* **2003**, *5*, 3843.
- (16) Hashmi, A. S. K. In *Silver in Organic Chemistry*; Harmata, M., Ed.; John Wiley & Sons: Hoboken, 2010, p 357.
- (17) Camasso, N. M.; Sanford, M. S. *Science* **2015**, *347*, 1218.
- (18) Bour, J. R.; Camasso, N. M.; Sanford, M. S. *J. Am. Chem. Soc.* **2015**, *137*, 8034.
- (19) Zhou, W.; Schultz, J. W.; Rath, N. P.; Mirica, L. M. *J. Am. Chem. Soc.* **2015**, *137*, 7604.
- (20) Zhou, W.; Zheng, S.; Schultz, J. W.; Rath, N. P.; Mirica, L. M. *J. Am. Chem. Soc.* **2016**, *138*, 5777.
- (21) Schultz, J. W.; Fuchigami, K.; Zheng, B.; Rath, N. P.; Mirica, L. M. *J. Am. Chem. Soc.* **2016**, *138*, 12928.

- (22) Ribas, X.; Calle, C.; Poater, A.; Casitas, A.; Gómez, L.; Xifra, R.; Parella, T.; Benet-Buchholz, J.; Schweiger, A.; Mitrikas, G.; Solà, M.; Llobet, A.; Stack, T. D. P. *J. Am. Chem. Soc.* **2010**, *132*, 12299.
- (23) Colpas, G. J.; Maroney, M. J.; Bagyinka, C.; Kumar, M.; Willis, W. S.; Suib, S. L.; Mascharak, P. K.; Baidya, N. *Inorg. Chem.* **1991**, *30*, 920.
- (24) Yang, C.; Wu, W.-D.; Zhao, L.; Wang, M.-X. *Organometallics* **2015**, *34*, 5167.
- (25) Kau, L. S.; Spira-Solomon, D. J.; Penner-Hahn, J. E.; Hodgson, K. O.; Solomon, E. I. *J. Am. Chem. Soc.* **1987**, *109*, 6433.
- (26) Martin-Diaconescu, V.; Gennari, M.; Gerey, B.; Tsui, E.; Kanady, J.; Tran, R.; Pécaut, J.; Maganas, D.; Krewald, V.; Gouré, E.; Duboc, C.; Yano, J.; Agapie, T.; Collomb, M.-N.; DeBeer, S. *Inorg. Chem.* **2015**, *54*, 1283.
- (27) Westre, T. E.; Kennepohl, P.; DeWitt, J. G.; Hedman, B.; Hodgson, K. O.; Solomon, E. I. *J. Am. Chem. Soc.* **1997**, *119*, 6297.
- (28) Klein, A.; Kaiser, A.; Wielandt, W.; Belaj, F.; Wendel, E.; Bertagnolli, H.; Zálíš, S. *Inorg. Chem.* **2008**, *47*, 11324.
- (29) DeBeer George, S.; Brant, P.; Solomon, E. I. *J. Am. Chem. Soc.* **2005**, *127*, 667.
- (30) Martin-Diaconescu, V.; Chacón, K. N.; Delgado-Jaime, M. U.; Sokaras, D.; Weng, T.-C.; DeBeer, S.; Blackburn, N. J. *Inorg. Chem.* **2016**, *55*, 3431.
- (31) Sarangi, R. *Coord. Chem. Rev.* **2013**, *257*, 459.
- (32) Grove, D. M.; Van Koten, G.; Ubbels, H. J. C.; Zoet, R.; Spek, A. L. *Organometallics* **1984**, *3*, 1003.
- (33) Cloutier, J.-P.; Vabre, B.; Moungang-Soumé, B.; Zargarian, D. *Organometallics* **2015**, *34*, 133.
- (34) Stol, M.; Snelders, D. J. M.; Godbole, M. D.; Havenith, R. W. A.; Haddleton, D.; Clarkson, G.; Lutz, M.; Spek, A. L.; van Klink, G. P. M.; van Koten, G. *Organometallics* **2007**, *26*, 3985.
- (35) van de Kuil, L. A.; Veldhuizen, Y. S. J.; Grove, D. M.; Zwikker, J. W.; Jenneskens, L. W.; Drenth, W.; Smeets, W. J. J.; Spek, A. L.; van Koten, G. *Recl. Trav. Chim. Pays-Bas* **1994**, *113*, 267.
- (36) Martinez, G. E.; Ocampo, C.; Park, Y. J.; Fout, A. R. *J. Am. Chem. Soc.* **2016**, *138*, 4290.
- (37) Schley, N. D.; Fu, G. C. *J. Am. Chem. Soc.* **2014**, *136*, 16588.
- (38) He, Z.; Huang, Y. *ACS Catal.* **2016**, *6*, 7814.
- (39) Mougang-Soumé, B.; Belanger-Gariépy, F.; Zargarian, D. *Organometallics* **2014**, *33*, 5990.
- (40) Bour, J. R.; Camasso, N. M.; Meucci, E. A.; Kampf, J. W.; Canty, A. J.; Sanford, M. S. *J. Am. Chem. Soc.* **2016**, *138*, 16105.
- (41) Golub, G.; Cohen, H.; Paoletti, P.; Bencini, A.; Bertini, L. M.; Meyerstein, D. *J. Am. Chem. Soc.* **1995**, *117*, 8353.
- (42) Mizuta, S.; Verhoog, S.; Wang, X.; Shibata, N.; Gouverneur, V.; Médebielle, M. *J. Fluorine Chem.* **2013**, *155*, 124.
- (43) Güell, I.; Ribas, X. *Eur. J. Org. Chem.* **2014**, *2014*, 3188.

- (44) Jiang, Y.; Xu, L.; Zhou, C.; Ma, D. In *C-H and C-X Functionalization. Transition Metal Mediation*; Ribas, X., Ed.; RSC Publishing: Cambridge, UK, 2013; Vol. Catalysis Series 11, p 1.
- (45) Cai, Q.; He, G.; Ma, D. *J. Org. Chem.* **2006**, *71*, 5268.
- (46) Ma, D.; Cai, Q. *Org. Lett.* **2003**, *5*, 3799.
- (47) Zhang, H.; Cai, Q.; Ma, D. *J. Org. Chem.* **2005**, *70*, 5164.
- (48) Altman, R. A.; Shafir, A.; Choi, A.; Lichtor, P. A. and Buchwald, S. L. *J. Org. Chem.* **2008**, *73*, 284.
- (49) Cohen, T.; Cristea, I. *J. Am. Chem. Soc.* **1975**, *40*, 3649.
- (50) Tye, J. W.; Weng, Z.; Johns, A. M.; Incarvito, C. D.; Hartwig, J. F. *J. Am. Chem. Soc.* **2008**, *130*, 9971.
- (51) Shafir, A.; Lichtor, P. A.; Buchwald, S. L. *J. Am. Chem. Soc.* **2007**, *129*, 3490.
- (52) Yu, H.-Z.; Jiang, Y.-Y.; Fu, Y.; Liu, L. *J. Am. Chem. Soc.* **2010**, *132*, 18078.

CHAPTER VIII.

GENERAL CONCLUSIONS



In the past years, the catalysis research community got interested in first-row transition metal-assisted cross-coupling chemistry providing more effective and more sustainable procedures, which emerged as powerful synthetic strategies in many areas. However, a clear understanding of the fundamental reactivity of metal-assisted cross-coupling reactions remains a challenge due to the occurrence of mechanisms highly dependent on the reactants and experimental conditions used.

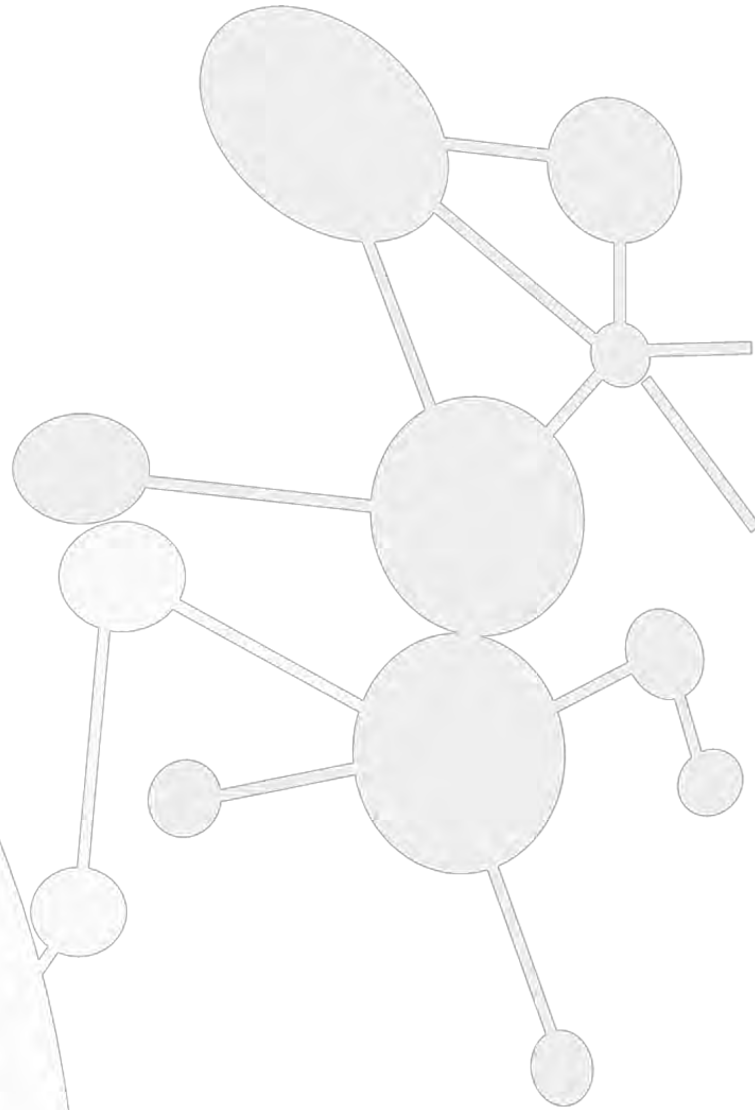
In this thesis we used a well-defined aryl-Cu^{III} macrocyclic model system as starting point on the mechanistic study of C(sp²)-C(sp³) (Hurtley-type coupling) and C(sp²)-C(sp) (Stephens-Castro-type coupling) bond formation, and studied the putative role of these high-valent copper species (Chapter III and Chapter IV, respectively). In **Chapter III**, studies conducted with well-defined aryl-Cu^{III} species reveal their capability to undergo C(sp²)-C(sp³) bond formation *via* reductive elimination process in presence of several activated methylenes (malononitrile, dimethyl malonate and acetylacetone), which interestingly undergo a very favourable intramolecular spontaneous reorganization step to afford the final heterocyclic products 1,2-dihydroisoquinoline (**P1** and **P2**) and 1,2-dihydroisoquinolin-3(4H)-one (**P3**). Moreover, the exploration of catalytic copper-catalysed version of this transformation provided the formation of desired compounds in good yields. In order to gain mechanistic insight, we monitored the catalytic transformations by UV/Vis and ¹H NMR (at low temperature). All the data obtained clearly points towards the intermediacy of aryl-Cu^{III} species in the coupling reactions within our model platform, providing the first evidence of the direct engagement of a redox Cu^I/Cu^{III} catalytic cycle, involving oxidative addition and reductive elimination steps for Cu-catalysed Hurtley-type coupling reactions.

In **Chapter IV** we studied the feasibility of aryl-Cu^{III} species as a key intermediates in copper-assisted Stephens-Castro reaction for C(sp²)-C(sp) bond formation, by exploring their reactivity with terminal *p*-R-phenylacetylene derivatives (R = NO₂, CF₃, H) at room temperature. Interestingly, the final products afforded also contained heterocyclic 2*H*-isoindole (**P**_{NO₂}, **P**_{CF₃}, **P**_{Ha}), or 1,2-dihydroisoquinoline (**P**_{Hb}) scaffolds, which are formed through the nucleophilic attack of one secondary amine moiety of the macrocyclic system to the biaryl acetylene intermediate species (**I**_R). As we expected, the nucleophilic attack is facilitated by the electrophilic activation of triple bond by the coordination of Cu^I cation. However, the use of **L5-Cl** substrate with *p*-CF₃-phenylacetylide copper(I) complex precluded the intramolecular reorganization step, affording the **I'**_{CF₃} as a final stable product. In addition, the representation of the frontier molecular orbitals for **I**_H·Cu^I and **I**_{NO₂}·Cu^I species explained the divergence on the formation of the 5-membered ring and the 6-membered ring scaffolds. Moreover, both DFT calculations and the experimental data obtained nicely correlate, providing a strong evidence for the involvement of an organometallic aryl-Cu^{III}-acetylide intermediate species in these transformations. Nevertheless, catalytic turnover was not possible in this model system due to inhibition or entrapment of Cu^I released upon reductive elimination. Altogether, the formation of heterocyclic scaffolds also constitute a valuable knowledge for synthetic organic chemistry.

In **Chapter V** we turned our attention to the redox chemistry of Ni-mediated transformations, aiming at understanding the fundamental steps in coupling transformations. To that end, we took advantage of our experience in model substrates for copper catalysis, and we studied in depth the synthesis and reactivity of well-defined aryl-Ni^{II} complexes. Organometallic square planar aryl-Ni^{II} complexes can be synthesised through oxidative addition of Ni⁰ to macrocyclic aryl halide model substrates or through the direct C-H activation of macrocyclic arene model substrates by Ni^{II} salts. [L_nNi^{II}](X) complexes have been exhaustively characterised by crystallographic and spectroscopic techniques, showing one of the shortest Ni-C bond (1.83 Å) reported to date. The strength of the Ni-C bond precludes their direct reactivity with nucleophiles *via* reductive elimination. Nevertheless, we have proved their reactivity in the presence of a 2 e-redox oxidant as an electrophilic CF₃⁺ source, obtaining quantitative yields of the trifluoromethylated aryl-CF₃ compounds. Furthermore, DFT calculations and experimental mechanistic investigations pointed towards the feasibility of an initial SET step followed by a recombination of aryl-Ni^{III}/CF₃[•] adduct to form an aryl-Ni^{IV}-CF₃ intermediate species, which easily underwent the formation of trifluoromethylated product through reductive elimination. To the best of our knowledge, this constitutes the first example of square planar model platform that allows to travel through the rich redox chemistry of nickel, from Ni⁰ to Ni^{IV}, gaining insight into its geometry-dependent reactivity of multiple oxidation states in a single model system.

In **Chapter VI** we turned our attention to the standard Ullmann-Goldberg systems by studying the effect of the ligand choice on the chemoselectivity and on the operative mechanism of a multiple combinations of amides, amines and phenols in competitive reactions. High selective arylation with high yields of a wide range of O-based and N-based nucleophiles using a common experimental methodology and a preferred auxiliary ligand for each nucleophile were obtained in the most of the cases. However, the exact role of these auxiliary ligands on the chemoselective arylation is not well understood and an in-depth mechanistic studies should be done. Indeed, the reactions conducted using a radical clock as a substrate did not reveal the formation of radical intermediates during the reaction course, indicating the thermal-based Cu^I/Cu^{III} redox catalytic cycle as the operative mechanism in such coupling reactions. So far, the precise methodologies to be used for the arylation of any of the nucleophiles tested should be a precious practical guide in organic synthesis laboratories.

ANNEX 1.



Supplementary Information Chapter III

Model C_{sp2}-C_{sp3} Hurtley coupling catalysis operating via a well-defined Cu^I/Cu^{III} mechanism

Mireia Rovira, Marc Font and Xavi Ribas *

QBIS Research Group, Departament de Química, Universitat de Girona, Campus Montilivi, Girona E-17071, Catalonia, Spain.

CONTENTS

1. Materials and Methods	157
1.1. Materials and methods	157
1.2. Instrumentation.....	157
1.3. Synthesis of aryl-Cu ^{III} complex 1 _{ClO₄}	158
1.4. Synthesis and characterization of C _{sp2} -C _{sp3} coupling products P1-P3	158
1.5. General procedure for catalytic reactions	160
1.6. Procedure for UV-Vis monitoring of the catalytic reactions.....	160
1.7. NMR Structural determination of P1-P3 final products	161
2. Supplementary References	163
3. Supplementary Figures	163

1. Materials and Methods

1.1. Materials and methods

Commercially available reagents were used as received, unless otherwise noted. Solvents were purchased from SDS-Carlo Erba and Scharlab and were purified and dried by passing through an activated alumina purification system (MBraun SPS-800). Preparation and handling of air-sensitive materials were carried out in a N₂ drybox (Jacomex) with O₂ and H₂O concentrations < 1 ppm. Ligand **L1-Br**, and aryl-Cu^{III} complex **1**_{ClO₄} were synthesized following published procedures.^[1-3]

1.2. Instrumentation

NMR data concerning product identity were collected with a Bruker 400 or 300 AVANCE spectrometer in the corresponding deuterated solvent (CDCl₃, CD₃CN) and calibrated relative to an external reference (1,3,5-trimethoxybenzene). ESI-MS experiments were collected and analyzed on a Bruker Daltonics Esquire 6000 mass spectrometer with acetonitrile as the mobile

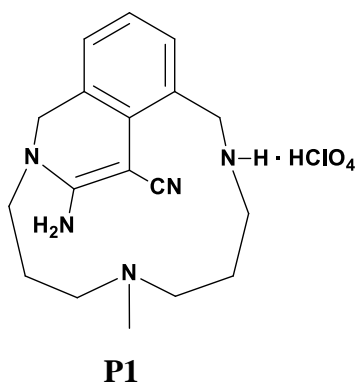
phase. UV-Vis spectroscopy was performed on an Agilent-UV-Visible-8453 spectrophotometer using 1 cm quartz cuvettes. Temperature control was achieved with a cryostat from Unisoku Scientific Instruments, Japan.

1.3. Synthesis of aryl-Cu^{III} complex **1**_{ClO₄}

Caution: Perchlorate salts are potentially explosive and should be handled with care! Arylcopper(III) complex **1**_{ClO₄} was prepared following procedures described in the literature previously.^[1,2]

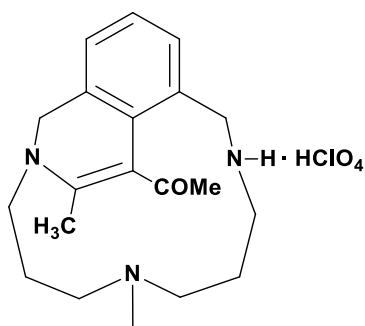
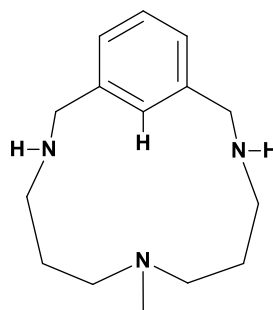
1.4. Synthesis and characterization of C_{sp2}-C_{sp3} coupling products **P1-P3**

In an inert-atmosphere glove box, a sample of the aryl-Cu^{III} complex **1**_{ClO₄} (14.2 mg, 28 μmol) was dissolved in CD₃CN (1.6 mL) and 0.4 mL of a solution of 1,3,5-trimethoxybenzene was added as an internal standard. A portion of this solution (0.6 mL) was loaded into a NMR tube, and 2 equivalents of the corresponding activated methylene nucleophile were added to the tube (0.1 mL, 168 mM). Final concentrations: [**1**_{ClO₄}] = 12 mM and [active methylene nucleophile] = 24 mM. The tube was sealed with a screw-cap and the reaction was allowed to react at room temperature (for malononitrile) or at 50°C (for acetylacetone and dimethyl malonate) and monitored by ¹H-NMR spectroscopy until reaction completion. Final yields were: **P1** (99%), **P2** (80%) and **P3** (37%). In the reaction of dimethyl malonate the presence of Cs₂CO₃ (8.8 eq.) enhances the yield of **P3** from 37% to 56%. ¹H, COSY, NOESY, TOCSY, ¹H-¹³C HSQC, ¹H-¹³C HMBC and ¹³C-NMR spectra and mass spectrometric analysis were obtained directly from crude reactions. Reaction yields were obtained by relative integration of the ¹H-NMR signals to the internal standard.

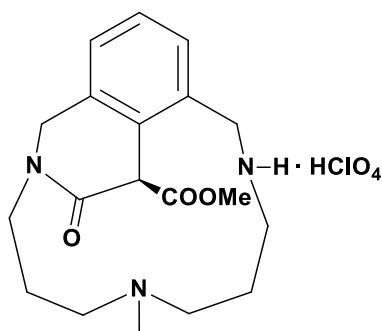
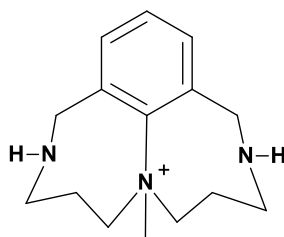
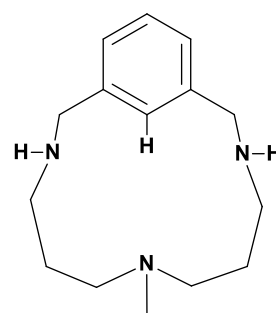


P1. (yield: 99%) ¹H-NMR (400 MHz, CD₃CN, 25 °C) δ, ppm: 7.25-7.11 (m, 3H, H^a, H^b), 5.61 (s, 2H, NH₂), 4.98 (d, 1H, *J* = 13.8 Hz, H^c or H^d), 4.21 (m, 2H, H^r, H^s), 3.92 (d, 1H, *J* = 13.64 Hz, H^c or H^d), 3.88- 3.83 (m, 1H, H^p or H^q), 3.11 (ddd, 1H, *J* = 15.24 Hz *J* = 6.88 Hz, *J* = 2.6 Hz, H^p or H^q), 2.83-2.76 (m, 1H, H^e or H^f), 2.63-2.37 (m, 3H, Hⁱ or H^j, H^e or H^f, H^l or H^m), 2.30- 2.22 (m, 1H, Hⁱ or H^j), 2.12 (s, 3H, H^k), 2.06- 2.01 (m, 1H, H^l or H^m), 1.81-1.71 (m, 1H, Hⁿ or H^o), 1.58-1.47 (m, 1H, H^g or H^h), 1.39-1.29 (m, 1H, Hⁿ or H^o), 1.22-1.12 (m, 1H, H^g or H^h). ¹³C-NMR (100 MHz, CD₃CN, 25 °C) δ, ppm: 162.4 (C₁₄), 132.2 (C₁), 130.7 (C₃ or C₄), 127.5 (C₁₆), 124.7 (C₂), 123.8

(C₃ or C₄), 54.6 (C₈), 52.9 (C₁₃), 52.9 (C₁₀), 49.8 (C₁₂), 48.9 (C₅), 44.4 (C₆), 40.4 (C₉), 26.4 (C₁₁), 22.8 (C₇). **ESI-MS** (CH₃CN, m/z): 312.2 (100) [C₁₈H₂₅N₅ + H⁺]⁺.

**P2****L1-H**

P2. (yield: 80%) **¹H-NMR** (400 MHz, CD₃CN, 25 °C) δ, ppm: 7.32-7.25 (m, 3H, H^a, H^b), 4.37 (d, 1H, *J* = 14 Hz, H^r), 4.24 (d, 1H, *J* = 13.7 Hz, H^d), 4.12 (d, 1H, *J* = 13.7 Hz, H^c), 4.06 (d, 1H, *J* = 14 Hz, H^s), 3.94-3.74 (m, 1H, H^q), 3.35 (dt, 1H, *J* = 14.7 Hz, *J* = 3.8 Hz, H^p), 2.65-2.54 (m, 1H, H^e or H^f), 2.54 (s, 3H, H^t), 2.29-2.21 (m, 2H, H^e or H^f, Hⁱ or H^j), 2.23 (s, 3H, H^u), 2.00 (s, 3H, H^k), 1.99-1.92 (m, 1H, Hⁱ or H^j), 1.90-1.87 (m, 1H, H^l), 1.73-1.68 (m, 2H, H^m, H^o), 1.52-1.44 (m, 1H, Hⁿ), 1.32-1.22 (m, 1H, H^g or H^h), 1.10-1.02 (m, 1H, H^g or H^h). **¹³C-NMR** (100 MHz, CD₃CN, 25 °C) δ, ppm: 190.9 (C₁₇), 163.5 (C₁₅), 134.6 (C₁), 128.8 (C₄), 126.7 (C₂), 124.6 (C₃), 113.3 (C₁₄), 55.0 (C₈), 53.9 (C₁₃), 51.2 (C₁₀), 48.8 (C₅), 48.1 (C₁₂), 43.7 (C₆), 41.3 (C₉), 29.1 (C₁₆), 26.5 (C₁₁), 23.9 (C₇), 19.1 (C₁₈). **ESI-MS** (CH₃CN, m/z): 328.2 (100) [C₂₀H₂₉N₃O + H⁺]⁺. *This reaction generates the byproduct L1-H* (**ESI-MS** (CH₃CN, m/z): 248.1 (20.1) [C₁₅H₂₅N₃ + H⁺]⁺).

**P3****BP1****L1-H**

P3. (yield: 56%) **¹H-NMR** (400 MHz, CD₃CN, 25 °C) δ, ppm: 7.35-7.29 (m, 3H, H^a, H^b), 5.75 (s, 1H, Hⁱ), 4.88 (d, 1H, *J* = 16 Hz, H^r or H^s), 4.38 (d, 1H, *J* = 12.8 Hz, H^d), 4.25 (d, 1H, *J* = 16.4 Hz, H^r or H^s), 4.27-4.18 (m, 1H, Hⁱ or H^m), 3.65 (s, 3H, H^u), 3.61 (d, 1H, *J* = 13.2 Hz, H^c), 3.10-3.04 (m, 2H, Hⁱ or H^m, H^p or H^q), 2.81-2.70 (m, 2H, Hⁱ or H^j, H^e or H^f), 2.48 (s, 3H, H^k), 2.48-2.41 (m, 1H, Hⁱ or H^m), 2.17-2.08 (m, 2H, H^e or H^f, Hⁿ or H^o), 1.80-1.75 (m, 2H, Hⁿ or H^o, Hⁱ or H^j), 1.37-1.29 (m,

^1H , H^{a} or H^{b}), 0.72-0.59 (m, ^1H , H^{a} or H^{b}). ^{13}C -NMR (100 MHz, CD_3CN , 25 °C) δ , ppm: 169.0 (C_{14}), 167.2 (C_{16}) 136.4 (C_2), 132.6 (C_1) 129.5 (C_3), 125.7 (C_4), 55.0 (C_{10}), 52.6 (C_{15}), 52.5 (C_{17}), 51.6 (C_5), 51.3 (C_{13}), 45.3 (C_{12}), 43.7 (C_6), 40.3 (C_9), 25.6 (C_7), 24.2 (C_8), 22.3 (C_{11}). **ESI-MS** (CH_3CN , m/z): 346.1 (54.6) [$\text{C}_{19}\text{H}_{27}\text{N}_3\text{O}_3 + \text{H}^+$] $^+$. *This reaction generates byproduct BP1* (**ESI-MS** (CH_3CN , m/z): 246.1 (100) [$\text{C}_{15}\text{H}_{24}\text{N}_3$] $^+$).

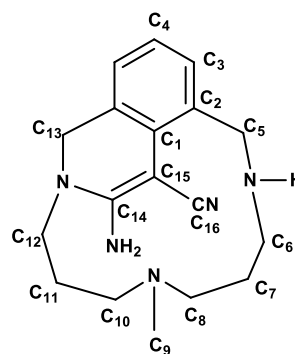
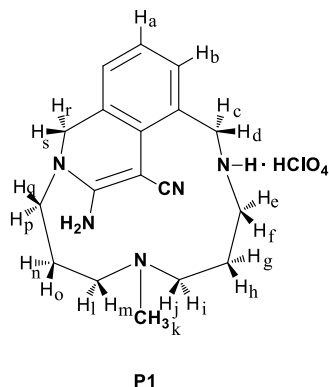
1.5. General procedure for catalytic reactions

In an inert-atmosphere glove box, a vial was loaded with 0.5 mL of ligand **L1-Br** 30 mM in CH_3CN and 10 mol % of $[\text{Cu}^{\text{I}}(\text{CH}_3\text{CN})_4](\text{CF}_3\text{SO}_3)$ was added (0.2 mL of stock solution 7.5 mM in CH_3CN). The colourless solution becomes slightly red indicating that oxidative addition takes place obtaining the corresponding complex $\text{arylCu}^{\text{III}}\text{-Br}$, complex **2_{Br}**. Then 2.3 mL of active methylene nucleophile solution 13 mM in CH_3CN were added by syringe pump in a period of 3 hours. For the dimethyl malonate and acetylacetone couplings the presence of K_2CO_3 (8.8 equivalents and 2.2 equivalents respectively) is needed and for acetylacetone coupling the presence of molecular sieves increases the yield of the catalysis. Final concentrations: [**L1-Br**] = 5 mM, [$[\text{Cu}^{\text{I}}(\text{CH}_3\text{CN})_4](\text{CF}_3\text{SO}_3)$] = 0.5 mM, [active methylene nucleophile] = 10 mM. After stirring the mixture crude, at room temperature for 24 hours, 150 μL of 1,3,5-trimethoxybenzene 1.67 mM in CH_3CN as internal standard is added and the solvent is removed. The sample is re-dissolved in 0.5 mL of CD_3CN and NMR yields were obtained by ^1H -NMR using integration of benzylic protons respect to trimethoxybenzene. The obtained yields are 95%, 37% and 67% for **P1**, **P2** and **P3** respectively.

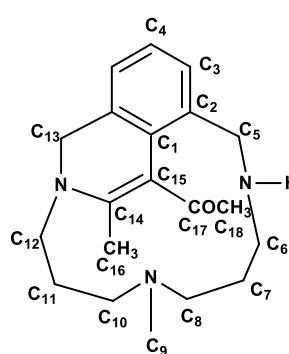
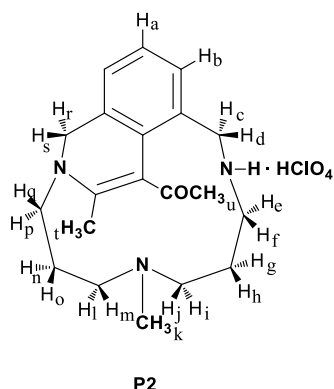
1.6. Procedure for UV-Vis monitoring experiments

A UV-Visible cuvette equipped with a Teflon stopcock was dried in an oven and cooled under vacuum. Stock solutions of malononitrile (3 M), **L1-Br** (17 mM) and $[\text{Cu}^{\text{I}}(\text{CH}_3\text{CN})_4](\text{CF}_3\text{SO}_3)$ (3.6 mM) were prepared in dry CH_3CN . After backfilling the cuvette with dry N_2 , 1.75 mL of **L1-Br** stock solution was added via syringe. The cuvette was inserted into the spectrophotometer and the temperature was allowed to equilibrate at 40°C. 1.15 mL of $[\text{Cu}^{\text{I}}(\text{CH}_3\text{CN})_4](\text{CF}_3\text{SO}_3)$ stock solution were added to the cuvette. The reaction was initiated by adding malononitrile (0.1 mL) to the cuvette followed by rapid mixing of the combined solutions. Final concentrations: [**L1-Br**] = 10 mM, [$[\text{Cu}^{\text{I}}(\text{CH}_3\text{CN})_4](\text{CF}_3\text{SO}_3)$] = 1.4 mM, [malononitrile] = 100 mM, CH_3CN , 40°C. The appearance of a band at 550 nm confirmed the formation of the $\text{aryl-Cu}^{\text{III}}\text{-Br}$ species.^[4] The reaction progress was monitored by following the decay of the absorbance at 550 nm (see Figure S1).

1.7. NMR Structural determination of P1-P3 final products

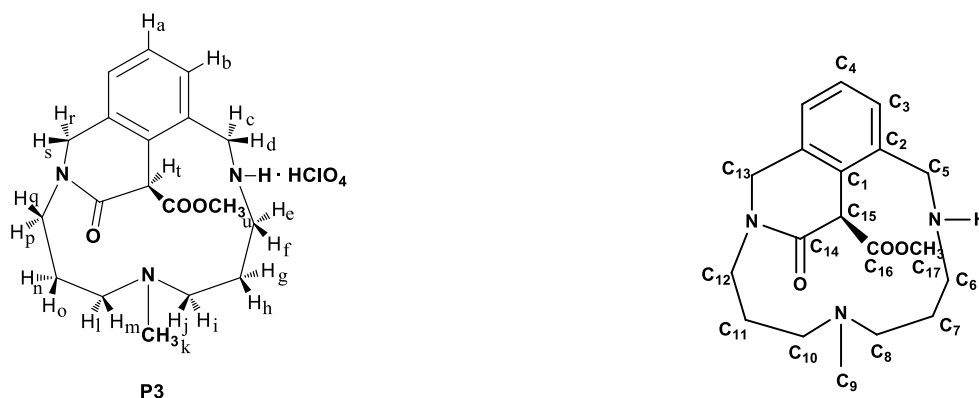


P1. By means of the ^1H - ^{13}C HMBC experiment, the two benzylic protons present in the ^1H -NMR spectrum, appearing as a multiplet at 4.21 ppm and corresponding to the H^r and H^s protons, along with the multiplet and the double double doublet at 3.88-3.83 respectively, that corresponds to H^p and H^q , show a coupling with the alkenylic carbon C_{14} at 162.4 ppm in the ^{13}C -NMR. Moreover, the benzylic protons in the other side of the molecule H^c and H^d , that appear in the ^1H -NMR as two doublets at 4.98 and 3.92 ppm, couple with a peak at 127.5 ppm in the ^{13}C -NMR, assigned to the carbon of the nitrile group (C_{16}). The NOESY experiment allowed us to assign H^p and H^q due to its coupling through space with H^r and H^s protons. Using the TOCSY experiment the protons corresponding to each aliphatic chain (H^e , H^f , H^g , H^h , H^i & H^j for the aliphatic chain on the right of the central N-CH_3 group and H^n , H^o , H^p , H^q , H^r , H^s for the left chain) are determined. The COSY and ^1H - ^{13}C HSQC experiments allowed us to determine the ^{13}C NMR peaks for each proton. The NOESY also enabled the assignation of the benzylic protons H^r and H^s with H^p or H^q and H^b . ^1H - ^{13}C HMBC experiments were critical to distinguish between protons H^e , H^f and H^i , H^j , since only H^i or H^j show coupling with the peak at 40.4 ppm in the ^{13}C -NMR assigned to the methyl of the tertiary central amine (C_9). With this information in hand and using the NOESY experiment we assigned the peaks in the two aliphatic chains. Furthermore, the ^1H - ^{13}C HMBC experiment allowed us to assign the quaternary carbons of the molecule using H^a , H^b , H^c , H^d , H^r and H^s to identify them.



P2. The ^1H - ^{13}C HMBC spectrum shows a coupling of the singlet corresponding to the methyl group of the ketone (H^u) at 2.54 ppm in the ^1H -NMR with the carbonylic carbon (C_{17}) in the ^{13}C -NMR. With regard to the singlet corresponding to the 3H of the methyl group H^t at 2.23 ppm in the ^1H -NMR, the ^1H - ^{13}C HMBC spectrum shows its coupling with the two alkenylic carbons (C_{14}

& C₁₅) at 113.3 ppm and 163.5 respectively. On the other hand, the NOESY experiment reveals a coupling between H^t and the multiplet signal corresponding to 1H at 3.94-3.74 ppm in the ¹H-NMR that is assigned to H^q, because the proton facing upwards is in closer proximity than the one facing downwards (H^p). Using the TOCSY experiment the protons corresponding to the aliphatic chain on the left side of the central tertiary amine (H^l, H^m, Hⁿ, H^o, H^p & H^q) are determined. The COSY and ¹H-¹³C HSQC experiments allowed us to determine the couples of protons bound to the same carbon in the aliphatic chain and again, the NOESY experiment allowed us to identify which protons are facing upwards and downwards. The NOESY also enabled the differentiation of the benzylic protons H^r and H^s due to the coupling of H^p with H^r. The identification of the protons from the aliphatic chain on the right side of the molecule (H^e, H^f, H^g, H^h, Hⁱ & H^j) was done as described for the left chain. ¹H-¹³C HMBC experiments were critical to distinguish between protons H^p, H^q and H^l, H^m, since H^l along with Hⁱ or H^j shows coupling with the peak at 41.3 ppm in the ¹³C-NMR assigned to the methyl of the tertiary central amine (C₉). Moreover, the ¹H-¹³C HMBC experiment allowed us to assign the quaternary carbons of the molecule.



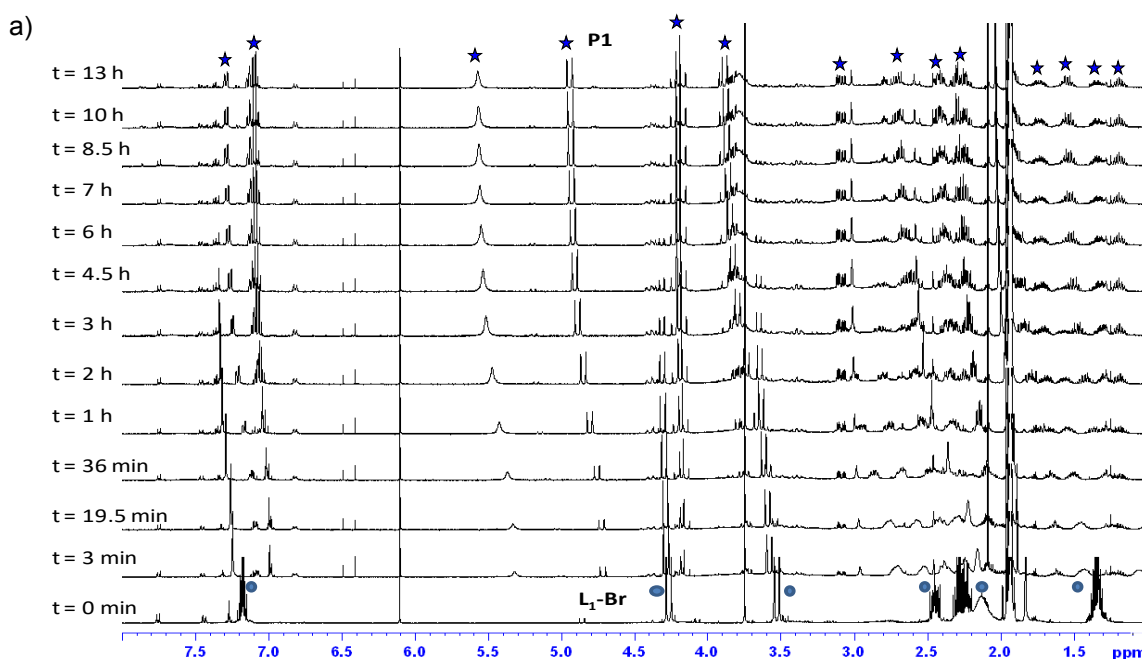
P3. The ¹H-¹³C HMBC spectrum shows a coupling of the singlet corresponding to the proton α -dicarbonylic (H^t) at 6.11 ppm in the ¹H-NMR with the carbonylic carbons of the amide (C₁₄) and the ester (C₁₆) appear at 169.0 ppm and 167.2 ppm respectively. With regard to the singlet corresponding to the 3H of the methyl group H^u at 3.65 ppm in the ¹H-NMR, ¹H-¹³C HMBC spectrum shows its coupling with the carbonylic carbon of the amide (C₁₄). On the other hand, the NOESY experiment reveals a coupling between H^t and the doublet signal corresponding to 1H at 4.38 ppm in the ¹H-NMR that is assigned to the benzylic H^c. The only conformation presenting the close proximity necessary to observe a NOE for these two protons, is the one in which the proton H^t faces downwards and the benzylic proton H^d faces upwards. Using the TOCSY experiment the protons corresponding to each aliphatic chain (H^e, H^f, H^g, H^h, Hⁱ & H^j for the aliphatic chain on the right of the central amine and Hⁿ, H^o, H^p, H^q, H^r, H^s for the left chain) are determined. The COSY and ¹H-¹³C HSQC experiments allowed us to determine the couples of protons bound to the same carbon in the aliphatic chain. The ¹H-¹³C HMBC allowed us to distinguish between protons H^p, H^q and H^l, H^m, since H^l or H^m show coupling with the peak at 40.3 ppm in the ¹³C-NMR assigned to the methyl of the tertiary central amine (C₉).

2. Supporting References

1. Ribas, X.; Jackson, D. A.; Donnadiou, B.; Mahía, J.; Parella, T.; Xifra, R.; Hedman, B.; Hodgson, K. O.; Llobet, A.; Stack, T. D. P. *Angew. Chem. Int. Ed.* **2002**, *41*, 2991.
2. King, A. E.; Huffman, L. M.; Casitas, A.; Costas, M.; Ribas, X.; Stahl, S. S. *J. Am. Chem. Soc.* **2010**, *132*, 12068.
3. Casitas, A.; Canta, M.; Solà, M.; Costas, M.; Ribas, X. *J. Am. Chem. Soc.* **2011**, *133*, 19386.
4. A. Casitas, A. E. King, T. Parella, M. Costas, S. S. Stahl, X. Ribas, *Chem. Sci.* **2010**, *1*, 326-330

3. Supporting Figures

Figure S1. ^1H NMR monitoring of the Cu^{I} -catalyzed coupling of **L₁-Br** and malononitrile to produce **P1** quantitatively. a) Overlaid spectra showing the consumption of substrate **L₁-Br** signals (circles) and growing of **P1** signals (stars). b) Plot of the concentration changes of both substrate **L₁-Br** and product **P1** based on the integration of selected peaks. Conditions (equivalents to those of Scheme 6 in the manuscript): $[\text{L}_1\text{-Br}] = 9.6 \text{ mM}$, $[[\text{Cu}^{\text{I}}(\text{CH}_3\text{CN})_4](\text{CF}_3\text{SO}_3)] = 0.9 \text{ mM}$, $[\text{malononitrile}] = 17 \text{ mM}$, $[\text{TMB}] = 0.76 \text{ mM}$, CH_3CN , 40°C , N_2 atmosphere. Spectra registered every 15 min (selected spectra are shown for clarity).



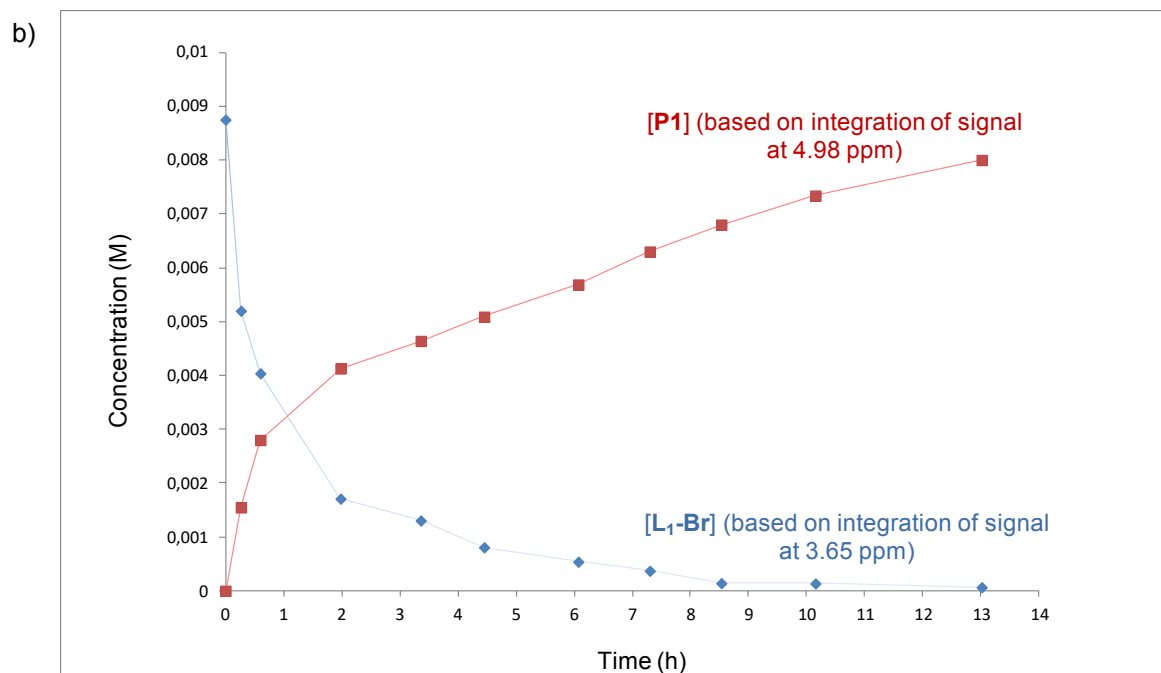


Figure S2. ESI-MS spectrum of compound **P1** ($m/z = 312.2$) in CH_3CN .

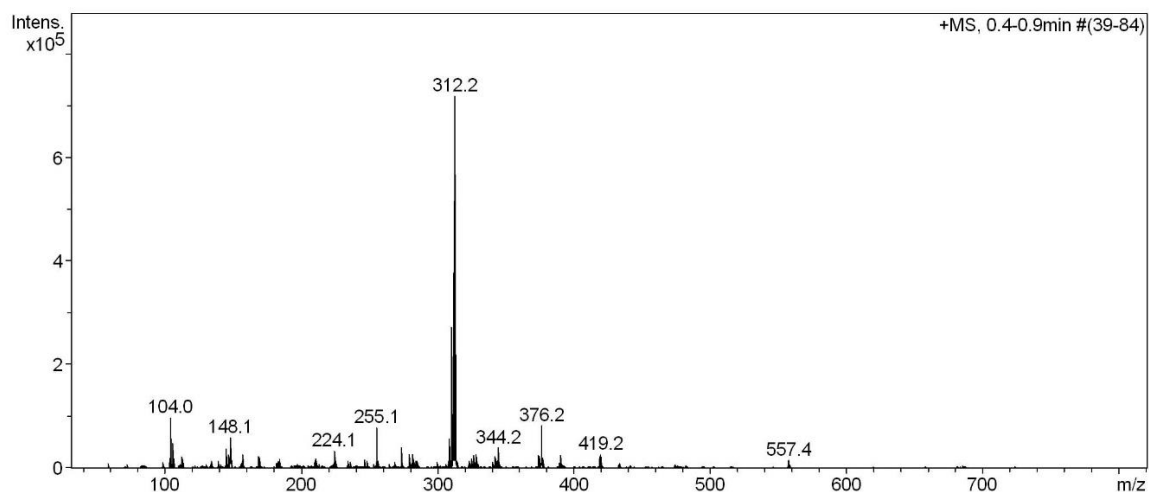
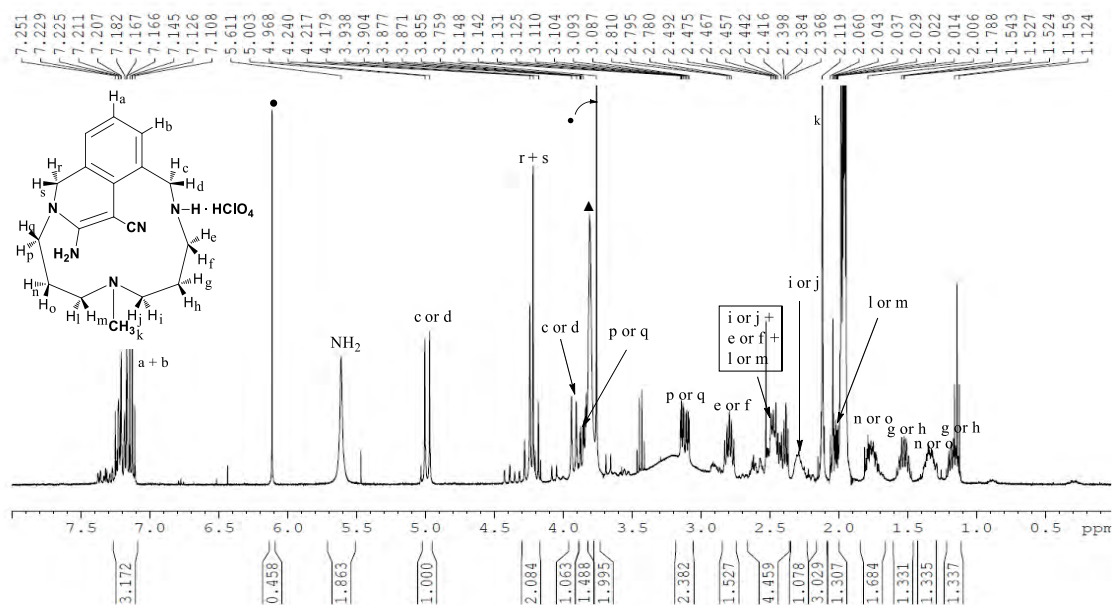


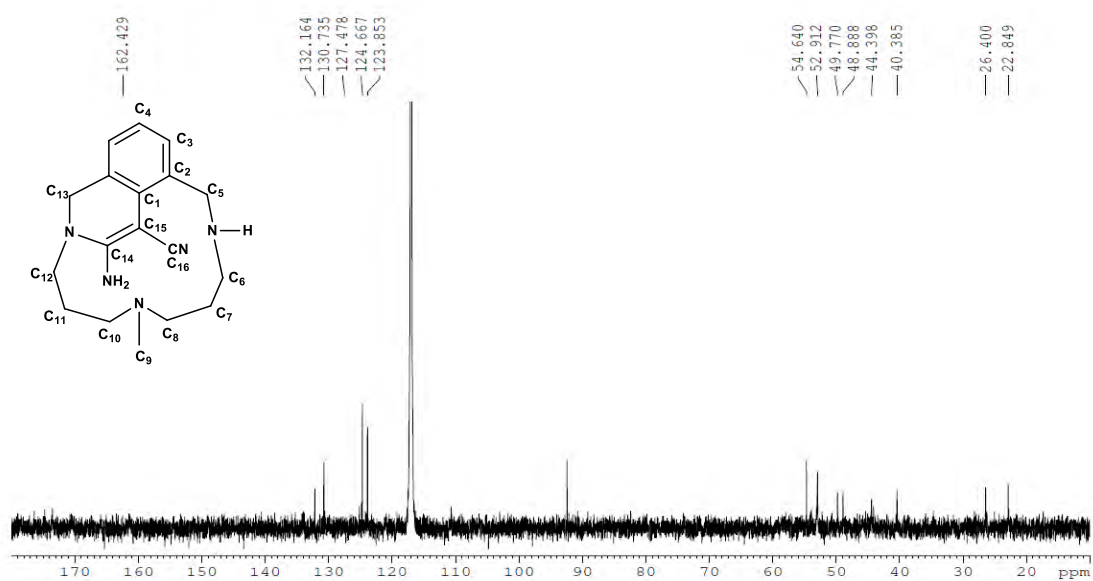
Figure S3. NMR characterization of P1: a) ^1H -NMR spectrum (400 MHz, CD_3CN , 25 °C). b) $^{13}\text{C}\{^1\text{H}\}$ -NMR spectrum (100 MHz, CD_3CN , 25 °C). c) ^1H - ^1H COSY spectrum (400 MHz, CD_3CN , 25°C). d) ^1H - ^1H NOESY spectrum (400 MHz, CD_3CN , 25°C). e) ^1H - ^{13}C HSQC_ed spectrum (400 MHz, CD_3CN , 25°C). f) ^1H - ^{13}C HMBC spectrum (400 MHz, CD_3CN , 25°C). g) ^1H - ^1H TOCSY spectrum (400 MHz, CD_3CN , 25°C).

a)

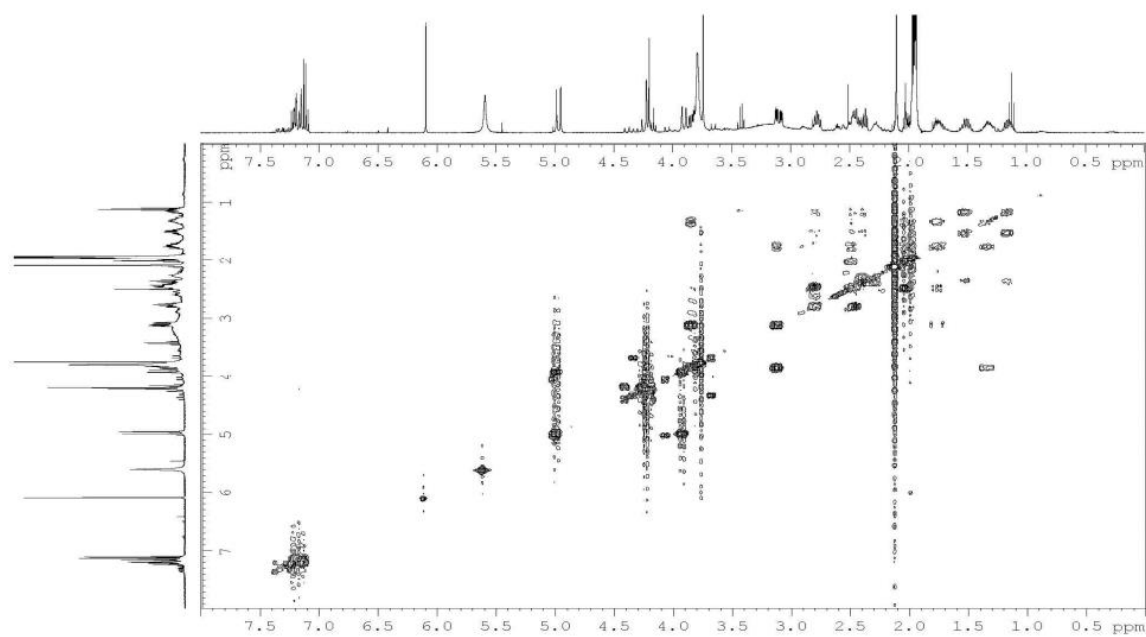


● 1,3,5-trimethoxybenzene (std.). ▲ excess malononitrile.

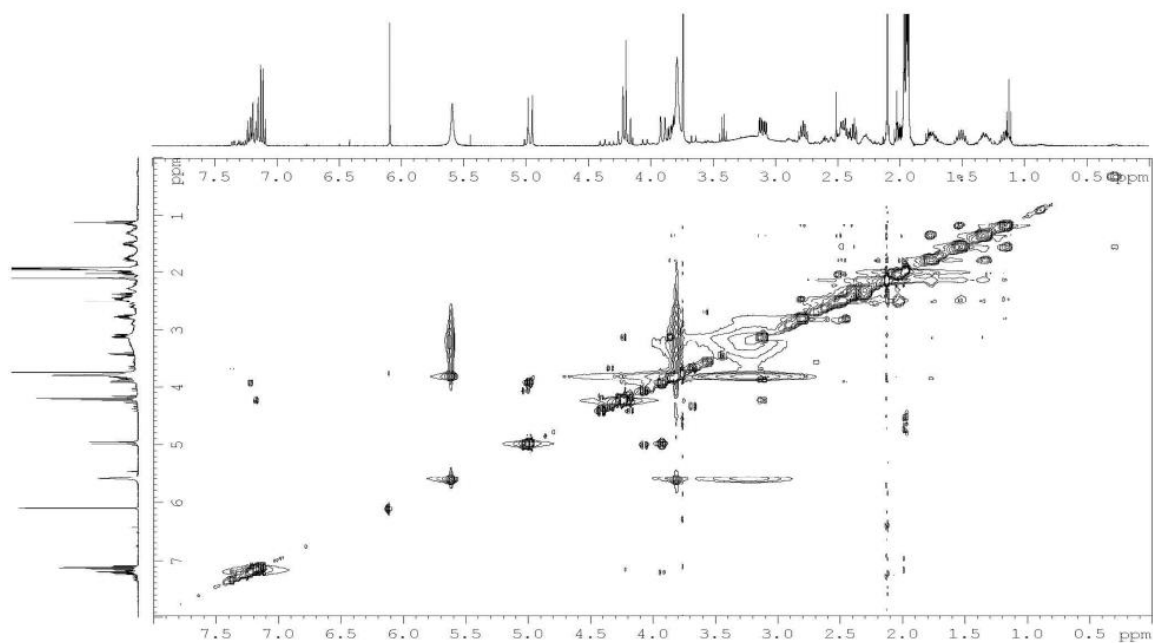
b)



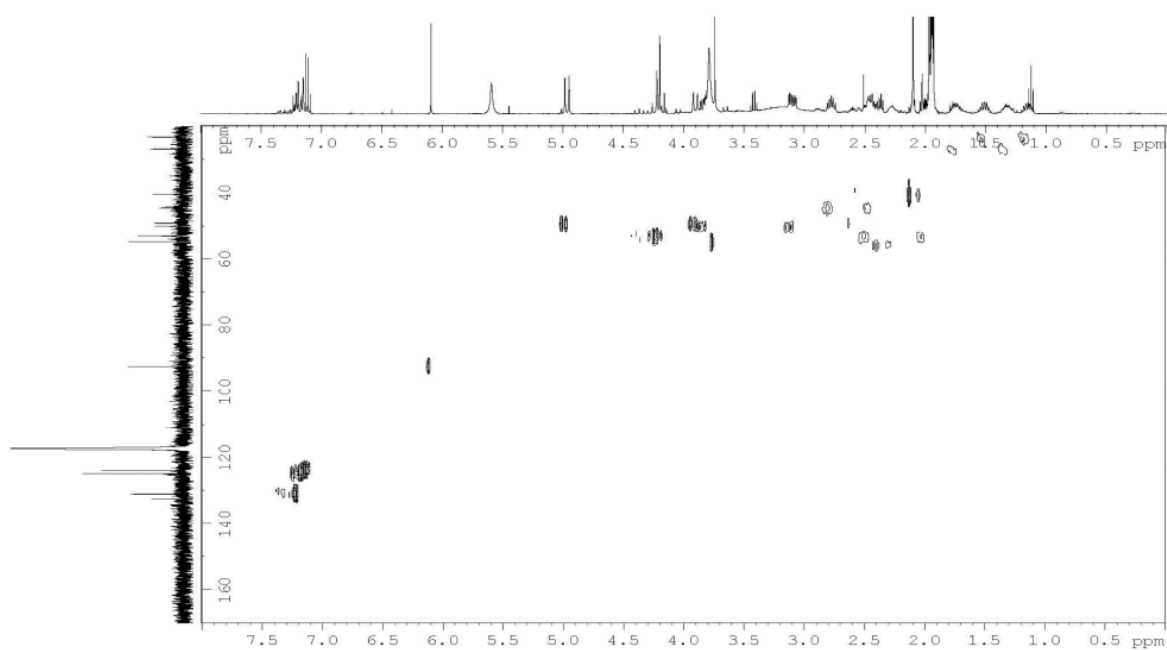
c)



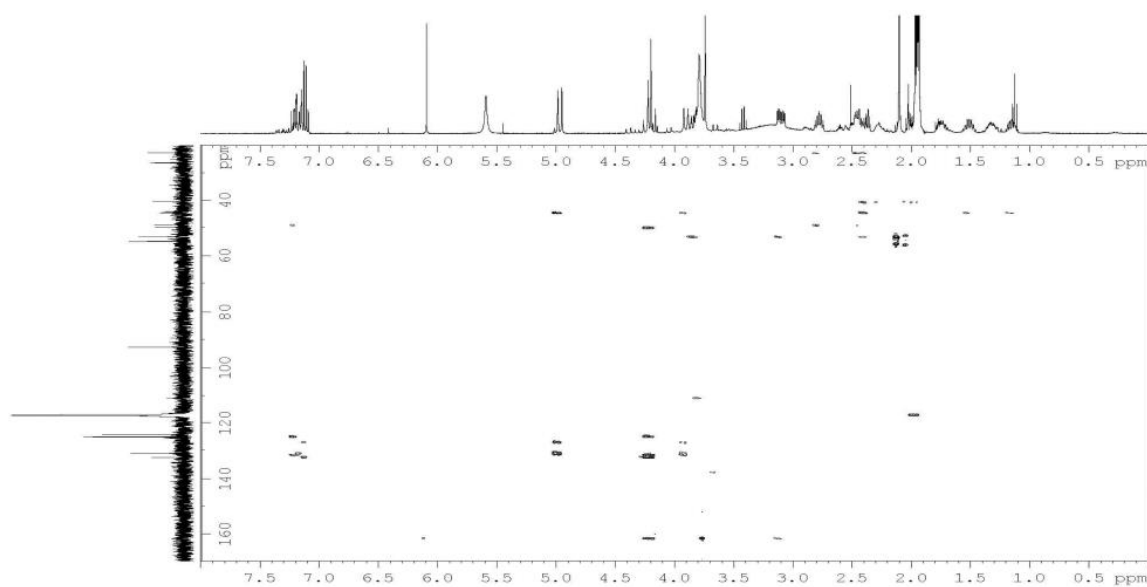
d)



e)



f)



g)

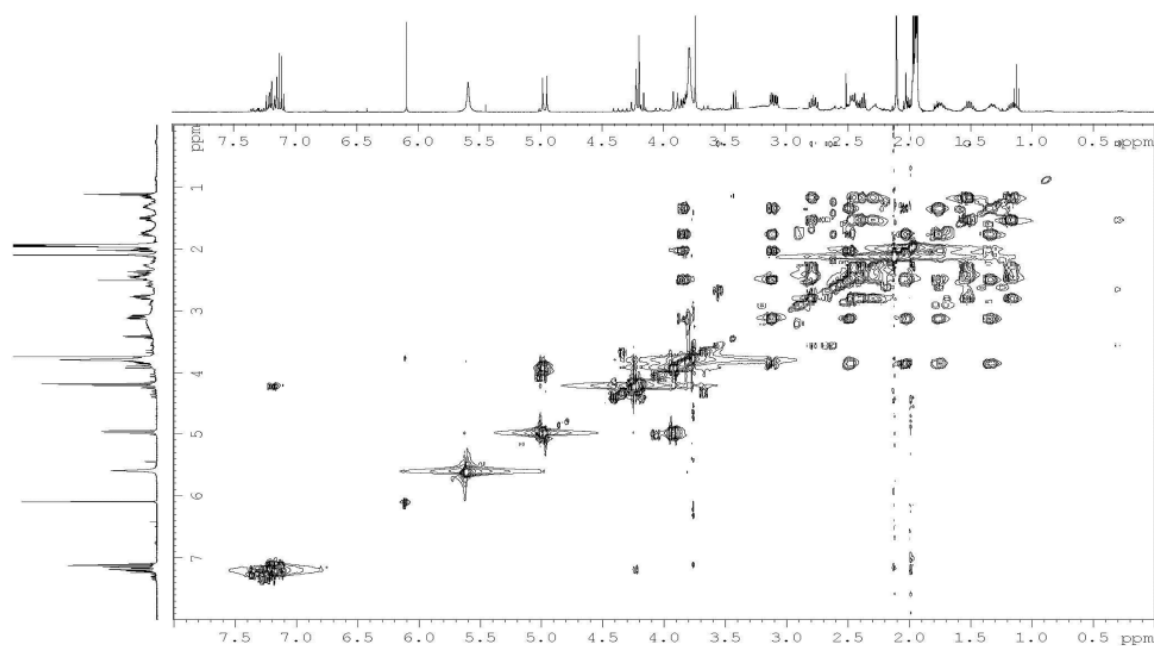


Figure S4. ESI-MS spectrum of compound **P2** (m/z 328.2) and byproduct **L1-Br** (m/z 248.2) in CH_3CN .

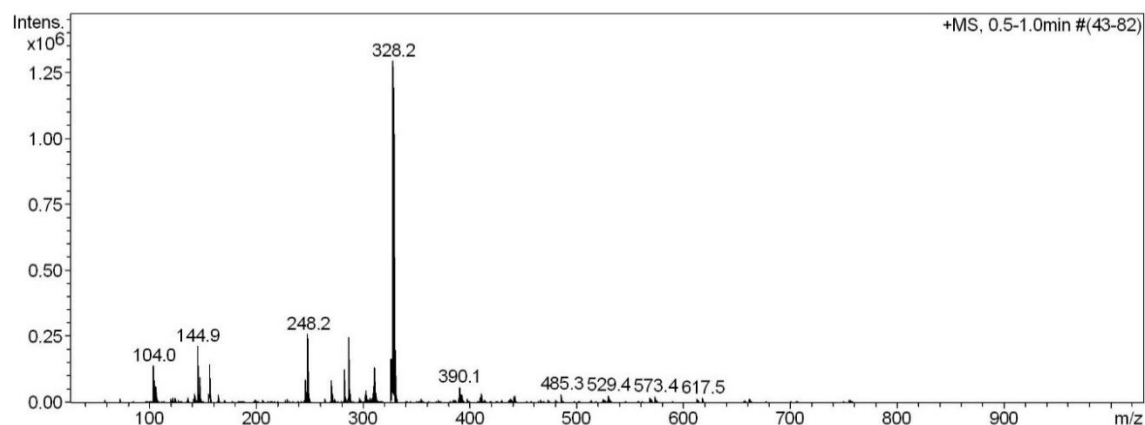
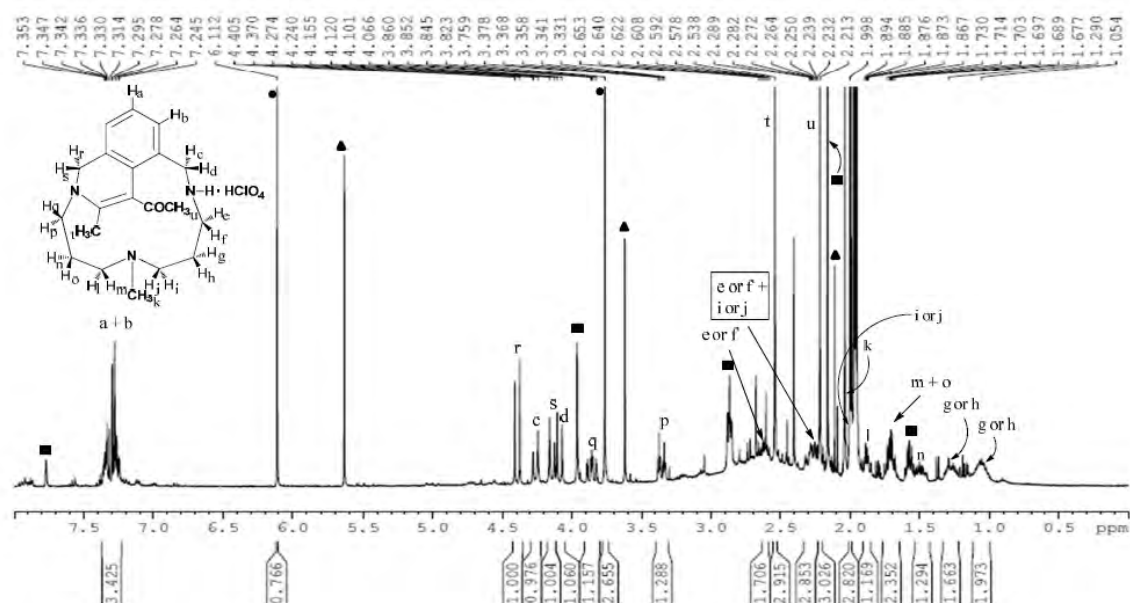


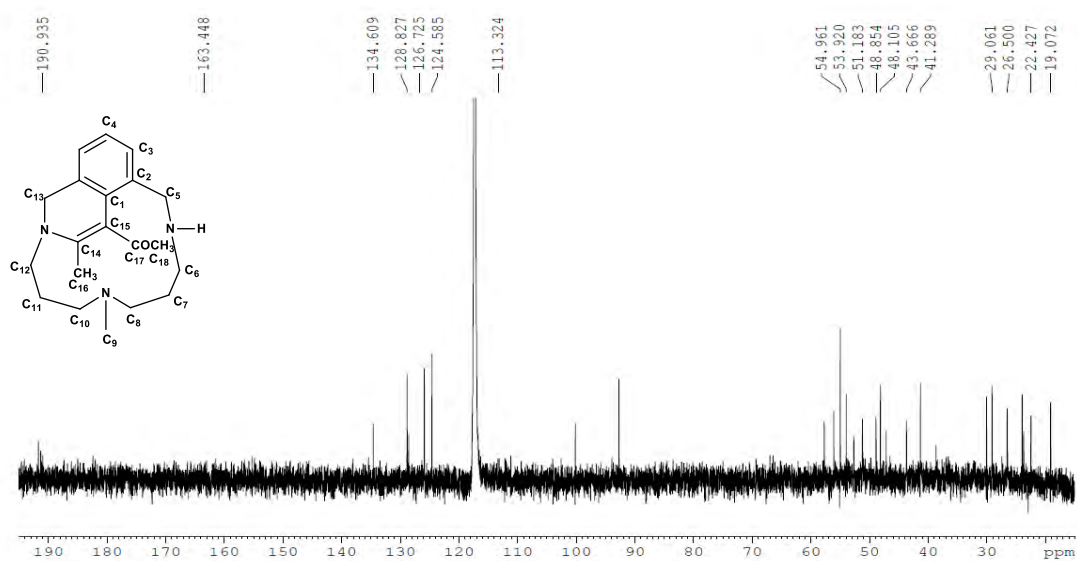
Figure S5. NMR characterization of **P2**: a) ^1H -NMR spectrum (400 MHz, CD_3CN , 25 °C). b) $^{13}\text{C}\{^1\text{H}\}$ -NMR spectrum (100 MHz, CD_3CN , 25 °C). c) ^1H - ^1H COSY spectrum (400 MHz, CD_3CN , 25°C). d) ^1H - ^1H NOESY spectrum (400 MHz, CD_3CN , 25°C). e) ^1H - ^{13}C HSQC_ed spectrum (400 MHz, CD_3CN , 25°C). f) ^1H - ^{13}C HMBC spectrum (400 MHz, CD_3CN , 25°C). g) ^1H - ^1H TOCSY spectrum (400 MHz, CD_3CN , 25°C).

a)

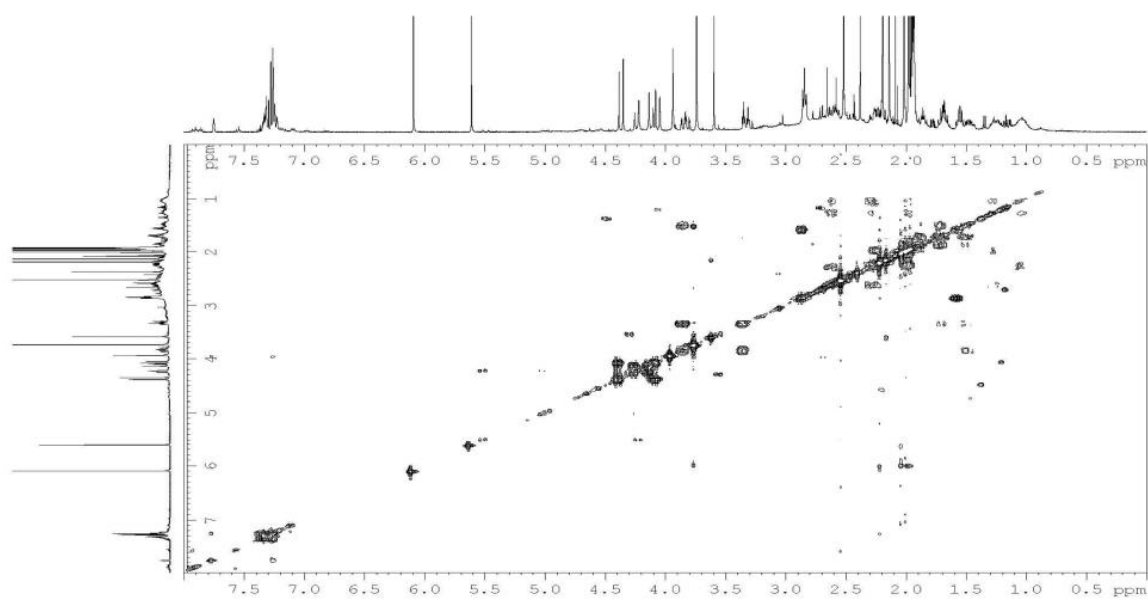


■ byproduct L1-H. ● 1,3,5-trimethoxybenzene (std.). ▲ excess acetylacetone.

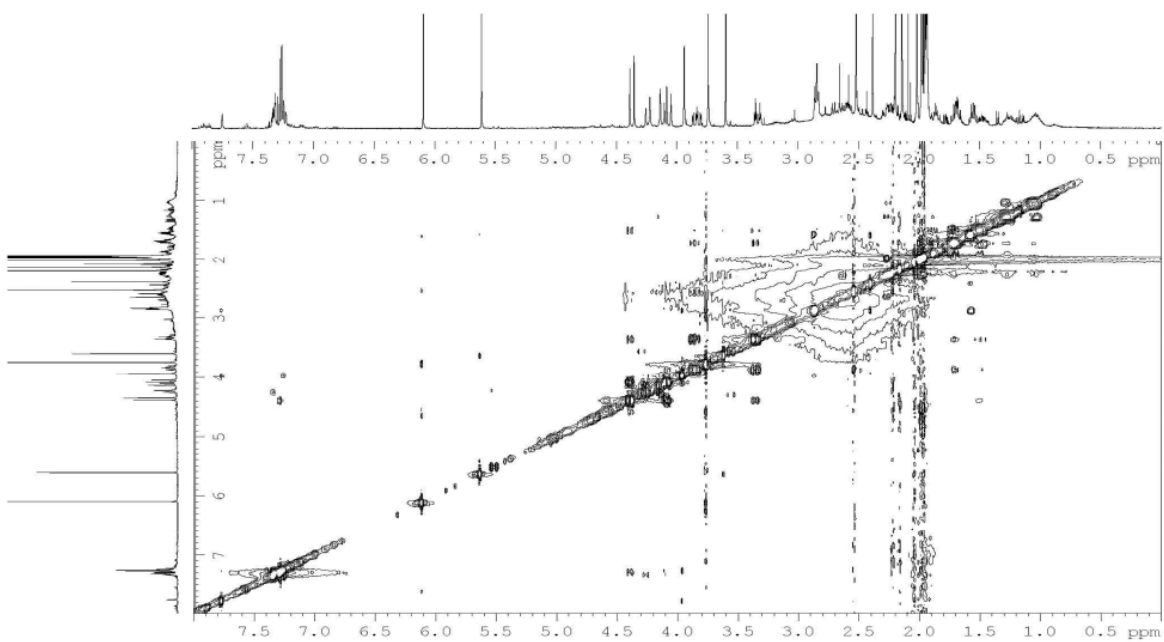
b)



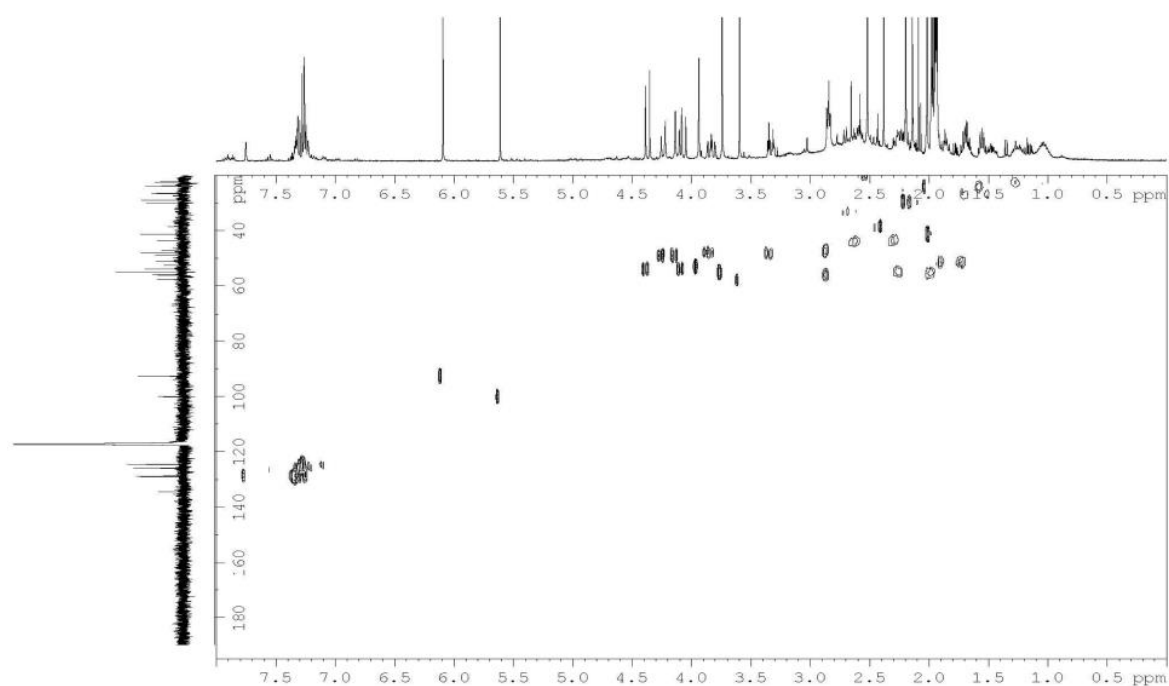
c)



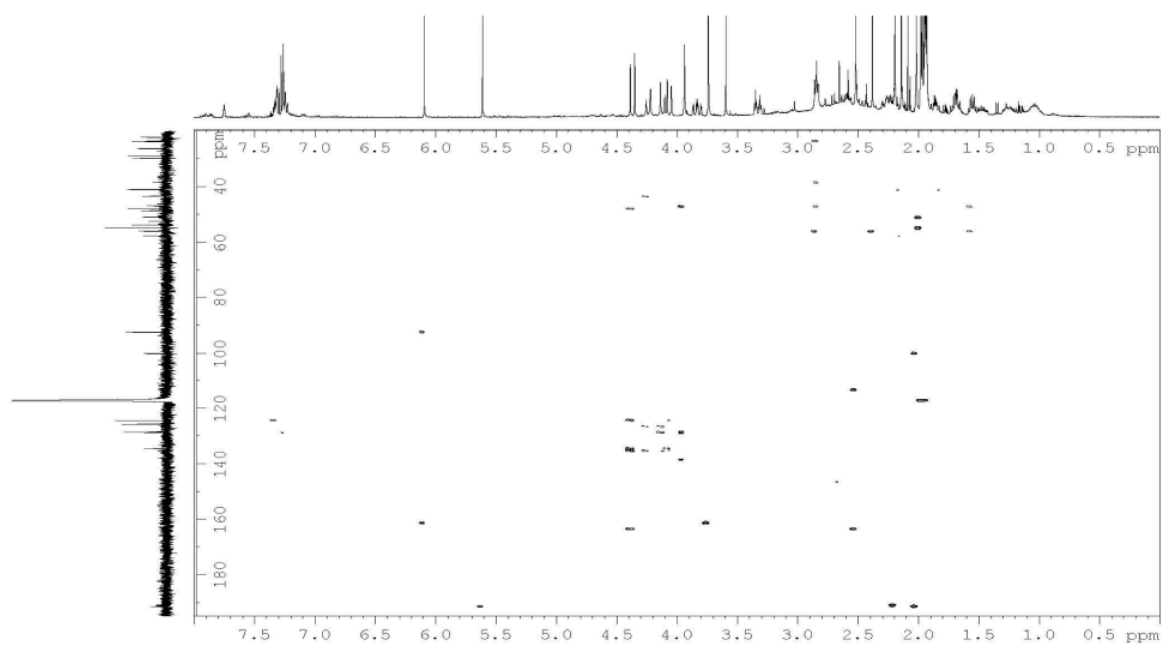
d)



e)



f)



g)

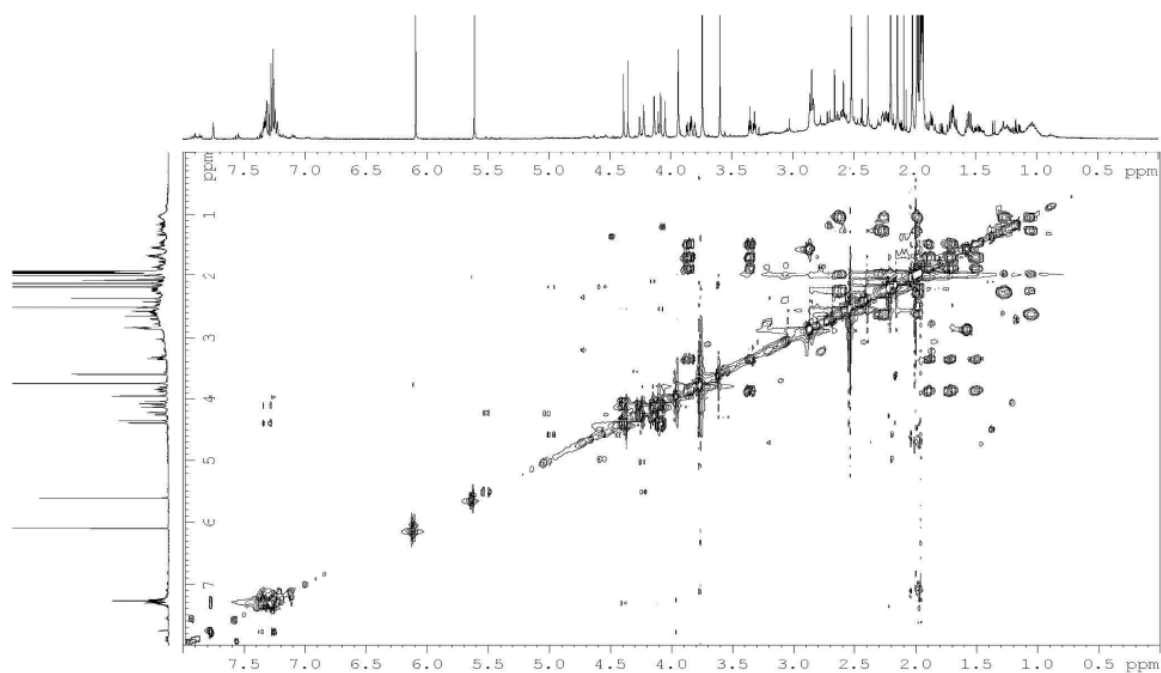


Figure S6. ESI-MS spectrum of compound **P3** ($m/z = 346.1$) and byproduct **BP1** ($m/z = 246.1$) in CH_3CN .

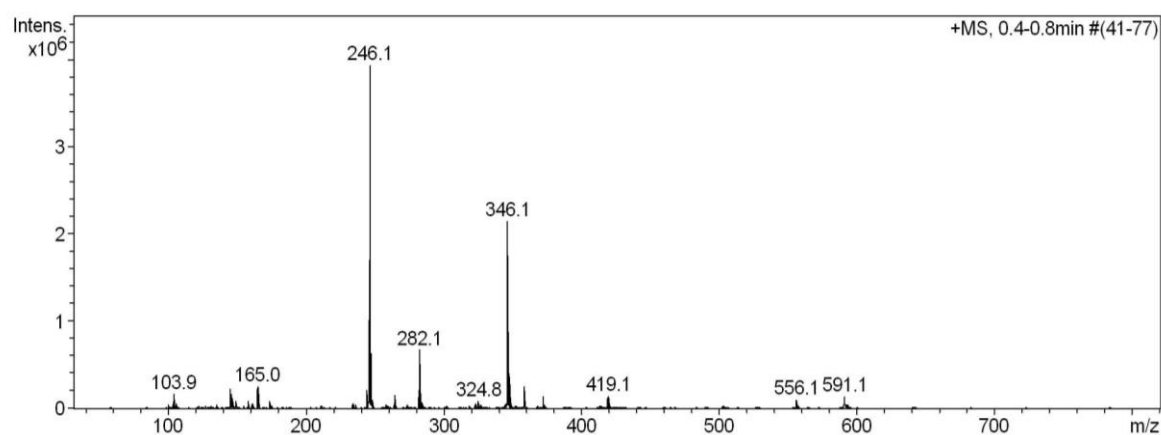
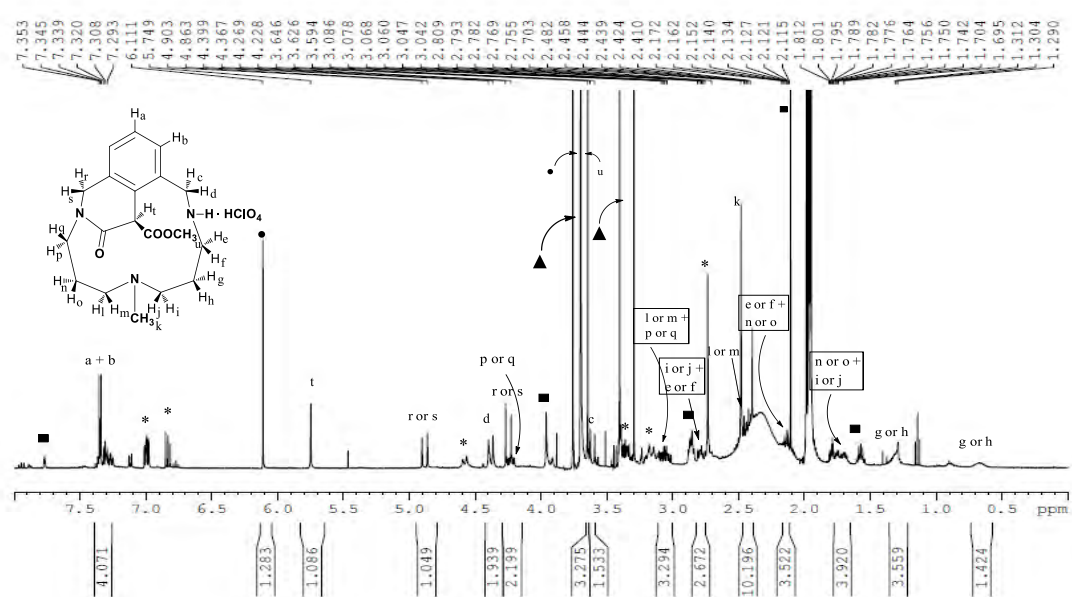


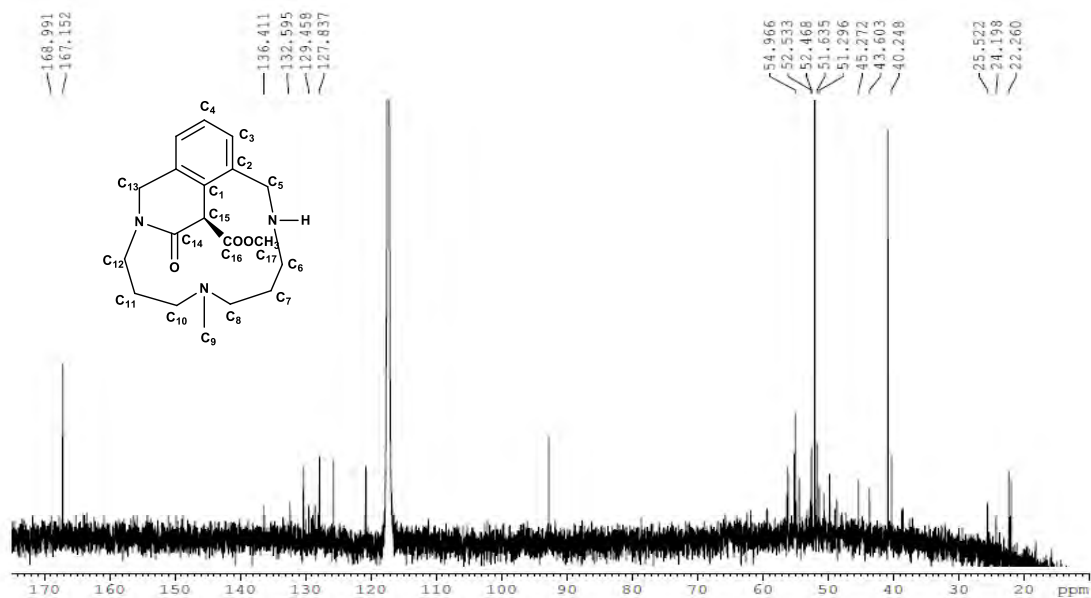
Figure S7. NMR characterization of P3: a) ^1H -NMR spectrum (400 MHz, CD_3CN , 25 °C). b) $^{13}\text{C}\{^1\text{H}\}$ -NMR spectrum (100 MHz, CD_3CN , 25 °C). c) ^1H - ^1H COSY spectrum (400 MHz, CD_3CN , 25°C). d) ^1H - ^1H NOESY spectrum (400 MHz, CD_3CN , 25°C). e) ^1H - ^{13}C HSQC_ed spectrum (400 MHz, CD_3CN , 25°C). f) ^1H - ^{13}C HMBC spectrum (400 MHz, CD_3CN , 25°C). g) ^1H - ^1H TOCSY spectrum (400 MHz, CD_3CN , 25°C).

a)

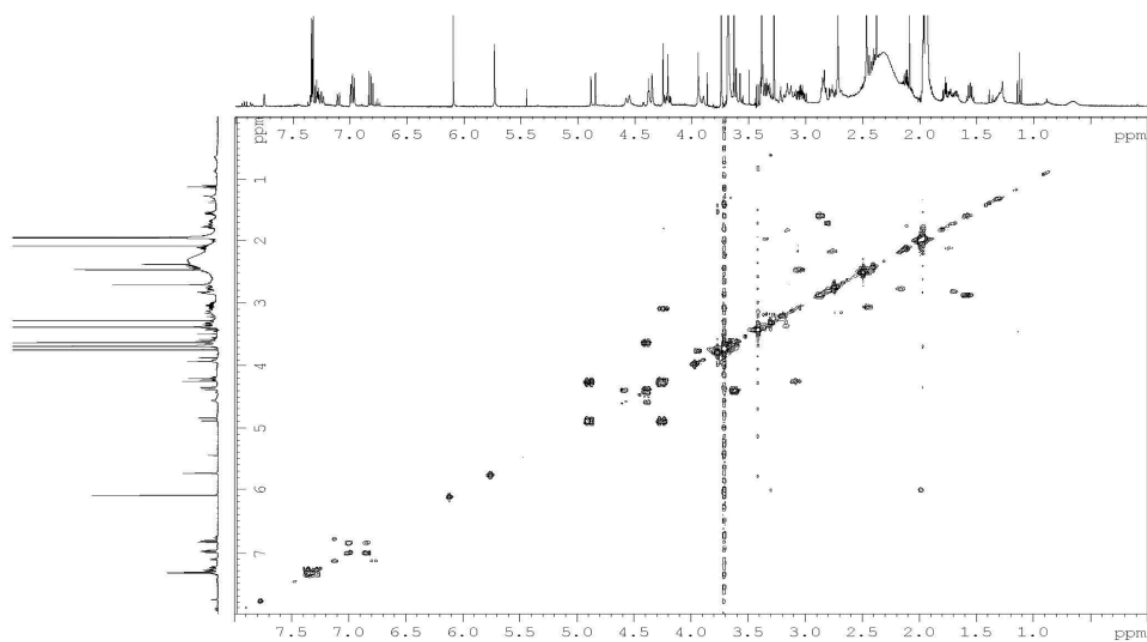


* byproduct BP1. ■ byproduct L₁-H. ● 1,3,5-trimethoxybenzene (std.). ▲ excess dimethyl malonate.

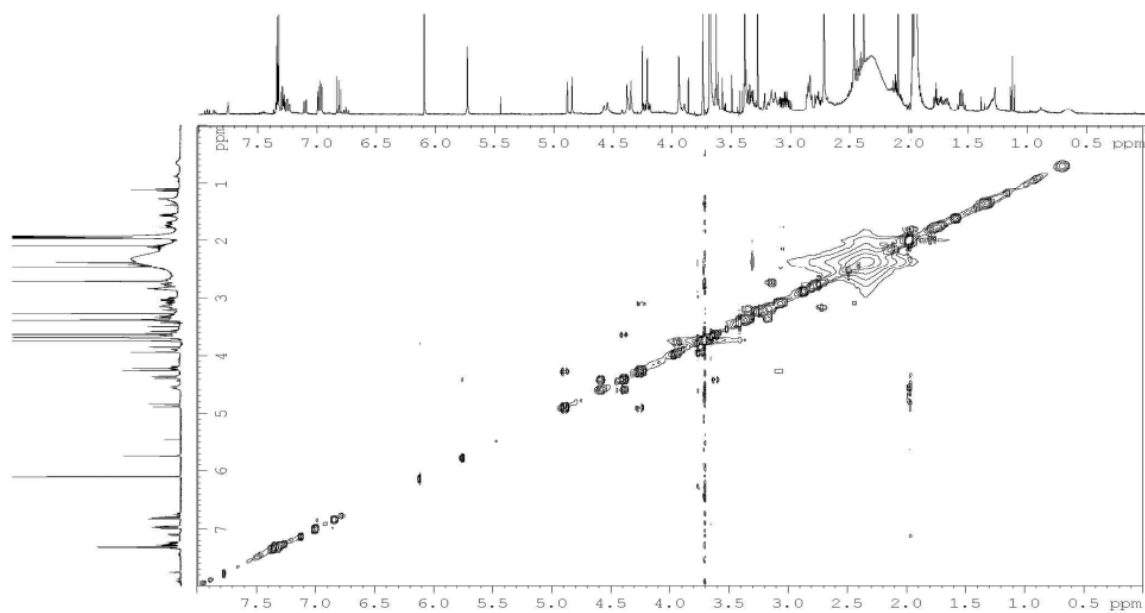
b)



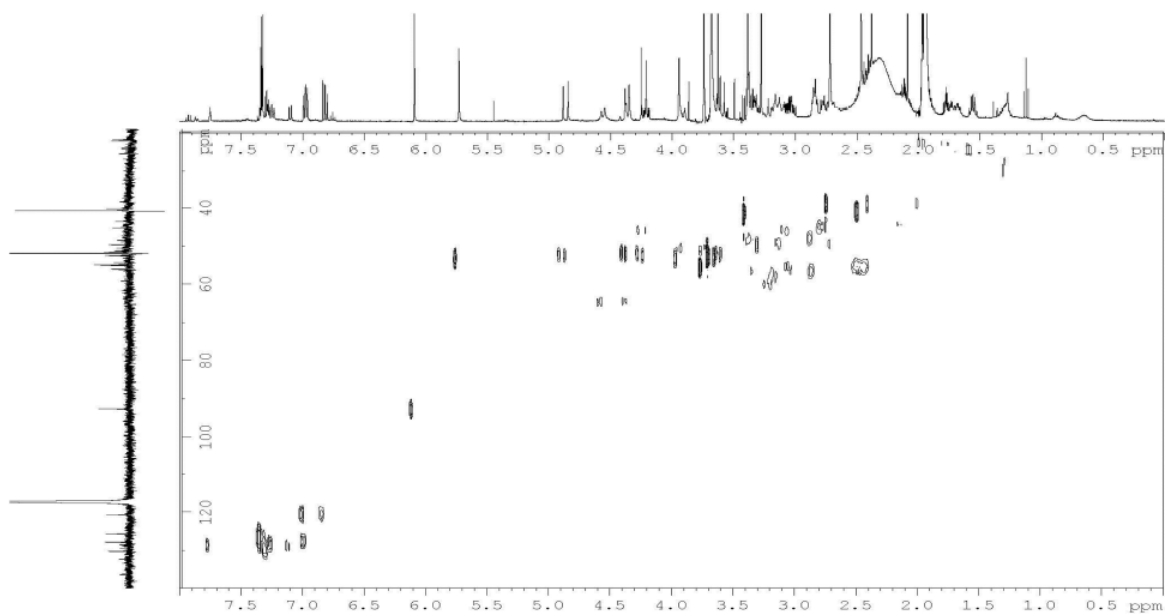
c)



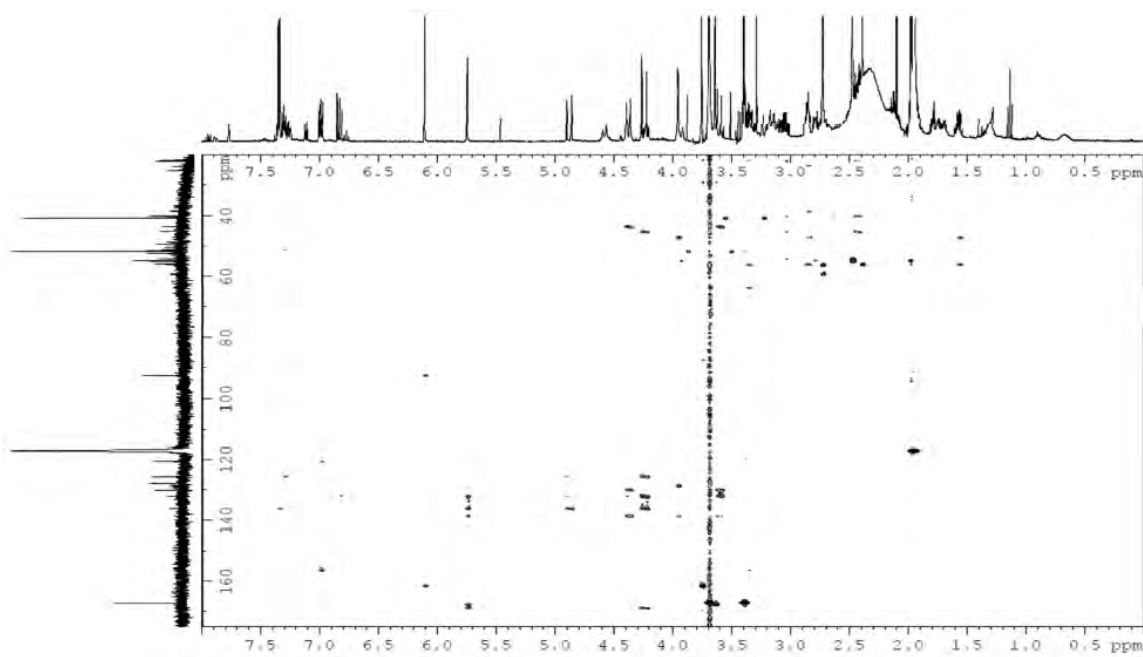
d)



e)



f)



g)

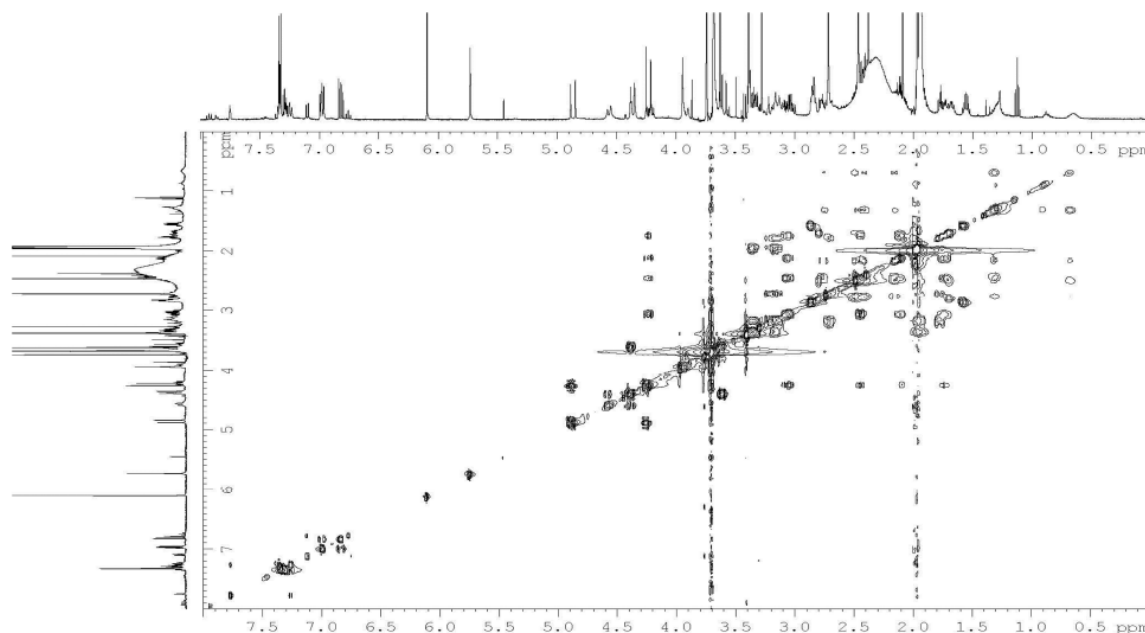
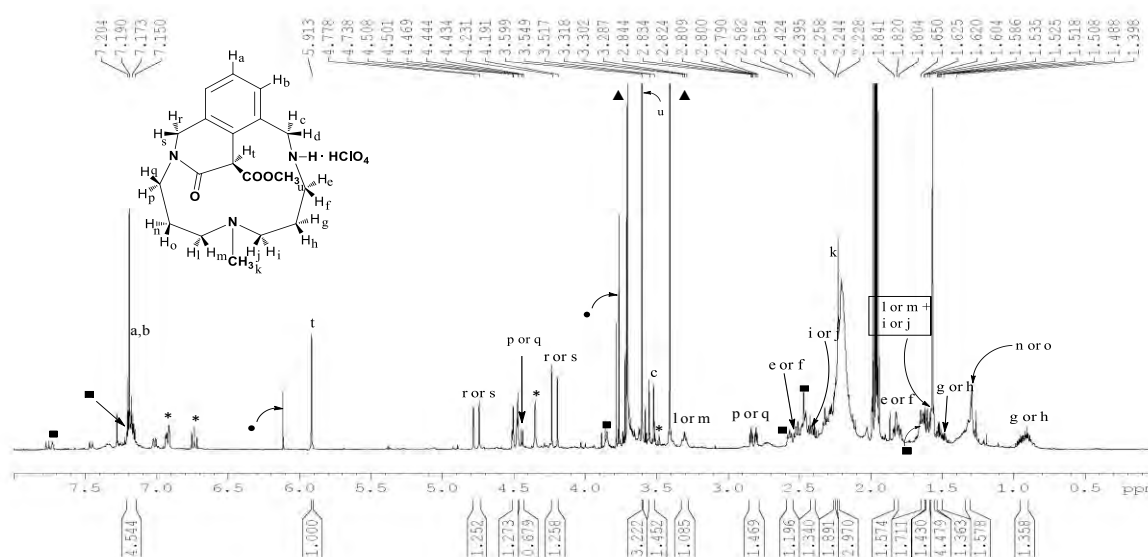


Figure S8. ^1H -NMR spectrum of the final crude of the copper-catalyzed reaction to obtain compound **P3** in CD_3CN , 400 MHz, at 298 K.



* byproduct BP1. ■ byproduct L1-H. ● 1,3,5-trimethoxybenzene (std.). ▲ excess dimethyl malonate

Peaks of **P3** under the experimental catalytic conditions show shifting of peaks with respect to the same compound obtained under stoichiometric conditions (Figure S18). To clarify the assignment of peaks, again 2D NMR experiments were conducted and the proton characterization is listed below. Moreover, the ESI-MS spectrum ($m/z = 346.1$) unambiguously confirmed the identity of **P3**. The amount of byproducts can cause a significant increase in pH, and that might be the explanation for the observed peak shifting.

P3 obtained under catalytic conditions. (yield: 67%) **¹H-NMR** (400 MHz, CD₃CN, 25 °C) δ , ppm: 7.20-7.15 (m, 3H, H^a, H^b), 5.91 (s, 1H, Hⁱ), 4.76 (d, 1H, $J = 16$ Hz, H^r or H^s), 4.49 (d, 1H, $J = 13$ Hz, H^d), 4.44 (d, 1H, $J = 4$ Hz, H^l or H^m), 4.21 (d, 1H, $J = 16$ Hz, H^r or H^s), 3.60 (s, 3H, H^u), 3.53 (d, 1H, $J = 13$ Hz, H^c), 3.32-3.29 (m, 1H, H^p or H^q), 2.82 (dd, 1H, $J = 13.6$ Hz, $J = 4$ Hz, H^l or H^m), 2.58-2.55 (m, 1H, H^e or H^f), 2.42- 2.39 (m, 1H, Hⁱ or H^j), 2.26- 2.24 (m, 1H, Hⁿ or H^o) 2.23 (s, 3H, H^k), 1.84-1.80 (m, 1H, H^e or H^f), 1.65-1.20 (m, 1H, H^p or H^q), 1.60-1.59 (m, 1H, Hⁱ or H^j), 1.53- 1.49 (m, 1H, H^g or H^h), 1.34-1.31 (m, 1H, Hⁿ or H^o), 0.72-0.59 (m, 1H, H^g or H^h).

Figure S9. Proposed mechanism for the synthesis of **P2**.

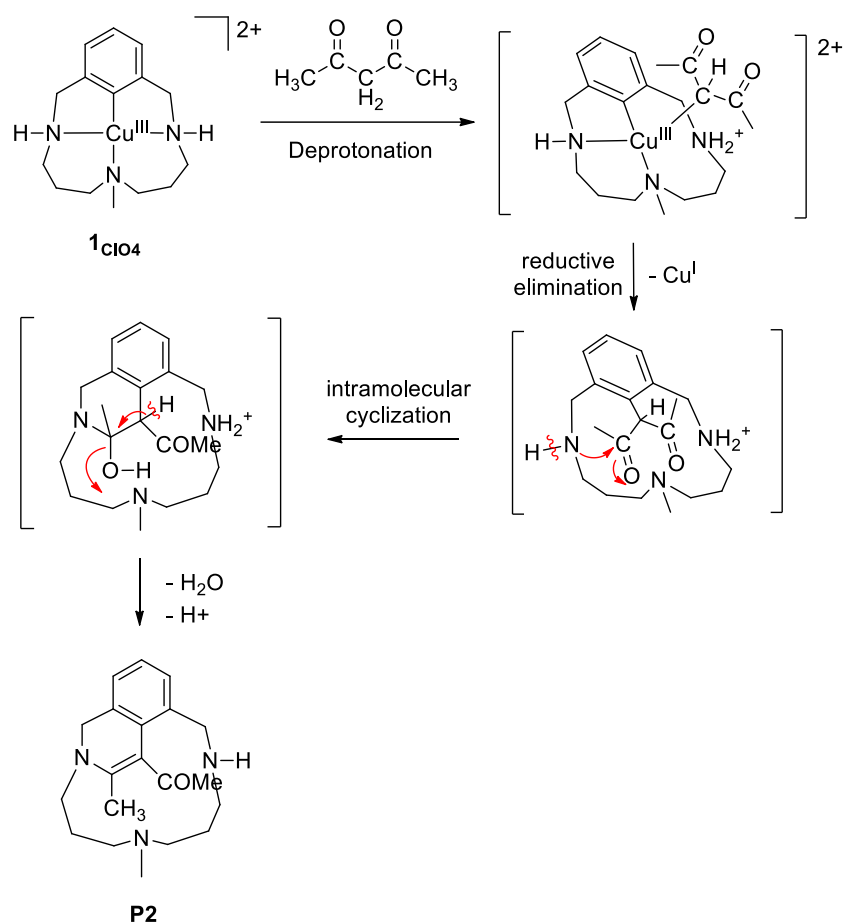
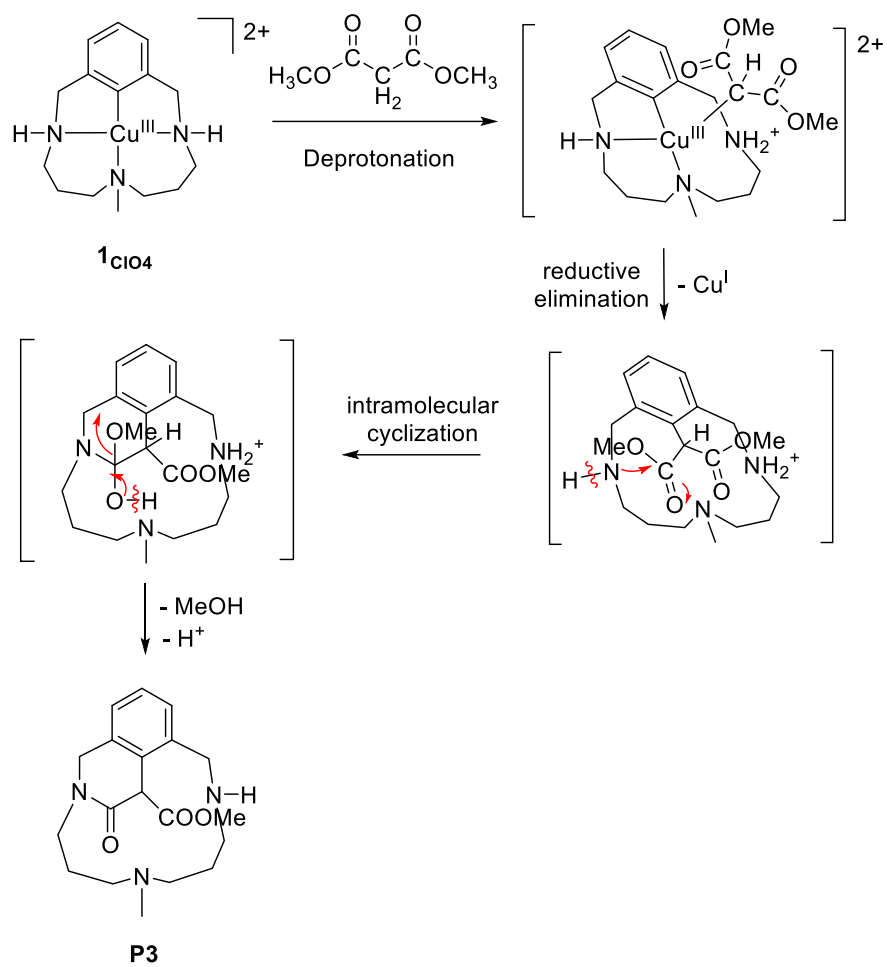
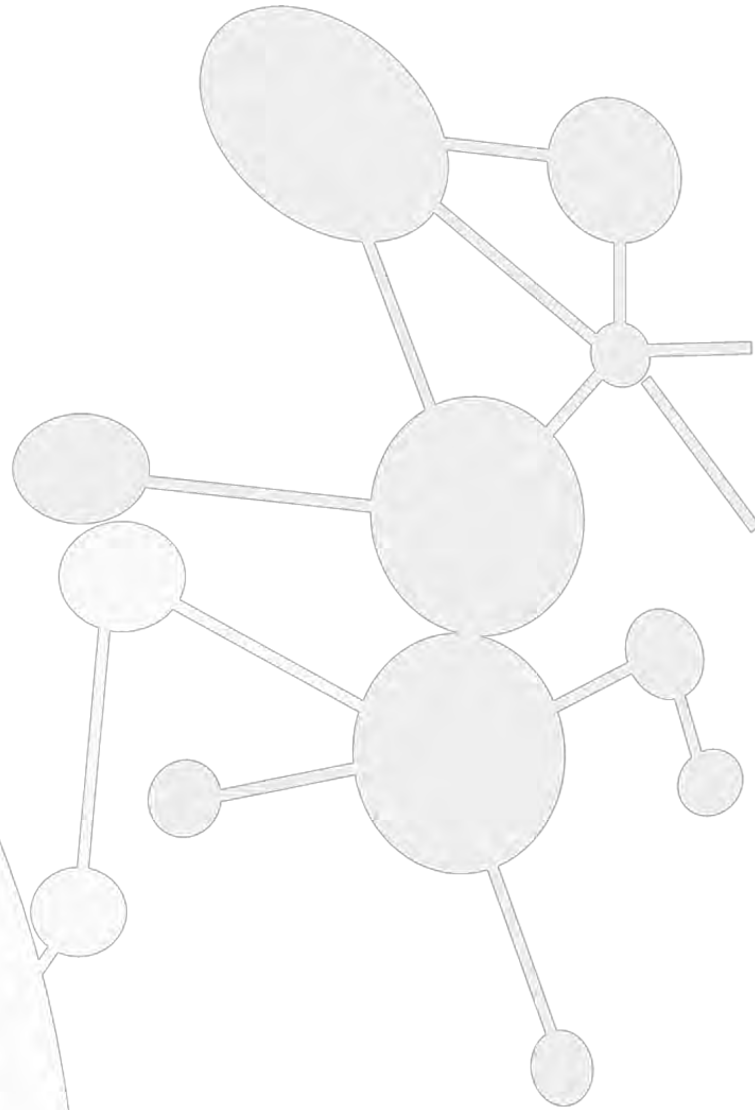


Figure S10. Proposed mechanism for the synthesis of **P3**.

ANNEX 2.



Supporting Information Chapter IV

Aryl-Copper(III)-acetylides as key intermediates in C_{sp^2} - C_{sp} model couplings under mild conditions

*Mireia Rovira, Marc Font, Ferran Acuña-Parés, Teodor Parella, Julio Lloret-Fillol, Josep M. Luis and Xavi Ribas **

Institut de Química Computacional i Catàlisi (IQCC) and Departament de Química, Universitat de Girona, Campus Montilivi, Girona E-17071, Catalonia, Spain.

Servei de RMN, Facultat de Ciències, Universitat Autònoma de Barcelona (UAB), Campus UAB, E-08193 Bellaterra (Catalonia, Spain)

CONTENTS

1. Materials and Methods	181
1.1. Materials and methods	181
1.2. Instrumentation	182
1.3. Synthesis of aryl-Cu ^{III} complex 1 _{ClO₄}	182
1.4. Synthesis and characterization of C_{sp^2} - C_{sp} coupling products P _{NO₂} , P _{CF₃} and P _{Ha} / P _{Hb}	182
1.5. Synthesis and characterization of C_{sp^2} - C_{sp} reaction intermediate I _{CF₃}	184
1.6. General procedure for synthesis of I ' _{CF₃} (alkynylation of L ₅ -Cl using alkynylcopper reagents).....	185
1.7. 1D and 2D NMR structural determination of P _{NO₂} , P _{CF₃} , P _H final products	184
1.8. Experimental details for the attempts to perform C_{sp^2} - C_{sp} couplings under catalytic conditions on Cu ^I	187
1.9. Computational details	188
2. Supplementary Figures	188
3. Supplementary Tables	207
4. Supplementary References	208

1. Materials and Methods

1.1. Materials and methods

Commercially available reagents were used as received, unless otherwise noted. Solvents were purchased from SDS-Carlo Erba and Scharlab and were purified and dried by passing through an activated alumina purification system (MBraun SPS-800). Preparation and handling of air-sensitive materials were carried out in a N₂ drybox (Jacomex) with O₂ and H₂O concentrations <

1 ppm. Ligand **L₁-Br**, **L₅-Cl**, **L₅-Br**, **alkynylcopper reagents** and aryl-Cu^{III} complex **1_{ClO₄}** were synthesized following published procedures.^[1-5]

1.2. Instrumentation

NMR data concerning product identity were collected with a Bruker 400 or 300 AVANCE spectrometer in the corresponding deuterated solvent (CDCl₃, CD₃CN) and calibrated relative the residual protons of the solvent or added tetramethylsilane. Quantification is performed using an internal reference (1,3,5-trimethoxybenzene). High resolution mass spectra (HRMS) were recorded on a Bruker MicrOTOF-Q IITM instrument using ESI or Cryospray ionization sources at Serveis Tècnics of the University of Girona.

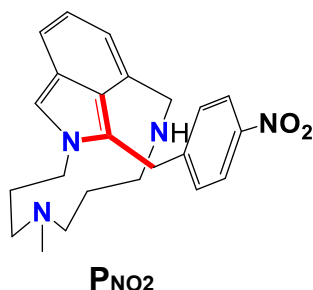
1.3. Synthesis of aryl-Cu^{III} complex **1_{ClO₄}**

Caution: *Perchlorate salts are potentially explosive and should be handled with care!*

Arylcopper(III) complex **1_{ClO₄}** was prepared following procedures described in the literature previously.^[1,2]

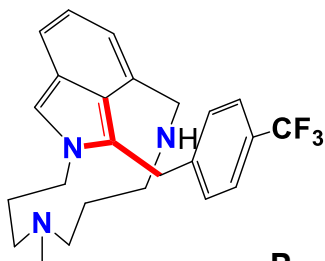
1.4. Synthesis and characterization of C_{sp2}-C_{sp} coupling products **P_{NO₂}**, **P_{CF₃}** and **P_{Ha}/P_{Hb}**

In an inert-atmosphere glove box, a sample of the aryl-Cu^{III} complex **1_{ClO₄}** (14.2 mg, 28 μmol) was dissolved in CD₃CN (1.6 mL) and 0.4 mL of a solution of 1,3,5-trimethoxybenzene was added as an internal standard. A portion of this solution (0.6 mL) was loaded into a NMR tube, and 2 equivalents of the corresponding acetylene nucleophile were added to the tube (0.1 mL, 168 mM). Final concentrations: [**1_{ClO₄}**] = 12 mM, [acetylene nucleophile] = 24 mM. The tube was sealed with a screw-cap and the reaction was allowed to react at room temperature and monitored by ¹H-NMR spectroscopy until reaction completion. Final yields were: **P_{NO₂}** (98%), **P_{CF₃}** (98%), **P_{Ha}** (42%) and **P_{Hb}** (36%). ¹H, ¹³C, and two-dimensional COSY, NOESY, TOCSY, ¹H-¹³C HSQC, ¹H-¹³C HMBC -NMR spectra and mass spectrometric analysis were obtained directly from crude reactions. Reaction yields were obtained by relative integration of the ¹H-NMR signals to the internal standard.

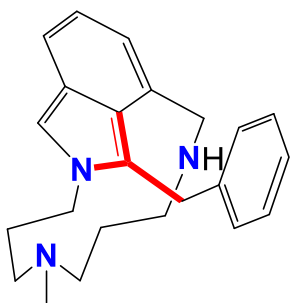
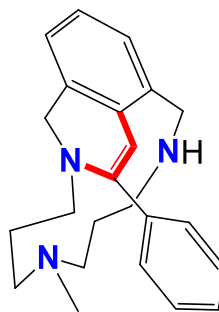


P_{NO₂}: (yield: 98% (by NMR)) ¹H-NMR (400 MHz, CD₃CN, 320 °C) δ, ppm: 8.06 (d, *J* = 8.8 Hz, 2H, H^v), 7.52 (d, *J* = 8.8 Hz, 1H, H^u), 7.47 (s, 1H, H^l), 7.06 (d, *J* = 8.8 Hz, 2H, H^b), 6.91 (d, *J* = 7.5 Hz, 1H, H^b), 6.90 (t, 1H, H^a), 5.12- 5.00 (m, 1H, H^s), 4.65 (d, 1H, *J* = 17.8 Hz, H^t), 4.51- 4.50 (m, 1H, H^m), 4.43 (d, 1H, *J* = 13.1 Hz, H^d), 4.40- 4.32 (m, 1H, Hⁿ), 4.13 (m, 1H, H^e), 3.90- 3.83 (m, 1H, H^f), 3.68 (d, 1H, *J* = 13.1 Hz, H^c), 3.12 (m, 1H, Hⁱ), 2.70- 2.62 (m, 1H, H^o), 2.37- 2.30 (m, 1H, H^r),

2.28- 2.15 (m, 3H, H^k), 2.12- 2.07 (m, 1H, H^q), 1.90- 1.80 (m, 1H, H^p), 1.71- 1.62 (m, 2H, H^h and Hⁱ) and 1.15- 1.10 (m, 1H, H^g). **¹³C-NMR** (100 MHz, CD₃CN, 25 °C) δ, ppm: 149.1 (C₁₈), 146.2 (C₂₁), 129.3 (C₄), 128.3 (C₁₉), 127.5 (C₁₄), 124.4 (C₁), 124.2 (C₁₅), 123.0 (C₂₀), 122.0 (C₁₆), 121.1 (C₂), 120.2 (C₃), 115.6 (C₁₃), 55.7 (C₆), 52.2 (C₅), 46.1 (C₁₂), 42.7 (C₁₁), 39.9 (C₁₀), 38.8 (C₉), 31.9 (C₁₇), 24.9 (C₈) and 23.5 (C₇). **ESI-MS** (CH₃CN, m/z): 393.2304 (100) [C₂₃H₂₈N₄O₂ + H⁺]⁺.

**P_{CF3}**

P_{CF3}. (yield: 98% (by NMR)) **¹H-NMR** (400 MHz, CD₃CN, 25 °C) δ, ppm: 7.53 (m, 1H, H^b), 7.50 (d, 1H, *J* = 8.06 Hz, H^v), 7.45 (s, 1H, Hⁱ), 7.04 (d, 1H, *J* = 8.06 Hz, H^u), 6.86 (t, 2H, H^a, H^b), 5.10- 4.90 (m, 1H, H^s), 4.65 (d, 1H, *J* = 17.2 Hz, H^t), 4.56-4.49 (m, 1H, H^m), 4.45 (d, 1H, *J* = 12.7 Hz, H^d), 4.39- 4.29 (m, 1H, Hⁿ), 4.20- 4.13 (m, 1H, H^e), 3.90- 3.85 (m, 1H, H^f), 3.66 (d, 1H, *J* = 13.3 Hz, H^c), 2.90-2.81 (m, 1H, H^j), 2.72- 2.62 (m, 1H, H^o), 2.35-2.26 (m, 1H, H^r), 2.20 (s, 3H, H^k), 2.19-2.10 (m, 1H, H^q), 1.90-1.83 (m, 1H, H^p), 1.73-1.61 (m, 1H, H^h), 1.60-1.51 (m, 1H, Hⁱ) and 1.20-1.09 (m, 1H, H^g). **¹³C-NMR** (100 MHz, CD₃CN, 25 °C) δ, ppm: 145.6 (C₁₈), 128.0 (C₁₉), 125.6 (C₂₀), 125.4 (C₂₂), 124.8 (C₁₄), 124.5 (C₄), 123.3 (C₂₁), 123.0 (C₁), 122.8 (C₁₅), 120.5 (C₃), 120.2 (C₂), 118.3 (C₁₆), 116.6 (C₁₃), 52.4 (C₆), 52.0 (C₅), 45.9 (C₁₂), 42.2 (C₁₁), 31.5 (C₁₇), 30.0 (C₉), 24.5 (C₁₀), 24.3 (C₈) and 23.2 (C₇). **¹⁹F-NMR** (282.4 MHz, CD₃CN, 25°C) δ, ppm: -61.1 ppm. **ESI-MS** (CH₃CN, m/z): 416.2291 (100) [C₂₄H₂₈N₃F₃ + H⁺]⁺.

**P_{Ha}****P_{Hb}**

P_{Ha}. (yield: 42% (by NMR)) **¹H-NMR** (400 MHz, CD₃CN, 320 °C) δ, ppm: 7.52- 7.47 (m, 5H, H^a, H^b), 7.41 (s, 1H, Hⁱ), 7.24- 7.20 (m, 4H, H^v, H^w), 6.90 (d, 2H, *J* = 6.3 Hz, H^u), 6.86 (d, 1H, *J* = 7.8 Hz, H^b), 4.92- 4.74 (m, 1H, H^s), 4.56- 4.50 (m, 4H, H^t, Hⁿ and H^d), 4.38 (m, 2H, H^m), 4.24 (m, 1H, H^e), 3.92- 3.90 (m, 1H, H^f), 3.67 (d, 1H, *J* = 13 Hz, H^c), 3.07- 2.99 (m, 3H, H^j), 2.69- 2.63 (m, 2H, H^o), 2.39- 2.33 (m, 2H, H^r), 2.20- 2.16 (m, 5H, H^k and H^q), 1.90- 1.85 (m, 1H, H^p), 1.70- 1.62 (m, 1H, H^h), 1.61- 1.51 (m, 1H, Hⁱ), 1.19- 1.12 (m, 1H, H^g). **¹³C-NMR** (100 MHz, CD₃CN, 25 °C) δ, ppm: 140 (C₁₈), 129.3 (C₂₁), 129.3 (C₄), 128.6 (C₁₄), 127.1 (C₁₉), 126.4 (C₂₀), 124.9 (C₁₅), 123.9

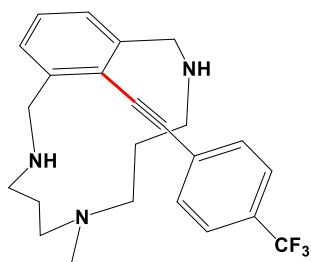
(C1), 120.5 (C2), 120.2 (C3), 119.7 (C₁₆), 114.7 (C₁₃), 56.2 (C₆), 52.3 (C₅), 46.5 (C₁₂), 41.3 (C₁₁), 40 (C₉), 31.7 (C₁₇), 25.7 (C₁₀), 24.2 (C₈), 23.4 (C₇). **ESI-MS** (CH₃CN, m/z): 348.2455 (100) [C₂₃H₂₉N₃ + H⁺]⁺.

P_{Hb}. (yield: 36% (by NMR)) **¹H-NMR** (400 MHz, CD₃CN, 25 °C) δ, ppm: 7.89 (d, 2H, *J* = 7.5 Hz, H^u), 7.52- 7.46 (m, 5H, H^v, H^w), 7.24- 7.20 (m, 4H, H^b), 7.18- 7.11 (m, 2H, H^a, H^p), 6.96 (s, 1H, H^t), 4.56- 4.50 (m, 4H, H^c or H^d), 4.38 (s, 1H, H^m), 4.34- 4.30 (m, 1H, H^l), 3.74 (s, 1H, H^d), 3.24- 3.20 (m, 1H, H^o), 3.07- 2.99 (m, 3H, Hⁿ and H^e), 2.69- 2.63 (m, 2H, H^f), 2.53- 2.50 (m, 1H, Hⁱ), 2.47- 2.42 (m, 1H, H^j), 2.39- 2.33 (m, 2H, H^s), 2.21 (s, 3H, H^k), 2.20- 2.16 (m, 5H, H^r), 1.82- 1.74 (m, 1H, H^g), 1.51- 1.41 (m, 2H, H^h and H^p), 0.94- 0.82 (m, 1H, H^p or H^q). **¹³C-NMR** (100 MHz, CD₃CN, 25 °C) δ, ppm: 148.4 (C₁₇), 129.0 (C₂₁), 134.6 (C₁₄), 132.3 (C₁₅), 132.0 (C₁₈), 129.0 (C₄), 128.5 (C₁₉), 128.5 (C₂), 129.0 (C₂₀), 126.0 (C₁), 125.5 (C₃), 109.8 (C₁₆), 56.3 (C₈), 55.6 (C₁₃), 55.6 (C₁₀), 51.9 (C₁₂), 49.0 (C₅), 46.8 (C₆), 39.8 (C₉), 27.1 (C₁₁), 22.1 (C₇). **ESI-MS** (CH₃CN, m/z): 348.2455 (100) [C₂₃H₂₉N₃ + H⁺]⁺.

P_{Hb} NMR characterization: P_{Hb} has been characterized by NMR as containing a 6-membered 1,2-dihydroisoquinoline moiety (Figures S16-21). The most relevant ¹H signals as described below: two pairs of benzylic protons, H^c/H^d and H^l/H^m, are found. Another important signal was the singlet corresponding to H^t located at 6.96 ppm; ¹H-¹³C HSQC experiment allowed us to determine its ¹³C-NMR peak (C₁₆, 109.8 ppm), with a value characteristic of a C_{sp2}. The NOESY experiment determined its dipolar coupling with H^c and H^d, H^u and H^e and H^f. Moreover, the ¹H-¹³C HMBC experiment gives correlations of H^t with C₁₅, C₁₇, C₁₈, C₁₉ i C₁₄. Also, benzylic H^l and H^m protons exhibited NOESY interactions with Hⁿ, H^o and H^b. In addition, the ¹H-¹³C HMBC experiment indicates coupling of H^l and H^m with C₁₇, C₁₄, C₁₅, C₃ and C₁₂. Finally, the proton H^u presents a NOE contact with H^t and HMBC cross-peaks with C₁₇ and C₁₈. Another aromatic proton, H^b has HMBC correlations with C₁₄, C₁₅ and C₁₃.

1.5. Synthesis and characterization of C_{sp2}-C_{sp} reaction intermediate I_{CF3}

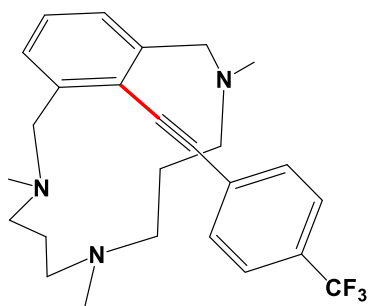
In an inert-atmosphere glove box, a sample of aryl-Cu^{III} complex **1_{ClO4}** (20 mg, 39 μmol) was dissolved in CD₃CN (0.1 mL) and 0.2 mL of a solution of 1,3,5- trimethoxybenzene was added as an internal standard. All the solution was transferred to a NMR tube. The reaction was initiated by adding 2 equivalents of the *p*-CF₃-phenylacetylene were added to the tube (0.2 mL, 392.5 μmol). In this case, the reaction was allowed to react at 0°C and monitored by ¹H-NMR spectroscopy until the reaction intermediate was formed. At this point, the NMR spectrometer temperature was decreased to -35°C to block the reaction advancement and to favor the accumulation of the intermediate species.



I_{CF3}. ¹H-NMR (400 MHz, CD₃CN, -35 °C) δ, ppm: 7.84 (d, 2H, *J* = 7.9 Hz, H^l), 7.77 (d, 2H, *J* = 8.3 Hz, H^m), 7.40- 7.31 (m, 3H, H^a and H^b), 4.44 (d, 2H, *J* = 12.5 Hz, H^d), 3.60- 3.52 (m, 2H, H^c), 3.07- 2.91 (m, 2H), 2.87- 2.76 (m, 2H), 2.72- 2.59 (m, 2H), 2.57- 2.43 (m, 2H), 2.35 (s, 3H, H^k), 1.66- 1.49 (m, 1H), 0.78- 0.50 (m, 2H). ¹³C-NMR (100 MHz, CD₃CN, -35 °C) δ, ppm: 146.2 (C₃), 132.3 (C₁₄), 131.8 (C₁₂), 129.6 (C₁), 126.9 (C₂), 126.6 (C₁₁), 125.7 (C₁₃), 125.4 (C₁₅), 122.5 (C₉), 97.1 (C₁₀), 59.1 (C₅), 52.7 (C₄), 45.6 (C₇), 40.7 (C₈), 23.9 (C₆). ¹⁹F-NMR (282.4 MHz, CD₃CN, 25°C) δ, ppm: -61.6 ppm. **ESI-MS** (CH₃CN, *m/z*): 416.2360 (100) [C₂₄H₂₈N₃F₃ + H⁺]⁺.

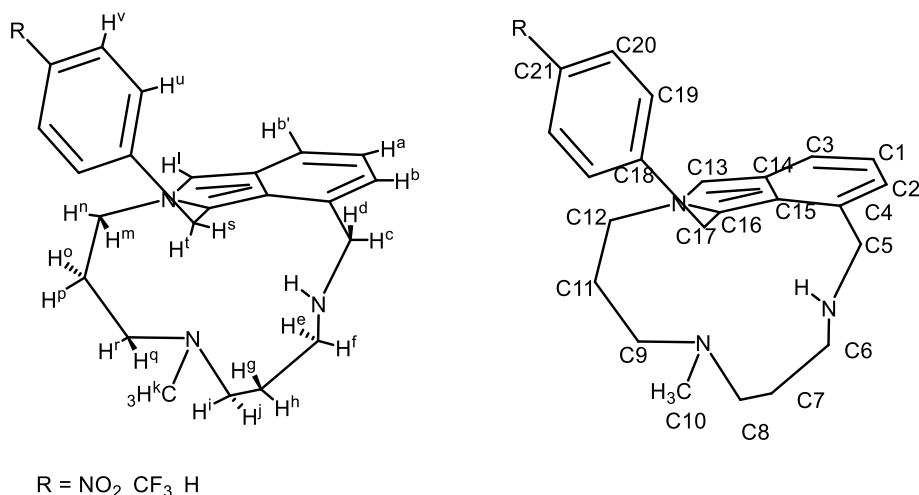
1.6. General procedure for synthesis of I'CF₃ (alkynylation of L₅-Cl using alkynylcopper reagents)

Ligand L₅-Cl, 1,3,5-trimethoxybenzene and Cu^I-(C≡C-Ph-*p*CF₃) were weighted in and then entered into inert-atmosphere glove box, were the stock solutions of L₅-Cl (16.8 mM), 1,3,5-trimethoxybenzene (2 mM) and Cu^I-(C≡C-Ph-*p*CF₃) (0.084 M) were prepared in CD₃CN. The L₅-Cl/1,3,5-trimethoxybenzene stock (0.5 mL) and 0.2 mL of Cu^I-(C≡C-Ph-*p*CF₃) were loaded into a NMR tube. The final concentrations were as follows: [L₅-Cl] = 12 mM and [Cu^I-(C≡C-Ph-*p*CF₃)] = 24 mM. The reaction was monitored by ¹H-NMR spectroscopy until the reaction completion, and the yield was obtained using 1,3,5-trimethoxybenzene as internal standard (Figure S27).

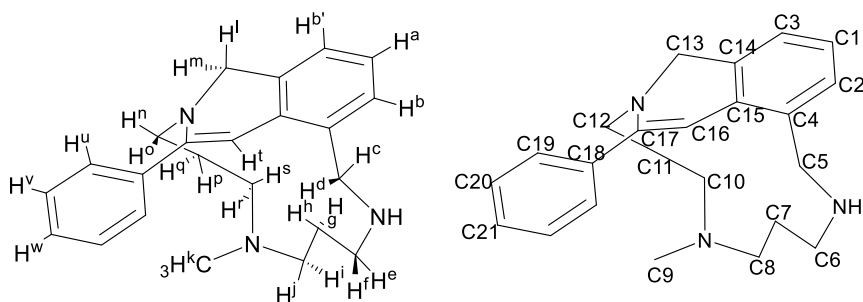


I'CF₃. (yield: 73% (by NMR)) ¹H-NMR (400 MHz, CD₃CN, 25 °C) δ, ppm: 8.02 (d, 2H, *J* = 7.9 Hz, H^m), 7.75 (d, 2H, *J* = 8.3 Hz, Hⁿ), 7.37 (t, 1H, H^a), 7.30 (d, 2H, *J* = 7.9 Hz, H^b), 4.25 (d, 2H, *J* = 12.5 Hz, H^d), 3.31 (d, 2H, *J* = 12.5 Hz, H^c), 2.85 (t, 2H), 2.49- 2.40 (m, 2H), 2.37 (s, 6H, H^l), 1.88- 1.82 (m, 2H), 1.81- 1.77 (m, 2H), 1.75 (s, 3H, H^k), 1.66- 1.52 (m, 2H), 1.46- 1.32 (m, 2H). ¹³C-NMR (100 MHz, CD₃CN, 25 °C) δ, ppm: 140.6 (C₃), 132.1 (C₁₃), 130.8 (C₁₂), 130.3 (C₂), 128.9 (C₁), 128.4 (C₁₅), 125.4 (C₁₆), 125.1 (C₁₄), 122.9 (C₁₀), 121.8 (C₁₁), 63.8 (C₄), 56.2 (C₆), 51.4 (C₇), 44.9 (C₅), 39.3 (C₉), 24.1 (C₈). ¹⁹F-NMR (282.4 MHz, CD₃CN, 25°C) δ, ppm: -63.6 ppm. **ESI-MS** (CH₃CN, *m/z*): 444.2610 (100) [C₂₆H₃₂F₃N₃ + H⁺]⁺.

1.7. 1D and 2D NMR structural determination of P_{NO_2} , P_{CF_3} , P_{Ha} and P_{Hb} final products



P_{NO_2} / P_{CF_3} / P_{Ha} . These compounds have been characterized by NMR as containing a common heterocyclic 2H-isoindole moiety (Figures S2-S15 and S17-S21). The most relevant couples of protons found are the coupling formed by the benzylic H^c/H^d, H^s/H^t and the aliphatic H^m/Hⁿ proton pairs. NOESY experiment allowed us to assign H^c and H^d due to its dipolar coupling with H^e, H^f and also, H^b protons. NOE were also observed between the H^s and H^t protons with the aromatic H^u proton. This fact was indicative of the loss of the triple bond of acetylene. Finally, H^m and Hⁿ show NOE interactions with Hⁱ, H^r and H^q. Another important signal found in the ¹H-NMR spectrum was Hⁱ proton showing a singlet located at 7.47 ppm (¹H-¹³C HSQC spectrum allowed us to determine its directly attached carbon (C₁₃) at 115.6 ppm) which show NOE contacts with H^b, H^m and Hⁿ protons. Finally, ¹H-¹³C HMBC experiment was crucial to afford the structural determination. We found that H^s and H^t showed correlations with C₁₉, C₂₀, C₁₆ and C₁₅, whereas Hⁱ correlated with C₁₂, C₁₄, C₁₅ and C₁₆. These results suggested a formation of 5-member heterocyclic substructure corresponding to a 2H-isoindole. Similar NMR pattern for 2H-isoindoles had been described previously.⁶ To conclude the assignment of aliphatic protons in each chain, NOESY spectrum show connectivities between H^k (N-CH₃ group) with H^p and H^o and H^q and H^r. The same experiment exhibits NOE between Hⁱ and H^j with H^r and H^q. The COSY and ¹H-¹³C HSQC allowed us to determine the couple of protons bound to the same carbon in the aliphatic chain. Moreover, the ¹H-¹³C HMBC experiment provided the assignment of quaternary carbons and the aliphatic chain.



P_{Hb}. This product has been characterized by NMR as containing a 6-membered 1,2-dihydroisoquinoline moiety (Figures S16-21). The most relevant couples of protons found are the pairs formed by the benzylic H^c/H^d and Hⁱ/H^m protons. An important signal found in the ¹H-NMR spectrum was the singlet located in 6.96 ppm and ¹H-¹³C HSQC experiment allowed us to determine its ¹³C-NMR peak (C₁₆, 109.8 ppm). The NOESY experiment shows connectivities with H^c and H^d, H^u and H^e and H^f. Moreover, the ¹H-¹³C HMBC spectrum gives correlations with C₁₅, C₁₇, C₁₈, C₁₉ and C₁₄. These results indicated the formation of another species in the reaction crude. We also found other indicative protons, which supported this hypothesis like Hⁱ and H^m. This couple of protons showed NOE contact between Hⁿ, H^o and H^b. In addition, the ¹H-¹³C HMBC experiment showed correlations with C₁₇, C₁₄, C₁₅, C₃ and C₁₂. Finally, the proton H^u present a NOE with H^t and HMBC cross-peaks with C₁₇ and C₁₈. Another aromatic proton, H^b presented HMBC connectivities with C₁₄, C₁₅ and C₁₃. These experiments allowed us to determine the 6 members ring formation during the reaction outcomes. NOESY experiment also determined a NOE contact between H^c and H^d protons and between H^e and H^f, Hⁱ and H^b. Additionally, HMBC experiment showed cross-peaks between C₄, C₁₅ and C₆. COSY and ¹H-¹³C HSQC allowed us to determine the couple of protons bound to the same carbon in the aliphatic chain. Moreover, the ¹H-¹³C HMBC experiment provided the necessary clues for the assignment of quaternary and aliphatic chain carbons.

1.8. Experimental details for the attempts to perform C_{sp2}-C_{sp} couplings under catalytic conditions on Cu^I

1.8.1. General procedure for the catalytic reactions using L₁-X as a ligand

In an inert-atmosphere glove box, ligand L₁-X (X = I or Cl or Br) (16.9 mg, 6 μmol) was dissolved in CH₃CN (2 mL). 0.5 mL of this solution was loaded in a vial and 0.5 mol% of Cu(CH₃CN)₄(CF₃SO₃) was added (0.2 mL of stock solution 7.5 mM in CH₃CN). The colourless solution becomes slightly red indicating that oxidative addition takes place obtaining the corresponding complex arylCu^{III}-X (X = Cl, Br). Then 2.3 mL of 13- 65 mM of *p*-R-phenylacetylene (R = NO₂, CF₃) in CH₃CN was added. Final concentrations: [L₁-X] = 5 mM, [Cu] = 0.5 mM and [*p*-R-phenylacetylene] = 10 - 50 mM (Table S2). For the catalysis carried out in presence of a base, 2.2 equivalents were added in the reaction mixture. For the soluble base (Et₃N) 1.15 ml of stock solution (28 mM in CH₃CN) were added into the stock solution of the *p*-R-phenylacetylene. Subsequently, a portion of this solution (3 mL) were added to the reaction mixture. Insoluble bases (K₂CO₃, K₃PO₄) were weighed directly into the reaction vial. For the catalysis conducted in presence of 2 equivalents of AgOTf or GaCl₃, 1.15 mL of a stock solution (26 mM) were added into the reaction mixture. After stirring the mixture crude, at room temperature for 24 hours, 150 μL of 1,3,5-trimethoxybenzene 3 mM in CH₃CN as internal standard were added and the solvent was removed. The sample was re-dissolved in 0.5 mL of CD₃CN and NMR yields were obtained by ¹H-NMR by integration of the benzylic protons with respect to the internal standard.

1.8.2. General procedure for the catalytic reactions using L_5-X as a ligand

In an inert-atmosphere glove box, ligand L_5-X ($X = Cl$ or Br) (38.7 mg, 5 μ mol) was dissolved in CD_3CN (1 mL) and 0.5 mL of a solution of 1,3,5- trimethoxybenzene was added as an internal standard. 0.4 mL of this solution was loaded in a vial and 0.5-1 mol% of $Cu(CH_3CN)_4(CF_3SO_3)$ or $Cu^I-(C\equiv C-Ph-pCF_3)$ was added (0.2 mL of stock solution 2.5 mM in CD_3CN). The colourless solution becomes yellow indicating the formation of $Cu^I-(C\equiv C-Ph-pCF_3)$ species. Then 0.4 mL of 250 mM of p - CF_3 -phenylacetylene in CD_3CN was added. Final concentrations: $[L_5-X] = 5$ mM, $[Cu] = 0.5-1$ mM and $[p$ - CF_3 -phenylacetylene] = 10 mM. For the catalysis carried out in presence of a base, 4 equivalents of the base were added in the reaction mixture. Insoluble bases (K_2CO_3 , K_3PO_4 , $tBuOK$) were weighed directly into the reaction vial. Reactions were conducted at different temperatures (25-70°C) under stirring for 24 hours. NMR yields were obtained by 1H -NMR by integration of the benzylic protons with respect to the internal standard.

1.9. Computational details (For more details see CD-ROOM)

The DFT-B3LYP hybrid exchange-correlation functional^[7-9] was used to explore the $C_{aryl}-C_{sp}$ coupling mechanism conducted by copper species, All DFT calculations were performed out using the Gaussian09 program package.^[10] The molecular orbitals and geometry visualizations presents in the main text have been generated with the Chemcraft program.^[11] Optimizations were performed with no symmetry restrictions, using the 6-31G* basis set for the all atoms. The effect of acetonitrile solvent in the energy and geometry optimization calculations was modeled by the SMD method.^[12] Dispersion effects were also introduced employing the Grimme's DFT-D₂ correction.^[13] Mulliken and natural-population analysis (NPA)^[14] Weinhold charges were calculated for some species in solution to understand their reactivity trend.

Vibrational frequency calculations based on analytical second derivatives to obtain the enthalpy and entropy corrections at $T = 298.15$ K were performed at the same level of theory. Stationary points were established by frequency calculations in solvent-phase, where minima have no imaginary frequencies and transition states only one.

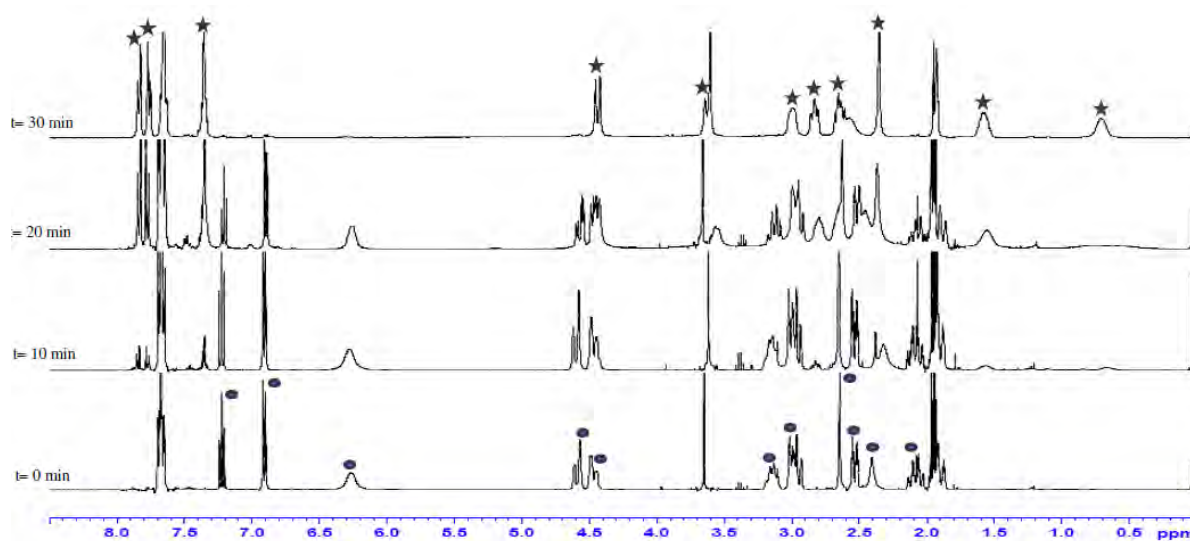
Solvent-phase free energies are corrected with the free-energy change associated with moving from a standard-state gas-phase pressure of 1 atm to a standard-state gas-phase concentration of 1M, $\Delta G^{o/g}$.^[15] Thus, the final free energies use a standard state of an ideal gas at a gas-phase concentration of 1 mol L⁻¹ dissolving as an ideal dilute solution at a liquid-phase concentration of 1 mol L⁻¹. The value of $\Delta G^{o/g}$ at 298 K is 1.9 kcal mol⁻¹ for 1M standard state solutes.

2. Supporting Figures

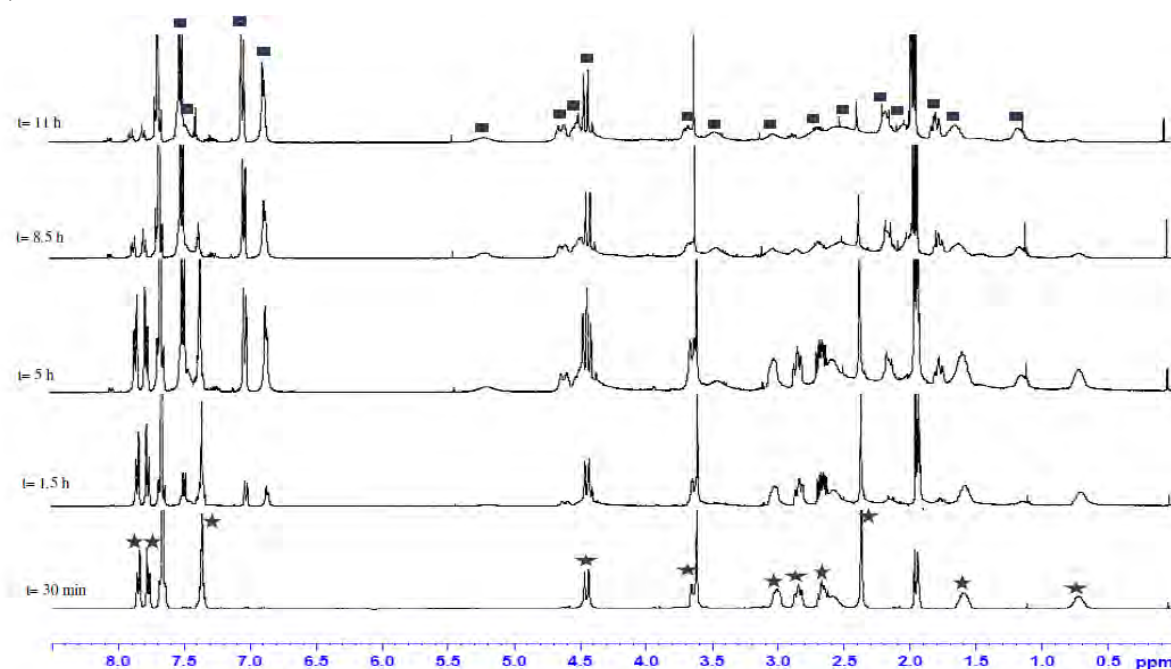
Figure S1. 1H NMR monitoring of the reaction between a well-defined aryl- Cu^{III} complex (**1**_{ClO₄}) with 4-Ethynyl- α,α,α - trifluorotoluene (**S**_{CF₃}) to produce the **I**_{CF₃} and **P**_{CF₃} quantitatively. a) Overlaid spectra showing the consumption of substrate **1**_{ClO₄} signals (circles) and growing of **I**_{CF₃} signals

(stars). b) Overlaid spectra showing the consumption of reaction intermediate I_{CF_3} signals (stars) and growing of P_{CF_3} signals (squares). The doublet at 7.67 ppm and the singlet at 3.63 ppm, these signals correspond to S_{CF_3} excess. c) Overlaid spectra showing the consumption of reaction intermediate I_{CF_3} signals (stars) and growing of P_{CF_3} signals (squares) upon addition of 2.5 eq. of 1,10-phenanthroline to sequester Cu^I . Signals at 8.98 ppm, 8.57 ppm, 8.02 ppm and 7.89 ppm correspond to 1,10-phenanthroline excess. d) Plot of the concentration changes versus time of both I_{CF_3} and product P_{CF_3} , with and without sequestering Cu^I by the addition of phen. Conditions (equivalents to those of Scheme 2 in the manuscript): $[1_{ClO_4}] = 78.6$ mM, $[S_{CF_3}] = 157.2$ mM, CH_3CN , $0^\circ C$, N_2 atmosphere.

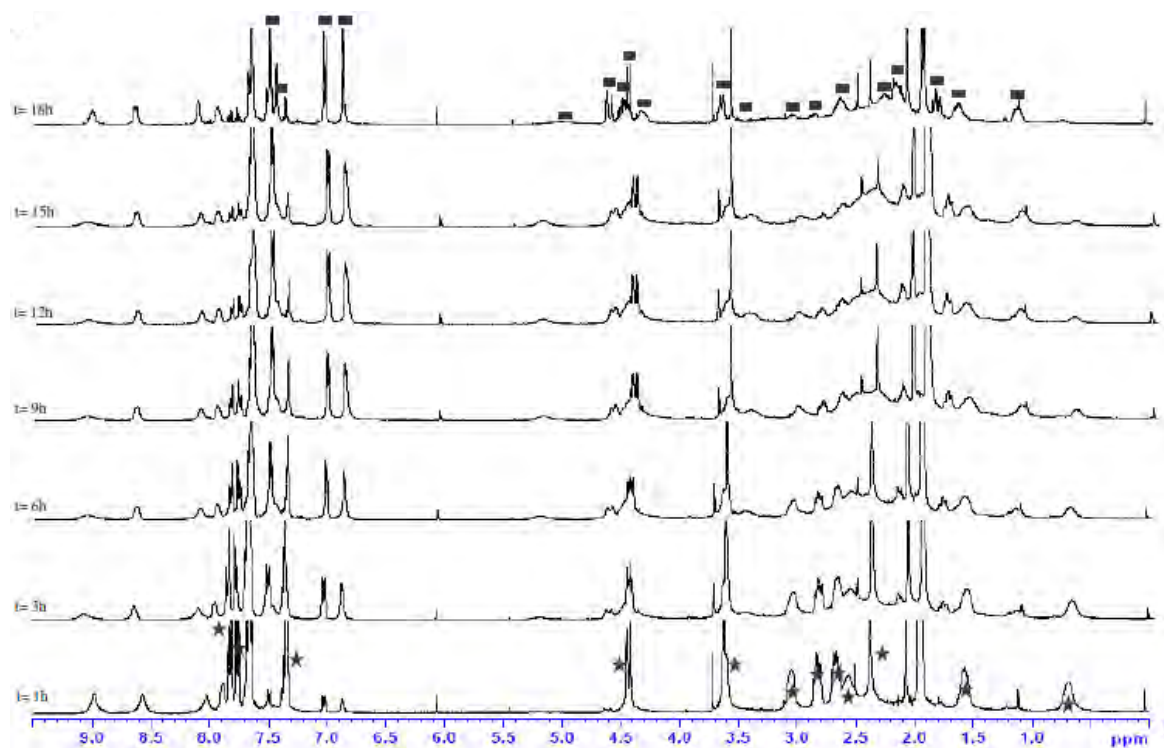
a)



b)



c)



d)

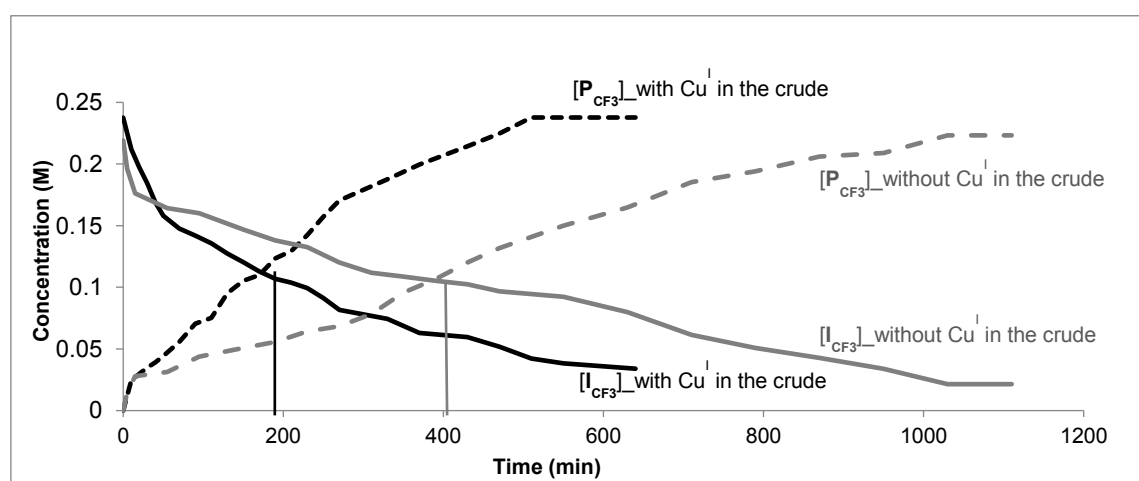


Figure S2. ESI-MS spectrum of compound **P_{NO2}** ($m/z = 393.2300$), byproduct **L₁-H** ($m/z 248.2116$) in CH₃CN.

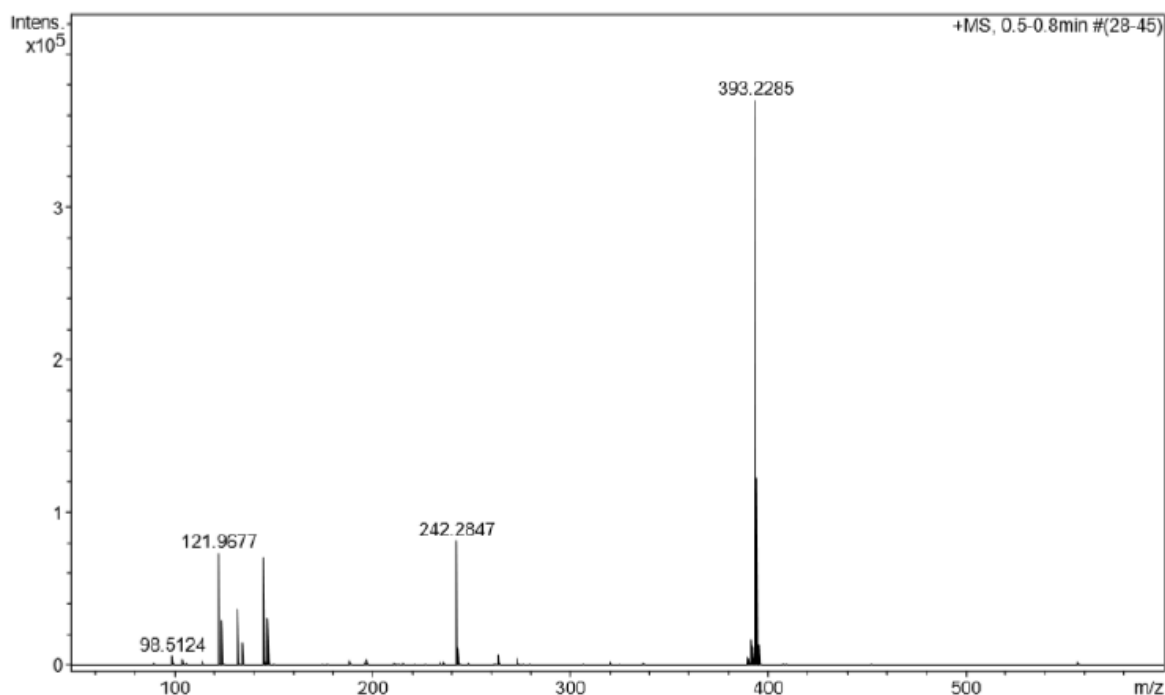
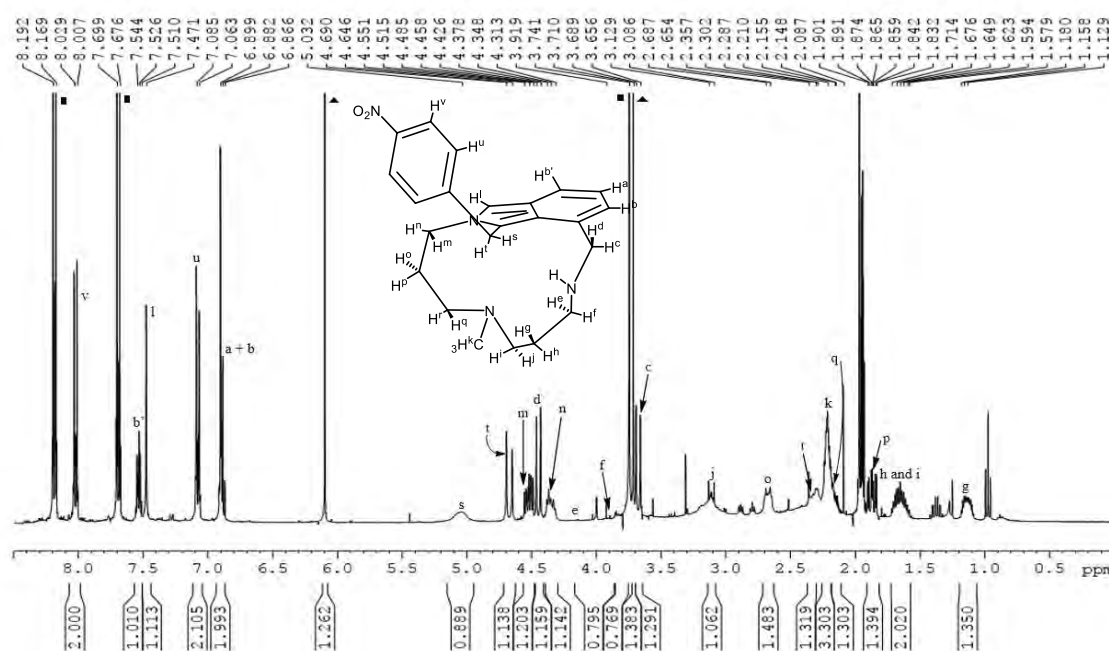


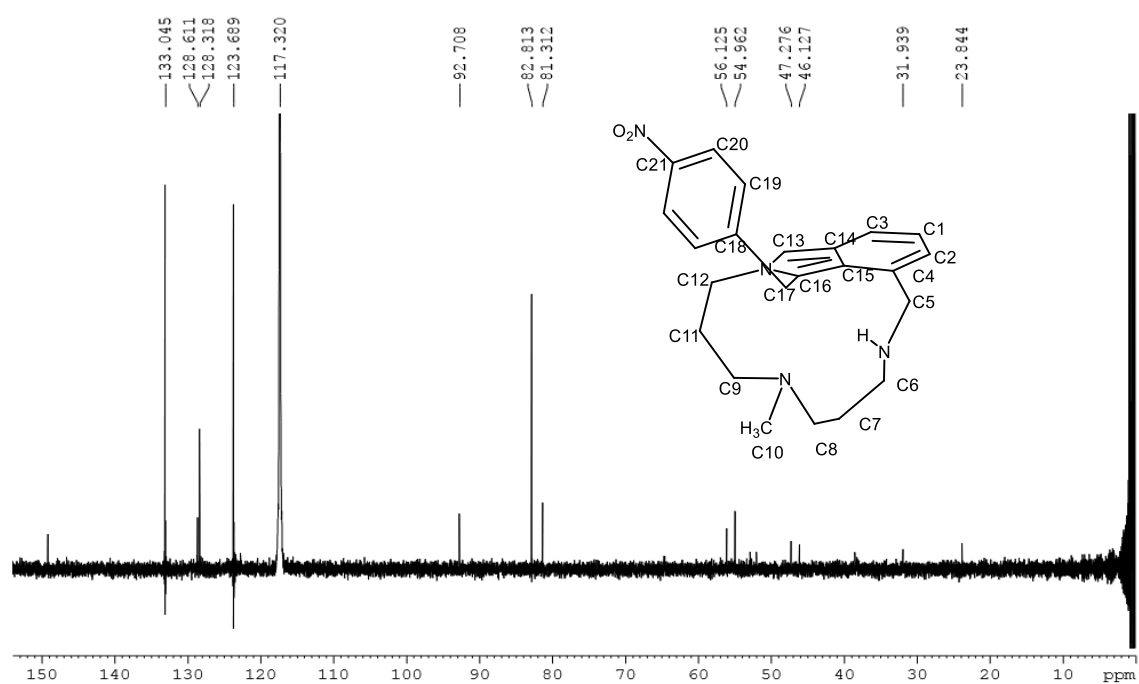
Figure S3. NMR characterization of **P_{NO2}:** a) ¹H-NMR spectrum (400 MHz, CD₃CN, 47 °C). b) ¹³C{¹H}-NMR spectrum (100 MHz, CD₃CN, 47 °C). c) ¹H-¹H COSY spectrum (400 MHz, CD₃CN, 47 °C). d) ¹H-¹H NOESY spectrum (400 MHz, CD₃CN, 47 °C). e) ¹H-¹³C HSQC_ed spectrum (400 MHz, CD₃CN, 47 °C). f) ¹H-¹³C HMBC spectrum (400 MHz, CD₃CN, 47 °C). g) ¹H-¹H TOCSY spectrum (400 MHz, CD₃CN, 47 °C).

a)

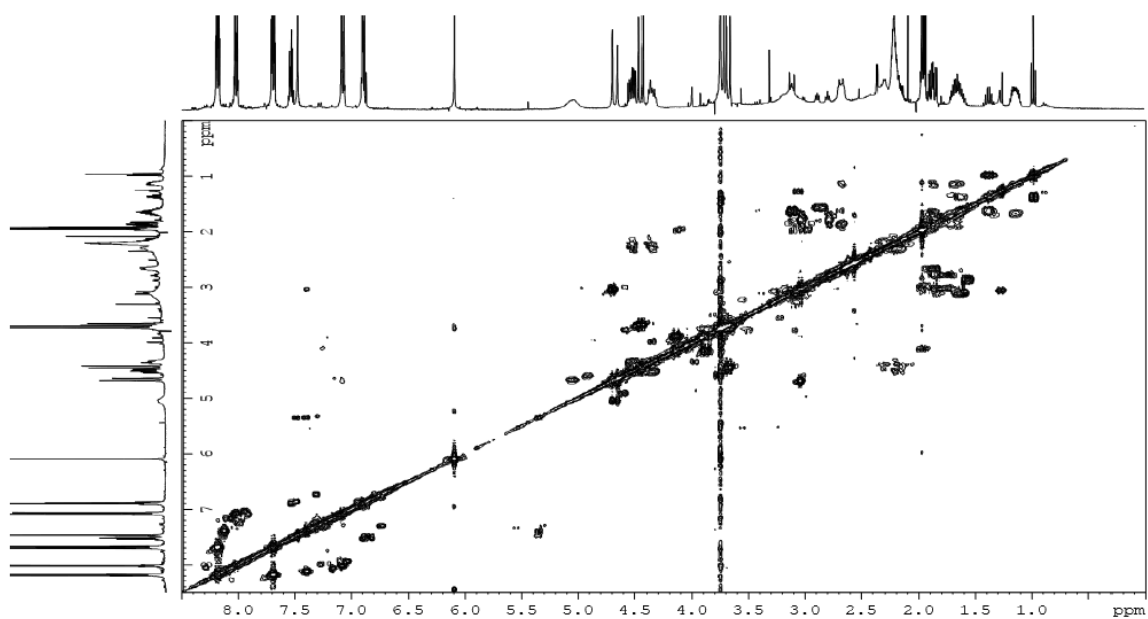


▲ 1,3,5-trimethoxybenzene (std.). ■ excess nitrophenyl acetylene.

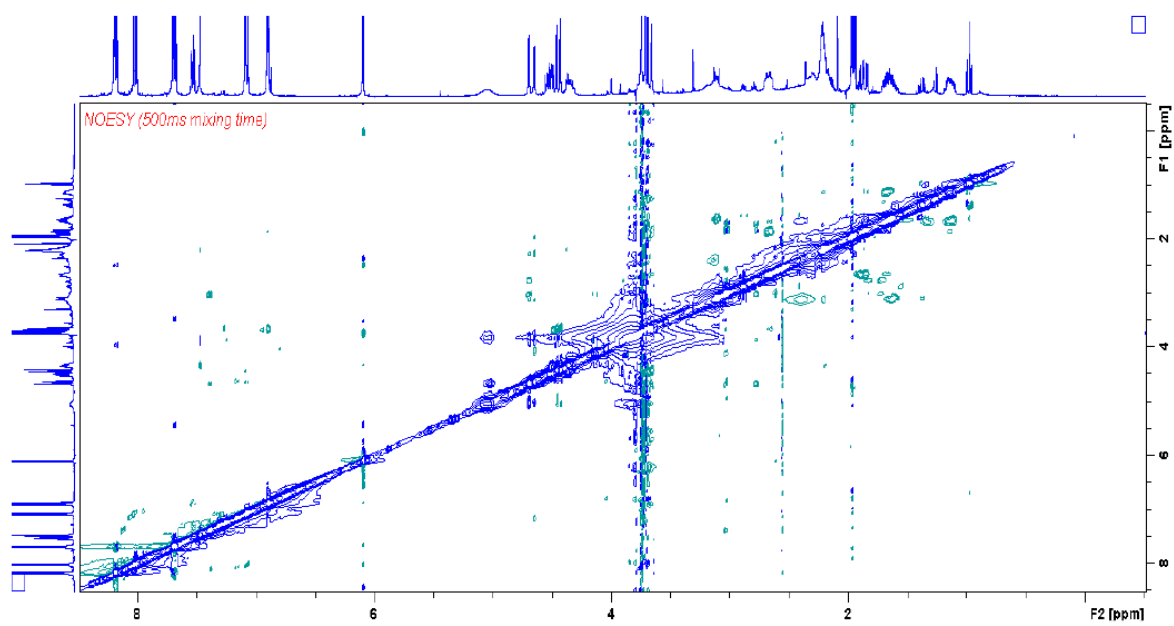
b)



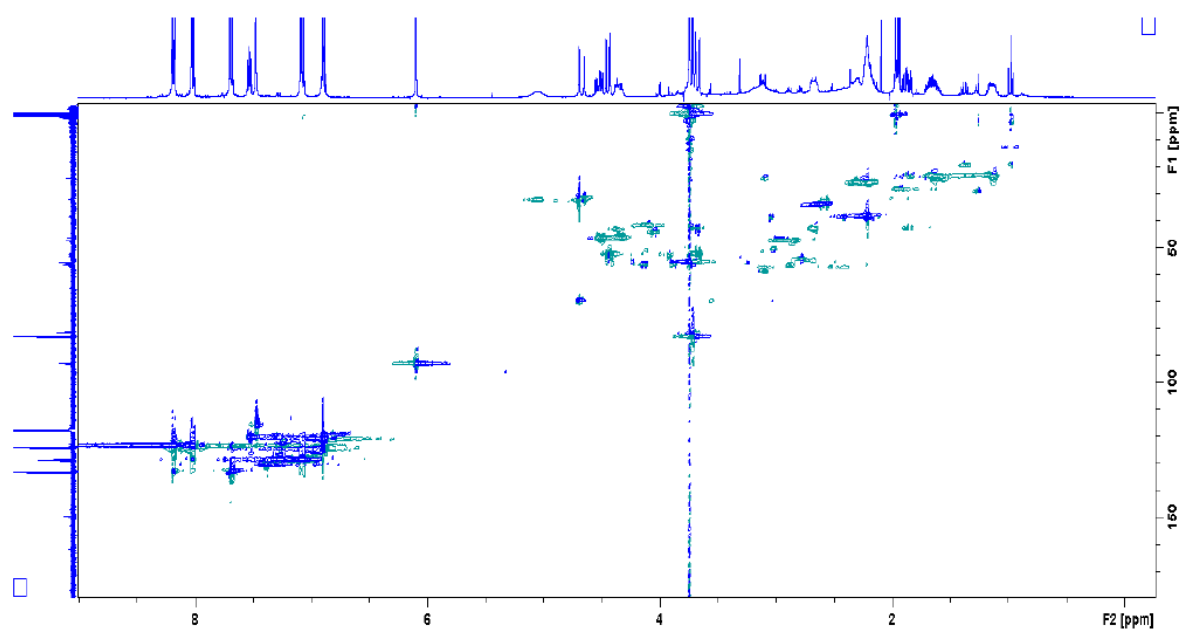
c)



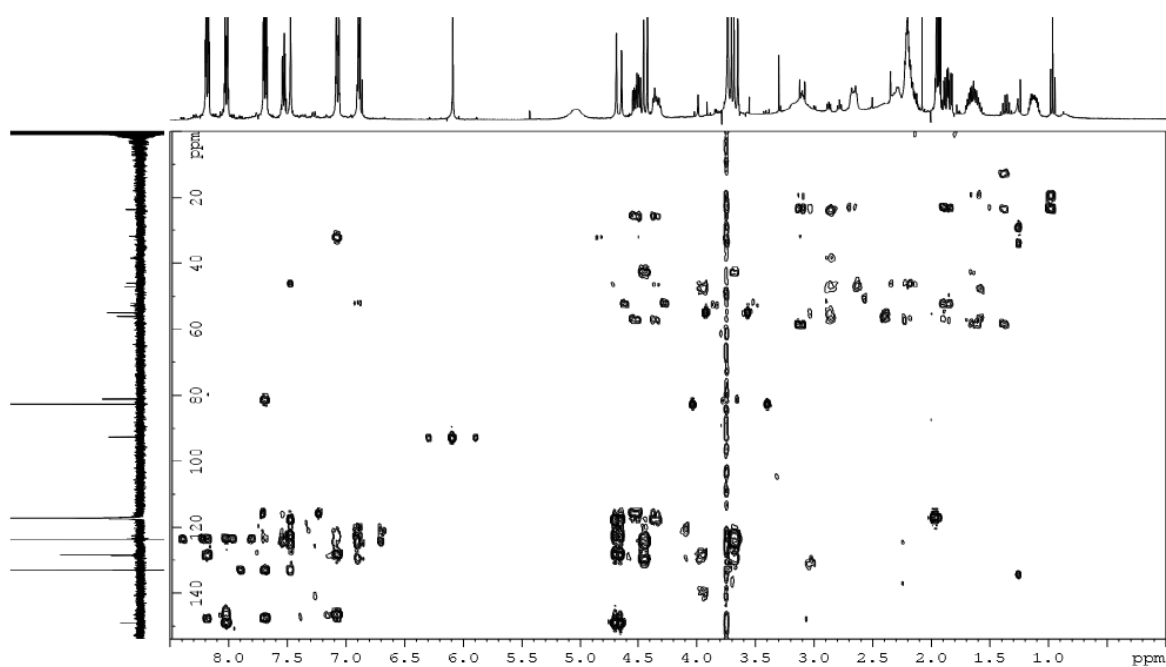
d)



e)



f)



g)

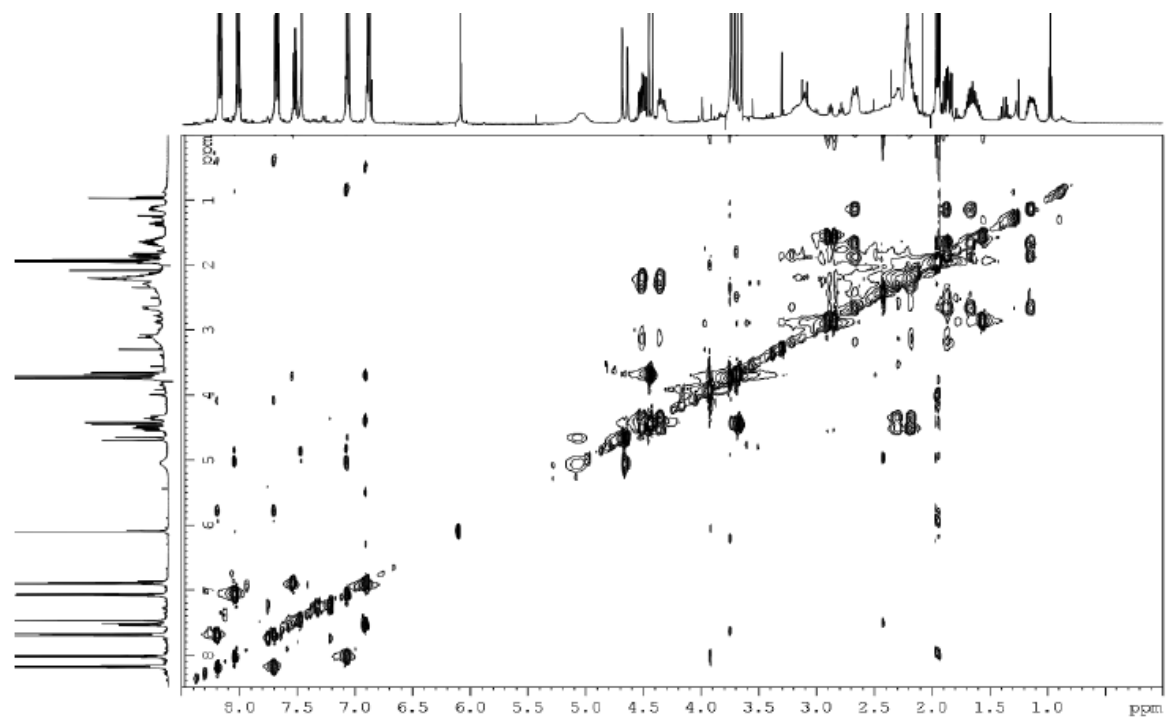
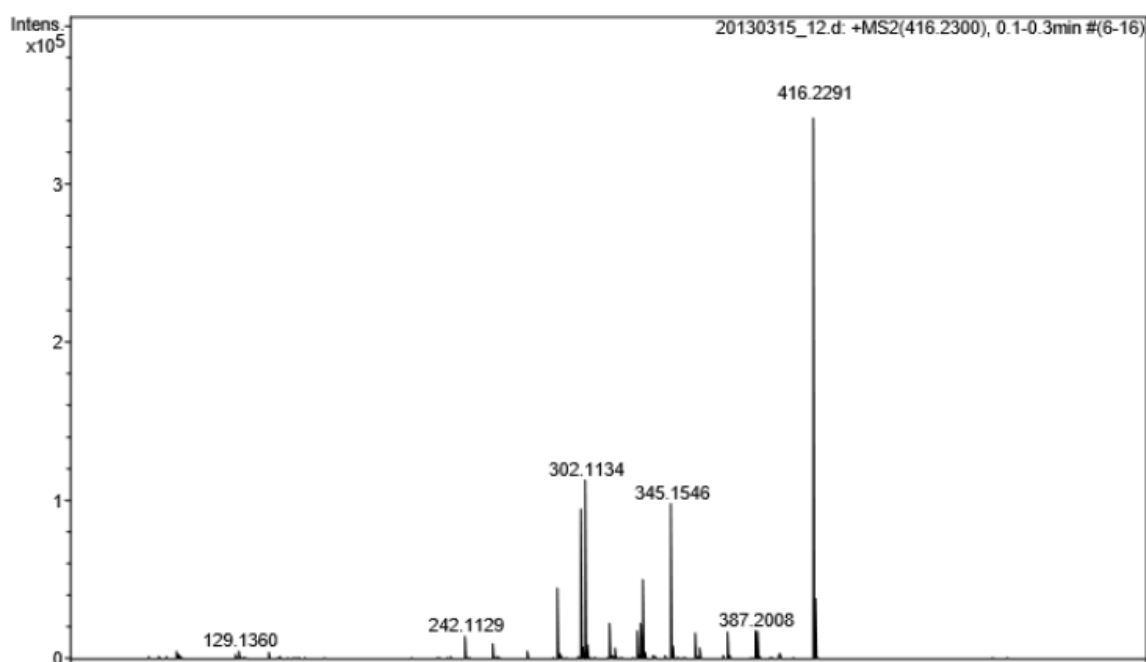
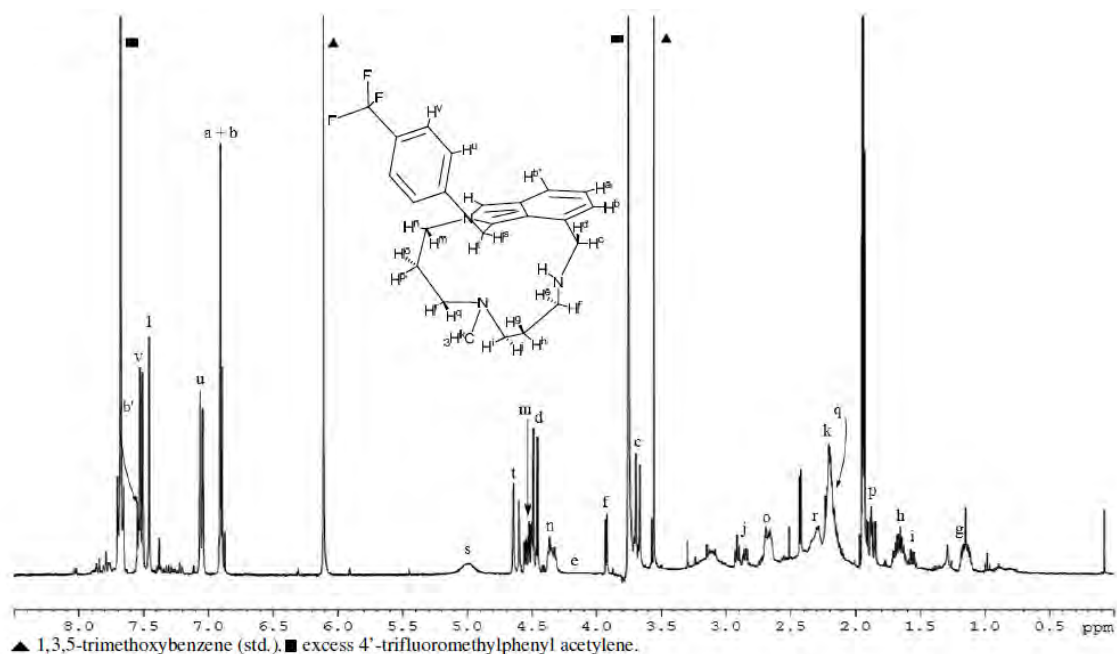
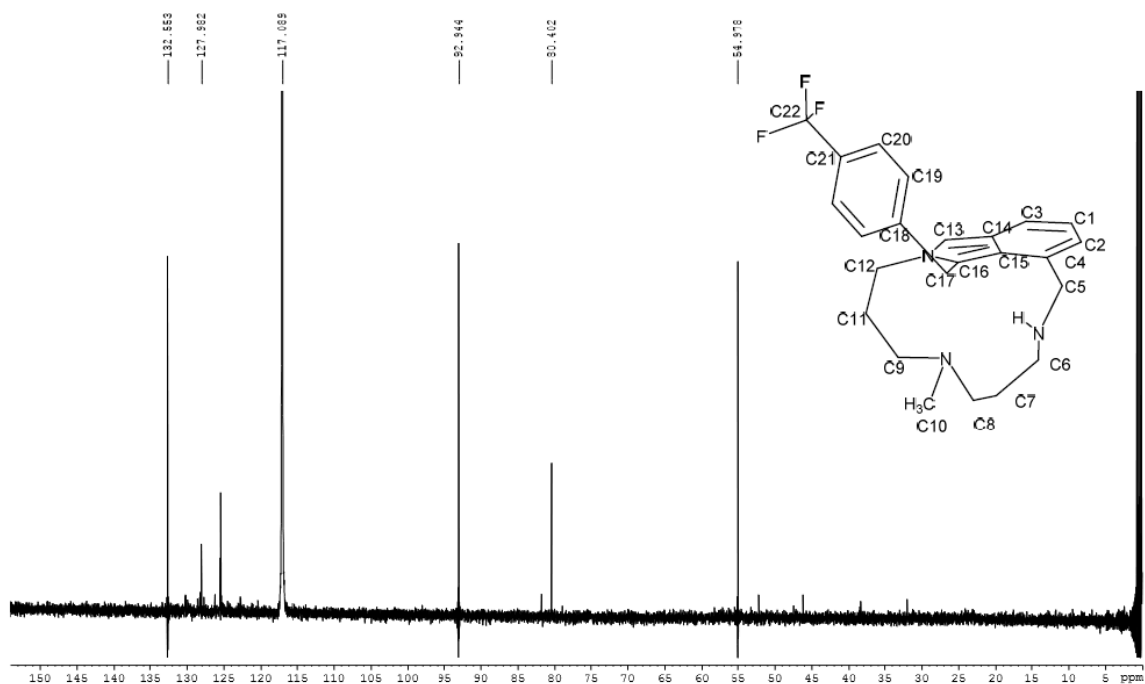


Figure S4. ESI-MS spectrum of compound **P_{CF₃}** ($m/z = 416.2291$) in CH₃CN.**Figure S5.** NMR characterization of **P_{CF₃}**: a) ¹H-NMR spectrum (400 MHz, CD₃CN, 47 °C). b) ¹³C{¹H}-NMR spectrum (100 MHz, CD₃CN, 47 °C). c) ¹H-¹H COSY spectrum (400 MHz, CD₃CN, 47 °C). d) ¹H-¹H NOESY spectrum (400 MHz, CD₃CN, 47 °C). e) ¹H-¹³C HSQC_ed spectrum (400 MHz, CD₃CN, 47 °C). f) ¹H-¹³C HMBC spectrum (400 MHz, CD₃CN, 47 °C).

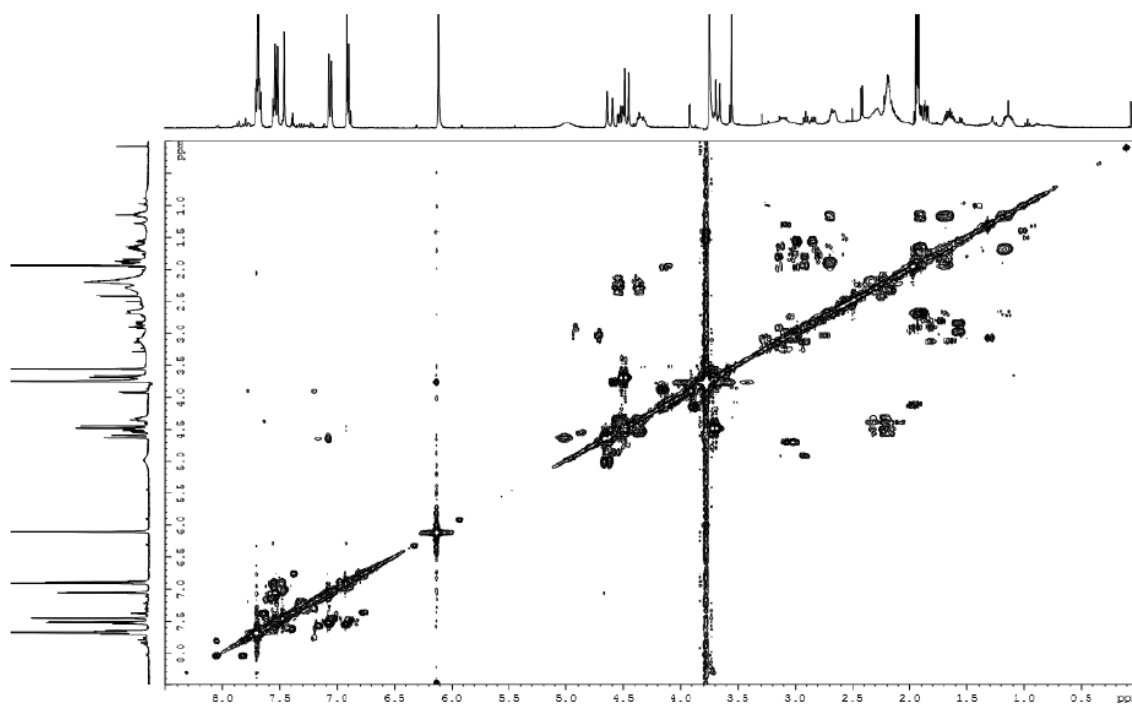
a)



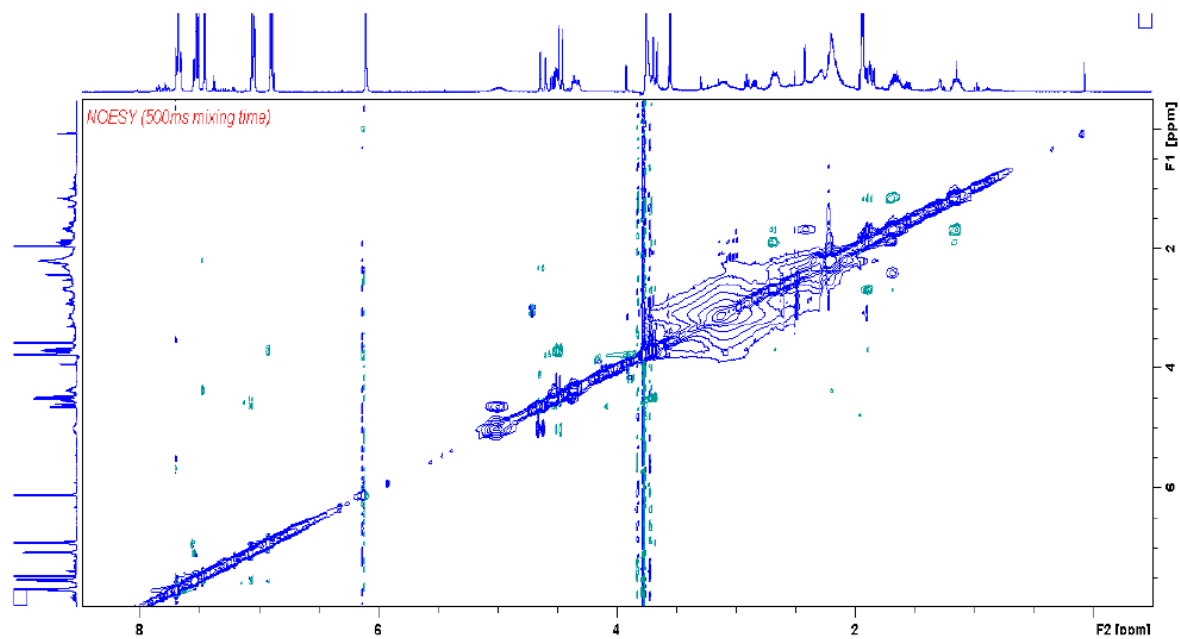
b)



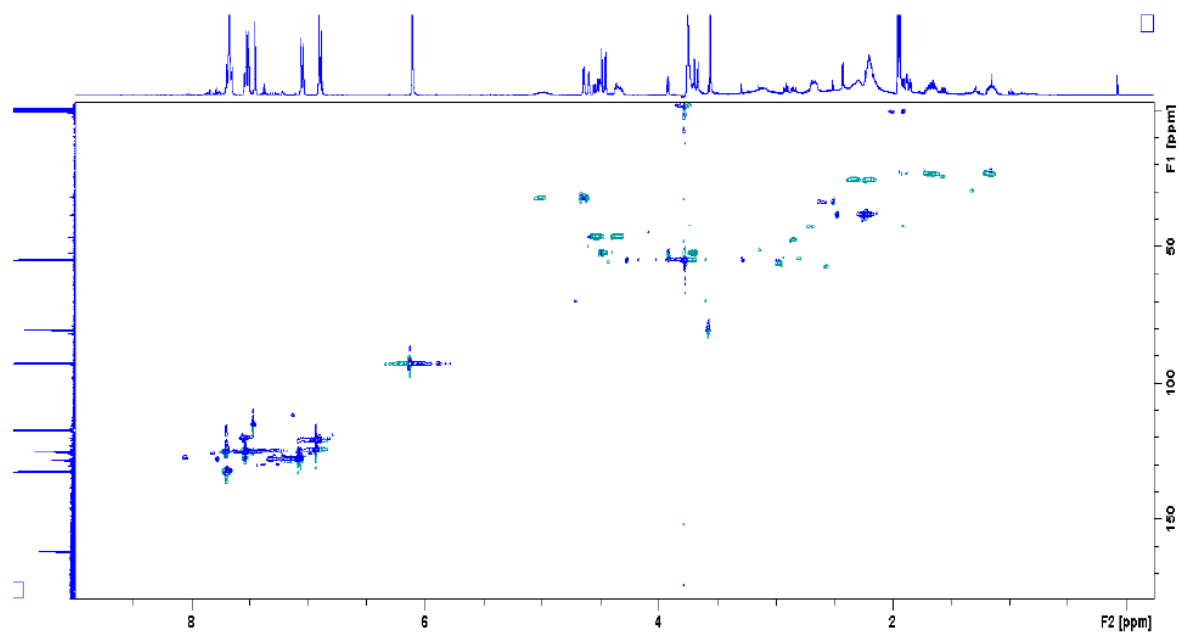
c)



d)



e)



f)

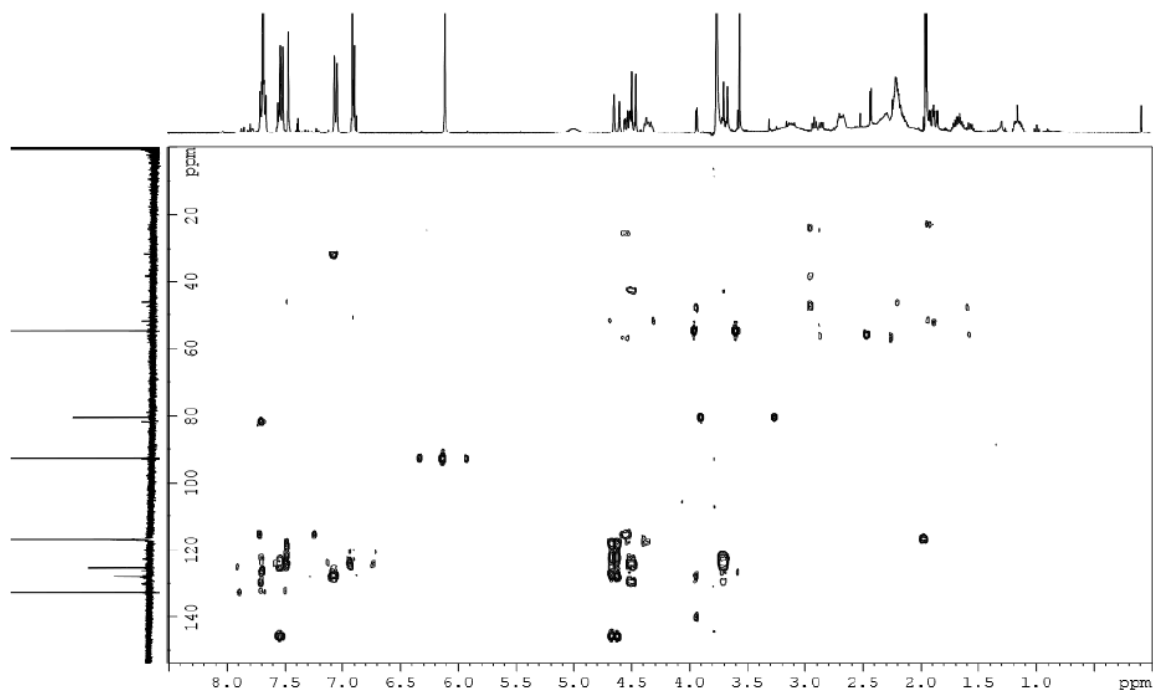


Figure S6. ESI-MS spectrum of compound **P_{Ha}** and **P_{Hb}** ($m/z = 348.2437$) in CH_3CN .

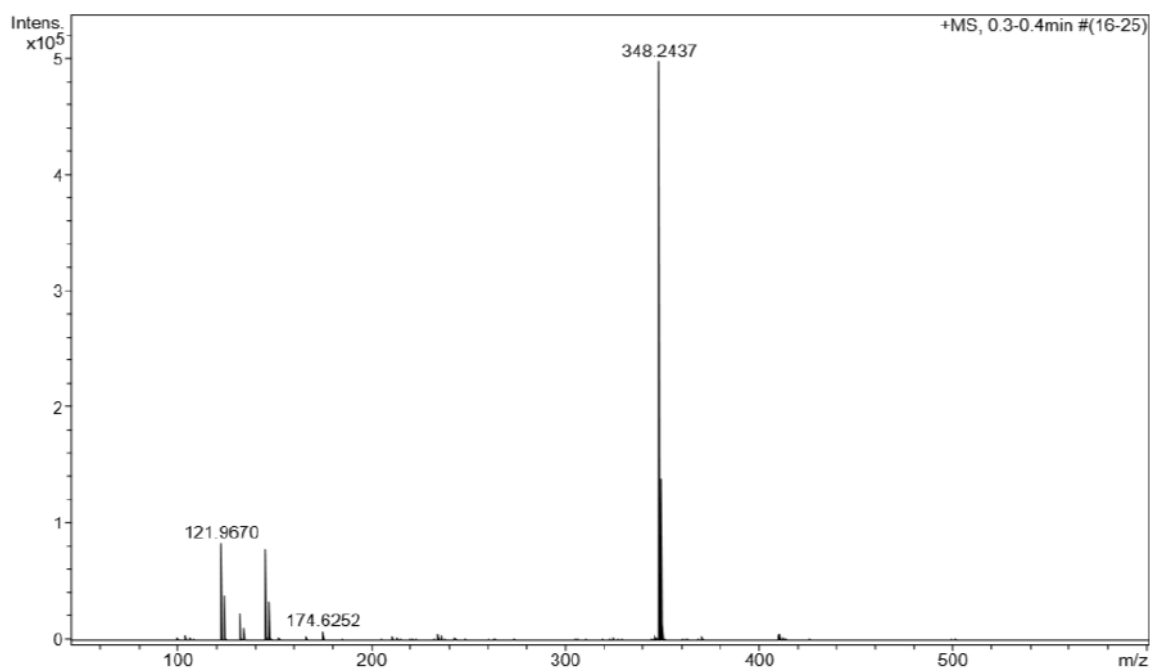
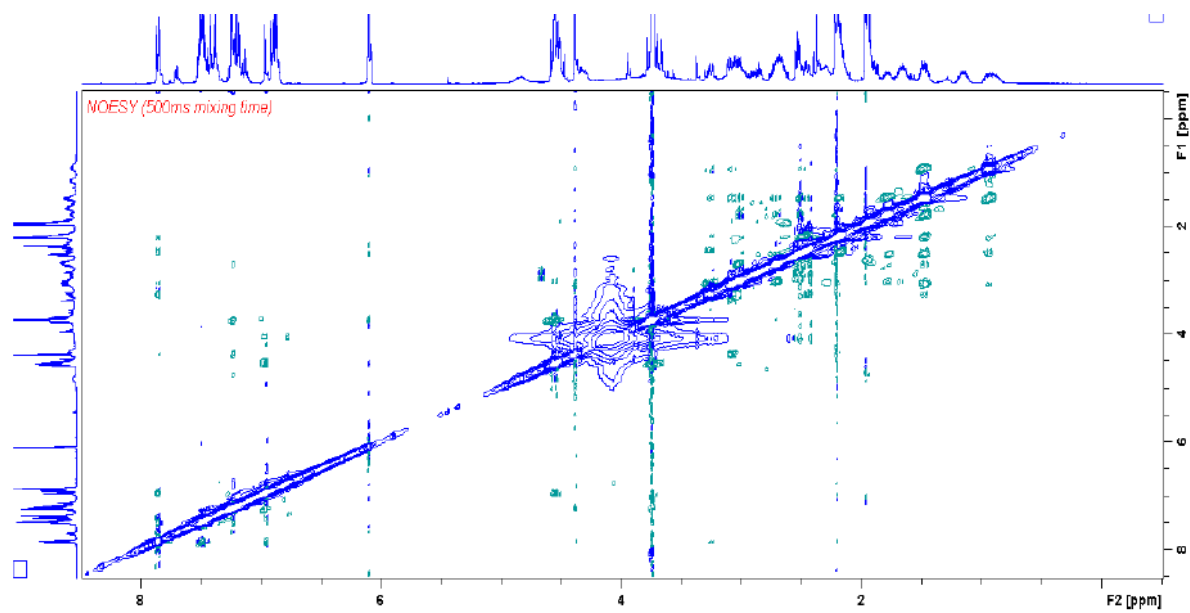


Figure S6. NMR characterization of **P_{Ha}** and **P_{Hb}**: a) ^1H -NMR spectrum of **P_{Ha}** (400 MHz, CD_3CN , 47 °C). b) ^1H -NMR spectrum of **P_{Hb}** (400 MHz, CD_3CN , 47 °C). c) $^{13}\text{C}\{^1\text{H}\}$ -NMR spectrum (100 MHz, CD_3CN , 47 °C). d) ^1H - ^1H COSY spectrum (400 MHz, CD_3CN , 47 °C). e) ^1H - ^1H NOESY spectrum (400 MHz, CD_3CN , 47 °C). f) ^1H - ^{13}C HSQC_ed spectrum (400 MHz, CD_3CN , 47 °C). g) ^1H - ^{13}C HMBC spectrum (400 MHz, CD_3CN , 47 °C).

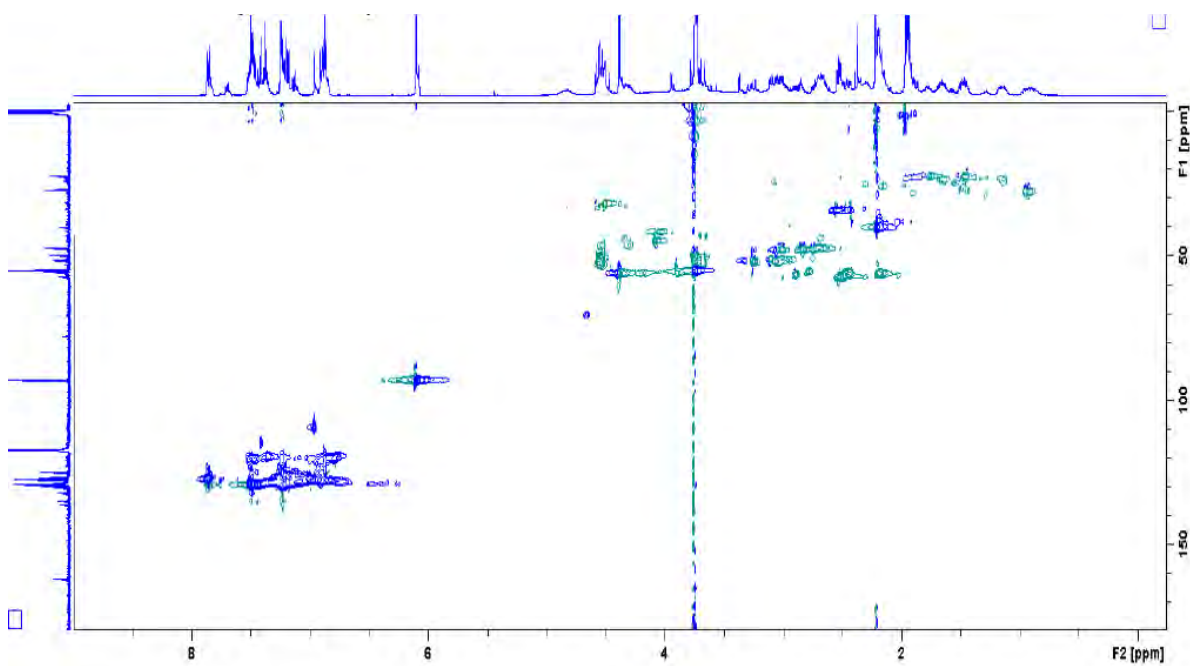
a)

c)

e)



f)



g)

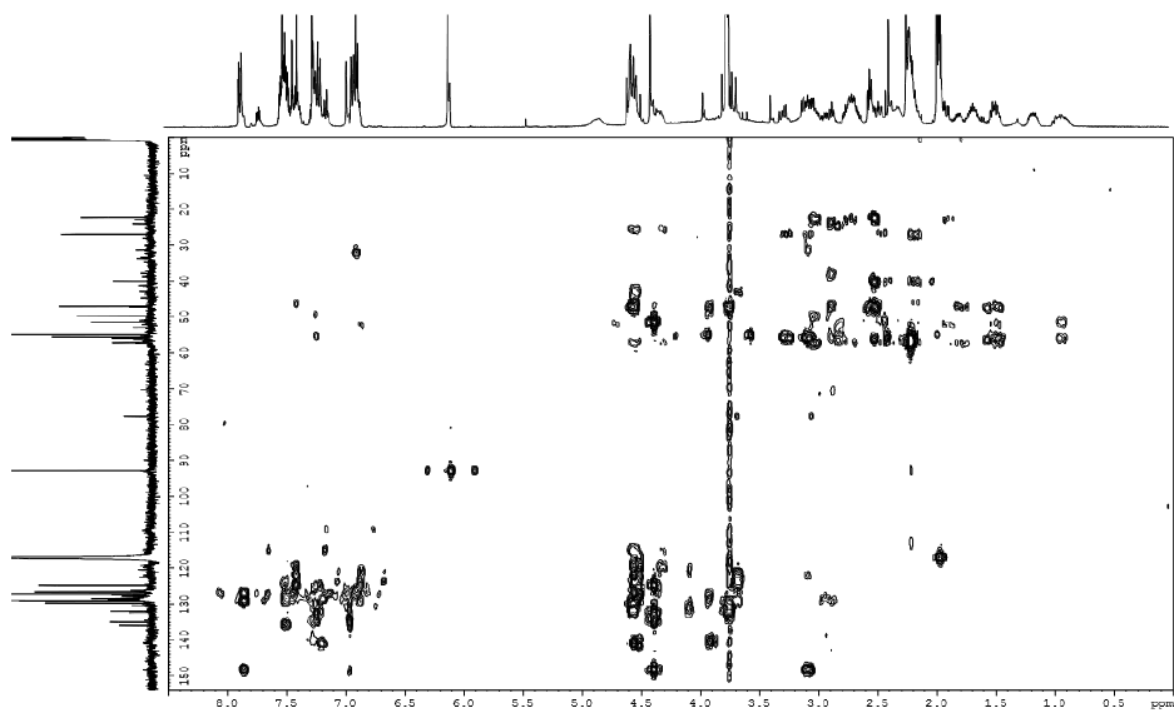


Figure S7. HRMS spectrum of compound **1cF₃** (*m/z* 416.2360), using Cryospray device at -40°C, in CH₃CN

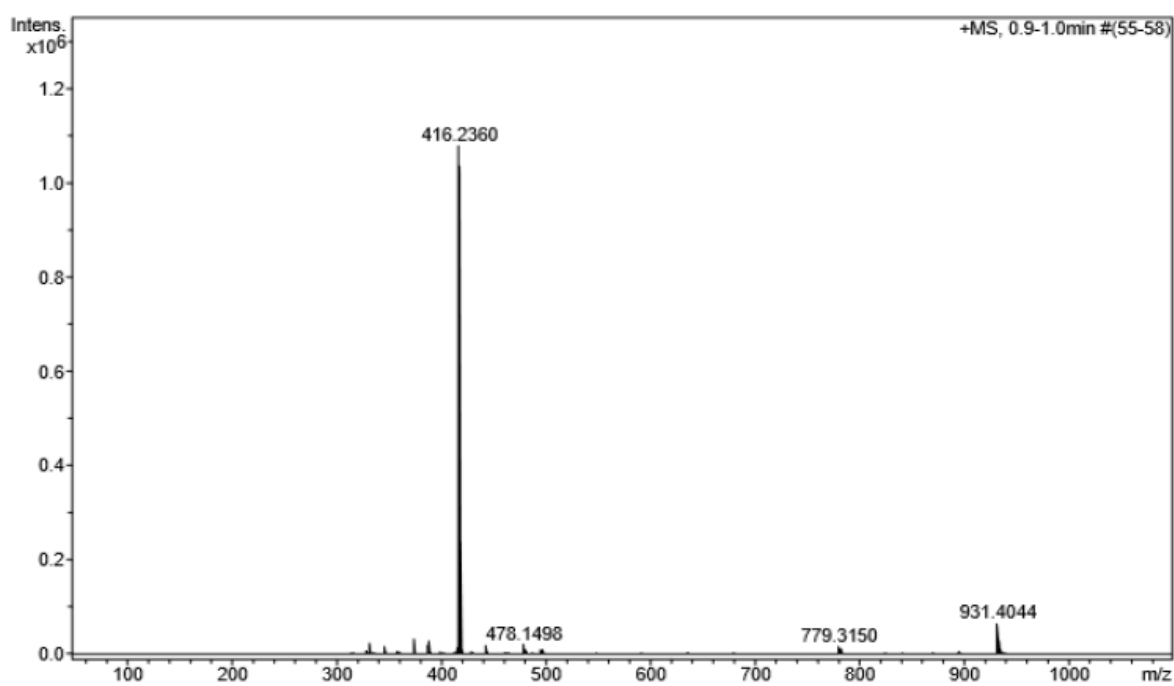


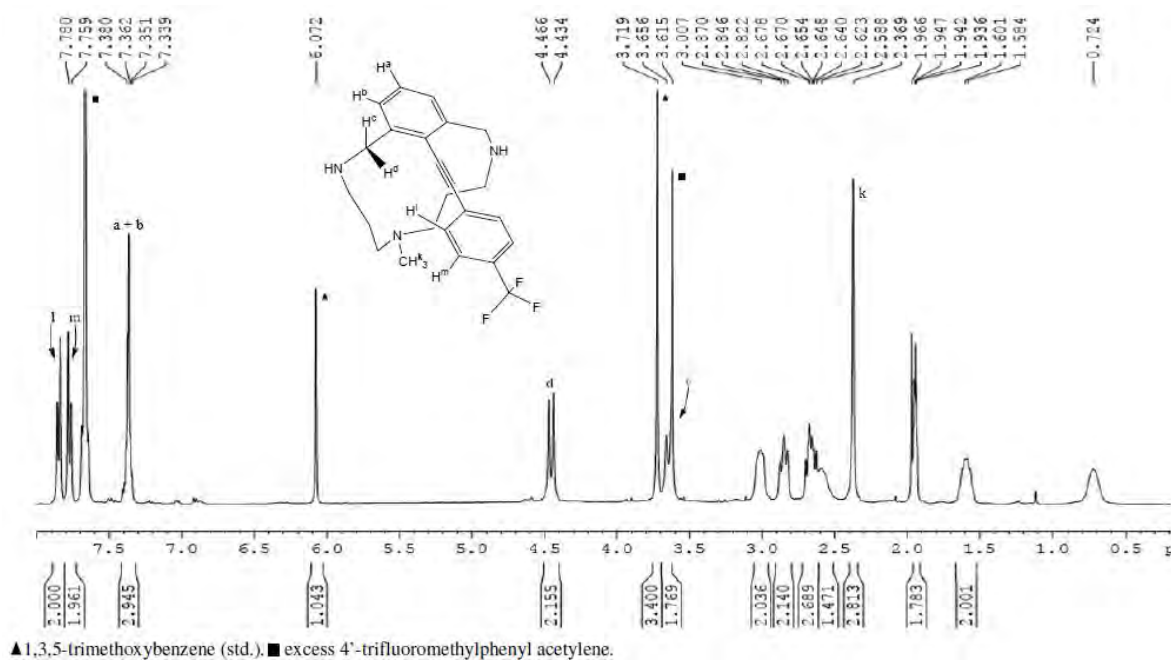
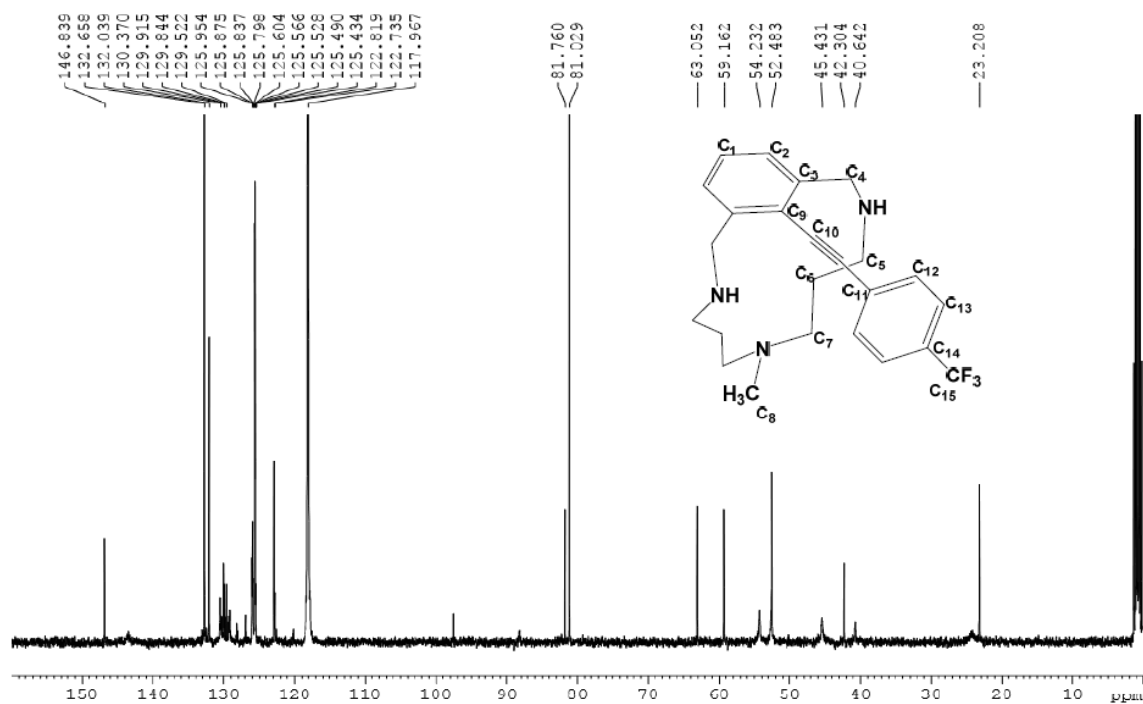
Figure S8. ^1H -NMR spectrum of compound **1cF₃** in CD_3CN , 400 MHz, at -10°C .**Figure S9.** $^{13}\text{C}\{^1\text{H}\}$ -NMR spectrum of compound **1cF₃** in CD_3CN , 400 MHz, at -10°C . (For 2D spectras see CD-ROOM)

Figure S10. ESI-MS spectrum of compound **I_{CF3}** with **Cu^I** (m/z 478.1498) in CH_3CN .

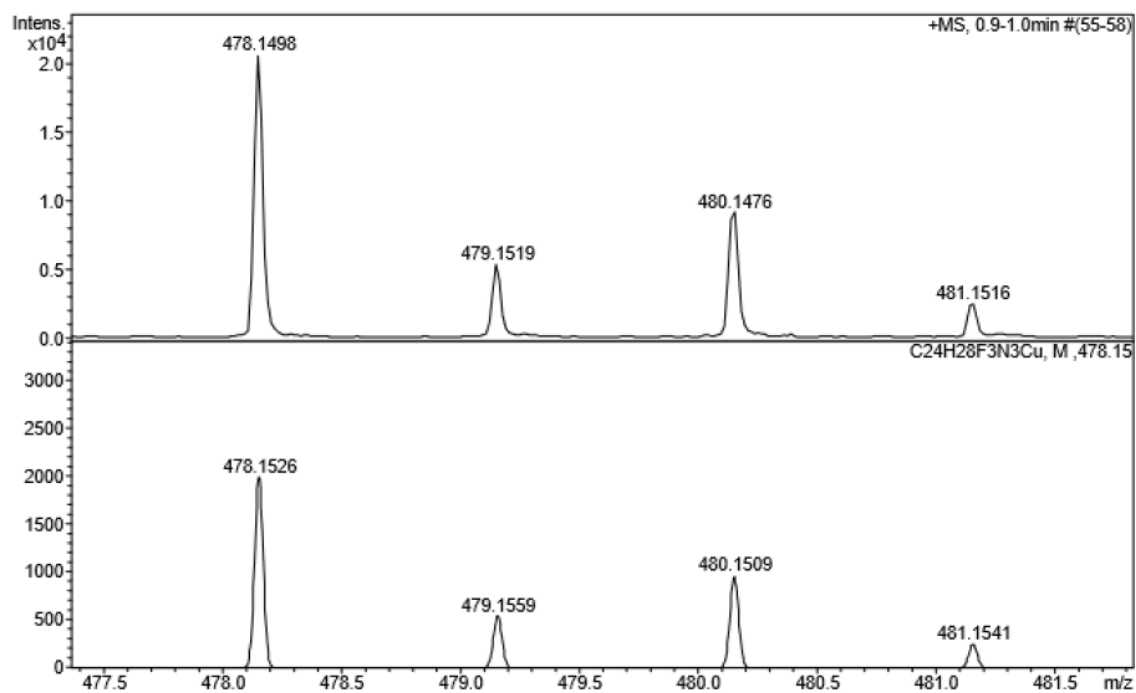


Figure S11. ESI-MS spectrum of compound **I'CF₃** (m/z 444.2610) and **L₅-Cl** (m/z 310.2019) in CH_3CN .

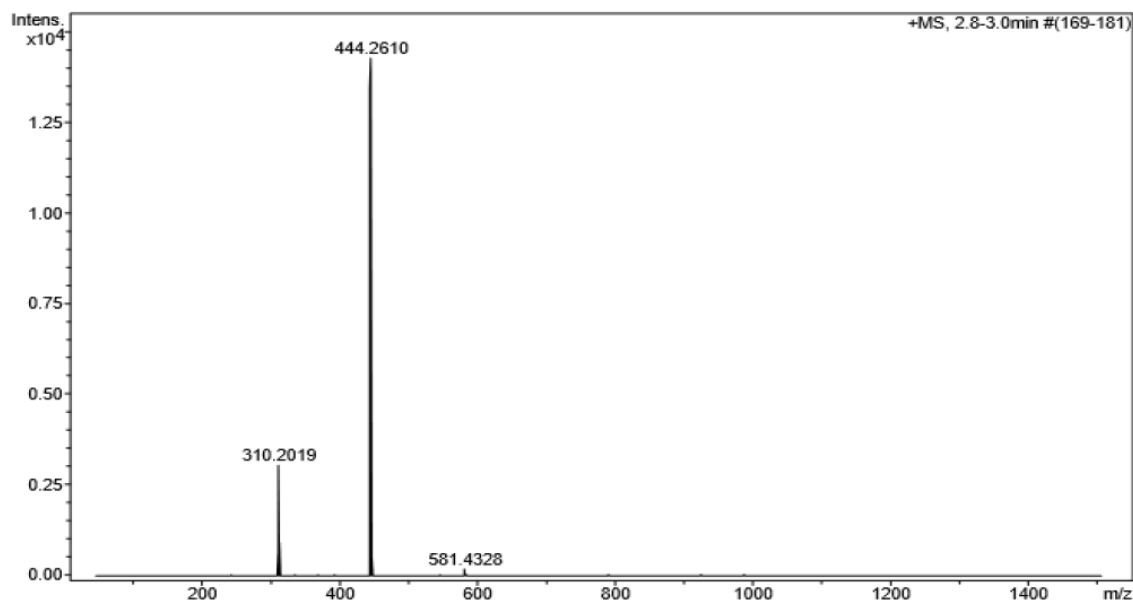


Figure S12. ^1H -NMR spectrum of compound **I'** CF_3 in CD_3CN , 400 MHz, at 25 °C. (For 2D spectras see CD-ROOM)

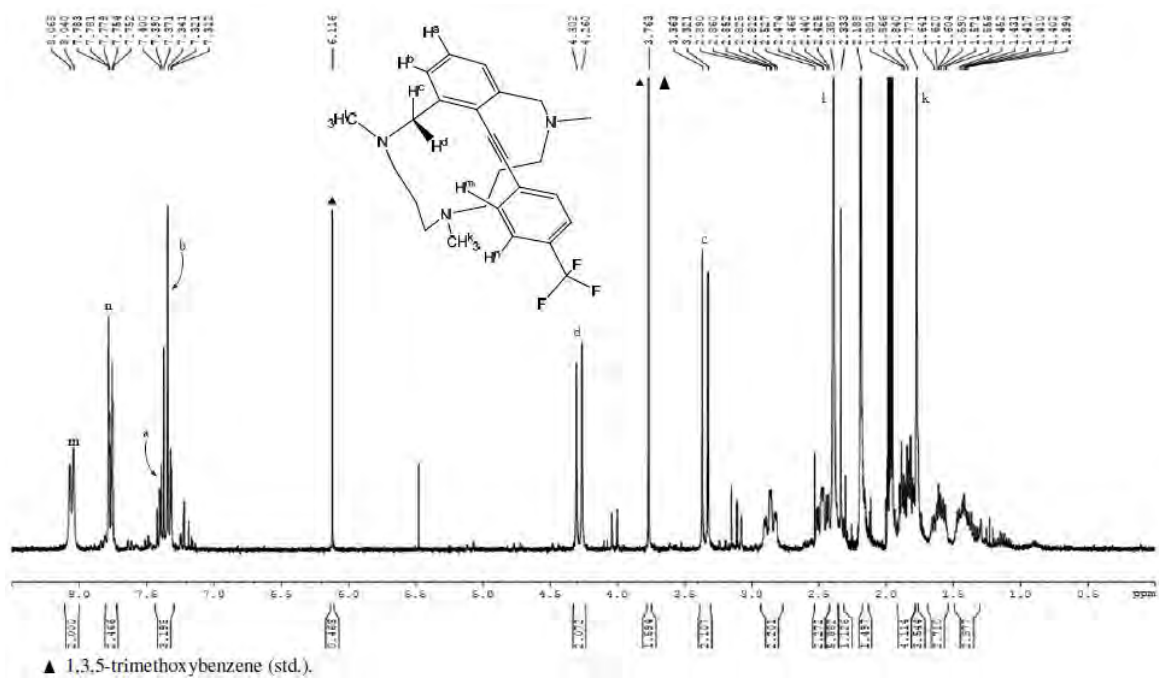


Figure S13. $^{13}\text{C}\{^1\text{H}\}$ -NMR spectrum of compound **I'** CF_3 in CD_3CN , 400 MHz, at 25 °C.

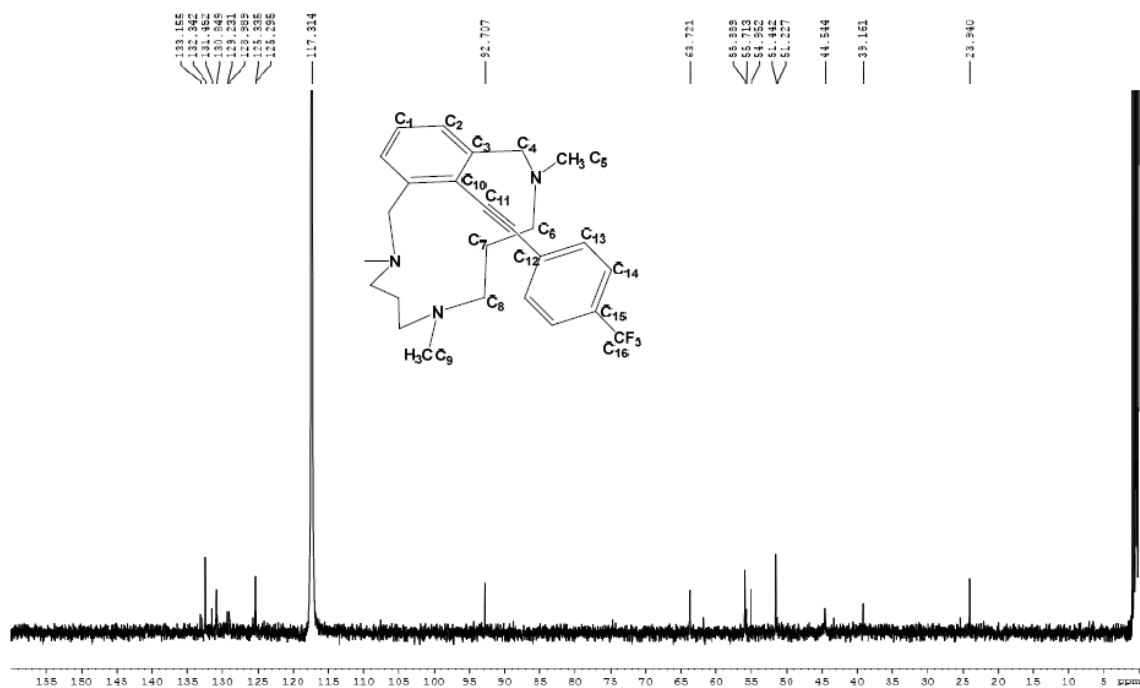


Figure S14. B3LYP-D₂/6-31G*/SMD optimized geometry for the transition state involving the intramolecular proton transfer from the phenylacetylene moiety to one of the secondary amines of the aryl-Cu^{III} complex. Selected bond distances are in Å (irrelevant hydrogen atoms are omitted for clarity).

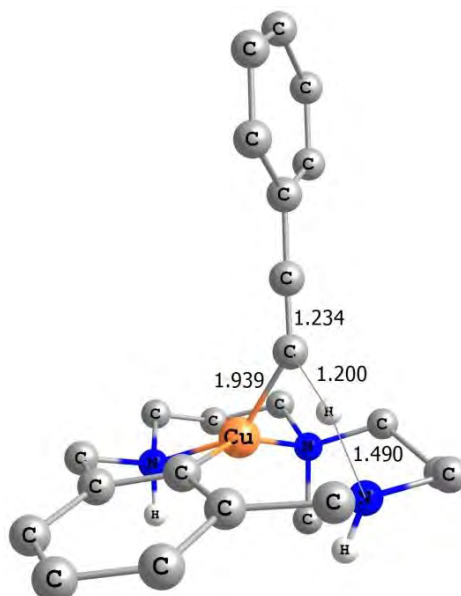
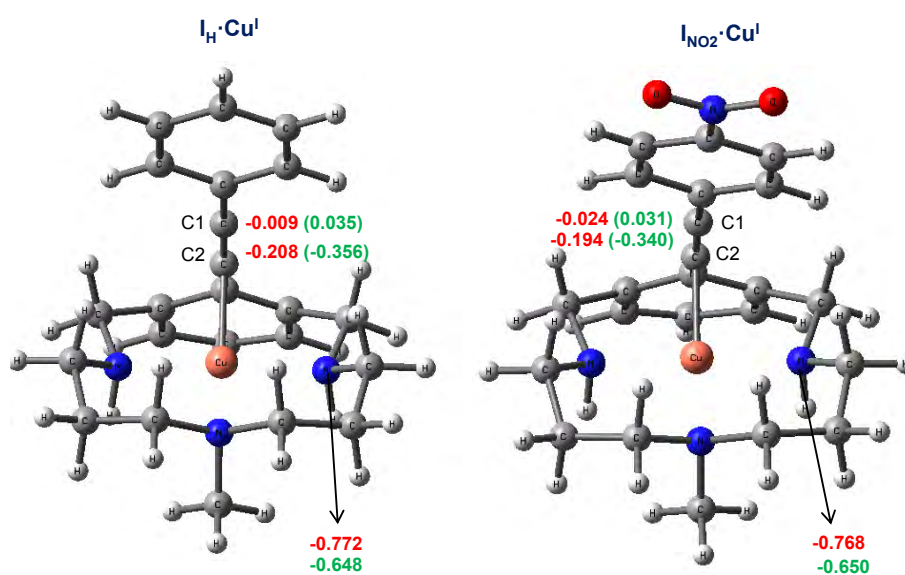


Figure S15. Mulliken (green) and NPA (red) charges on the alkyne and amine moieties for $I_H \cdot Cu^I$ and $I_{NO_2} \cdot Cu^I$ species.



3. Supporting Tables

Table S1. Attempts to synthesize **P_{NO2}** under catalytic amounts of Cu^I sources.

Ligand	Cu ^I (mol%)	Base (equiv)	S _{NO2} (equiv)	Additive (equiv)	T (°C)	Yield P _{NO2} (%)	Conversion (%)
L₁-Br	Cu ^I (CH ₃ CN) ₄ OTf (10)	-	2*	-	25	0	64%
	Cu ^I (CH ₃ CN) ₄ OTf (10)	Proton Sponge (4)	2	-	25	0	100%
	Cu ^I (CH ₃ CN) ₄ OTf (10)	-	2*	Ag(OTf) (2)	25	0	100%
	Cu ^I (CH ₃ CN) ₄ OTf (10)	-	2*	-	50	0	82%
	Cu ^I (CH ₃ CN) ₄ OTf (10)	Et ₃ N (2.2)	2*	-	25	0	100%
	Cu ^I (CH ₃ CN) ₄ OTf (10)	K ₂ CO ₃ (2.2)	2	-	25	0	100%
	Cu ^I (CH ₃ CN) ₄ OTf (10)	-	10*	-	25	0	75%
L₁-I	Cu ^I (CH ₃ CN) ₄ OTf (10)	-	2*	-	25	0	30%
	Cu ^I (CH ₃ CN) ₄ OTf (10)	K ₂ CO ₃ (2.2)	2	-	50	0	100%
	Cu ^I (CH ₃ CN) ₄ OTf (10)	K ₃ PO ₄ (2.2)	2	-	25	0	100%
L₁-Cl	Cu ^I (CH ₃ CN) ₄ OTf (10)	-	2*	GaCl ₃ (2)	25	0	0%
	Cu ^I (CH ₃ CN) ₄ OTf (10)	-	10*	GaCl ₃ (2)	25	0	0%
	Cu ^I (CH ₃ CN) ₄ OTf (10)	-	10	GaCl ₃ (2)	50	0	0%

(General conditions for catalytic reactions: [L₁-X] = 5 mM, [nucleophile] = 10 mM, [Cu^I source] = 0.5 mM and 1mM, N₂, CD₃CN). *added by syringe pump in 3 hours.

Table S2. Attempts to synthesize **I'_{CF3}** under catalytic amounts of Cu^I sources.

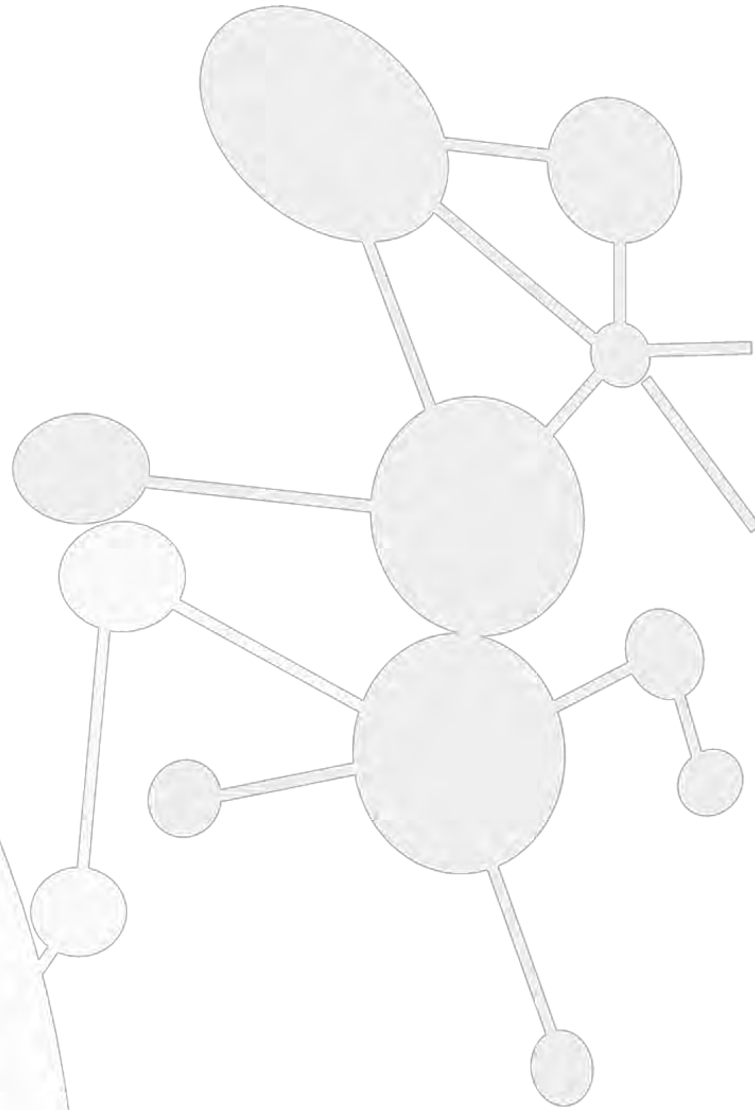
Ligand	Cu ^I (mol%)	Base (equiv)	S _{CF3} (equiv)	T (°C)	Yield I' _{CF3} (%)
L₅-Cl	Cu ^I (CH ₃ CN) ₄ OTf (10)	-	2	25	10%
	Cu ^I (CH ₃ CN) ₄ OTf (10)	K ₂ CO ₃ (4)	2	25	15%
	Cu ^I (CH ₃ CN) ₄ OTf (10)	K ₃ PO ₄ (4)	2	60	0%
	Cu ^I -(C≡C-Ph- <i>p</i> CF ₃) (20)	^t BuO ⁻ K ⁺ (0.2)	0.2	25	23%
L₅-Br	Cu ^I -(C≡C-Ph- <i>p</i> CF ₃) (20)	K ₃ PO ₄ (4)	2	70	0%
	Cu ^I (CH ₃ CN) ₄ OTf (20)	^t BuO ⁻ K ⁺ (4)	2	50	0%

(General conditions for catalytic reactions: [L₅-X] = 5 mM, [nucleophile] = 10 mM, [Cu^I source] = 0.5 mM and 1mM, N₂, CD₃CN).

4. Supporting References

1. Ribas, X.; Jackson, D. A.; Donnadiou, B.; Mahía, J.; Parella, T.; Xifra, R.; Hedman, B.; Hodgson, K. O.; Llobet, A.; Stack, T. D. P. *Angew.Chem. Int. Ed.* **2002**, *41*, 2991.
2. King, A. E.; Huffman, L. M.; Casitas, A.; Costas, M.; Ribas, X.; Stahl, S. S. *J. Am. Chem. Soc.* **2010**, *132*, 12068.
3. Casitas, A.; Canta, M.; Solà, M.; Costas, M.; Ribas, X. *J. Am. Chem. Soc.* **2011**, *133*, 19386.
4. A. Casitas, A. E. King, T. Parella, M. Costas, S. S. Stahl, X. Ribas, *Chem. Sci.* **2010**, *1*, 326-330.
5. Jouvin, K.; Heimbürger J.; Evano, G. *Chem. Sci.* **2012**, *3*, 756-760.
6. Wojciechowski, K. *Liebigs Ann. Chem.* **1991**, 831- 832.
7. Becke, A. D. *J. Chem. Phys.* **1993**, *98*, 1372-1377.
8. Becke, A. D. *J. Chem. Phys.* **1993**, *98*, 5648-5652.
9. Lee, C. T.; Yang, W. T.; Parr, R. G. *Phys. Rev. B* **1988**, *37*, 785-789.
10. Gaussian 09, Revision C.01, M. J. Frisch, G. W. Trucks, H. B. Schlegel, G. E. Scuseria, M. A. Robb, J. R. Cheeseman, G. Scalmani, V. Barone, B. Mennucci, G. A. Petersson, H. Nakatsuji, M. Caricato, X. Li, H. P. Hratchian, A. F. Izmaylov, J. Bloino, G. Zheng, J. L. Sonnenberg, M. Hada, M. Ehara, K. Toyota, R. Fukuda, J. Hasegawa, M. Ishida, T. Nakajima, Y. Honda, O. Kitao, H. Nakai, T. Vreven, J. A. Montgomery, Jr., J. E. Peralta, F. Ogliaro, M. Bearpark, J. J. Heyd, E. Brothers, K. N. Kudin, V. N. Staroverov, T. Keith, R. Kobayashi, J. Normand, K. Raghavachari, A. Rendell, J. C. Burant, S. S. Iyengar, J. Tomasi, M. Cossi, N. Rega, J. M. Millam, M. Klene, J. E. Knox, J. B. Cross, V. Bakken, C. Adamo, J. Jaramillo, R. Gomperts, R. E. Stratmann, O. Yazyev, A. J. Austin, R. Cammi, C. Pomelli, J. W. Ochterski, R. L. Martin, K. Morokuma, V. G. Zakrzewski, G. A. Voth, P. Salvador, J. J. Dannenberg, S. Dapprich, A. D. Daniels, O. Farkas, J. B. Foresman, J. V. Ortiz, J. Cioslowski, and D. J. Fox, Gaussian, Inc., Wallingford CT, 2010.
11. <http://www.chemcraftprog.com>
12. Marenich, A. V.; Cramer, C. J.; Truhlar, D. G. *J. Phys. Chem. B* **2009**, *113*, 6378-6396.
13. Schwabe, T.; Grimme, S. *Phys. Chem. Chem. Phys.* **2007**, *9*, 3397-3406.

ANNEX 3.



Supporting Information for Chapter V

Mechanistic insight in the trifluoromethylation of a well-defined aryl-Ni^{II} complex involving a SET step and a Ni^{IV}-CF₃ intermediate species

Mireia Rovira, Steven Roldán-Gómez, Vlad Martin-Diaconescu, Christopher J. Whiteoak, Anna Company, Josep M. Luis* and Xavi Ribas *

Institut de Química Computacional i Catàlisi (IQCC) and Departament de Química, Universitat de Girona, Campus de Montilivi, E-17071 Girona, Catalonia, Spain

CONTENTS

1. Materials and Methods	212
1.1 Materials and methods.....	212
1.2. Instrumentation.....	212
1.3. Synthesis of aryl-Ni ^{II} complexes.....	212
2. Crystallographic data information	216
2.1. X-Ray crystal structure of [Ni ^{II} (L ₁)](NO ₃) (1 _{NO3}).....	216
2.2. X-Ray crystal structure of [Ni ^{II} (L ₁)](ClO ₄) (1 _{ClO4}).....	217
2.3. X-Ray crystal structure of [Ni ^{II} (L ₅)](OTf) (5 _{OTf}).....	218
3. Electrochemical measurements	219
3.1. Cyclic voltammetry of [Ni ^{II} (L ₁)](OTf).....	219
3.2. Cyclic voltammetry of [Ni ^{II} (L ₅)](OTf).....	220
4. Reactivity studies of aryl-Ni complexes	220
4.1. Model C-CF ₃ bond-forming cross-coupling reactions using 1 _{OTf}	220
4.2. Model C-CF ₃ bond-forming cross-coupling reactions using 5 _{OTf}	222
4.3. Spin trapping experiments.....	223
5. XAS studies	223
5.1. Sample preparation, data acquisition and processing.....	224
5.2. XANES Analysis.....	224
5.3. EXAFS Analysis.....	224
6. Computational Studies	225
6.1. Single Electron Transfer.....	226
6.2. Supplementary Energy profiles.....	228
6.3. Trifluoromethyl radical addition to aryl-Ni ^{III} complex 6	227
6.4. Energy profiles of complex [L ₁ -H···Ni ^{II} -solv] ²⁺ (solv = H ₂ O or MeCN exogenous ligands).....	230
7. Supplementary Figures	230
8. References	245

1. Materials and Methods

1.1. Materials and methods

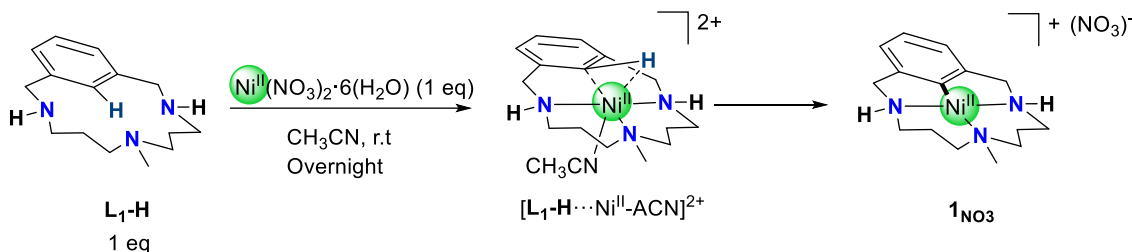
Commercially available reagents were used as received, unless otherwise noted. Solvents were purchased from SDS-Carlo Erba and Scharlab and were purified and dried by passing through an activated alumina purification system (MBraun SPS-800). Preparation and handling of air-sensitive materials was carried out in a N₂ drybox (Jacomex) with O₂ and H₂O concentrations < 1 ppm. Ligand **L₁-Br**, **L₁-H** and **L₅-Br** were synthesized following published procedures.^[1-3]

1.2. Instrumentation

NMR data were collected on a Bruker 400 or 300 AVANCE spectrometer in the corresponding deuterated solvent (CDCl₃, CD₃CN) and calibrated with either the residual protons of the solvent or added tetramethylsilane. NMR yields were calculated relative to an internal reference (1,3,5-trimethoxybenzene). High resolution mass spectra (HRMS) were recorded on a Bruker MicroTOF-Q IITM instrument using ESI or Cryospray ionization sources by Serveis Tècnics at the University of Girona.

1.3. Synthesis of aryl-Ni^{II} complexes

1.3.1 Via C-H Activation – L₁-H

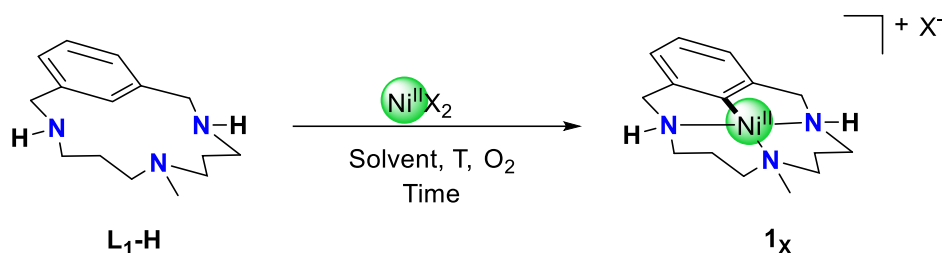


Aryl-Ni(II) complex **1_{NO3}** was prepared following a procedure described in the literature previously.^[4]

¹H NMR (400 MHz, CD₃CN, ppm), δ: 6.93 (t, ³J_H = 8.16 Hz, 1H), 6.65 (d, ³J_H = 7.75 Hz, 2H), 4.20 (bs, 2H, N-H), 4.13 (d, ²J_H = 16.51 Hz, 2H), 3.62 (dd, ²J_H = 14.96 Hz, ³J_H = 7.76 Hz, 2H), 3.00 (td, ²J_H = 12.45 Hz, ³J_H = 2.92 Hz, 2H), 2.70- 2.65 (m, 4H), 2.62 (s, 3H), 1.79- 1.73 (m, 2H) and 1.68 (dt, ²J_H = 16.76 Hz, ³J_H = 3.34 Hz, 2H)

¹³C {¹H} NMR (100 MHz, CD₃CN, ppm), δ: 152.0, 147.9, 125.2, 117.7, 62.7, 61.4, 51.1, 41.2 and 23.7.

HRMS (ESI) calcd. for C₁₅H₂₄N₃Ni⁺ [M]⁺: 304.1318; found: 304.1310.

1.3.1.1. Optimization of Reaction Conditions for the C-H Activation of L₁-H

In a 2 mL vial, macrocyclic ligand L₁-H (0.11 mmol) and Ni(X)₂ (0.11 mmol) were mixed in 1 mL of solvent. The vial was then capped and sealed. After the required reaction time the solvent was removed and the product mixture was analyzed using ¹H NMR techniques and/or ESI-HRMS-QTOF. The resulting complexes were isolated and fully characterized. Results obtained are summarized in **Table S1**.

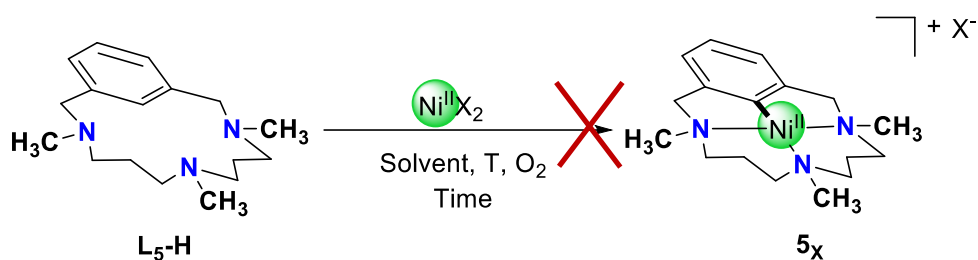
Table S1. Reaction of L₁-H with different Nickel (II) salts under different conditions.

Entry	Eq ligand	Ni salt	Eq Ni(II)	Solvent	T (°C)	Reaction time	Yield (%) ^a
1	1	Ni(NO ₃) ₂ ·6H ₂ O	1	CH ₃ CN	r.t	Overnight	55
2	1	Ni(OAc) ₂ ·4H ₂ O	1	CH ₃ CN	r.t	Overnight	<20
3	1	Ni(ClO ₄) ₂ ·6H ₂ O	1	CH ₃ CN	r.t	Overnight	aprox 50
4	1	Ni(OAc) ₂ ·4H ₂ O	1	MeOH	r.t	Overnight	<20
5	1	Ni(OAc) ₂ ·4H ₂ O	1	MeOH/ CH ₃ CN	r.t	Overnight	<20
6	1	Ni(NO ₃) ₂ ·6H ₂ O	2	CH ₃ CN	r.t	Overnight	No reaction
7	2	Ni(NO ₃) ₂ ·6H ₂ O	1	CH ₃ CN	r.t	Overnight	50
8	1	Ni(NO ₃) ₂ ·6H ₂ O	1	TFE	50	Overnight	No reaction
9	1	Ni(NO ₃) ₂ ·6H ₂ O	1	CH ₃ CN	60	Overnight	No reaction
10 ^b	1	Ni(NO ₃) ₂ ·6H ₂ O	1	CH ₃ CN	r.t	Overnight	No reaction
11 ^c	1	Ni(OAc) ₂ ·4H ₂ O	1	CH ₃ CN	r.t	Overnight	No reaction

^a Isolated yield. ^b Addition of 1 equiv of CsOAc as an additive after 1 hour from the beginning of the reaction.

^c Addition of 1 equiv of sodium benzoate as an additive.

1.3.1.2. Optimization of Reaction Conditions for the C-H Activation of L₅-H



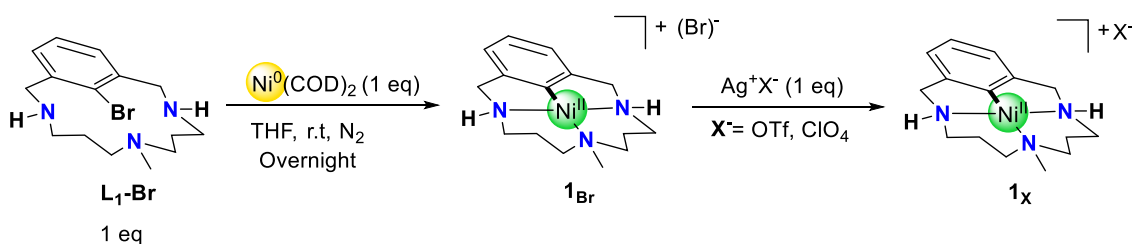
In a 2 mL vial, macrocyclic ligand L₅-H (0.11 mmol) and Ni(X)₂ (0.11 mmol) were mixed in 1 mL of solvent. The vial was capped and sealed. After the required reaction time the solvent was removed and the product mixture was analyzed using ¹H NMR and/or ESI-HRMS-QTOF. The resulting complexes were isolated and fully characterized. Results obtained are summarized in **Table S2**.

Table S2. Reaction of L₅-H with different Nickel (II) salts under different conditions.

Entry	Eq ligand	Ni salt	Eq. Ni(II)	Solvent	T	Reaction time	Yield (%)
1	1	Ni(NO ₃) ₂ ·6H ₂ O	1	CH ₃ CN	r.t	24 h	No Reaction
2	1	Ni(NO ₃) ₂ ·6H ₂ O	1	CH ₃ CN	100°C	24 h	No Reaction
3*	1	Ni(NO ₃) ₂ ·6H ₂ O	1	CH ₃ CN	80°C	24h	No Reaction
4 [‡]	1	NiBr ₂	1	THF	65°C	overnight	No Reaction

*Addition of 2 equiv of Na(OAc) as an additive. [‡] Conditions used in similar work reported by Mirica and co-workers (*J. Am. Chem. Soc.* **2016**, *138*, 5777-5780).

1.3.2 Via Oxidative addition – L₁-Br



The synthesis of aryl-Ni(II) complex **1_{OTf}** was achieved by reacting the model aryl-halide ligand L₁-Br with 1 equiv. of Ni(COD)₂ in dry THF under a N₂ atmosphere overnight, affording [Ni^{II}(L₁)]Br (**1_{Br}**, >98% yield). A counter anion exchange was performed in order to improve the solubility of the complex using 1 eq. of AgOTf or AgClO₄. This complex is benchtop stable and has been fully characterized spectroscopically and crystallographically. The structure obtained by X-ray diffraction studies of compounds **1_{OTf}** and **1_{ClO4}** shows that the Ni(II) centre is tetracoordinated

and exhibits a nearly square planar geometry, in which the aryl moiety and three amine N atoms are co-planar with the nickel centre.

• **$[\text{Ni}^{\text{II}}(\text{L}_1)]\text{OTf}$**

^1H NMR (400 MHz, CD_3CN , ppm), δ : 6.93 (t, $^3J_{\text{H}} = 7.39$ Hz, 1H), 6.64 (d, $^3J_{\text{H}} = 7.37$ Hz, 2H), 4.13 (d, $^2J_{\text{H}} = 16.60$ Hz, 2H), 4.06 (bb, 2H, N-H), 3.64 (dd, $^2J_{\text{H}} = 15.70$ Hz, $^3J_{\text{H}} = 7.63$ Hz, 2H), 3.01 (td, $^2J_{\text{H}} = 12.66$ Hz, $^3J_{\text{H}} = 7.63$ Hz, 2H), 2.71- 2.64 (m, 4H), 2.61 (s, 3H), 2.20 (ddd, $^2J_{\text{H}} = 12.76$ Hz, $^3J_{\text{H}} = 6.68$ Hz, $^4J_{\text{H}} = 2.45$ Hz, 2H) and 1.77- 1.65 (m, 4H).

^{13}C $\{^1\text{H}\}$ NMR (100 MHz, CD_3CN , ppm), δ : 152.0, 147.9, 125.3, 117.6, 62.8, 61.3, 51.2, 41.4 and 23.6.

HRMS (ESI) calcd. for $\text{C}_{15}\text{H}_{24}\text{N}_3\text{Ni}^+$ $[\text{M}]^+$: 304.1318; found: 304.1310.

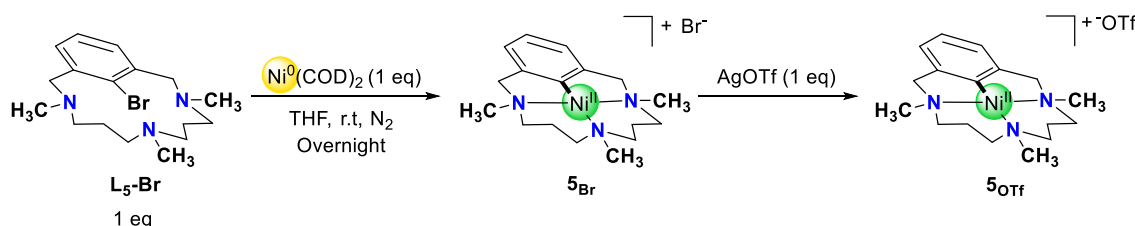
• **$[\text{Ni}^{\text{II}}(\text{L}_1)](\text{ClO}_4)$**

^1H NMR (400 MHz, CD_3CN , ppm), δ : 6.94 (t, $^3J_{\text{H}} = 7.75$ Hz, 1H), 6.66 (d, $^3J_{\text{H}} = 7.88$ Hz, 2H), 4.15 (d, $^2J_{\text{H}} = 17.42$ Hz, 2H), 4.08 (bb, 2H, N-H), 3.64 (dd, $^2J_{\text{H}} = 14.72$ Hz, $^3J_{\text{H}} = 6.62$ Hz, 2H), 3.01 (td, $^2J_{\text{H}} = 12.71$ Hz, $^3J_{\text{H}} = 2.89$ Hz, 2H), 2.69- 2.65 (m, 4H), 2.62 (s, 3H), 2.20 (ddd, $^2J_{\text{H}} = 13.18$ Hz, $^3J_{\text{H}} = 6.53$ Hz, $^4J_{\text{H}} = 2.90$ Hz, 2H) and 1.79- 1.69 (m, 4H).

^{13}C $\{^1\text{H}\}$ NMR (100 MHz, CD_3CN , ppm), δ : 147.8, 147.6, 125.3, 117.5, 62.7, 61.3, 51.1, 41.4 and 23.8.

HRMS (ESI) calcd. for $\text{C}_{15}\text{H}_{24}\text{N}_3\text{Ni}^+$ $[\text{M}]^+$: 304.1318; found: 304.1310.

1.3.3 Via Oxidative addition – $\text{L}_5\text{-Br}$



Aryl-Ni^{II} complex **5OTf** was prepared following procedures previously described, using **L₅-Br** as a model aryl-halide, affording bright yellow crystals of $[\text{Ni}^{\text{II}}(\text{L}_5)]\text{OTf}$ (**5OTf**, 80% yield).

^1H NMR (400 MHz, CD_3CN , ppm), δ : 6.99 (t, $^3J_{\text{H}} = 7.52$ Hz, 1H), 6.73 (d, $^3J_{\text{H}} = 7.52$ Hz, 1H), 6.66 (d, $^3J_{\text{H}} = 7.52$ Hz, 1H), 4.23 (dd, $^2J_{\text{H}} = 21.28$ Hz, $^2J_{\text{H}} = 14.14$ Hz, 1H), 3.90 (d, $^2J_{\text{H}} = 15.02$ Hz, 1H), 3.56 (d, $^2J_{\text{H}} = 15.63$ Hz, 1H), 3.40 (d, $^2J_{\text{H}} = 13.25$ Hz, 1H), 3.27 (t, $^2J_{\text{H}} = 13.25$ Hz, 1H), 3.24- 3.15 (m, 2H), 3.15- 3.06 (m, 4H), 2.87 (td, $^2J_{\text{H}} = 13.10$ Hz, $^3J_{\text{H}} = 3.09$ Hz, 1H), 2.62 (d, $^3J_{\text{H}} = 9.19$ Hz, 3H), 2.56 (s, 1H), 2.49 (s, 2H), 2.41- 2.26 (m, 6H) and 1.62- 1.54 (m, 2H).

^{13}C $\{^1\text{H}\}$ NMR (100 MHz, CD_3CN , ppm), δ : 152.9, 145.6, 125.6, 119.3, 74.9, 74.3, 73.5, 62.8, 62.2, 61.8, 60.9, 54.9, 52.8, 46.8, 43.5, 41.6 and 21.3.

HRMS (ESI) calcd. for $\text{C}_{17}\text{H}_{28}\text{N}_3\text{Ni}^+$ $[\text{M}]^+$: 332.1620; found: 332.1631.

2. Crystallographic data information

2.1. X-Ray crystal structure of $[\text{Ni}^{\text{II}}(\text{L}_1)](\text{NO}_3)$ (**1**_{NO3})

Yellow crystals of $\text{C}_{15}\text{H}_{24}\text{N}_3\text{NiClO}_4$, were grown by slow diffusion of ethyl ether in an acetonitrile solution of the compound, and used for low temperature (100(2) K) X-ray structure determination. The measurement was carried out on a *BRUKER SMART APEX CCD* diffractometer using graphite-monochromated $\text{Mo } K\alpha$ radiation ($\lambda = 0.71073 \text{ \AA}$) from an x-Ray Tube. The measurements were made in the range 1.631 to 27.596° for θ . Hemi-sphere data collection was carried out with ω and ϕ scans. A total of 11206 reflections were collected of which 4238 [$R(\text{int}) = 0.0523$] were unique. Programs used: data collection, Smart^[5]; data reduction, Saint+^[6]; absorption correction, SADABS^[7]. Structure solution and refinement was done using SHELXTL^[8]. The structure was solved by direct methods and refined by full-matrix least-squares methods on F^2 . The non-hydrogen atoms were refined anisotropically. The H-atoms were placed in geometrically optimized positions and forced to ride on the atom to which they are attached. Spurious electron density peaks non attributable to any solvent molecule were removed using the SQUEEZE option in PLATON^[8].

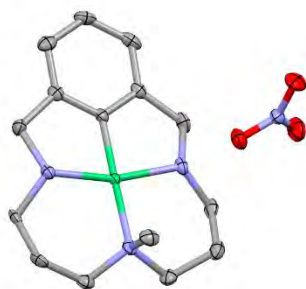


Figure S1. X-Ray crystal structure of $[\text{Ni}^{\text{II}}(\text{L}_1)](\text{NO}_3)$ (**1**_{NO3}) at 50% probability level. H atoms were omitted for clarity.

Table S3. Crystallographic parameters for $[\text{Ni}^{\text{II}}(\text{L}_1)](\text{NO}_3)$ (**1**_{NO3}) (CCDC code: 1526514)

Chemical formula	$\text{C}_{15}\text{H}_{24}\text{N}_4\text{NiO}_3$
fw (g mol⁻¹)	367.08
T (K)	100 (2)
Space group	Monoclinic, $P 2_1/c$
a (Å)	10.806(2)
b (Å)	15.026(3)
c (Å)	10.763(2)
α (deg.)	90
β (deg.)	114.601(3)
γ (deg.)	90
V (Å³)	1588.97(15)
$\rho_{\text{calcd.}}$ (g cm⁻³)	1.549

λ (Å)	0.71073
R_1 [$I > 2\sigma(I)$]	0.0330
wR_2 [$I > 2\sigma(I)$]	0.0887

2.2. X-Ray crystal structure of $[\text{Ni}^{\text{II}}(\text{L}_1)](\text{ClO}_4)$ (1_{ClO_4})

Yellow crystals of $\text{C}_{15}\text{H}_{24}\text{N}_3\text{NiClO}_4$, were grown by slow diffusion of ethyl ether in an acetonitrile solution of the compound, and used for low temperature (100(2) K) X-ray structure determination. The measurement was carried out on a *BRUKER SMART APEX CCD* diffractometer using graphite-monochromated $\text{Mo } K\alpha$ radiation ($\lambda = 0.71073$ Å) from an x-Ray Tube. The measurements were made in the range 1.631 to 27.596° for θ . Hemi-sphere data collection was carried out with ω and ϕ scans. A total of 11206 reflections were collected of which 4238 [$R(\text{int}) = 0.0523$] were unique. Programs used: data collection, Smart^[5]; data reduction, Saint+^[6]; absorption correction, SADABS^[7]. Structure solution and refinement was done using SHELXTL^[8]. The structure was solved by direct methods and refined by full-matrix least-squares methods on F^2 . The non-hydrogen atoms were refined anisotropically. The H-atoms were placed in geometrically optimized positions and forced to ride on the atom to which they are attached. Spurious electron density peaks non attributable to any solvent molecule were removed using the SQUEEZE option in PLATON^[8].

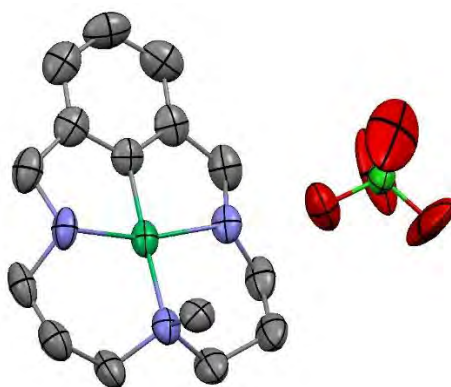


Figure S2. X-Ray crystal structure of $[\text{Ni}^{\text{II}}(\text{L}_1)](\text{ClO}_4)$ (1_{ClO_4}) at 50% probability level. H atoms omitted for clarity.

Table S4. Crystallographic parameters for $[\text{Ni}^{\text{II}}(\text{L}_1)](\text{ClO}_4)$ (1_{ClO_4}) (CCDC code 1526515)

Chemical formula	$\text{C}_{15}\text{H}_{24}\text{N}_3\text{NiClO}_4$
fw (g mol⁻¹)	404.53
T (K)	100 (2)
Space group	Monoclinic, C 2/c
a (Å)	22.827(5)
b (Å)	14.924(4)

c (Å)	10.947(3)
α (deg.)	90
β (deg.)	92.888(5)
γ (deg.)	90
V (Å³)	3724.7(15)
ρ_{calcd.} (g cm⁻³)	1.443
λ (Å)	0.71073
R₁ [I>2σ(I)]	0.0633
wR₂ [I>2σ(I)]	0.1337

2.3. X-Ray crystal structure of [Ni^{II}(L₅)](OTf) (**5_{OTf}**)

Yellow crystals of **C₁₈H₂₈F₃N₃NiO₃S**, were grown from slow diffusion of ethyl ether in an acetonitrile solution of the compound, and used for low temperature (100(2) K) X-ray structure determination. The measurement was carried out on a *BRUKER SMART APEX CCD* diffractometer using graphite-monochromated Mo *Kα* radiation (λ = 0.71073 Å) from an x-Ray Tube. The measurements were made in the range 1.656 to 26.979° for θ . Hemi-sphere data collection was carried out with ω and ϕ scans. A total of 6534 reflections were collected of which 4152 [R(int) = 0.0270] were unique. Programs used: data collection, Smart^[5]; data reduction, Saint⁺^[6]; absorption correction, SADABS^[7]. Structure solution and refinement was done using SHELXTL^[8].

The structure was solved by direct methods and refined by full-matrix least-squares methods on F^[6]. The non-hydrogen atoms were refined anisotropically. The H-atoms were placed in geometrically optimized positions and forced to ride on the atom to which they are attached. The structure was refined as a 2-component inversion twin.

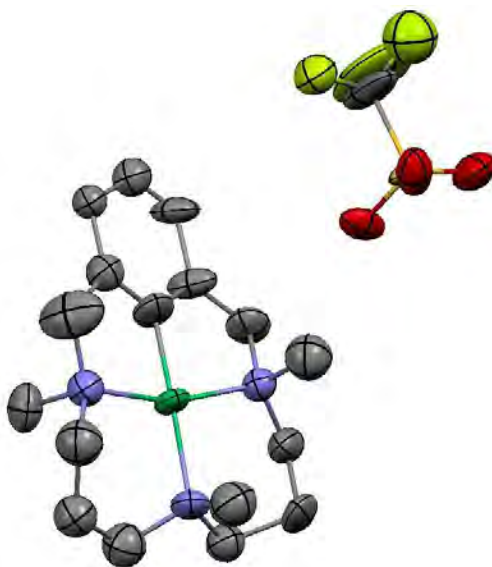


Figure S3. X-Ray crystal structure of [Ni^{II}(L₅)](OTf) (**5_{OTf}**) at 50% probability level. H atoms omitted for clarity.

Table S5. Crystallographic parameters for $[\text{Ni}^{\text{II}}(\text{L}_5)](\text{OTf})$ (**5_{OTf}**) (CCDC code 1526516)

Chemical formula	$\text{C}_{18}\text{H}_{28}\text{F}_3\text{N}_3\text{NiO}_3\text{S}$
fw (g mol⁻¹)	482.20
T (K)	100 (2)
Space group	Monoclinic, P21
a (Å)	9.287(3)
b (Å)	8.926(3)
c (Å)	12.462(4)
α (deg.)	90
β (deg.)	99.363(5)
γ (deg.)	90
V (Å³)	1019.4(5)
ρ_{calcd.} (g cm⁻³)	1.571
λ (Å)	0.71073
R₁ [I > 2σ(I)]	0.0627
wR₂ [I > 2σ(I)]	0.1487

3. Electrochemical measurements

Electrochemical grade *n*-Bu₄NPF₆ was used as the supporting electrolyte. Cyclic voltammetry measurements were carried out in a glovebox under an inert atmosphere in a one-compartment cell using a CH Instruments electrochemical analyzer. A glassy carbon electrode and platinum wire were used as the working and auxiliary electrodes, respectively. The pseudo reference electrode was an Ag/AgNO₃ wire.

3.1. Cyclic voltammetry (versus Ag/AgNO₃) of **1_{OTf}**

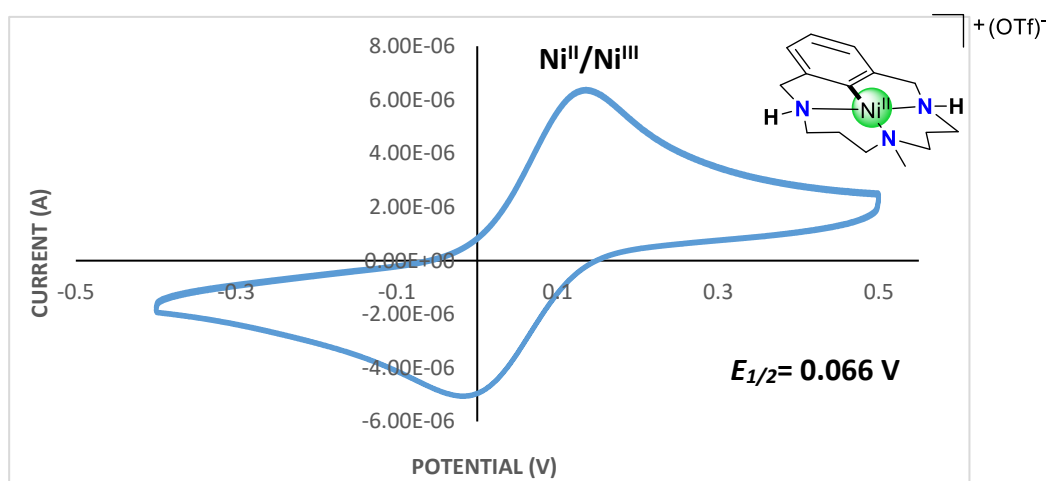


Figure S4. Cyclic Voltammogram of complex $[\text{Ni}^{\text{II}}(\text{L}_1)](\text{OTf})$ = 0.5 mM, $[n\text{-Bu}_4\text{NPF}_6]$ = 0.1 M, CH₃CN, 298 K, scan rate = 0.1 V/s, using non-aqueous Ag/AgNO₃ reference electrode.

3.2. Cyclic voltammetry (versus Ag/AgNO₃) of 5_{OTf}

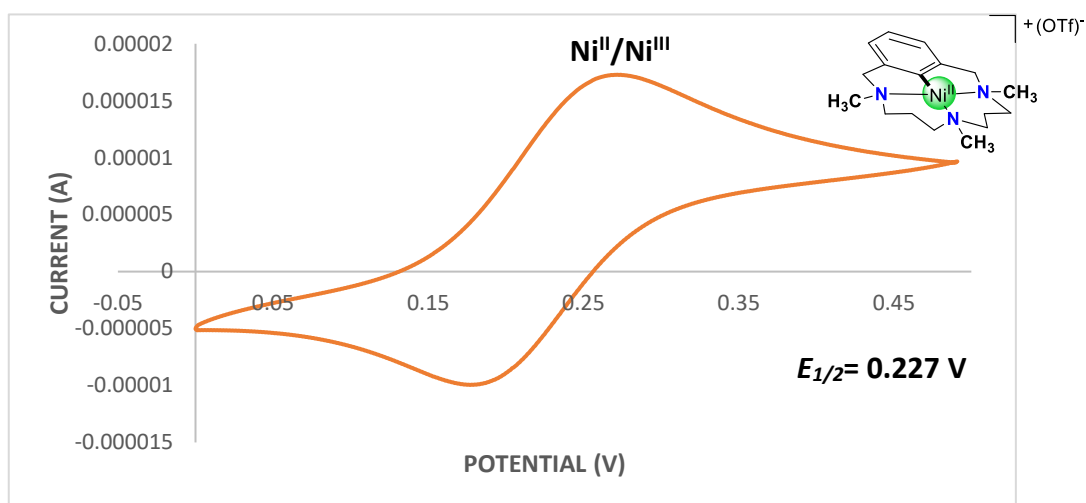
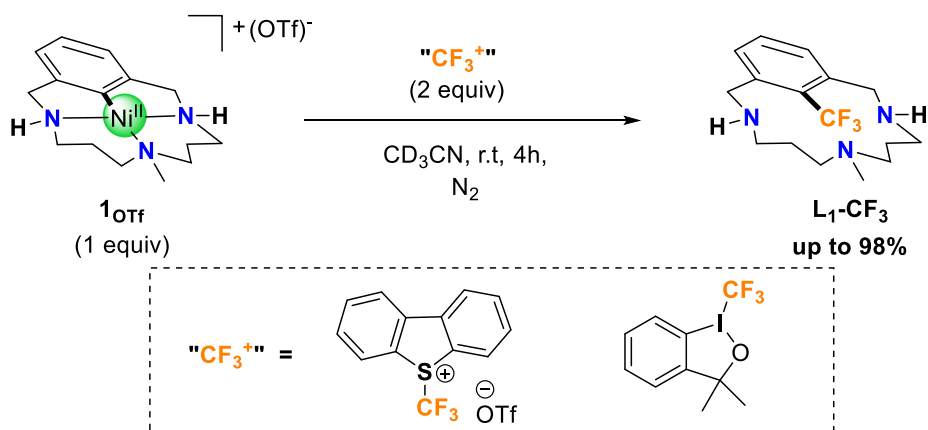


Figure S5. Cyclic Voltammogram of complex $[[\text{Ni}^{\text{II}}(\text{L}_5)](\text{OTf})] = 1 \text{ mM}$, $[\textit{n}\text{-Bu}_4\text{NPF}_6] = 0.1 \text{ M}$, CH_3CN , 298 K, scan rate = 0.1 V/s, using non-aqueous Ag/AgNO₃ reference electrode.

4. Reactivity studies of Ni complexes

4.1 Model C–CF₃ bond-forming cross-coupling reactions using 1_{OTf}



A screw cap NMR tube was charged with $[\text{Ni}^{\text{II}}(\text{L}_1)](\text{OTf})$ (**1_{OTf}**) complex (8 mg, 0.0176 mmol, 1 equiv) in 0.3 ml CD_3CN , a solution of 5-(Trifluoromethyl)dibenzothiophenium trifluoromethanesulfonate (TDTT) (14.6 mg, 0.035 mmol, 2 eq.) in 0.3 ml CD_3CN was subsequently added at room temperature, and the reaction remained light yellow. In a separate experiment, the hypervalent iodine reagent, 3,3-Dimethyl-1-(trifluoromethyl)-1,2-benziodoxole (12.2 mg, 0.035 mmol, 2 eq.) were added to $[\text{Ni}^{\text{II}}(\text{L}_1)](\text{OTf})$ complexes in CD_3CN at room temperature for 12 hours. Under these conditions, the yellow solution turned orange. ^1H NMR spectroscopic analyses of the crude reaction mixtures were consistent with the formation of the trifluoromethylated product in more than 99% of yield.

^1H NMR (400 MHz, CDCl_3 , ppm) δ 7.33 (t, $^3J_{\text{H}} = 7.60$ Hz, 1H, H^{a}), 7.21 (d, $^3J_{\text{H}} = 7.44$ Hz, 2H, H^{b}), 4.61 (d, $^2J_{\text{H}} = 14.24$ Hz, 2H, H^{c} or H^{d}), 3.55 (d, $^2J_{\text{H}} = 14.33$ Hz, 2H, H^{c} or H^{d}), 2.39- 2.24 (m, 6H, H^{e} , H^{f} and H^{i} or H^{j}), 1.94 (dt, $^2J_{\text{H}} = 12.40$ Hz, $^3J_{\text{H}} = 5.11$ Hz, 2H, H^{i} or H^{j}), 1.86 (s, 3H, H^{k}) and 1.38- 1.29 (m, 4H, H^{g} or H^{h}).

^{13}C $\{^1\text{H}\}$ NMR (100 MHz, CDCl_3 , ppm) δ 142.4 (C3), 131.6 (C2 and C4), 130.0 (C1), 127.3 (CF_3), 55.1 (C8), 53.9 (C5), 44.3 (C6), 40.3 (C9) and 27.4 (C7)

^{19}F $\{^1\text{H}\}$ NMR (282.4 MHz, CDCl_3 , ppm) δ -53.2 ppm

HRMS (ESI) calcd. for $\text{C}_{16}\text{H}_{24}\text{N}_3\text{F}_3^+$ $[\text{M}]^+$: 316.1995; found: 316.2007.

Monitoring of the Crude Reaction Mixture by ^1H NMR Spectroscopy at Low Temperature

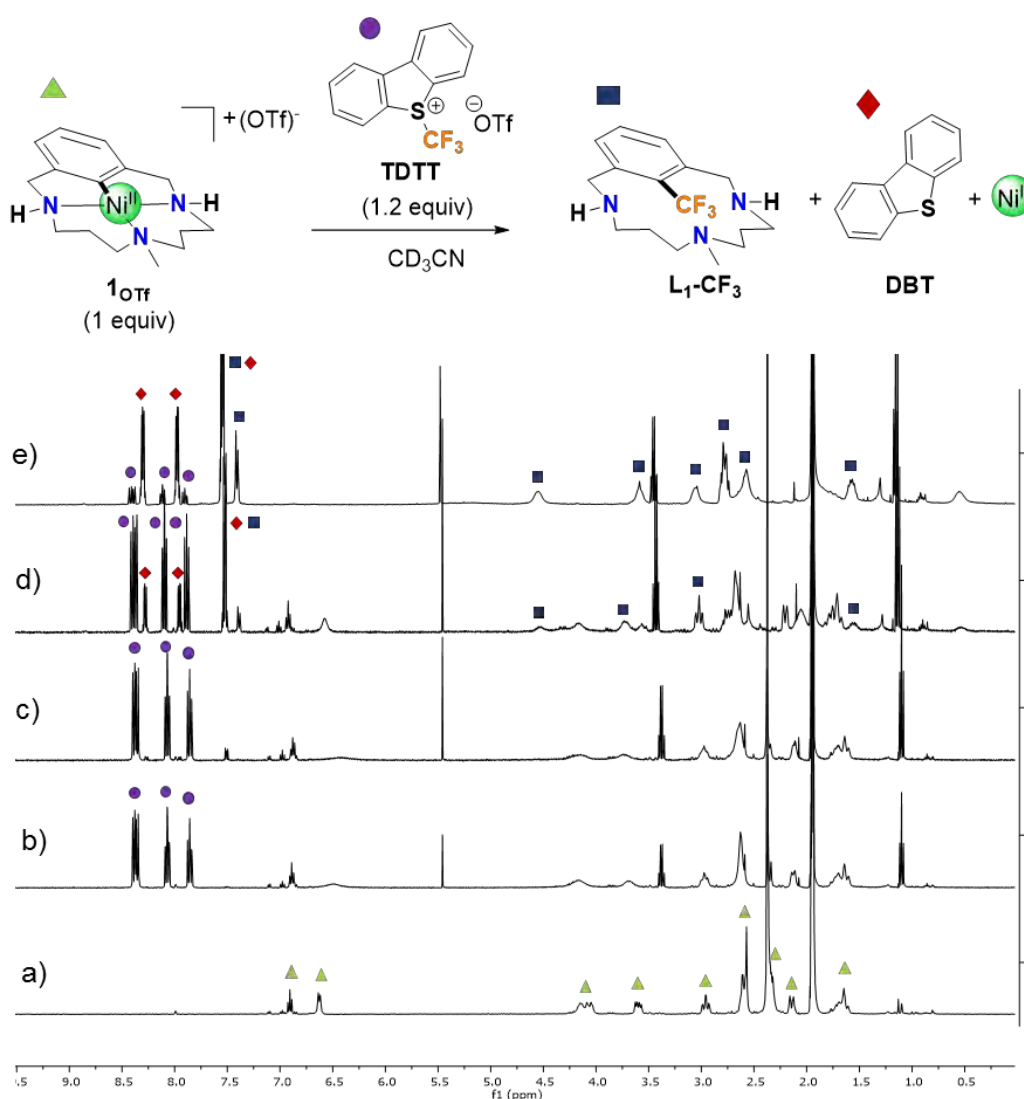
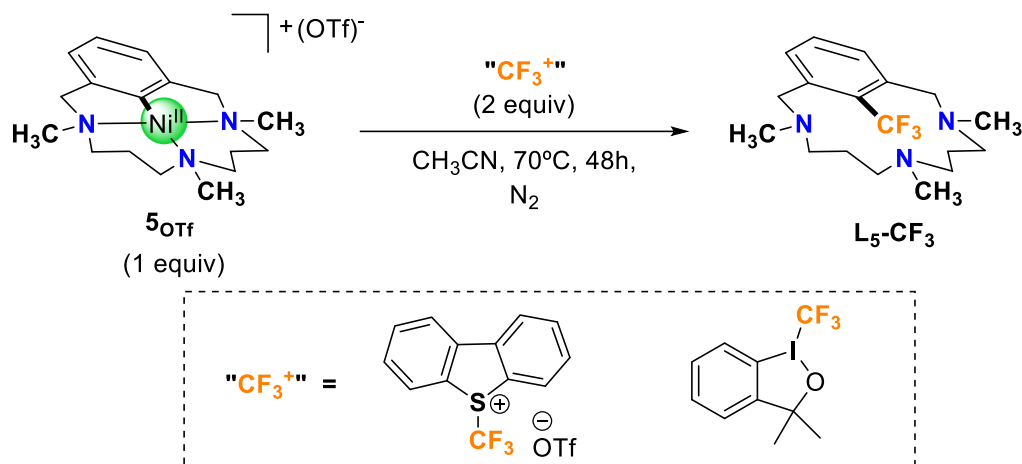


Figure S6. Reaction progress of the formation of trifluoromethylated compound and consumption of 1_{OTf} complex monitored by ^1H NMR spectroscopy at low temperature in CD_3CN . Compounds 1_{OTf} complex, TDDT, trifluoromethylated compound and the byproduct of the oxidant,

dibenzothiophene, are marked. (a) complex **1_{OTf}** at -40°C; (b) Reaction crude, 45 min, -40°C; (c) 1.45 h, 0°C; (d) 4.45 h, 0°C and (e) Overnight, 0°C.

4.2 Model C–CF₃ bond-forming cross-coupling reactions using **5_{OTf}**



A screw cap NMR tube was charged with [Ni^{II}(L₅)](OTf) (**5_{OTf}**) complex (8 mg, 0.0166 mmol, 1 equiv) in 0.3 ml CD₃CN, a solution of 5-(Trifluoromethyl)dibenzothiophenium trifluoromethanesulfonate (TDTT) (13.8 mg, 0.033 mmol, 2 eq.) in 0.3 ml CD₃CN was subsequently added at 70°C for 48h, and the reaction remained light yellow. In a separate experiment, the hypervalent iodine reagent, 3,3-Dimethyl-1-(trifluoromethyl)-1,2-benziodoxole (11.5 mg, 0.033 mmol, 2 eq.) was added to [Ni^{II}(L₅)](OTf) complexes in CD₃CN at 70°C for 48 hours. Under these conditions, the yellow solution turned to orange. ¹HNMR spectroscopic analyses of the crude reaction mixtures were consistent with the formation of the trifluoromethylated product in more than 99% of yield.

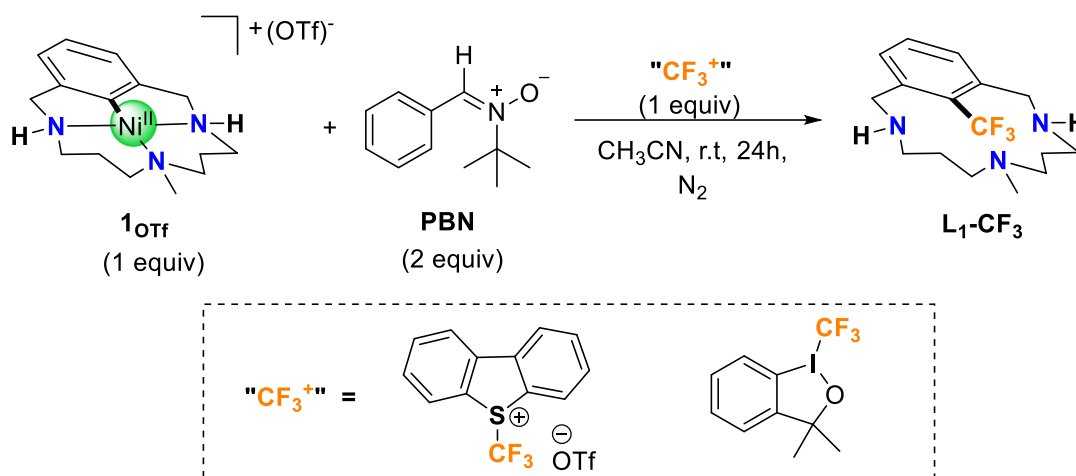
¹H NMR (400 MHz, CDCl₃, ppm) δ 7.27 (s, 3H, H^a and H^b), 4.11 (d, ²J_H = 13.13 Hz, 2H, H^c or H^d), 3.19 (d, ²J_H = 13.13 Hz, 2H, H^c or H^d), 2.35 (s, 6H, Hⁱ), 2.31- 2.21 (m, 5H, H^e, H^f and Hⁱ or H^j), 1.89 (s, 3H, H^k), 1.37- 1.28 (m, 4H, Hⁱ and H^j and H^g or H^h) and 0.92- 0.80 (m, 3H, H^g and H^h).

¹³C {¹H} NMR (100 MHz, CDCl₃, ppm) δ 140.4 (C3), 132.6 (C1 and C2), 131.9 (C4), 129.5 (CF₃), 62.4 (C5), 53.8 (C9), 53.6 (C6), 44.6 (C10), 29.9 (C7) and 20.6 (C8).

¹⁹F {¹H} NMR (282.4 MHz, CDCl₃, ppm) δ -53.8 ppm.

HRMS (ESI) calcd. for C₁₈H₂₈N₃F₃⁺ [M]⁺: 344.2308; found: 344.2318.

4.3. Spin trapping experiments



In an inert-atmosphere glove box, a sample of the $[\text{Ni}^{\text{II}}(\text{L}_1)](\text{OTf})$ complex (5 mg, 0.01 mmol, 1 eq.) were dissolved in 100 μL of degassed $\text{d}^6\text{-DMSO}$ and 100 μL of a solution of 1,3,5-trimethoxybenzene was added as an internal standard, a solution of 5-(Trifluoromethyl)dibenzothiophenium trifluoromethanesulfonate (TDTT) (4.6 mg, 0.01 mmol, 1 eq.) in 0.3 mL of $\text{d}^6\text{-DMSO}$ was subsequently added at room temperature. After few seconds stirring a solution of the spin trap *N*-tert-butyl- α -phenylnitron (BPN) (3.9 mg, 0.02 mmol, 2 equiv) in 0.2 mL $\text{d}^6\text{-DMSO}$ was added. In a separate experiment, the hypervalent iodine reagent, 3,3-Dimethyl-1-(trifluoromethyl)-1,2-benziodoxole (3.9 mg, 0.01 mmol, 1 eq.) were used as a trifluoromethyl source. Under these conditions, the yellow solutions turned to orange. After 24 hours, ^1H NMR spectroscopic analyses of the crude mixture was consistent with the absence of radical intermediates in the product formation. Products yields were determined by integration of the corresponding ^1H NMR peaks relative to the internal standard.

5. XAS studies

5.1. Sample preparation, data acquisition and processing

A 10 mM solution sample of $[\text{L}_1\text{-H--Ni}^{\text{II}}]^{+2}$ was prepared in butyronitrile by mixing 1 eq. of nickel (II) perchlorate with $\text{L}_1\text{-H}$ and immediately freezing the mixture upon loading into a sample cell. Similarly a 10mM solution of the 1_{NO_3} was formed by reacting two eq. of the $\text{L}_1\text{-H}$ with 1 eq. of nickel(II) nitrate in acetonitrile. The reaction was stirred overnight and then filtered. A solid sample was also obtained by slow diffusion of diethyl ether into the filtrate. The 1_{ClO_4} was formed by reaction of 1 eq. of $\text{L}_1\text{-Br}$ with 1 eq. of $\text{Ni}(0)(\text{COD})_2$. The precipitate was collected and suspended in dichloromethane with 1 eq. of silver (I) perchlorate. The solution was filtered and the solvent removed from the filtrate to yield an off-yellow powder which was recrystallized from acetonitrile:diethyl ether.

Solution samples of $[L_1-H--Ni^{II}]^{+2}$ and 1_{NO_3} were run on the XAFS beamline at Elettra Sincrotrone Trieste equipped with a Si(111) double crystal monochromator. Solution data was collected in fluorescence mode and samples were kept at ~90 K using a liquid nitrogen finger dewar. Solid samples of 1_{NO_3} and 1_{ClO_4} were diluted in boron nitride and were run at the ALBA synchrotron, CLAESS beamline, equipped with a Si(111) double crystal monochromator. A liquid nitrogen flow cryostat was again used to maintain samples at liquid nitrogen temperatures and data was collected in transmission mode.

Background subtraction and normalization was carried out using the Athena software package.^[9] The energies were calibrated to the first inflection point of Ni foil taken as 8331.6 eV. EXAFS were extracted using the AUTOBK algorithm having a spline with a k range of 1 to 12.5 \AA^{-1} and a R_{bkg} value of 1.1 \AA . EXAFS analysis was carried out with the Artemis software program employing the IFFEFIT engine and the FEFF6 code.^[9-11] Fits were carried out on k^2 -weighted data in r-space using a Hannings window ($dk=2$), with the S_0^2 value set to 0.9, and a global ΔE_0 with the initial E_0 value set to the inflection point of the rising edge. As previously described, single and multiple scattering paths were fit in terms of a Δr_{eff} and σ^2 and to assess the goodness of the fits the R_{factor} (%R) was minimized.^[12,13]

5.2. XANES Analysis

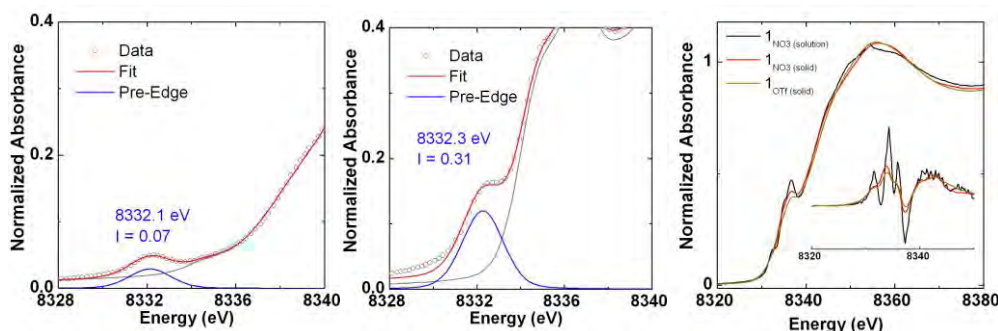


Figure S7: (left) $[L_1-H--Ni^{II}]^{+2}$ XANES pre-edge fit; (center) 1_{NO_3} in acetonitrile solution XANES pre-edge fit; (right) comparison of solid and solution samples of 1_{NO_3} and 1_{OTf} .

5.3. EXAFS Analysis

Table S6: EXAFS fits carried out in r-space with a Hanning window (dk 2), a k -weight = 2 and $S_0^2 = 0.9$. Bond distances and disorder parameters (Δr_{eff} and σ^2) were allowed to float having initial values of 0.0 \AA and 0.003 \AA^2 respectively (σ^2 reported as $\times 10^3 \text{\AA}^2$).

$[L_1-H--Ni^{II}]^{+2}$ series

MODEL	k-range	r-range	Var.	%R _{FACTOR}	DE ₀	Ni-N/C		Ni-C/N		Ni-C/N		Ni-C/N		Ni-N/C-N/C-Ni		Ni-N/C-N/C-Ni		Ni-C/N		Ni-N/C-N/C-Ni						
						N	r(Å)	S ²⁰	N	r(Å)	S ²⁰	N	r(Å)	S ²⁰	N	r(Å)	S ²⁰	N	r(Å)	S ²⁰	N	r(Å)	S ²⁰	N	r(Å)	S ²⁰
[L ₁ -H-Ni ^{II}] ⁺²	2-12.0	1-3.2	4	4.967	0	4	2.09(1)	1(1)	1	2.28(2)	1(1)	2	2.75(2)	1(1)	6	3.14(3)	1(1)	3	3.32(3)	1(1)	4	3.40(3)	1(1)	12	3.47(3)	1(1)
	2-12.0	1-3.2	4	4.100	0	4.5	2.09(1)	2(1)	1	2.29(2)	2(1)	2	2.77(2)	2(1)	6	3.14(3)	2(1)	3	3.31(3)	2(1)	4	3.40(3)	2(1)	12	3.47(3)	2(1)
	2-12.0	1-3.2	4	4.124	0	5	2.09(1)	2(1)	1	2.31(2)	2(1)	2	2.78(2)	2(1)	6	3.14(3)	2(1)	3	3.31(3)	2(1)	4	3.39(3)	2(1)	2	3.42(3)	2(1)

Ni-aryl series

MODEL	k-range	r-range	Var.	%R _{ACTOR}	DE ₀	Ni-N/C		Ni-C/N		Ni-C/N		Ni-C/N		Ni-N/C-N/C-Ni		Ni-N/C-N/C-Ni		Ni-C/N	
						N	r(Å) S ^{2o}	N	r(Å) S ^{2o}	N	r(Å) S ^{2o}	N	r(Å) S ^{2o}	N	r(Å) S ^{2o}	N	r(Å) S ^{2o}	N	r(Å) S ^{2o}
1 _{NO3} (solution)	2-11.0	1-3.0	4	4.406	-3.2(1.4)	3	1.97(2) 6(1)	1	1.79(2) 3(2)	2	2.75(2) 3(2)	4	2.89(2) 6(1)	4	2.97(2) 3(2)	8	3.18(2) 6(1)	2	3.33(2) 6(1)
1 _{NO3} (solid)	2-12.0	1-3.2	5	3.208	-3.5(1.1)	3	1.96(2) 6(1)	1	1.83(2) 6(1)	2	2.79(1) 5(2)	4	2.89(1) 5(2)	4	3.00(1) 5(2)	8	3.18(1) 5(2)	2	3.34(1) 5(2)
1 _{OTf} (solid)	2.12.0	1-3.2	5	2.729	-3.8(1.1)	3	1.97(2) 5(1)	1	1.83(2) 5(1)	2	2.79(1) 5(2)	4	2.90(1) 5(2)	4	3.01(1) 5(2)	8	3.19(1) 5(2)	2	3.34(1) 5(2)

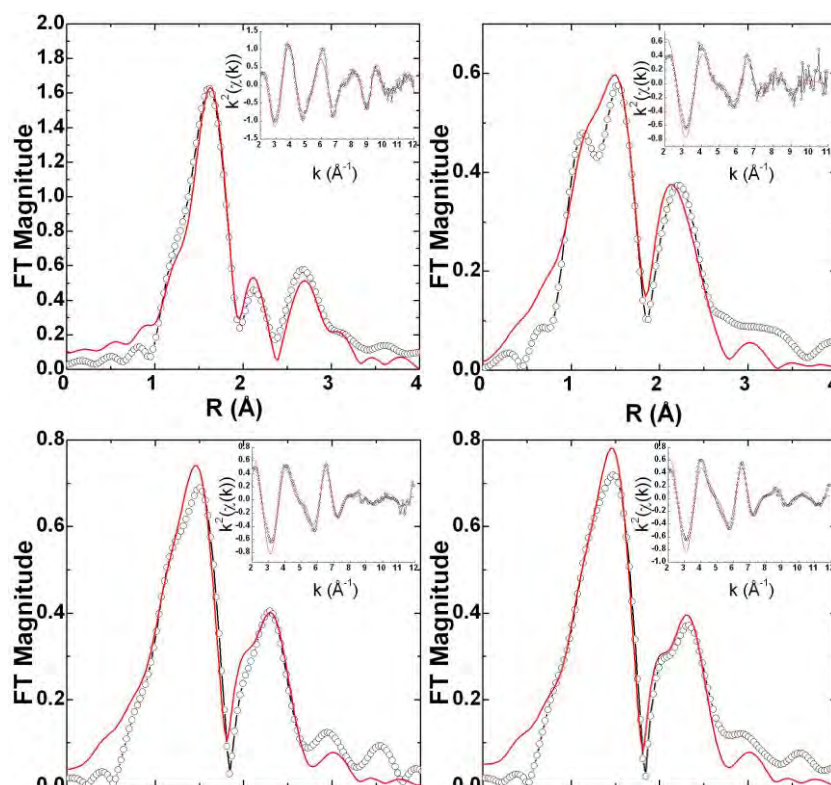


Figure S8: Fourier-transformed EXAFS spectra (no phase correction, FT, window as shown in the inset); Inset: k^2 -weighted unfiltered EXAFS spectra. (top left) 10 mM $[L_1-H--Ni^{II}]^{+2}$; (top right) 10 mM 1_{NO3} (bottom left) 1_{NO3} solid in boron nitride matrix; (bottom right) 1_{OTf} solid in boron nitride matrix.

6. Computational Studies

All calculations of the mechanism A, B, and C (**Scheme 4** main text) were performed with Gaussian 09 program.^[14] Geometry optimizations were obtained using the Becke three-parameter functional with the Becke 88 exchange functional and the Lee, Yang, and Parr correlation functional (B3LYP)^[15-18] along with the **TZPV** basis set developed by Ahlrichs^[19-20]. The empirical dispersion was described using the D3 version of Grimme's model with Becke-Johnson damping algorithm (**GD3BJ**)^[21] approach and the solvation effects in **Acetonitrile** were simulated using PCM-SMD method developed by Truhlar *et al*^[22]. Subsequent frequency calculations at the same level of theory were performed to evaluate enthalpy and entropy and entropy corrections at 298.15 K (**G_{corr.}**) and ensured that all local minima had only real frequencies while a single imaginary frequency confirmed the presence of transition states. All the transition states were connected to the corresponding reactants and products with IRC calculations. Finally, single point energy

calculations were done with a more flexible basis set, **cc-pVTZ**^[23,24], including also the solvent effects and GD3BJ dispersion corrections (**E_{cc-pVTZ}**).

The change of conventional 1 atm standard state for gas-phase calculations to a standard-state gas-phase concentration of 1.0 M requires the introduction of a concentration-change term of 1.89 kcal/mol at 298.15 K, $\Delta G^{o/*}$. Then, the final total Gibbs free energy (G) was given by:

$$G = E_{cc-pVTZ} + G_{corr.} + \Delta G^{o/*} \quad (\text{Equation S1})$$

6.1. Single Electron Transfer

For the single electron transfer (SET) processes, the free energy barrier (ΔG_{SET}) was calculated with the formalism of the Marcus approximation (commonly known as Marcus Theory for Single electron transfer)^[25-27], in which the barrier is defined by the Gibbs Energy of the redox reaction (ΔG_{redox}) and the reorganization energy (λ) with the expression:

$$\Delta G_{SET} = \frac{(\Delta G_{redox} + \lambda)^2}{4\lambda}, \quad \lambda = \lambda_{is} + \lambda_{os}$$

Where λ describes the sum of the inner sphere reorganization energy (λ_{is}) and the outer sphere reorganization energy (λ_{os}). The former (λ_{is}) describes the contribution due to the slight geometrical change of the molecules when the electronic states change, *i.e.*, the energy to reorganize the geometry caused by the electron transfer; And the latter (λ_{os}) corresponds to the energy require to rearrange the surrounding solvent molecules of the system.

We can calculate λ_{is} as the total reorganization energy for products(λ_{isP}) and reactants(λ_{isR}).

$$\lambda_{is} = (\lambda_{isP} + \lambda_{isR})/2$$

Then, these energies can be computed as the energy difference between the ground state products with reactants' geometry ($E(PRO)_R$) and the ground state products at their optimized geometry ($E(PRO)_{OPT}$), and the energy difference between the ground state reactants with product's geometry ($E(RE)_P$) and the ground state reactants at their optimized geometry ($E(RE)_{OPT}$). In Figure S9 this approach is shown in a clearer way.

$$\begin{aligned} \lambda_{isP} &= E(PRO)_R - E(PRO)_{OPT} \\ \lambda_{isR} &= E(RE)_P - E(RE)_{OPT} \end{aligned}$$

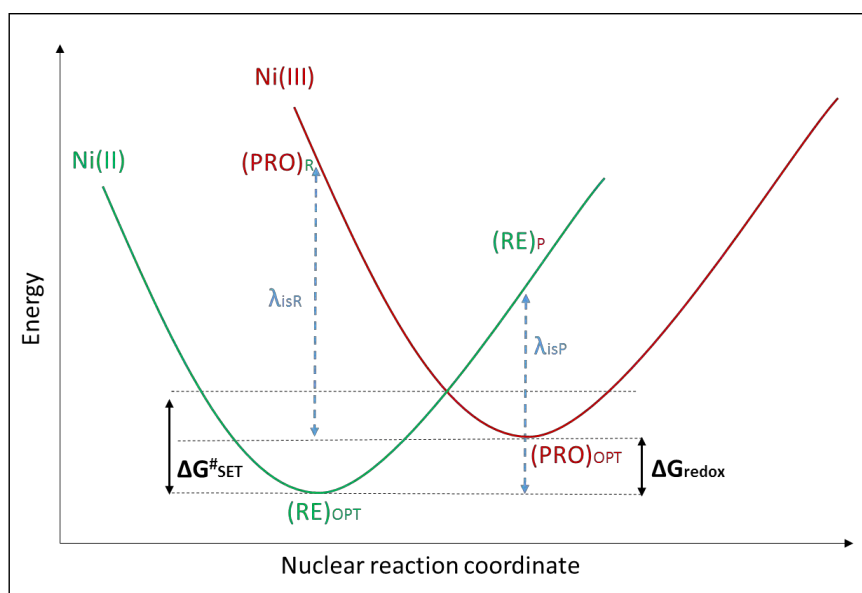


Figure S9. The plot illustrates the Marcus approach to calculate the inner sphere reorganization energy. It shows a typical electron transfer free-energy profile for reactants and products within the Marcus model of two spheres, being $\Delta G^{\#}_{\text{SET}}$ the Marcus barrier.

In the other hand, the expression to describe λ_{os} in a continuum solvent models is as follows:

$$\lambda_{os} = (\Delta q)^2 \left(\frac{1}{2r_1} + \frac{1}{2r_2} - \frac{1}{R} \right) \left(\frac{1}{D_{op}} - \frac{1}{\epsilon_s} \right)$$

Where Δq is the charge transferred, r_1 and r_2 are the radii of the reactant molecules, R is the radius of the reactant adduct, and D_{op} and ϵ_s are the static and optical dielectric constants of the solvent. The radii are computed from the sphere that corresponds to the molecular volume defined as the volume inside a contour of 0.001 electrons/Bohr³ density.

6.2 Supplementary Energy profile

The Gibbs free energy profile for the mechanism **A** computed at B3LYP/cc-pVTZ//B3LYP/TZPV level is described in the Figure S10. We compared the free energies of all the species at infinite distance with their respective adduct complexes with TDT⁺(S-(Trifluoromethyl)dibenzothiophenium) or DBT (Dibenzothiophene) and selected the most stable species. The Energy profile of the mechanism **B** is not shown due to the trifluoromethyl radical preference for the Nickel(III).

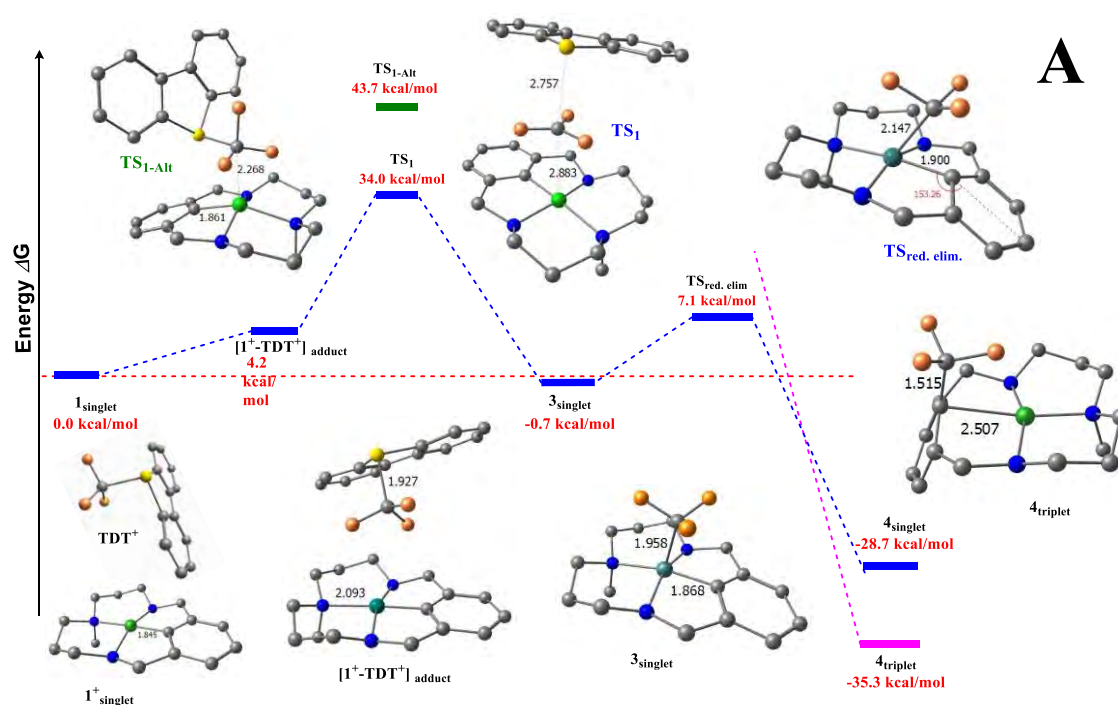


Figure S10: Free energy profile for the proposed mechanism **A** computed at B3LYP/cc-pVTZ//B3LYP/TZPV level. TS₁ and TS_{1-Alt} correspond to the two plausible transition states that connects the Ni (II) and Ni (IV) species through an oxidative addition-like step. The former represents an S_N2-like attack between the species, while the latter describes a sort-of-lateral attack. TS₂ is the transition state of the reductive elimination final step of the pathway A. **Blue** lines represent the singlet state pathway, whereas **magenta** ones describe the triplet profile. Atomic color code: **Carbon**, **Nitrogen**, **Fluorine**, **Sulphur**; In the case of Nickel, different colors are assigned to different oxidation states: **Nickel (II)**, **Nickel (IV)**.

6.3. Trifluoromethyl radical addition to aryl-Ni^{III} complex 6

Using IRC calculations at B3LYP-GD3BJ/TZPV level, we were able to explore the PES of the CF₃· addition to the nickel complex to find the lowest energy barrier for the radical attack. As we stated in the paper, our initial guess was that the most vulnerable position could be the aromatic carbon bonded to the Ni center. However, after a thorough search we found that the CF₃· attack occurs at the Ni itself in a barrierless way (see Figure S10). Some snapshots of these IRCs were taken to illustrate how the attack is on the Ni. Even if ·CF₃ is placed over the aromatic carbon as starting point of the IRC calculation (see Figure S10B), the CF₃· pass close over the aromatic carbon and attack the metal. During the pathway, we used the spin density as an indicator of the radical character of the ·CF₃ species.

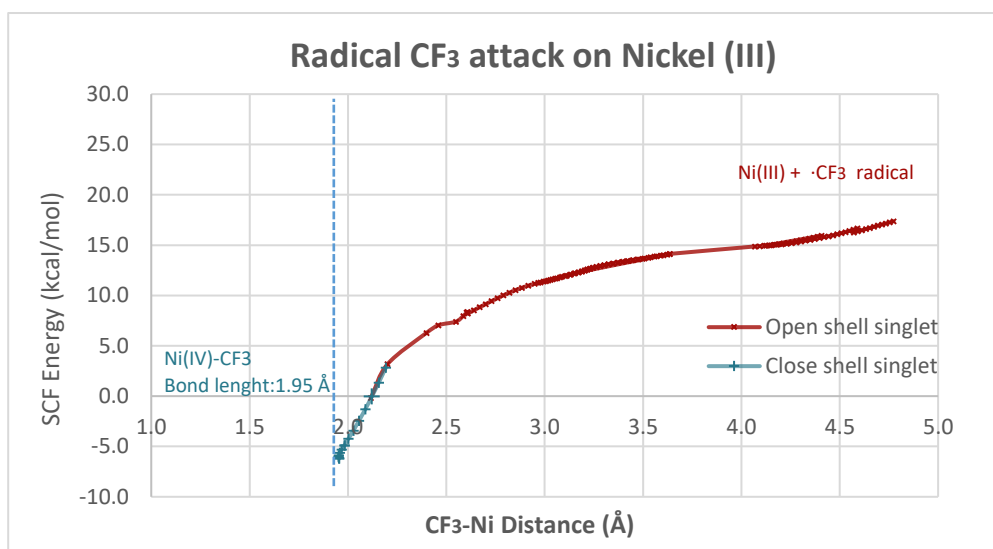
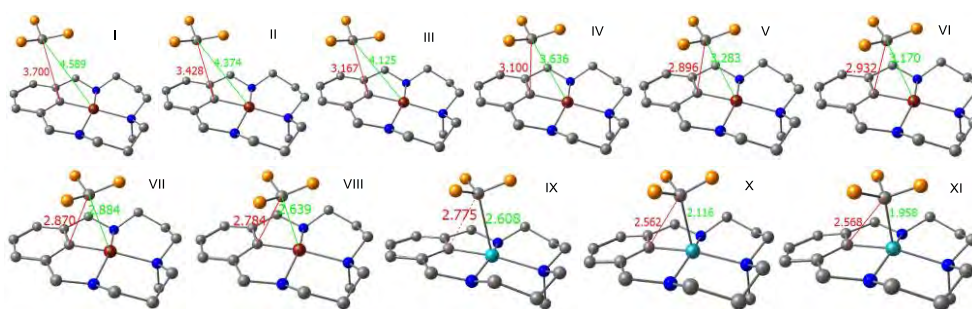
A**B**

Figure S11. Energy profile computed at B3LYP-GD3BJ/TZPV level and snapshots sequence of the CF₃· attack to the Ni^{III} to generate Ni^{IV}-CF₃. The plot **A** shows the electronic energy profile of the barrierless approach of the radical to the Ni^{III}. The spin density allowed us to locate the bond distance at which the Ni^{IV}-CF₃ can be formally considered initially formed (no spin density on the CF₃). The sequence of IRC snapshots in scheme **B** illustrates the attack on the Nickel center. Color code: Carbon, Nitrogen, Fluorine, Sulphur; In the case of Nickel, different colors are assigned to different oxidation states: Ni^{III}, Ni^{IV}.

6.4 Comparative Energy profiles of complex $[L_1-H-Ni^{II}-solv]^{2+}$ (solv = H_2O or MeCN exogenous ligands)

Table S7. The Gibbs free energies of $[L_1-H-Ni^{II}-solv]^{+2}$ having either a water exogenous ligand ($[L_1-H-Ni^{II}-H_2O]^{+2}$) or an acetonitrile ligand ($[L_1-H-Ni^{II}-MeCN]^{+2}$) were investigated and it was found that ligation of the Ni center by acetonitrile (MeCN) is favored.

uB3LYP/ TZPV	Electronic Energy (a.u)	Gibbs (a.u.) ^{a)}
Acetonitrile (MeCN)	-132.821896	-132.793964
Water (H ₂ O)	-76.470309	-76.464298
$[L_1-H-Ni^{II}-H_2O]^{+2}$	-2335.928727	-2335.552166
$[L_1-H-Ni^{II}-MeCN]^{+2}$	-2392.287198	-2391.890017
(1) $[L_1-H-Ni^{II}-H_2O]^{+2} + (MeCN)$	-2468.750623	-2468.346130
(2) $[L_1-H-Ni^{II}-MeCN]^{+2} + (H_2O)$	-2468.757507	-2468.354315
Difference (kcal/mol) for (1)-(2)	4.32	5.14

^{a)} The final total Gibbs free energy (G) was given by $G = E_{TZPV} + G_{corr.} + \Delta G^{0/*}$, where the calculation of $\Delta G^{0/*}$ has been done considering the standard-state concentration of 10mM for the complexes $[L_1-H-Ni^{II}-H_2O]^{+2}$ and $[L_1-H-Ni^{II}-MeCN]^{+2}$, 50 mM for Water, and 19 M for the Acetonitrile (solvent).

7. Supplementary Figures

Figure S12. HRMS (ESI-MS) spectrum of complex $[Ni^{II}(L_1)](OTf)$ (**1_{OTf}**). Experiment performed in CH_3CN (spectrum at the bottom corresponds to the simulated peak).

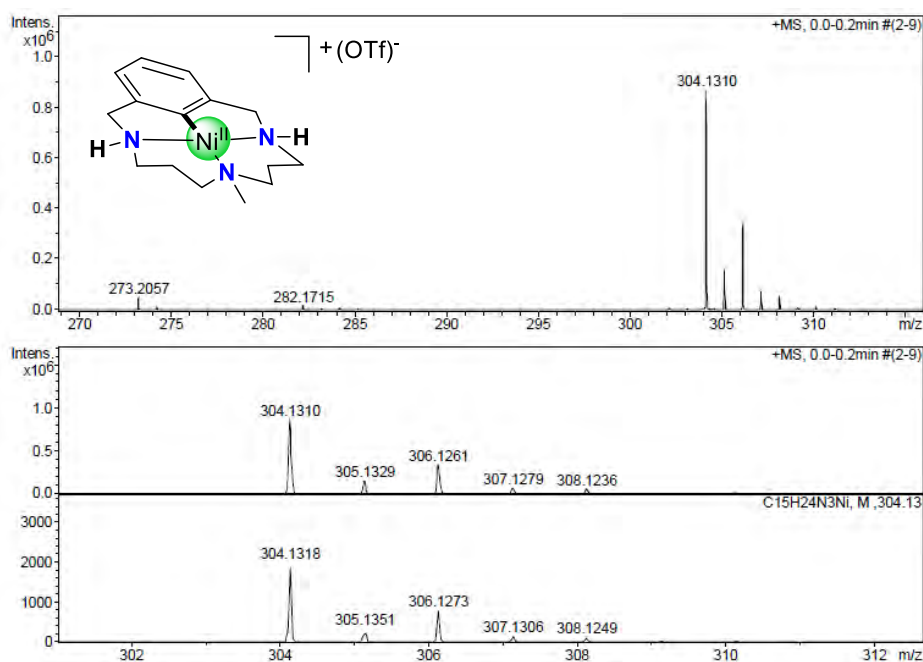
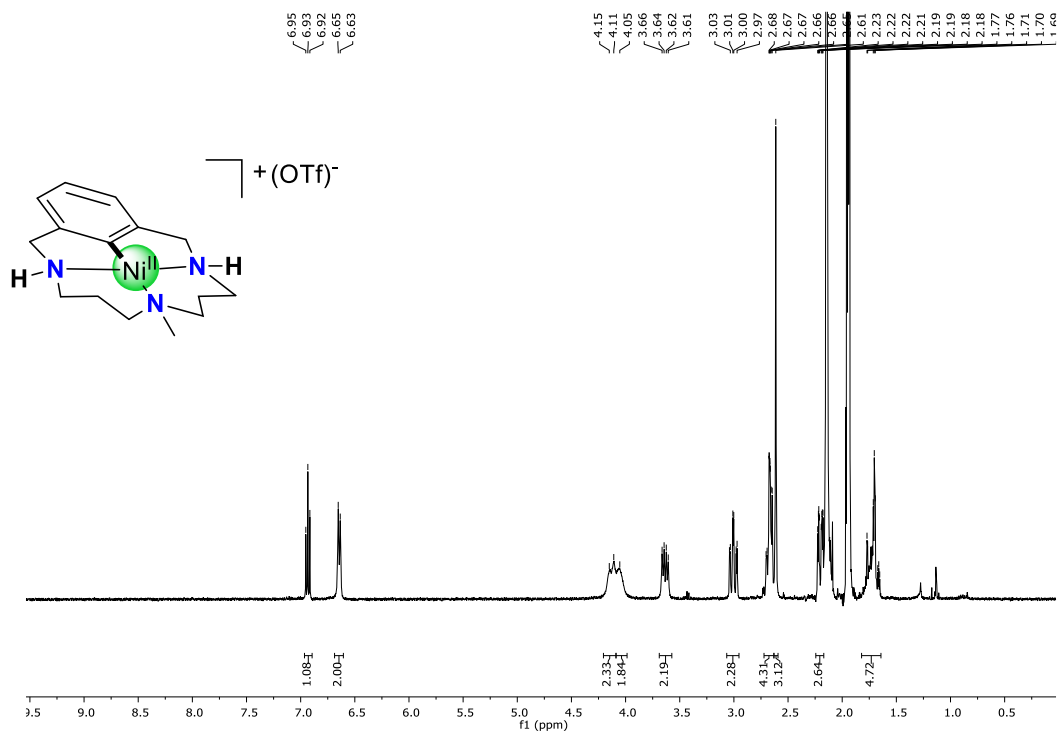
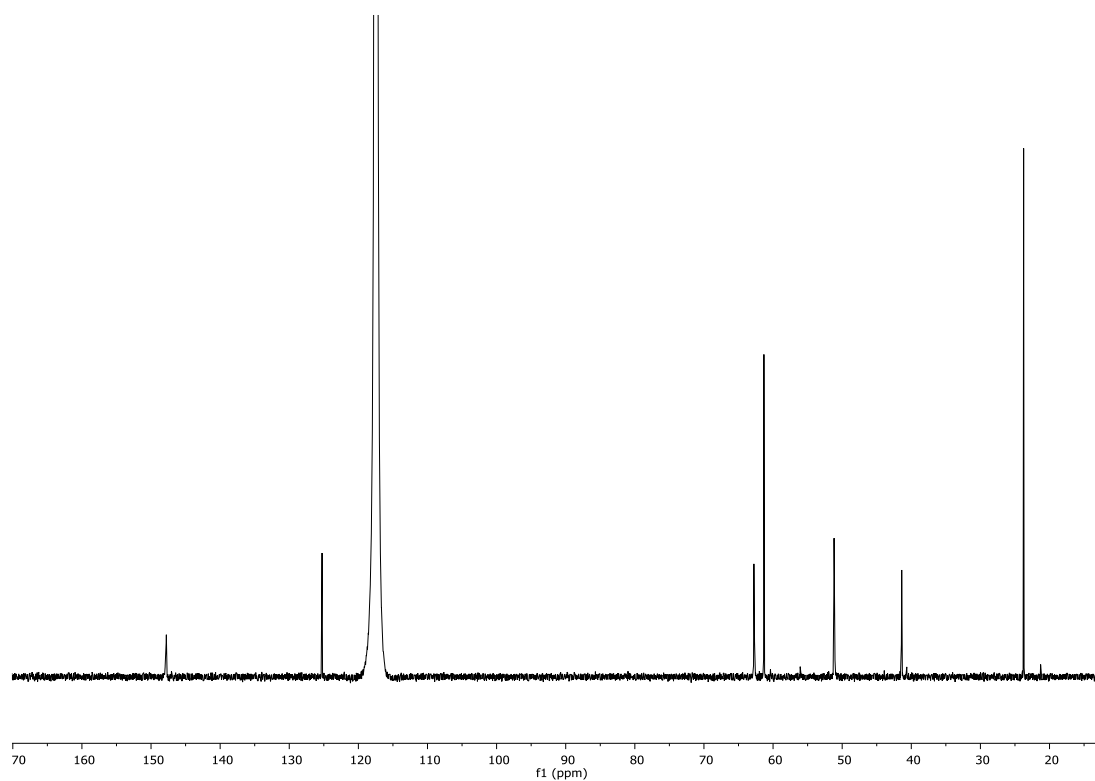


Figure S13. Complex $[\text{Ni}^{\text{II}}(\text{L}_1)]\text{OTf}$ (1_{OTf}): a) ^1H -NMR spectrum (400 MHz, CD_3CN , 25 °C). b) ^{13}C -NMR spectrum (100 MHz, CD_3CN , 25 °C). c) ^1H - ^{13}C COSY spectrum (400 MHz, CD_3CN , 25°C). d) ^1H - ^{13}C HSQC_ed spectrum (400 MHz, CD_3CN , 25°C). e) ^1H - ^{13}C HMBC (400 MHz, CD_3CN , 25°C).

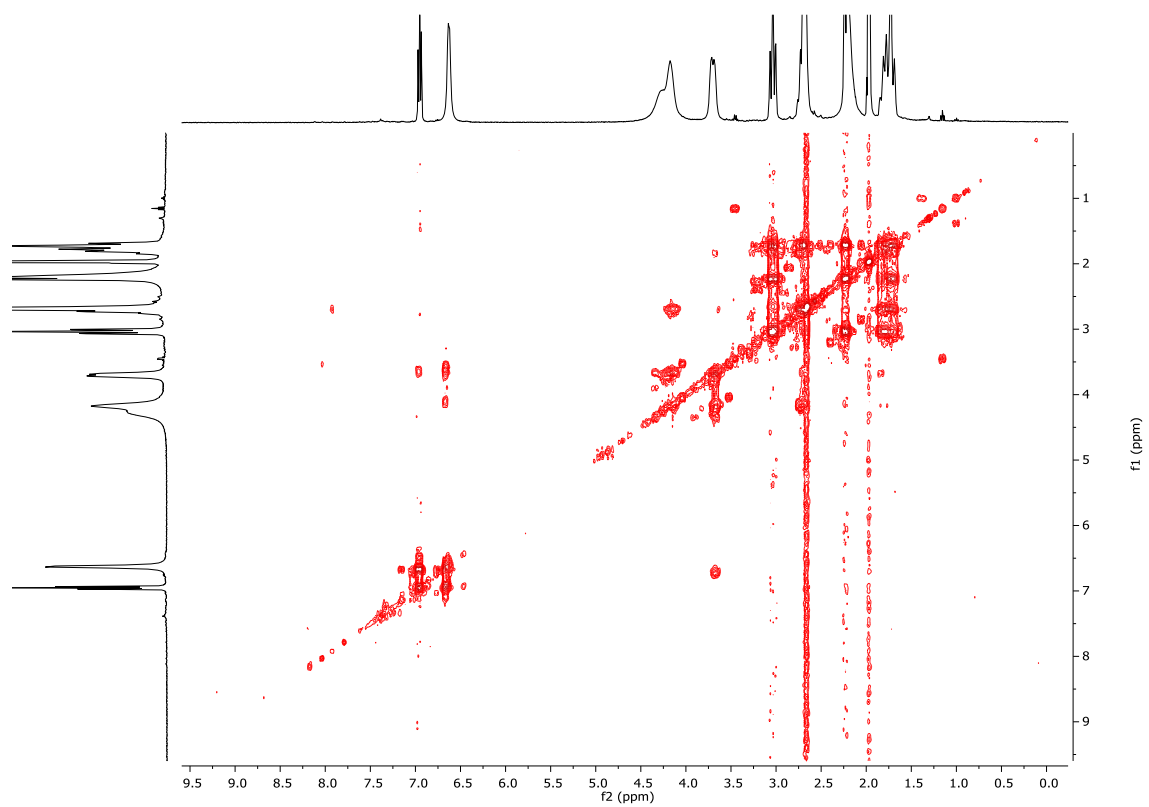
a)



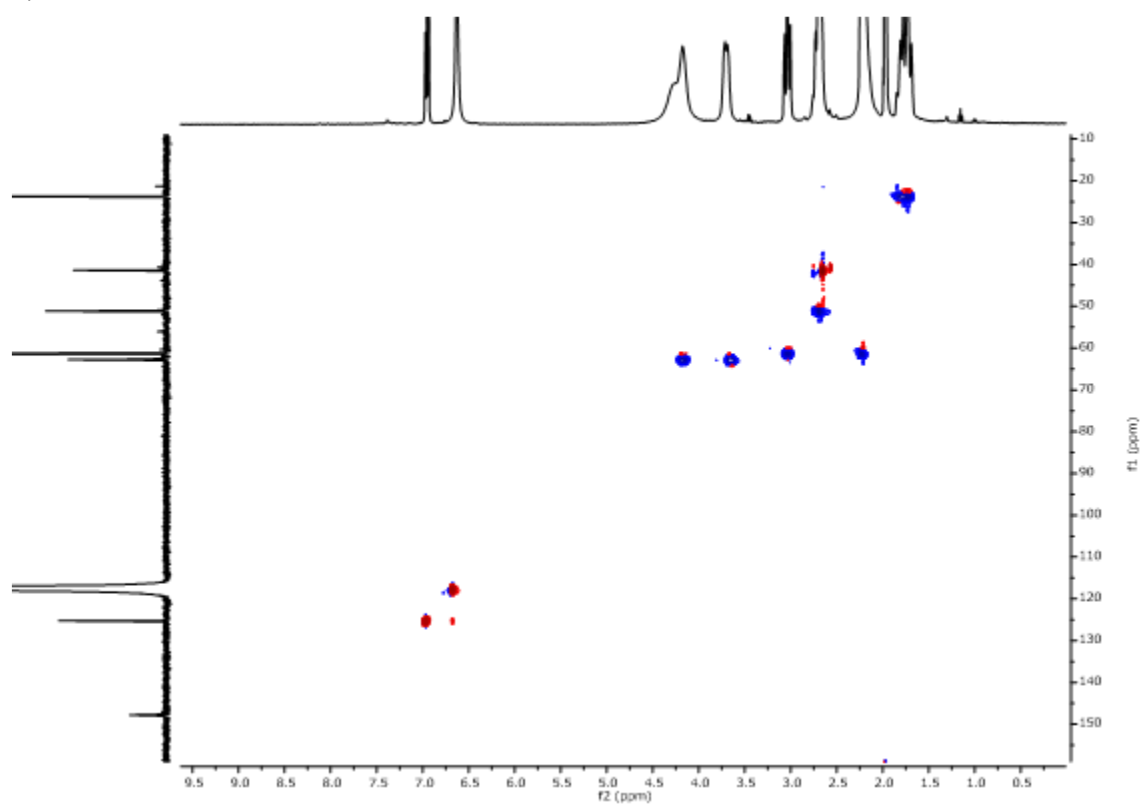
b)



c)



d)



e)

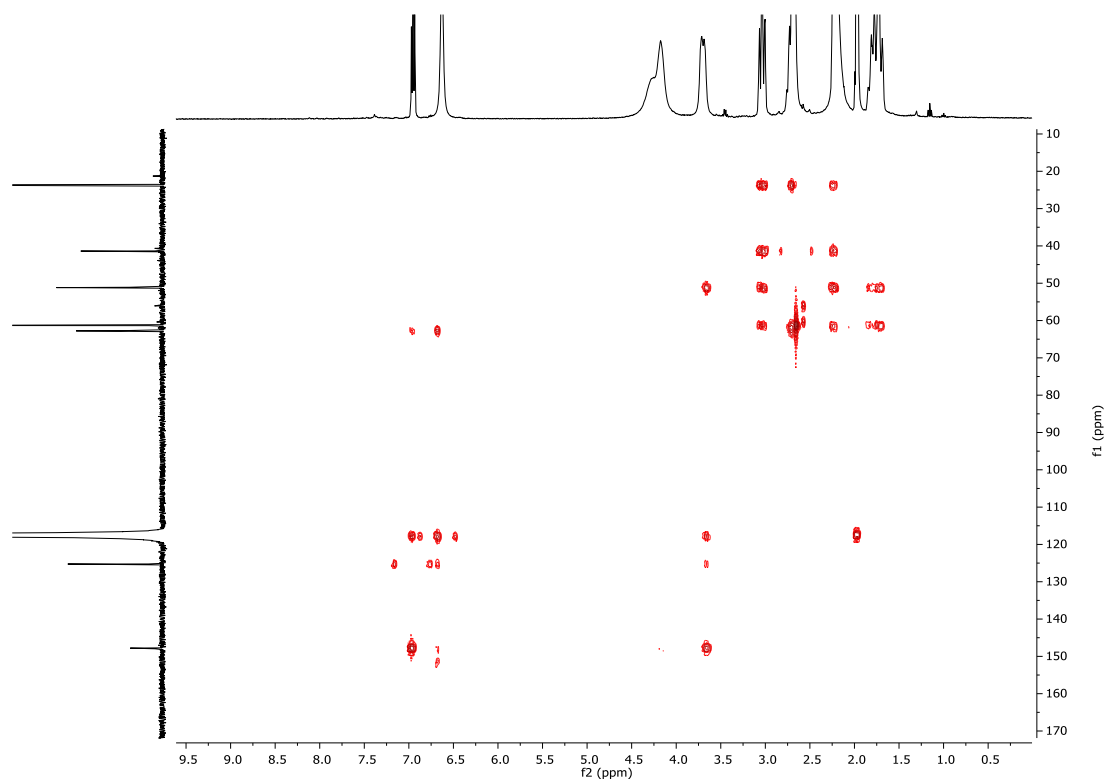


Figure S14. HRMS (ESI-MS) spectrum of complex $[\text{Ni}^{\text{II}}(\text{L}_5)](\text{OTf})$ (5_{OTf}). Experiment performed in CH_3CN (spectrum at the bottom corresponds to the simulated peak)

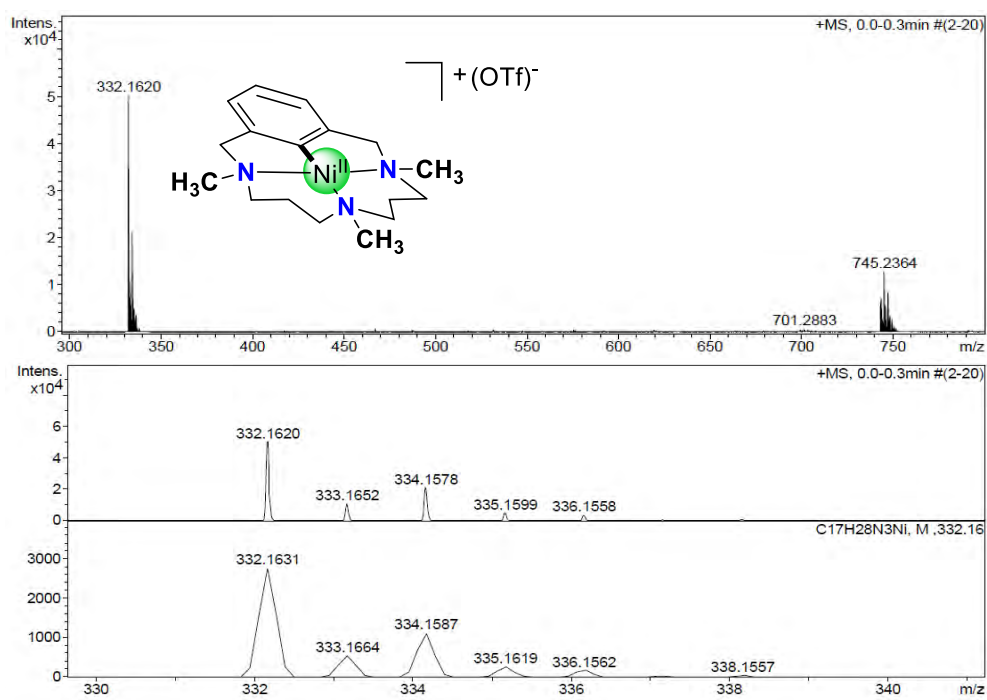
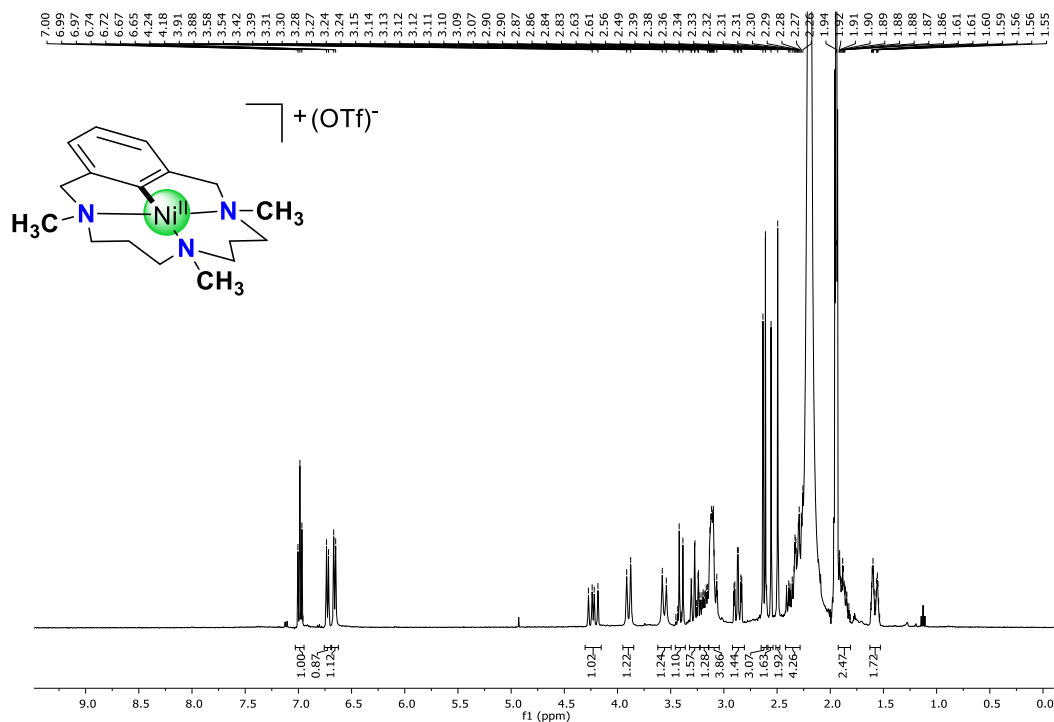
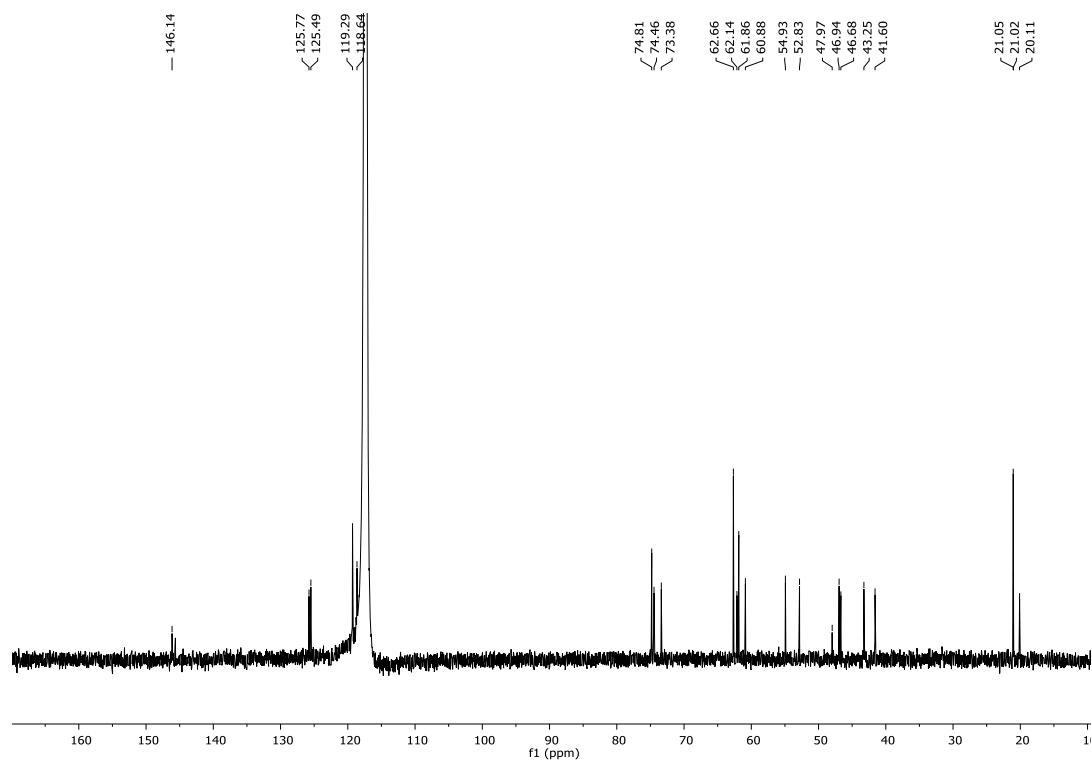


Figure S15. Complex $[\text{Ni}^{\text{II}}(\text{L}_5)]\text{OTf}$ (5_{OTf}): a) ^1H -NMR spectrum (400 MHz, CD_3CN , 25 °C). b) ^{13}C -NMR spectrum (100 MHz, CD_3CN , 25 °C). c) ^1H - ^1H COSY spectrum (400 MHz, CD_3CN , 25°C). d) ^1H - ^{13}C HSQC_ed spectrum (400 MHz, CD_3CN , 25°C). e) ^1H - ^{13}C HMBC (400 MHz, CD_3CN , 25°C).

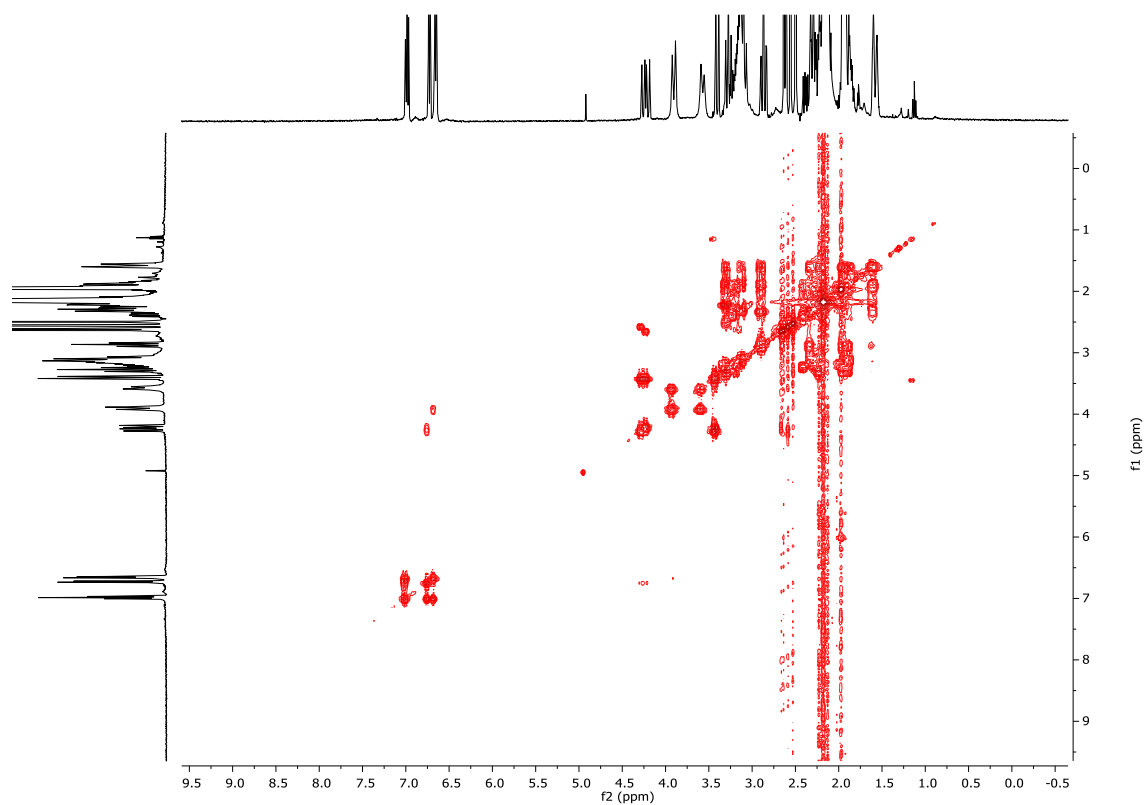
a)



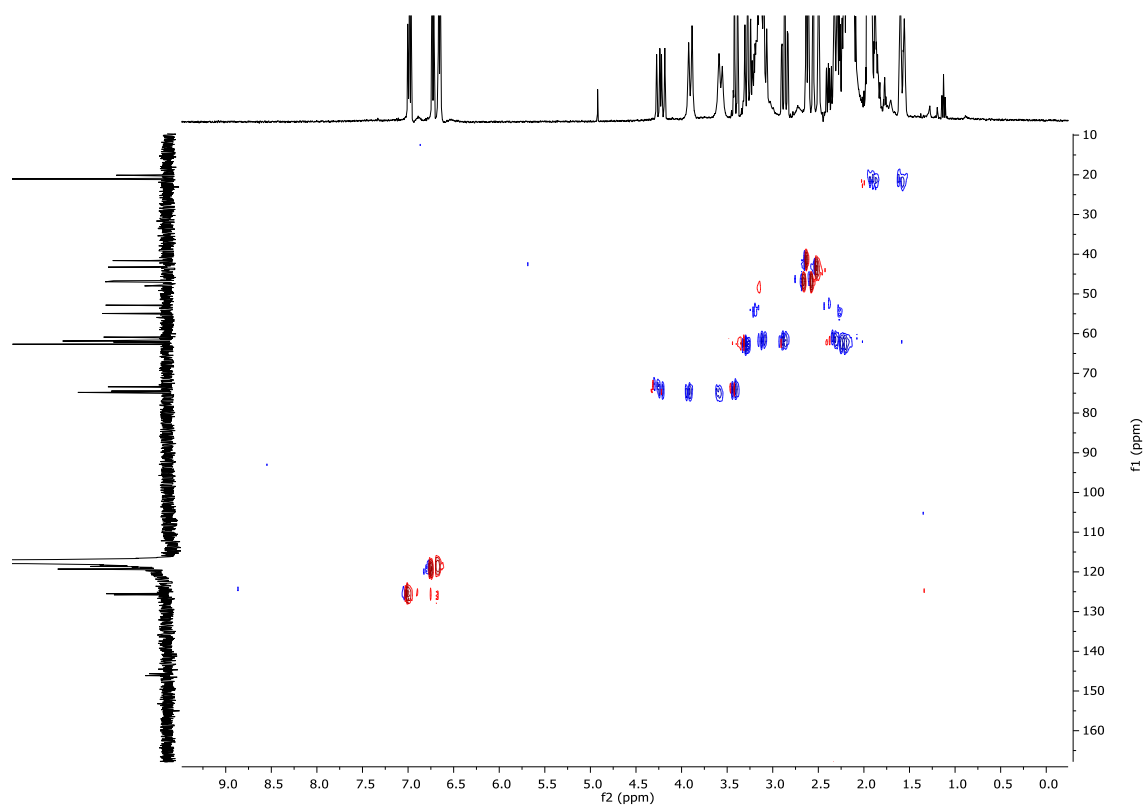
b)



c)



d)



e)

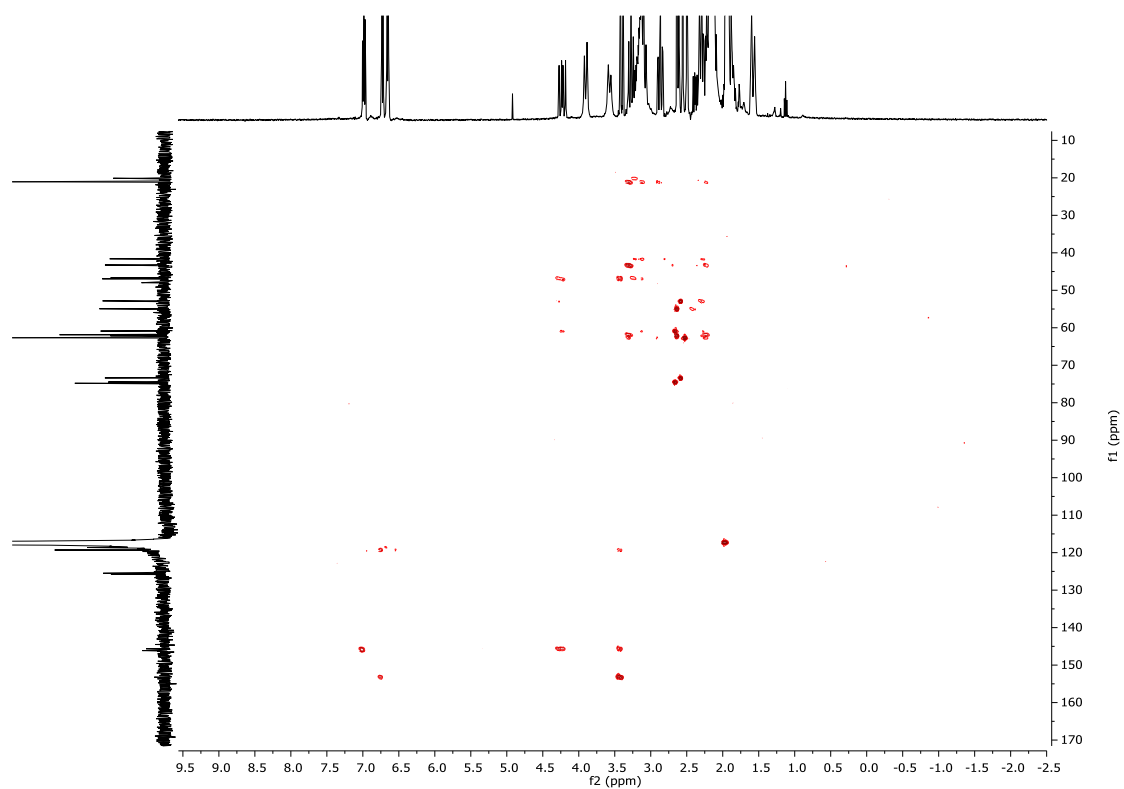


Figure S16. HRMS (ESI-MS) spectrum of the coupling product L₁-CF₃. Experiment performed in CHCl₃ (spectrum at the bottom corresponds to the simulated peak)

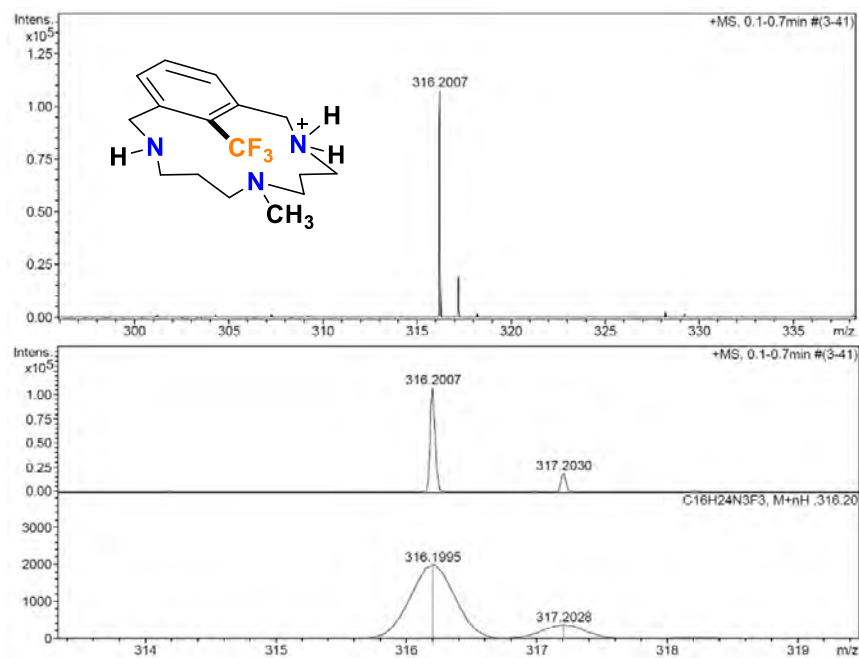
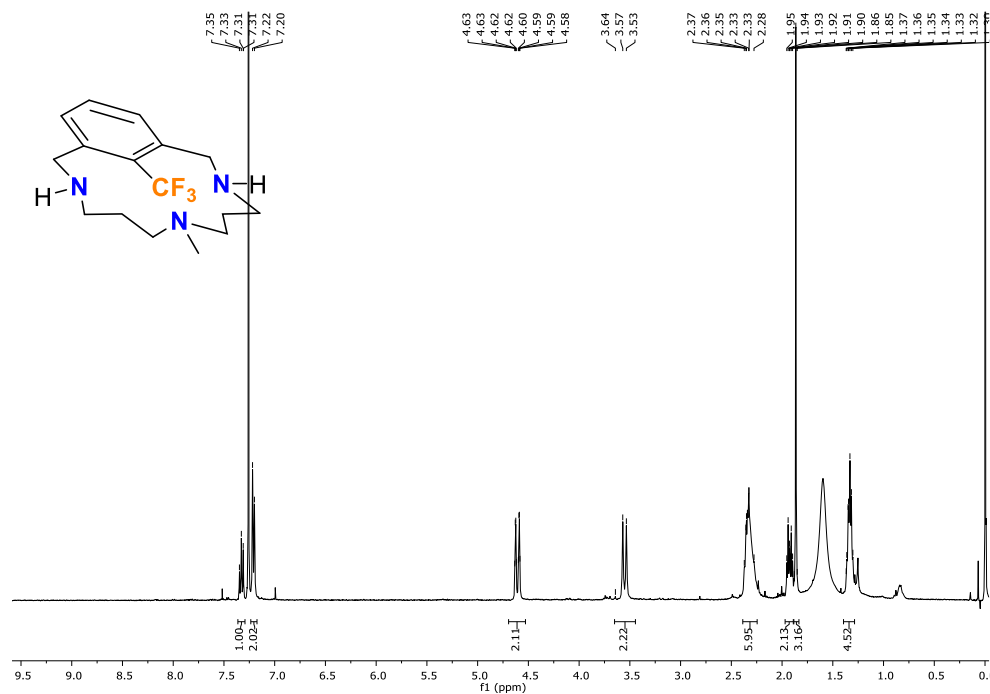
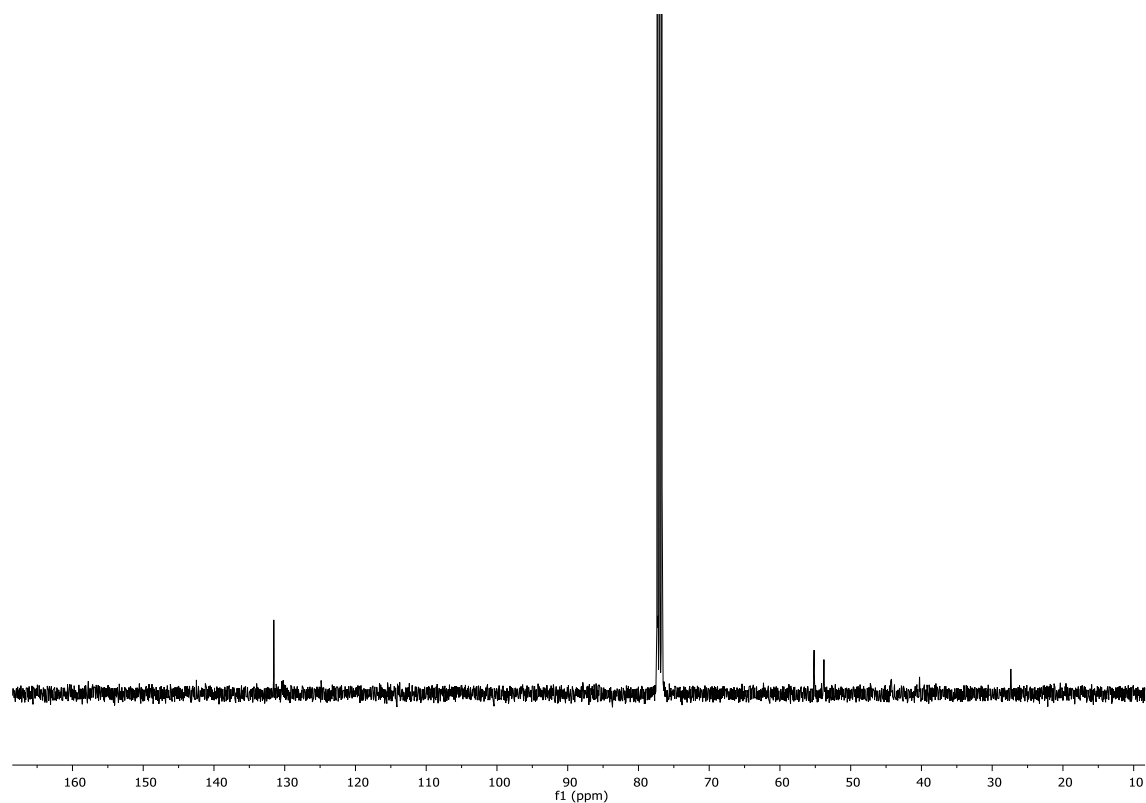


Figure S17. L₁-CF₃ coupling product: a) ¹H-NMR spectrum (400 MHz, CD₃CN, 25 °C). b) ¹³C-NMR spectrum (100 MHz, CD₃CN 25 °C). c) ¹H-¹H COSY spectrum (400 MHz, CD₃CN, 25°C). d) ¹H-¹H NOESY spectrum (400 MHz, CD₃CN, 25°C). e) ¹H-¹³C HSQC_ed spectrum (400 MHz, CD₃CN, 25°C). f) ¹H-¹³C HMBC (400 MHz, CD₃CN, 25°C).

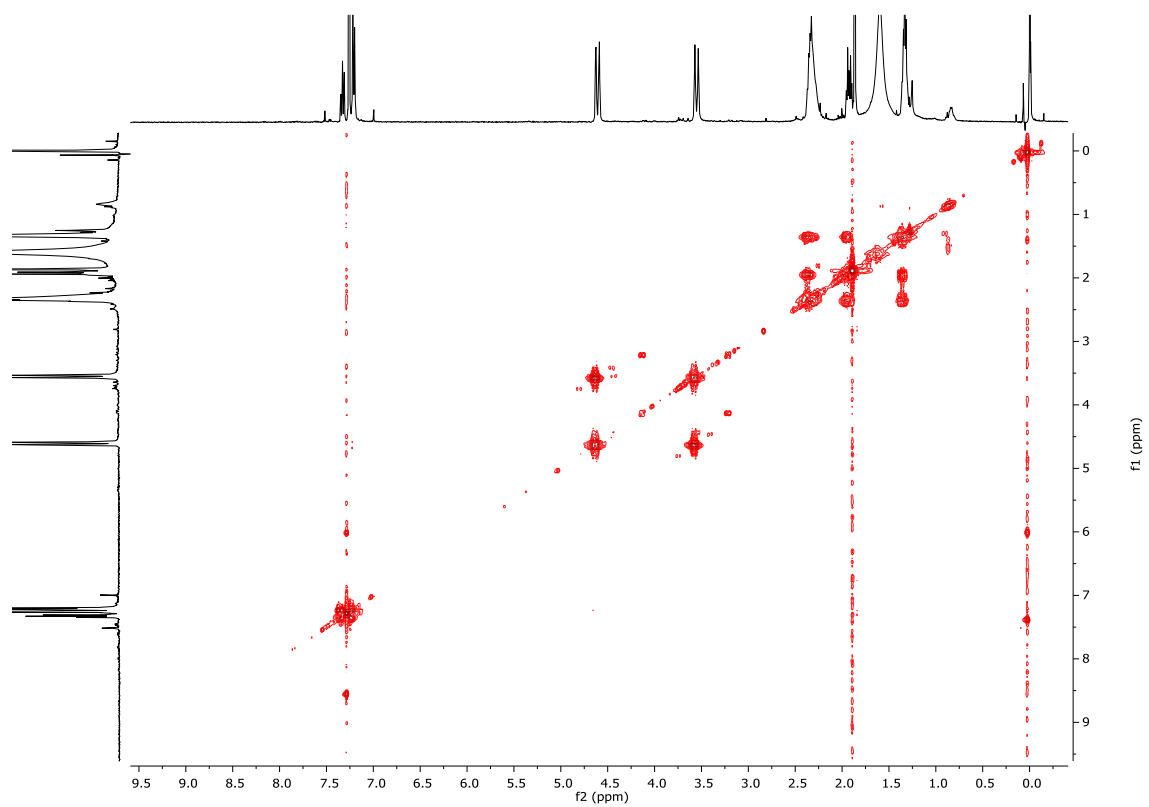
a)



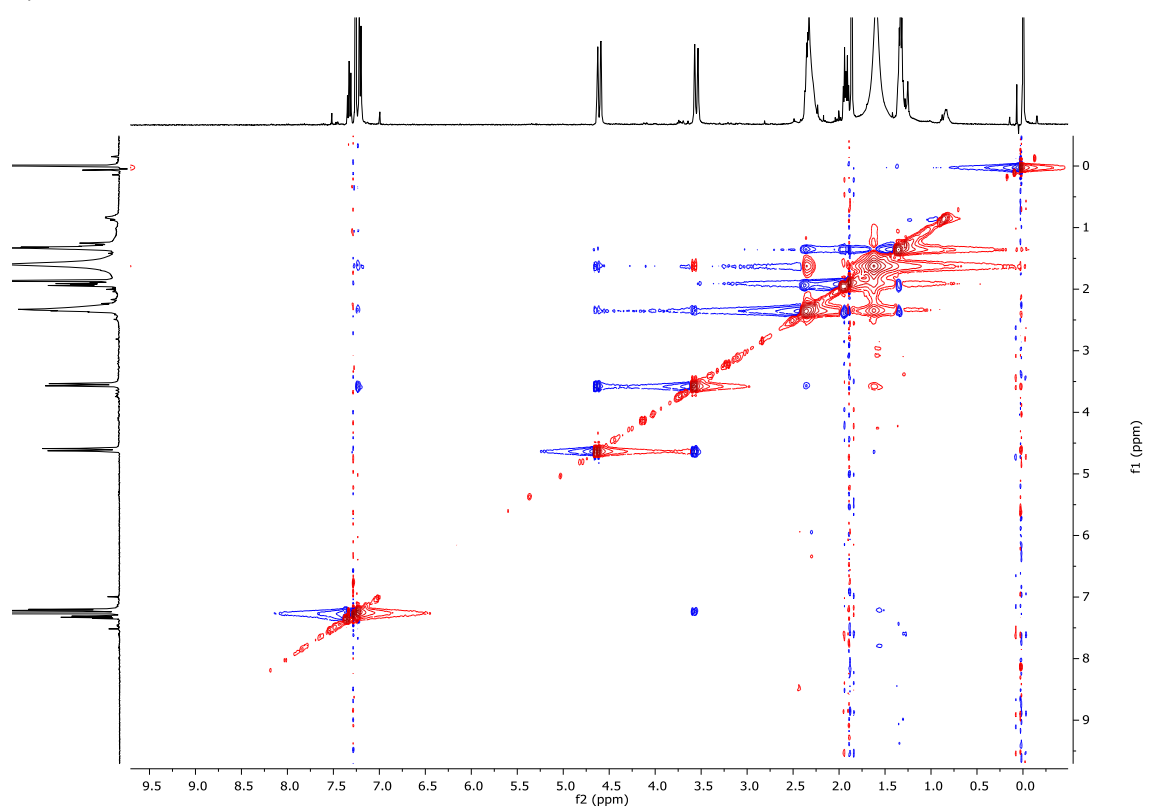
b)



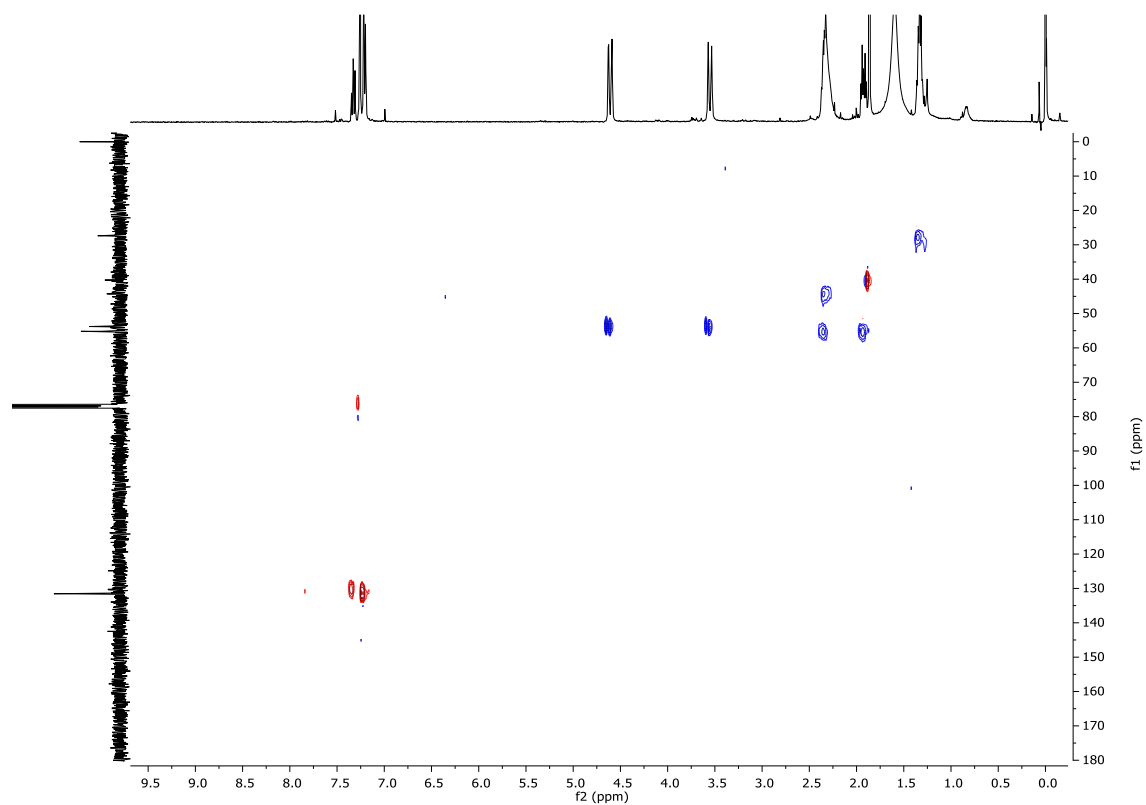
c)



d)



e)



f)

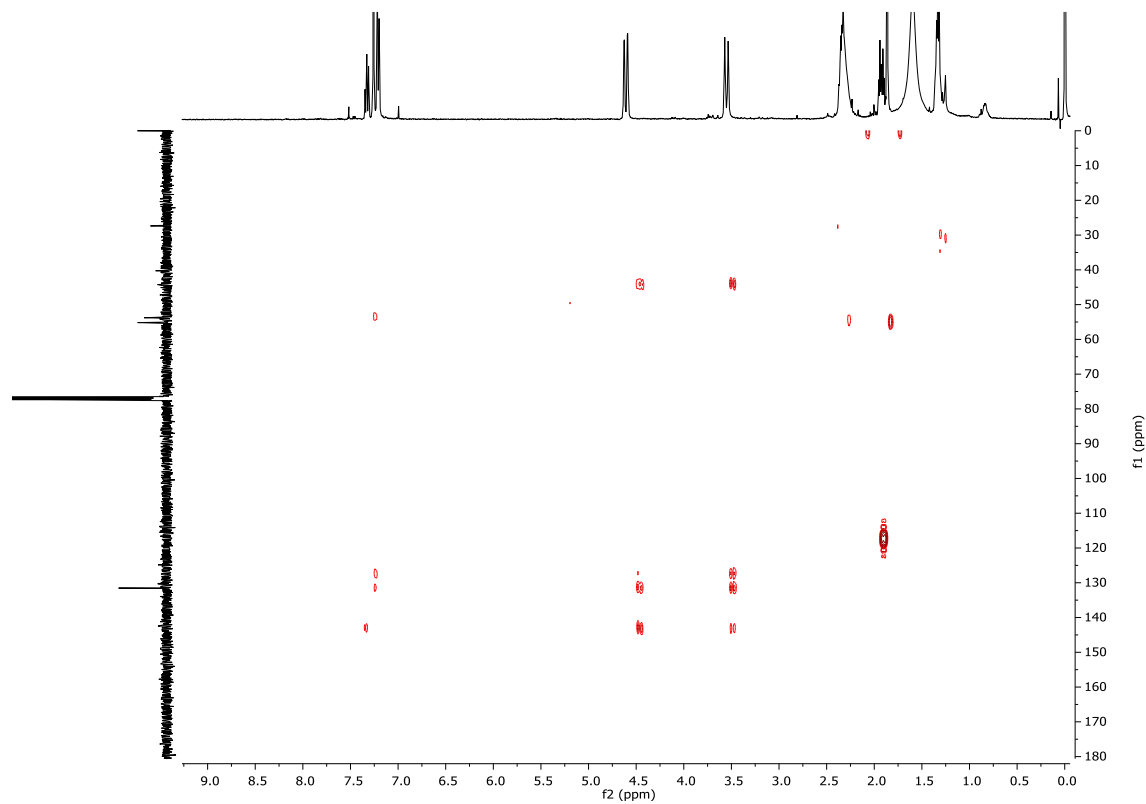


Figure S18. HRMS (ESI-MS) spectrum of the coupling product **L₅-CF₃**. Experiment performed in CHCl₃ (spectrum at the bottom corresponds to the simulated peak).

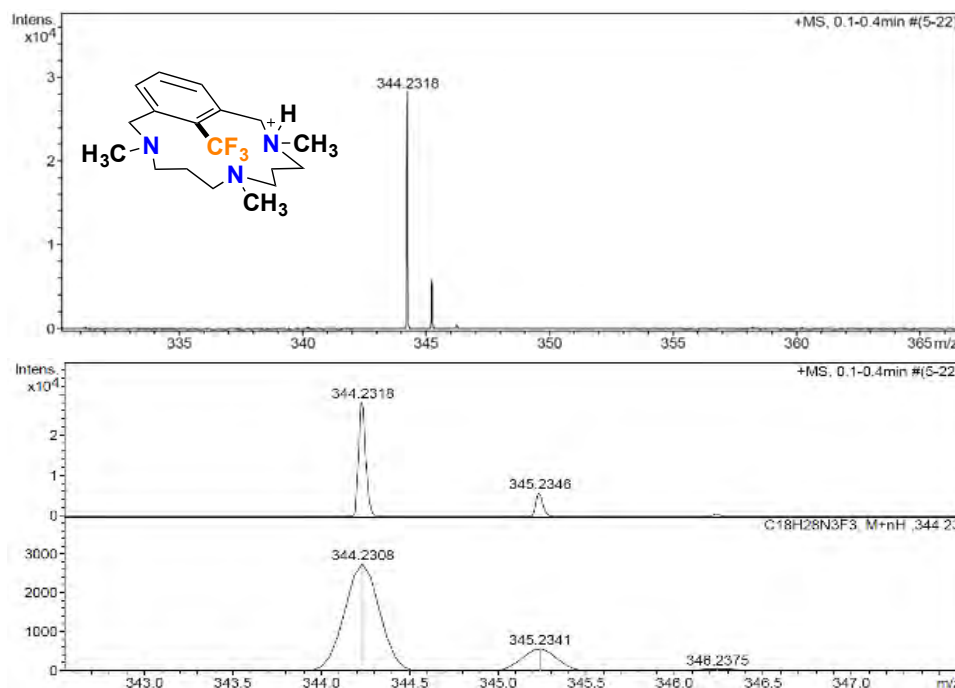
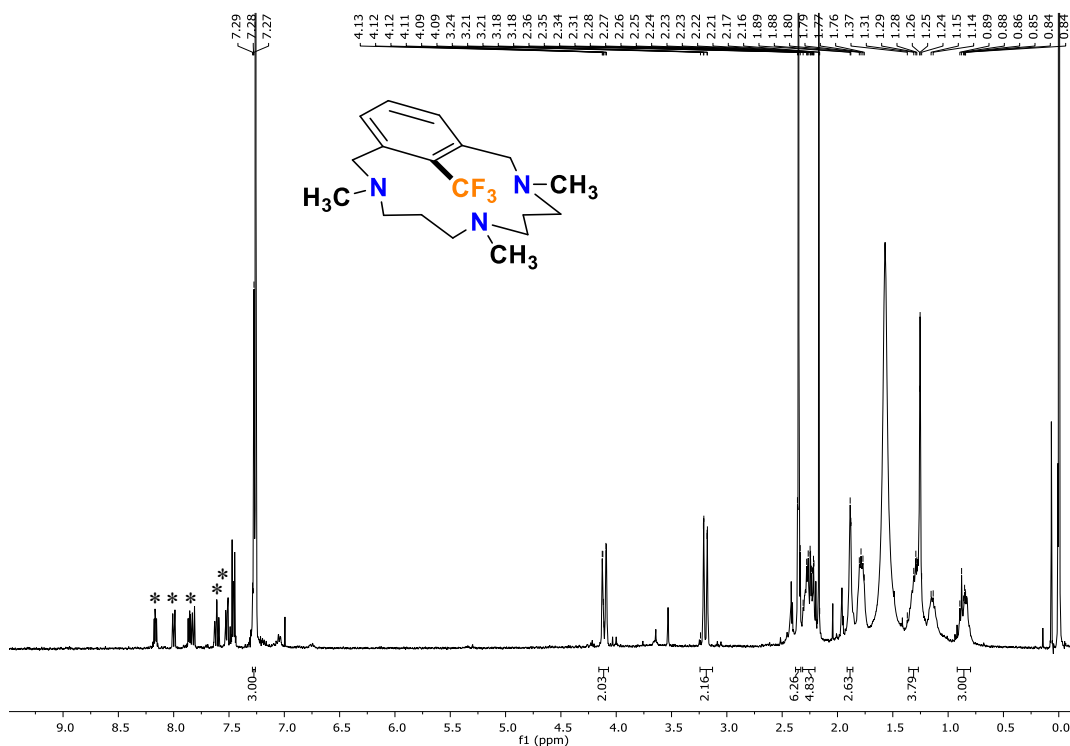


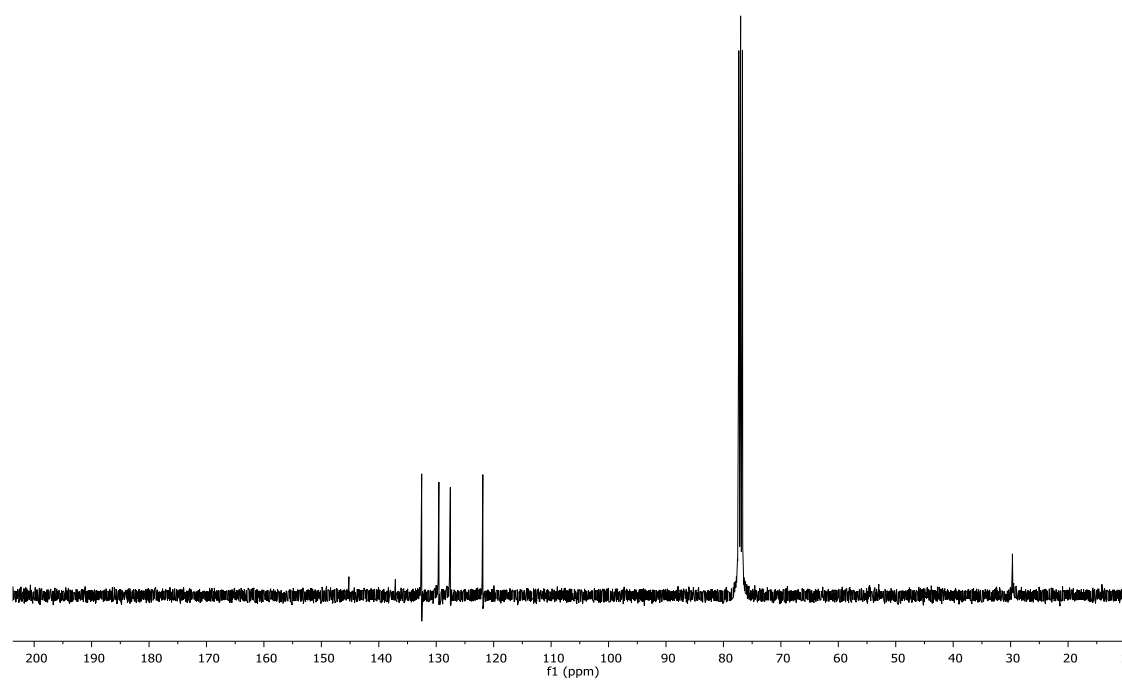
Figure S19. **L₅-CF₃** coupling product: a) ¹H-NMR spectrum (400 MHz, CD₃CN, 25 °C). b) ¹³C-NMR spectrum (100 MHz, CD₃CN 25 °C). c) ¹H-¹H COSY spectrum (400 MHz, CD₃CN, 25°C). d) ¹H-¹H NOESY spectrum (400 MHz, CD₃CN, 25°C). e) ¹H-¹³C HSQC_ed spectrum (400 MHz, CD₃CN, 25°C). f) ¹H-¹³C HMBC (400 MHz, CD₃CN, 25°C).

a)

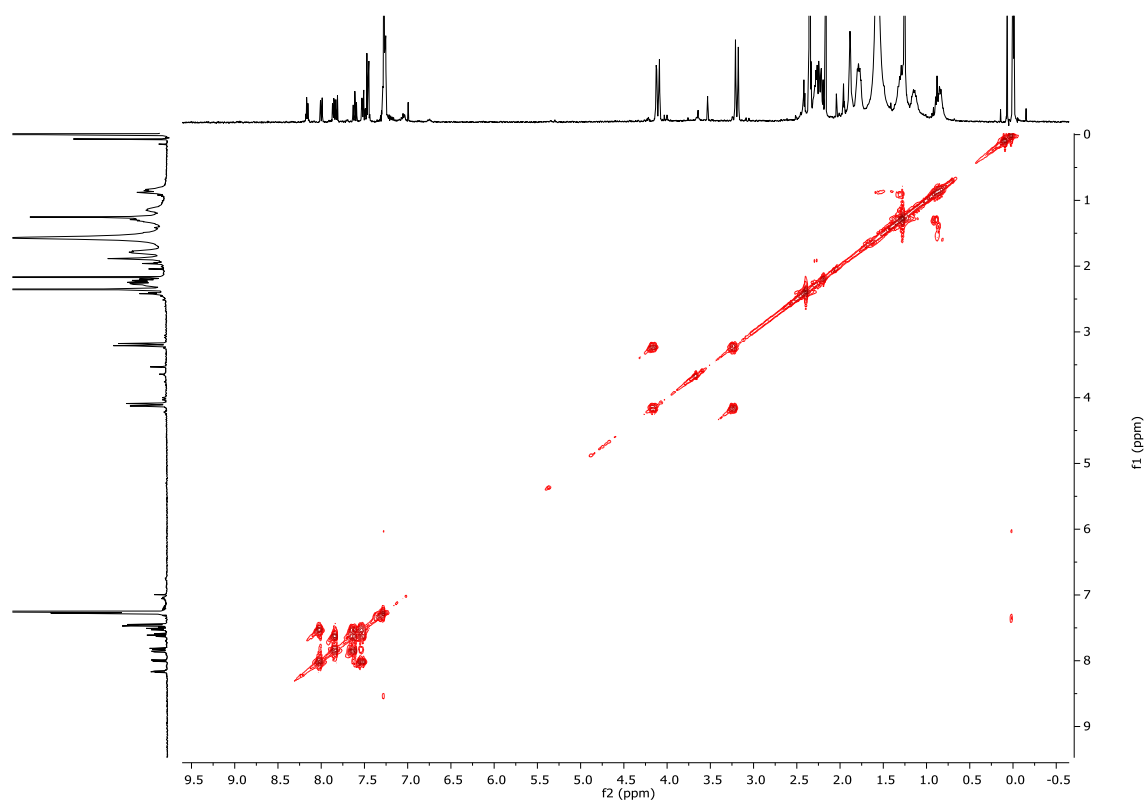


* residual signals of TDDT and DBT, which could not be removed

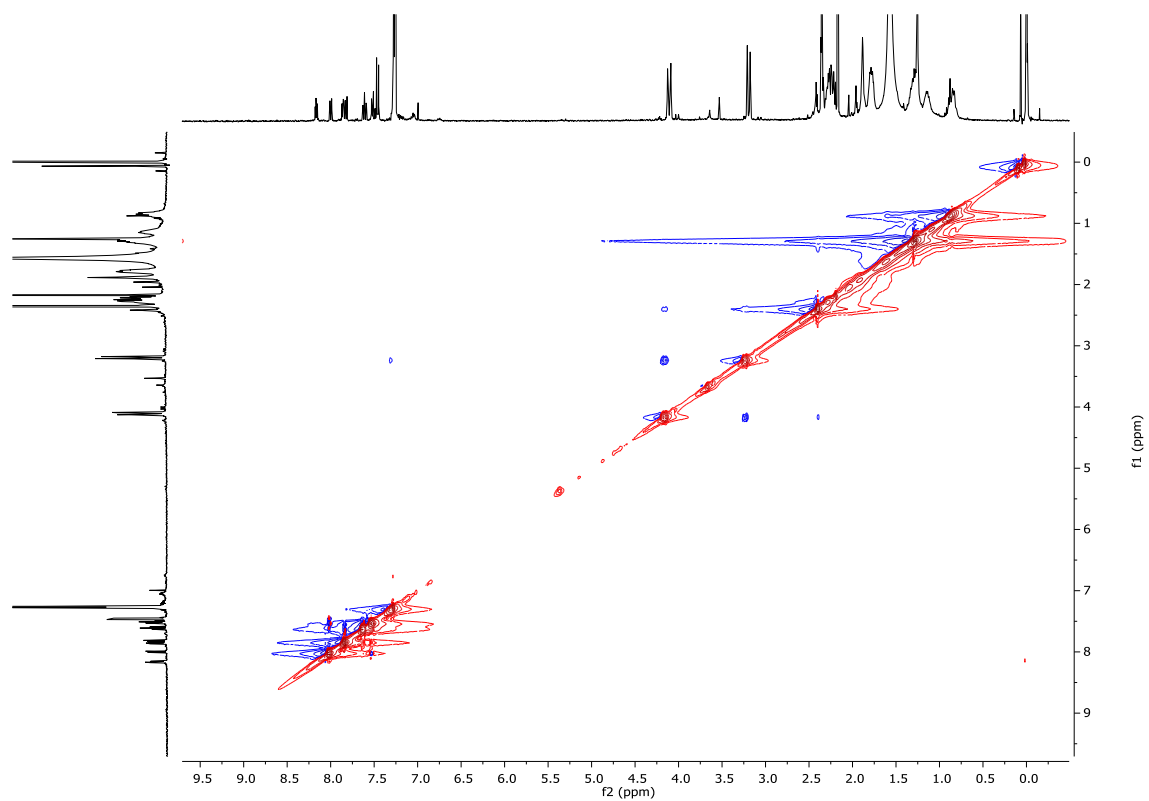
b)



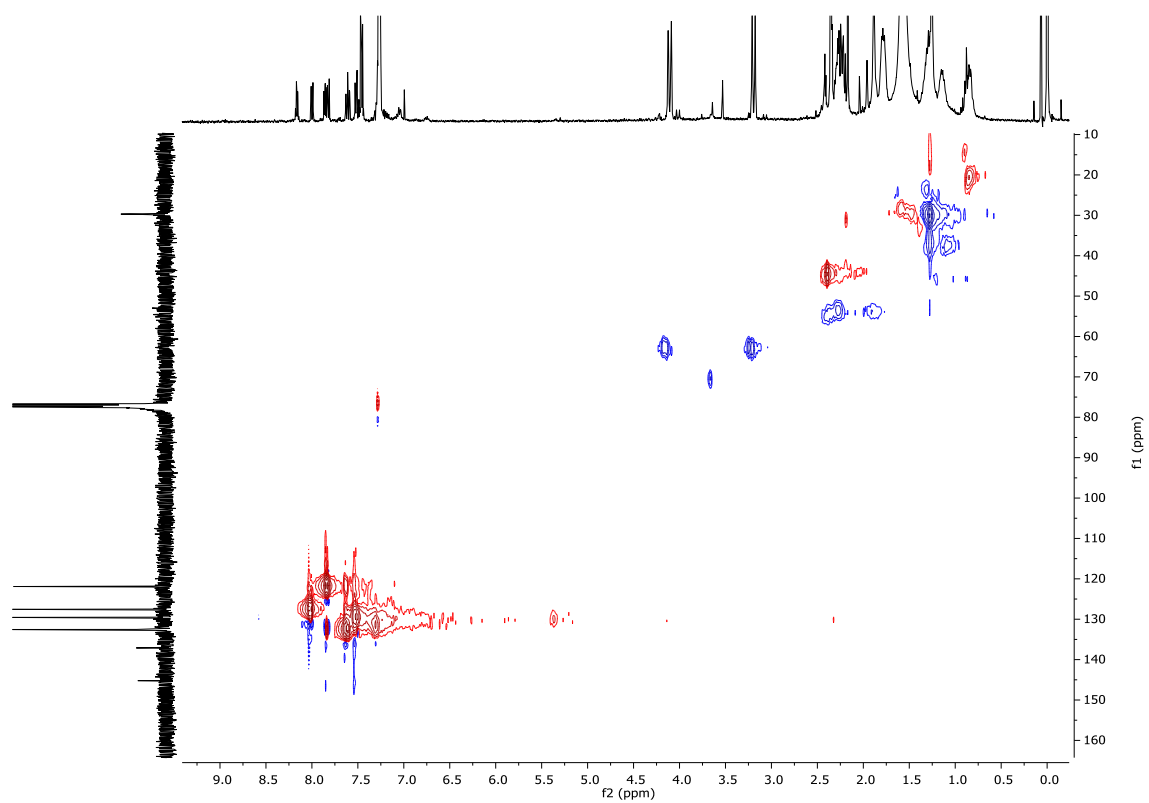
c)



d)



e)



f)

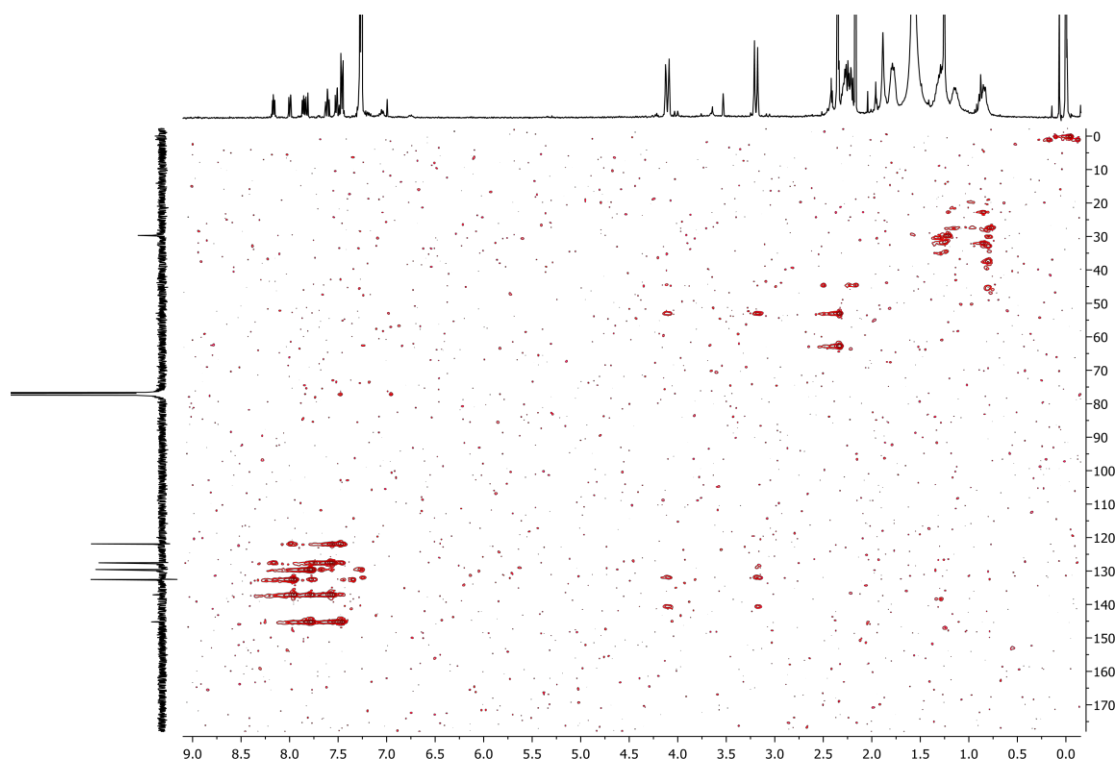


Figure S20. ^1H NMR spectrum of complex $[\text{Ni}^{\text{II}}(\text{L}_1)](\text{OTf})$ (1_{OTf}) upon the addition of 1 equiv of TDDT and 2 equiv of the radical trap BPN.

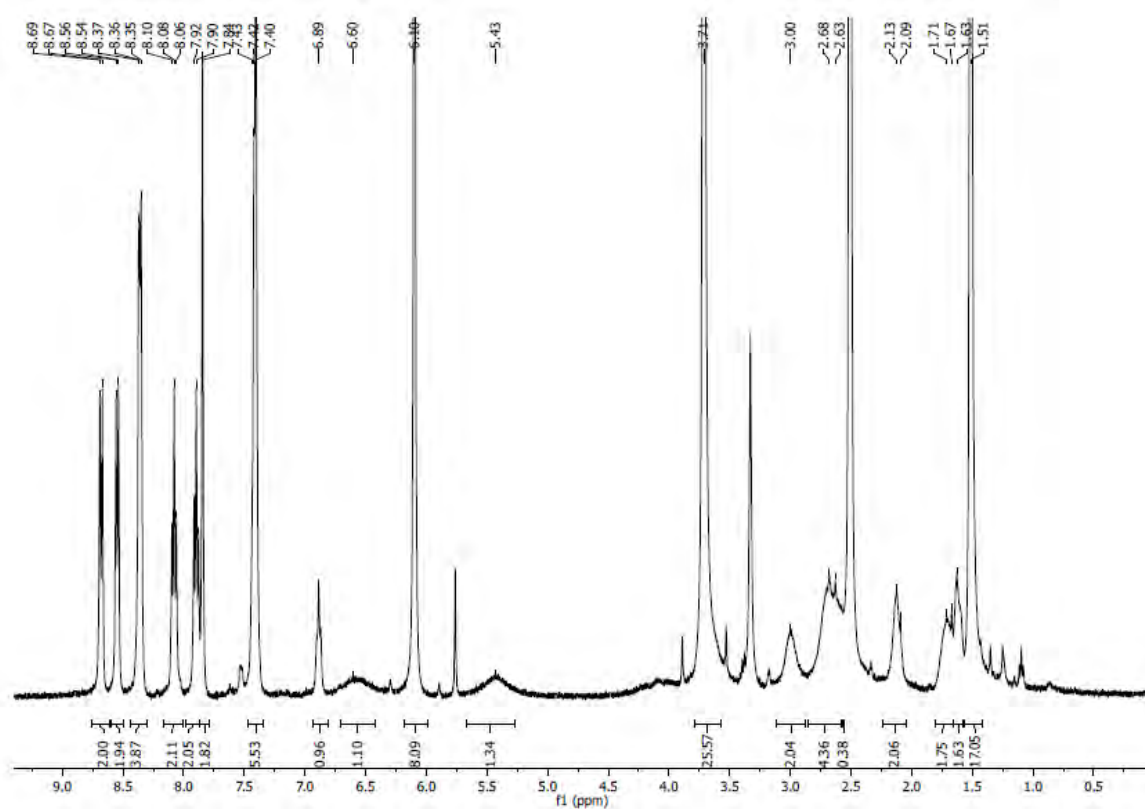


Figure S20. ^1H NMR spectrum of the formation of the coupling product after 24h of the addition to 1_{OTf} of 1 equiv of TDDT and 2 equiv of the radical trap BPN.

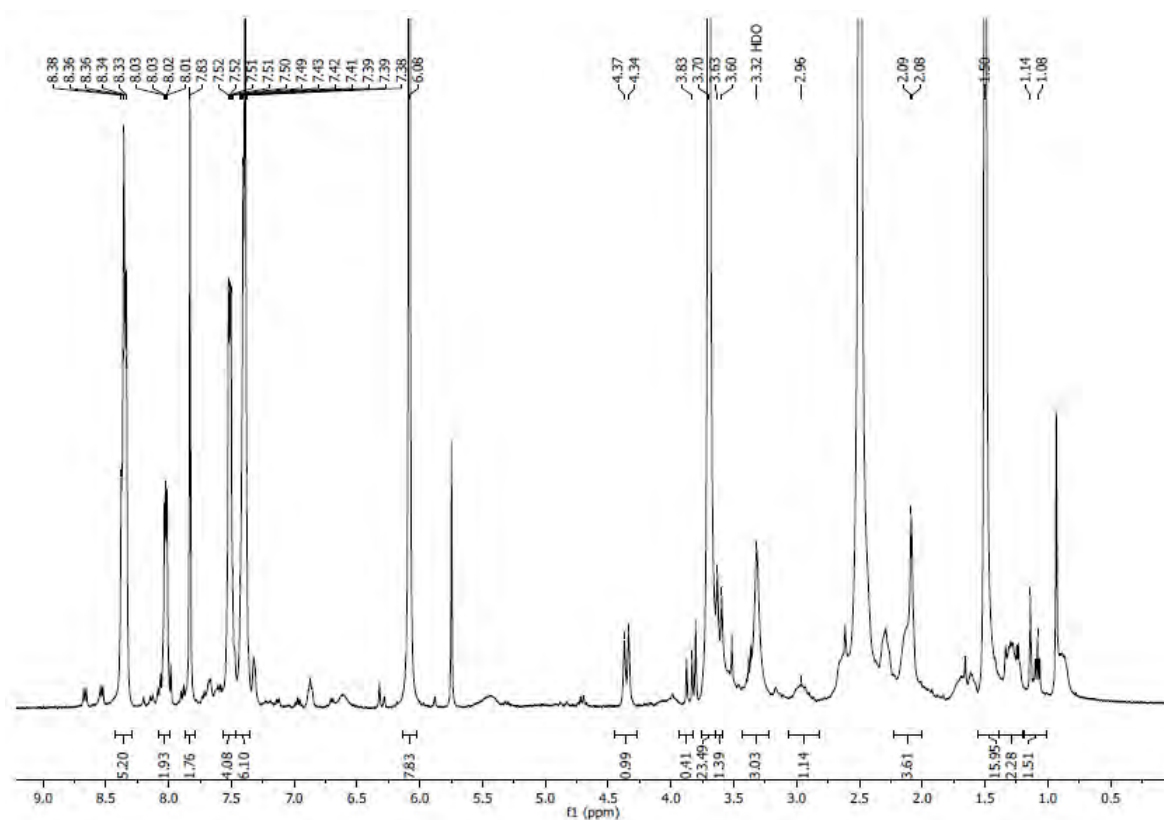


Figure S22. ¹H NMR spectrum of complex [Ni^{II}(L₁)](OTf) (**1OTf**) upon the addition of 1 equiv of the hypervalent iodine reagent and 2 equiv of the radical trap BPN.

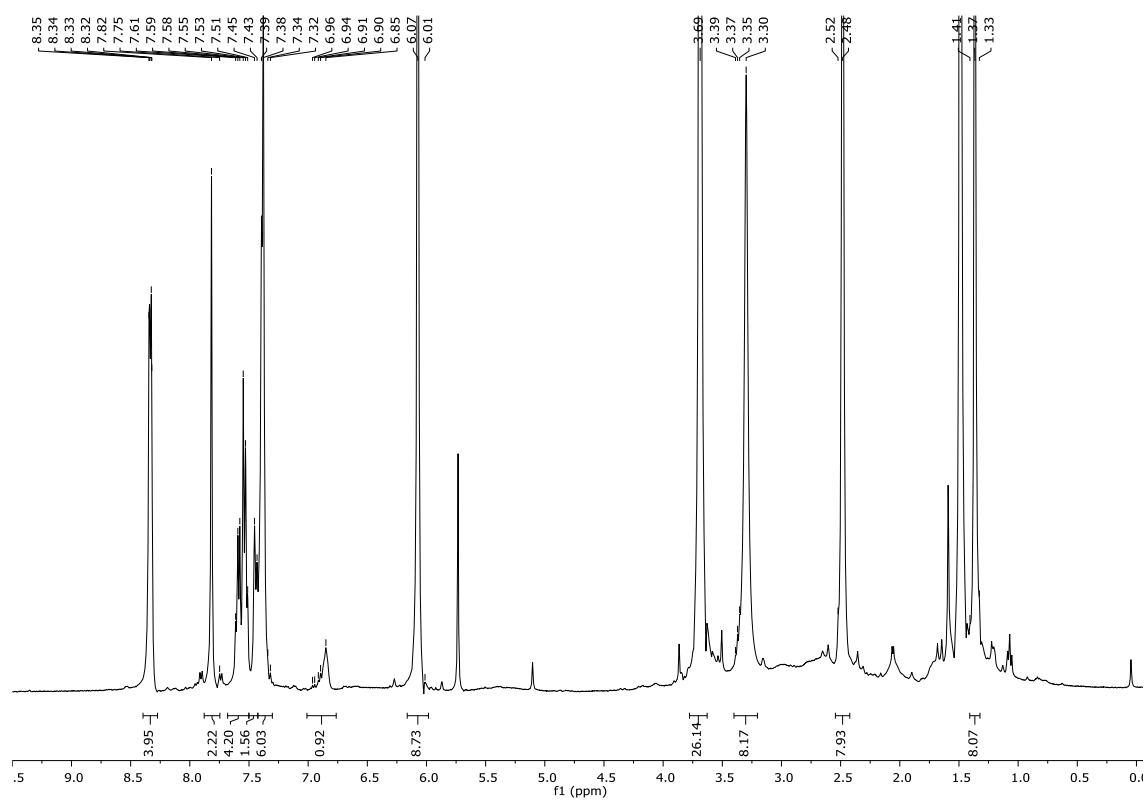
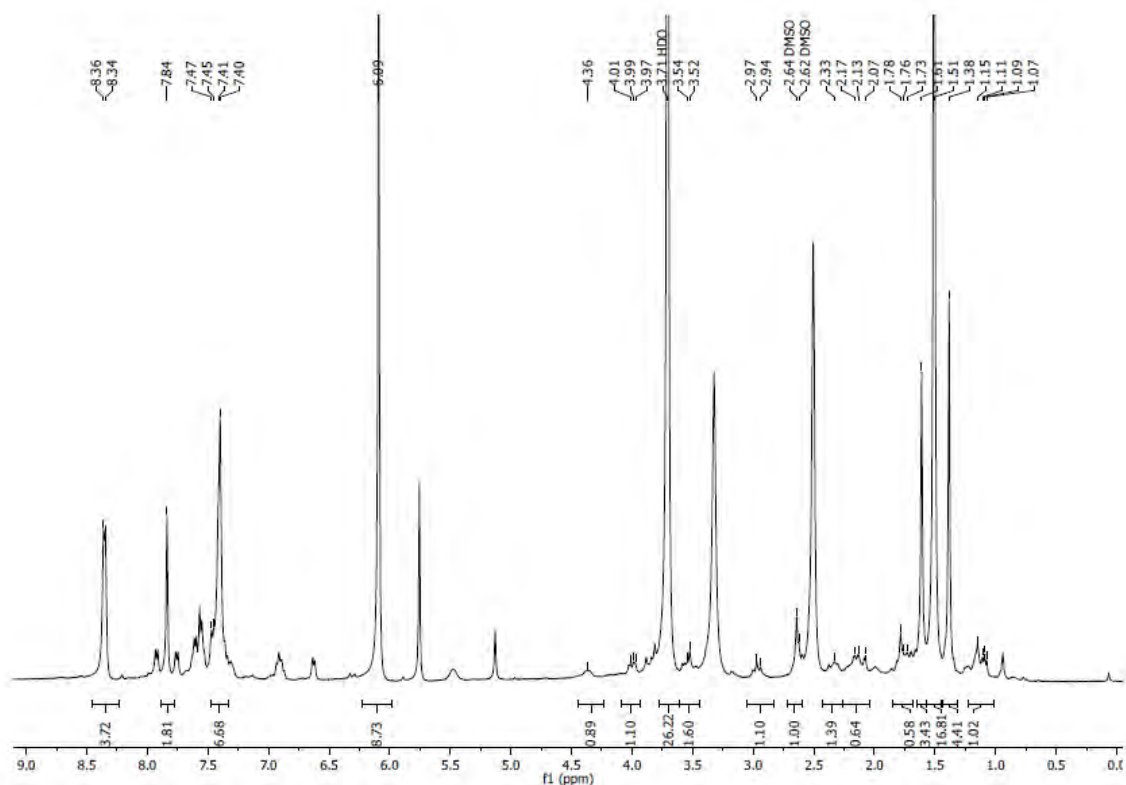


Figure S23. ^1H NMR spectrum of complex $[\text{Ni}^{\text{II}}(\text{L}_1)](\text{OTf})$ (**1_{OTf}**) after 48h of the addition of 1 equiv of the hypervalent iodine reagent and 2 equiv of the radical trap BPN.

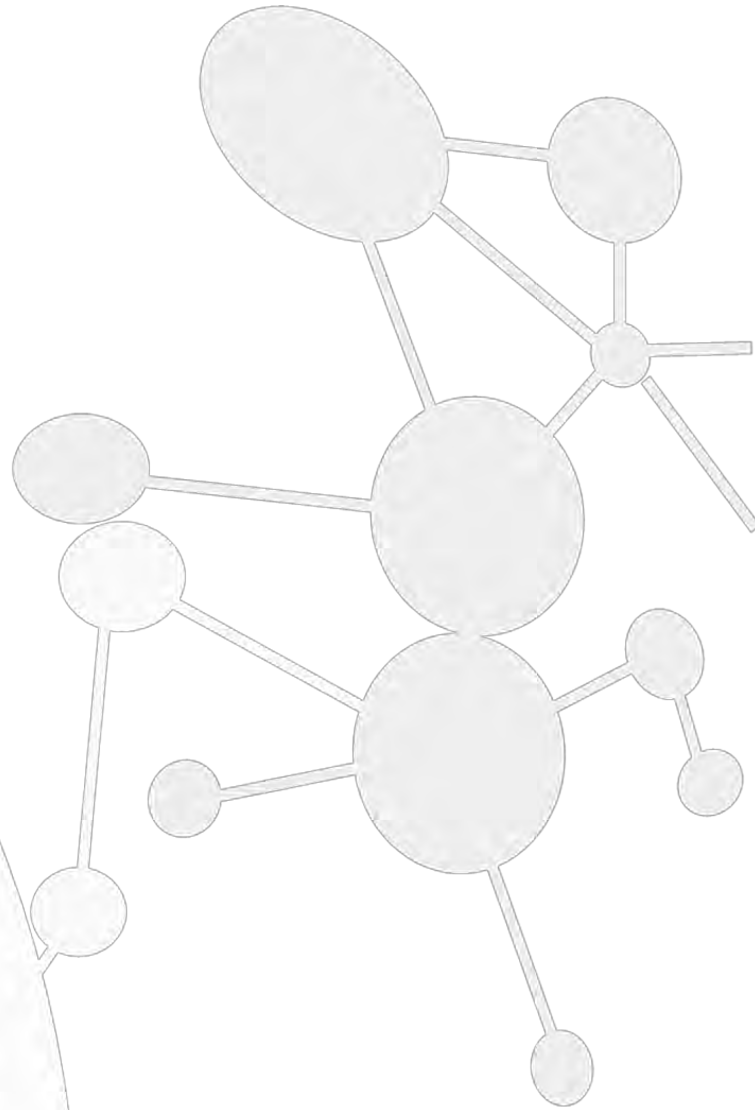


8. Supplementary references

1. Ribas, X.; Jackson, D. A.; Donnadieu, B.; Mahía, J.; Parella, T.; Xifra, R.; Hedman, B.; Hodgson, K. O.; Llobet, A.; Stack, T. D. P. *Angew. Chem. Int. Ed.* **2002**, *41*, 2991.
2. King, A. E.; Huffman, L. M.; Casitas, A.; Costas, M.; Ribas, X.; Stahl, S. S. *J. Am. Chem. Soc.* **2010**, *132*, 12068.
3. A. Casitas, A. E. King, T. Parella, M. Costas, S. S. Stahl, X. Ribas, *Chem. Sci.* **2010**, *1*, 326-330.
4. Ribas, X.; Calle, C.; Poater, A.; Casitas, A.; Gómez, L.; Xifra, R.; Parella, T.; Benet-Buchholz, J.; Schweiger, A.; Mitrikas, G.; Solà, M.; Llobet, A. and Stack, T.P. *J. Am. Chem. Soc.* **2010**, *132*, 12299
5. Bruker Advanced X-ray Solutions. SMART: Version 5.631, 1997-2002.
6. Bruker Advanced X-ray Solutions. SAINT +, Version 6.36A, 2001.
7. G. M. Sheldrick, *Empirical Absorption Correction Program*, Universität Göttingen, 1996
Bruker Advanced X-ray Solutions. SADABS Version 2.10, 2001.
8. G. M. Sheldrick, *Program for Crystal Structure Refinement*, Universität Göttingen, 1997
Bruker Advanced X-ray Solutions. SHELXTL Version 6.14, 2000-2003. SHELXL-2013 (Sheldrick, 2013)
9. Ravel, B.; Newville, M. *J. Synch. Rad.* **2005**, *12*, 537.
10. Newville, M. *J. Synch. Rad.* **2001**, *8*, 96.

11. Rehr, J. J.; Albers, R. C. *Rev. Modern Phys.* **2000**, 72, 621.
12. Martin-Diaconescu, V.; Bellucci, M.; Musiani, F.; Ciurli, S.; Maroney, M. J. *J. Biol. Inorg. Chem.* **2012**, 17, 353.
13. Zambelli, B.; Berardi, A.; Martin-Diaconescu, V.; Mazzei, L.; Musiani, F.; Maroney, M. J.; Ciurli, S. *J. Biol. Inorg. Chem.* **2014**, 19, 319.
14. Frisch, M. J.; Trucks, G. W.; Schlegel, H. B.; Scuseria, G. E.; Robb, M. A.; Cheeseman, J. R.; Scalmani, G.; Barone, V.; Mennucci, B.; Petersson, G. A.; Nakatsuji, H.; Caricato, M.; Li, X.; Hratchian, H. P.; Izmaylov, A. F.; Bloino, J.; Zheng, G.; Sonnenb, D. J. *Gaussian, Inc.*: Wallingford CT 2013.
15. Becke, A. D. *J. Chem. Phys.* **1993**, 98, 1372.
16. Lee, C.; Yang, W.; Parr, R. G. *Phys. Rev. B* **1988**, 37, 785.
17. Vosko, S. H.; Wilk, L.; Nusair, M. *Can. J. Phys.* **1980**, 58, 1200.
18. Stephens, P. J.; Devlin, F. J.; Chabalowski, C. F.; Frisch, M. J. *J. Phys. Chem.* **1994**, 98, 11623.
19. Schäfer, A.; Huber, C.; Ahlrichs, R. *J. Chem. Phys.* **1994**, 100, 5829.
20. Schäfer, A.; Horn, H.; Ahlrichs, R. *J. Chem. Phys.* **1992**, 97, 2571.
21. Grimme, S.; Ehrlich, S.; Goerigk, L. *J. Comput. Chem.* **2011**, 32, 1456.
22. Marenich, A. V.; Cramer, C. J.; Truhlar, D. G. *J. Phys. Chem. B.* **2009**, 113, 6378.
23. Kendall, R. A.; Dunning, T. H.; Harrison, R. J. *J. Chem. Phys.* **1992**, 96, 6796.
24. Davidson, E. R. *Chem. Phys. Lett.* **1996**, 260, 514.
25. Marcus, R. a. *J. Chem. Phys.* **1956**, 24, 966.
26. Postils, V.; Company, A.; Solà, M.; Costas, M.; Luis, J. M. *Inorg. Chem.* **2015**, 54, 8223.
27. Amini, A.; Harriman, A. J. *Photochem. Photobiol. C Photochem. Rev.* **2003**, 4, 155.

ANNEX 4.



Supplementary Information Chapter VI

Orthogonal discrimination among functional groups in Ullmann-type C-O and C-N couplings

Mireia Rovira, Marta Soler, Imma Güell, Ming-Zheng Wang, Laura Gómez, Xavi Ribas*

QBIS Research Group, Departament de Química, Universitat de Girona, Campus Montilivi, Girona E-17071, Catalonia, Spain.

CONTENTS

1. Supplementary methods	249
1.1. Instrumentation	249
2. Supplementary Schemes	251
Scheme S1. Competition reactions using iodobenzene	251
Scheme S2 and S3. Competition reactions using <i>p</i> -iodotoluene and <i>p</i> -iodonitrobenzene	252
Scheme S4. Competition reactions using bromobenzene	253
Scheme S5. Competition reactions using chlorobenzene	255
Scheme S6. Selected coupling reactions with significant formation of benzene via protodecupration	256
3. Supplementary Figures	257
3.1. Supplementary Figures S3	257
3.2. Supplementary Figures. Auxiliary ligand	274
4. Supplementary tables	277
5. Supplementary references	281

1. Supplementary methods

1.1 Instrumentation

^1H and ^{13}C NMR spectra were recorded with a 400 MHz or 300 MHz NMR spectrometer. Chemical shifts (δ) are reported in ppm and were directly referenced to the solvent signal. GC product analyses were performed with a gas chromatograph equipped with an HP-5 capillary column (30 m \times 0.32 mm \times 0.25 μm) and a flame ionization detector. GC–MS analyses were performed with a gas chromatograph equipped with an HP-5 capillary column interfaced with a mass spectrometer. The electron ionization (EI) source was set at 70 eV.

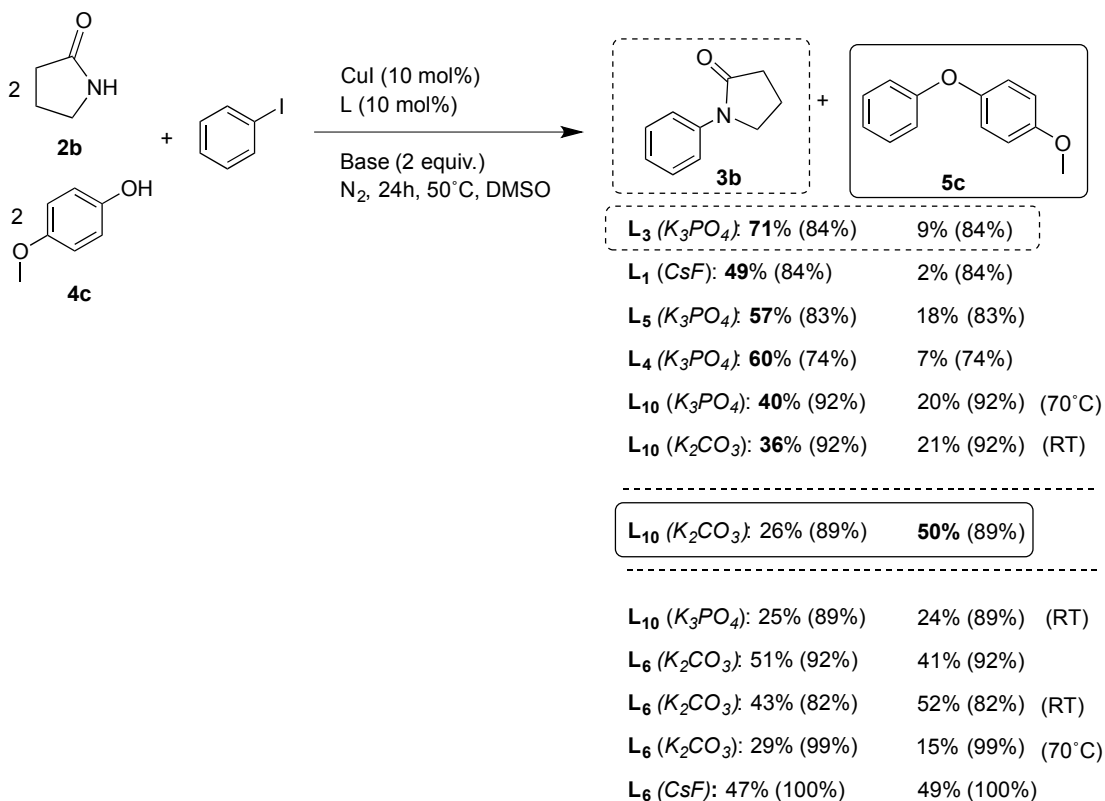
High resolution mass spectra (HRMS) were recorded with MicrOTOF-Q IITM instrument with ESI or Cryospray ionization sources. Samples were introduced into the mass spectrometer ion source by direct injection through a syringe pump and were externally calibrated by using sodium formate.

All analyses were carried out on gas chromatography instrument GC-System equipped with a fused silica capillary column HP-5 19091J-102 (25m x 200 μ m x 0.33 μ m). The stationary phase used is 5%-phenylmethylpolysiloxane. Temperatures range, in which the column is working, cannot be higher than 325°C. The injection was carried out on a split/splitless automatic injector at 275°C, in split mode with ratio 100:1 and volume injected was 1 μ L. Helium was the carrier gas at a rate of 2ml/min in inlet. The detection was conducted by a FID, which temperature was 300°C, and the hydrogen flow rate was 40mL/min and air flow rate was 350 mL/min, respectively, with a makeup flow of 20 mL/min. The temperature program was as follows: starting at 75°C for 0.5 min and then raised to 190°C at 10°C/min. A ramp to 300°C at 20°C/min and 1 min hold was needed to purge the system. The analysis time was 18.5 min.

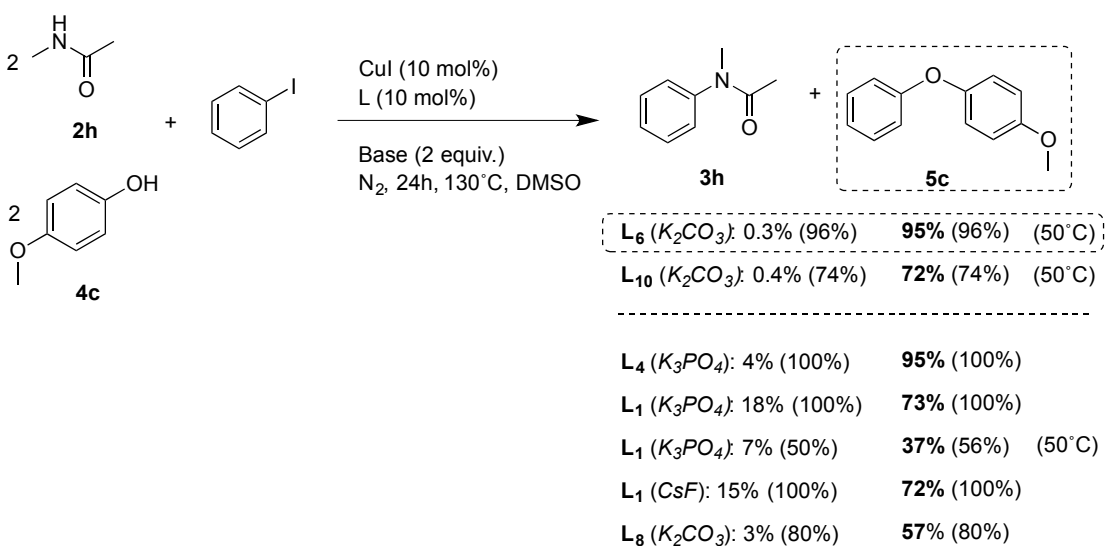
2. Supplementary Schemes

Scheme S1. Competitive reactions using iodobenzene (conversions are given in parenthesis).

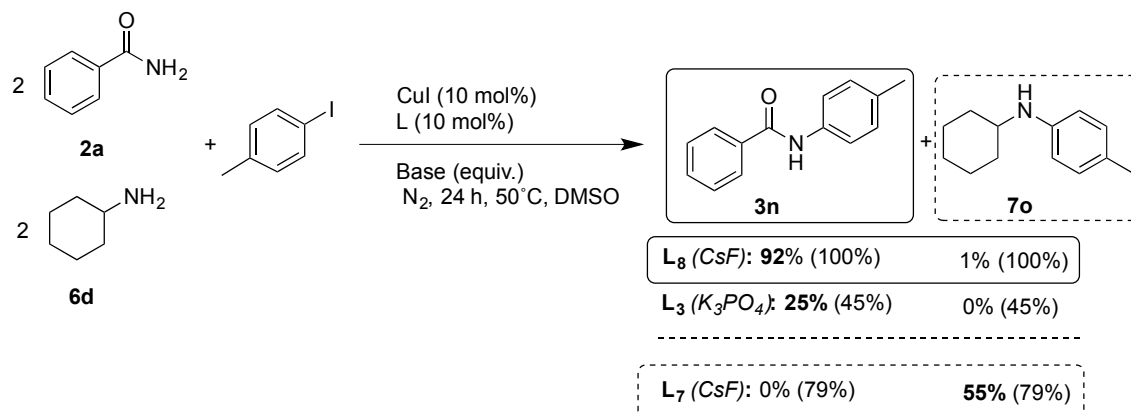
A) (expanded Scheme 7M, main text)



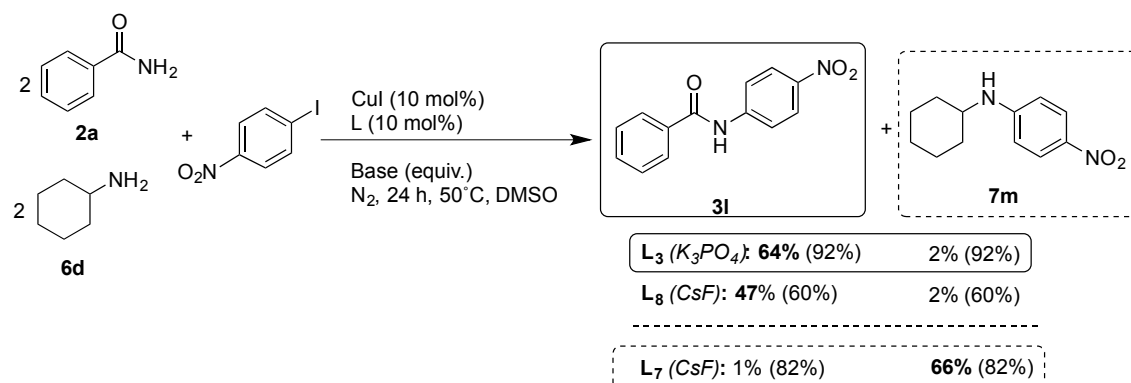
B) (expanded Scheme 8C, main text)

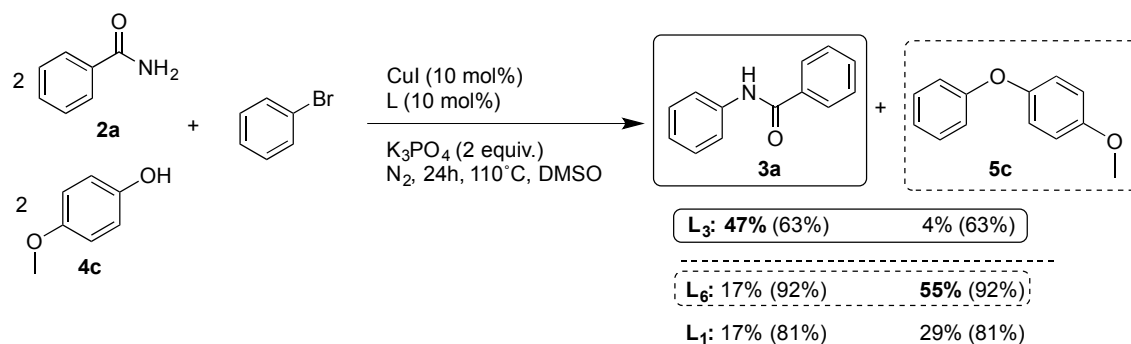
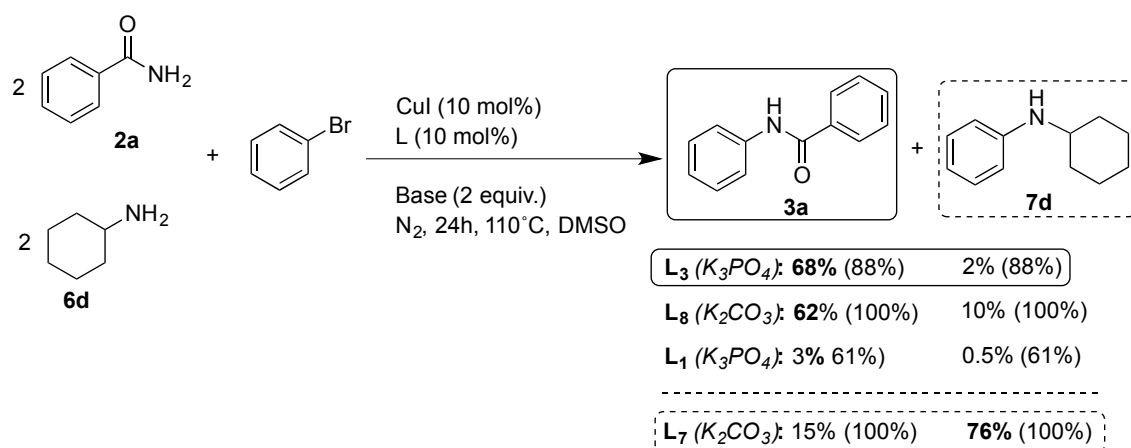
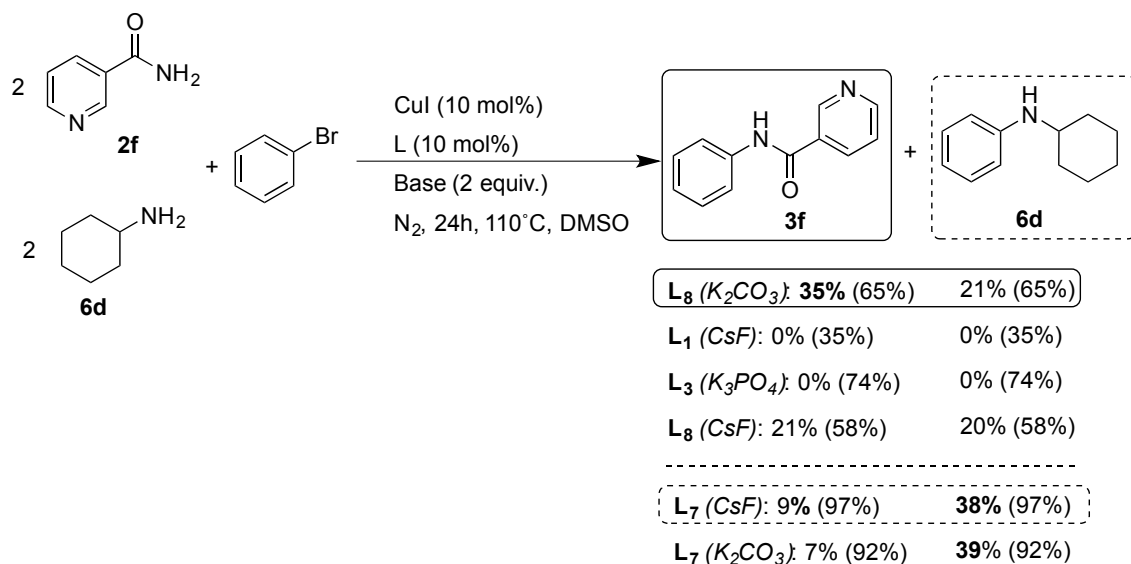


Scheme S2. Competitive reactions using *p*-iodotoluene (conversions are given in parenthesis). Characterization of **3n** and **7o** has been performed following the experimental description published in ref [1].

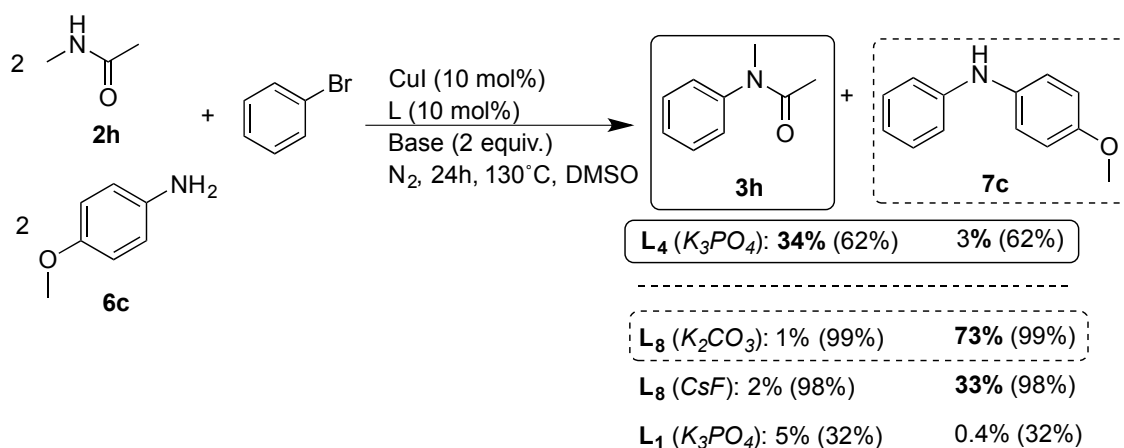


Scheme S3. Competitive reactions using *p*-iodonitrobenzene (conversions are given in parenthesis). Characterization of **3l** and **7m** has been performed following the experimental description published in ref [1].

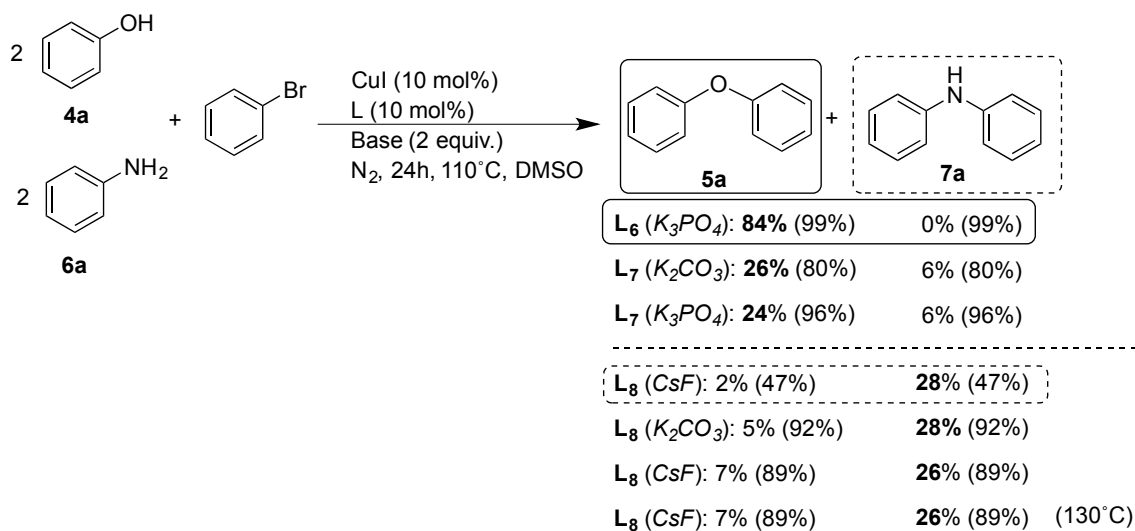
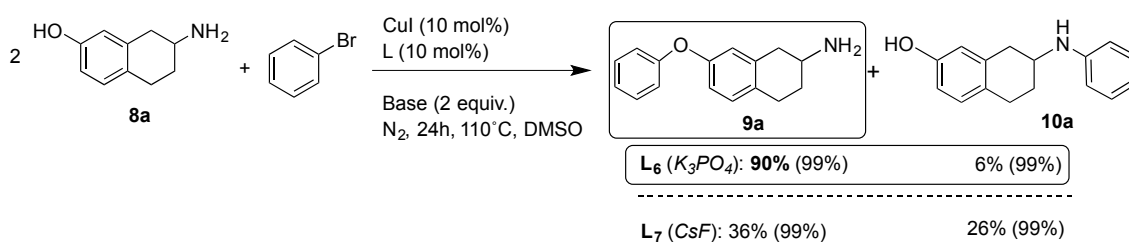


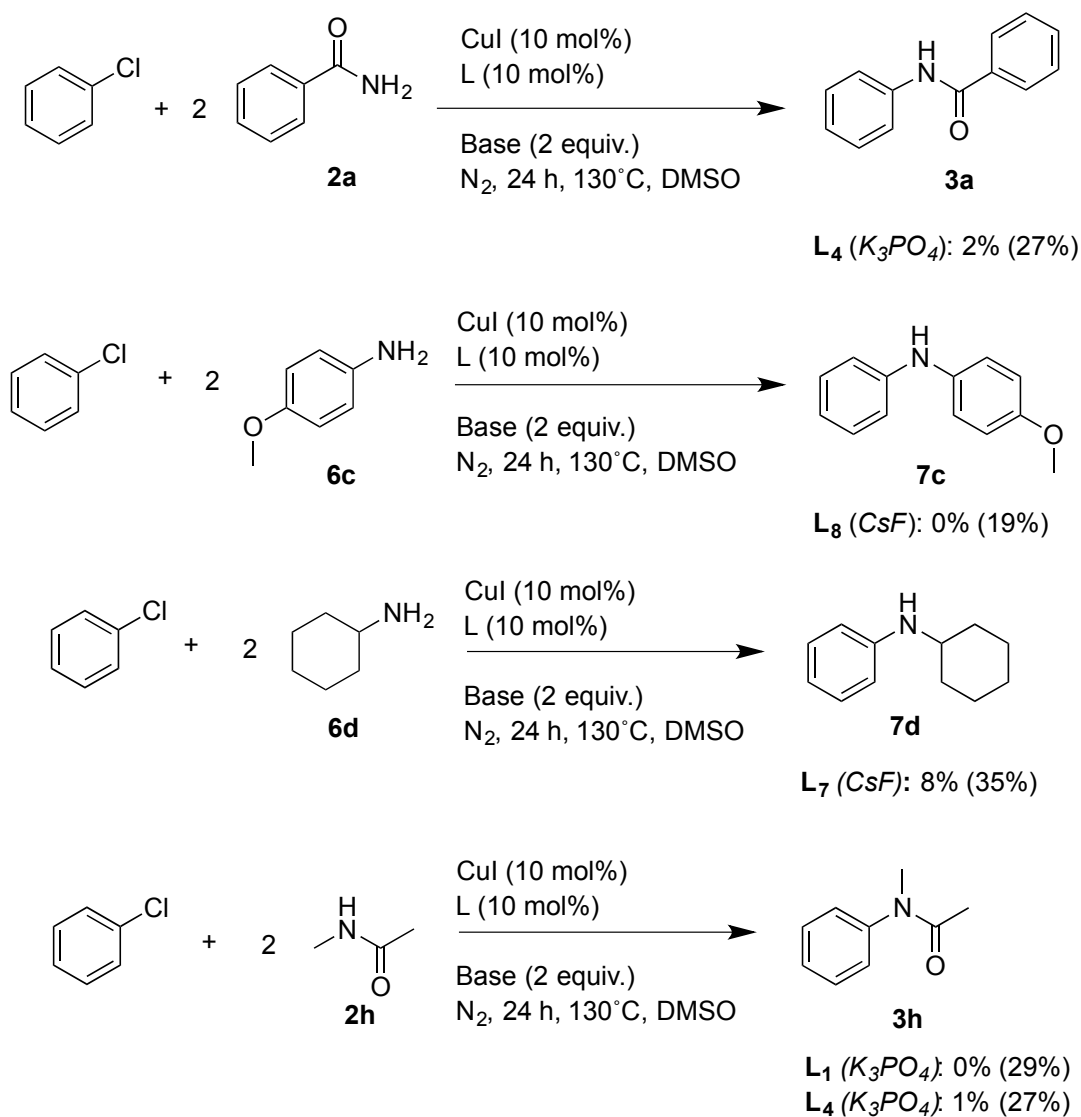
Scheme S4. Competition reactions using bromobenzene (conversions are given in parenthesis).Competition A' (analogous to Scheme 7A, main text)Competition C' (analogous to Scheme 7C, main text)Competition D' (analogous to Scheme 7D, main text)

Competition G' (analogous to Scheme 7G, main text)

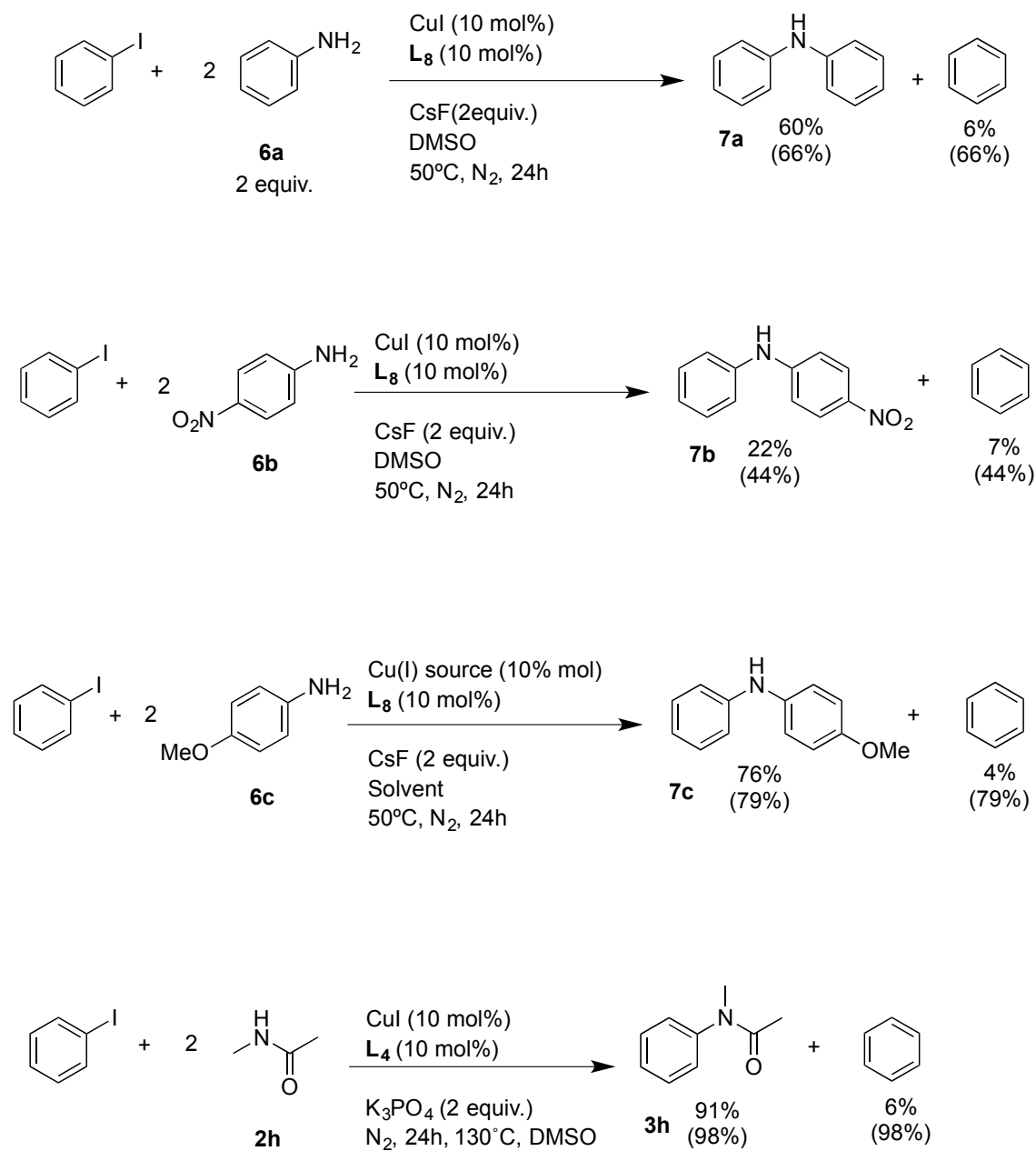


Competition J' (analogous to Scheme 7J, main text)

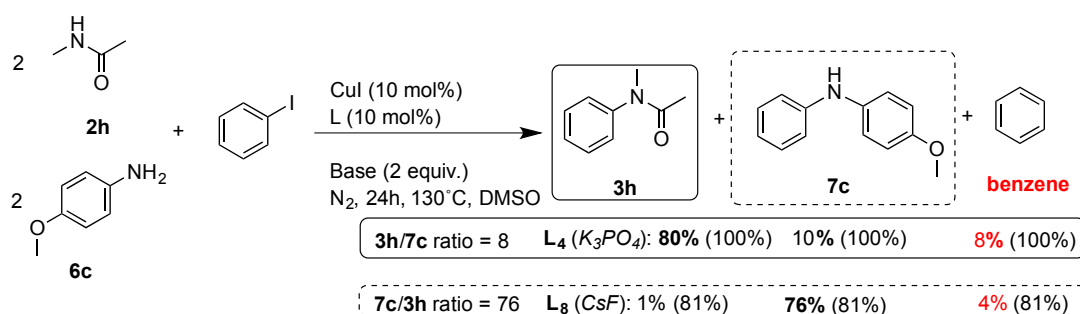
Bifunctional **8a** (analogous to Scheme 9A, main text)

Scheme S5. Reactions with chlorobenzene (conversions are given in parenthesis).

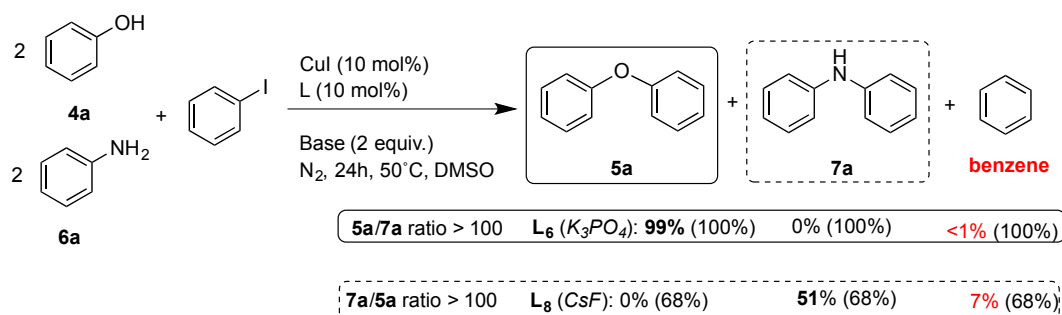
Scheme S6. Selected coupling reactions with significant formation of benzene via protodecupration (conversions are given in parenthesis).



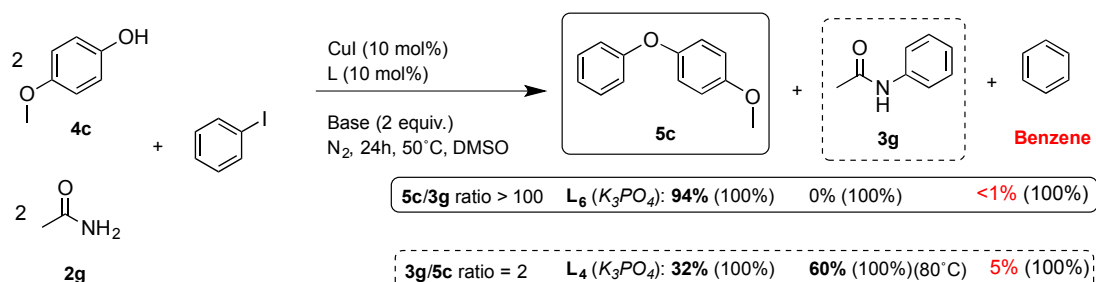
Expanded Scheme 7G, main text



Expanded Scheme 7J, main text



Expanded Scheme 7L, main text



3. Supplementary Figures (For more NMR spectra see CD-ROOM)

3.1 Supplementary Figures S3: ¹H NMR, ¹³C{¹H}NMR and ESI-TOF or GC-MS spectra

Conditions A: 10 mol% CuI, 10 mol% L, 2 eq. K₃PO₄, 50°C, 24h, N₂, DMSO.

Conditions C: 10 mol% CuI, 10 mol% L, 2 eq. K₃PO₄, 130°C, 24h, N₂, DMSO.

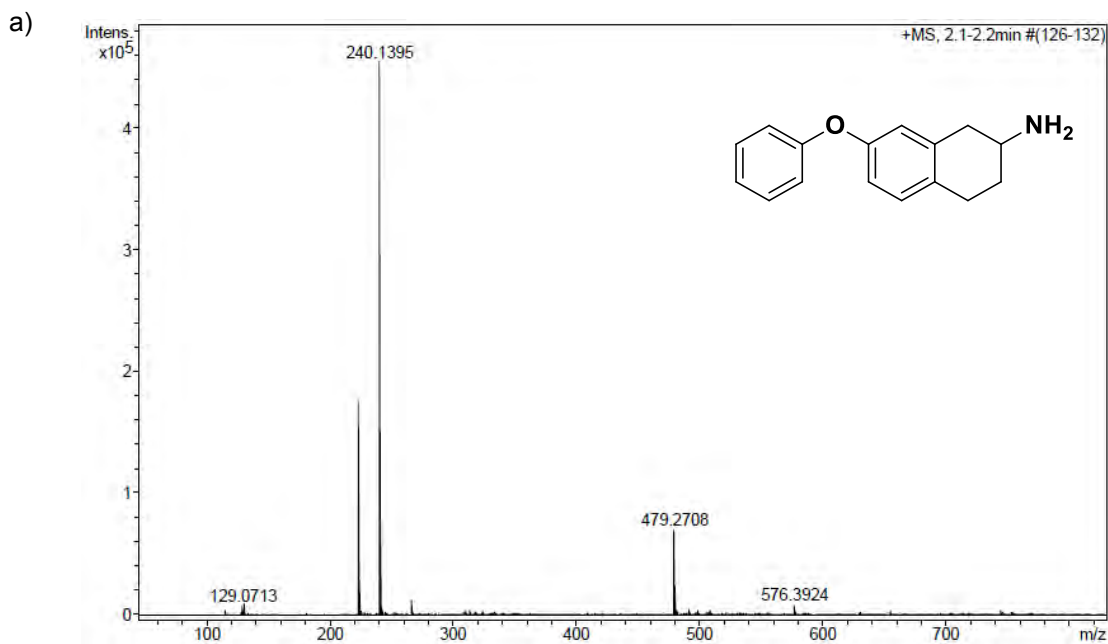
Conditions D: 10 mol% CuI, 10 mol% L, 2 eq. CsF, 50°C, 24h, N₂, DMSO.

Conditions F: 10 mol% CuI, 10 mol% L, 2 eq. K₃PO₄, 70°C, 24h, N₂, DMSO.

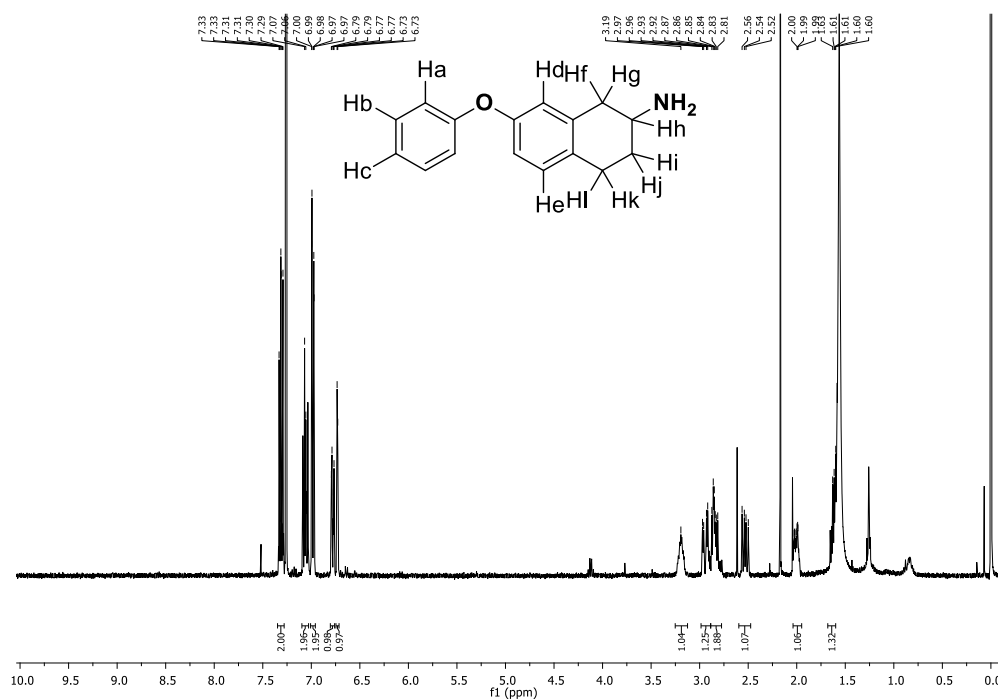
Conditions G: 10 mol% CuI, 10 mol% L, 2 eq. CsF, 70°C, 24h, N₂, DMSO.

Bifunctionals Substrates

Figure S1. 7-phenoxy-1,2,3,4-tetrahydronaphthalen-2-amine (9a): synthesized using conditions A and L_6 as an auxiliary ligand; a) HRMS (ESI-TOF) (m/z). b) ^1H -NMR spectrum (400 MHz, CDCl_3 , 25 °C). c) $^{13}\text{C}\{^1\text{H}\}$ -NMR spectrum (100 MHz, CDCl_3 , 25 °C).



b)



c)

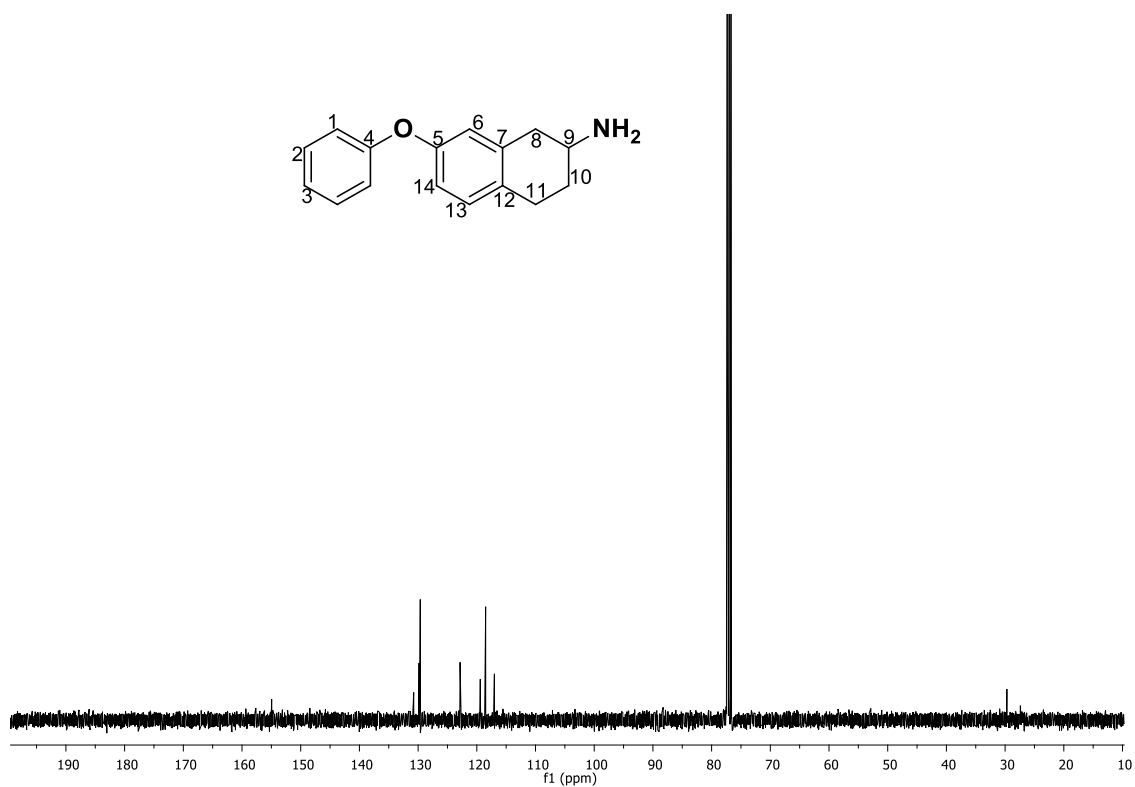
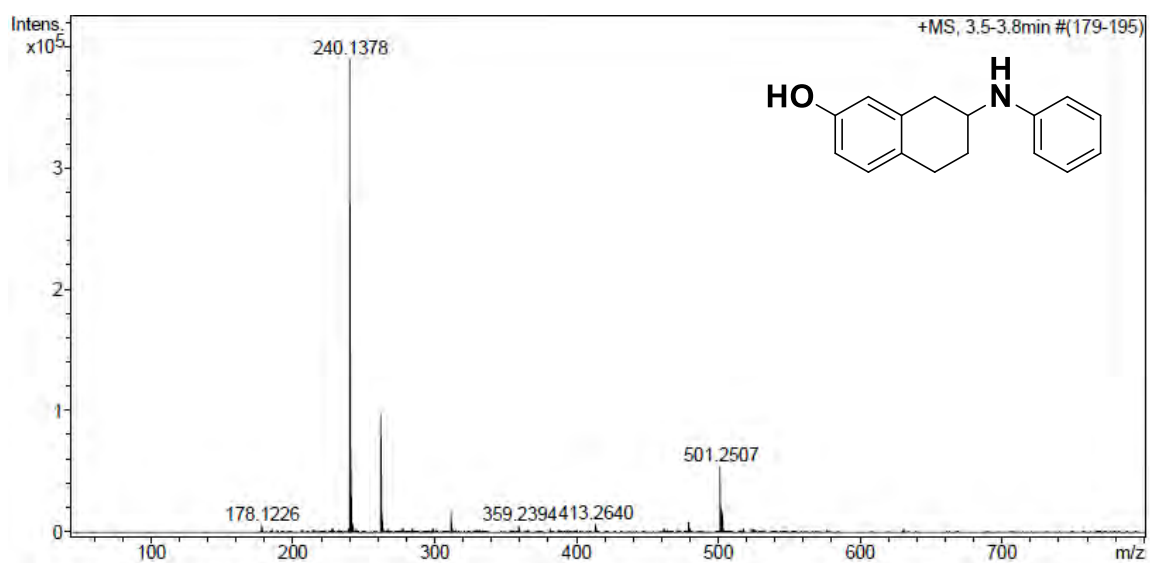
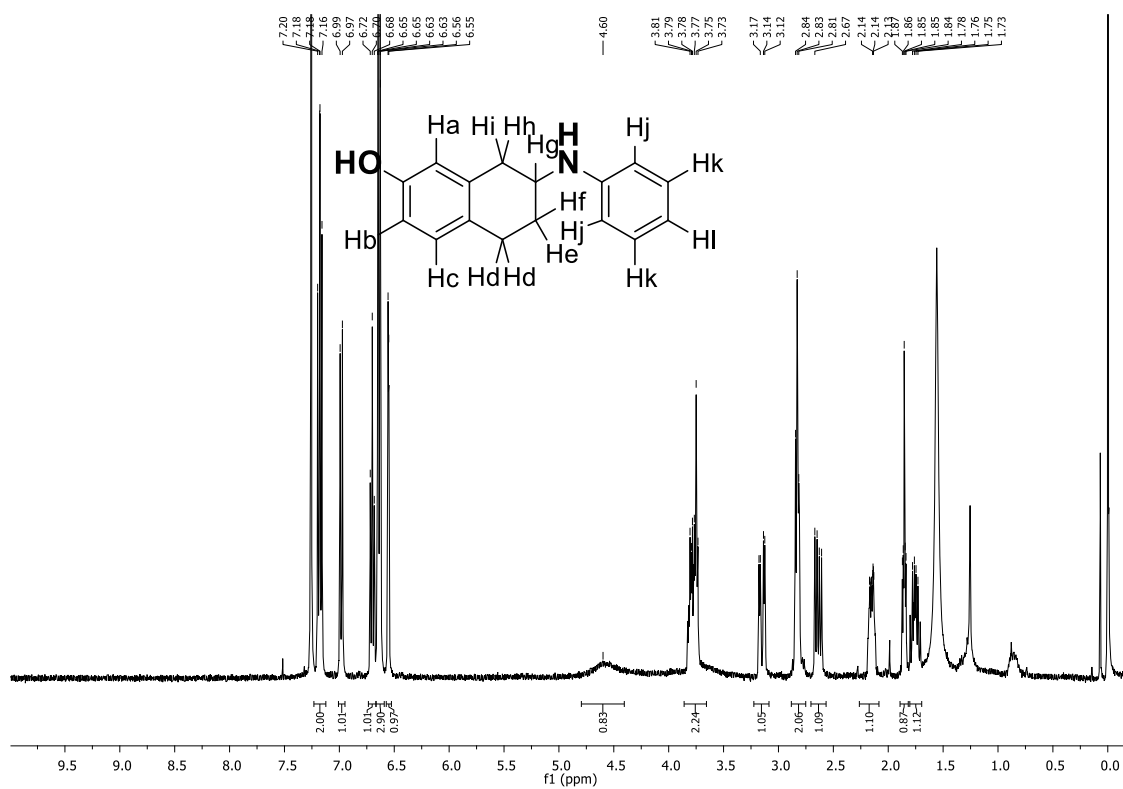


Figure S2. 7-(phenylamino)-5,6,7,8-tetrahydronaphthalen-2-ol (10a): synthesized using conditions D and 20 mol% of L_9 as an auxiliary ligand; a) HRMS (ESI-TOF) (m/z). b) ^1H -NMR spectrum (400 MHz, CDCl_3 , 25 °C). c) $^{13}\text{C}\{^1\text{H}\}$ -NMR spectrum (100 MHz, CDCl_3 , 25 °C).



b)



c)

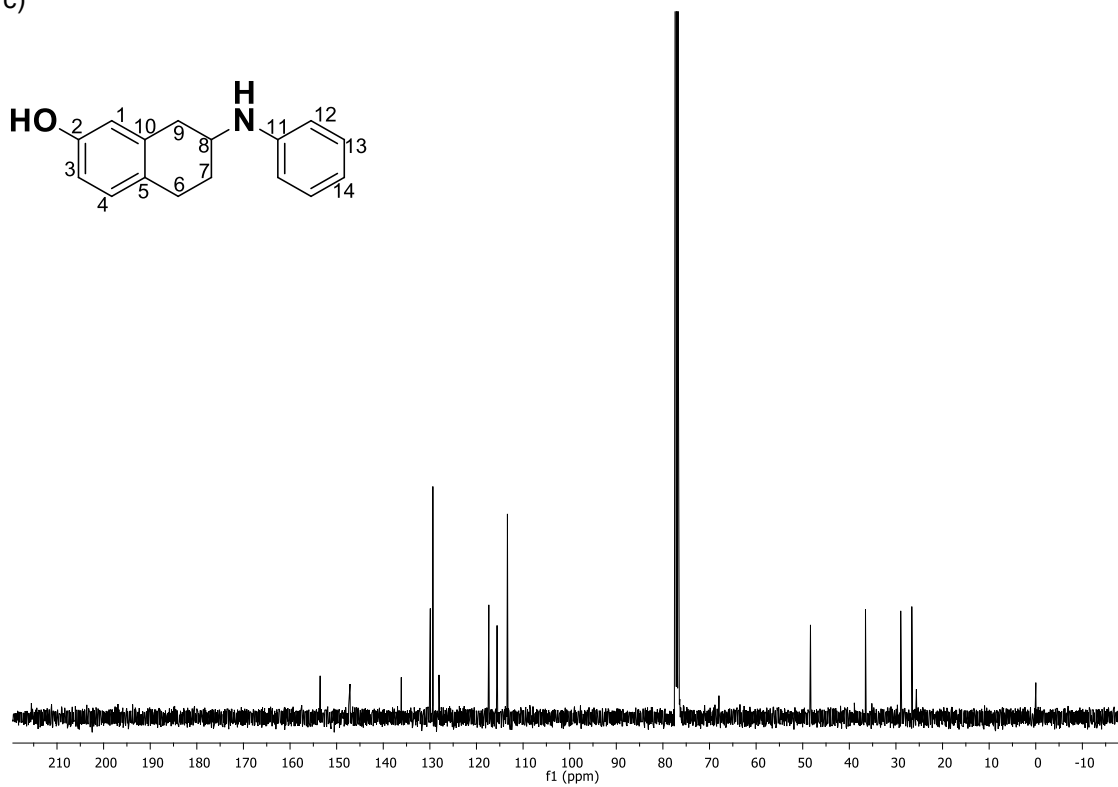
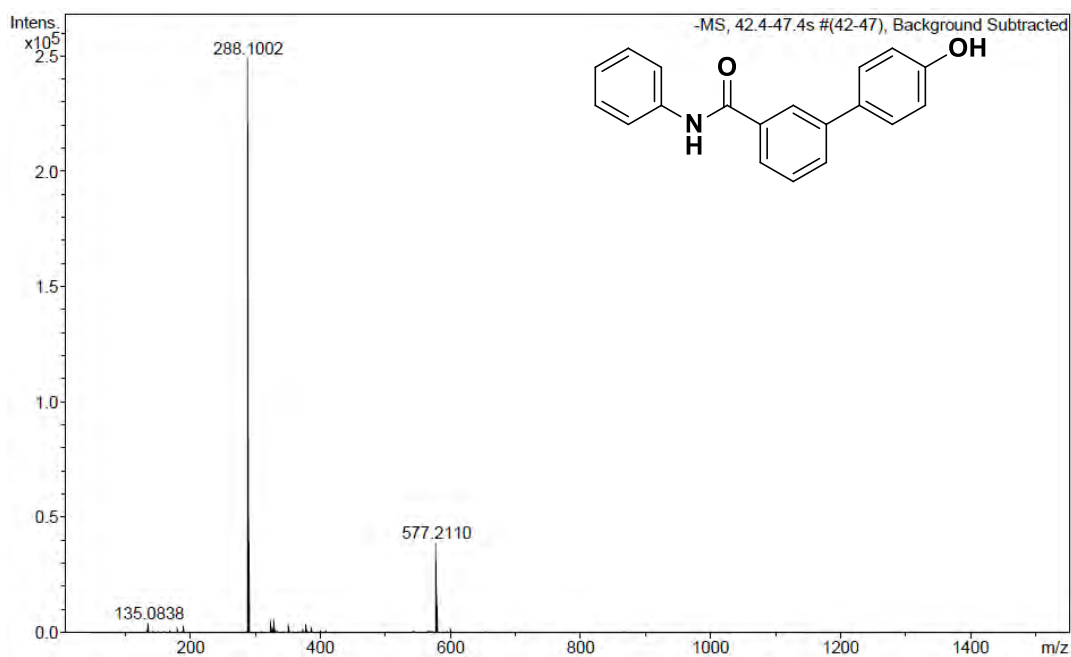
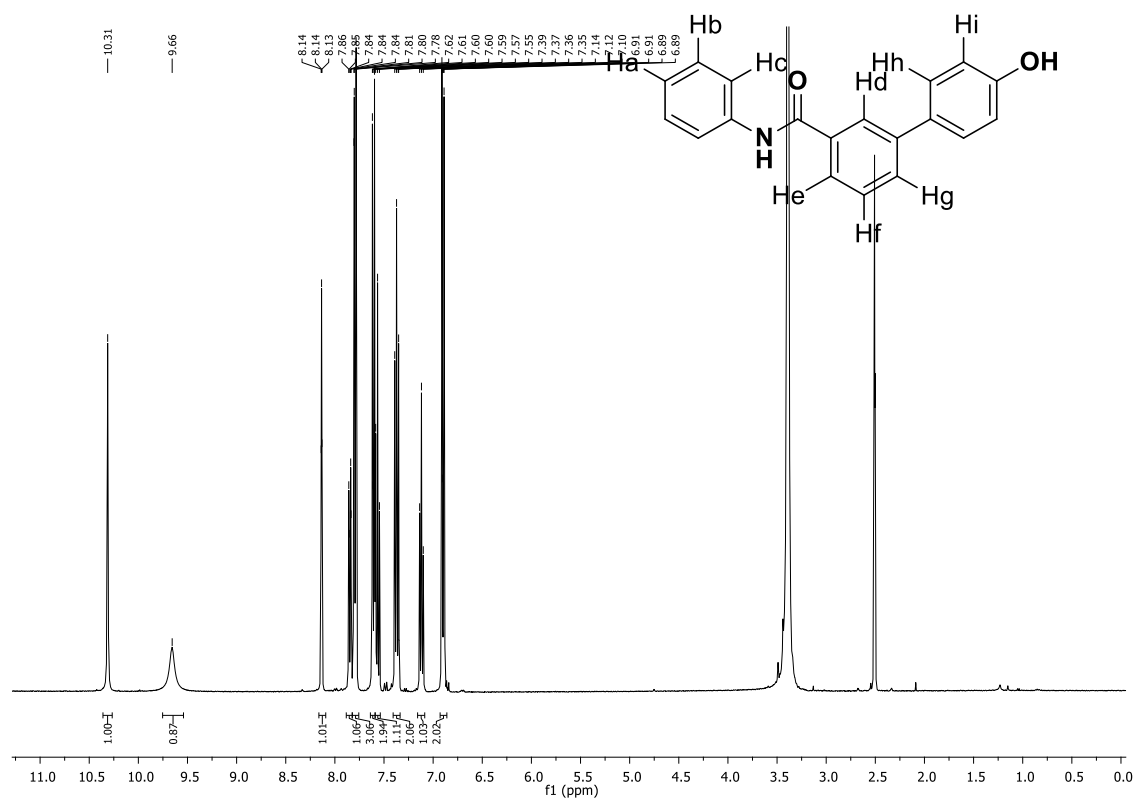


Figure S3. 4'-hydroxy-N-phenyl-[1,1'-biphenyl]-3-carboxamide (**9b**): synthesized using conditions A and L_3 as an auxiliary ligand; a) HRMS (ESI-TOF) (m/z). b) ^1H -NMR spectrum (400 MHz, DMSO-d_6 , 25 °C). c) $^{13}\text{C}\{^1\text{H}\}$ -NMR spectrum (100 MHz, DMSO-d_6 , 25 °C).

a)



b)



c)

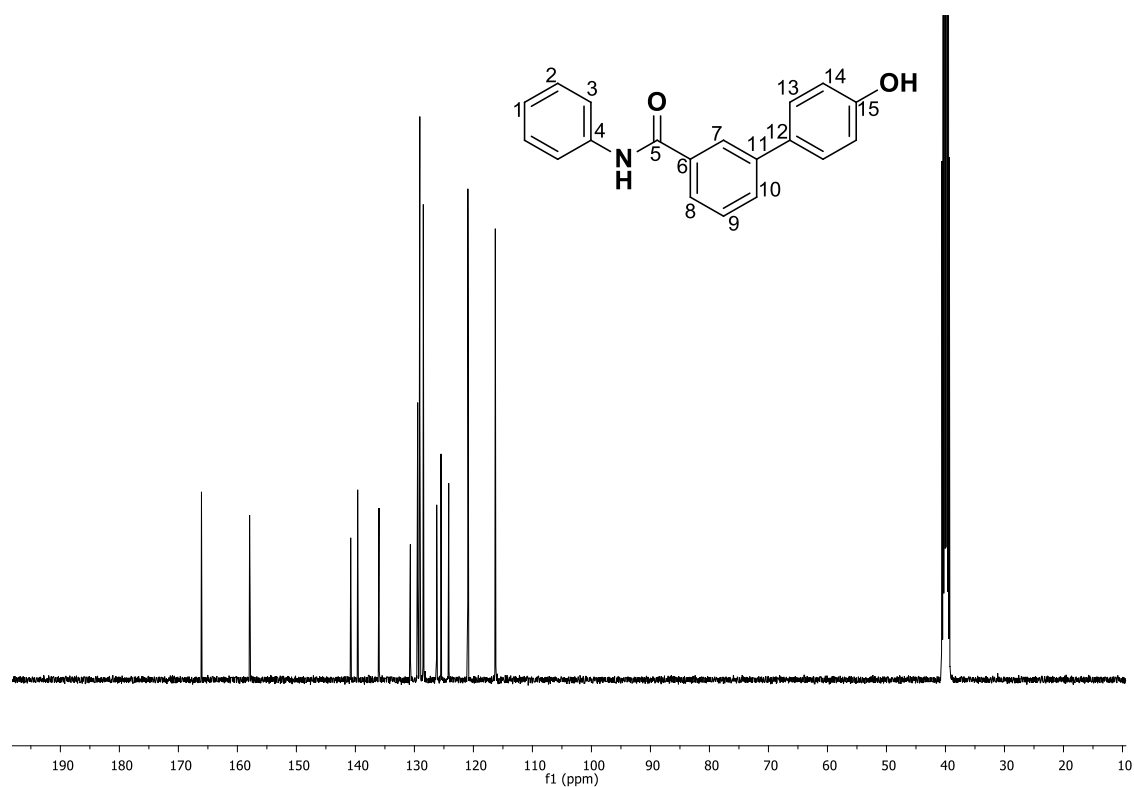
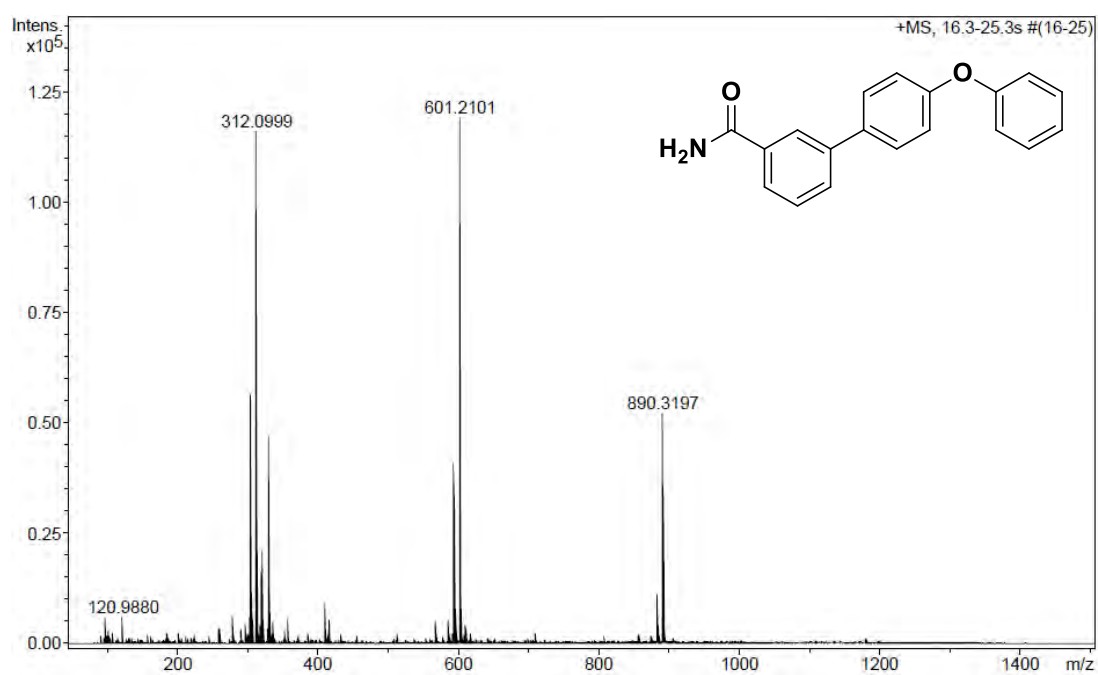
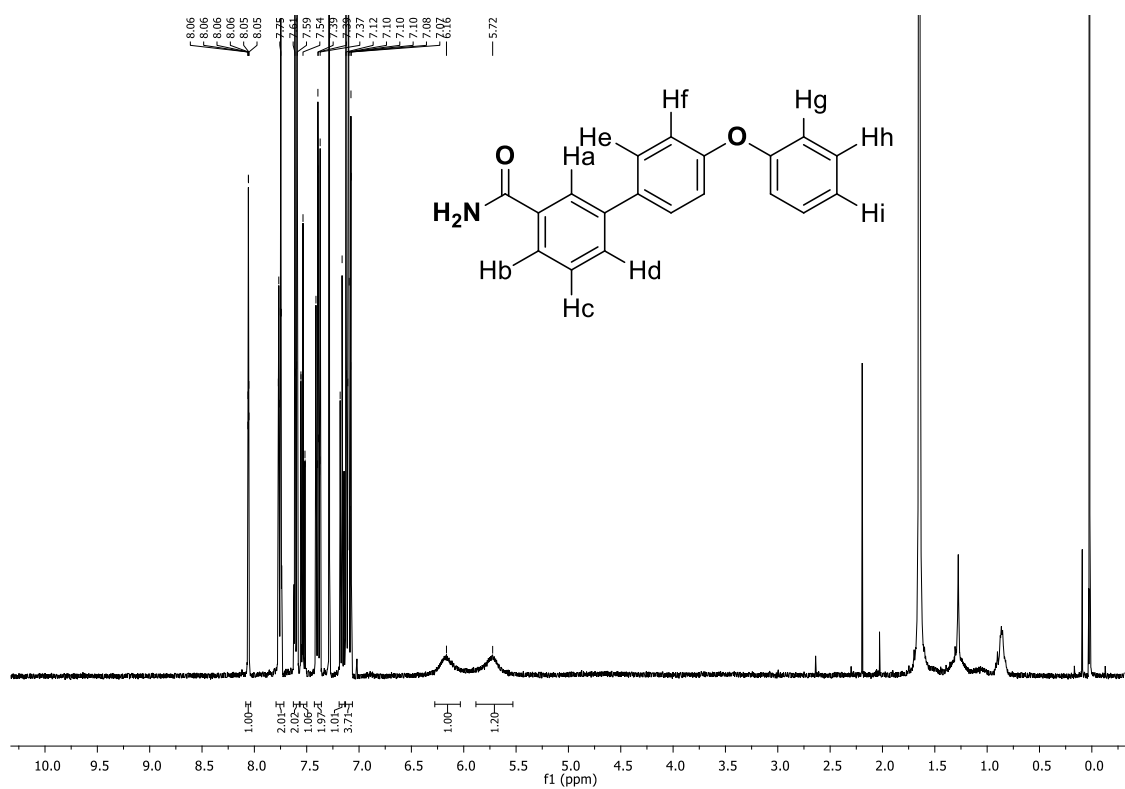


Figure S4. 4'-phenoxy-[1,1'-biphenyl]-3-carboxamide (**10b**): synthesized using conditions *F* and *L*₆ as an auxiliary ligand; a) HRMS (ESI-TOF) (*m/z*). b) ^1H -NMR spectrum (400 MHz, CDCl_3 , 25 °C). c) $^{13}\text{C}\{^1\text{H}\}$ -NMR spectrum (100 MHz, CDCl_3 , 25 °C).

a)



b)



c)

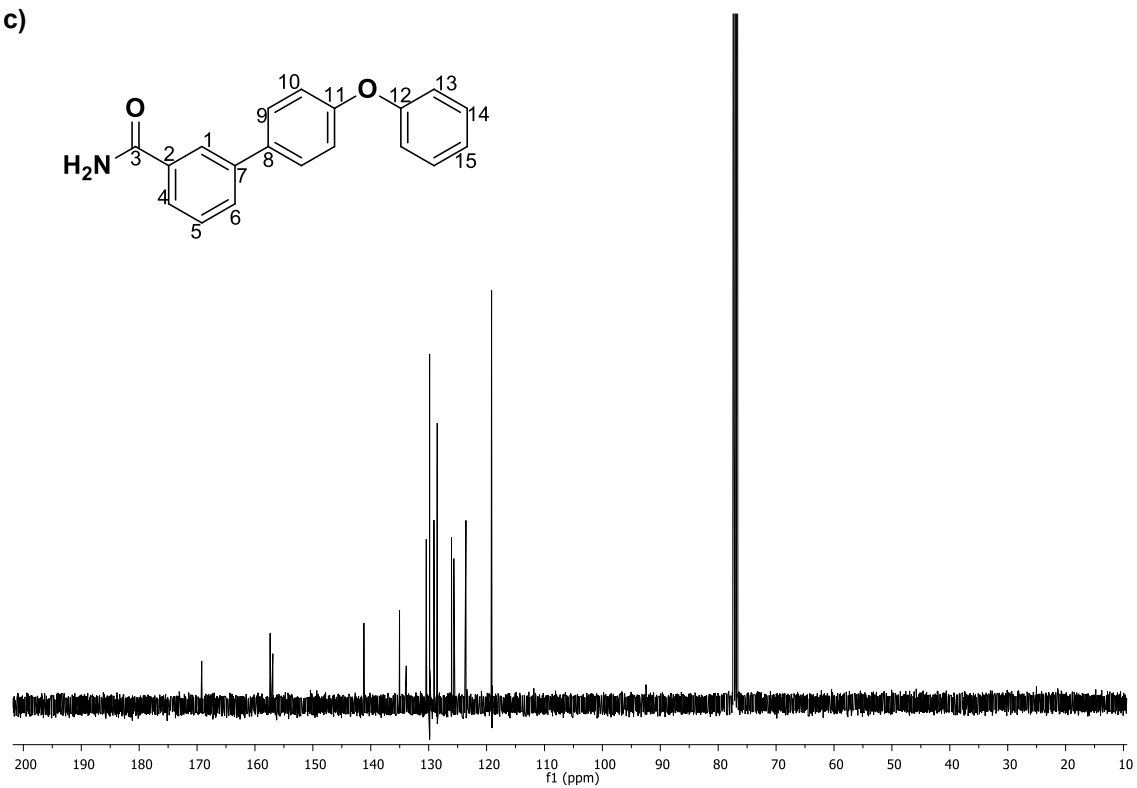
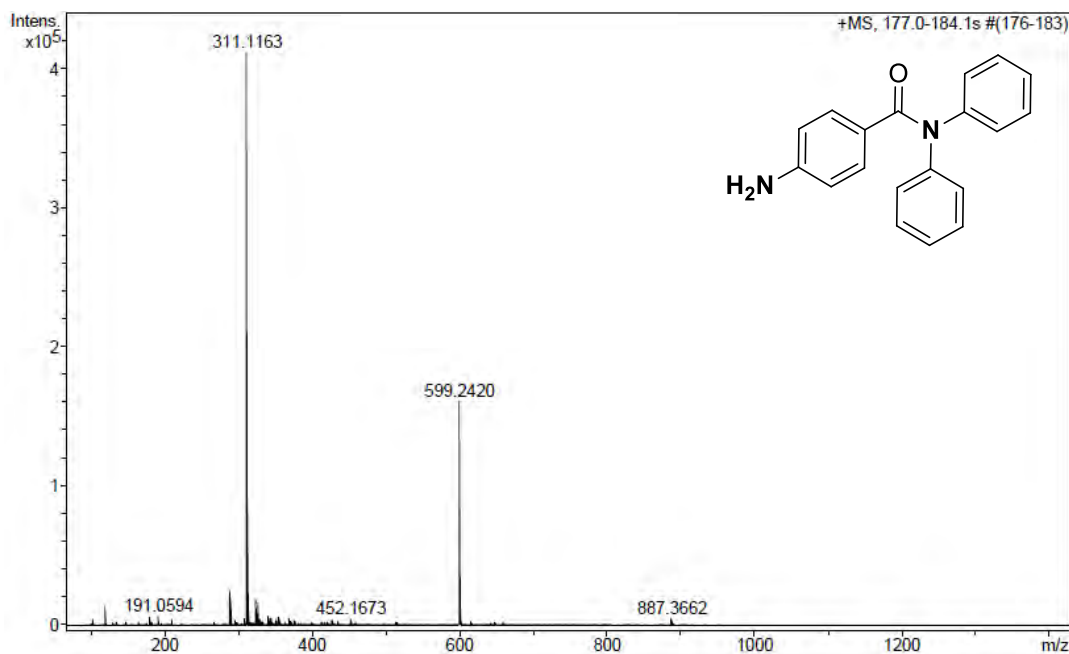
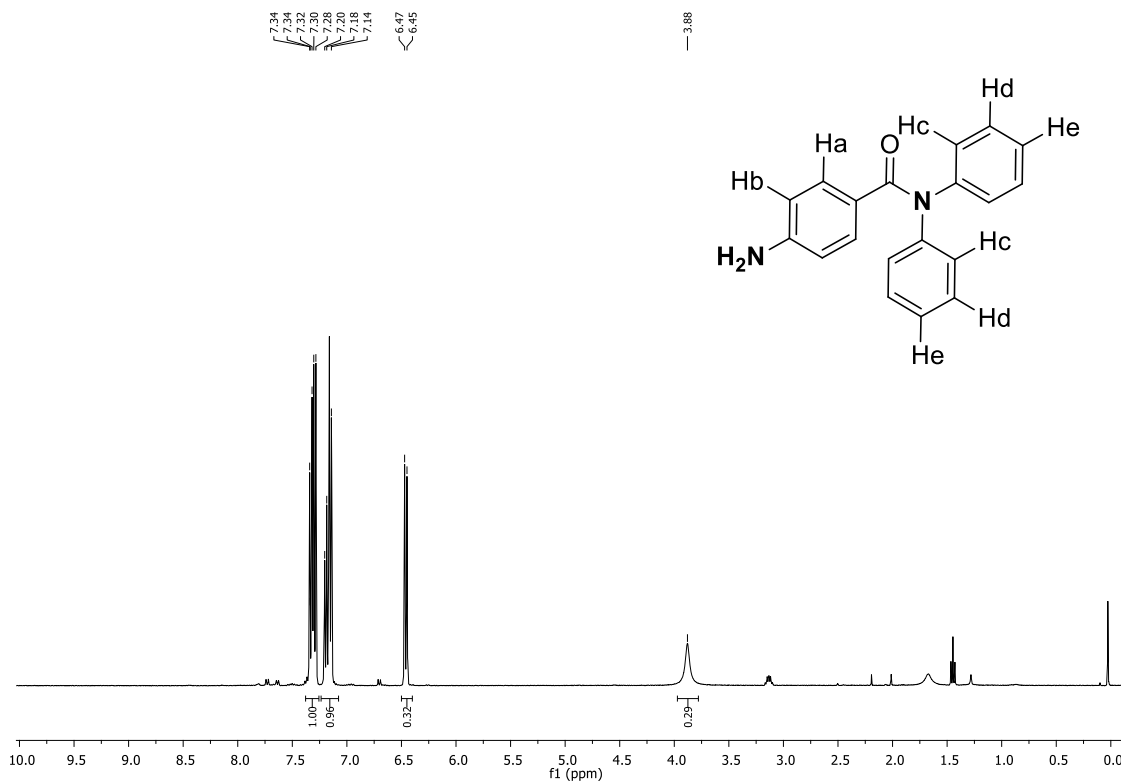


Figure S5. 4-amino-N,N-diphenylbenzamide (9c): synthesized using conditions C and L_4 as an auxiliary ligand; a) HRMS (ESI-TOF) (m/z). b) ^1H -NMR spectrum (400 MHz, CDCl_3 , 25 °C). c) $^{13}\text{C}\{^1\text{H}\}$ -NMR spectrum (100 MHz, CDCl_3 , 25 °C).

a)



b)



c)

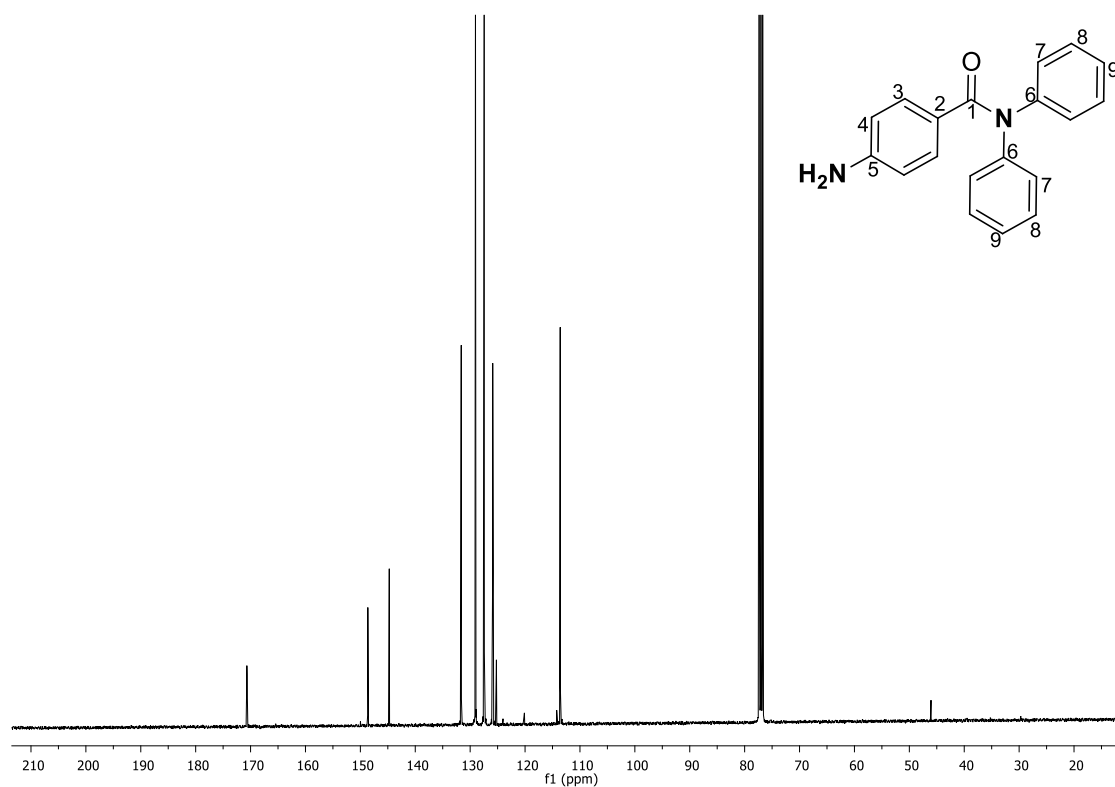
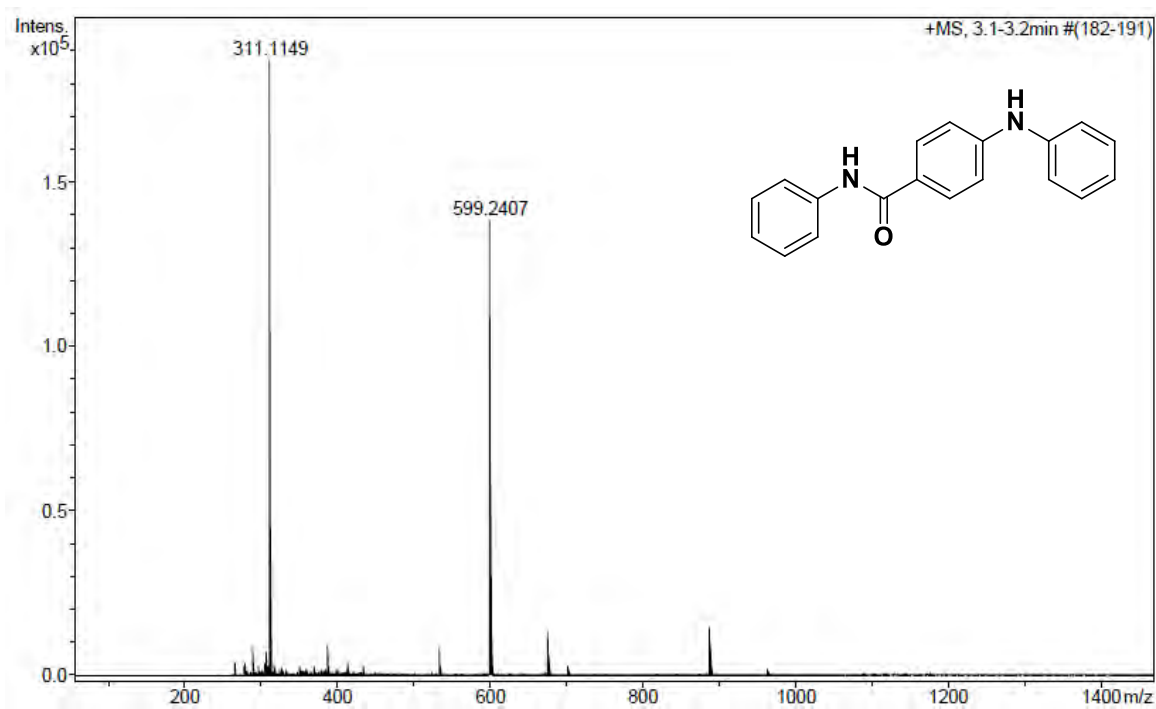
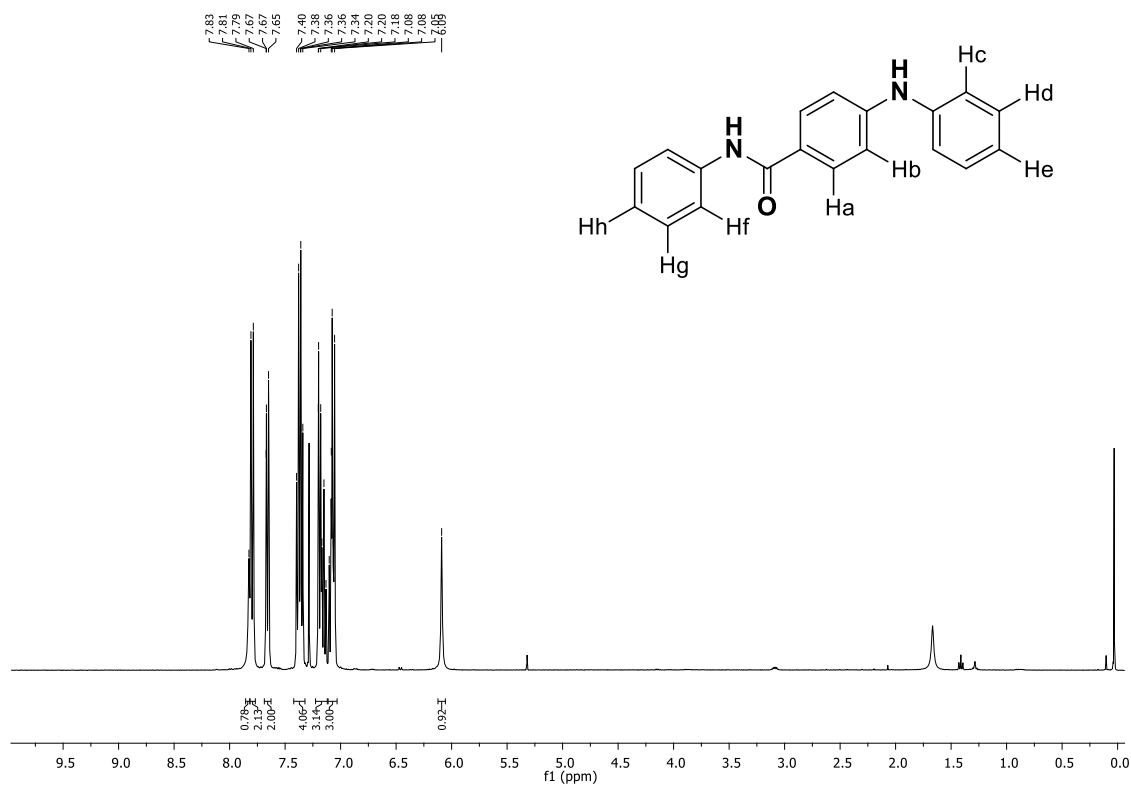


Figure S6. N-phenyl-4-(phenylamino)benzamide (10c): synthesized using conditions G and L₈ as an auxiliary ligand; a) HRMS (ESI-TOF) (m/z). b) ^1H -NMR spectrum (400 MHz, CDCl₃, 25 °C). c) $^{13}\text{C}\{^1\text{H}\}$ -NMR spectrum (100 MHz, CDCl₃, 25 °C)

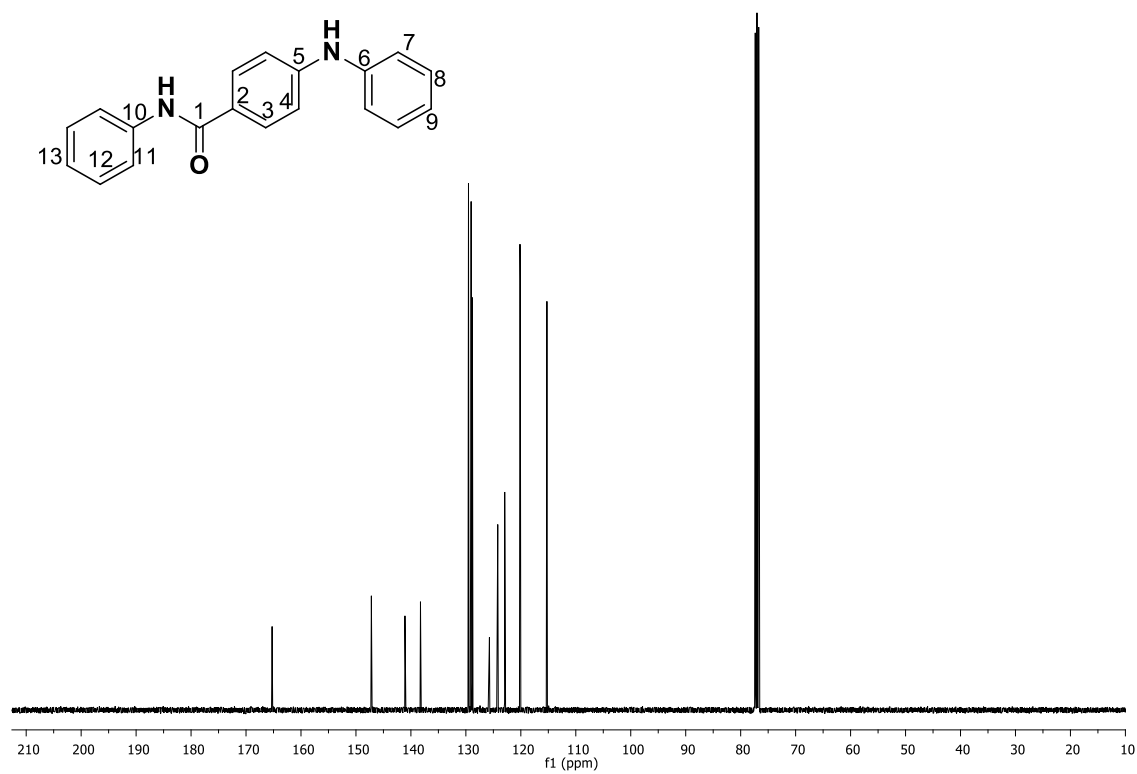
a)



b)



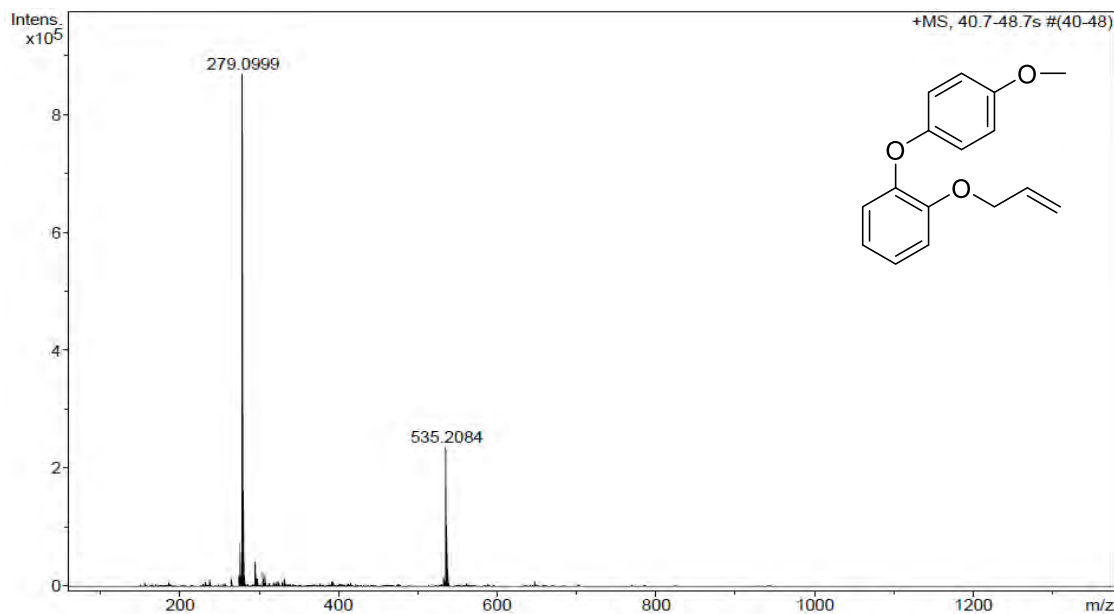
c)



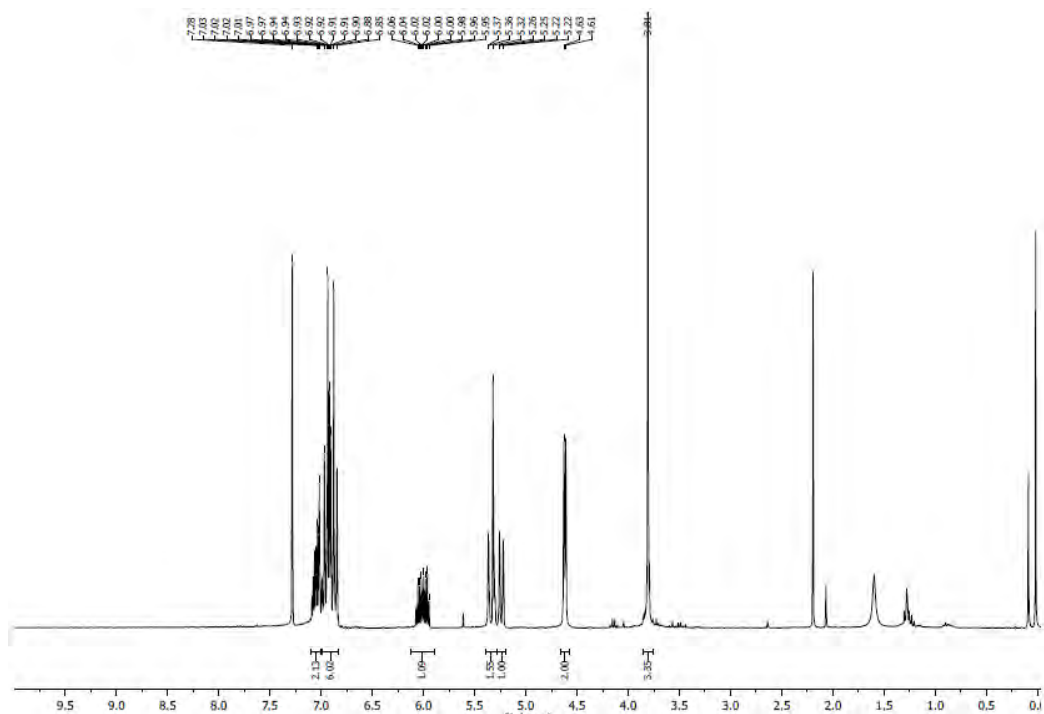
1-(allyloxy)-2-iodobenzene (rc) derivatives

Figure S7. 1-(allyloxy)-2-(4-methoxyphenoxy)benzene (rc-5c): synthesized using conditions A and L_6 as an auxiliary ligand; a) HRMS (ESI-TOF) (m/z). b) ^1H -NMR spectrum (300 MHz, CDCl_3 , 25 $^\circ\text{C}$). c) $^{13}\text{C}\{^1\text{H}\}$ -NMR spectrum (75 MHz, CDCl_3 , 25 $^\circ\text{C}$).

a)



b)



c)

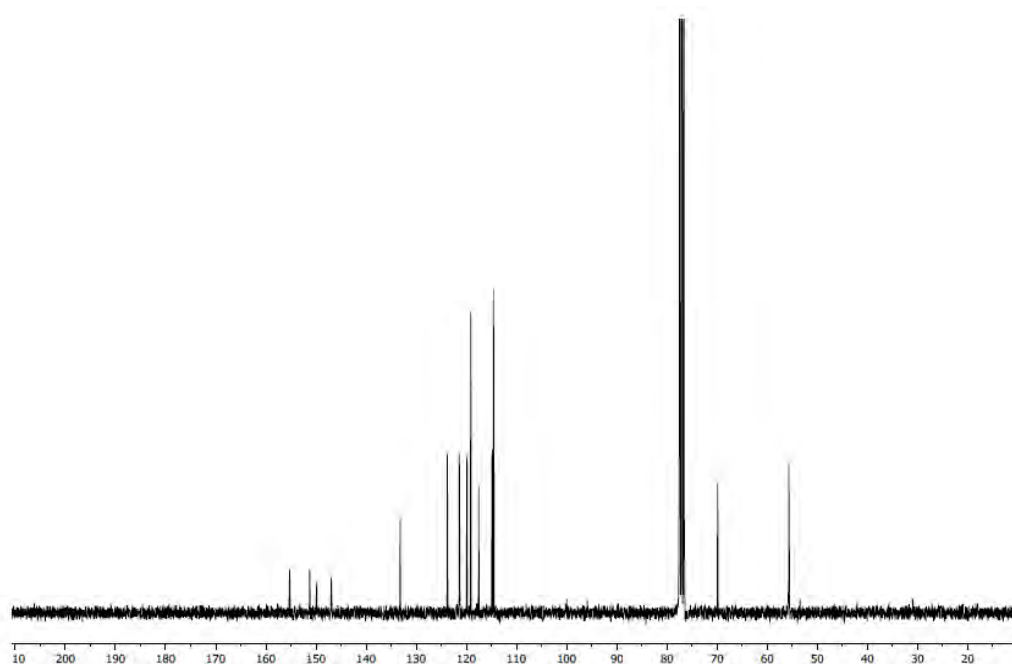
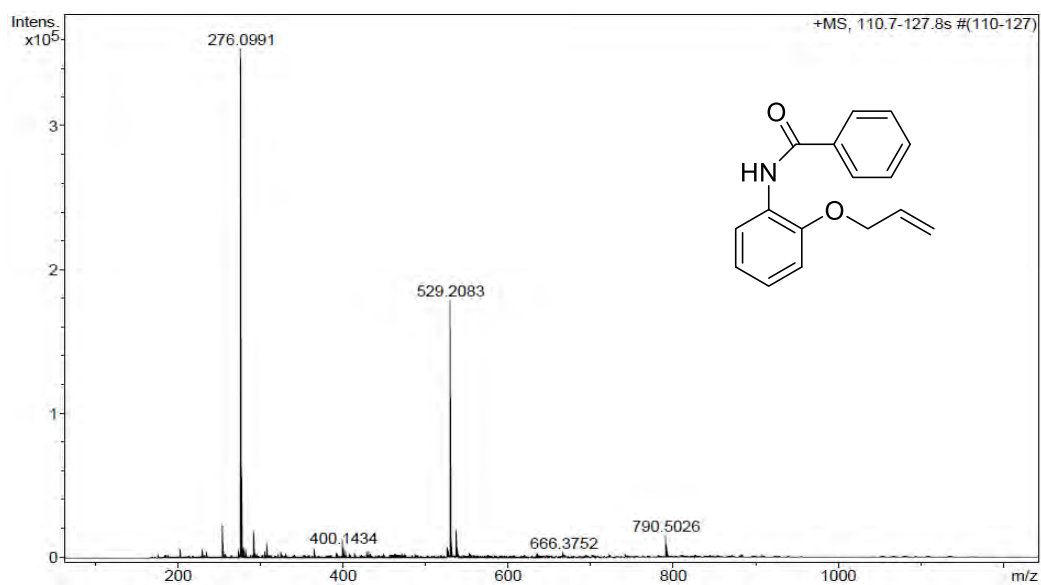
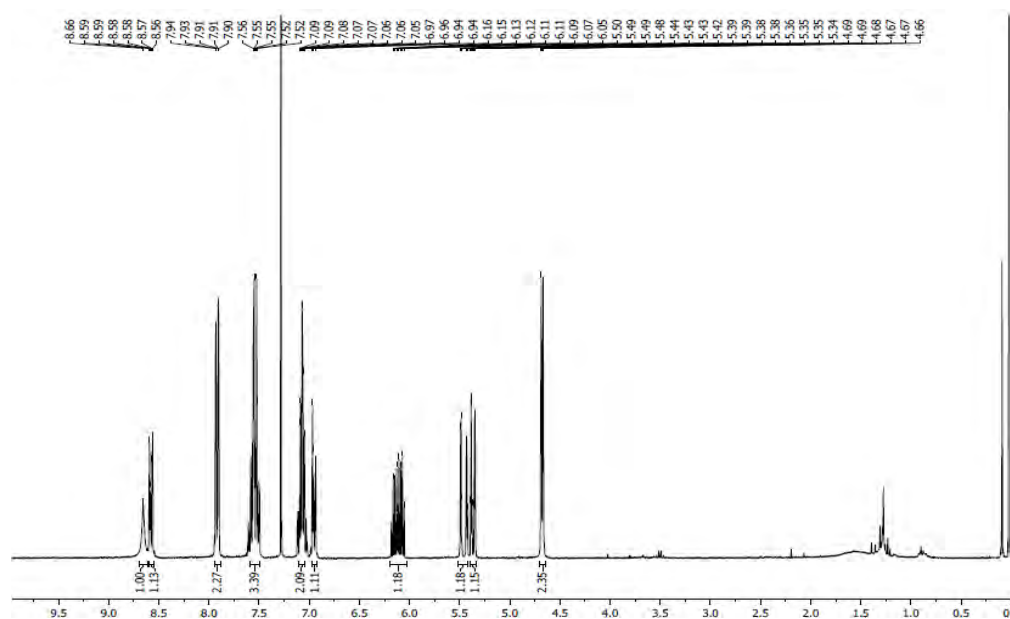


Figure S8. N-(2-(allyloxy)phenyl)benzamide (rc-3a): synthesized using conditions A and L_1 as an auxiliary ligand; a) HRMS (ESI-TOF) (m/z). b) ^1H -NMR spectrum (300 MHz, CDCl_3 , 25 °C). c) $^{13}\text{C}\{^1\text{H}\}$ -NMR spectrum (75 MHz, CDCl_3 , 25 °C).

a)



b)



c)

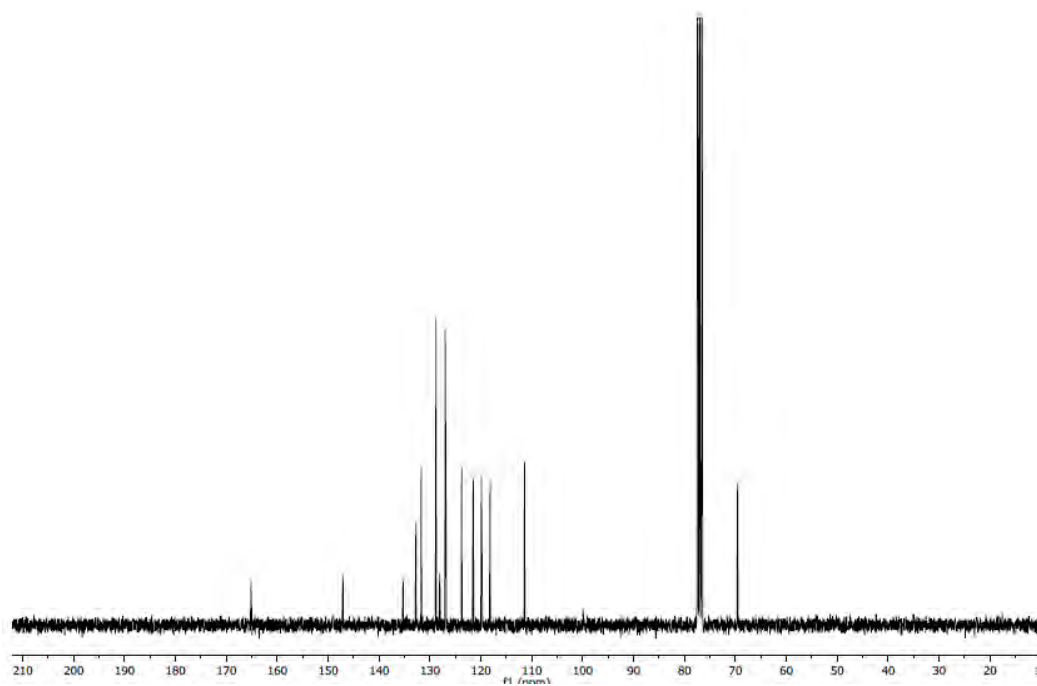
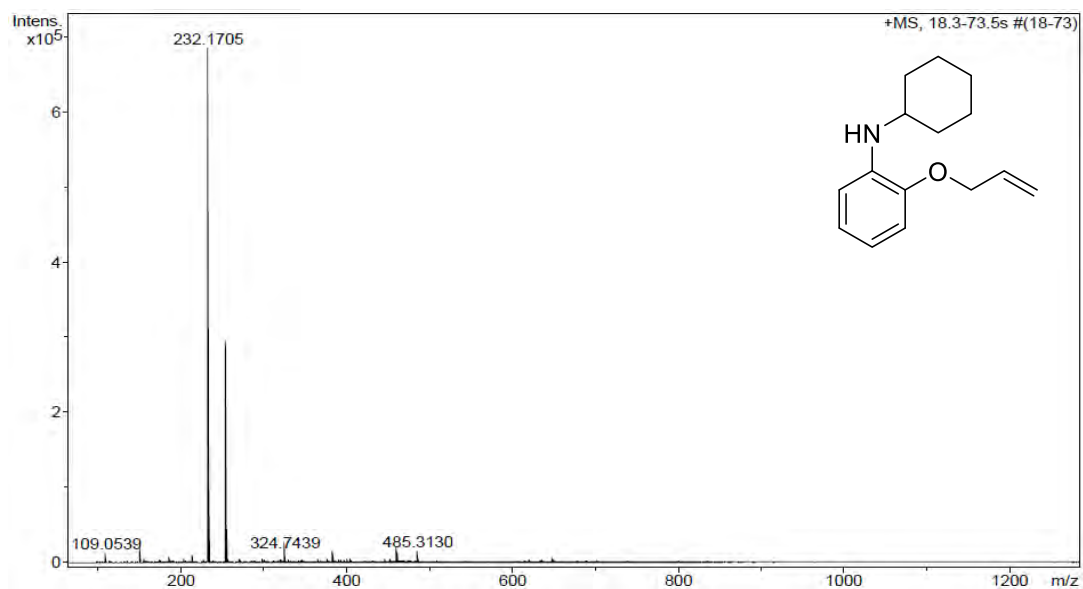
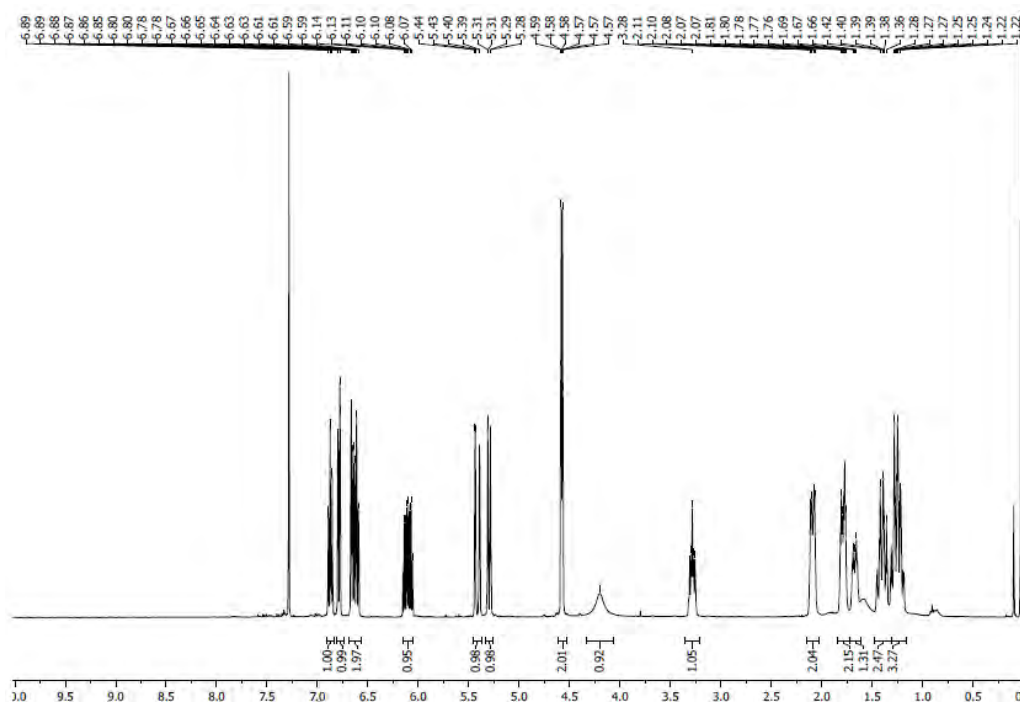


Figure S9. 2-(allyloxy)-N-cyclohexylaniline (rc-7d): synthesized using conditions H and L₇ as an auxiliary ligand; a) HRMS (ESI-TOF) (*m/z*). b) ¹H-NMR spectrum (400 MHz, CDCl₃, 25 °C). c) ¹³C{¹H}-NMR spectrum (100 MHz, CDCl₃, 25 °C).

a)



b)



c)

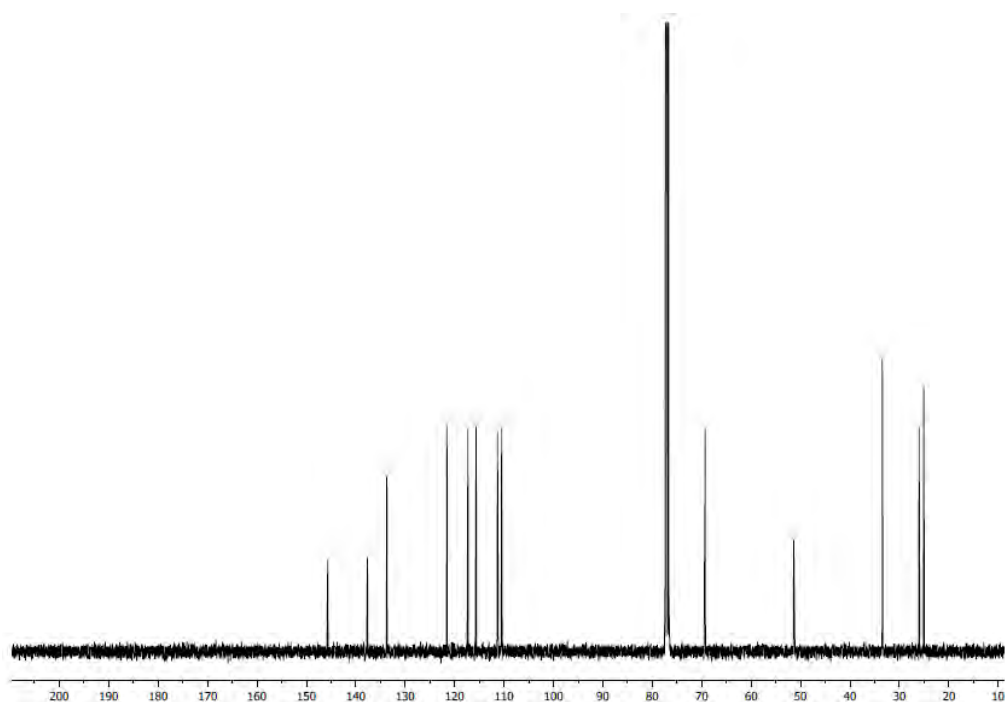
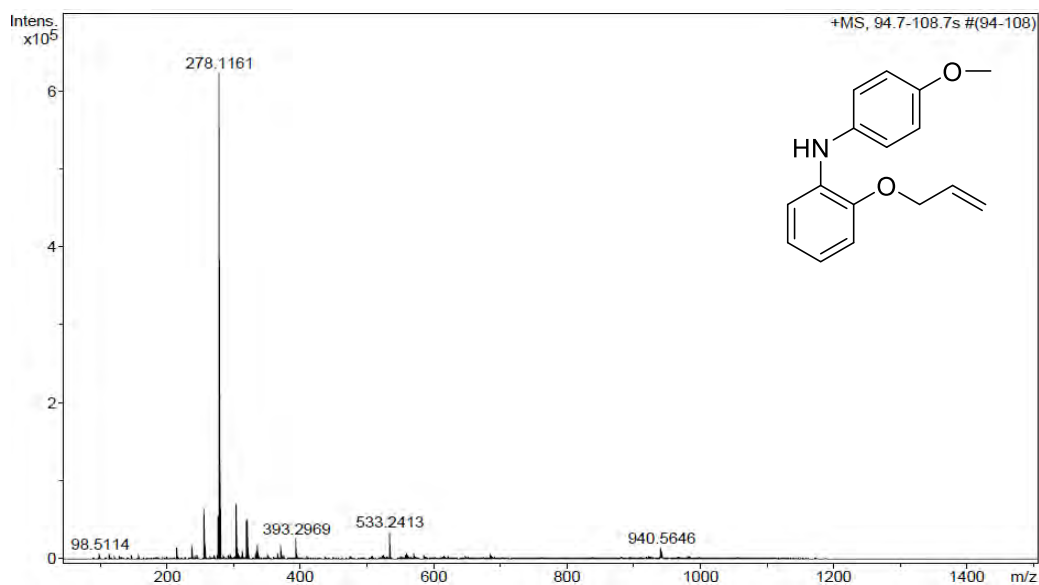
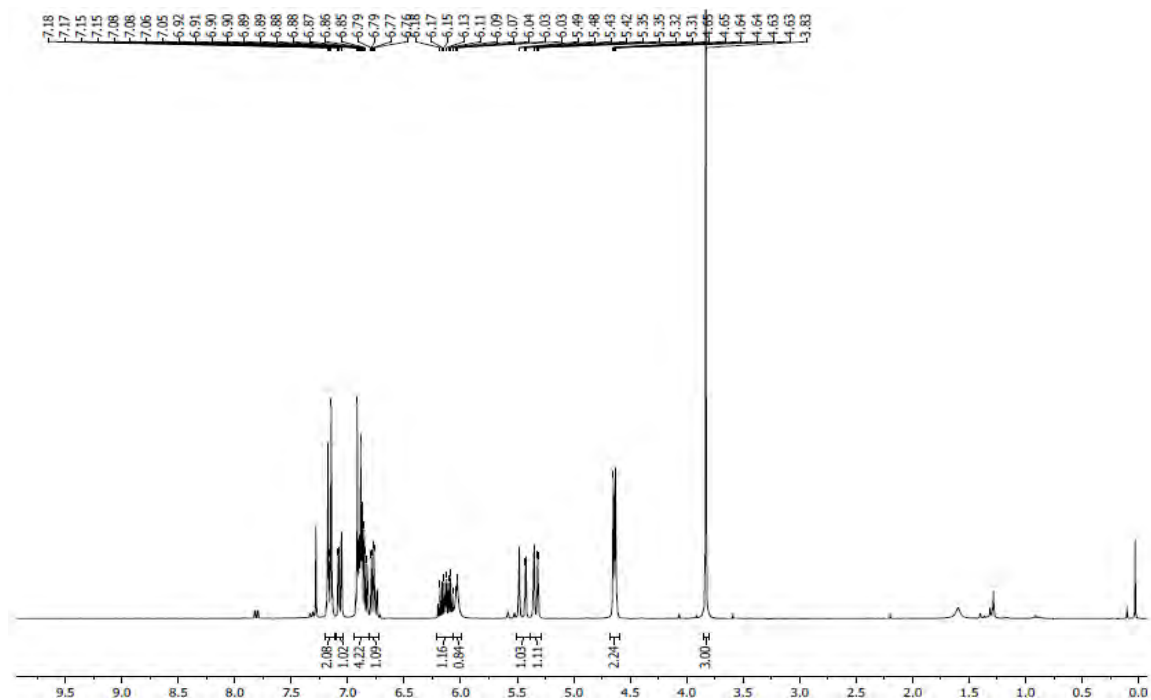


Figure S10. 2-(allyloxy)-N-(4-methoxyphenyl)aniline (**rc-7c**): synthesized using conditions *H* and *L₈* as an auxiliary ligand; a) HRMS (ESI-TOF) (*m* synthesized *z*). b) ^1H -NMR spectrum (400 MHz, CDCl_3 , 25 $^\circ\text{C}$). c) $^{13}\text{C}\{^1\text{H}\}$ -NMR spectrum (100 MHz, CDCl_3 , 25 $^\circ\text{C}$).

a)





c)

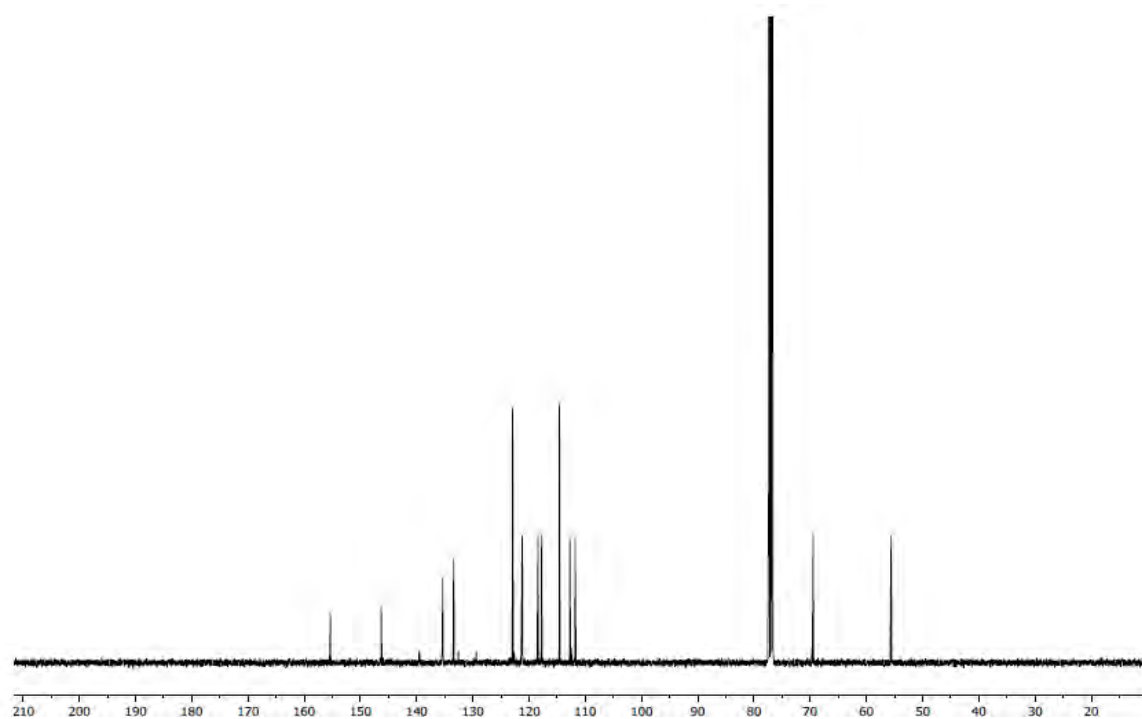
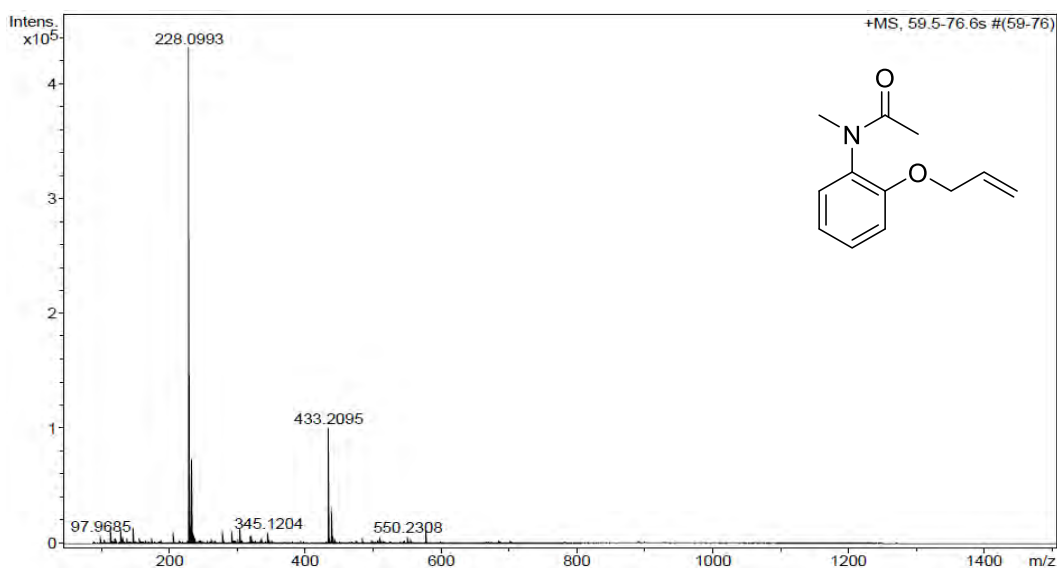
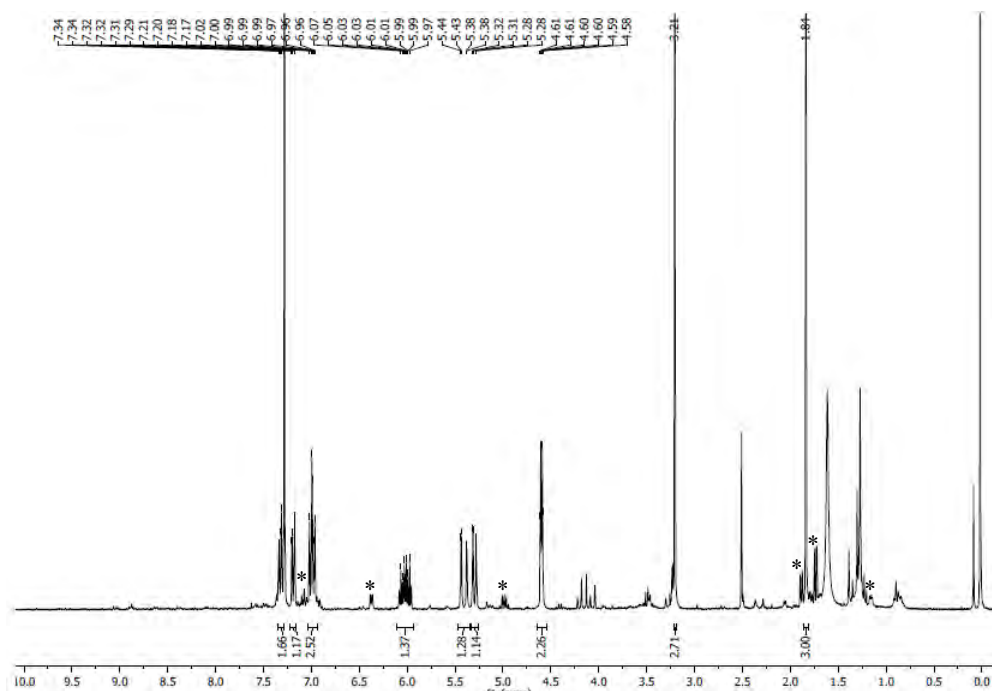


Figure S11. N-(2-(allyloxy)phenyl)-N-methylacetamide (rc-3h): synthesized using conditions C and L_4 as an auxiliary ligand; a) HRMS (ESI-TOF) (m/z). b) ^1H -NMR spectrum (300 MHz, CDCl_3 , 25 $^\circ\text{C}$). c) $^{13}\text{C}\{^1\text{H}\}$ -NMR spectrum (75 MHz, CDCl_3 , 25 $^\circ\text{C}$).

a)

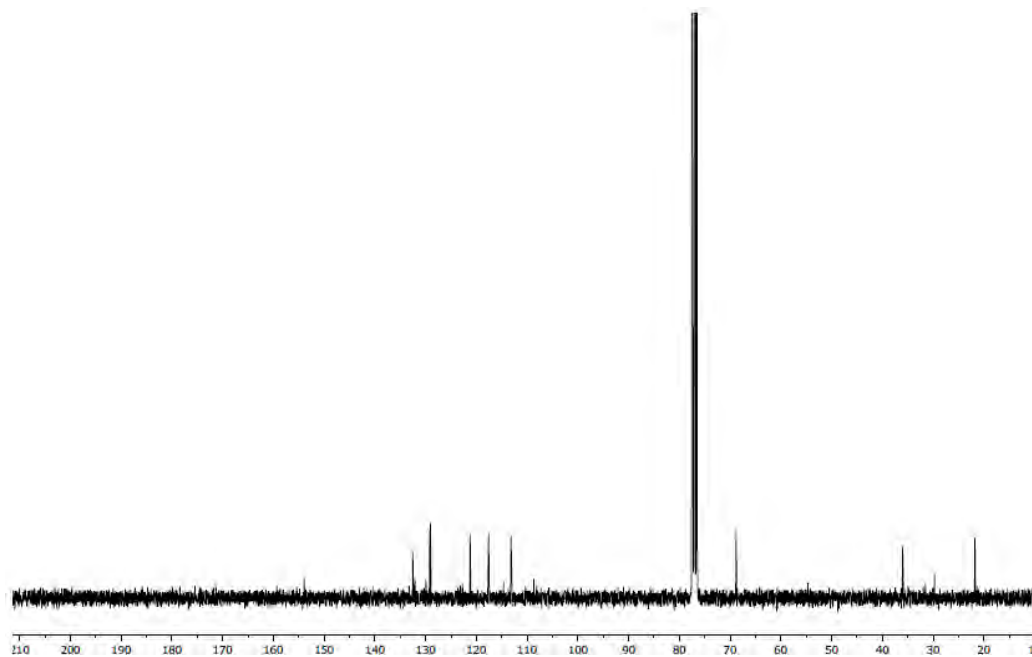


b)



*Minor amounts of the isomerization product (E)-N-methyl-N-(2-(prop-1-en-1-yl)oxy)phenylacetamide, identified by 1D-2D-NMR and GC-MS, and quantified by ^1H -NMR.

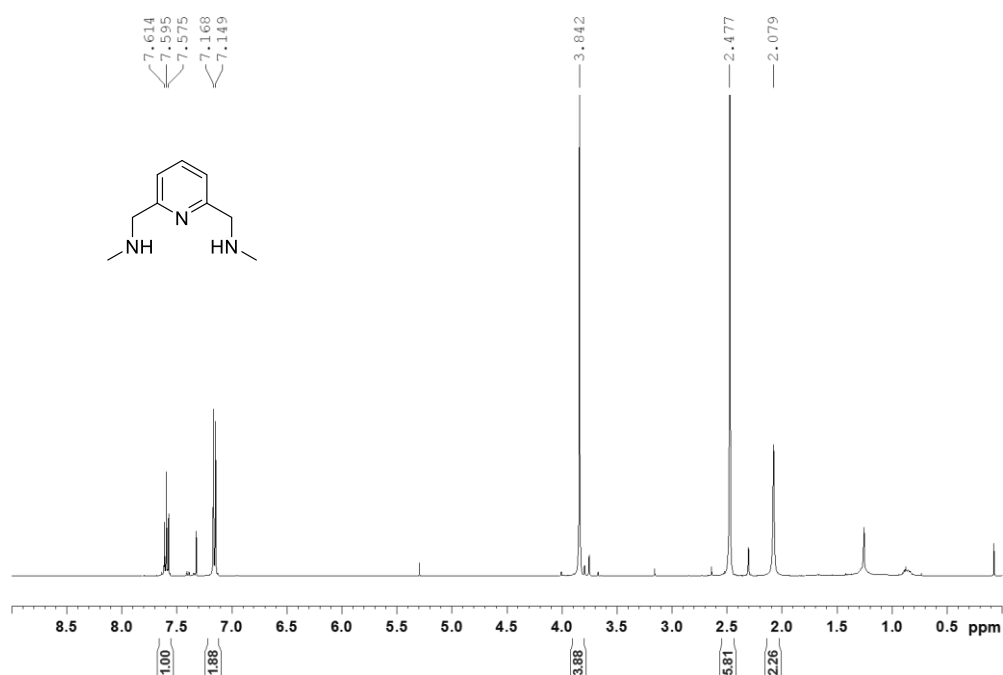
c)



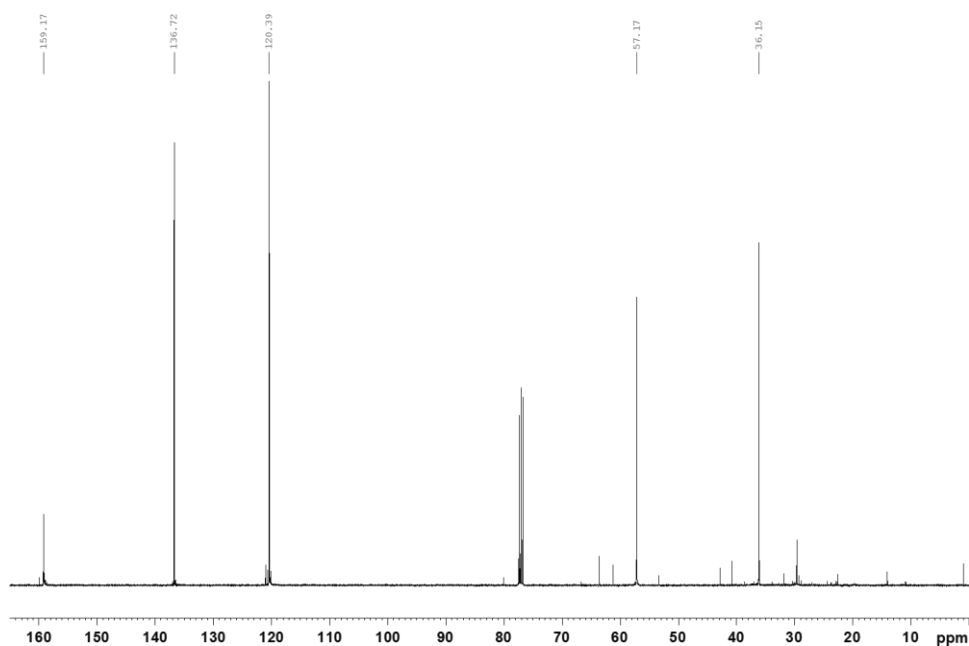
3.2. Supplementary figures S4. Auxiliary ligand L₃

Figure S12. L₃: *N,N'*-dimethyl-2,6-bis(aminomethyl)pyridine; a) ¹H-NMR spectrum (400 MHz, CDCl₃, 25 °C), b) ¹³C{¹H}-NMR spectrum (100 MHz, CDCl₃, 25 °C), c) HRMS (ESI-TOF (*m/z*)).

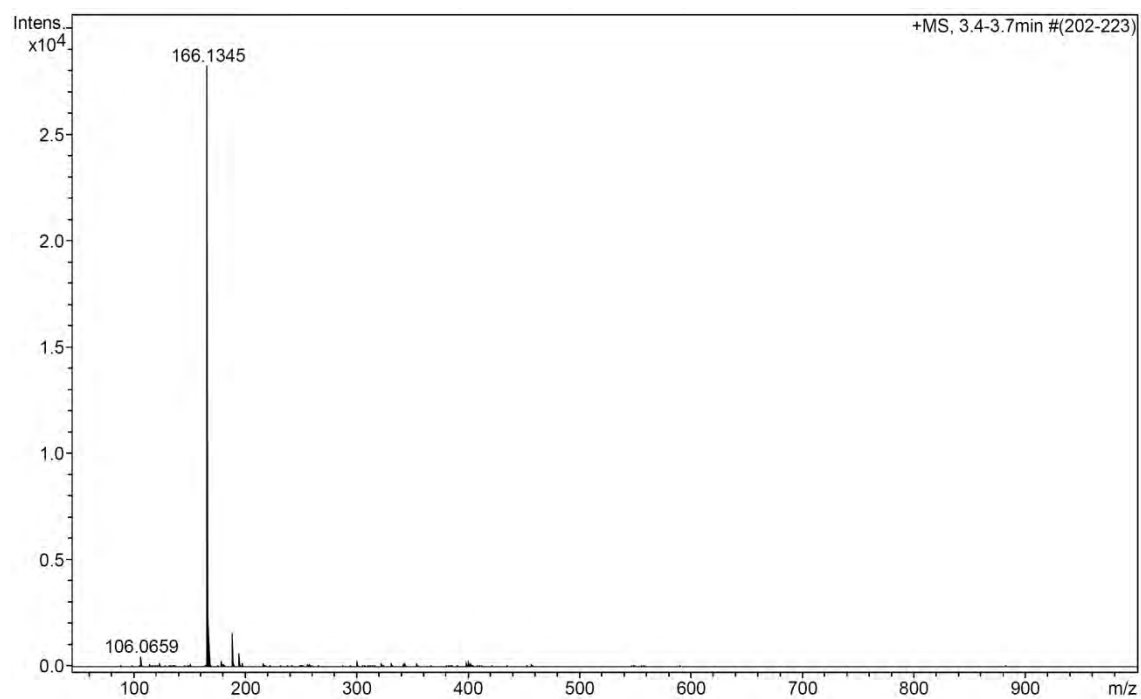
a)

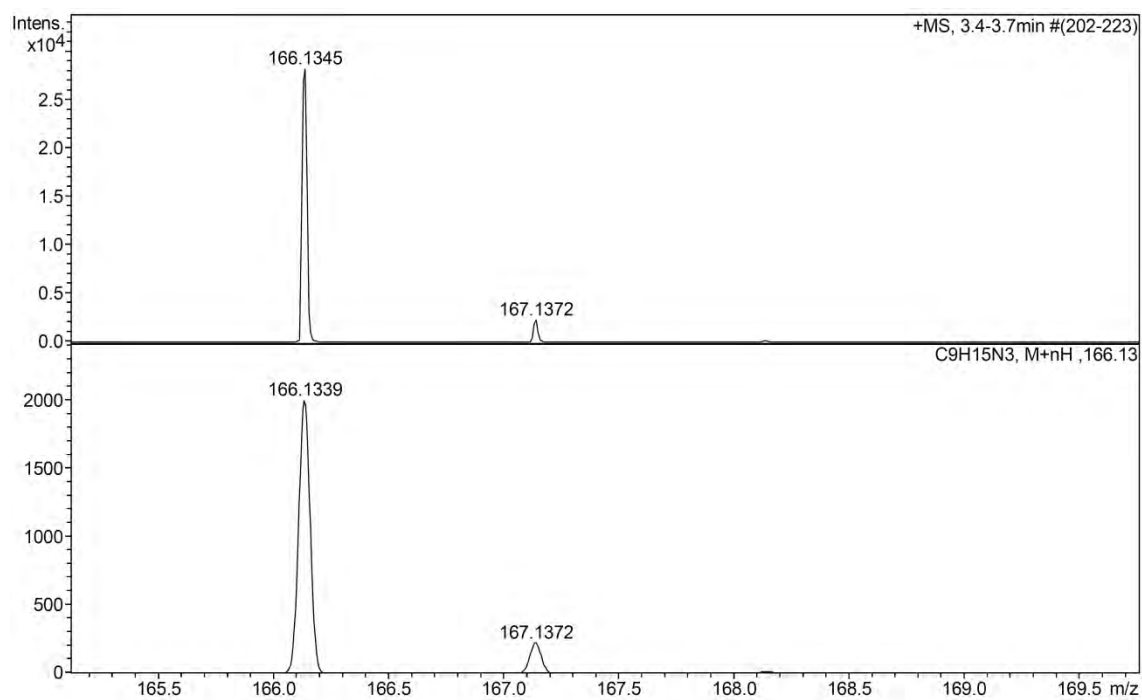


b)

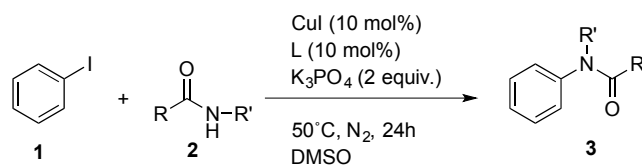


c)





4. Supplementary Tables

Table S1. Screening of amides for N-arylation with iodobenzene.

R, R' = H-, aryl-, alkyl-

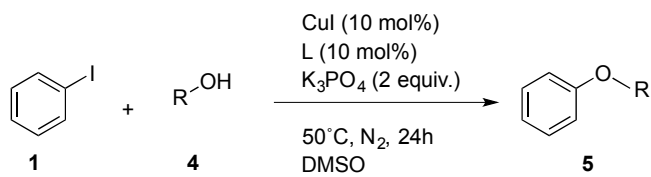
Preferred Auxiliary Ligands: **L**₁, **L**₂, **L**₃ (for primary aromatic amides)
L₇ (for primary aliphatic amides)
L₄/130°C (for secondary amides)

Entry ^[a]	Amides	Product	Ligand [†]	Conv. (%)	Yield (%) ^l
1			L ₁ , L ₂ , L ₃	100	100, 98, 75
2			L ₁ , L ₂ , L ₃ , L ₄	90-100	91, 79, 80, 88
3			L ₂	44	27
4			L ₁	62	46
5			L ₁ , L ₂ , L ₃	50	1, 3, 6
6			L ₁ , L ₂	100	100, 76
7 ^[c]			L ₇	96 ^[e]	91 ^[f]
8 ^[d]			L ₄	98	91
9 ^[d]			L ₄	84	62
10 ^[d]			L ₄	100	52

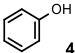
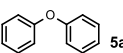
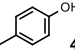
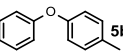
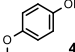
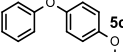
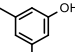
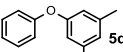
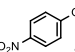
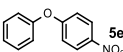
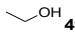
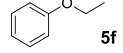
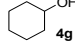
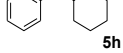
[a] Reaction conditions: **1** (0.88 mmol, 0.9 M), **2** (1.79 mmol); [b] Yield was determined by GC.

[c] Reaction temperature of 80°C. [d] Reaction temperature of 130°C. [e] 2% yield N,N-

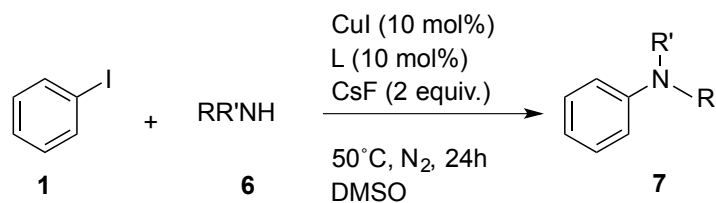
diphenylacetamide. [f] Isolated yield. [†] **L**₃ refers to the hydrochloric salt **L**₃·(HCl)₂. * **2i**=**3a**.

Table S2. Mild O-arylation of alcohols with iodobenzene.

R = aromatic, aliphatic
 Preferred auxiliary ligand: **L₆**

Entry ^[a]	Alcohols	Product	Ligand	Conv. (%)	Yield (%) ^[b]
1	 4a	 5a	L₆	93	82
2	 4b	 5b	L₆	98	92
3	 4c	 5c	L₆	100	97
4	 4d	 5d	L₆	94	94
5	 4e	 5e	L₆	3	3
6	 4f	 5f	L₅	50	27
7	 4g	 5h	L₅	2	traces

[a] Reaction conditions: **1** (0.88 mmol, 0.9 M), **4** (1.79 mmol); [b] Yield was determined by GC.

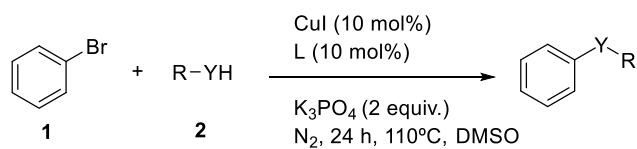
Table S3. Mild N-arylation of amines with iodobenzene.

R, R' = H-, aromatic, aliphatic

Preferred auxiliary ligands: **L₇**, **L₈**

Entry ^[a]	Amines	Product	Ligand	Conv (%)	Yield (%) ^[b]
1	6a	7a	L₈	66	62
2	6b	7b	L₈	44	22
3	6c	7c	L₈	79	76
4	6d	7d	L₇	93	89
5 ^[c]	6e	7e	L₇	100	95
6	6f	7f	L₇	19	13
7	6g	7g	L₇	99	86
8	6h	7h	L₁	98	96

[a] Reaction conditions: **1** (0.88 mmol, 0.9 M), **6** (1.79 mmol); [b] Yield was determined by GC.[c] Yield was determined by ¹H-NMR.

Table S4. Arylation of different nucleophiles with bromobenzene.

Entry ^[a]	Nucleophile	Product	Ligand	Conv. (%)	Yield ^[b] (%)
1			L ₁	7	1
2			L ₈	47	26
3			L ₈	18	0
4			L ₇	21	0
5			L ₈	38	0
6			L ₅	100	100
7			L ₅	95	88
8 ^[c]			L ₇	85	80
9 ^[c]			L ₈	76	50
10 ^[c]			L ₈	79	51

[a] Reaction conditions: **1** (0.88 mmol, 0.9 M), **6** (1.79 mmol, 1.84 M). [b] Yield was determined by GC using 1,3,5-trimethoxybenzene as an internal standard. [c] CsF was used as the base.

5. Supplementary references

- [1] Güell, I.; Ribas, X., *Eur. J. Org. Chem.* **2014**, 3188-3195.

